Regional Geology and Tectonics: Phanerozoic Rift Systems and Sedimentary Basins

Regional Geology and Tectonics: Phanerozoic Rift Systems and Sedimentary Basins

Volume 1B

Editors

D.G. Roberts*

Dept of Earth Sciences, Royal Holloway, University of London, Egham, Surrey, UNITED KINGDOM.
*d.roberts@robertsgeosciences.com

A.W. Bally*

Dept of Earth Sciences, Rice University, Houston, Texas, USA.
*albertwbally@gmail.com

ELSEVIER

AMSTERDAM • BOSTON • HEIDELBERG • LONDON • NEW YORK • OXFORD
PARIS • SAN DIEGO • SAN FRANCISCO • SYDNEY • TOKYO

Elsevier
Radarweg 29, PO Box 211, 1000 AE Amsterdam, The Netherlands
The Boulevard, Langford Lane, Kidlington, Oxford OX5 1 GB, UK
525 B Street, Suite 1900, San Diego, CA 92101-4495, USA
225 Wyman Street, Waltham, MA 02451, USA

First edition 2012

Notice

No responsibility is assumed by the publisher for any injury and/or damage to persons or property as a matter of products liability, negligence or otherwise, or from any use or operation of any methods, products, instructions or ideas contained in the material herein.

British Library Cataloguing in Publication Data
A catalogue record for this book is available from the British Library

Library of Congress Cataloging-in-Publication Data
A catalog record for this book is available from the Library of Congress

ISBN: 978-0-444-56356-9

For information on all Elsevier publications
visit our web site at www.elsevierdirect.com

Printed and bound in China
12 13 14 15 10 9 8 7 6 5 4 3 2 1

Contributors for Volumes 1A, 1B and 1C

A.A. Antobreh
Department of Geosciences, University of Oslo, PO Box 1047, Blindern, N-0316 Oslo, Norway

I.M. Artemieva
Geological Institute, University of Copenhagen, Oster Voldgade 10, DK-1350 Copenhagen K, Denmark

P. Aukes
Kinwest 2008 Energy, 218, 309-2nd Avenue SW, Calgary, AB T2P 0C5, Canada

A.W. Bally
Dept of Earth Sciences, Rice University, Houston, Texas, USA

Y. Bartov
Ministry of National Infrastructures, 234 Jaffa Street, Jerusalem, Israel

Z. Ben-Avraham
Department of Geophysics and Planetary Sciences, Tel Aviv University, Tel Aviv 69978, Israel

G.T. Bertram
Stratigraphic Research International UK Ltd, 41 Braehead Avenue, Milngavie, Glasgow G62 6DH, Scotland, United Kingdom

T.G. Bevan
BP Exploration Libya Ltd., Sunbury-on-Thames, Middlesex, United Kingdom

K.M. Bohacs
ExxonMobil Production Research, PO Box 2189, Houston, TX 77252-2189, United States

W. Borkowski
ExxonMobil Production Research, PO Box 2189, Houston, TX 77252-2189, United States

D. Bosence
Department of Earth Sciences, Royal Holloway University of London, Egham, Surrey, United Kingdom

W. Bosworth
Apache Corporation Egypt, 11, Street 281 New Maadi, Cairo, Egypt

R. Bourrouilh
Laboratoire Cinematique Bassin et Marges, CIBAMAR, Avenue des Facultes, Université Bordeaux 1, 33405 Talence, France

T.A. Brent
Geological Survey of Canada, 3303-33rd Street, NW, Calgary, AB T2E 0Z5, Canada

D.S. Broad
Petroleum Agency SA, PO Box 1174, Parow 7499, Cape Town, South Africa

D. Brown
Canada Nova Scotia Offshore Petroleum Board, i8th floor, TD Centre, 1791 Barrington Street, Halifax NSB3J 3K9, CANADA

P.M. Burgess
Dept of Earth Sciences, Royal Holloway, University of London, Egham. Surrey TW20 0EX, United Kingdom

T. Burke
ExxonMobil Production Research, PO Box 2189, Houston, TX 77252-2189, United States

E. Carminati
Dipartimento di Scienze della Terra, Universita' La Sapienza, P. le A. Moro, Box 11, 00185 Roma, Italy

J. Cartwright
Department of Earth Sciences, Cardiff University, Main Building, Park Place, Cardiff CF10 3YE, Wales, United Kingdom

O. Catuneanu
University of Alberta, Department of Earth and Atmospheric Sciences, Edmonton, Alberta, Canada

J.A. Chalmers
GEUS, Geologiske Undersogelse, Oster Voldgade 10, DK-1350 Copenhagen K, Denmark

F. Charlet
Renard Centre of Marine Geology (RCMG), Universiteit Gent, Gent, Belgium, Dredging International, Scheldedijk, Zwijndrecht, Belgium

F.A. Cook
Department of Geology and Geophysics, University of Calgary, Calgary, AB T2N 1N4, Canada

T. Cope
Department of Geosciences, DePauw University, Greencastle, Indiana, USA

B. Corner
Corner Geophysics Namibia cc., PO Box 2055, Swakopmund, Namibia

J.A. Cupertino
Petrobras/E&P-EXP, Av. Repú blica do Chile 330, Centro, Rio de Janeiro, Brazil

J. Craig
ENI E&P, Via Emilia 1, San Donato Milanese, MI 20097, Italy

L. Desheng
Chinese Academy of Geosciences, 20, Institution Road, P.O. Box 910, Beijing, China

E. Deville
Division Geologie, Institut Francais de Petrole, 1-4 Av. de Bois – Preau, 92852 Rueil Malmaison, France

M. De Batist
Renard Centre of Marine Geology (RCMG), Universiteit Gent, Gent, Belgium

P.W. Dickerson
Department of Geological Sciences, University of Texas at Austin, 1, University Station, Austin, TX 78712-0254, United States

C. Doglioni
Dipartimento di Scienze della Terra, Universita' La Sapienza, P. le A. Moro, Box 11-00185, 00185 Roma, Italy

T. Dooley
Bureau of Economic Geology, Jackson School of Geosciences, University of Texas at Austin, University Station, Box X, Austin, TX 78713-8924, United States

D. Druesne
Total SA, 2, Place Jean Millier La Defense 6, 92078 Paris, La Defense Cedex, France

C. Ebinger
Department of Earth and Environmental Sciences, University of Rochester, Rochester, NY USA

O. Eldholm
Department of Earth Science, University of Bergen, Allegaten 41, N-5007, Bergen, Norway

A-J. Everts
Sarawak Shell Berhad, Sabah Shell Petroleum Co. Ltd., Locked Bag No 1, 98009 Miri, Sarawak, Malaysia

J. Eyer
6 Chantilly Place, Hendersonville, NC 28739, United States

R. Fainstein
Schlumberger, Rio de Janeiro, Brazil

J.D. Fairhead
GETECH PLC, Kitson House, Elmete Hall, Elmete Lane, Roundhay, Leeds LS8 2LJ, United Kingdom

J.I. Faleide
Department of Geosciences, University of Oslo, PO Box 1047, Blindern, N-0316 Oslo, Norway

C.M.R. Fowler
Department of Earth Sciences, Royal Holloway, University of London, Egham, Surrey TW20 0EX, United Kingdom

D. Franke
Bundesanstalt für Geowissenschaften und Rohstoffe (BGR), Hannover, Germany

U. Frieslander
Geophysical Institute of Israel, PO Box 182, Lod 71100, Israel

S. Galeazzi
Total Austral SA, Moreno 877, Ciudad de Buenos Aires 1091, Argentina

K. Gallagher
UMR 6118- Géosciences Rennes, Université de Rennes 1, Campus de Beaulieu, 35042 Rennes Cedex, France

Y. Garfunkel
Institute of Earth Science, Hebrew University of Jerusalem, Givat Ram, Jerusalem 91904, Israel

B. Gelabert
Departament Ciències de la Terra, Universitat de les Illes Balears, 07071-Palma de Mallorca, Spain

R.G. Gibson
Apache Corporation, 6120 S. Yale#1500, Tulsa, OK, 74136, USA

D. Gilbert
ExxonMobil Production Research, PO Box 2189, Houston, TX 77252-2189, United States

A. Ginzburg
Department of Geophysics and Planetary Sciences, Tel Aviv University, Tel Aviv 69978, Israel

S. Graham
Department of Geological and Environmental Sciences, Stanford University, Stanford, California, USA

S.A. Graham
Department of Geological and Environmental Sciences, Stanford University, Stanford, California, USA

N. Haddadi
Retired 11, Avenue Marengo, 77500 Chelles, France

M. Hafid
Dept of Geology, Ibn Tofail University, Kenitra, Morocco

J.C. Harrison
Geological Survey of Canada, 3303-33rd Street, NW, Calgary, AB T2E 0Z5, Canada

K. Hinz
Bundesanstalt für Geowissenschaften und Rohstoffe (BGR), Hannover, Germany

L-Y. Hsiao
Department of Geological and Environmental Sciences, Stanford University, Stanford, California, USA

P. Huchon
Laboratoire de Tectonique, Université Pierre et Marie Curie, Paris, France

M.R. Hudec
Bureau of Economic Geology, Jackson School of Geosciences, University of Texas at Austin, University Station, Box X, Austin, TX 78713-8924, United States

R. Hus
Renard Centre of Marine Geology (RCMG), Universiteit Gent, Gent, Belgium; BHP Billiton, Newman, Australia

H. Jabour
ONHYM, 34, Avenue Alfadila, Rabat 10050, Rabat - Sale - Zemmour-Zaer, MOROCCO

M.P.A. Jackson
Bureau of Economic Geology, Jackson School of Geosciences, University of Texas at Austin, University Station, Box X, Austin, TX 78713-8924, United States

C.L. Johnson
Department of Geology and Geophysics, University of Utah, Salt Lake City, Utah, USA

E.H.A. Jungslager
Tullow Oil, Cape Town, South Africa

M. Kennedy
Department of Earth Science, University of California, Riverside 900 University Avenue, Riverside, CA 92521, United States

A.C. Kerr
Department of Earth Sciences, Cardiff University, Main Building, Park Place, Cardiff CF10 3YE, Wales, United Kingdom

S.M. Khalil
Fault Dynamics Research Group, Department of Earth Sciences, Royal Holloway, University of London, Egham, Surrey TW20 OEX, United Kingdom

O. Khlystov
Limnological Institute of the Siberian Branch of the Russian Academy of Sciences, Irkutsk, Russia

J. Klerkx
International Bureau of Environmental Studies (IBES), Brussels, Belgium

M. Lazar
Dr. Moses Strauss Department of Marine Geosciences, University of Haifa, Mount Carmel, Haifa 31905, Israel

D.P. Le Heron
Department of Earth Sciences, Royal Holloway, Egham, Surrey TW20 0EX, United Kingdom

K. Louden
Dalhousie University, Halifax, Nova Scotia, Canada B3H 4J1

L.P. Magnavita
Petrobras/E&P-EXP, Av. República do Chile 330, Centro, Rio de Janeiro, Brazil

G. Manatschal
CGS-EOST, CNRS-ULP, University of Strasbourg, 1 Rue Blessig, F-67084 Strasbourg, France

M.A. Martins-Neto
Vale E&P – Av. Graça Aranha 26, ZIP 20020-900, Rio de Janeiro, Brazil; Federal University of Ouro Preto, Geology Department, Ouro Preto/MG, Brazil

A. Mascle
Division Geologie, Institut Francais de Petrole, 1-4 Av. de Bois – Preau, 92852 Rueil Malmaison, France

J. Mather
Total E&P Australia, Level 13 – BGC Centre 28, The Esplanade, Perth, WA 6000, Australia

K.R. McClay
Fault Dynamics Research Group, Department of Earth Sciences, Royal Holloway, University of London, Egham, Surrey TW20 0EX, United Kingdom

I.R. McLachlan
Petroleum Agency SA, PO Box 1174, Parow 7499, Cape Town, South Africa

K.E. Meisling
BP Exploration, 200 Westlake Boulevard, Houston, TX 77079, United States

M.A. Menzies
Department of Earth Sciences, Royal Holloway, University of London, Egham, Surrey TW20 0EX, United Kingdom

W.U. Mohriak
Petroleo Brasiliero SA, Exploration Division, Av. Republica do Chile, 65 RJ, PO Box 15515, Rio de Janeiro, 20031-912, Brazil

A.R. Moustafa
Department of Geology, Ain Shams University, Cairo, Egypt

W.R. Muehlberger
Department of Geological Sciences, University of Texas at Austin, 1, University Station, Austin, TX 78712-0254, United States

N. Destro
Petrobras/E&P-EXP, Av. Repú blica do Chile 330, Centro, Rio de Janeiro, Brazil

L. Naudts
Renard Centre of Marine Geology (RCMG), Universiteit Gent, Gent, Belgium; Management Unit of the North Sea Mathematical Models and the Scheldt Estuary (MUMM), Brussels, Belgium

J.E. Neal
ExxonMobil Production Research, PO Box 2189, Houston, TX 77252-2189, United States

R. Newton
50 Santos Haven, Schoeman Street, Heiderand 6511, South Africa

A.A. Nezhdanov
OOO TyumenNIIgiprogas, 2, Vorovskogo Street, Tyumen 625019, Russia

A. Nicolas
Laboratoire de Tectonophysique, ISTEEM (CNRS-UM2), Cc 49 – Universite Montpellier 11, 34095 Montpellier Cedex 05, France

I.O. Norton
ExxonMobil Production Research, PO Box 2189, Houston, TX 77252-2189, United States

P.E. Olsen
Department of Earth and Environmental Sciences and Lamont-Doherty Earth Observatory of Columbia University, Palisades, New York, USA

G. Panza
Dipartimento Scienze Terra, Università di Trieste, Trieste, Italy The Abdus Salam International Center for Theoretical Physics – SAND Group, Trieste, Italy

J.A.M.M. Peijs
BP Exploration Operating Co. Ltd., Sunbury-on-Thames, Middlesex, United Kingdom

J.T. Piombino
BP Egypt, Digla, Maadi, Cairo, Egypt

S. Planke
Volcanic Basins Petroleum Research AS, Oslo Innovation Centre, N-0349 Oslo, Norway

O. Point
Total SA, 2, Place Jean Millier La Defense 6, 92078 Paris, La Defense Cedex, France

J. Poort
Renard Centre of Marine Geology (RCMG), Universiteit Gent, Gent, Belgium; ISTeP, Université Pierre et Marie Curie, Paris, France

B.E. Prather
Shell International E&P, Shell BTC, 3737 Bellaire Boulevard, Houston, TX 77025, United States

D. Procaccanti

R.B. Raykova
Geophysical Institute, Bulgarian Academy of Sciences, Sofia, Bulgaria

T.C. Redshaw
BP Exploration, Chertsey Road, Sunbury on Thames, Middlesex TW16 7LN, United Kingdom

M. Reshef
Department of Geophysics and Planetary Sciences, Tel Aviv University, Tel Aviv 69978, Israel

B. Ritts
Chevron, 60001 Bollinger Canyon Road, San Ramon, CA 94583, United States

B. Ritts
Chevron Asia Pacific Exploration and Production, Singapore

D.G. Roberts
Dept of Earth Sciences, Royal Holloway, University of London, Egham, Surrey, UNITED KINGDOM

H.H. Roberts
Coastal Studies Institute, Department of Oceanography and Coastal Sciences, Louisiana State University, E-235 Howe-Russell, Baton Rouge, LA 70803, United States

E. Roca
Departament Geodinàmica-Geofísica, Universitat de Barcelona, Barcelona, Spain

D. Roeder
Murnau Geodynamics, 9225 West Jewell Place #107, Lakewood, CO 80227, United States

Y. Rotstein
Geophysical Institute of Israel, PO Box 182, Lod 71100, Israel

M. Rottman
ExxonMobil Production Research, PO Box 2189, Houston, TX 77252-2189, United States

J. Roux
Petroleum Agency SA, PO Box 1174, Parow 7499, Cape Town, South Africa

F. Sabat
Departament Geodinàmica-Geofísica, Universitat de Barcelona, Barcelona, Spain

D. Sawyer
Department of Earth Sciences, Rice University, MS 126, 6100 Main Street, Houston, TX 77005, United States

W. Schlager
Faculty of Earth and Life Sciences, Department of Sedimentary and Marine geology, Vrije Universiteit, De Boelelaan 1085, 1081 HV Amsterdam, The Netherlands

R.W. Schlische
Department of Earth and Planetary Sciences, Rutgers University, Piscataway, New Jersey, USA

D. Scrocca
Istituto di Geologia Ambientale e Geoingegneria – CNR, Roma, Italy

H. Shulman
Department of Geophysics and Planetary Sciences, Tel Aviv University, Tel Aviv 69978, Israel

A. Sinkewich
Department of Earth Sciences, Rice University, MS 126, 6100 Main Street, Houston, TX 77005, United States

C. Sladen
BP Mexico, Av. Santa Fe NO 505, Piso 10, Col. Cruz Manca Santa Fe, 05390 Mexico DF, Mexico

R.M. Slatt
School of Geology and Geophysics, University of Oklahoma, 100 E Boyd Street, Ste 210, OK, United States

R. Stephenson
School of Geosciences, University of Aberdeen, Aberdeen, Scotland

E. Stettler
Council for Geoscience, Private Bag X112, Pretoria 0001, South Africa

S. Stovba
SPK-Geoservice, Kyiv, Ukraine

O.E. Sutcliffe
Neftex Petroleum Consultants Ltd, 97, Milton Park, Abingdon OX14 4RY, United Kingdom

R. Swart
Namcor, Private Bag 13196, Windhoek, Namibia

J.C. Sydow
BP Trinidad and Tobago, Port of Spain, Trinidad and Tobago

P. Szatmari
Petrobras/CENPES/PDGEO, Ilha do Fundão, Rio de Janeiro, Brazil

A. Tankard
Tankard Enterprises, Calgary, Alberta, Canada

G. Tari
OMV E&P, Trabrennstrasse 6-8, 1020 Vienna, Austria

F. Tsikalas
Department of Geosciences, University of Oslo, PO Box 1047, Blindern, N-0316 Oslo, Norway ENI Norge, PO Box 101, Forus, N-4064 Stavanger, Norway

B.E. Tucholke
Department of Geology and Geophysics, Woods Hole Oceanographic Institution, Woods Hole, MA 02543, United States

C.I. Uruski
GNS Science, PO Box 30368, Lower Hutt 5010, New Zealand

D. van der Spuy
Petroleum Agency SA, PO Box 1174, Parow 7499, South Africa

A.J. van der Velden
Department of Geology and Geophysics, University of Calgary, Calgary, AB T2N 1N4, Canada

J-H. van Konijnenburg
Sarawak Shell Berhad, Sabah Shell Petroleum Co. Ltd., Locked Bag No 1, 98009 Miri, Sarawak, Malaysia

A.V. Vyssotski
Chevron North America Exploration and Production, Midcontinent/Alaska Business Unit, 15, Smith Road, Room 2101, Midland TX 79705, USA

V.N. Vyssotski
TNK-BP, 1 Arbat Street, Moscow 119019, Russia

A.B. Watts
Department of Earth Sciences, University of Oxford, South Parks Road, Oxford OX1 3AN, UK

P. Weimer
Department of Geological Sciences, 339 UCB, University of Colorado, 2200, Colorado Avenue, Benson Building, Boulder, CO 80309-0399, United States

H. Welsink
Repsol Exploración SA, Madrid, Spain

J. Wendebourg
Shell International E&P BV, Volmerlaan 8, Postbus 60, 2280 AB Rijswijk, The Netherlands

R.S. White
Bullard Laboratories, Department of Earth Sciences, University of Cambridge, Madingley Rise, Madingley Road, Cambridge CB3 0EZ, United Kingdom

P. Whitehouse
Hess Ltd., Level 9, The Adelphi Building, 1-11 John Adam Street, London WC2N 6AG, United Kingdom

R.B. Whitmarsh
Challenger Division, National Oceanography Centre, European Way, Southampton SO14 3ZH, United Kingdom

R. Whittington
IGES, Aberystwyth University, Ceredigion SY23 3DB, United Kingdom

E.L. Winterer
Department of Geological Sciences, Scripps Institution of Oceanography, Geological Division, University of California, San Diego, 9500 Gilman Drive, La Jolla, CA 92093, United States

M.O. Withjack
Department of Earth and Planetary Sciences, Rutgers University, Piscataway, New Jersey, USA

L.J. Wood
Bureau of Economic Geology, Jackson School of Geosciences, University of Texas at Austin, University Station, Box X, Austin, TX 78713-8924, United States

J.E. Wu
Department of Earth Sciences, Royal Holloway, University of London, Egham, Surrey TW20 0EX, United Kingdom

V. Zampetti
Faculty of Earth and Life Sciences, Department of Sedimentary and Marine geology, Vrije Universiteit, De Boelelaan 1085, 1081 HV Amsterdam, The Netherlands

M. Zizi
Ziz Geoconsulting, Rabat, Morocco

Foreword and Introduction

Both the petroleum industry and academia continue to undergo a transition whereby active knowledge transfer by experienced earth scientists represented by faculty teachers and researchers, Chief geoscientists, etc. is rapidly changing to passive knowledge (or data transfer) through a variety of electronic media and systems. Over the recent past, the broad experience base in both industry and academia has been phased out through retirement, redundancy and focus on specific research areas. In the case of industry, a new generation of younger specialists, sometimes called Nintendo geoscientists, are trained to solve specific practical problems based on highly focussed data acquisition and interpretation using work stations. In academia, an increasingly holistic focus on earth systems science is eroding the broader geological base that has hitherto underpinned scholarly research.

As a result, there is a new generation of geoscientists in academia and industry who are insufficiently aware of the various regional geological settings of our planet to separate and differentiate essential from unimportant information. Because the regional context is now deemed to be of much lesser importance, we see a rapid loss of memory, perhaps disinterest (?), in academia and the loss of corporate memory in industry is now legendary. In oil exploration, the lack of regional background is commonly alleviated by expensive multi-client and proprietary consulting reports of variable breadth and depth. However, such reports are only of restricted availability in industry and inaccessible to academia. While the Memoirs of the AAPG and GSA, and Special Publications of the Geological Society provide useful summaries of different aspects of regional geology, in reality these are typically collected thematic sets of papers that do not always provide a systematic overview of a given subject. In addition, academic training does not provide the broader skills to judiciously pick, choose and analyse these publications to provide the adequate background for work in academia or industry.

In conclusion, we believe there is a clear need for a "how to do regional geology" book that provides a useful and insightful overview of what we know and how to think about what we know, and illustrates the characteristics of various geological provinces at different levels of abstraction designed to appeal to a broad readership. In addition, such a book will relate the observed evolution of selected areas to theoretical models. In planning this book, we envisaged illustration with the best possible examples drawn from new and more widely available industry seismic data. To save valuable space that would be taken up by comprehensive lists of references, we have encouraged authors to use key references that allow the reader to pursue further lines of enquiry. In addition, we have tried to ensure that

the book is not overly burdened with theory, detailed methodological discussion and superfluous jargon such as formation and stage names as well as local geographic names. The up to date list of general and specific references will allow the first edition to be archived in digital form, thereby facilitating revision and ultimately the production of a second edition at some future date.

The scope of Phanerozoic Regional Geology of the World is defined by "regional scale". A set of introductory chapters together with overviews that preface the major sections provide the reader with the basic principles allowing exploration of the book at various levels of detail. It should be stressed that the book is not about methods. The introductory chapters are intended to provide nutshell overviews of some of the different methods useful for regional analysis with the main emphasis throughout on the importance of integration as well as its limitations. Summaries of analogue and theoretical models are provided as an essential backdrop to structure and stratigraphy. Chapters in Volume 1A thus provide a global overview of the Earth, principles and methods for regional analysis and a summary of the physical and theoretical basis for some types of geological modelling.

In seeking contributions for these introductory chapters, we encountered difficulty, and did not succeed, in securing, for example, chapters on theoretical models of rifting and passive margin evolution as well as analogue models of extension despite their obvious relevance to offshore deep-water exploration. We find this surprising as we had deemed these chapters to be essential. It may perhaps indicate that the theoretical models have yet to be firmly grounded in terms of the integrated data sets, still sparse, that describe the deep structure of rifts and passive margins despite being more than 30 years since McKenzie formulated his theoretical model of basin extension. We were unable to secure chapters on clastic sedimentation in rifts and carbonate platform evolution possibly because much information already lies in the public domain. In some cases, we were also obliged to seek alternative contributors of chapters. All the above factors, including the effort to compile the Global Maps, resulted in considerable delays in compiling this book for which we apologise to all the contributors.

Perhaps inevitably, the work has proven too large to be published as a single volume and it has now been divided into three volumes 1A, 1B and 1C. Volume 1A deals mainly with principles of regional geological analysis, Volume 1B with rifts and 1C with passive margins and cratonic basins. Our original intent was to include the major chapter on the Global Maps in Volume 1A. However, to achieve a better balance in the length of each of the three volumes, and to herald a fourth volume on compressional basins and folded belts, it is now included in Volume 1C.

Following the introductory chapters in Volume 1A, the main body of Volumes 1B and 1C deals with extensional basins including rifts, passive margins and inverted extensional basins. Each chapter has a broadly similar layout and, where appropriate, includes a section on the petroleum system. We have briefly prefaced each of

the main sections with a short introduction to provide additional context. The examples described in this volume are not exhaustive and have been consciously chosen for diversity as well as importance. Passive margins are reviewed to address commonality of structure and stratigraphic process.

Who is the book for? We envisage that the book will be valuable to all professional geoscientists in the petroleum industry as well as academia who wish to examine, understand and compare the tectonics and stratigraphy of a large variety of basins formed by extension.

Because our background is both the oil industry and academia, we have designed this book to appeal to both constituencies. In the case of the petroleum industry, regional geological understanding that underpins play-based exploration is a prerequisite for any new exploration venture. In this context, the book provides simple analysis and documentation of a variety of extensional basins and thus the basis for comparison in strategic decision ranking as well as an analogue approach.

In terms of academia, we believe that the book will have wide appeal to final year undergraduates, MSc and PhD students because the book can be used at a variety of different levels. For final year undergraduates as well as post-graduate students, the book will be an essential introduction to the geology and analysis of extensional basins. For research workers, we expect that the book will stimulate future research by providing the geological context and relevance for future research projects

About A.W Bally and D.G. Roberts

A.W. (Bert) Bally is Emeritus Professor at Rice University Houston. Before joining Rice, he was Chief Geologist and Exploration Advisor to Shell Us and Pecten. Bert is a past President of the Geological Society of America and is the holder of many major awards including the Sydney Powers Award of the AAPG, the Penrose medal of the Geological Society of America and the William Smith medal of the Geological Society of London to name but a few of his awards. In particular, he is internationally recognised for his early work on cross section balancing in the Canadian Rockies and for several major books notably the Seismic Stratigraphy and Structural Styles Atlases published by the AAPG and the Stratigraphic Atlas of North America. As well as initiating the DNAG set of volumes on the Geology of North America, he was also major contributor to the set.

D.G. Roberts was formerly Distinguished Exploration Advisor at British Petroleum. He is a visiting professor at Royal Holloway, the National Oceanography Centre Southampton and the IFP School Paris. He is Founder and Emeritus Editor of Marine and Petroleum Geology. He co-edited the AAPG Memoir on Salt Tectonics for which he received the R.H. Dott Memorial Award. He is an Honorary Fellow of the Geological Society of America and AAPG. He was awarded the Coke and Petroleum Group medals of the Geological Society of London.

Acknowledgements*

We particularly wish to thank all the authors who have contributed to this volume for producing the excellent chapters that comprise this book. Their patience during the very long gestation period has been very gracious and we believe that their efforts are more than well rewarded by the book and its valuable content. We also wish to thank Elsevier for their forbearance and patience.

A.W. Bally and D.G. Roberts 2011

**The majority of the manuscripts were submitted for the book over a five year period and some even later and are based on information available before the date of submission of manuscript.*

In this chapter

1

Regional geology and tectonics of sedimentary basins

A Prologue

D.G. Roberts, A.W. Bally†*

*Department of Earth Sciences, Royal Holloway, University of London, Egham, Surrey, United Kingdom
†Department of Earth Sciences, Rice University, Houston, Texas, USA

1.1 Introduction

Regional geology forms an essential bridge between local and continental/global geology. Its purpose should be to simplify local surface and subsurface data to a scale that aids prediction and further illuminates the broader brush generalisations implicit in continent-wide and global syntheses.

Regional and supra-regional (e.g., continent-wide) geology thus connects global plate tectonics, global climate changes, global eustatic sea-level changes and underpinning studies in geoscience to the more pragmatic applications associated with the search and conservation of natural resources, that is, water, ore deposits and solid earth energy resources. For example, the steadily evolving seismic technology developed by both academia and the oil industry over the past 50 decades provides ever more detailed subsurface images. As a result, for selected areas there are now very detailed 3D seismic images available, but equally important are the available much longer and more widely spaced 2D profiles. Crustal scale seismic profiles, mostly acquired by academic institutions are even longer and typically have less detailed resolution, but have much deeper penetration as they are intended to map the base of the crust and parts of the upper mantle. Each of these and many other geophysical maps and profiles have their proper role. The same can be said for the large spectrum of geochemical/isotope studies. The purpose and scope of regional geology is to judiciously reconcile insights obtained by studies and surveys of the various geoscience disciplines and to end up with a coherent, observation/data-based narrative that explains the geologic evolution of larger regions and is also tied to a narration of evolving, frequently changing global concepts, models and theories. In the process, it will be inevitable that there

Phanerozoic Rift Systems and Sedimentary Basins DOI:10.1016/B978-0-444-56356-9.00028-6

will be unexpected surprises. These may range from lessons learned from expensive dry holes drilled by petroleum explorers all the way to lofty global hypotheses that fail when tested by incoming new data.

1.2 A historical perspective

There is a widespread perception that the dawn of the geosciences was associated with William Smith, Lyell, Darwin and others. In actuality, geological observations were first and widely used by the earliest civilizations to identify water and mineral resources for bronze, iron, precious metals and coal (see e.g., Agricola, 1556). By the time of William Smith (see Winchester, 2001), the earth sciences were firmly established as observation-based, enabling of the first theories on the evolution of the earth to be drawn directly from observations (see Hutton, 1795; Lyell, 1830–1833). The map developed by William Smith was a direct outcome of the engineering surveys of canals and tunnels. In consequence, by the end of the 1800s, geology had become well established as an applied science, providing services to civil engineering works including roads, tunnels and canals for the military as well as a tool to explore for natural resources.

The parallel exploration of the New Worlds of North and South America and also of Africa by individuals as well as government explorers allowed access to hitherto unknown lands and to new mineral resources. Among exemplary early works are the first map of North America (Guettard, 1752) and the results of the major expeditions by Powell and Hayden in the American West. Ami Boué (Johnson, 1856), followed later by Berghaus (1892), published the first geological map of the world.

About 1700 years ago, exploration and drilling for hydrocarbons probably began with the Chinese who used bamboo casings for their wells. Around the sixteenth century "naphtha" was produced from shallow pits in Baku, Azerbaijan. Drilling for oil in 1813 near Pechelbronn (Alsace, France) marked the inception of petroleum exploration in Europe.

The first modern oil well in North America was drilled by Colonel Drake in Pennsylvania in 1858. Much early oil exploration was focused on areas and surface structures associated with natural oil seepage. It was not until the advent of the internal combustion engine and the change to oil as fuel for cargo and naval ships that there began to be significant demand for oil resulting in systematic onshore oil exploration worldwide initially focused on fold belts and the coastal plains of Texas and Louisiana where there were many natural seeps.

In the late nineteenth and early twentieth centuries, major global syntheses were written first by Suess (1885–1909) followed by Argand (1916, 1922), and later by Stille (1924) and Staub (1928), among many others who contributed significant milestones in regional geology.

They all had the means, intellect and incentive to think big. For example, Suess, in his seminal global geology summary (1885), noted that "the possibility was recognised of deducing from the uniform strike of the folds of a mountain chain, a mean general direction or trend line: such trend lines were seldom seen to be straight but consisted of arcs or curves, often violently bent curves of accommodation; the trend lines of central Europe were observed to possess a certain regular arrangement and to be traceable in part as far as Asia. It was further recognised that the ocean from the mouth of the Ganges to Alaska and to Cape Horn is bordered by folded mountain chains while in the other hemisphere this is not the case so that **Pacific and Atlantic types** may be recognised."Suess thus recognised, over a hundred years ago, the fundamental differences between the active (Pacific) and passive (Atlantic) continental margins. He noted the continuity of the circum-Pacific and Alpine–Himalayan fold belts whose association with calc alkaline volcanism and deep earthquakes is now very well known and understood. Suess was also well aware of the problems of major marine transgressions, especially that of the Late Cretaceous. However, Suess thought that the ocean crust was similar to that of the continents and that the oceans owed their origins to "subsidence and collapse."

The enormous thicknesses of sediments documented in fold belts and their adjacent basins caused major difficulties reconciled in the "geosynclinal" theory of Hall (1882) and Dana (1873). These thicknesses far exceeded the depths of the modern oceans and the sediments typically consisted of shallow marine deposits. Obviously, subsidence had to have taken place to allow the accumulation of such thicknesses. Dana used the term "geosynclinal" with reference to a subsiding and infilling basin resulting from his concept of crustal contraction due to a cooling earth.

The Western Alpine structural zones (see De Graciansky et al., 2011; Trümpy, 2001) soon came to be interpreted in terms of Dana's geosynclinal model. In this way, Emile Haug (1925) added extra detail by invoking an elongate narrow trough between the continents whose erosion supplied the sediment. Two belts of sedimentary rocks were thought to accumulate in troughs separated by an intervening ridge called a "geanticline." He designated the Dauphine geosyncline; the volcanic rocks and deep water sediments were termed a "eu-geosyncline" while the trough with mainly shallow water sediments was called a "miogeosyncline" (see Chapter 4 for a comparison of old and modern definitions). The driving mechanism was thought to be compression between two colliding continents.

A little later, Steinmann (1927) considered that the Alpine ultrabasic and basic igneous rock suites called "ophiolites" (see Chapter 25) were emplaced by injection and differentiation of basic and ultrabasic magmas under marine sediments well before dissection by later thrusts. Today, these ophiolites are known to be fragments of oceanic lithosphere or sub-continental mantle entrained in thrust sheets (see Manatschal and Whitmarsh Chapter 9 and Chapter 25).

The geosynclinal view of the earth seemed comprehensive where mapped in detail but was less than convincing in explaining the relationship between fold belts, volcanoes and seismicity as well as the new data from passive margins in several respects.

Application of the geosynclinal model was valuable in that it provided guidelines for geological exploration and thinking in different fold belts worldwide and particularly those surrounding the Mediterranean. The geosyncline model was classically taught worldwide and remained a mainstay of geology until the 1960s. Notwithstanding the recognition of oceanic and continental crust and the first primitive studies of the deep structure of continental margins in the 1950s, strenuous efforts were made to apply geosynclinal theory to these new and later confirmatory observations. See, for example, Marshall Kay (1951), Drake et al. (1959) and Aubouin (1965).

However, it should be borne in mind that the nineteenth and early twentieth centuries saw the flowering of worldwide geological exploration and the development of many of the sub-disciplines that are embodied in geoscience today. The observations made during this period remain good even though interpretations have changed radically.

At the turn of the nineteenth century, inferences from gravity observations were used to compare the gross crustal structure of the continents and oceans. Airy (1855) proposed that the weaker gravity anomalies associated with mountain belts were caused by a low density root, a hypothesis later known as "isostasy." In 1909, Helmert showed that the gravity anomaly across continental margins exhibited a characteristic edge effect marked by a gravity high on the outer shelf and a low on the continental rise: away from the rise, gravity values returned to the worldwide norm. Wegener (1924), the main proponent of continental drift, recognised the significance of this and concluded continental crust was absent in the ocean basins and that the underlying crust must be very thin. He also inferred that a large pressure differential between continents and oceans would be a consequence of this variation, speculating that this might cause the step faulting observed on the coastal segments of margins such as South Africa and eastern South America.

Laborious measurements of gravity in submarines by Vening Meinesz (1941) among others resulted in the conclusion that the cause of the gravity variation was abrupt thinning of the sialic continental crust across the continental margin.

Early systematic seismic refraction measurements at sea were made in the Atlantic, Pacific, and Indian oceans by Gaskell et al. (1959) during the postwar HMS Challenger expedition complemented by groups at Scripps Institute of Oceanography and Lamont Geological Observatory. Collectively, the results showed that continental crust was completely absent in all the ocean basins and that the ocean basins were characterised by thin sediments overlying a simple tripartite

layered ocean crust quite different from that observed beneath the continents. The transition from continental to oceanic crust was thought to occur beneath the continental rise.

The problem posed by the presence of only thin sediments on oceanic crust was already recognised by Kuenen (1950). He queried the absence of thick sediment accumulations that must have been eroded from folded belts and the continents during previous geological time, assuming continental margins were Tertiary and Mesozoic in age. In the western Alps, for example, in the post Hercynian Mesozoic succession, siliciclastic sediments that would have been eroded from Hercynian terranes are almost absent and the sedimentary record is dominated by carbonates and marls. Kuenen's question thus impacts fundamentally on the processes that formed the oceanic crust.

The first results from seismic refraction studies and their value in defining the nature of the oceanic crust have been mentioned above. Allied to these studies was an explosion in mapping of the sea floor of the world's oceans using modern echo sounding equipment from 1945 onward. The general division of passive margin bathymetry into continent shelf, slope, rise and adjoining abyssal plain was soon recognised as was the presence and worldwide extent of the mid-ocean ridge system although its presence had been inferred earlier by oceanographers. Heezen (1960) recognised that the mid-ocean ridges were characterised by an axial median valley which was the loci of shallow earthquakes. They were able to demonstrate the continuity of the mid-ocean ridge in the Indian Ocean with the East African rift system in Ethiopia. However, they felt unable to offer an explanation of their findings at that time although Heezen later proposed expansion of the earth. In a similar way, mapping of Pacific active margins had identified a shelf, slope and adjacent trench associated with shallow, intermediate and deep earthquakes adjoined onshore by either island arcs or Andean fold belts along with volcanoes.

At the same time, refraction-based sections of the passive margin off North America by Drake et al. (1959) prompted comparison with geosynclines and especially Kay's reconstruction (1951) of the mio-geosyncline and eu-geosyncline of the Appalachian system in middle Ordovician time. The comparison showed as many differences as similarities. While sediment thicknesses were broadly comparable, there were also differences in structural style and overall basin shape. In short, it was difficult to construct a section across a passive margin that resembled a classic geosyncline.

Since the advent of modern cartography, the similarity in shape of the coastlines of the Atlantic had resulted in speculation that they might once have been joined together. The idea of continental drift was first suggested by Taylor (1910) and then Wegener (1924, 1966), who also suggested a means of accounting for the major differences between Atlantic- and Pacific-type margins. Later seminal work by Du Toit (1937), which compared Atlantic margins with rifts and noted

the continuity of the Samfrau "geosyncline" in the now separated continents of the Southern Hemisphere, was ignored in common with other supporting evidence as was Holmes' (1928) avowal of continental drift. At the time, the idea of continental drift was correctly rejected on the grounds that Wegener's mechanism, which proposed continents ploughing through the ocean floors, was physically untenable. Indeed from the viewpoint of geologists in Central Eurasia or on the west, Pacific, coast of the United States, continental drift seemed intrinsically unreasonable. As a result, vertical and compressional tectonics held sway despite being under increasing challenge from marine geophysical studies that blossomed in the postwar years.

In the early 1950s, under the direction of Maurice "Doc" Ewing, at the Lamont, Doherty Observatory, marine geology, geophysics and geochemistry became the focus of a broad data acquisition effort. A prodigious set of cores from the deep-sea floor was acquired using the research vessel Vema. It was the time when detailed surveys revealed the rifted nature of the mid-ocean ridge (e.g., Heezen et al.,1959; Heezen and Tharp, 1961; for additional background, see Doel et al., 2006). About the same time V. Vacquier (e.g., Vacquier et al., 1951; Vacquier, 1972) at Scripps developed the tools and a geomagnetics program that eventually would lead to the early maps that showed linear magnetic anomalies as well (e.g., Raff and Mason, 1961). The results of these early magnetic surveys were followed by the formal introduction of transform faults by Wilson (1965). Eventually, systematic surveys of geomagnetic anomalies covered much of the oceans of the world. In our zeal to elevate the scientists who developed important conceptual breakthroughs, we tend to overlook the foresight of leaders who recognised the need for new kinds of data and measurements that led to the ensuing explosion of novel observations. These, in turn, allowed formulation of many, often competing, new concepts. In short, these studies enabled the hitherto unmapped floors of the oceans, covering two-thirds of the earth, to be mapped in terms of topography and age.

A major paradigm shift resulted from innovative paleomagnetic studies, notably those of Runcorn (1956) and Blackett et al. (1960), which showed that the continents had moved relative to each other. In addition, the celebrated, successful reconstruction of the North and South Atlantic oceans by Bullard et al. (1965), using rotation about Euler poles, confirmed the former conjugation of Africa with South America, Africa with North America and North America with Eurasia.

Although continental drift was from then on regarded as proven, the exact mechanism remained uncertain. For example, Carey (1958), in a paper that anticipated plate reconstructions by 10 years, asserted that the fits of the continents could be readily explained by an expanding earth. However, Hess (1960, 1962), and also Dietz (1961), proposed the sea floor spreading hypothesis as a basis for understanding of sea floor tectonics and in consequence the margins of the ocean basins. This simple and elegant hypothesis states that new oceanic crust is formed

at the axis of mid-ocean ridges by upwelling and injection of magma as dykes, with conservation of the earth's surface N–S of the Pacific for the most part. Passive margins were therefore considered to have formed by crustal extension that led to complete rupture of the continental crust and the formation of ocean crust by spreading as is shown by the continuity of the mid-ocean ridge in the Gulf of Aden with the actively extending northern Ethiopian rift.

In 1963, Vine and Matthews developed a critical corollary to the sea floor spreading hypothesis. They proposed that the, by then, well-mapped pattern of magnetic lineations in the ocean basins could be explained by formation of new oceanic crust during periods of normal and reversed magnetic polarity. The magnetic lineations thus preserved both a record of the history of reversals and also the rate of sea floor spreading. Their hypothesis initially used the precise chronology of magnetic reversals in the late Neogene to calibrate spreading rates. The systematic increase in age of the ocean floor away from the mid-ocean ridge axis was later confirmed by one of the first voyages of the Deep Sea Drilling ship Glomar Challenger in 1968. Le Pichon (1968) showed from a summation of global rates of plate divergence and convergence that the earth was neither contracting nor expanding.

Another key step was made by McKenzie and Parker (1967), who were able to describe the movement of the North Pacific in terms of tectonics on a sphere, thus founding plate tectonics. Isacks et al. (1986) incorporated global seismologic data to complete the formulation of modern plate tectonics. (For a review of the history of plate tectonics see Oreskes, 2003, and Chapter 25.)

From earthquake mechanism studies and the recognition of transform faults, three types of plate boundaries were defined and used by Bally and Snelson (1980) in their classification of sedimentary basins (see Chapter 4):

Extensional, corresponding to active rifts, mid-ocean ridges and their fossil trace represented by *passive margins* and failed rifts such as the North Sea.

Convergent, represented by the subduction zones of the Pacific and the collisional fold belts of the Andes, Himalayas and Alps. Convergence first results in the formation of an accretionary prism and associated trench (e.g., Timor wedge, Chapter 25). Shortening progressively leads to emergence and the construction of fold belts by collision. Flexural loading by the fold belt creates the adjacent foreland basin.

Strike slip, represented by oceanic transform faults, which describe plate trajectories and intracontinental transform faults such as the Dead Sea transform and the San Andreas Fault; transfer faults observed in rift systems are commonly precursors to oceanic fracture zones (Wilson, 1965).

All past and present sedimentary basins can be described in terms of formation at one or the other of these plate boundary types (see McKenzie, 1978; Stockmal et al., 1986).

It should be stressed that the postwar explosion in marine and geophysical research, the results from the Deep Sea Drilling Project and the increasing use of multi-channel seismic data, first in industry and later in academia, had two consequences. First, a much simpler understanding of the way the earth works developed in a plate tectonics context and allowed geoscientists for the first time to address the continuum of evolution from rifting through to passive margins and into folded belts and foreland basins, thus harmonising the modern marine geoscience data with the legacy of 150 years of field-based studies. Second, new observation platforms such as satellites and a radical increase in computing power have resulted in increased sophistication in data manipulation and theoretical modelling of processes that have further enabled understanding of basin evolution. It can be argued that the impact of the post-1950 era of geoscience research, especially in marine geosciences and hydrocarbon exploration, had as broad and deep an impact on regional geology as did the syntheses of Argand and others earlier in the century.

1.3 Some remarks on regional geology and tectonics

The chapters in these volumes, combined with the tables in Chapter 4 and maps in Chapter 25, attempt to simplify what obviously is a very complex geologic world. Hierarchic tables that list orogens, their bounding folds and their thrust belts as well as tables listing sedimentary basins are merely an attempt to assign each of these regional provinces to proper overriding regional themes, which in turn need to be fitted into a global/plate tectonic context.

In reality, no two orogenic systems or sedimentary basins have had the same evolution. Only oceans formed since the Jurassic until today display a remarkably simple tectonic evolution despite complications associated with varying spreading rates and directions, the complexities of transform fault systems, passive and active margins, diffuse oceanic plate boundaries and the emplacement of oceanic plateaus and island chains. The complexities of continental evolution are primarily due to a 4.5-Ga-long history that includes the assembly and then break-up of several supercontinents that become less well defined backward in time. While the reconstruction of Neo-Proterozoic and Paleozoic supercontinents remains debatable, the Phanerozoic is luckily much better constrained than the reconstructions of earlier supercontinents.

Perennial recycling of continental material, through surface erosion and redeposition along former passive margin/oceanic domains, is followed by oceanic and/or continental subduction along active margins. This process also includes subduction of attenuated continental wedges of present and former continental passive margins, and decoupling of some or all of the overlying sediments to form

foreland fold and thrust belts. In addition, crust–mantle transitions in continental arc/backarc domains may modify the crust–mantle boundary and so reset the age of the Moho. All these processes challenge researchers who try to understand the evolution and growth rates of continents, their "stable" cratons, their complex orogens and their overlying sedimentary basins. Continents are always "a work in progress." In this context, it does not help not to be excessively pedantic about definitions. Earth scientists with different backgrounds often use the same terms quite differently—for example, the term "craton," or the notion of the North Sea being a rift versus a cratonic basin. Understanding the different perspectives is important although often well-intentioned new terms and definitions (e.g., "megasutures"; Bally and Snelson, 1980) only add to a confusion that is rarely clarified by committees and resolutions.

In the past, geologists were accused of being mere stamp collectors, while more ambitious "global geo-thinkers" pursued ever better and more refined conceptual/quantitative models. Ordered regional and supra-regional classifications of folded belts and sedimentary basins will always be debatable and ephemeral. Even so, such basins and tectonic systems, etc., in ways similar to well-ordered stamp collections, need to be rationally and thematically systematised if we are to understand the history of the long evolution of our earth, its basins and orogens. Regional and supra-regional classifications need to remain flexible and allow for change.

The mixing of different criteria leads to obvious overlaps as shown by the various rift classifications and the reappearance of the same rifts in so many different tectonic settings (see Chapter 25). Consequently, in our basin classification scheme, rifts are classified separately and the some of the same rifts re-appear as part of yet another basin class. As introduced here and elaborated in Chapter 4, our basin classification proceeds from simple rifts, to passive margins and cratonic basins to increasingly more complex foreland basins, and finally to the most complex and variable episutural basins.

Petroleum explorers know that for each basin type there are representative hydrocarbon-rich "prolific" basins and there are "poor" counterparts; for example, the prolific Gulf of Mexico passive margin basin contrasts with the "poor" Namibia passive margin, the "prolific" West Siberian cratonic basin versus the less productive East Siberia cratonic basin, the prolific Arabian Gulf/foreland basin versus the poor Tindouf basin of Morocco and Algeria, and the episutural Los Angeles basin and Indonesian basins versus the much less prospective basins along the east coast of Canada and Washington and Oregon. Clearly, other geological factors like climate, the paleogeography of basins and, above all, the presence or absence of prolific source beds also matter greatly. However, and clearly so, the main reasons for "rich basins" versus "poor basins" are almost always geological. Basin classifications are of very limited use when evaluating various opportunities or else trying to choose the highest ranked basin for further exploration. Nonetheless, classifications and

ranking of basins are quite helpful in guiding exploration programs from frontier exploration into more mature phases of exploration. In other words, comparing and contrasting well-known basins with a less explored basin of a similar type helps in planning long-range exploration strategies, which include appropriate back-out points when results do not confirm the original ideas that were on the basis of perceived analogues. "Analogy remains demonstration and not proof."

Some of the examples alluded to in Chapter 25 are intended to show the appropriate use and also the limitations of simplified maps and classifications within the more complex scope of regional geology. Regional and supra-regional (e.g., continent-wide) geology serve as a bridge that connects global plate tectonics, global climate changes, global eustatic sea-level studies, etc., to the more pragmatic applications associated with the search and conservation of natural resources, that is, water, ore deposits and solid earth energy resources. For example, the steadily evolving and innovative seismic technology developed by both academia and the oil industry over the past 50 decades now provides ever more detailed subsurface images. As a result, for selected areas, there are now very detailed 3D seismic images available, but of equal importance in regional geological analysis is the use of available, much longer and more widely spaced 2D profiles. Crustal scale seismic profiles, mostly acquired by academic institutions, are even longer, with typically less detailed resolution but have much deeper penetration as they are intended to map the base of the crust and parts of the upper mantle. Each of these and many other geophysical maps and profiles have their proper role as can be said for the large spectrum of geochemical/isotope research studies. The purpose and scope of regional geology is to judiciously reconcile insights obtained by studies and surveys of the various geoscience disciplines and to end up with a coherent, observation/data-based narrative that explains the geologic evolution of larger regions and is also tied to a narration of evolving, frequently changing, global concepts, models and theories. In the process, it will be inevitable that there will be unexpected surprises. These may range from lessons learned from expensive dry holes drilled by petroleum explorers all the way to a global hypothesis that fails when tested by incoming new data. The book that elevates serendipity through exploration as perhaps the most successful "scientific method" has yet to be written! In the meantime, comparative regional geology may help to prepare earth scientists for seminal new insights.

The foundations of regional geology lie in global and regional earth science–related surface and subsurface maps at various scales with varying degrees of simplification ranging from simple sketches to more refined larger scale printed maps to GIS-compatible global databases that allow retrieval of well-defined geological themes. Much as seismic profiles illuminate the subsurface, digital elevation maps combined with geological, geophysical and geochemical maps and seismic lines display the products of the evolution of our $\pm$4.5-Ga-year-old planet. The scope of regional geology not only involves the integration of these maps with other geological, geochemical and geophysical data but also includes communications

between often highly specialised geoscientists and their contacts with colleagues with widely differing backgrounds, students and also outsiders who need and want their advice in practical matters. The chapters in the various volumes and our simplified thematic global maps are intended to support the dialogue between different earth science specialists and also with interested non-geologists such as engineers, managers, academics, administrators and even politicians who require an overview firmly based on a first class regional geological understanding.

Finally, our global maps are not GIS based much as we would like them to be. However, it is hoped that the maps and the tables in Chapters 4 and 25 may guide the design of a future GIS-based thematic map system that would guide users to ask the right, that is, properly focused, questions that would permit easy and swift retrieval relevant of recent and older publications, including the key publications that constitute the large earth science legacy acquired over so many years. Not all countries have adequate geological map coverage and older, say, pre–plate tectonic maps, are often very informative and detailed even though commonly forgotten. Here, the observations remain good even though the interpretation may change later.

Hierarchical tables in Chapters 4 and 25 that list folded belts, their bounding fold and thrust belts as well as sedimentary basins are merely an attempt to assign each of these regional provinces to their proper overriding regional themes, which in turn need to be fitted into a global plate tectonic context. The tables are intended to be flexible and also modified and replaced by geoscientists with different and/or more advanced perspectives. Tables allow the reader to recognise deficiencies that may be modified or else be an incentive to promote a different perspective.

1.4 Conclusion

Where do we stand in the twenty-first century, almost 200 years after William Smith? Today, earth science is burdened by a profusion of constituencies, each characterised with its own specialist jargon. In particular, local geologists use a jargon that differs fundamentally from that used in global geoscience studies. Regional syntheses have an important role to play in aiding translation of local jargon that will benefit global specialists. An interesting example is the widely popular use of local formation names such as the *scisti a fucoidi* or *scaglia cinerea* of central Italy, the Kekituk and Tiglukpuk of northern Alaska, the Tamaulipas of Mexico, and the Kujung and Tuban units of eastern Java. There were and are good reasons for the use of formation names and there is little point ignoring them as worldwide they represent a huge legacy. Yet there is a need to translate them in a common language that will make that heritage accessible to a large majority of geoscientists who do not have meaningful relationships to stratigraphy let alone any kind of paleontology. This emphasises the importance of using tectono-stratigraphic megasequences as a common and consistent communication channel.

Formation names are less commonly used in many offshore areas probably because regional seismic profiles have a built-in stratigraphic continuity. Modern seismic-based sequence stratigraphy, with biostratigraphic control supplemented by a variety of subsurface logs enables lithostratigraphy to be correctly and rigorously placed in a chronostratigraphic context. However, sequence stratigraphic concepts have been so focused on sea-level changes that, in addition, it is very desirable to primarily focus on basin formation processes emphasised by the use of tectono-stratigraphic megasequences. Put in a hierarchical sense, tectono-stratigraphic megasequences define the basin evolution and its building blocks while sequences depict the architecture of the infill of the megasequences.

Common use of the megasequence–sequence hierarchy allows comparison of significant geological themes between regions as well as other parts of the world that appear analogous. The ability to compare and contrast using a common tectonic and stratigraphic framework will be as important as a deeper understanding of the differences is likely to lead to new insights and, in the case of the petroleum explorationists, to new exploration plays and concepts.

Regional geology aims to be a communication bridge between local and global geoscientists. In addition, thematic meetings of earth science societies contribute significantly to improving communications between wider groups of geoscientists as do publications that synthesise various aspects of the earth sciences, and in this context regional geology occupies a special niche. Even so, highly specialised geoscientists need regional geology to provide context to ensure that their models are on target.

For administrators/managers and interested non–earth scientists, regional geology offers a way to summarise and communicate the relationship of local geology with a broader perspective of the earth.

Global perspectives and models, that is, plate tectonics, climatology, paleoceanography, etc., are important. However, these higher levels of abstraction tend to obscure the complexities of the real world, which is the subject of a four-dimensional evolution that began over 4.5 Ga ago, whereas the important subject of this book is only limited to the relatively much more recent record of the past 550 Ma.

We subscribe not only to the classical notion that the recent is a good key to understanding past processes but also to the notion that the past is an important key to the understanding of the present.

References

Agricola, G., De re metallica. Basileae M.D.LVI Froben, Basel 586 pp (http://archimedes.mpiwg-berlin.mpg.de/cgi-bin/toc/toc.cgi?step=thumb). Translated to English by Hoover, H., Hoover, L.H. (1912) 1556 The Mining Magazine in London. 585 pp; reprinted in 1950 by Dover 638 pp.

Agricola, G., 1556. De Re Metallica. English translation by Hoover, H.C. and Hoover, L.H. The Mining Magazine. London. Reprinted by Dover Publications 1950, 672 pp.

Airy, G.B., 1855. On the compilation of the effect of the attraction of mountain ranges as disturbing the apparent astronomical latitude of stations in geodetic surveys. Proc. R. Soc. Lond. 7, 51–75.

Argand, E., 1916. Sur l'arc des Alps Occidentales. Ecl. Geol. Helvet. 14, 145–192.

Argand, E., 1922. La tectonique de l'Asie. Compte Rendu du 13ème Congrès Géologique International, Belgique. Vaillant-Carmanne, Liège, pp. 171–372. In: Carozzi, A.V. (Ed. and translator). Emile Argand: Tectonics of Asia. Hafner, New York, 218 pp and 1 Tectonic Map.

Aubouin, J., 1965. Geosynclines. Developments in Geotectonics. Elsevier, Amsterdam, 335 pp.

Bally, A.W., Snelson, S., 1980. Realms of subsidence. In: Miall, A.D. (Ed.), Facts and Principles of World Petroleum Occurrence. Can. Petrol. Geol. Mem. vol. 6. pp. 6–94.

Berghaus, H., 1892. Atlas der Geologie der Welt. 15 colored maps and text. Justus Perthes, Gotha.

Blackett, P.M.S., Clegg, J.A., Stubbs, P.H.S., 1960. An analysis of rock magnetic data. Proc. R. Soc. Lond. A 256 (1286), 291–322.

Bullard, E.C., Everett, J.E., Smith, A.G., 1965. The fit of the continents around the Atlantic. Phil. Trans. R. Soc. Lond. A 258 (1088), 291–322.

Carey, S.W., 1958. Continental Drift – a symposium. University of Hobart, 375 pp.

Dana, J.D., 1873. On some results of the Earth's contraction from cooling. Am. J. Sci. 5 (3), 423–443.

De Graciansky, P.C., Roberts, D.G., Tricart, P., 2011. The Western Alps, From Rift to Passive Margin to Orogenic Belt: An Integrated Geoscience Overview. Developments in Earth Surface Processes, vol. 14. (Series Ed. J.F. Schroder Jr.). Elsevier, 398 pp.

Dietz, R.S., 1961. Continent and ocean basin evolution by spreading of the sea floor. Nature 190, 854–857.

Doel, R.E., Levin, T.J., Marker, M.K., 2006. Extending modern cartography to the ocean depths: military patronage, Cold War priorities and the Heezen-Tharp mapping project 1092–1959. J. Histor. Geogr. 605–626.

Drake, C.L., Ewing, M., Sutton, G.H., 1959. Continental margins and geosynclines, the east coast of North America north of Cape Hatteras. Physics and Chemistry of the Earth, vol. 5. Pergamon Publishers, New York, pp. 110–198.

Du Toit, A., 1937. Our Wandering Continents. Oliver and Boyd Publishers, London/Edinburgh, 366 pp.

Gaskell, T.F., Hill, M.N., Swallow, J.C., 1959. Seismic measurements made by H.M.S. Challenger in the Atlantic, Pacific and Indian Oceans, and in the Mediterranean Sea, 1950–1953. Phil. Trans. R. Soc. Lond. A 251, 23–85.

Guettard, J.E., 1752. Mémoire dans lequel on compare le Canada a la Suisse, par rapport a ses minéraux. Hist. Acad. R. Sci. In 3 parts: pp. 189–220, 323–360, and 524–538; 4 plates and 2 maps.

Hall, J., 1882. Physical conditions in Paleozoic Seas. 1857-Presidential address. American Association for the Advancement of Science, 31, 29–63.

Hall, J., 1883. Contribution to the geological history of the American continent. American Association for the Advancement of Science, 32, 29–67.

Heezen, B.C., 1960. The rift in the ocean floor. Sci. Am. 203, 98–110.

Heezen, B.C., Tharp, M., 1961. Physiographic Diagram of the South Atlantic, the Caribbean, the Scotia Sea, and the Eastern Margin of the South Pacific Ocean. The Geological Society of America, Boulder, CO.

Heezen, B.C., Tharp, M., Ewing, M., 1959. The Floor of the Oceans. 1: the North Atlantic. Geol. Soc. Am. Special Paper 65, 122 pp.

Helmert, F.R., 1909. Die Tiefe der Ausgleichfläche bei der Prattschen Hypothese für das Gleichgewicht der Erdkruste und dem Verlauf der Schwerestörung von Innern der Kontinente und Ozeane nach den Küsten: Sitzungs Bericht der Königlichen Preussischen Akademie der Wissenschaften. 18, 1192–1198.

Hess, H.H., 1960. Evolution of Ocean Basins. Report to Office of Naval Research. Contract No. 1858 (10), NR 081-067. 38 p.

Hess, H.H., 1962. History of the Ocean Basins. Petrologic Studies – A Volume in Honour of A.F. Buddington. Memoir Geological Society of America, vol. 55, pp. 599–620.

Holmes, A., 1928. Radioactivity and earth movements. Trans. Geol. Soc. Glasg. 18 (3). 559–608.

Hutton, J., 1795. Theory of the Earth, with Proofs and Illustrations, vols. I & II. Cadell & Davies/ William Creech, London/Edinburgh; vol 3, Geological Society, London.

Isacks, B., Oliver, J., Sykes, L.R., 1986. Seismology and the new global tectonics. J. Geophys. Res. 73, 5855–5900.

Johnston, A.K., 1856. The Geological Structure of the Globe According to Ami Boué, with Additions to 1855. Blackwood and Son's, Edinburgh/London, 1 sheet.

Kuenen, Ph., 1950. Marine Geology. Wiley, 568 pp.

Le Pichon, X., 1968. Seafloor spreading and continental drift. J. Geophys. Res. 12, 3661–3697.

Le Pichon, Franchteau, J. Bonnin, 1973. J. Plate tectonics. Elsevier, Amsterdam, 300 pp.

Lyell, C., 1830–1833. Principles of Geology, Being an Attempt to Explain the Former Changes of the Earth's Surface, by Reference to Causes Now in Operation, 3 vols. John Murray, London. Re-issued by Secord, J.E. (Ed.), 1997. Penguin Classics. With Introduction. 48 pp. Text 475 pp.

Marshall Kay, 1951. North American Geosynclines, vol. 151, Geological Society of America, 143 pp.

McKenzie, D.P., 1978. Some remarks on the development of sedimentary basins. Earth Planet. Sci. Lett. 40, 25–32.

McKenzie, D.P., Parker, R.L., 1967. The North Pacific: an example of tectonics on a sphere. Nature 216, 1276–1280.

Oreskes, N. (Ed.), 2003. Plate Tectonics: An Insider's History of the Modern Theory of the Earth. Westview Press, 448 pp.

Raff, A.D., Mason, R.G., 1961. Magnetic survey off the West Coast of North America. 40° Latitude to 52° N Latitude. Geol. Soc. Am. Bull. 72, 1004–1007 (before Hess and Dietz).

Runcorn, S.K., 1956. Paleomagnetism, polar wandering and continental drift. Geologie en Mijnbouw, Amsterdam, 8, 253–256.

Staub, R., 1928. Der Bewegungsmechanismus der Erde. Gebrüder Borntraeger, Berlin. 270 pp. 1 colored map, 44 Figs.

Steinmann, G., 1927. Die ophiolotischen Zonen in den mediterranen Kettengebirgen. Comptes Rendus XIVème Congrès Geologique International, vol. 2. Graficas Reunidas, Madrid. pp. 637–667.

Stille, H., 1924. Grundfragen der vergleichenden Tektonik. Bornträger, Berlin, 443 pp.

Stockmal, G.S., Beaumont, C., Boutilier, R., 1986. Geodynamic models of convergent margin tectonics: Transition from rifted margin to overthrust belt and consequences for Foreland-basin development. Am. Assoc. Petr. Geol. Bull. 70 (2), 181–190.

Suess, E., 1885–1909. Das Antlitz der Erde. Prag and Vienna, Tempsky, V.1(1885) 778 p; V.2 (1888) 703 p; V.3, part 1(1901), 508 pp, and part 2 (1909) 789 pp. Translated by Sollas, H.B.C., Sollas, W.J. (1904–1924). The Face of the Earth (*authorized English translation*). Oxford, Clarendon. V.1 (1904) 104 pp; V.2 (1906) 556 pp; V.3 (1908) 400 pp; and V.4. (1924) 170 p. Translated by E. de Margerie E. 1921. (*authorized French translation*), v. 1–4, 3079 p. Paris, Librairie Armand Colin, 4 vols. 3079 pp.

Taylor, F.B., 1910. Bearing of the Tertiary Mountain Belt on the Origin of the Earth's Plan. Bulletin Geological Society of America 21, 179–226.

Trümpy, R., 2001. Why plate tectonics was not invented in the Alps. Int. J. Earth Sci. 90, 477–483.

Vacquier, V., 1972. Geomagnetism in Marine Geology. Elsevier Oceanography Series, Amsterdam, 185 pp.

Vacquier, V., Steenland, N.C., Henderson, R.G., Zietz, I., 1951. Interpretation of aeromagnetic maps. Geol. Soc. Am. Memo. 47, 151 pp.

Vening Meinesz, F.A., 1941. Gravity over the continental edges. Koninkl. Ned. Akad. Wetenschap. Proc. V. 44.

Vine, F.J., Matthews, D.H., 1963. Magnetic anomalies over mid-ocean ridges. Nature 199, 947–949.

Wegener, A., 1922. Die Enstehung de Kontinente und Ozeane. Geologische Rundschau, 276–292.

Wegener, A.,1966. The origins of the continents and Oceans (translated form the 4th revised German Edition (1929) Dover, 272 pp.

Wilson, T.J., 1965. A new class of faults and their bearing on continental drift. Nature 207, 343–347.

Winchester, S., 2001. The Map that Changed the World. Harper Viking, New York, 352 pp.

In this chapter

2

From rifts to passive margins: A continuum of extension

D.G. Roberts, A.W. Bally†*

*Dept of Earth Sciences, Royal Holloway, University of London, Egham, Surrey, TW20 0EX, UNITED KINGDOM. email:d.roberts@robertsgeosciences.com

†Dept of Earth Sciences, Rice University, MS126, 6100 Main Street, Houston, TX 77005, USA.

Basins formed by stretching of the continental lithosphere comprise a continuum from rifts on continental lithosphere to passive margins formed by the opening of new oceans. The process of rifting that leads to spreading and the formation of passive margins through geological time from the Proterozoic to the Present is an integral part of the 'Wilson cycle' whose parts occur today, side by side in varying areas on our Earth. Rifts are the loci of crustal extension and occur in a variety of tectonic settings ranging from cratonic crust to orogenic settings. Rifts may be abortive or successful leading to the formation of passive margins. Both rifts and passive margins host major hydrocarbon provinces (Fraser et al., 2007) whose petroleum systems are a direct consequence of their structural and stratigraphic evolution.

The succeeding sections provide overviews of rifts, passive margins and their conjugates generally grouped by age and type so that the reader can sensibly compare and contrast.

It is not the intent of this introduction to document the processes that control extension and its reflection in the geological record. There are many useful texts that summarise the geological and physical processes that shape rifts and passive margins (e.g., Allen and Allen, 1990; Busby and Ingersoll, 1995; Fowler, 1990; Kearey et al., 2009; Leeder, 1999; Windley, 1995; Sengör and Natal'in, 2001). However, some commentary is necessary on important advances made in the past 10 years and some outstanding problems.

It is now generally accepted that rifts and passive margins form by extension and cooling of the lithosphere. Both can be broadly divided into magmatic or amagmatic types and examples are described in the following chapters. There may be a continuum between these two end members and also along strike transitions

Phanerozoic Rift Systems and Sedimentary Basins DOI:10.1016/B978-0-444-56356-9.00001-8

from one margin type to another as perhaps exemplified by the Nova Scotian and Moroccan margins (Funk et al., 2004; Maillard et al., 2006). Both types exhibit fundamental differences in structural style and subsidence histories which impact on the evolution of palaeoenvironments from rifting through to passive thermal subsidence.

Relevant to this introduction are the following global maps (Bally et al., Chapter 25, Vol.1C)

Plate 2: Age of rift and age of basement
Plate 3: Tertiary rifts and recent plate motions
Plate 6: Passive margins, age of basement and Cenozoic-Mesozoic rifts
Plate 7: Cenozoic radiating dyke swarms and rifts

2.1 Rifts (Chapters 2–17)

Reporting on East Africa, Gregory (1896) introduced the commonly accepted term 'Rift', fully realising that his rift valleys were the equivalent of the 'graben' (an old German mining term) described earlier by Suess (1883). Quennell (1982, 1985) collected and commented on many earlier publications on rifts. Landon (1994) edited an informative volume on rifts. Letourneau and Olsen (2005) assembled and edited a substantial amount of information on the early Mesozoic rift systems of Eastern N. America. A book edited by Olsen (1995) and its introduction (Olsen and Morgan, 1995) reviews many aspects of rifting including techniques commonly used in the investigation of rifts. A number of papers in Morley (1999) illustrate East African rifts in substantial seismic detail.

Among others, Lambiase (1995) reviews hydrocarbon occurrences in rift systems. Of these, the North Sea is an example of an intracratonic rift whose structure, stratigraphy and petroleum systems are very well documented from oil and gas exploration (Glennie, 1998; Millennium Atlas, 2000).

Syn-rift sediments range from lacustrine to continental (e.g., Graham et al., Chapter 17 Vol 1b; Li Desheng Chapter 9, Vol.1B; Szatmari et al., Chapter 15, Vol.1B) and marine. Hydrocarbon source beds may be lacustrine, coastal swamp and marine. While clastic sequences commonly dominate the syn-rift fill, carbonates are also known to be deposited in rifts, on rift flanks and shoulder shoulders (see, e.g., Bosence, Chapter 6 Vol.1B; Peijs et al., Chapter 8, Vol.1B). Volcanics may comprise part of the syn-rift sequence and less commonly the post-rift sequence (Withjack and Schlische, Chapter 13, Vol.1B).

Sengör and Natal'in (2001) in a detailed and broad review of nearly all known rift systems propose that 'Rifts are fault bounded elongate troughs, under or near which the entire lithosphere have been reduced in extension during their formation'. Rifts are typically bounded by major border faults whose polarity commonly flips along the rift in association with transfer zones. Such transfers often herald transform zones in passive margins.

Based on this reasonable first-order definition, Sengör (1995) also proposed classification of rifts that was re-formatted (as Table 3 and reproduced here) to supplement our overall basin classification and as a guide to some of the jargon in use. Their studies and particularly their maps are the main basis of Plates 1 and 2.

Plate 3 places Tertiary rift systems in a neotectonic plate motion perspective (greatly simplified from Chamot-Rooke and Rabaute, 2006) that allows differentiation between the various tectonic settings of rift systems (see Table 2.1). These settings are controlled by varying directions and convergence rates, leading to complex strain partitioning within Cenozoic and Mesozoic orogens. Most rift systems are also associated with varying degrees of crustal and lithospheric thinning. In addition, a significant number of Tertiary rift systems superimposed on Cenozoic/Mesozoic orogens are linked to low-angle listric faults overlying metamorphic core complexes. For an in-depth discussion of transition of rifting to the opening of an ocean, see Karner et al. (2007a,b), Tucholke et al. (2007) Tucholke and Whitmarsh, Chapter 10 Vol.1C.

Table 2.1 Classification of rifts after Sengör (1995)

1. Rifts
1.1. Active rifts (D)[a]
1.1.1. Intra-plate rifts
1.1.2. Divergent plate boundary rifts (a) with previous doming (b) without previous doming
1.2. Passive Rifts (D)[a]
1.2.1. Divergent plate boundary rifts – associated with strike-slip faults (a) with previous doming (b) without previous doming
1.2.2. Conservative Plate boundary rifts (a) Transtensional rifts (b) Pull-apart rifts (c) Sphenochasms
1.2.3. Convergent plate boundary rifts
1.2.3.1. Subduction-related rifts (a) Extensional arc rifts (b) neutral arc rifts (c) compressional arc rifts
1.2.3.2. Continental collision-related rifts (a) Impactogens (b) Intracontinental convergence-related rifts (c) Pack-ice type rifts
GEOMETRIC TYPES (G) TYPES
G-1 Solitary rifts G-2 Radiating rift stars G-3 Rift chains G-4 Clusters of subparallel rifts (Diffuse Rifts of some authors) G-5 Rift nets

[a](D) Designates the primary Dynamic classification. The other subclasses are secondary kinematic subdivisions.

Comparison of Plate 3 with Plate 6 shows the obvious dominance of Mesozoic passive margin rift systems, but also the widespread distribution of aborted Mesozoic Rifts on the African Craton (Table 2.2).

A glance at the digital elevation map of Plate 1 and Plates 2 and 3 Bally et al., Chapter 25, Vol.1C & Roberts and Bally Chapter 3, Vol.1A shows that many Neogene rifts are associated with a high topographic elevation that extends well beyond the immediate location of specific rifts. This is also the case for the East African Rifts that are located on Precambrian basement, as well as the diffuse rift family of the Basin and Range that is superposed on highly deformed Mesozoic to Palaeogene Cordilleran folded belts. The suggestion is that syn-rift to late-rift regional uplift is not confined to the narrow shoulder regions of rifts but also affects very large adjacent areas that are less deformed.

The duration of rifting ranges from about 9 Ma (Provencal Ligurian basin) to, say, 280 Ma for the Norwegian Greenland Sea, whereby synrift-magmatic events typically are shorter (Ziegler, 1996).

Most Palaeozoic, Mesozoic and a number of Tertiary rifts are buried and separated by a post-rift unconformity that does not preserve the shoulders of specific rifts. This suggests extensive post-rift peneplanation that precedes the deposition of a new megasequence. The erosion of rift shoulders may be more limited in marine rifts covered by a marine post-rift sequence. Consequently, the hiatus separating syn-rift from post-rift megasequences covers a more limited time.

Table 2.2 Tertiary rifts and neotectonics[a,b]

1 Rifts on cratonic crust (e.g., East African Rifts, Bresse/Rhone-Rhine graben system)
2 Rifts associated with the opening of a passive margin (e.g., Offshore Lena Delta)
3 Rifts superimposed on Cenozoic/Mesozoic orogenic systems
3.1 Associated with W. Pacific slab roll back and the coeval opening marginal back-arc seas (e.g., [b]East Asia onshore and offshore)
3.2 Associated with Indian Ocean slab roll back (e.g., Indonesian back arc basins)
3.3 Associated with Transtensional/Transpressional West Pacific/N. America Plate Boundary (e.g., [b]Basin and Range rift system, California pull-apart basins)
3.4 Associated with overall compressional Andean Plate boundary
3.5 Associated with Africa Eurasia collision (e.g., [b]Alboran Sea, [b]Tyrrhenian Sea and [b]Central Apennines, and the [b]Aegean Sea/Eastern Anatolia diffuse rift systems)
3.6 Associated with India/Eurasia collision ([b]Himalaya/Tibetan Plateau)

[a]*Rift systems associated with thickened crust/lithosphere (all other systems are associated with varying degrees of crustal/lithospheric extension (stretching)).*
[b]*Associated with Tertiary extensional metamorphic core complexes.*

The rifts shown on Plate 2 are not easily combined in the context of the comprehensive basin classification shown on Plate 4 (see also Tables 1 and 3 in Chapter 4 on Basin Classification and Tectonostratigraphic Megasequences Roberts and Bally Chapter 4, Vol 1A).

Many, if not most, basins are underlain by rift systems, suggesting that extension has acted as an initial driving mechanism for many basins. However, the presence or absence of evidence supporting rifting is often easily explained. When the syn-rift fill overlies basement, while the rift shoulders are in turn overlain by the post-rift sequence, the implied hiatus may well be in order of several tens or over 100 My. Pre-rift erosion is fairly common and the presence of a pre-rift sequence may or may not narrow the stratigraphic hiatus underlying the rift sequence. Without a fairly accurate idea of the missing time associated with the hiatuses that underlie and overly the rift fill, it is often difficult to estimate how much of the rift system and the surrounding region has been eroded before and after the rifting. Diachronous rifting further complicates the situation as does the inversion of rifts during their late stages in that it sometimes precedes post-rift erosion.

2.2 Passive margins

Passive margins can be divided into *amagmatic* (Chapters 9–11 Vol 1C), *magmatic* (Chapters 4–8, Vol.1C) and *transform* (Chapters 15–18, Vol.1C) margin types.

In the context of the length of passive margins worldwide, amagmatic margins now seem to be in a minority and magmatic margins of various ages (see Plate 7) may be more common. Examples of amagmatic passive margins include the conjugate margins of Newfoundland and Iberia, the Labrador Sea and the transform margins of the Equatorial Atlantic. We suspect the proportion may decrease further as deeper seismic imaging becomes more available across poorly known margins. There seems to be no correlation between the presence or absence of amagmatic and magmatic margins with underlying basement structure or age.

2.3 Amagmatic margins

In the case of amagmatic rifts and passive margins, a variety of kinematic models have been developed which describe the stretching process in terms of uniform simple shear (McKenzie, 1978), asymmetric simple shear (Wernicke, 1985), detachment faulting (Lister et al., 1986) and depth-dependent stretching (Davis and Kusznir, 2004; Keen and Dehler, 1993). As first noted by McKenzie (1978), the variation in the thickness of the crust and lithosphere across rifts and passive margins controls heat flow, subsidence and melting by decompression (Watts, this volume). The variation in heat flow through time in response to cooling is of course the foundation of predictive petroleum systems modelling (e.g., Doligez et al., 1986; Welte et al., 1997). An updated 2002 version of Ziegler (1996) provides a good overview of the dynamics of rifting.

Through integration of deep-sea drilling, seismic reflection and refraction studies, the best-documented amagmatic passive margins are those of western Iberia and Newfoundland (Holker et al. 2003; see Tucholke and Whitmarsh Chapter 10, Vol.1C). Studies of the continent ocean transition zone on these margins have been aided by study of the exhumed Tethyan passive margin in the Swiss Alps which exhibits many closely comparable features. More recently, Leslie (2009) has reported the results of a 2008 workshop on the Highland Boundary Fault Zone of Scotland which has comparable features to the Iberian margin and the Tethyan margin in the Alps, suggesting these results widen applicability to Palaeozoic passive margins and thus emphasising the similarity of process during the Phanerozoic.

The new observations of the conjugate but asymmetric margins of Iberia and Newfoundland and in particular the presence of exhumed serpentinised subcontinental mantle (Tucholke and Whitmarsh; Whitmarsh and Manatschal, this volume) have widened discussion of the spatial variant of crustal and lithospheric extension on highly extended amagmatic passive margins (see Huismans and Beaumont, 2008). More information on the topic of lithosphere extension and breakup can be found in Karner et al. (2007a,b) and papers therein.

There are several major issues. Davis and Kusznir (2004) have noted that there is a common and significant discrepancy between the amount of extension measured from upper crustal extensional faults and the amount of extension inferred from crustal thickness. Secondly, the nature of the upper crustal extension process observed from normal fault geometries and how it evolves to control the exhumation of subcontinental mantle is not understood (Huismans and Beaumont, 2008). Both problems are related intimately.

A variety of papers document the overall geometry of extensional faults on passive margins and in the field. There is little doubt in our view that these faults are truly listric as well documented by De Charpal et al. (1978), Perez-Gussiniye and Reston (2001), Holker et al. (2003), Reston (2007) and also see Welsink and Tankard, Chapter 14, Vol.1B. The Monte Generoso fault, exposed near Lugano, Switzerland, is a particularly fine and well-documented example of an exhumed listric fault with its associated rollover (Bernouilli et al., 1990). The Jean D'Arc graben on the eastern Grand Banks is similar but crustal in scale (Welsink and Tankard, Chapter 14, Vol.1B).

The classical approach to measurement of extension is to make detailed measurements of the heaves of upper crustal faults and to then compare the results with those made from crustal thickness measurements. That the fault plane trajectories flatten with depth close to the brittle ductile transition in the continental crust of highly extended margins persuasively argues for depth-dependent stretching (Chenet et al., 1982). However, it has been argued that multiple generations of faulting at subseismic scales conceal perhaps as much as 40–70% of the deformation (Marrett and Allmendinger, 1992).

Crosby et al. (2008) have inversely modelled strain in a manner that does not prescribe the presence or absence of depth-dependent stretching. Their work, based on conjugate reflection and refraction and deep-sea drilling data from Newfoundland and Iberia, shows that strain rate distributions are depth dependent, suggesting that the lithospheric mantle thins over a wider region than the crust. Their strain rate histories have been tested by comparing total horizontal extension with that inferred from normal faults to find that both agree within the margins of error. It is important to note that it is likely that the stretching behaviour may have varied through time. As the crust is initially thinned by small amounts, depth-dependent stretching is unlikely to occur as is observed in failed rifts such as the North Sea. However, as strain rates increase and stretching evolves to higher extension factors, depth-dependent stretching becomes progressively more important. In the case of the Iberia–Newfoundland, strain rates are initially high but decrease significantly in the past 10 Ma before the first formation of oceanic crust whose spreading rates are also very low. In this period, exhumation of serpentinised subcontinental mantle seems to have taken place. While it is obvious that the exhumed lithospheric upper mantle deforms in a ductile manner, the evolution and position of the detachment during the transition from brittle extension to ductile deformation are not clear. Development of an admissible balanced cross-section seems problematic (Lavier and Manatschal, 2006; Whitmarsh and Manatschal, Chapter 9, Vol.1C).

While several problems remain, the existence of broad zones of exhumed upper mantle has considerable implications for heat flow and temperature gradients on the outer parts of amagmatic margins relevant to petroleum generation. In addition, initial water depths at the time of exhumation of the subcontinental mantle were probably in the region of 2000 m, resulting in deposition of condensed pelagic marls and shales in this distal setting.

2.4 Magmatic margins

Magmatic passive margins which are more widespread exhibit quite different characteristics. Following the inception of magmatic activity increases with initial emplacement of radiating dyke swarms and associated volcanic plateaus (see Plates 25 and 7 Bally et al., Chapter Vol.1C), the radiating dyke swarms may be viewed as roots surrounding a hot spot. The Central Atlantic Magmatic province (CAMP) is perhaps the best-documented magmatic event of this type (see Hames et al., 2003; Withjack and Schlische, Chapter 13, Vol 1B). The inferred centre of the hotspot is placed east of northern Florida (see Global map B-10), but this is sensitive to the pre-drifting fit of the peri-Atlantic continents and the hyper-extended continental margin. Centres of radiating dyke swarms associated with volcanic plateaus have also been established for the Parana/Etendeka Plateaus of Brazil and southern Africa. These early magmatic events are known to be active during the very early rifting phases of passive margins (e.g., Hafid et al., 2000).

It is plausible to assume that the subaerial volcanics revealed as seaward dipping reflectors (see Global map C-7) along magmatic margins of laterally propagating opening oceans would be more likely to be linked more to coast–parallel dyke systems that were emplaced after the initial emplacement of radial dyke swarms.

First reported by Hinz (1981) and drilled during DSDP leg 81 (Roberts et al., 1984), they are now known to consist of subaerial basalts whose internal velocity and density structure results in the suites of seaward-dipping reflectors (SDRs) commonly observed on seismic profiles (Mutter and Zehnder, 1988; Mutter et al., 1982). The seaward downdip tips of these reflectors are thought to correspond to dyke swarms which source the magma forming subaerial lavas extruded along dyke parallel fissures. Onshore, large igneous provinces are generally associated with magmatic margins as are major regional dyke swarms and sills observed both at outcrop (e.g., East Greenland) and on seismic profiles in adjoining sedimentary basins.

The magmatism is voluminous and in the case of East Greenland and Western India took place about 2 Ma ago.

This narrow age span coupled with the linearity and length of magmatic margins implies very rapid rift propagation and transition to spreading: transform faults are rare, an exception being the Jan Mayen fracture zone. Conjugate margins show complete symmetry in the oceanward dips of the SDR suites.

Modern refraction and reflection profiles across such margins are few and among the best known are those off eastern North America, where the prominent East Coast Magnetic Anomaly defines the zone of SDRs (Talwani et al., 1994) although quality refraction data are now also available for Greenland, Norway, Namibia, the Rockall Plateau and the Faeroes. These refraction data share common features. An underplated body, represented by high-velocity lower crust, is always present and located between continental and oceanic crust (Mjelde et al., 2005; Mutter and Zehnder, 1988). The SDRs can be shown to straddle the continent–ocean boundary. Unlike amagmatic margins, the continent–ocean transition zone is abrupt and relatively narrow, perhaps as little as 20 km (see, e.g., Mjelde et al., 2004; White et al., 2008) and separates relatively thick, though thinned, continental crust from oceanic crust. Because the width of the zone of SDRs may be much wider than the width of the continent ocean transition noted earlier, there is a significant uncertainty to pre-spreading continental rifts in the case of magmatic margins.

This narrow age span coupled with the linearity and length of magmatic margins implies very rapid rift propagation and transition to spreading: transform faults are rare, an exception possibly being the Jan Mayen fracture zone. Conjugate margins show complete symmetry in the oceanward dips of the SDR suites.

The thermal conditions and tectonic processes that give rise to magmatic margins are open to question. Clearly, the formation of enormous amounts of basalt

in short geological time spans requires anomalous, large and rapid amounts of melting in the upper mantle. Asthenospheric temperatures higher than those at mid-ocean ridges are necessary. In this context, White and McKenzie (1989) discussed magmatism at rift zones. White (1989) proposed that magmatic margins are associated with mantle plumes. White et al. (2008) review the emplacement of lower crustal intrusions on the North Atlantic continental passive margin. Indeed, plume-related uplift of Scotland has been proposed as the explanation for its exhumation during the Palaeocene and deposition of the prolific reservoir sands of the Early Tertiary in the North Sea. However, very high rates of upwelling of mantle material may be an alternative mechanism. The latter has some appeal as a mechanism that may explain the length and linearity of many magmatic margins but may require initiation by plume impingement in the upper mantle (Simon et al., 2009).

Another problem concerns the conditions within the crust that permit massive dyke intrusion. While it is well established that dyke intrusion is aided by fluid pressure, we offer the view that the crust may be weakened through prior rifting that heralds magmatism. Work in the Afar depression of Ethiopia (Wolfenden and Ebinger, 2005; Ebinger, Chapter 7, vol.1B) shows that a major initial phase of brittle extension which formed the rift margin is followed by dyke intrusion and fissure eruption in the rift axis: the outcrop pattern of the lavas is similar to the SDRs observed on seismic profiles.

Less well understood is the along-strike segmentation of magmatic margins. Off Nova Scotia, for example, the East Coast Magnetic Anomaly and its associated underplated body die out and the margin apparently has the structure of an amagmatic margin (Funk et al., 2004) though new refraction data suggest this may not be the case (Makris, 2010, personal communication). The same transition has also been reported on the conjugate margin of Morocco (Maillard et al., 2006) and is also possibly observed in the northern Red Sea. However, as noted earlier, the thermal and kinematic evolution of amagmatic and magmatic margins is incompatible. This is a problem requiring further research.

2.5 Transform passive margins

Transform margins mark the location of transform faults that define the tangential trace of movement between diverging plates. The relative motion of the plates is deemed by convention to be parallel to the fault trace. Transform faults commonly inherit the fabric of major transfer faults in rifts which control the polarity of extension on rift border faults. Commonly, as the trailing edges of the diverging plates separate, transform faults evolve into oceanic fracture zones with which they are contiguous.

Despite their obvious importance in passive margin evolution, until recently comparatively little was known about the stratigraphy and structure of transform passive margins. Large transforms such as the active San Andreas Fault system,

developed in an orogenic setting, were much better understood due to a combination of outcrop geology and hydrocarbon exploration in the associated transtensional basins. The Dead Sea–Jordan valley transform (Avraham et al., Chapter 17, Vol 1C) offers a useful insight into a long offset passive margin transform in the early phases of development. Along the line of this system, transtensional basins represented by the Gulf of Aqaba, Dead Sea and Sea of Galilee are present as well as major transpressionally elevated areas such as Mt. Hermon. Such features bear useful consideration in examining transform passive margins.

The best-known transform margins are in the Equatorial Atlantic between Guinea and Nigeria and also along the conjugate margin of Northern Brazil, Surinam (Blaich et al., 2009) and South Africa (Broad et al., Chapter 15, Vol.1C). Although earlier information on the Guinea and Ghana fracture zone of the Atlantic was reported by Jones and Mgbatogu (2007), Benkhehil et al. (1995) and Basile et al. (2005), only since 2000 has much new seismic information become available from oil exploration in the Equatorial basins of West Africa; recently, the giant Jubilee-Mahogany discoveries were made off Ghana. The role of the transform systems in controlling both structure and sedimentation is of obvious exploration importance in transform margins. Antobreh et al., Chapter 16, Vol.1C document, from multichannel seismic and potential field data, a complex pattern of evolution involving changing plate boundary geometry, transtension and transpression in configuring the structural architecture of the margin. This may pertain more widely as better-quality data become available. A less complex pattern of evolution is demonstrated in the hydrocarbon-bearing transtensional basins developed along the Agulhas transform margin of South Africa: Broad et al., Chapter 15, Vol.1C.

References

Allen, P.A., Allen, J.R., 1990. Basin Analysis. Blackwell Science, Oxford, UK, 451pp.

Basile, C., Mascle, J., Guiraud, R., 2005. Phanerozoic geological evolution of the Equatorial Atlantic domain. J. Afr. Earth. Sci. 43, 275–282.

Benkhehil, J., Mascle, J., Tricart, P., 1995. The Guinea continental margin: an example of a structurally complex transform margin. Tectonophysics 248, 117–137.

Bernouilli, D., Bertotti, G., Froitzheim, N., 1990. Mesozoic faults and associated sediments in the Austro-Alpine and South Alpine passive continental margin. In: The Geology of Italy Since 1990. Memoria della Societa Geologica Italiana, vol. 45, pp. 25–38.

Blaich, O.A., Tsikalas, F., Faleide, J.I., 2009. Northeastern Brazilian margin: regional evolution based on integrated analysis of seismic reflection and potential field data and modeling. Tectonophysics. doi:10.1016/j.tecto2008.02.011.

Busby, C.J., Ingersoll, R.V. (Eds.), 1995. Tectonics of Sedimentary Basins. Blackwell Science, Oxford, UK, 579pp.

Chamot-Rooke, N., Rabaute, A., (compilers). 2006. Plate Tectonics from Space, 1:50,000,000. CGMW (Commission of the Geological Map of the World), UNESCO, Paris.

Chenet, P., Giraud, H., Montadert, L., Roberts, D.G., 1982. Extension ratio measurements on the Galicia, Portugal and northern Biscay margins: implications for evolutionary models of passive margins. In: Studies of Continental Margin Geology. AAPG Mem., 34, pp. 703–715.

Crosby, A., White, N., Edwards, G., Shillington, D.J., 2008. Evolution of the Newfoundland-Iberia conjugate margins. Earth Planet. Sci. Lett. 273, 214–226.

Davis, M., Kusznir, N.J., 2004. Depth-dependent lithospheric stretching at rifted continental margins. In: Karner, G.D. (Ed.), Proceedings of NSF Rifted Margins Theoretical Institute. Columbia University Press, pp. 92–136.

De Charpal, O., Guennoc, P., Montadert, L., Roberts, D.G., 1978. Rifting, subsidence and crustal attenuation in the Bay of Biscay. Nature 275, 706–711.

Doligez, B., Bessis, F., Burrus, F., 1986. Integrated numerical simulation of sedimentation, heat transfer, hydrocarbon formation and fluid migration in a sedimentary basin: the THEMIS model. In: Thermal Modelling of Sedimentary Basins. Ed Technip, Paris, France , pp. 173–195.

Fowler, C.M.R., 1990. The Solid Earth. Cambridge University Press, Cambridge, UK, 472pp.

Fraser, S.J., Fraser, A.J., Lentini, M.R., Gawthorpe, R.L., 2007. Return to rifts – the next wave: fresh insights into the petroleum geology of global rift basins. Petrol. Geosci. 13, 99–104.

Funk, T., Jackson, H.R., Louden, K.E., Dehler, S.A., Wu, Y., 2004. Crustal structure of the northern Nova Scotia rifted continental margin (eastern Canada). J. Geophys. Res. 109, BO9102. doi:10.1029/2004JB003008.

Glennie, K.W. (Ed.), 1998. Petroleum Geology of the North Sea. Blackwell Science, Oxford, UK, 636pp.

Gregory, J.W., 1896. The Great Rift Valley. John Murray, London, UK.

Hafid, M., Ait Salem, A., Bally, A.W., 2000. The Western Termination of the Atlas system – offshore Essaouira Basin. Mar. Petrol. Geol. 17 (3), 431–443.

Hames, W.E., McHone, J.G., Renne, P.R., Ruppel, C. (Eds.), 2003. The Central Atlantic Magmatic Province. Insight from Fragments of Pangaea. American Geophysical Union. Geophysical Monograph, 136, p. 267.

Hinz, K., 1981. A hypothesis of terrestrial catastrophes: wedges of very thick oceanward dipping reflectors beneath passive continental margins: their origin and environmental significance. Geologisches Jahrbuch, Reihe E Geophysik, 3–28.

Holker, A.B., Manatschal, G., Holliger, K., Bernouilli, D., 2003. Tectonics, nature and seismic response of top-basement detachment faults in magma poor rifted margins. Tectonics 22. doi:10.1029/2001TC001347.

Huismans, R., Beaumont, C., 2008. Complex rifted continental margins explained by dynamical models of depth-dependent extension. Geology 36, 163–166.

Jones, E.J.W., Mgbatogu, C.C.S., 2007. The structure and evolution of the West African margin of Guinea Bissau, Guinea and Sierra Leone. In: Scrutton, R.A., Talwani, M. (Eds.), The Ocean Floor. Wiley, New York, pp. 165–202.

Karner, G.D., Manatschal, G., Pinheiro, L.M. (Eds.), 2007a. Imaging, Mapping and Modelling Continental Lithosphere Extension and Breakup. An introduction, Geol. Soc. Sp. Publ., 282, p. 482.

Karner, G.D., Manatschal, G., Pinheiro, L.M. (Eds.), 2007b. Imaging, Mapping and Modelling Continental Lithosphere Extension and Breakup. An introduction, Geol. Soc. Sp. Publ., 282, pp. 1–8.

Kearey, P., Klepeis, K.A., Vine, F.J., 2009. Global Tectonics. third ed. Blackwell-Wiley, Chichester, UK, 482pp.

Keen, C.E., Dehler, S.A., 1993. Stretching and subsidence of conjugate margins in the North Atlantic region. Tectonics 12, 1201–1229.

Lambiase, J.J. (Ed.), 1995. Hydrocarbon Habitat in Rift Basins, Geol. Soc. Sp. Publ., 80, p. 380.

Landon, S. (Ed.), 1994. Interior Rift Basins, AAPG Mem., 59, 276.

Lavier, L.L., Manatschal, G., 2006. A mechanism to thin the crust at magma poor margins. Nature 440, 324–328.

Leeder, M., 1999. Sedimentology and Sedimentary Basins: From Turbulence to Tectonics. Blackwell Science, Oxford, UK, 591pp.

Leslie, G., 2009. Border skirmish. Geoscientist 19, 16–20.
Letourneau, P.M., Olson, P.E. (Eds.), 2005. Flood Basalt Provinces of the Pangean Atlantic Rift: Regional Extent and Environmental Significance. Columbia University Press, New York, USA.
Lister, G.S., Etheridge, M.A., Symonds, P.A., 1986. Application of the detachment fault model to the formation of passive continental margins. Geology 14, 246–250.
Maillard, A., Malod, J., Thiebot, E., Klingelhofer, F., Rehault, J.P., 2006. Imaging a lithospheric detachment at the continent–ocean transition off Morocco. Earth Planet. Sci. Lett. 241, 686–698.
Marrett, R., Allmendinger, R.W., 1992. Amount of extension on"small" faults: an example from the Viking graben. Geology 20, 47–50.
McKenzie, D.P., 1978. Some remarks on the development of sedimentary basins. Earth. Planet. Sci. Lett. 40, 25–32.
Mjelde, R., Raum, T., et al., 2005. Continent-ocean transition on the Voring Plateau, NE Atlantic, derived from densely sampled bottom seismometer data. J. Geophys. Res. 110, B5.
Mjelde, R., Raum, T., Myrhen ,B., Shimamura, H., Murai, Y., Takanami, T., Karpuz, R. And Naess, U. (2001). Continent- ocean transition on the Voring Plateau, NE Atlantic derived from densely sampled ocean bottom seismometer data. Journal of Geophysical Research,110, (B05101), 1–19.
Morley, C.K. (Ed.), 1999. Geoscience of rift systems – evolution of East Africa, AAPG Studies in Geology 44, p. 242.
Mutter, J.C., Zehnder, C.M., 1988. Deep crustal structure and magmatic processes: the inception of seafloor spreading in the Norwegian Sea. Early Tertiary volcanism and the Opening of the NE Atlantic, Geol. Soc. Sp. Publ., 39, pp. 35–48.
Mutter, J.C., Talwani, M., Stoffa, P., 1982. Origin of seaward dipping reflectors in oceanic crust off the Norwegian margin by "subaerial sea floor spreading". Geology 10, 353–357.
Olsen, K.H. (Ed.), 1995. Continental Rifts: Evolution, Structure, Tectonics. Elsevier, Developments in Geotectonics 25, Elsevier, Amsterdam, pp. xxiii+466.
Olsen, K.H., Morgan, P., 1995. Introduction: progress in understanding continental rifts. In: Olsen, K.H. (Ed.), Continental Rifts: Evolution, Structure, Tectonics. Elsevier, Developments in Geotectonics 25. Elsevier, Amsterdam, pp. 3–26.
Perez-Gussiniye, M., Reston, T.J., 2001. Rheological evolution during extension at non volcanic rifted margins: onset of serpentinisation and development of detachments leading to continental breakup. J. Geophys. Res. 106, 3961–3975.
Quennell, A.M. (Ed.), 1982. Rift Valleys: Afro-Arabia. Hutchinson Ross, Stroudsburg, PA, USA, 419pp.
Quennell, A.M., 1985. Continental Rifts. Van Nostrand Reinhold, New York NY, USA, 349pp.
Reston, T.J., 2007. Extension discrepancy at North Atlantic non volcanic rifted margins; depth dependent or unrecognized faulting. Geology 35, 285–301.
Roberts, D.G., Backman, J., Morton, A.C., Murray, J.W., Keene, J.B., 1984. Evolution of volcanic rifted margins: synthesis of Leg 81 results on the west margin of Rockall Plateau. In: Roberts, D.G., Schnitker, D., et al., (Eds.), Initial Reports of the Deep Sea Drilling Project. Leg 81, vol. 81, US Government Printing Office, Washington, DC, pp. 883–911.
Sengör, A.M.C., 1995. Sedimentation and tectonics of fossil rifts. In: Busby, C.J., Ingersoll, R.V. (Eds.), Tectonics of Sedimentary Basins. Blackwell Science, Oxford, UK, pp. 53–118.
Sengör, A.M.C., Natal'in, B.A., 2001. Rifts of the World. Mantle Plumes: Their Identification Through Time, Geol. Soc. Am. Sp. Paper, 352, pp. 183–225.
Simon, K., Huismans, R.J., Beaumont, C., 2009. Dynamical modelling of lithospheric extension and small scale convection: implications for magmatism during the formation of volcanic rifted margins. Geophysical Journal,176,1,327–350.
Suess, E., 1883. Der Antlitz der Erde. 1A. Tempsky, Prague, p. 310.
Talwani, M., Ewing, J., Sheridan, R.E., Holbrook, W.S., Smithson, S.B., 1994. The EDGE experiment and the US East Coast magnetic anomaly. In: Banda, E., Torne, M., Talwani, M. (Eds.), Rifted Ocean-Continent Boundaries. Kluwer Academic Publishers, Dordrecht, Netherlands, , pp. 155–182.

Tucholke, B.E., Sawyer, D.S., Sibuet, J.C., 2007. Breakup of the Newfoundland Iberia Rift. In: Karner, G.D., Manatschal, G., Pinheiro, L.M. (Eds.), Imaging, Mapping and Modelling Continental Lithosphere Extension and Breakup. Geol. Soc. Sp. Publ., 282, pp. 9–47.

Welte, D., Horsfield, B., Baker, D.R., 1997. Petroleum and Basin Evolution: Insights from Geochemistry, Geology and Basin Modeling. Springer, Berlin, Germany.

Wernicke, B.P., 1985. Uniform-sense normal simple shear of the continental lithosphere. Canad. J. Earth Sci. 22, 108–124.

White, R.S., 1989. Initiation of the Iceland Plume and opening of the North Atlantic. In: Tankard, A.J., Balkwill, H.R. (Eds.), Extensional Tectonics and Stratigraphy of North Atlantic Margins, Am. Assoc. Petrol. Geol. Mem., 46, pp. 149–154.

White, R.S., McKenzie, D.P., 1989. Magmatism at rift zones: the generation of volcanism at continental margins and flood basalts. J. Geophys. Res. 94B, 7685–7729.

White, R.S., Smith, L.K., et al., 2008. Lower crustal intrusion on the North Atlantic continental margin. Nature 452, 460–464.

Windley, B., 1995. The Evolving Continents. John Wiley, Chichester, UK, 526pp.

Wolfenden, E., Ebinger, C., 2005. Evolution of a volcanic rifted margin, southern Red Sea, Ethiopia. Bull. Geol. Soc. Am. 117, 7–8, 846–864.

Ziegler, P.A., 1996. Geodynamic processes governing the development of rifted basins. In: Roure, F., Ellouz, N., Shein, V.S., Skvortsov, I. (Eds.), Geodynamic Evolution of Sedimentary Basins. Technip, Paris, pp. 85–94. An updated 2002 version of this paper is available on: http://com1.geol.unibas.ch/downloads/ziegler.pdf.

Millennium Atlas (2003). Petroleum Geology of the Central and Northern North Sea. Eds. Evans, D., Graham, C., Armour, A. and Bathurst, P. Geological Society London, pp. 389.

In this chapter

3

Models for the evolution of passive margins

A.B. Watts
Department of Earth Sciences, University of Oxford, South Parks Road, Oxford OX1 3AN, UK

3.1 Introduction

It has been more than 30 years since Sleep (1971) first proposed that passive continental margins form by thermal contraction following rifting and continental breakup. According to his model, the lithosphere is heated during rifting which causes thermal expansion and uplift over a broad region. Cooling restores the uplifted lithosphere to its pre-rift level, but sub-aerial erosion thins it. The net result is that the lithosphere subsides below its initial level, thereby forming a marginal depression for continental-derived sediments to infill.

Sleep (1971) assumed that margin evolution could be modelled by the cooling of a plate from an initially high temperature and an erosion rate that was proportional to the regional elevation. He substantiated his model by showing that the depth to horizon tops in wells in the coastal plain of the East Coast, USA, when normalised to a particular depth (in his case the top of the Woodbine) followed an exponential curve with a thermal time constant of about 50 Myr. A similar time constant characterises the subsidence of oceanic lithosphere away from a mid-ocean ridge.

Walcott (1972) showed that although thermal contraction and erosion may indeed combine to produce a marginal depression, sediments act as a load on the surface of the lithosphere and cause additional subsidence. He demonstrated that if sediments prograded into a 5 km deep basin, the lithosphere (which includes the crust) would bend or flex by as much as 8 km, depending on the density of the sediment and, importantly, the flexural rigidity of the underlying lithosphere.

Sleep and Snell (1976) constructed a model that combined thermal contraction, erosion and flexure and showed that it explained many features of the stratigraphic architecture of the coastal plain of the East Coast, USA. One problem with the model, however, was that it was based on a viscoelastic rather than an elastic plate. Flexure studies (e.g., Watts and Cochran, 1974) had earlier

Phanerozoic Rift Systems and Sedimentary Basins DOI:10.1016/B978-0-444-56356-9.00002-X

suggested that the oceanic lithosphere is elastic, rather than viscoelastic, and that if there is any load-induced stress relaxation, it occurs on short time-scales (i.e., $<$1 Myr) rather than on the long time-scales ($\sim$10–50 Myr) that had been assumed by Sleep and Snell (1976).

Nevertheless, Sleep's model was instrumental in focussing attention on the structural styles of passive margins. In two seminal papers, Montadert et al. (1977) and de Charpal et al. (1978) showed that the Bay of Biscay and Rockall Plateau (eastern North Atlantic) margins were underlain by tilted and rotated 'blocks' that were bounded by listric faults. These authors noted that there was little evidence for sub-aerial erosion preceding rifting. They suggested that the tilted blocks formed in response to extension during rifting and that it was brittle deformation, together with ductile flow, that thinned the crust and caused subsidence.

These observations, together with the lack of evidence for erosion in the deeper parts of the North Sea basin, led McKenzie (1978) to develop an alternative model. He proposed that the subsidence of rift-type basins was caused partly by stretching of the crust during extension (the 'initial subsidence') and partly by thermal cooling of the thinned sub-crustal lithosphere (the 'thermal subsidence'). The McKenzie stretching model, as it is now known, and its modifications for the effects of finite rifting and lateral heat flow (e.g., Cochran, 1983), have subsequently enjoyed much success in explaining the subsidence and uplift history of rift-type basins in both continental interior and passive margin settings.

While stretching is a highly effective way to extend the crust and lithosphere, precisely how it occurs is in dispute. The McKenzie model assumes 'pure-shear' which predicts that the geometry of the thinned crust either side of a rift zone would show a high degree of symmetry. Wernicke (1985), however, suggested an alternative 'simple shear' model based on field observations of highly extended terranes that are now juxtaposed to metamorphic core complexes in the Basin and Range province of the western USA. The main feature of his model is a 'detachment surface' that separates an 'upper plate' consisting of a weakly structured rifted upper continental crust from a 'lower plate' dominated by a highly deformed lower crust. The model predicts spatial variations in the proportion of crust to mantle thinning and, hence, a high degree of asymmetry in the subsidence and uplift history either side of a continental rift zone (e.g., Wernicke, 1985) or newly formed ocean basin (e.g., Lister et al., 1986).

Since about the mid-1980s, there has been a rapid increase in the amount and, importantly, the quality of multichannel seismic (MCS) reflection profile data acquired over the world's ocean basins and their margins. These data have imaged not only the sediments, but also the rift structures that underlie them. The increase has been led by the oil and gas industry as exploration has shifted from the continental shelf to deep-water slope and rise regions. The industry

activity has been supplemented by academic groups interested in rifting processes, sedimentary products and fluid flow (e.g., US MARGINS, UK Ocean Margins, France 'Marges', EUROMARGINS) and by government-led groups (e.g., Geoscience Australia) involved in the mapping of the Economic Exclusion Zone.

The new MCS data have shown increasing complexities in passive margins, especially as regards their across-strike and along-strike structure. As a result, a new generation of thermal and mechanical models based on numerical and analogue techniques has been constructed. In this chapter, we will review some of the new observations and the models that have been developed to explain them. We begin, as did Sleep, by considering the subsidence and uplift history as this is still one of the most important data sets against which the predictions of new models need to be tested.

3.2 Subsidence and uplift history

Passive margins are characterised by large thicknesses of sediments (up to ~12 km) that obscure and make it difficult to use structural styles alone to distinguish between the various rifting models. The development of techniques such as backstripping (e.g., Watts and Ryan, 1976), however, has enabled the subsidence and uplift history to be determined directly from stratigraphic data. These data may then be compared to the predictions of different rifting models.

The backstripping of biostratigraphic data from commercial wells shows that the tectonic subsidence (i.e., the subsidence not caused by sediment and water loading) of passive margins decreases with time following rifting (e.g., Watts and Ryan, 1976). The subsidence is exponential in form and bears a striking resemblance to that of oceanic crust away from a mid-ocean ridge.

Unfortunately, commercial wells tend to be drilled on structural 'highs' and so relatively few of these wells penetrate both the syn-rift (i.e., the sediments that form during rifting) and the post-rift (i.e., the sediments deposited after rifting). As a result, there is still much uncertainty about the tectonic subsidence during the syn-rift and post-rift. Some margins (e.g., South China Sea – Lin et al., 2003) appear to have an equal amount of syn-rift and post-rift subsidence. Others, however, exhibit either more syn-rift than post-rift subsidence (e.g., Western Mediterranean – Watts et al., 1993) or less syn-rift than post-rift subsidence (e.g., Labrador, Canada – Royden et al., 1980; northwest Australia – Driscoll and Karner, 1998).

The proportion of syn-rift to post-rift sediments is a useful constraint on rifting models. The instantaneous, uniform extension, McKenzie stretching model, for example, predicts an approximately equal amount of syn-rift and post-rift subsidence, irrespective of the actual amount of crustal heating and thinning. Variations therefore suggest refinements to the model. The large proportion of

syn-rift to post-rift subsidence in Western Mediterranean margins, for example, has been explained by a finite rifting model in which the majority of the thinning and, hence, subsidence occurs during the syn-rift rather than the post-rift (e.g., Cochran, 1983). The small proportion of syn-rift to post-rift subsidence in the Labrador, Canada and Northwest Australia margins has been attributed to a greater amount of extension in the mantle than in the crust (Royden et al., 1980). The latter model, however, causes a 'space problem' if the *total* amount of extension is not constrained in depth (e.g., White and McKenzie, 1988). Driscoll and Karner (1998) therefore proposed another model in which extension in the upper mantle and lower crust was partitioned from the upper crust by an intra-crustal detachment.

A critical question is whether the pattern of tectonic subsidence and uplift deduced from backstripping is similar at *conjugate* passive margins (i.e., the margins that form on opposing sides of a new ocean basin). The 'pure shear' model predicts a symmetric pattern of subsidence and uplift patterns in each margin. The 'simple shear' model, however, predicts an asymmetric, spatially varying, pattern.

While both 'pure shear' (e.g., White, 1989) and 'simple shear' (e.g., Lister et al., 1986) models have been applied to passive margins, there is presently too few well data to be able to distinguish between them. The best constraints on the amount of thinning have come instead from seismic reflection and refraction data. Keen et al. (1989), for example, argued that while the pattern of faulting at the Flemish Cap, Canada and Goban Spur (Southwest Approaches, UK) conjugate margin pair is asymmetric, the amount of crustal thinning shows a high degree of symmetry. Recently, Louden and Chian (1999) using better data have questioned the degree of symmetry at this margin pair. Moreover, these workers have shown that the Labrador–southwest Greenland conjugate margin pair is initially symmetric, but shows progressively more asymmetry as the locus of rifting shifts to one side of the rift system.

Backstripping of restored stratigraphic cross-sections of ancient passive margins that have been preserved in deformed orogenic belts reveals patterns of tectonic subsidence and uplift that resemble those in modern margins. The Canadian and U.S. Rockies (e.g., Armin and Mayer, 1983; Bond and Kominz, 1984), Alps (e.g., Wooler et al., 1992), Betics (e.g., Peper and Cloetingh, 1992) and Himalaya (e.g., Corfield et al., 2005), for example, show examples where there is an equal amount of syn-rift to post-rift subsidence. By backstripping restored stratigraphic sections and comparing them to the predictions of the 'pure shear' and 'simple shear' models, it has been possible to place constraints on the age of rifting, the distribution of stretched crust, and the orientation (e.g., of the proximal and distal facies) of ancient margins.

Not all passive margin backstrip curves reveal the smooth exponential shape expected of thermal and mechanical models. Some show departures due to

uncertainties in the parameters used in backstripping (e.g., the compaction depth constant, paleobathymetry and magnitude of sea-level changes in the past). Others, however, show departures due to basin-wide tectonic events and post-depositional sedimentary processes. The tectonic subsidence and uplift of the Tethyan margin in the Betics, for example, show changes in the subsidence rate during the Middle Triassic, Early Jurassic and Callovian–Hauterivian, which Peper and Cloetingh (1992) attributed to multiple rifting events. The Northeast Atlantic margin (Clift et al., 1995) shows excess uplift early on in its evolution that has been attributed to dynamic topography due to plume-related processes. In contrast, the Northwest Australia margin (Muller et al., 2000) shows excess subsidence later in its evolution that has been attributed to dynamic topography due to subduction-related processes. Finally, the eastern seaboard of Canada (Watts and Steckler, 1979) and northern Gulf Coast (Diegel et al., 1995) margins show similar magnitude excesses of uplift and subsidence. The excesses have been interpreted, however, not as tectonic in origin, but as a result of post-depositional processes associated with salt migration.

The departures in the backstrip from simple exponential curves make it difficult to invert subsidence and uplift history data *directly* for the amount of stretching and, hence, the strain rate history of a passive margin. Nevertheless, White (1994) has attempted such inversions on the basis that they are able to discriminate between extensional rifting events from other events, such as those associated with thrust/fold loading, flexure and foreland basin formation. As Newman and White (1997) have demonstrated, the strain rate and its relationship to the amount of stretching, β, is a potentially important constraint on the rheology of extended continental lithosphere.

The Wilson Cycle implies that passive margins ultimately become the sites of orogeny. Although the mechanisms by which this transition takes place are unclear (e.g., Erickson, 1993), there is evidence from backstripping of biostratigraphic data that foreland basins are underlain by stretched crust (e.g., the western deep Gulf of Mexico basin which overlies the western Gulf Coast margin (Feng et al., 1994), the Papuan basin which overlies the Northwest Australia margin (Haddad and Watts, 1999) and the west Taiwan basin which overlies the South China Sea margin (Lin and Watts, 2002)).

Figure 3.1 shows an example of one such backstrip curve from the Colville Trough (north slope, Alaska), a flexural foreland basin that formed as a result of thrust/fold loading in the Brooks Ranges. The figure shows that during the Carboniferous to Jurassic the well site was the location of an exponentially decreasing passive margin type subsidence. The decrease can be explained by a McKenzie stretching model with an initial rifting age of 360 Ma and $\beta = 1.5$, although a finite rifting model with an older rifting age and higher β could explain the subsidence equally well. Irrespective of that, the exponentially decreasing subsidence is interrupted during the Late Jurassic and mid-Cretaceous by an accelerating subsidence that is typical of foreland basins.

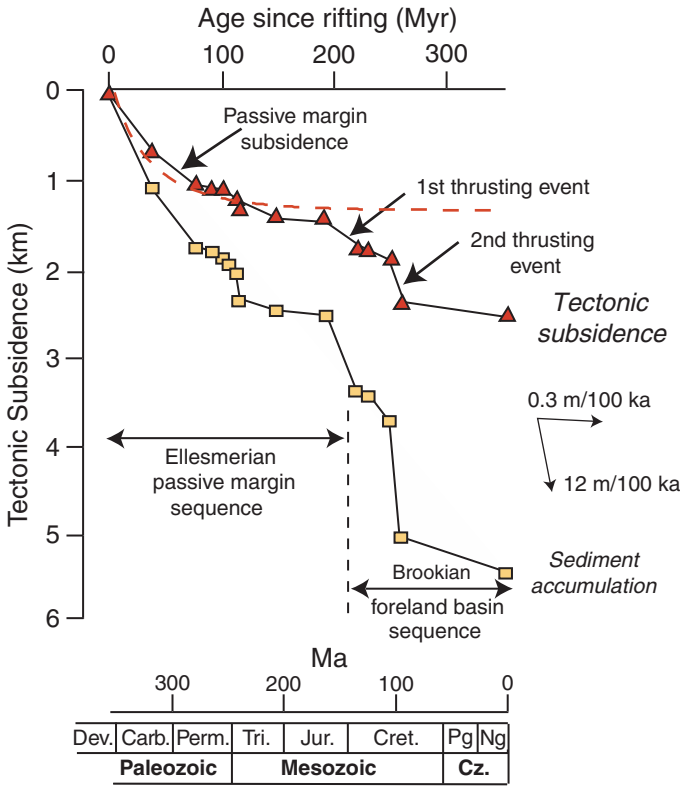

Figure 3.1 Tectonic subsidence and uplift at the Inigok-1 well in the Colville Trough, National Petroleum Reserve, Alaska. Yellow filled squares show the sediment accumulation based on data in Armagnac et al. (1988) and references therein. Red filled triangles show the tectonic subsidence and uplift obtained by progressively backstripping individual sediment layers through time. The dashed line shows the calculated subsidence based on the McKenzie 'pure shear' model with initial rifting at 360 Ma, a stretching factor, β, of 1.5, an initial crust and lithosphere thickness of 31.2 and 125 km respectively, a 0°C crust and sub-crustal mantle density of 2800 and 3330 kg m^{-3} respectively, a coefficient of volume expansion of 3.28 $\times$ 10^{-5}°C^{-1}, an isothermal mantle temperature of 1333°C and a thermal diffusivity of 8.0 $\times$ 10^{-7} m^2 s^{-1}.

The evolution of a passive margin into a foreland basin has important implications for the petroleum system. In Eastern Venezuela, for example, the subsidence caused by thrust/fold loading has taken the otherwise immature Guyana passive margin sequence into the petroleum window (Summa et al., 2003).

3.3 Thermal and mechanical structure

The main result of backstripping (e.g., Fig. 3.1) has been to show that the accumulation of sediments at passive margins is the result of two main factors: cooling following heating of the lithosphere at the time of rifting and loading due to the sediment flux. Other factors (e.g., sea-level, compaction, salt tectonics, magmatism) contribute, but it is generally agreed that these are of secondary importance. We now consider some observational constraints on the thermal and mechanical structure of passive margins.

Heat flow

An important constraint on the thermal structure of a passive margin is the present day heat flow. Of particular significance is the heat flow away from a margin, and such regions are indicative of the pre-rift 'background' heat flow of the continental crust. A comparison between the heat flow at the margin and surrounding regions is indicative of whether or not a margin is still experiencing thermal subsidence.

Unlike other marine geophysical data, there are still relatively few heat flow measurements at passive margins. Della Vedova and Herzen (1987) and Ruppel et al. (1995) have shown that the heat flow over the old (rifting ~180 Ma) East Coast, USA, margin is in the range 30–49 m Wm^{-2}. Louden et al. (1991) have shown that heat flows across the intermediate age (rifting ~100 Ma) Goban Spur and Galicia Bank margins average 50–55 and 30–35 m Wm^{-2}, respectively. Finally, Nissen et al. (1995) have shown that the heat flow over the young (rifting ~56–36 Ma) South China Sea margin averages 75–79 m Wm^{-2}. These estimates (which include, where applicable, corrections for the effects of sediment blanketing) suggest that young margins have a high overall basement heat flow while old margins have low heat flow.

Whether a margin is presently 'hot' or 'cold', however, depends on the 'background' heat flow. The old East Coast, USA, margin, for example, appears to have a similar heat flow to the adjacent crust. The intermediate age Goban Spur has higher heat flow than adjacent oceanic crust while Galicia Bank has a lower heat flow. Interestingly, *both* Goban Spur and Galicia Bank margins have a lower heat flow than the flanking continental crust. This is probably because of the relatively high radioactive heat content of the Variscan terranes that extend from Brittany and southwest England, across the Southwestern Approaches to the English Channel and into the Iberian peninsula. Finally, the young South China Sea margin heat flow is similar to that of adjacent oceanic crust, but higher than that of flanking continental crust.

Various models have been proposed to explain heat flow data at passive margins. Thermal models predict that during rifting heat flow should increase in

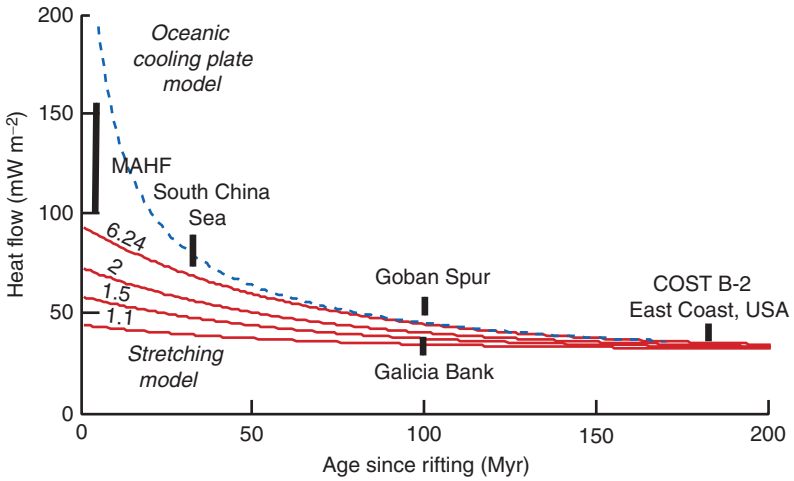

Figure 3.2 Comparison of the observed average surface heat flow over stretched continental crust at the East Coast, USA, South China Sea and Bay of Biscay margin to predictions based on a stretching model. The observed data (thick bars) is based on Nissen et al. (1995), Louden et al. (1991), Della Vedova and Von Herzen (1987) and Ruppel et al. (1995). MAHF, mean axial heat flow at the ridge crest is based on Sclater et al. (1980). The calculated solid lines are based on the McKenzie stretching model with $\beta = 1.1$, 1.5, 2 and 6.24, assuming no radiogenic heat production from the crust. Other parameters are as assumed in the subsidence calculations in Fig. 3.1. The calculated dashed lines are based on the Parsons and Sclater (1977) cooling oceanic plate model.

an oceanward direction from relatively low values over unstretched crust to relatively high values over the stretched crust. Once seafloor spreading begins, heat flow over stretched continental crust may increase, in part, due to lateral heat flow from the relatively hot oceanic crust into the relatively cold stretched crust. The increase in heat flow across a margin may persist for a few tens of Myr, but model calculations suggest that it will probably have decayed by about 50 Myr following rifting.

Probably the most detailed comparison that has been carried out to date of observed and calculated heat flow is that by Nissen et al. (1995) at the South China Sea margin. These authors used seismic refraction data to determine the amount of thinning along transects of the South China Sea margin. By using rift models (e.g., Fig. 3.2) to compute the heat flow from the amount of crustal thinning and comparing it to observed values, Nissen et al. (1995) were able to constrain parameters such as the initial lithospheric thickness and radiogenic heat production.

The South China Sea is a relatively young margin that underwent rifting during the early Paleogene (~65–35 Ma) and seafloor spreading during the late Paleogene (~35–17 Ma). The 'pure-shear' model predicts that despite oceanic crust generation ending at ~17 Ma, there should be an increase in present day heat flow across the margin. Observations, however, do not show an increase; heat flow being high over both stretched crust (Fig. 3.2) and adjacent oceanic crust. Nissen et al. (1995) suggested that this was due to either a thinner initial lithosphere (50–60 km instead of a 'standard' thickness of 125 km) or high radiogenic heat production. This would require, however, too high a heat flow at the margin prior to rifting. Their preferred model therefore was a combined one of a 'standard' initial lithosphere thickness and a moderate radiogenic heat production.

In summary, heat flow data provide useful constraints on the thermal structure of passive margins. Unfortunately, there are only a small number of heat flow transects of margins. In most margins, other observations (e.g., seismic refraction, gravity anomaly, subsidence history) are used to constrain the amount of thinning and thermal models are used to *predict* the basement heat flow. While such models have been useful in calculating the temperature structure of the sediments and thermal maturity, they are limited. Heat flow observations are crucial, therefore, not only to constrain thermal models, but also to understand the contribution of the various processes not included in these models such as radioactive heat production, deep flow of hot fluids and salt diapirism.

Elastic thickness

An important constraint on the mechanical structure of a passive margin is the elastic thickness, T_e, which is a proxy for the long-term (i.e., $>10^5$ a) strength of the lithosphere. Simple models (e.g., Watts et al., 1982) show that T_e exerts a strong control on the overall stratigraphic 'architecture' of a passive margin, explaining the existence, for example, of a coastal plain at old margins. Furthermore, there is evidence that flexure may account for some of the stratigraphic patterns that are observed in passive margins, such as onlap and offlap (e.g., Watts, 1989).

There have been a number of estimates of T_e at passive margins. Some are based on reconstructions of the footwall uplift and hanging-wall geometry of syn-rift basins (e.g., Clift et al., 2002). The majority, however, are based on gravity anomaly data (e.g., Cochran, 1973) which are sensitive not only to the local rift geometry, but also to the deformation that is caused by all the sediment and other (e.g., magmatic underplate) loads that have been applied to a margin during its evolution.

One problem in using the gravity anomaly is the requirement that all the loads acting on the crust (and lithosphere) be specified. This may not be a problem with magmatic underplating, the geometry of which is usually constrained by seismic refraction data, but it is a problem with sediments where it is difficult to determine the pre-load configuration of the margin. Holt and Stern (1991), for example, used the paleobathymetry derived from biostratigraphic data to define the base of the sediment load and present day bathymetry to derive the top of the load.

Watts (1988) suggested a method, dubbed Process-Oriented Gravity Modelling (POGM), that does not require *a priori* estimates of the paleobathymetry. The method regards passive margins as simple mechanical systems (e.g., Fig. 3.3) in which the crust thinned during rifting is subsequently subject to sediment (i.e., the non-volcanic type passive margin), volcanic (i.e., volcanic margin) or some combination of these loads. Flexural backstripping (i.e., backstripping that explicitly takes into account the strength of the lithosphere) of the sediment

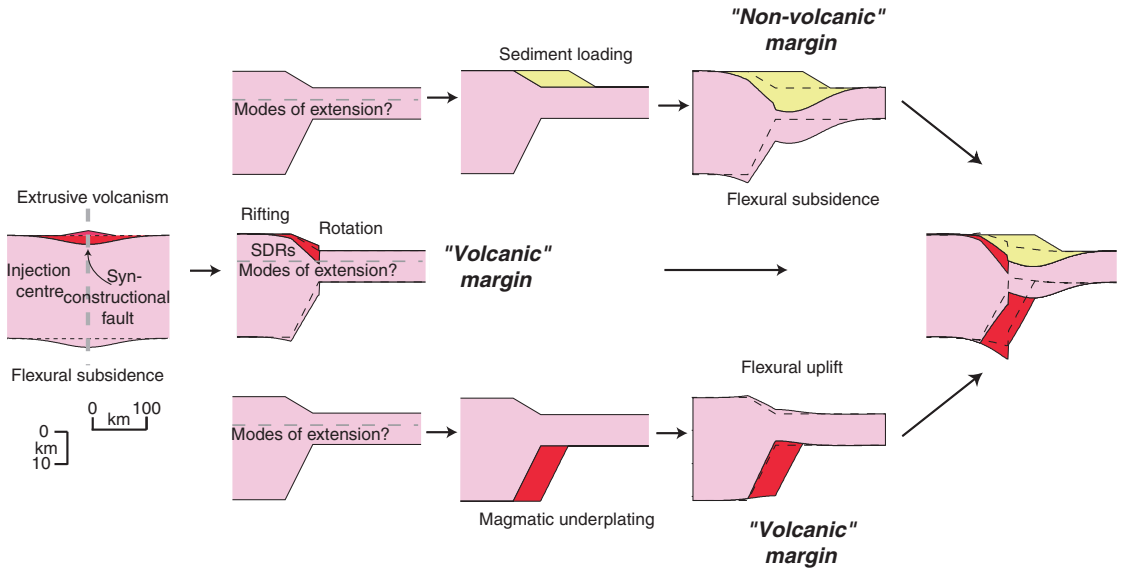

Figure 3.3 Simple models for the mechanical evolution of passive margins. The models view that passive margins form by a combination of rifting, which thins the crust and sediment loading, sub-aerial volcanic loading and magmatic underplating which deforms it. Seaward dipping reflectors (SDRs) refer to the material that initially infilled the flexural moats that flanked the main region of extrusive volcanism and has since subsided (and rotated) following rifting. The pre-rift crust is assumed to have a zero elevation thickness of 31.2 km.

reveals the Total Tectonic Subsidence (TTS) at a margin and, hence, the geometry of the rifted crust for different assumed values of T_e. By calculating the 'sum' gravity anomaly due to the combined effects of the restored rifted crust (the 'rifting anomaly') and sediments (the 'sedimentation anomaly') and comparing it to observations, it is possible to constrain T_e at the margin. The effects of magmatic underplating and sub-aerial volcanism can be included in POGM by computing their flexural loading effect on both the TTS and the gravity anomaly.

Figure 3.4 shows a compilation of T_e estimates over passive margins based on POGM, as well as other forward models. The figure shows a wide range of values and there is no simple relationship between T_e and age since the initiation of rifting. However, when margins are considered that have been loaded at some stage during their evolution by a large discreet load, there is evidence that T_e may depend on the age. The South China Sea, for example, is a young margin that was loaded by thrust/fold loads in Taiwan during the Pliocene and has a low T_e while Northeast Brazil is an old margin that was loaded by the Amazon Cone deep-sea fan system during the late Miocene and has a high T_e. The increase appears to follow the depth to the 450°C isotherm and is in accord with the earlier suggestions of Karner and Watts (1982) based on spectral studies and of

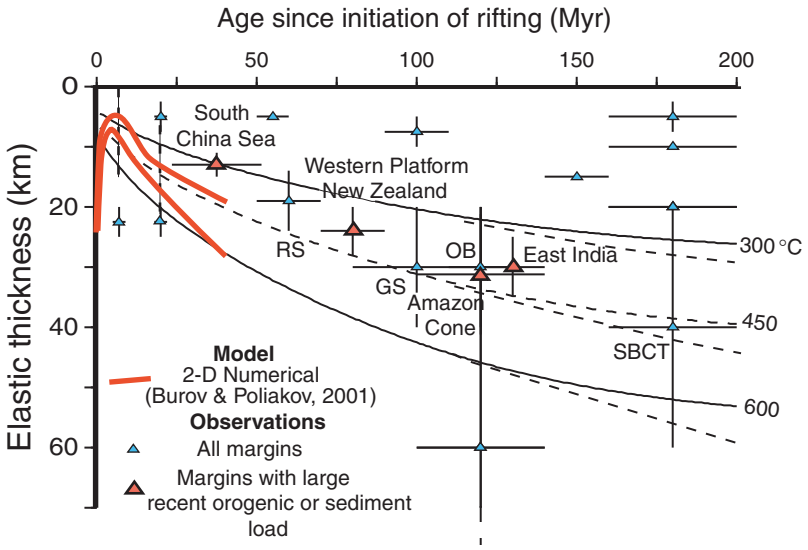

Figure 3.4 Plot of elastic thickness, T_e versus age since the initiation of rifting at passive margins. The T_e estimates are based on Table 6.3c in Watts (2001) with additional estimates from Cochran (1973), Lin and Watts (2002) and Krishna et al. (2000). The ages are also based on Watts (2001) except that ages for the Goban Spur, Jeanne d'arc, Nova Scotia and Grand Banks margins have been amended to 100, 180, 180 and 180 Ma respectively. RS, Ross Sea, GS, Goban Spur, OB, Orphan Bank (Canada), SBCT, southern Baltimore Canyon Trough (East Coast, USA). The solid and dashed black lines show the depth to the 300, 450 and 600°C isotherms based on the cooling oceanic plate model. The thick red lines show the predicted relationship between T_e and age since the initiation of rifting on the basis of the numerical models of Burov and Poliakov (2001).

Burov and Poliakov (2001) based on numerical models that stretched continental lithosphere may increase its strength with age as it cools following rifting.

There are, as Fig. 3.5 shows, a number of T_e estimates that are less than the depth to the 450°C isotherm. They suggest that if the sub-crustal (stretched) continental mantle gains strength following rifting, then there are processes that might act to weaken it. Possible processes include fluidisation of the sub-crustal mantle (e.g., Pérez-Gussinyé and Reston, 2001), thermal blanketing (e.g., Lavier and Steckler, 1997) and load-induced increases in curvature and, hence, yielding (e.g., Wyer, 2003).

Data from experimental rock mechanics suggest that the strength of the lithosphere is limited by brittle deformation and ductile flow (e.g., Kirby and Kronenberg, 1987). Moreover, they suggest that it might be possible to construct a Yield Strength Envelope (YSE) that is applicable to the lithosphere. Although the YSE has a number of limitations (Rutter and Brodie, 1991), it has proved a useful way to quantitatively evaluate the strength of the lithosphere for different strain rates, compositions and geothermal gradients and, importantly, tectonic stresses (including the stresses generated by flexure).

Unfortunately, the YSE does not explicitly define the strength of stretched continental lithosphere. This is because heating at the time of rifting increases the geothermal gradient and, hence, may reduce the strength of the lithosphere while crustal thinning replaces weak crust by strong mantle and, hence, strengthens it. There is therefore a 'competition' between heating that weakens the lithosphere and crustal thinning that strengthens it.

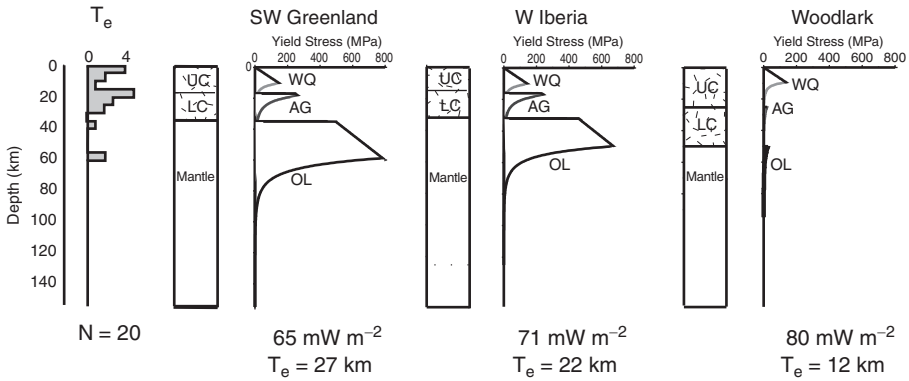

Figure 3.5 Comparison of the observed distribution of T_e at passive margins to calculations of the YSE at selected margins. T_e based on Table 6.3 in Watts (2001). Heat flow and YSE for the SW Greenland, W. Iberia and Woodlark passive margins based on Pérez-Gussinyé et al. (2001). The numbers below each YSE show the heat flow and the T_e estimated from the YSE using the method described by Burov and Diament (1995).

Irrespective of the amount of heating and thinning, YSE considerations suggest that the strength of stretched continental lithosphere will depend not only on the rheological properties of the initial, pre-rift lithosphere, but on its thermal state (e.g., Buck, 1991). Figure 3.5 shows, for example, the YSE for the southwest Greenland, west Iberia and Woodlark margins according to Pérez-Gussinyé et al. (2001). The Greenland and Iberia margins have relatively thin crust and are strong ($22 < T_e < 27$ km) compared to the Woodlark margin which has relatively thick crust and is weak ($T_e \sim 12$ km). A thicker initial crust is not the only reason, however, that the Woodlark margin appears weaker. The background heat flow, according to Pérez-Gussinyé et al. (2001), is high (Fig. 3.5) which implies a higher geothermal gradient and, hence, a lower T_e than for the Greenland and Iberia margins.

3.4 Models

These considerations of heat flow and elastic thickness data suggest that the thermal and mechanical structure of passive margins should be combined in some way. The thermal structure determines heat flow in the cooling basement and, hence, the amount of tectonic subsidence and uplift whereas the mechanical structure determines how it responds to sediment and other loads imposed on it during and following rifting.

Early attempts to combine the thermal and mechanical structure were based on relatively simple kinematic models. Watts and Thorne (1984), for example, used the uniform and depth-dependent extension models to estimate the thermal structure of the cooling basement and a Finite Difference model to compute the flexure. They linked the thermal and mechanical structure by assuming that T_e is given by the depth to a particular isotherm (450°C). The stratigraphy was calculated by assuming that the sediment load could be determined from the *difference* between an old sediment surface and a new surface, the depth to which could be estimated from the paleobathymetry (assumed fixed through time) and the relative height of sea level.

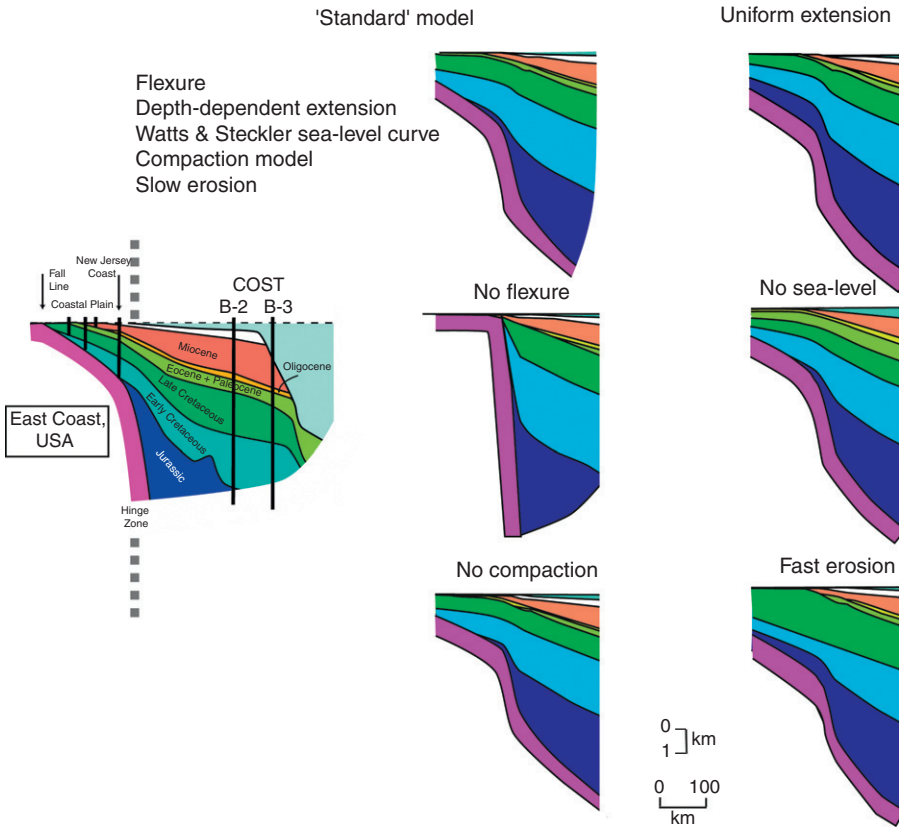

Figure 3.6 Comparison of the observed and calculated stratigraphy at the East Coast, USA, passive margin (modified from Watts and Thorne, 1984). The left panel shows the observed stratigraphy based on well and seismic data along a transect of the margin that intersects the coast near Long Beach, New Jersey. The middle and right panels show the calculated stratigraphy based on a model in which the thermal structure is defined by either a uniform or depth-dependent extension model and a T_e that is given by the depth to the 450° isotherm. The top section in the middle panel shows the 'standard model'. The other sections show the sensitivity of the 'standard model' to the different types of extension model, flexure, sea-level changes, erosion rate and compaction.

Figure 3.6 compares the observed stratigraphy at the East Coast, USA, margin to the calculated stratigraphy based on a combined thermal and mechanical model. The figure shows that the models explain well the overall stratigraphic 'architecture' of the margin. However, their real significance is in determining the role of the various input parameters that control the stratigraphic 'architecture' of the margin. The early history of the margin is determined, for example, mainly by the mode of extension (i.e., whether it is uniform or varies with depth) and flexure. Together, these tectonic controls determine whether or not Jurassic sediments underlie the coastal plain and the extent to which they onlap the basement. The later history, in contrast, is determined less by tectonics, and more by other factors, such as changes in sea level.

Similar models have subsequently been constructed by Lawrence et al. (1990), Kendall et al. (1991) and Reynolds et al. (1991). The main difference between them and earlier models was the inclusion of a variable sediment flux. Reynolds et al. (1991) assumed, for example, a constant continental shelf water depth

(0 km) and slope angle (2.2°) and showed that sediment flux determined the position of the Depositional Shelf Break (DSB) separating the shelf and slope. By tracking the DSB during evolution of the margin they were able to determine the role of sediment flux compared to that of other factors such as tectonics and sea level in determining the nature of the control on the development of the stratigraphic record.

Later models, especially those developed as part of the STRATAFORM programme (Steckler et al., 1996), have incoporated increasingly sophisticated ways of modelling the sediment dynamics. Steckler (1999), for example, included a shoreface which moved independently of the DSB. He showed that, unlike the DSB, the shoreface was more sensitive to first-order sea-level changes.

While the models discussed thus far have provided important insights into passive margin evolution, they are limited to a kinematic description of their thermal and mechanical structure. The structure in the Reynolds et al. (1991) model, for example, is based on a uniform elastic plate that ignores the effect of a vertically layered rheology. Weissel and Karner (1989) and Kusznir et al. (1991) constructed a thermal and mechanical model for rift-type basins that combined brittle deformation in the crust and ductile flow in the sub-crustal mantle. However, their models did not incorporate the YSE, which suggests (e.g., Fig. 3.5) one or more strength maxima in the pre-rift lithosphere.

The effect of a strength 'maxima' on the response of continental lithosphere to extension has been investigated by Kooi et al. (1992). They pointed out that the region of a strength 'maxima' would be difficult to deform and so acts to vertically partition the strain that results from rifting. The depth to a strong zone, dubbed by Kooi et al. (1992) as the depth of necking, determines the magnitude of a basin that overlies it and the uplift of the mantle that underlies it. Shallow depths predict a shallow basin and a large amount of mantle uplift whereas greater depths predict a deep basin and a small amount of mantle uplift. The isostatic response to such a crust/mantle geometry depends on the T_e during rifting. If $T_e = 0$, then the depth of the basin for a particular mantle uplift will be as predicted by an Airy model, irrespective of the depth of necking. If $T_e > 0$, however, then shallow depths of necking predict a broad flexural downwarp at a basin margin while deep depths predict flexurally supported rift flank uplifts.

Although the depth of necking model has been applied with some success (e.g., Kooi et al., 1992 – Gulf of Lyon margin; Keen and Dehler, 1997 – Canada and southwest Greenland margins; Watts and Stewart, 1998 – Gabon margin), Govers and Wortel (1999) have criticised it as well as other kinematic models. They preferred a Finite Element Method (FEM) to solve the coupled heat flow and mechanical equilibrium equations and showed that while T_e during rifting may indeed be finite, the depth of necking is not constant and varies both spatially and temporally. They used a brittle strength failure criterion to represent

Byerlee's law and an effective viscosity to simulate power law creep to show that the depth of necking at a rift axis only approaches a constant depth after a certain transient period (up to a few Myr). Moreover, they argued that the depth of necking does not actually coincide with the strength maxima, but rather occurs above it. Thus, in their view, the depth of necking parameter cannot be used in the same way as, for example, T_e in inferring information about rifted continental lithosphere.

Dynamical models of the type used by Govers and Wortel (1999) have, in fact, been applied to passive margins since the late 1980s (e.g., Bassi et al., 1993; Braun and Beamount, 1987; Dunbar and Sawyer, 1989; Harry and Sawyer, 1992). These models track temperatures using an FEM 'mesh' that includes the thermal lithosphere and at least part of the hot upwelling asthenosphere. The mechanical structure is approximated by experimentally constrained empirical laws for brittle and ductile deformation (e.g., Goetze and Evans, 1979) and isostasy is incorporated through a combination of gravitational body forces and forces on the base of the model that simulate buoyancy. Finally, forces on the side of the model simulate the in-plane extensional stresses.

Most dynamical models incorporate some sort of pre-rift weak zone (e.g., a thicker than normal crust or a thermal anomaly) that serves to focus the initial response of the lithosphere to extension. Despite this limitation, these models have provided useful constraints on the evolution of passive margin, especially the various factors that control the width of the transitional crust that separates unstretched continental and oceanic crust.

Bassi et al. (1993) showed, for example, that the width of stretched continental crust in passive margins depends strongly on the initial thermal conditions. Narrow margins (i.e., margins with widths of the stretched crust of up to 200 km), such as Flemish Cap, Canada, could be produced using models of a thick, cold, lithosphere, even after relatively small amounts of extension. In these models, the rapid localisation of strain is due mainly to the strong, plastic, part of the mantle necking almost to the point of rupture. The actual pattern of necking depends, however, on rheology, with a 'dry' rheology leading to a more rapid change in crust and mantle thinning than a 'wet' rheology. Wide margins (i.e., widths of up to 400 km), such as the Orphan Basin, Canada, could be produced using models of thin, hot lithosphere. In these models, there is a delocalisation of strain because of cooling at the rift axis that inhibits thinning and causes necking to take place along the edges of the deformed lithosphere.

During the past 8 years there has been a rapid development in both numerical (e.g., Bassi et al., 1993; Buck et al., 1999; Burov and Poliakov, 2001; Hopper and Buck, 1996; ter Voorde et al., 1998) and analogue (e.g., Brun and Besslier, 1996) models of rift basin evolution. Of particular interest have been models that determine the role of crust and mantle coupling, lower crustal flow and

crustal buoyancy in controlling the distribution of stretched crust, structural styles and the degree of along-strike segmentation at rifted margins.

Buck et al. (1999), for example, considered the forces involved in extension and the relative role of processes that serve to localise rifting and those that de-localise it. They argue that narrow rifts do not need a preexisting weakness and that necking, magmatic addition and cohesion loss on faults are all ways that rifting may be localised in narrow zones. Wide rifts, on the other hand, are produced by de-localising effects such as viscous flow, crustal buoyancy and flexure.

The role of buoyancy forces is a potentially important one given their association with the abrubt changes in the thickness and, hence, density of the crust and mantle that occur at passive margins. As pointed out by Newman and White (1999), lateral density variations generate buoyancy forces that may either oppose or enhance extension. These authors showed that a relationship exists between the amount of stretching and strain rate in continental rift basins. This suggests that extension ceases because the lithospheric mantle cools and strengthens following a rifting event, rather than because the extensional stresses have been removed.

Davis and Kusznir (2002) showed that despite their higher stretching factors (up to $\sim$3.5) and strain rates (up to $\sim 10^{-14}$ s^{-1}) a similar relationship exists between the amount of stretching and strain rate at passive margins as at continental rift basins. They took into account crustal and thermally driven buoyancy (dubbed by them 'rift push'). As crustal buoyancy forces oppose extension and 'rift push' forces enhance it, they argued that thermally driven buoyancy forces may dominate over crustal buoyancy forces.

While the models discussed thus far take into account the brittle and ductile deformation of rocks, they are mostly based on a single- rather than a multi-layer rheology. As pointed out by a number of workers (e.g., Burov and Diament, 1995) continents, unlike the oceans, comprise of more than one strong competent layer separated by weak layers. Multi-layer rheology lithosphere responds in fundamentally different ways to tectonic stresses than single-layer lithosphere.

ter Voorde et al. (1998) showed that a multi-layer rheology implies a different degree of coupling between the various competent layers. They showed that during rifting, the upper crust, lower crust and mantle could be either 'fully coupled', 'partly coupled', or 'fully decoupled', depending on the temperature structure in the lithosphere, especially the lower crust. The degree of coupling determines the thickness of the layer that supports flexural loading or unloading: fully decoupled indicates that the load is supported by the strength of the upper crust and that compensation takes place, at least in part, in the weak lower crust whereas fully coupled indicates that the lower crust is sufficiently strong that the load is supported by *both* the upper crust and the mantle and is compensated at greater depths.

ter Voorde et al. (1998), while discussing passive margins, suggested that the Bay of Biscay was an example of partially coupled margin, as is evidenced by the relatively short-wavelength (wavelength, λ, $\sim$30–40 km) of its syn-rift grabens and their associated hanging-walls and footwall uplifts, and the relatively long-wavelength ($\lambda > 80$ km) undulations of the underlying Moho.

A multi-layer rheology also implies, as Burov and Poliakov (2001) have pointed out, certain feedbacks, which involve a lower crust that either accelerates or retards subsidence during the syn-rift and post-rift. For example, while crustal thinning due to sub-aerial erosion increases subsidence, it decreases the distance between strong, competent, elastic 'cores' of the upper crust, lower crust, and mantle. This would cause T_e to increase which would arrest the subsidence. Other feedbacks could occur during the post-rift. For example, yielding during sediment loading would increase subsidence whereas the replacement of weak crust by strong mantle would decrease it. If such effects balance, then the subsidence history of a margin may be in accord with predictions of simple kinematic models such as 'pure shear' and 'simple shear'. Otherwise, they would disagree, which might help explain the observations at some margins of syn-rift sequences that greatly exceed the thickness of the post-rift (e.g., Grand Banks, Canada) and of post-rift sequences that greatly exceed the thickness of the syn-rift (e.g., East Coast, USA).

While the introduction of multi-layer rheologies and their associated feedbacks significantly complicates numerical models, advancements in computing may make it possible to take them into account in the future. An example of one such model is illustrated in Fig. 3.7. The main difference between this and previous models is that *both* the Brittle–Ductile Transition (BDT) and the Crust Mantle Boundary (CMB) can be tracked during rifting. Therefore, the pressure-temperature history of the crust (and lithosphere) can be determined.

One problem with the current generation of numerical models is that it has proved difficult to simulate faulting. Although several workers have traced faults through strain localisation (e.g., Behn et al., 2002), it is difficult to use numerical models to resolve between different extensional models (e.g., 'pure shear' and 'simple shear'). Laboratory experiments on brittle and ductile materials are unable to incorporate the temperature dependence of rock rheology though they have been useful to examine the structural styles that develop during extension, including core complexes.

Brun and Besslier (1996), for example, have used sand and silicone putty to represent the brittle and ductile layers of the lithosphere and a low-viscosity syrup to represent the underlying asthenosphere. They showed that by applying displacements at a constant rate along the edges of the model, necking of a multi-layer rheology lithosphere is nearly symmetric (i.e., 'pure shear'), but that asymmetrical structures develop internally, for example, because of faulting. As displacements increase and the brittle and ductile layers thin, lower crust

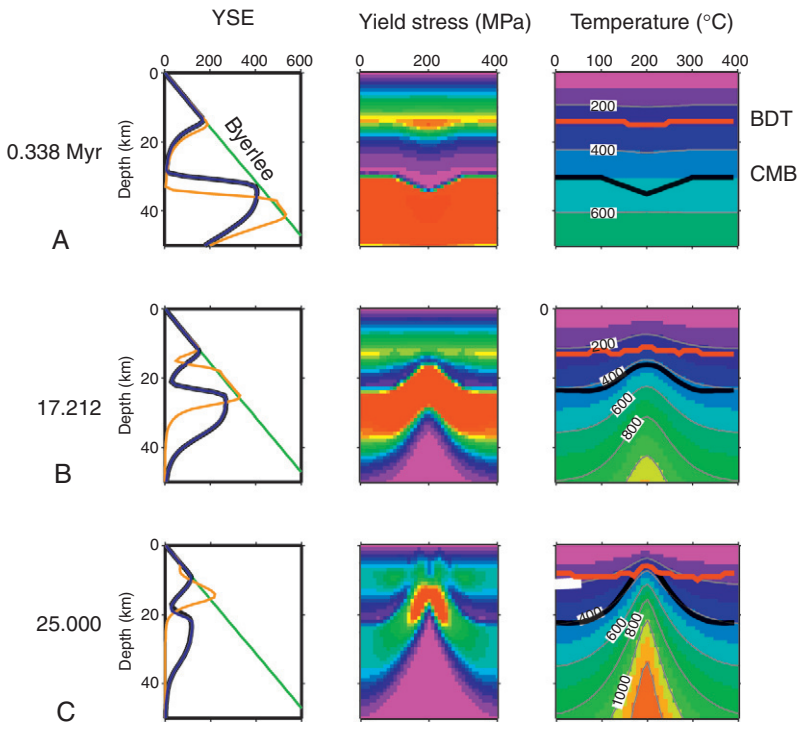

Figure 3.7 Numerical model for the response of the continental lithosphere to extension (Pérez-Gussinyé, pers. comm.). The model is based on a spatially and temporally varying multi-layer rheology and takes into account the heat consumed during rifting by melting. YSE, Yield Strength Envelope. Blue line = YSE at 100 and 300 km. Orange line = YSE at rift centre. Green line = Byerlee's law. BDT = Brittle–Ductile Transition. CMB = Crust/Mantle Boundary. A – 0.3 Myr after initial rifting. Extension is assumed to nucleate in a site of a previous weakness, simulated, in this case, by thicker than normal crust. B – 17.2 Myr. The CMB rises as extension proceeds. There is little change, however, in the depth to the BDT. C – 25.0 Myr. The CMB intersects the BDT such that the strong, cold, brittle upper crust now overlies weak, hot, upwelling mantle. Pérez-Gussinyé (pers. comm.) has used such models to study the onset of serpentinisation since it is likely to occur once faults which act as conduits for fluids can pass entirely through the crust and into the mantle.

and mantle may become juxtaposed. During extreme stretching, boudinage in the high strength sub-Moho layer allows ductile mantle to come into contact with ductile lower crust, leading to the exhumation of ductile material.

The occurrence of exhumed mantle rocks in the west Iberia margin has been interpreted as indicative of 'simple shear' with a detachment fault that cuts either the entire lithosphere (Boillot et al., 1988) or crust (Whitmarsh et al., 2001). However, multi-layer analogue models do not show any evidence of such

a large-scale fault (Brun, 1999). Moreover, seismic reflection profile data over passive margins show little evidence of the prominent reflectors expected of detachment faults.

A notable exception is the 'S-type' reflector observed on the north Biscay and Galicia Bank margins (de Charpal et al., 1978). Previous studies suggested that the reflector corresponds to the BDT, a detachment fault that penetrates the entire lithosphere, an intra-crustal detachment fault, a detachment between the upper crust and the serpentinised mantle. The most probable interpretation, however, (e.g., Louden and Chian, 1999; Reston et al., 1996) is that it marks the transition between a low velocity, highly faulted, upper crust and high velocity serpentinised peridotite.

One puzzling observation is that the width of the exhumed mantle at the west Iberia margin varies along-strike, being 10–20 km wide west of Galicia Bank (Pickup et al., 1996) and >100 km wide beneath the southern Iberia Abyssal Plain (Sibuet et al., 1995). Analogue modelling shows that wide regions of exhumed mantle can be produced if a low viscosity heterogeneity is placed below the lowest brittle-ductile interface in the central part of a developing rift (Brun, 1999). Such viscosity heterogeneities could arise from a zone of partial melting.

Callot and Geoffrey (2002) introduced heterogeneities (made of silicone putty) in their analogue models in order to simulate melting zones that locally weaken the extending lithosphere. They showed that such 'soft spots' within the brittle layer act to localise the strain and may control the along-strike magmatic segmentation that is observed in some passive margins (e.g., southwest Greenland – Geoffroy, 2001; and East Coast, USA – Behn and Lin, 2000).

The dynamical models discussed thus far have mainly been concerned with how the lithosphere responds to extension *during* rifting. While this is of fundamental importance to understanding the mechanisms of continental break-up, it sheds little light on the thermal and mechanical processes that occur during the post-rift when the margin is deformed by sediment and other types of loads.

An exception is the study of Kjeldstad et al. (2003) who used a numerical model to simulate the progradation of sediment loads across the Vøring Plateau margin, Norway, during the Pliocene–Pleistocene. They showed that the Helland Hansen Arch, a prominent anticlinal ridge in the outer part of the Vøring basin, could be explained, at least in part, by differential loading that pushes sediment downwards and laterally towards the front of the prograding wedge. Their conclusion, however, appears to be in conflict with recent analogue models for the arch. Leroy et al. (2004), for example, suggest that the Fles Fault Complex (which is located just to the north of the Helland Hansen Arch) is the consequence of incipient shortening, for example, because of 'ridge push' acting on preexisting lines of weakness.

3.5 Conclusions

We draw the following conclusions from this review:

1. The progressive backstripping of sediments though geological time reveals that the main factors controlling the subsidence of passive margins are sediment loading and thermal contraction following heating, thinning and cooling at the time of rifting.
2. Kinematic models suggest that tectonics (in the form of thermal contraction and uplift and flexure) are a major control on the early stratigraphic evolution of passive margins. Later stages, however, appear to be dominated more by changes in sediment flux and/or sea level than by tectonics.
3. The heat flow at young margins is generally higher than at surrounding cratonic areas whereas at old margins it is either similar or less. This suggests that the sub-crustal mantle at passive margins progressively cools with time.
4. The elastic thickness at young margins is generally lower than that at old margins, although there are a number of low values. This suggests that while the sub-crustal mantle at passive margins may increase in strength as it cools, other processes such as fluids, increases in loading, curvature and yielding and sediment blanketing act to weaken it.
5. Numerical and analogue models have provided new constraints on passive margin evolution, most notably on the factors that control their width, structural style and segmentation.
6. While preexisting zones of weakness act to localise strain in rifts, tectonic stresses appear to be large enough to cause stable lithosphere to neck almost to the point of rupture.
7. Necking is modulated by processes such as magmatic intrusion, which localise strain and processes such as viscous flow, crustal buoyancy and flexure, which delocalise it.
8. The net result is that while most conjugate passive margin pairs show a high degree of symmetry in their large-scale crust and mantle structure, they also show asymmetry, especially in their faulting styles, stratigraphic architecture and thermal and mechanical properties.

Acknowledgments

I thank Bert Bally, David Roberts, Tiago Cunha and Marta Pérez-Gussinyé for their discussion and helpful comments on an early version of this paper.

References

Armagnac, C., Bucci, J., Kendall, C.G.S., Lerche, I., 1988. Estimating the thickness of sediment removed at an unconformity using vitrinite reflectance data. In: Naeser, N.D., McCulloh, T.H. (Eds.), Thermal History of Sedimentary Basins, Springer-Verlag, New York, pp. 217–238.

Armin, R.A., Mayer, L., 1983. Subsidence analysis of the Cordillera miogeocline: implications for timing of late Proterozoic rifting and amount of extension. Geology 11, 702–705.

Bassi, G., Keen, C.E., Potter, P., 1993. Contrasting styles of rifting: models and examples from the eastern Canadian margin. Tectonics 12, 639–655.

Behn, M.D., Lin, J., 2000. Segmentation in gravity and magnetic anomalies along the U.S. East Coast passive margin: implications for incipient structure of the oceanic lithosphere. J. Geophys. Res. 105, 25769–25790.

Behn, M.D., Lin, J., Zuber, M.T., 2002. A continuum mechanics model for normal faulting using a strain-rate softening rheology: implications for thermal and rheological controls on continental and oceanic rifting. Earth Planet. Sci. Lett. 202, 725–740.

Boillot, G., Girardeau, J., Kornprobst, J., 1988. The rifting of the Galicia margin: crustal thinning and emplacement of mantle rocks on the seafloor. In: Boillot, G., Winterer, E.L. (Eds.), Proceedings of the Ocean Drilling Project Science Results, Washington, pp. 741–756.

Bond, G.C., Kominz, M.A., 1984. Construction of tectonic subsidence curves for the early Paleozoic Miogeocline, southern Canadian Rocky Mountains: implications for subsidence mechanisms, age of breakup and crustal thinning. Geol. Soc. Am. Bull. 95, 155–173.

Braun, J., Beamount, C., 1987. Styles of continental rifting: results from dynamic models of lithospheric extension. In: Beamount, C., Tankard, A.J. (Eds.), Sedimentary Basins and Basin-Forming Mechanisms, Can. Soc. Pet. Geol., Calgary, pp. 241–258.

Brun, J.P., 1999. Narrow rifts versus wide rifts: inferences for the mechanics of rifting from laboratory experiments. Phil. Trans. Roy. Soc. Lond. 357, 695–712.

Brun, J.P., Besslier, M.O., 1996. Mantle exhumation at passive margins. Earth Planet. Sci. Lett. 142, 161–173.

Buck, R., 1991. Modes of continental lithospheric extension. J. Geophys. Res. 96, 20,161–20,178.

Buck, W.R., Lavier, L.L., Poliakov, A.N.B., 1999. How to make a rift wide. Phil. Trans. R. Soc. Lond. 357, 671–693.

Burov, E., Poliakov, A., 2001. Erosion and rheology controls on synrift and postrift evolution: verifying old and new ideas using a fully coupled numerical model. J. Geophys. Res. 106, 16,461–16,481.

Burov, E.B., Diament, M., 1995. The effective elastic thickness (Te) of continental lithosphere: What does it really mean? J. Geophys. Res. 100, 3895–3904.

Callot, J.P., Geoffrey, L., 2002. Development of volcanic passive margins: three-dimensional laboratory models. Tectonics 21, doi:10.1029/2001TC901019.

Clift, P., Lin, J., Barckhausen, U., 2002. Evidence for low flexural rigidity and low viscosity lower continental crust during continental break-up in the South China Sea. Mar. Petrol. Geol. 19, 951–970.

Clift, P.D., Turner, J., and, Ocean Drilling Program Leg 152, 1995. Dynamic support by the Icelandic plume and vertical tectonics of the northeast Atlantic continental margins. J. Geophys. Res. 100, 24,473–24,486.

Cochran, J.R., 1973. Gravity and magnetic investigations in the Guiana Basin, Western Equatorial Atlantic. Geol. Soc. Am. Bull. 84, 3249–3268.

Cochran, J.R., 1983. Effects of finite extension times on the development of sedimentary basins. Earth Planet. Sci. Lett. 66, 289–302.

Corfield, R.I., Watts, A.B., Searle, M.P., 2005. Subsidence of the North Indian Continental Margin, Zanskar Himalaya, NW India. J. Geol. Soc. Lond. 162, 135–146.

Davis, M., Kusznir, N., 2002. Are bouyancy forces important during the formation of rifted margins? Geophys. J. Int. 149, 524–533.

Della Vedova, B., Von Herzen, R.P.V., 1987. Geothermal heat flux at the COST B-2 and B-3 Wells, U. S. Atlantic Continental margin, Woods Hole Oceanographic Institute, p. 80.

de Charpal, O., Guennoc, P., Montadert, L., Roberts, D.G., 1978. Rifting, crustal attenuation and subsidence in the Bay of Biscay. Nature 275, 706–711.

Diegel, F.A., Karlo, J.F., Schuster, D.C., Shoup, R.C., Tauvers, P.R., 1995. Cenozoic structural evolution and tectono-stratigraphic framework of the Northern Gulf Coast continental margin. In: Jackson, M.P.A., Roberts, D.G., Snelson, S. (Eds.), Salt Tectonics: A Global Perspective, AAPG, pp. 109–151.

Driscoll, N.W., Karner, G.D., 1998. Lower crustal extension across the Northern Carnarvon basin, Australia: evidence for an eastward dipping detachment. J. Geophys. Res. 103, 4975–4991.

Dunbar, J.A., Sawyer, D.S., 1989. How pre-existing weaknesses control the style of continental breakup. J. Geophys. Res. 94, 7278–7292.

Erickson, S.G., 1993. Sedimentary loading, lithospheric flexure, and subduction initiation at passive margins. Geology 21, 125–128.

Feng, J., Buffler, R.T., Kominz, M.A., 1994. Laramide orogenic influence on late Mesozoic-Cenozoic subsidence history, western deep Gulf of Mexico basin. Geology 22, 359–362.

Geoffroy, L., 2001. The structure of volcanic margins: some problematics from the North-Atlantic/Labrador-Baffin system. Mar. Pet. Geol. 18, 463–469.

Goetze, C., Evans, B., 1979. Stress and temperature in the bending lithosphere as constrained by experimental rock mechanics. Geophys. J. R. Astr. Soc. 59, 463–478.

Govers, R., Wortel, M.J.R., 1999. Some remarks on the relation between vertical motions of the lithosphere during extension and the necking depth parameter inferred from kinematic modelling studies. J. Geophys. Res. 104 (23), 245–325.

Haddad, D., Watts, A.B., 1999. Subsidence history, gravity anomalies, and flexure of the north-east Australian margin in Papua New Guinea. Tectonics 18, 827–842.

Harry, D.L., Sawyer, D.S., 1992. A dynamic model of lithospheric extension in the Baltimore Canyon Trough region. Tectonics 11, 420–436.

Holt, W.E., Stern, T.A., 1991. Sediment loading on the western platform of the New Zealand continent: implications for the strength of a continental margin. Earth Planet. Sci. Lett. 107, 523–538.

Hopper, J.R., Buck, W.R., 1996. The effect of lower crustal flow on continental extension and passive margin formation. J. Geophys. Res. 101, 20,175–20,194.

Karner, G.D., Watts, A.B., 1982. On isostasy at Atlantic-type continental margins. J. Geophys. Res. 87, 2923–2948.

Keen, C., Peddy, C., de Voogdl, B., Mathews, D., 1989. Conjugate margins of Canada and Europe: results from deep reflection profiling. Geology 17, 173–176.

Keen, C.E., Dehler, S.A., 1997. Extensional styles and gravity anomalies at rifted continental margins: some North Atlantic examples. Tectonics 16, 744–754.

Kendall, C.G.S.C., Strobel, J., Cannon, R., Bezdek, J., Biswas, G., 1991. The simulation of the sedimentary fill of basins. J. Geophys. Res. 96, 6911–6929.

Kirby, S.H., Kronenberg, A.K., 1987. Rheology of the lithosphere: selected topics. Rev. Geophys. 25, 1219–1244.

Kjeldstad, A., Skogseid, J., Langtangen, H.P., Bjorlykke, K., Hoeg, K., 2003. Differential loading by prograding sedimentary wedges on continental margins: an arch-forming mechanism. J. Geophys. Res. 108, doi: 10.1029/2001JB001145.

Kooi, H., Cloetingh, S., Burrus, J., 1992. Lithospheric Necking and Regional Isostasy at Extensional basins 1. Subsidence and Gravity Modeling with an Application to the Gulf of Lions Margin (SE France). J. Geophys. Res. 97 (17), 553–617.

Krishna, M.R., Chand, S., Subrahmanyam, C., 2000. Gravity anomalies, sediment loading and lithospheric flexure associated with the Krishna-Godavari basin, eastern continental margin of India. Earth Planet. Sci. Lett. 175, 223–232.

Kusznir, N.J., Marsden, G., Egan, S.S., 1991. A flexural-cantilever simple-shear/pure shear model of continental lithosphere extension: applications to the Jeanne d'Arc basin, Grand Banks and Viking Graben, North Sea. In: Roberts, A.M., Yielding, G., Freeman, B. (Eds.), The Geometry of Normal Faults, vol. 56, Geol. Soc. London, pp. 41–60.

Lavier, L.L., Steckler, M.S., 1997. The effect of sedimentary cover on the flexural strength of continental lithosphere. Nature 389, 476–479.

Lawrence, D.T., Doyle, M., Aigner, T., 1990. Stratigraphic simulation of sedimentary basins: concepts and calibration. Amer. Assoc. Pet. Geol. 74, 273–295.

Leroy, M., Dauteuil, O., Cobbold, P.R., 2004. Incipient shortening of a passive margin: the mechanical roles of continental and oceanic lithospheres. Geophys. J. Int. doi: 10.1111/j.1365–246X.2004.02400.x.

Lin, A.T., Watts, A.B., Hesselbo, S.P., 2003. Cenozoic stratigraphy and subsidence history of the South China Sea margin in the Taiwan region. Basin Res. 15, 453–478.

Lin, A.T., Watts, A.B., 2002. Origin of the West Taiwan basin by orogenic loading and flexure of a rifted continental margin. J. Geophys. Res. 107, doi: 10.1029/2001JB000669.

Lister, G.S., Etherridge, M.A., Symonds, P.A., 1986. Detachment faulting and the evolution of passive continental margins. Geology 12, 246–250.

Louden, K.E., Chian, D., 1999. The deep structure of non-volcanic rifted continental margins. Phil. Trans. Roy. Soc. Lond. 357, 767–804.

Louden, K.E., Sibuet, J.C., Foucher, J.P., 1991. Variations in heat flow across the Goban Spur and Galicia bank continental margins. J. Geophys. Res. 96, 16131–16150.

McKenzie, D.P., 1978. Some remarks on the development of sedimentary basins. Earth Planet. Sci. Lett. 40, 25–32.

Montadert, L., et al., 1977. Nature 268, 305–309.

Muller, R.D., Lim, V.S.L., Isern, A.R., 2000. Late Tertiary tectonic subsidence on the northeast Australian passive margin: response to dynamic topography? Mar. Geol. 162, 337–352.

Newman, R., White, N., 1997. Rheology of the continental lithosphere inferred from sedimentary basins. Nature 385, 621–624.

Newman, R., White, N., 1999. The dynamics of extensional sedimentary basins: constraints from subsidence inversion. In: White, R.S., Hardman, R.F.P., Watts, A.B., Whitmarsh, R.B. (Eds.), Response of the Earth's lithosphere to extension. The Royal Society, pp. 805–830.

Nissen, S.S., Hayes, D.E., Bochu, Y., Weijun, Z., Yongqin, C., Xiaupin, N., 1995. Gravity, heat flow, and seismic constraints on the processes of crustal extension: northern margin of the South China Sea. J. Geophys. Res. 100, 22,447–22,483.

Parsons, B.E., Sclater, J.G., 1977. An analysis of the variation of ocean floor bathymetry and heat flow with age. J. Geophys. Res. 82, 803–827.

Peper, T., Cloetingh, S., 1992. Lithosphere dynamics and tectono-stratigraphic evolution of the Mesozoic Betic rifted margin (southeastern Spain). Tectonophysics 203, 345–361.

Pérez-Gussinyé, M., Reston, T.J., 2001. Rheological evolution during extension at nonvolcanic rifted margins: onset of serpentinization and development of detachments leading to continental breakup. J. Geophys. Res. 106, 3961–3975.

Pérez-Gussinyé, M., Reston, T.J., Phipps Morgan, J., 2001. Serpentinization and magmatism during extension at non-volcanic margins: the effect of initial lithospheric structure. In: Wilson, R.C.L., Whitmarsh, R.B., Taylor, B., Froitzheim, M. (Eds.), Non-Volcanic Rifting of Continental Margins. Geological Society London, pp. 551–576.

Pickup, S.L.B., Whitmarsh, R.B., Fowler, C.M.R., Reston, T.J., 1996. Insight into the nature of the ocean-continent transition off West Iberia from a deep multichannel seismic reflection profile. Geology 24, 1079–1082.

Reston, T.J., Krawczyk, C., Klaeschen, D., 1996. The S reflector west of Galicia (Spain): evidence from prestack depth migration for detachment faulting during continental break-up. J. Geophys. Res. 101, 8075–8091.

Reynolds, D.J., Steckler, M.S., Coakley, B.J., 1991. The role of the sediment load in sequence stratigraphy: the influence of flexural isostasy and compaction. J. Geophys. Res. 96, 6931–6949.

Royden, L., Sclater, J.G., Von Herzen, R.P., 1980. Continental margin subsidence and heat flow: important parameters in formation of petroleum hydrocarbons. Am. Assoc. Petrol. Geol. Bull. 64, 173–187.

Ruppel, C., Von Herzen, R.P., Bonneville, A., 1995. Heat flux through an old (~175 Ma) passive margin: offshore southeastern United States. J. Geophys. Res. 100, 20,037–20,057.

Rutter, E.H., Brodie, K.H., 1991. Lithosphere rheology – a note of caution. J. Struct. Geol. 13, 363–367.

Sclater, J.G., Jaupart, C., Galson, D., 1980. The heat flow through oceanic and continental crust and the heat loss of the Earth. J. Geophys. Res. 18, 269–311.

Sibuet, J.C., Louvel, V., Whitmarsh, R.B., White, R.S., Horsefield, S.J., Sichler, B., Leon, P., Recq, M., 1995. Constraints on rifting processes from refraction and deep-tow magnetic data: the example of the Galicia continental margin (West Iberia). In: Banda, E., Torné, M., Talwani, M. (Eds.), Rifted Ocean–Continent Boundaries. Kluwer, Amsterdam, pp. 197–218.

Sleep, N.H., 1971. Thermal effects of the formation of Atlantic continental margins by continental breakup. Geophys. J. Roy. Astr. Soc. 24, 325–350.

Sleep, N.H., Snell, N.S., 1976. Thermal contraction and flexure of mid-continent and Atlantic marginal basins. Geophys. J. R. Astr. Soc. 45, 125–154.

Steckler, M.S., 1999. High-resolution sequence stratigraphic modelling 1: the interplay of sedimentation, erosion, and subsidence. In: Numerical Experiments in Stratigraphy: Recent Advances in Stratigraphic and Sedimentologic Computer Simulations. Society for Sedimentary Geology, pp. 139–149.

Steckler, M.S., Swift, D.J.P., Syvitski, J.P., Goff, J.A., Niedoroda, A.W., 1996. Modelling the sedimentology and stratigraphy of continental margins. Oceanography 9, 183–188.

Summa, L.L., Goodman, E.D., Richardson, M., Norton, I.O., Green, A.R., 2003. Hydrocarbon systems of Northeastern Venezuela: plate through molecular scale-analysis of the genesis and evolution of the Eastern Venezuela Basin. Mar. Petrol. Geol. 20, 323–349.

ter Voorde, M., van Balen, R.T., Bertotti, G., Cloetingh, S.A.P.L., 1998. The influence of a stratified rheology on the flexural response of the lithosphere to (un)loading by extensional faulting. Geophys. J. Int. 134, 721–735.

Walcott, R.I., 1972. Gravity, flexure, and the growth of sedimentary basins at a continental edge. Geol. Soc. Am. Bull. 83, 1845–1848.

Watts, A.B., 1988. Gravity anomalies, crustal structure and flexure of the lithosphere at the Baltimore Canyon Trough. Earth Planet. Sci. Lett. 89, 221–238.

Watts, A.B., 2001. Isostasy and Flexure of the Lithosphere, Cambridge University Press, Cambridge, p. 458.

Watts, A.B., Cochran, J.R., 1974. Gravity anomalies and flexure of the lithosphere along the Hawaiian-Emperor seamount chain. Geophys. J. R. Astr. Soc 38, 119–141.

Watts, A.B., Karner, G.D., Steckler, M.S., 1982. Lithospheric flexure and the evolution of sedimentary basins. In: Kent, P., Bott, M.H.P., McKenzie, D.P., Williams, C.A. (Eds.), The Evolution of Sedimentary Basins, vol. 305A. Phil. Trans. Roy. Soc. Lond., pp. 249–281.

Watts, A.B., Platt, J., Buhl, P., 1993. Tectonic Evolution of the Alboran Sea Basin. Basin Res. 5, 153–177.

Watts, A.B., Ryan, W.B.F., 1976. Flexure of the lithosphere and continental margin basins. Tectonophysics 36, 25–44.

Watts, A.B., Steckler, M.S., 1979. Subsidence and eustasy at the continental margin of eastern North America. In: Talwani, M., Hay, W., Ryan, W.B.F. (Eds.), Deep Drilling Results in the Atlantic Ocean: Continental Margins and Paleoenvironment. Maurice Ewing Series 3, Amer. Geophys. Union, Washington, D.C., pp. 218–234.

Watts, A.B., Stewart, J., 1998. Gravity anomalies and segmentation of the continental margin offshore West Africa. Earth Planet. Sci. Lett. 156, 239–252.

Watts, A.B., Thorne, J.A., 1984. Tectonics, global changes in sea-level and their relationship to stratigraphic sequences at the U.S. Atlantic continental margin. Mar. Pet. Geol. 1, 319–339.

Watts, A.B., 1989. Lithospheric flexure due to prograding sediment loads: implications for the origin of offlap/onlap patterns in sedimentary basins. Basin Res. 2, 133–144.

Weissel, J.K., Karner, G.D., 1989. Flexural uplift of rift flanks due to mechanical unloading of the lithosphere during extension. J. Geophys. Res. 94, 13,919–13,950.

Wernicke, B., 1985. Uniform sense normal simple shear of the continental lithosphere. Can. J. Earth Sci. 22, 108–125.
White, N., 1989. Nature of lithospheric extension in the North Sea. Geology 17, 101–106.
White, N., 1994. An inverse method for determining lithospheric strain rate variation on geological timescales. Earth Planet. Sci. Lett. 122, 351–371.
White, N., McKenzie, D.P., 1988. formation of the "steer's head" geometry of sedimentary basins by differential stretching of the crust and mantle. Geology 16, 250–253.
Whitmarsh, R.B., Manatschal, G., Minshull, T.A., 2001. Evolution of magma-poor continental margins from rifting to seafloor spreading. Nature 413, 150–154.
Wooler, D.A., Smith, A.G., White, N., 1992. Measuring lithospheric stretching on Tethyan passive margins. J. Geol. Soc. 149, 517–532.
Wyer, P.P.A., 2003. Gravity anomalies and segmentation of the eastern USA passive continental margin, Ph.D. thesis, Oxford.

In this chapter

4

Rift sequence stratigraphy

M.A. Martins-Neto,,† O. Catuneanu‡*

*Vale E&P – Av. Graça Aranha 26, ZIP 20020-900, Rio de Janeiro, Brazil,
†Federal University of Ouro Preto, Geology Department, Ouro Preto/MG, Brazil,
‡University of Alberta, Department of Earth and Atmospheric Sciences, Edmonton, Alberta, Canada

4.1 Introduction

Classic sequence stratigraphy has been developed within the context of passive-margin settings, which are tectonically stable areas where accommodation may be primarily attributed to global sea-level fluctuations on a background of longer term thermal subsidence (Posamentier and Vail, 1988; Posamentier et al., 1988; Vail et al., 1977). This method is useful for understanding the organization of the stratigraphic framework of sedimentary basins. It is also a powerful exploration tool since it characterizes the spatial and temporal distribution of depositional systems, with a component of predictability with regard to the distribution and geometry of reservoir, source, and seal facies.

Starting from the original model for passive margins, sequence stratigraphy continued to evolve during the past two decades (e.g., Catuneanu, 2002, 2006; Catuneanu et al., 2009; Emery and Myers, 1996; Loucks and Sarg, 1993; Posamentier and Allen, 1999; Weimer and Posamentier, 1993). However, despite the fundamental differences between the conditioning mechanisms of sequence development in tectonically stable versus tectonically active basins, many authors have attempted to apply the passive-margin model to all other tectonic settings. The variability of the sequence stratigraphic model with the tectonic setting has not yet been captured in any summary papers or textbooks, and this is arguably one of the "next frontiers" in sequence stratigraphy.

The purpose of this chapter is to present a sequence stratigraphic model for rift basins. The proposed model defines the dominant stratigraphic patterns that are commonly encountered in this tectonic setting, and it provides a framework for understanding the process–response relationship between the controls on accommodation and the resulting stratigraphic architecture of rift basins. This summary also provides a method for the definition of key surfaces for stratigraphic correlation in rift basins, and it highlights the predictive potential of the observed stratal stacking patterns in hydrocarbon exploration. The model

Phanerozoic Rift Systems and Sedimentary Basins DOI:10.1016/B978-0-444-56356-9.00003-1

proposed in this paper is based on case studies that include both marine and nonmarine depositional settings. However, whether the proposed model is general enough to apply to all rift basins remains to be tested.

4.2 Fundamental concepts

Sequence stratigraphy improves our understanding of the evolution and infill architecture of sedimentary basins, thus providing a methodology for predictive exploration of natural resources. The method of sequence stratigraphy emphasizes changes in depositional trends (i.e., progradation, retrogradation, aggradation, erosion) and the resulting stratal stacking patterns through time, which are controlled by shifts in the balance between accommodation (space available for sediments to fill) and sediment supply (Fig. 4.1; Catuneanu, 2002, 2006; Catuneanu et al., 2009; Emery and Myers, 1996; Posamentier and Allen, 1999; Weimer and Posamentier, 1993).

Accommodation is generated, or lost, primarily as a result of the interplay between tectonism (i.e., subsidence or uplift) and eustatic sea-level fluctuations

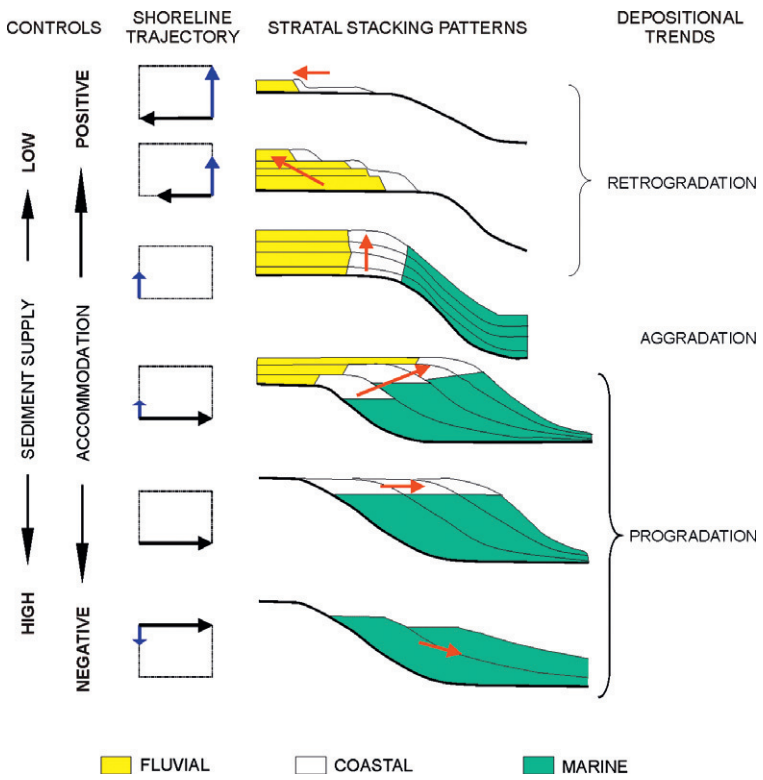

Figure 4.1
Depositional trends (progradation, retrogradation, aggradation) as a response of the interplay of accommodation and sediment supply *(modified from Van Wagoner et al., 1990)*. Black arrows represent the horizontal (progradational or retrogradational) component, blue arrows the aggradational component, and the red arrows the resultant shoreline trajectory.

(rise or fall). At the same time, sedimentation consumes available accommodation at rates that may or may not match the rates in which accommodation is created. The balance between the rates of accommodation change and the rates of sedimentation controls the manifestation of transgressions (coastal retrogradation) and regressions (coastal progradation) (Catuneanu, 2006; Posamentier and Allen, 1999, Fig. 4.1). In terms of vertical stacking patterns, progradation implies a facies succession where proximal facies gradually replace distal facies with time, generating a coarsening-upward succession in a shallow-water setting. Retrogradation results in a facies succession that displays proximal facies at the base, which grade upward to distal facies at the top (fining-upward trend in a shallow-water setting; Van Wagoner et al., 1990).

Temporal variations in sediment supply depend on a number of variables including climate, rock types available for weathering and erosion in the source areas, and the evolution of the differential relief between the source areas and the basin. Among these controls, the latter can be predictably linked to the tectonic evolution of a sedimentary basin, and hence to the change in accommodation that can be attributed to tectonic mechanisms. The role of tectonism as a control on accommodation is more significant in the case of tectonically active basins, such as rifts, while the role of eustasy is increasingly dominant in the case of tectonically stable basins such as the divergent continental ("passive") margins.

The ability of fluvial systems to transport sediment to the basin is proportional to the landscape gradients, which are affected both by the basin subsidence and by the source area tectonism. During times of base-level fall, a steepening of the fluvial gradient downstream leads to a negative adjustment of the graded profile (negative accommodation), resulting in an increase in sediment supply to the marine portion of the basin. By contrast, a positive adjustment during base-level rise causes sediment retention closer to the basin margin, within the fluvial portion of the sedimentary basin. In turn, this may lead to a decrease of sediment flux into the basin, and consequently to a decrease in the deposition of marine reservoir facies.

Passive-margin basins have their accommodation history and, consequently, their stratigraphic framework controlled mainly by sea-level fluctuations at different hierarchical scales (Posamentier and Allen, 1999; Posamentier and Vail, 1988; Posamentier et al., 1988). Depositional sequences on passive margins begin and end with stages of base-level fall that cause subaerial exposure, erosion, and clastic bypass of the continental shelf (sequence boundary) at the same time with the deposition of "lowstand fans" (i.e., forced regressive deposits) in the deep-water setting. Following this, a shift in the balance between the rates of positive accommodation and sediment supply leads to the classic arrangement of the stratigraphic record into lowstand normal regressive wedges, transgressive, and highstand systems tracts.

In a broader sequence stratigraphic approach, which could be generalized for all tectonic settings, a depositional sequence corresponds to a complete

stratigraphic cycle of changing depositional trends and stratal stacking patterns, generated by the interplay between the rates of creation/destruction of accommodation and sediment supply (Catuneanu, 2002, 2006; Catuneanu et al., 2009; Jervey, 1988; Posamentier and Allen, 1999).

4.3 Controls on the stratigraphic architecture of rift basins

Although climate-driven eustatic fluctuations may operate at a high-frequency level as a control on stratigraphic cyclicity in rifts, accommodation in these basins is generated mainly by tectonic subsidence. Rift basins are characterized by episodic subsidence with short stages of rapid creation of accommodation in response to pulses of extension and fault reactivation, commonly followed by longer periods of time of tectonic quiescence. During the latter stages, no new accommodation is generated and sediment supply gradually consumes the available space leading to a change from an underfilled to a filled or even overfilled basin. Typically, sediment supply increases soon after a tectonic pulse, when the newly created differential relief between the source area and the basin allows for a more efficient delivery of sediment to the basin.

The stratigraphic cycles observed in rift basins are dominated by progradational depositional trends, which describe coarsening-upward successions, as sediment supply fills the available accommodation after each stage of extensional subsidence (Fig. 4.2). A full cycle tends to include a short

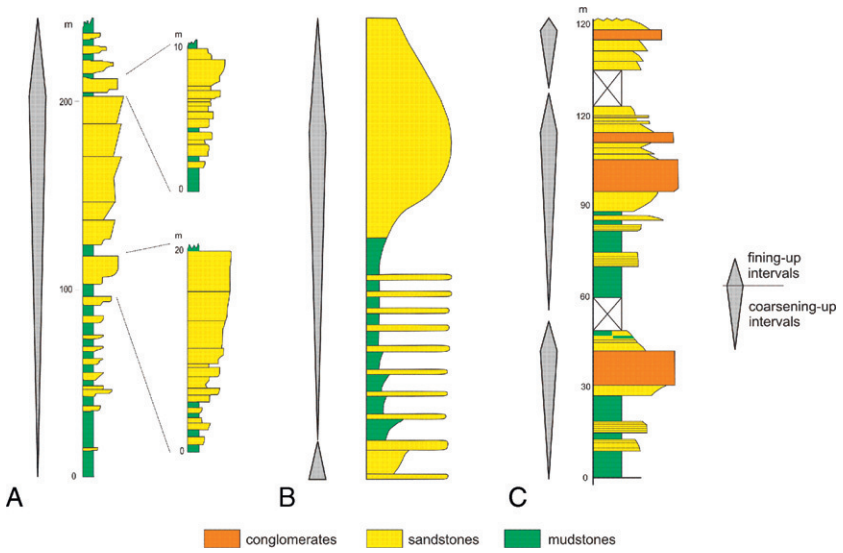

Figure 4.2 Stratigraphic columns showing the coarsening-upward vertical stacking pattern that is typical of sequences accumulated in rift basins. Columns (A) and (B) are conceptual, whereas column (C) illustrates the Proterozoic, lacustrine-alluvial deposits of the Sopa-Brumadinho sequence (part of the syn-rift stage, Espinhaço Basin, Brazil). The fining-upward trends that are observed at the tops of sequences may correspond to spans of time toward the end of each tectonic cycle when denudation of source areas, as well as the decrease in the differential relief between the source areas and the basin, combine to decrease the efficiency of sediment supply to the basin. References: (a) Frostick and Steel, 1993a; (b) Prosser, 1993; (c) Martins-Neto, 1993.

retrogradational portion (transgressive systems tract), which corresponds to the tectonic pulse of extensional subsidence, followed by a longer stage of progradation during tectonic quiescence (highstand systems tract). This stratal stacking pattern can be observed at different hierarchical levels. The first-order stratigraphic framework of the Early Cretaceous Recôncavo rift basin in northeast Brazil (Fig. 4.3), which is an aborted arm of the South Atlantic rift system, exemplifies the development of a coarsening-upward basin fill through the progradation of fluvial facies (Massacará Group) over the deltaic deposits of the Ilhas Group, which in turn overlie the source-rock lacustrine deposits of the Candeias Formation.

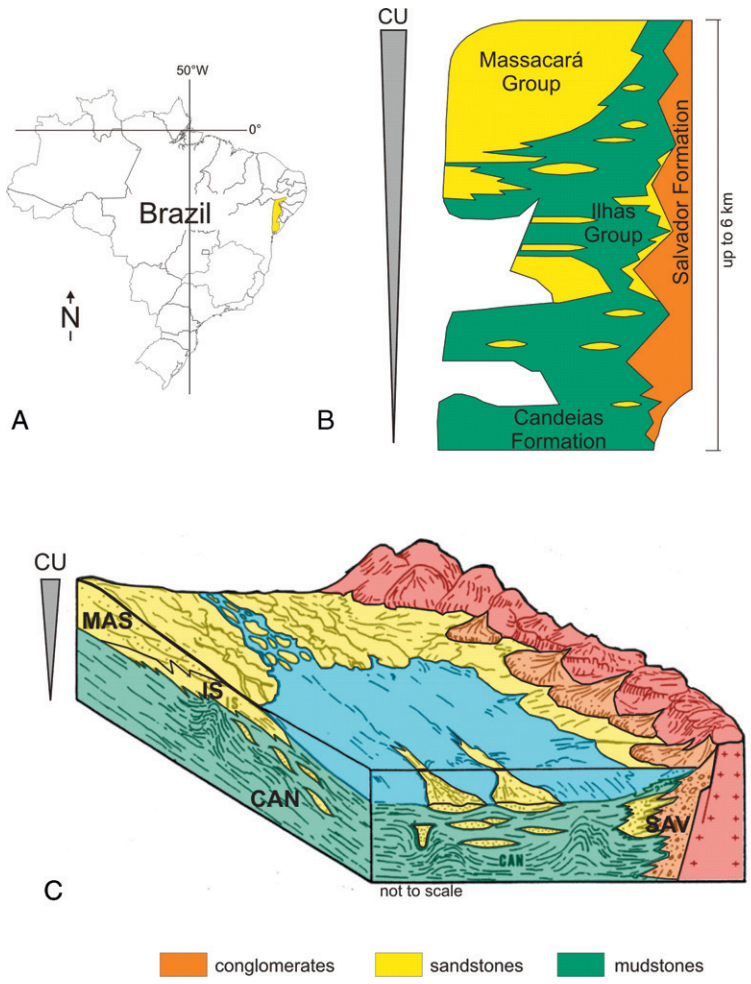

Figure 4.3
(A) Location of the Recôncavo–Tucano–Jatobá rift system (RTJ) in northeast Brazil. (B) Simplified stratigraphic chart of the Recôncavo rift basin, the southern segment of the RTJ, showing the overall coarsening-upward vertical stacking pattern. (C) Paleogeographic scenario for the Recôncavo rift basin *(modified after Da Silva, 1993)*, showing the development of the coarsening-upward (CU) stacking pattern through the progradation of fluvial facies (Massacará Group – MAS) over the deltaic deposits of the Ilhas Group (IS), which in turn overlie the source-rock bearing lacustrine deposits of the Candeias Formation (CAN). Note turbidite intercalations in the distal/deep portion of the Candeias lake. SAV, Salvador Formation.

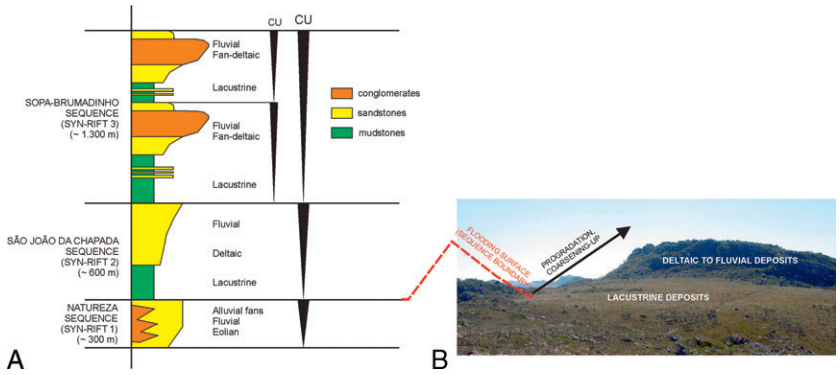

Figure 4.4
(A) Schematic stratigraphic column of the rift succession of the Proterozoic Espinhaço basin, southeastern Brazil, showing dominantly coarsening-upward depositional sequences. Note the recognition of sequences of different hierarchical orders in the Sopa-Brumadinho syn-rift 3 sequence. See text for details. (B) Panoramic view of the São João da Chapada sequence (syn-rift 2), Espinhaço basin, southeastern Brazil, showing the position of its basal flooding surface and the coarsening-upward stacking pattern.

Another example of this stratigraphic pattern can be seen in the Proterozoic Espinhaço rift basin of southeastern Brazil (Martins-Neto, 2000, 2007, 2009; Fig. 4.4). Two angular rift-propagation unconformities separate three syn-rift sequences within the rift succession. Flooding surfaces, reworking the unconformities, are overlain by lacustrine deposits, and define sequence boundaries. Each syn-rift sequence shows a stacking pattern of coarsening-upward, developed by the progradation of alluvial, fluvial, and deltaic depositional systems on top of the lacustrine system. Higher frequency sequences, interpreted to be the product of higher frequency faulting pulses, can be recognized in the Sopa-Brumadinho third syn-rift sequence (Figs. 4.2C and 4.4), and display the same internal architecture as the higher rank (lower frequency) sequences.

Owing to the specific subsidence patterns of rifts, sequence boundaries tend, therefore, to be marked by flooding surfaces, as rapid creation of accommodation leads to transgression in an underfilled (lacustrine or marine) setting. Flooding surfaces of different hierarchical orders can be identified in well logs and outcrops within rift basins, providing a powerful tool for stratigraphic correlation (Figs. 4.5 and 4.6).

The well-log cross-section of correlation in Fig. 4.5 exemplifies how flooding surfaces can be used as the key surfaces for stratigraphic correlation. The sequence boundary in Fig. 4.5 separates two syn-rift sequences, each of them displaying a coarsening-upward stacking pattern, which can be recognized both in the lithologic and gamma-ray logs. Similarly, the well-log cross-section in Fig. 4.6 shows a stratigraphic organization that supports the framework presented here, where syn-rift depositional sequences bounded by flooding surfaces can be recognized at different hierarchical levels.

Figure 4.7 illustrates a seismic section calibrated with well-log data, where a rift-propagation unconformity can be recognized using seismic-stratigraphic criteria (truncation at the top of syn-rift sequence 1 and onlap at the base of syn-rift sequence 2). The flooding surface at the base of syn-rift sequence 2 marks the sequence boundary, as documented by the well-log data.

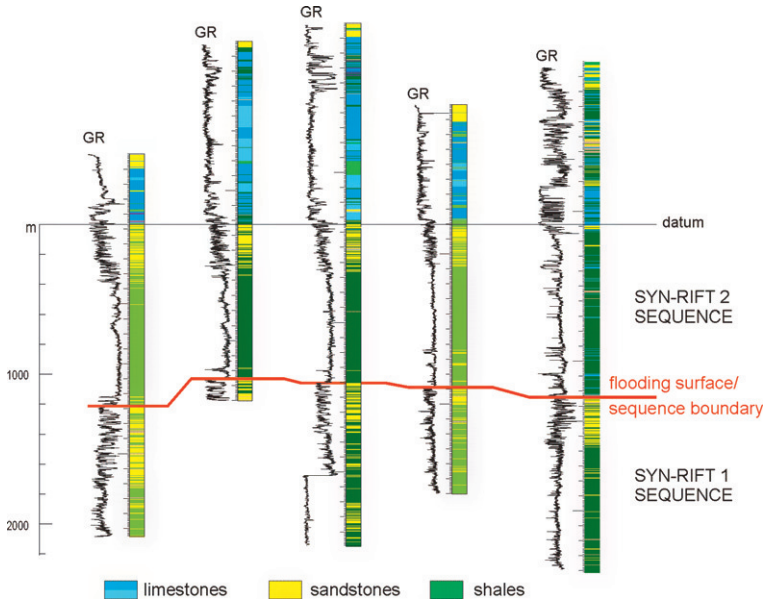

Figure 4.5 Well-log cross-section of correlation in the Proterozoic Espinhaço rift basin, southeastern Brazil, showing two depositional sequences separated by a flooding surface. The flooding surface is well defined in the lithologic and gamma-ray logs. Note the coarsening-upward stacking pattern of both sequences. The section is about 50 km long. GR, gamma ray.

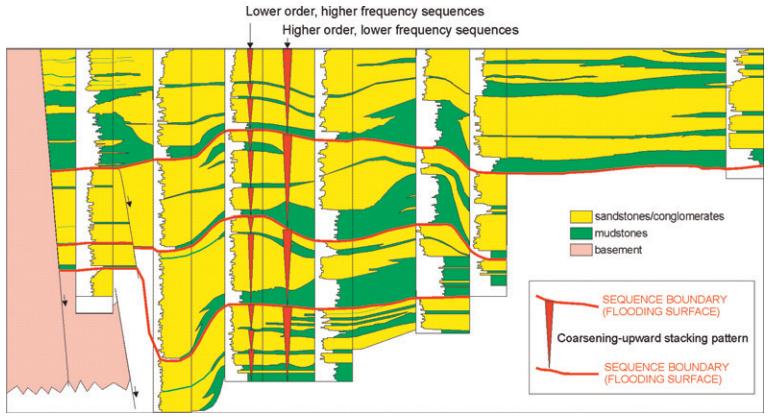

Figure 4.6 Well-log cross-section of correlation in the Viking graben, North-Sea rift *(modified after Frostick and Steel, 1993b)*, where four coarsening-upward depositional sequences, bounded by flooding surfaces, can be recognized. The sharp basal contacts of the deep-marine shales define flooding surfaces (sequence boundaries). The axial progradation of sandstones and conglomerates generates overall coarsening-upward stacking patterns. Note the recognition of lower order (higher frequency) sequences, which are bounded by lower order flooding surfaces.

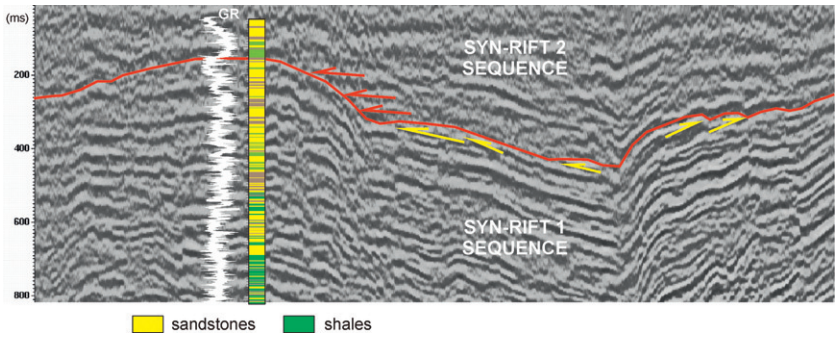

Figure 4.7 Seismic section calibrated with borehole data, showing a rift-propagation unconformity (red horizon) characterized by erosional truncation at the top of syn-rift sequence 1 (yellow arrows) and onlap at the base of syn-rift sequence 2 (red arrows) (the Proterozoic Espinhaço rift basin, southeastern Brazil; seismic data courtesy of Petrobras). The borehole data indicate that the unconformity (sequence boundary) is marked by a flooding surface. Abbreviations: GR, gamma ray; ms, milliseconds (two-way travel time).

4.4 Discussion and conclusions: A sequence-stratigraphic model for rift basins

A typical rift sequence tends to start with relatively deeper water deposits at the base, overlying a flooding surface, which are the product of rapid subsidence and consequent transgression (Figs. 4.2–4.8). A basal sandy interval can occur in some basins, below the initial flooding surface, representing the early stage of rift initiation, when accommodation is still limited (Prosser, 1993). Intercalations of turbidite facies within the basal fine-grained succession that overlies the first flooding surface may indicate the onset of progradation. The shale/turbidite package characterizes the underfilled phase in the evolution of the basin. With progradation, the succession passes upward to shallow-water and coastal systems (filled phase), which grade to alluvial facies at the top (overfilled phase). The general change from underfilled to overfilled conditions is attributed to a shift in the balance between accommodation and the ability of sedimentary systems to fill the available space.

A typical rift sequence consists of transgressive and highstand systems tracts. The transgressive systems tract includes the retrogradational facies that accumulate during the tectonically driven pulse of subsidence and flooding. The highstand systems tract forms the bulk of the sequence, and includes the progradational coarsening-upward succession that overlies the maximum flooding surface. Due to the strongly asymmetrical shape of the base-level (accommodation) curve, with fast rise (pulse of tectonic subsidence) followed by prolonged stillstand (tectonic quiescence), the lowstand systems tract tends to be poorly developed or absent. This marks a significant difference between rifts and tectonically stable basins such as those represented by continental shelves in passive-margin settings.

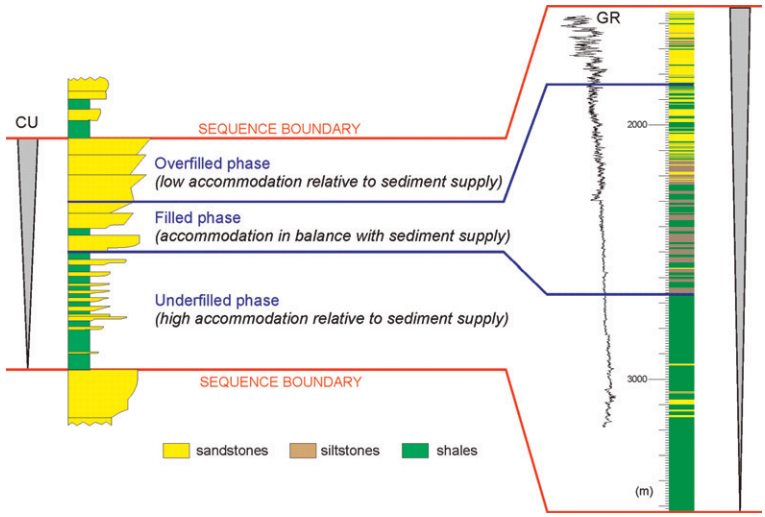

Figure 4.8
Internal architecture of a complete (ideal) rift sequence, showing the overall coarsening-upward (CU) vertical stacking pattern, as well as the shift from underfilled to filled and overfilled conditions during the accumulation of the sequence. The conceptual column to the left is correlated with a well log in a rift basin (GR, gamma-ray).

The tectonically controlled stratigraphic framework of rift depositional sequences bounded by flooding surfaces and arranged internally in dominantly coarsening-upward successions characterizes the architecture of sequences that develop at different hierarchical levels (Figs. 4.2, 4.4, and 4.6). Higher frequency sequences can be recognized in well logs, as shown in Fig. 4.9, where two smaller scale sequences display the same coarsening-upward character, with sequence boundaries marked by sharp flooding surfaces. Such higher frequency sequences (e.g., at third-order level) are attributed to smaller scale tectonic pulses of fault reactivation that occur between the higher magnitude (e.g., second-order) tectonic events, during a time of long-term (e.g., second-order) tectonic quiescence. A renewed subsidence pulse leads to the drowning of the previous deposits and the start of a new depositional sequence. The relative importance of sequences (e.g., based on thickness, or temporal scale) can be used to develop a hierarchy system for each rift basin fill. The entire basin fill of a rift can be taken as a first-order sequence, which represents the starting point for developing a hierarchy system for that basin (Catuneanu, 2006; Catuneanu et al., 2005).

Variations from the "typical sequence" can occur due to several factors such as the overprint of climate-driven sea/lake-level fluctuations, stretching rates during the evolution of the rift system, differences in the subsidence history between the various sub-basins of a rift system, and the location of the depocenters relative to the source areas and the sediment entry points into the basin.

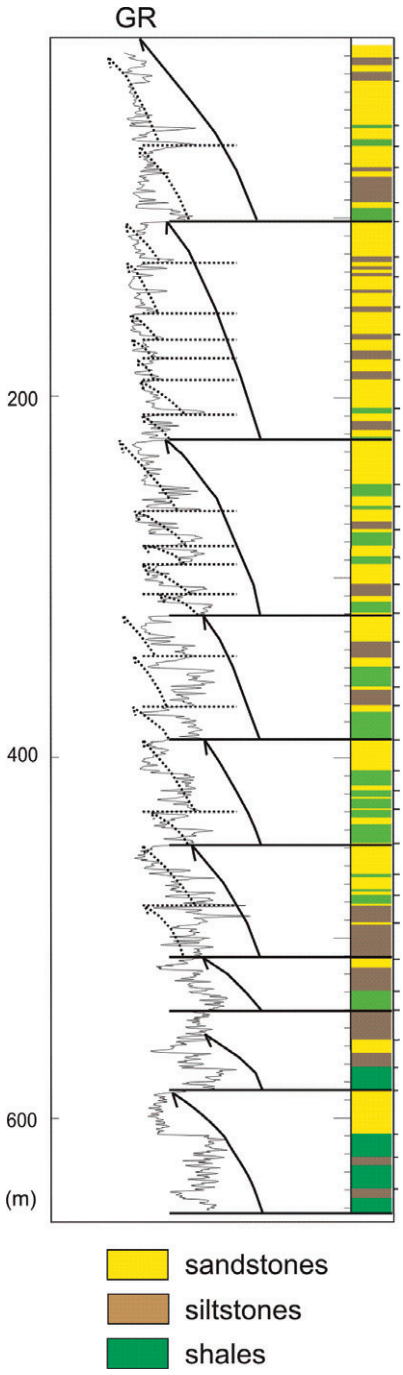

Figure 4.9 Well log (GR, gamma-ray) showing rift sequences of two hierarchical orders (solid arrows for lower order and dotted arrows for higher order). Regardless of their order of cyclicity, sequences are bounded by sharp flooding surfaces and display overall coarsening-upward vertical stacking patterns.

Acknowledgments

We thank Luiz Fernando Ev, Mariangela G.P. Leite (Federal University of Ouro Preto) and Frank Falkenhein (Petrobras) for their comments on earlier versions of this chapter. The research was funded by grants from CNPq (Brazilian National Research Council) and NSERC (Natural Sciences and Engineering Research Council of Canada). We thank Petrobras for providing data and feedback during a long-term collaboration that resulted, in part, in the publication of this chapter. We also express our thanks to the JMPG referees for their comments and suggestions.

References

Catuneanu, O., 2002. Sequence stratigraphy of clastic systems: concepts, merits and pitfalls. J. Afr. Earth Sc. 35, 1–43.

Catuneanu, O., 2006. Principles of Sequence Stratigraphy. Elsevier, Amsterdam, 375pp.

Catuneanu, O., Martins-Neto, M., Eriksson, P.G., 2005. Precambrian sequence stratigraphy. Sed. Geol. 176 (1–2), 67–95.

Catuneanu, O., Abreu, V., Bhattacharya, J.P., Blum, M.D., Dalrymple, R.W., Eriksson, P.G., Fielding, C.R., Fisher, W.L., Galloway, W.E., Gibling, M.R., Giles, K.A., Holbrook, J.M., Jordan, R., Kendall, C.G.S.t.C., Macurda, B., Martinsen, O.J., Miall, A.D., Neal, J.E., Nummedal, D., Pomar, L., Posamentier, H.W., Pratt, B.R., Sarg, J.F., Shanley, K.W., Steel, R.J., Strasser, A., Tucker, M.E., Winker, C., 2009. Towards the standardization of sequence stratigraphy. Earth Sci. Rev. 92, 1–33.

Da Silva, H.T.F., 1993. Flooding surfaces, depositional elements, and accumulation rates – characteristics of the Lower Cretaceous Tectonosequence in the Recôncavo Basin, northeast Brazil. Unpublished Ph.D. thesis, University of Texas, 312pp.

Emery, D., Myers, K.J., 1996. Sequence Stratigraphy. Blackwell, Oxford, 297 pp.

Frostick, L.E., Steel, R.J., 1993a. Tectonic signatures in sedimentary basin fills: an overview. International Association of Sedimentologists. Spec. Publ. 20, 1–9.

Frostick, L.E., Steel, R.J., 1993b. Sedimentation in divergent plate-margin basins. International Association of Sedimentologists. Spec. Publ. 20, 111–128.

Jervey, M.T. 1988. Quantitative geological modeling of siliciclastic rock sequences and their seismic expression. In: Wilgus, C.K., Hastings, B.S., Kendall, C.G., Posamentier, H.W., Ross, C.A., Va , Wagoner, J.C. (Eds.), Sea Level Changes – An Integrated Approach. SEPM Spec. Publ. 42, pp. 47–69.

Loucks, R.G., Sarg, J.F. (Eds.), 1993. Carbonate Sequence Stratigraphy, AAPG Memoir, 57, p. 545.

Martins-Neto, M.A., 1993. The sedimentary evolution of a Proterozoic rift basin: the basal Espinhaço Supergroup, southern Serra do Espinhaço. Brazil. Freiburger Geowissenschaftliche Beiträge, 155pp.

Martins-Neto, M.A., 2000. Tectonics and sedimentation in a Paleo/Mesoproterozoic rift-sag basin (Espinhaço Basin, southeastern Brazil). Precambrian Res. 103, 147–173.

Martins-Neto, M.A., 2007. Proterozoic first-order sedimentary successions of the São Francisco basin in eastern Brazil. Zeitschrift der Deutschen Gesellschaft für Geowissenschaften 158, 117–129.

Martins-Neto, M.A., 2009. Sequence stratigraphic framework of Proterozoic successions in eastern Brazil. Mar. Petrol. Geol. 26, 163–176.

Posamentier, H.W., Allen, G.P., 1999. Siliciclastic sequence stratigraphy: concepts and applications. SEPM Concepts Sedimentol. Paleontol. 7, 210pp.

Posamentier, H.W., Vail, G.P., 1988. Eustatic controls on clastic deposition II – sequence and systems tract models. In: Wilgus, C.K, Hastings, B.S., Kendall, C.G., Posamentier, H.W., Ross, C. A., Van Wagoner, J.C. (Eds.), Sea Level Changes – An Integrated Approach, SEPM Spec. Publ., vol. 42, pp. 125–154.

Posamentier, H.W., Jervey, M.T., Vail, P.R., 1988. Eustatic controls on clastic deposition I – conceptual framework. In: Wilgus, C.K., Hastings, B.S., Kendall, C.G., Posamentier, H.W., Ross, C.A., Van Wagoner, J.C (Eds.), Sea Level Changes – An Integrated Approach, SEPM Spec. Publ., vol. 42, pp. 109–124.

Prosser, S., 1993. Rift-related linked depositional systems and their seismic expression. Geological Society Special Publication, 71, 35–66.

Vail, P.R., Mitchum Jr., R.M., Todd, R.G., Widmier, J.M., Thompson, S.I.I.I., Sangree, J.B., Bubb, J.N., Hatlelid, W.G., 1977. Seismic stratigraphy and global changes of sea-level. In: Payton, C.E (Ed.), Seismic Stratigraphy – Applications to Hydrocarbon Exploration. AAPG Memoir 26, pp. 49–212.

Van Wagoner, J.C., Mitchum Jr., R.M., Campion, K.M., Rahmanian, V.D., 1990. Siliciclastic sequence stratigraphy in well logs, core, and outcrops: concepts for high-resolution correlation of time and facies. Am. Assoc. Pet. Geol. Methods Explor. Ser. 7, 55pp.

Weimer, P., Posamentier, H.W. (Eds.), 1993. Siliciclastic Sequence Stratigraphy, AAPG Memoir, vol. 58, 492pp.

In this chapter

5

Structural control on syn-rift sedimentation, northwestern Red Sea margin, Egypt

S.M. Khalil, K.R. McClay
Fault Dynamics Research Group, Department of Earth Sciences, Royal Holloway University of London, Egham, Surrey TW20 0EX, United Kingdom

5.1 Introduction

Recent studies in extensional settings have evaluated the relative roles of fault evolution and interaction in controlling the deposition, dispersal and architecture of syn-extensional sediments (Dart et al., 1994; Dawers and Underhill, 2000; Gawthorpe and Hurst, 1993; Gawthorpe et al., 1990, 1997; Gupta et al., 1999; Hardy et al., 1994; Ravnås and Steel, 1998; Scholz et al., 1990; Young et al., 2000). Structural and sedimentological field studies of ancient and active rift basins indicate that development of normal faults, their physiographic expressions and variations in fault slip rates are major factors influencing the spatial distribution and architecture of depositional systems adjacent to the fault zones (cf. Dart et al., 1994; Gawthorpe and Leeder, 2000; Leeder et al., 2002; Leppard and Gawthorpe, 2006; Seger and Alexander, 1993). In addition, seismic interpretations of rift structures in the East African rift system have shown that the primary control on syn-rift sedimentation is tectonic (Scholz et al., 1990, 1993), and it can be modified by pre-rift structural fabrics (cf. Lezzar et al., 2002; Versfelt and Rosendahl, 1989) and pre-rift topography (Crossley, 1984). In the northwestern Red Sea, early syn-rift clastics form coarse-grained fan deltas at key localities (these are recognised as sediment-input sites) along the coastal plain. The location, geometry and development of these fan delta systems in relation to the structural architecture and tectonic evolution of the northern Red Sea are still not fully understood. Understanding of the close relationship between rift fault architecture and syn-rift sedimentation patterns may help to predict clastic reservoir distribution, which is a key element of many hydrocarbon plays in rift basins. In this chapter, we present three detailed case studies to illustrate the structural control on deposition of the

Phanerozoic Rift Systems and Sedimentary Basins DOI:10.1016/B978-0-444-56356-9.00004-3

Early Miocene syn-rift coarse clastics and the influence of the structures on the localisation of sediment-input points in the northwestern margin of the Red Sea. This study was based on detailed field mapping (scale 1:20,000) and interpretation of Landsat and Spot Images of a 120-km-long segment of the northwestern Red Sea margin, between Safaga and just to the south of Quseir (Fig. 5.1).

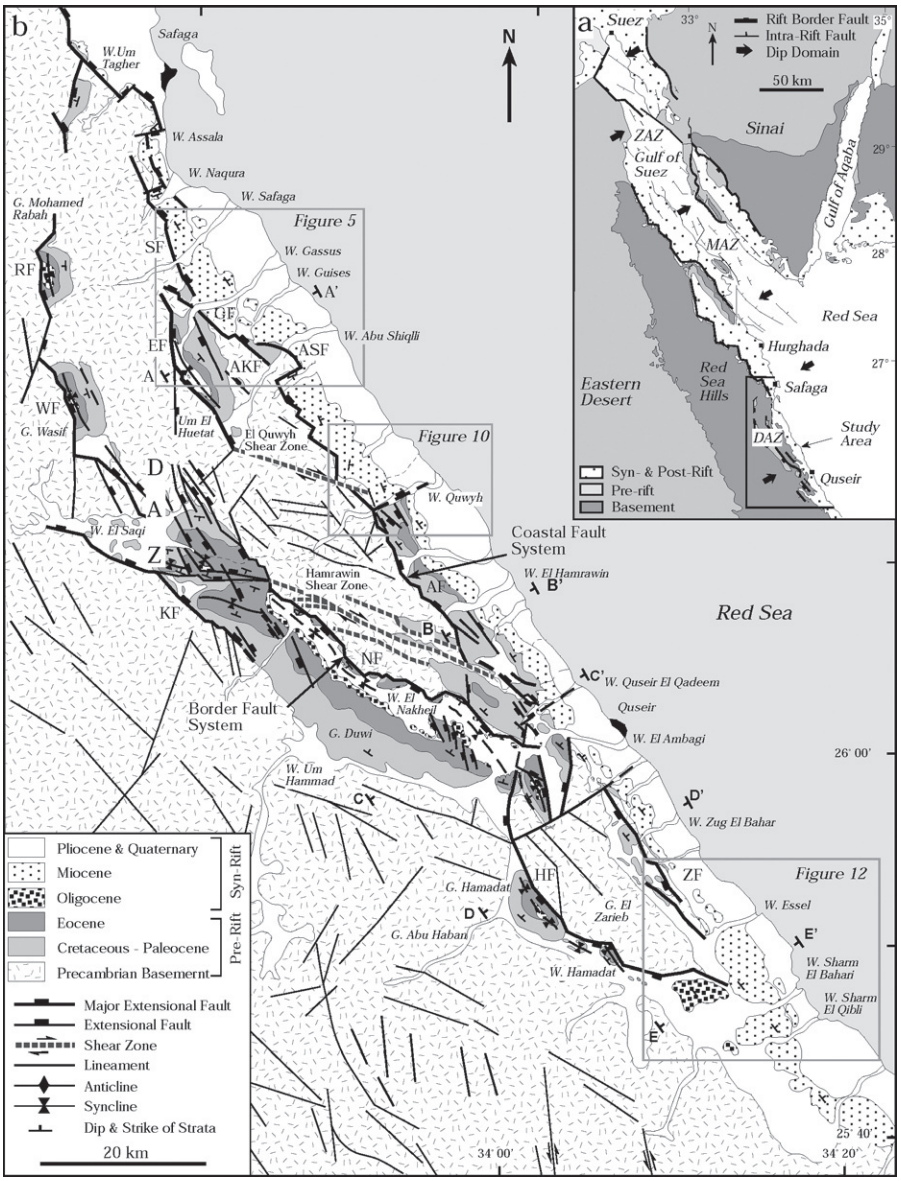

Figure 5.1 Surface geologic map of the northwestern Red Sea margin. Locations of cross-sections of Fig. 5.3 are labelled as A–A′ to E–E′. RF, WF, KF, NF and HF indicate the Rabah, Wasif, Kallahin, Nakheil and Hamadat segments of the Border Fault system, respectively. SF, EF, GF, AKF, ASF, AF and ZF indicate the Safaga, Um El Huetat, Gassus, Abu Kherfan, Abu Shiqlli, Anz and Zug El Bahar segments of the Coastal Fault system, respectively. Inset shows the tectonic setting of the Red Sea and location of the study area. ZAZ, MAZ and DAZ indicate the Zaafarana, Morgan and Duwi accommodation zones, respectively.

5.2 Stratigraphy and structure of the northwestern Red Sea

The Red Sea is a relatively young and active continental rift system that initiated in the Late Oligocene–Early Miocene (Bosworth et al., 2005; Cochran, 1983; Coleman, 1993; Le Pichon and Francheteau, 1978; Mckenzie et al., 1970; Steckler et al., 1988). It formed in response to the northeast separation of the Arabian plate from the African plate, and part of the plate movement was taken up by the opening of the Gulf of Suez rift during the Late Oligocene–Early Miocene (Coleman, 1993; Girdler and Southren, 1987; Hempton, 1987; Joffe and Garfunkel, 1987; Mckenzie et al., 1970). Part of the extension was taken by the sinistral strike-slip motion along the Aqaba–Dead Sea transform during the Mid Miocene–Quaternary times (Abdel Khalek et al., 1993; Bosworth et al., 2005; Freund, 1970; Mckenzie et al., 1970; Morgan, 1990; Quennell, 1984). In the Safaga–Quseir area, rotated extensional fault blocks expose pre- and syn-rift strata, together with large areas of the Precambrian basement, which form the Red Sea Hills on the rift margins (Fig. 5.1).

Stratigraphy of the northwestern Red Sea margin

Pre-rift strata

In the northwestern Red Sea, the pre-rift strata range in age from the Precambrian to the Eocene (Fig. 5.2). The Precambrian basement is heterogeneous in composition, and it consists of igneous, metamorphic, and sedimentary rocks deformed during the Pan-African orogeny (Akaad and Noweir, 1980; Kröner, 1984, 1993; Stern, 1981, 1994; Stoeser and Camp, 1985). The basement exhibits a strong fabric, which includes two major shear zones (Hamrawin and El Quwyh shear zones, Fig. 5.1B). These shear zones are oriented WNW, oblique to the NNW rift trend, and were reactivated during the Miocene rifting (Khalil and McClay 2001; Moustafa, 1997; Younes and McClay, 2002). Fracturing is well developed in the basement, and this, together with the lithological heterogeneities, produced easily eroded weak zones in the basement. These acted as source areas for the Early to Mid-Miocene sediments, which were transported to the Red Sea basin through a number of structurally controlled sediment-input sites located along the rift margin.

The Precambrian basement is unconformably overlain by a 500–700-m-thick section of Upper Cretaceous–Middle Eocene strata (Fig. 5.2). These sediments occur in a few isolated, fault-bounded sub-basins (e.g., Gebel Duwi and Gebel Hamadat; Fig. 5.1), as well as in relatively small tilted fault blocks along the coastal area (Figs. 5.1 and 5.3). The lower part of this pre-rift sedimentary section is predominantly siliciclastic, with the lowermost unit consisting of Upper Cretaceous, shallow marine to fluvial sandstones of the Nubia Formation. This is overlain by interbedded shales, sandstones and limestones with phosphate

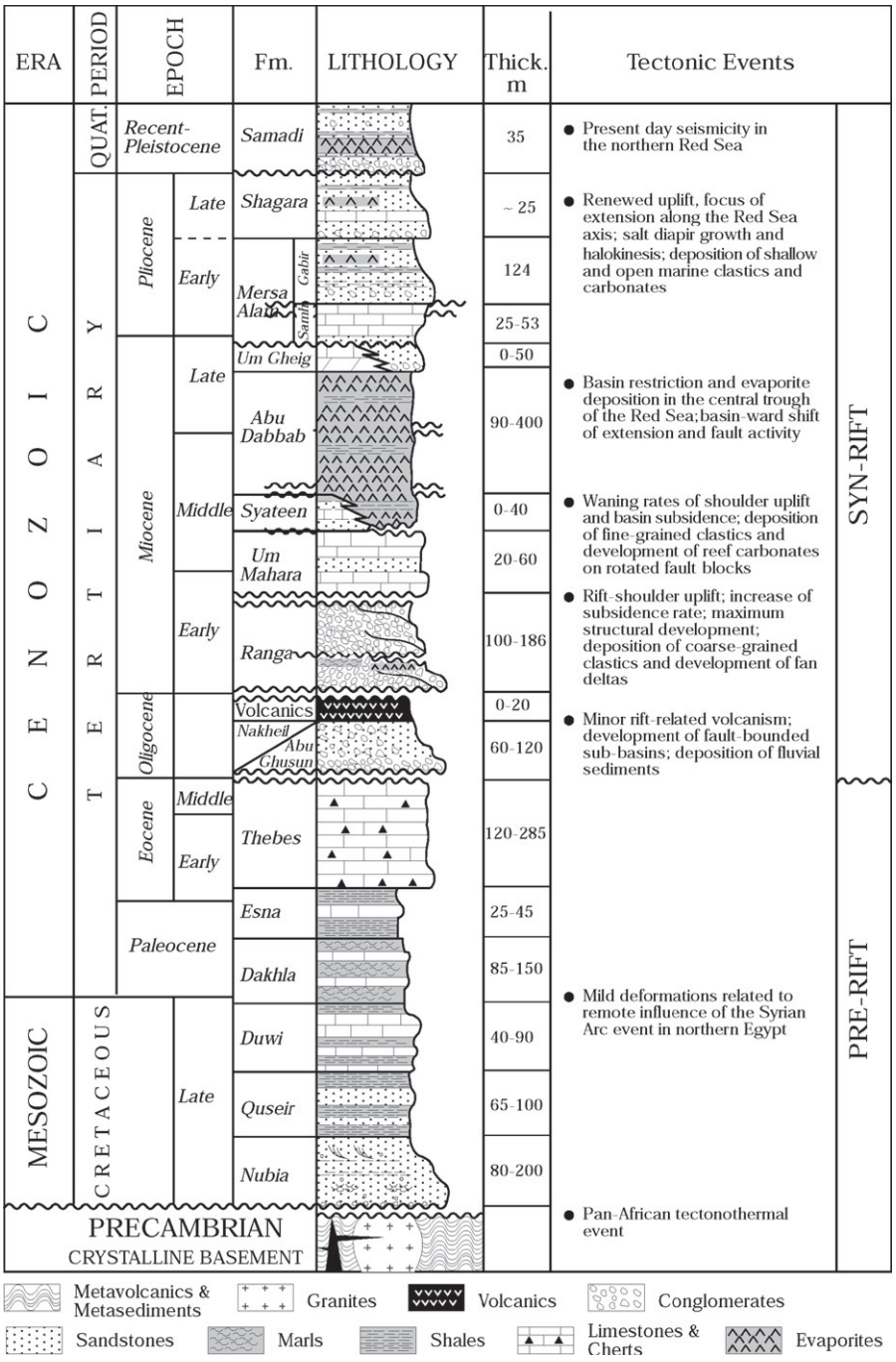

Figure 5.2 Summary stratigraphy of the northwestern Red Sea, based on data from Said (1990); Purser and Boscence (1998) and the authors' own work.

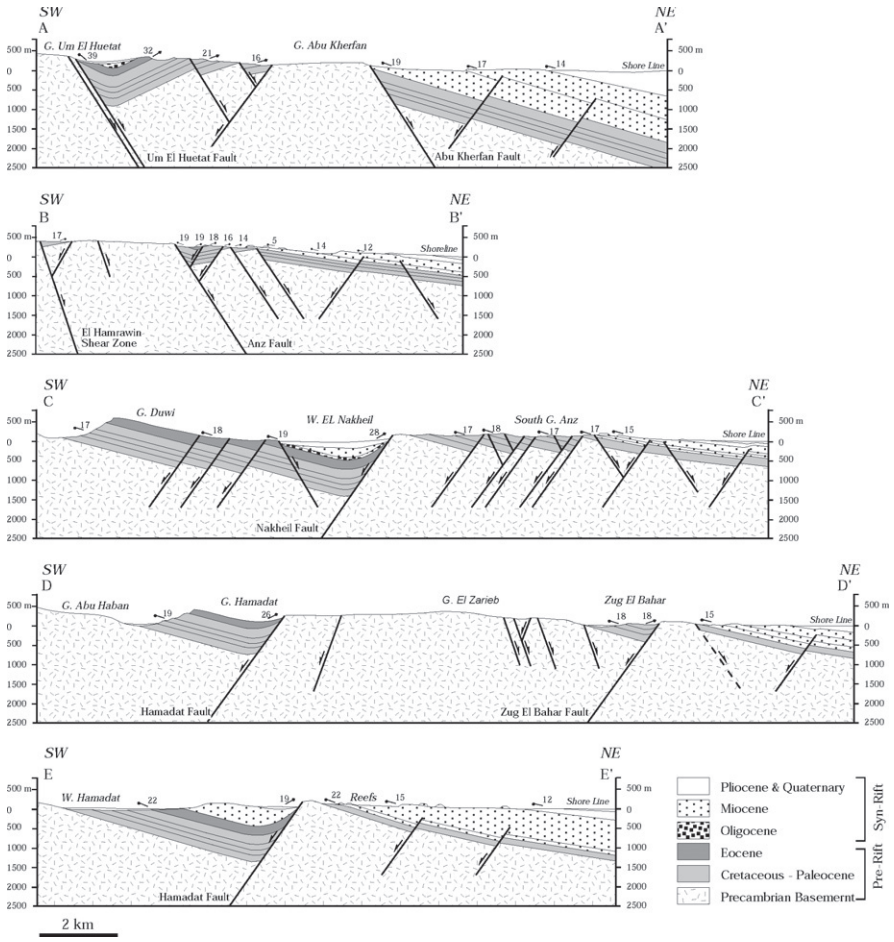

Figure 5.3 Cross-sections through the northwestern Red Sea margin, Egypt. The cross-sections illustrate the domino-style geometry of the fault blocks and change of polarity of the major block-bounding faults. Locations of cross-sections are shown in Fig. 5.1.

and oyster thin beds of the Upper Cretaceous to Paleocene Quseir, Duwi, Dakhla and Esna Formations, respectively (Fig. 5.2) (Abd El-Razik, 1967; Issawi et al., 1969; Said, 1990; Youssef, 1957). This Upper Cretaceous–Paleocene mixed clastic and carbonate section is overlain by a 120–280-m-thick section of chalky and cherty limestones of the Lower to Middle Eocene Thebes Formation (Fig. 5.2).

Syn-rift strata of the northwestern Red Sea margin

The earliest syn-rift sediments of the northwestern Red Sea margin are lacustrine red mudstones, sandstone, breccias and conglomerates of the Nakheil Formation (Fig. 5.2). The Nakeil Formation is Late Oligocene in age (Akkad and Dardir, 1966; Said, 1990) and is locally preserved in small hanging-wall synclines

formed along the Border Fault system (Fig. 5.1). In Wadi El Nakheil (Fig. 5.1), the Nakheil Formation is 60–120 m thick, and it unconformably overlies the pre-rift Eocene Thebes Formation. At this location, the Nakheil Formation is locally covered by Quaternary alluvium and terraces. The Nakheil breccias and conglomerates consist of reworked chert and limestone clasts derived from the underlying Eocene Thebes Formation. These grade upwards into reddish and varicoloured sandstones and mudstones interbedded with a few thin laminated carbonate beds. In the southern part of the study area (south Wadi Hamadat and Wadi Sharm El Bahari, Fig. 5.1), these conglomerates change to a polymict facies (referred to Abu Ghusun Formation; El Gezeery and Marzouk, 1974; Phillobbos et al., 1988) containing basement clasts, the proportion of which increases gradually upwards, alternating with red sandstones and mudstones locally interbedded with, and overlain by, Upper Oligocene thin basaltic flow (dated at 24.9–26 Ma; El Haddad, 1984; Roussel et al., 1986).

The coarse-grained sandstones and conglomerates of the Aquitanian–Burdigalian age Ranga Formation (El Bassyony, 1982) form a distinct syn-rift unit that unconformably overlies the pre-rift Precambrian to Eocene units and in places also overlies the Late Oligocene syn-rift red clastics. The Ranga Formation varies from 100 to 186 m in thickness (Fig. 5.2). Its lower part consists of continental red sandstones and conglomerates locally interbedded with a few gypsum thin beds (Fig. 5.4A) and marls, which contain Late Aquitanian–Burdigalian fauna (referred to as Rosa Member, Philobbos et al., 1993). The upper part of the Ranga Formation consists of shallow marine conglomerates and sandstones containing oyster shell fragments and patch reefs (Fig. 5.4B). The conglomerates are generally polymict, dominated by pebble- and boulder-size basement clasts in the area south of Safaga (Wadis Gassus, Guesis and Quwyh, Fig. 5.1) and dominated by chert clasts in the area south of Quseir (Wadi Sharm El Bahari, Fig. 5.1).

Unconformably overlying the Ranga conglomerates are reefal limestones and shallow marine fine-grained clastics of the Late Burdigalian–Langhian Um Mahara Formation (Fig. 5.2) (El Bassyony, 1982; Said, 1990). The thickness of Um Mahara Formation is 20–60 m in the study area, and it increases southwards to about 180 m at Wadi Abu Ghusun (Said, 1990). Along the coastal area, in the region of Safaga and Wadis El Ambagi and Zug El Bahar, the reefal limestone and sandy limestone of the Um Mahara Formation form local carbonate platforms with associated reef talus. These onlap the eastern slopes of exposed rotated basement blocks, which are topped in places by conglomerates and thin beds of detrital carbonates. The Middle–Late Miocene evaporite sequence of the Abu Dabbab Formation unconformably overlies the older syn-rift and pre-rift strata (Fig. 5.2). It consists of 90–400 m of massive to poorly bedded gypsum outcropping along the coastal plain, and it is up to 3 km in the offshore area (Said, 1990; Tewfik and Ayyad, 1982).

Overlying the evaporite sequence is a 200–300-m-thick succession of Upper Miocene–Quaternary sediments that are exposed along the coastal plain

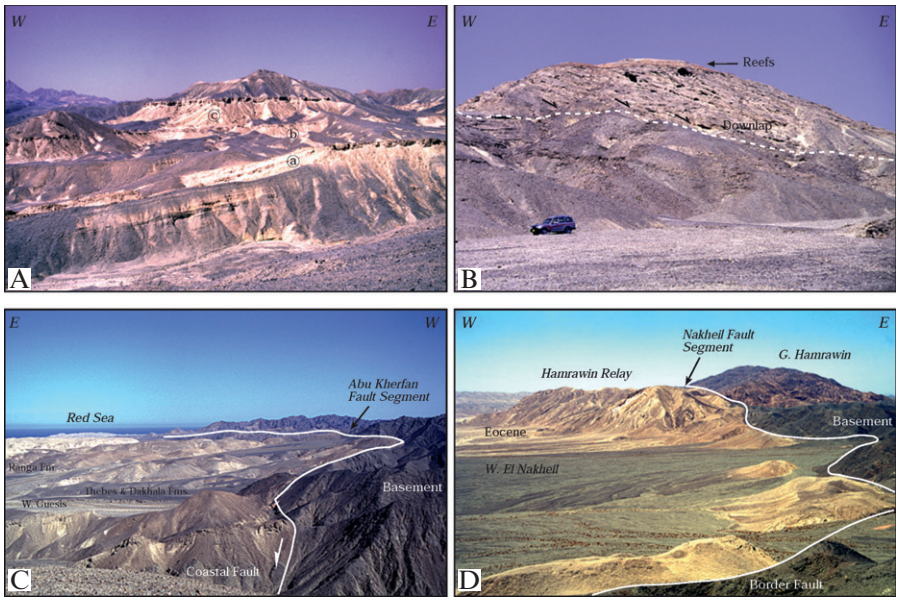

Figure 5.4
Outcrop examples of the stratigraphy and structure of the northwestern Red Sea. (A) Conglomerates and sandstones of the Ranga Formation, Wadi Gassus. The evaporite interbeds (A, B and C) of the Rosa Member separate fluvial conglomerates below and shallow marine conglomerates above. (B) Facies and stacking patterns of the upper part of the Ranga conglomerates, North Wadi Gassus. Foreset dip indicates eastward (basinward) propagation direction. Patch reefs are common in the topset beds. (C) Coastal Fault system (Abu Kherfan segment) juxtaposing pre- and syn-rift strata against the basement in Wadi Guesis. The Guesis fan delta occurs to the west of the photo. (D) Border Fault system (Nakheil segment) juxtaposing the Eocene strata against the basement, Wadi El Nakheil. Note the Hamrawin relay between the fault segments.

(Fig. 5.2). Offshore, these sediments can be up to 1000 m thick (Heath et al., 1998; Orszag-Sperber et al., 1998). They include Upper Miocene–Pliocene shallow to open marine sandstones and mudstones of the Mersa Alam Formation, interbedded limestone, coarse sandstones and conglomerates of the Shagara Formation, as well as Pleistocene conglomerates and coarse sands of the Samadi Formation (Fig. 5.2).

Structure of the northwestern Red Sea margin

The structural architecture of the northwestern margin of the Red Sea consists of two main extensional fault systems, together with a number of NW- and WNW-trending half graben basins (Figs. 5.1 and 5.3). The western fault system (herein called the Border Fault system) forms the western margin of the rift and juxtaposes the pre-rift Cretaceous–Eocene strata and syn-rift Nakheil Formation against Precambrian basement in the footwall of the extensional faults. The eastern fault system (herein called the Coastal Fault system) borders the Red Sea coastal plain, and it juxtaposes pre- and syn-rift Miocene strata against the Precambrian basement (Figs. 5.1 and 5.3). The Coastal Fault system generally trends NW, sub-parallel to the shoreline, and delineates the syn-rift exposures along the Red Sea coast (Fig. 5.4C). The Border Fault system is strongly segmented and trends oblique to the rift trend, reflecting the inherited basement fabric (cf. Khalil and McClay, 2002). Both of these fault systems consist dominantly of NW, WNW and NS fault segments that link through breached relay ramps and form a zig-zag fault pattern that bounds rhomboidal fault blocks

(Figs. 5.1 and 5.4C,D). The throw of the Border Fault system varies from 1.5 to 3.5 km and varies from 0.5 to 2 km along the Coastal Fault system (Khalil and McClay 2002) (Fig. 5.3).

In the northern part of the study area (between Safaga and the northern part of Gebel Duwi, Fig. 5.1), the Border Fault system dips northeastwards and bounds southwest-dipping half grabens (Mohamed Rabah and Wasif basins), whereas to the south, the Border Faults dip southwestwards and bound northeast-dipping half grabens (Duwi and Hamadat basins) (Figs. 5.1 and 5.3). This change in fault polarity and half-graben-dip direction occurs across a complex accommodation zone in the north of Gebel Duwi—called the Duwi accommodation zone (DAZ) (Khalil and McClay, 2001; Moustafa, 1997; Younes and McClay, 2002). The DAZ accommodates the transfer of displacement between the oppositely dipping fault segments of the Border Fault system and its location is controlled by reactivation of the WNW trending Precambrian Hamrawin shear zone (Fig. 5.1; Moustafa, 1997; Younes and McClay, 2002). Northeast–southwest cross-sections through the northwestern Red Sea (Fig. 5.3) show that the half grabens are dissected by intra-rift faults into 1–3-km-wide, domino-style fault blocks. These intra-rift faults are dominantly planar and have throws that range from tens of metres to a few hundreds of metres (Fig. 5.3).

5.3 Stratigraphic architecture and sedimentology of the Miocene syn-rift strata

In the Safaga–Quseir study area (Fig. 5.1), the Lower Miocene syn-rift clastics are localised in a number of structurally controlled sediment-input sites. Of particular importance are four sites that clearly show the inter-relationship between the structural architecture, and localisation and accumulation of syn-rift clastics. From north to south, these are located at Wadi Gassus, Wadi Guesis, Wadi Quwyh and Wadi Sharm El Bahari (Fig. 5.1). At these localities, the coarse-grained deposits of the Lower Miocene syn-rift Ranga Formation form fan-delta systems, which are dominated by pebble and cobble conglomerates, with minor amounts of pebbly and muddy sandstones. These Lower Miocene clastics unconformably overlie the pre-rift strata or Late Oligocene early syn-rift strata (Nakhiel and Abu Ghusun Formations), and are overlain by reef carbonates and/or evaporite successions of the Middle to Upper Miocene Um Mahara and Abu Dabbab Formations (Fig. 5.2).

Wadi Gassus–Wadi Guesis area

In the Wadi Gassus and Wadi Guesis area (Fig. 5.5), Lower Miocene clastics of the Ranga Formation develop kilometre-scale fan delta systems, formed in the hanging-wall of the fault segments of the Coastal Fault system. In these two

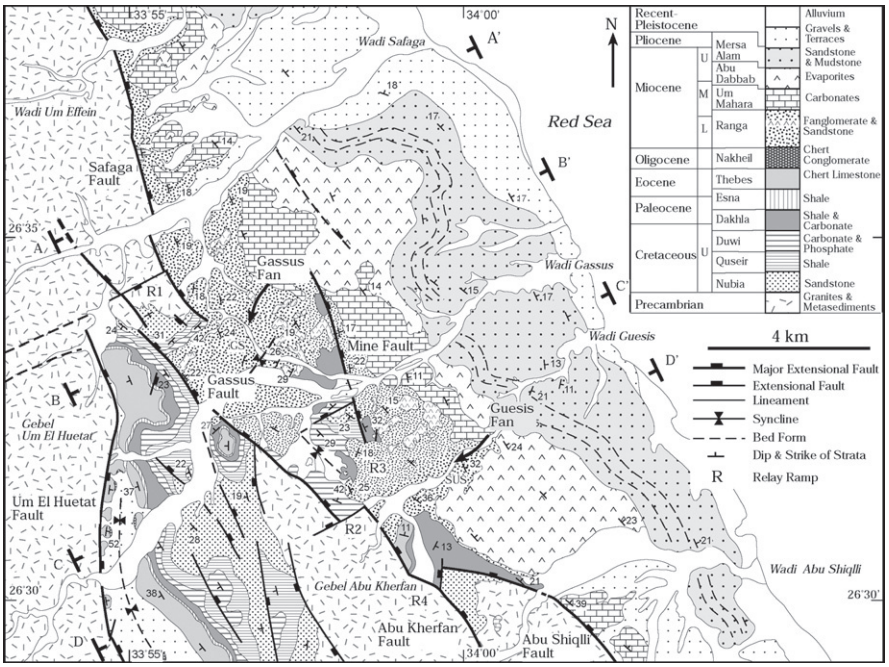

Figure 5.5
Detailed geologic map of the Wadi Gassus and Wadi Guesis area. R1, R2, R3 and R4 are relay ramps between the fault segments. GS and GUS indicate the locations of the measured log sections.

Wadis, the Ranga Formation consists of conglomerates and sandstones, with moderately to steeply dipping foresets prograding eastward (basin-ward). The structural setting and geometry of the Gassus and Guesis fan systems are shown in Figs. 5.5–5.7.

The Wadi Gassus fan delta is about 10 km^2 in outcrop area (Figs. 5.5 and 5.6), with a longitudinal length (parallel to the progradation direction) of 2 km and an average strike length of 5 km. The fan delta includes a pre-evaporite clastic section, which is 65–140 m in thickness (Fig. 5.8) and has a thickness/progradation ratio of 0.03–0.07. In Wadi Gassus, the conglomerates of the Ranga Formation are displaced against the Quseir and Duwi Formations, and in places unconformably overlie the Dakhla and Thebes Formations in the hanging-wall of the Gassus and Abu Kherfan fault segment (Fig. 5.4C).

On the northern flank of the Wadi Gassus (Figs. 5.1 and 5.5), the lower 30 m of the Ranga Formation consists of interbedded red siltstones and sandstones, and polymictic conglomerates that include chert and basement clasts. Palaeosols and red fine clastics in this part of the section indicate subarial exposure and deposition in continental environment. The remainder of the section consists of basement–clast conglomerates and includes sandstones and mudstones in thin beds and lenses. Within the clastic section, there are three to five evaporite

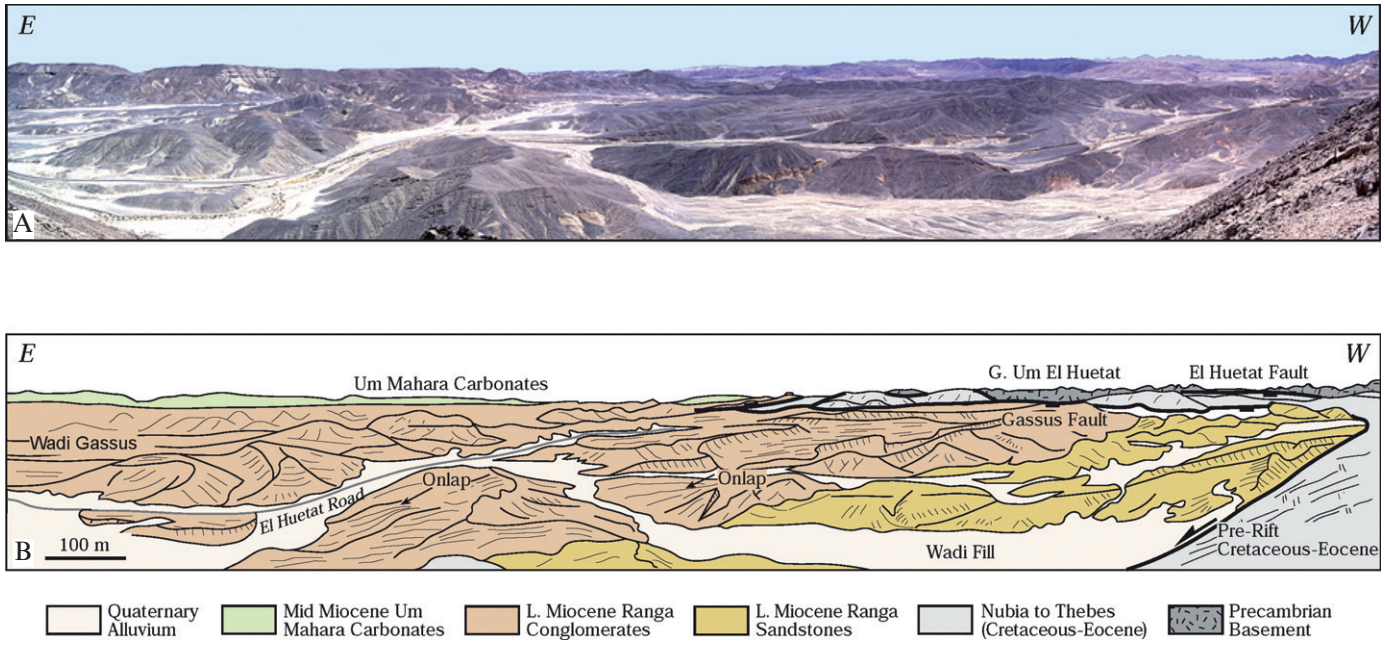

Figure 5.6 Field photo (A) and perspective sketch (B) showing the Wadi Gassus fan delta and the Gassus fault segment.

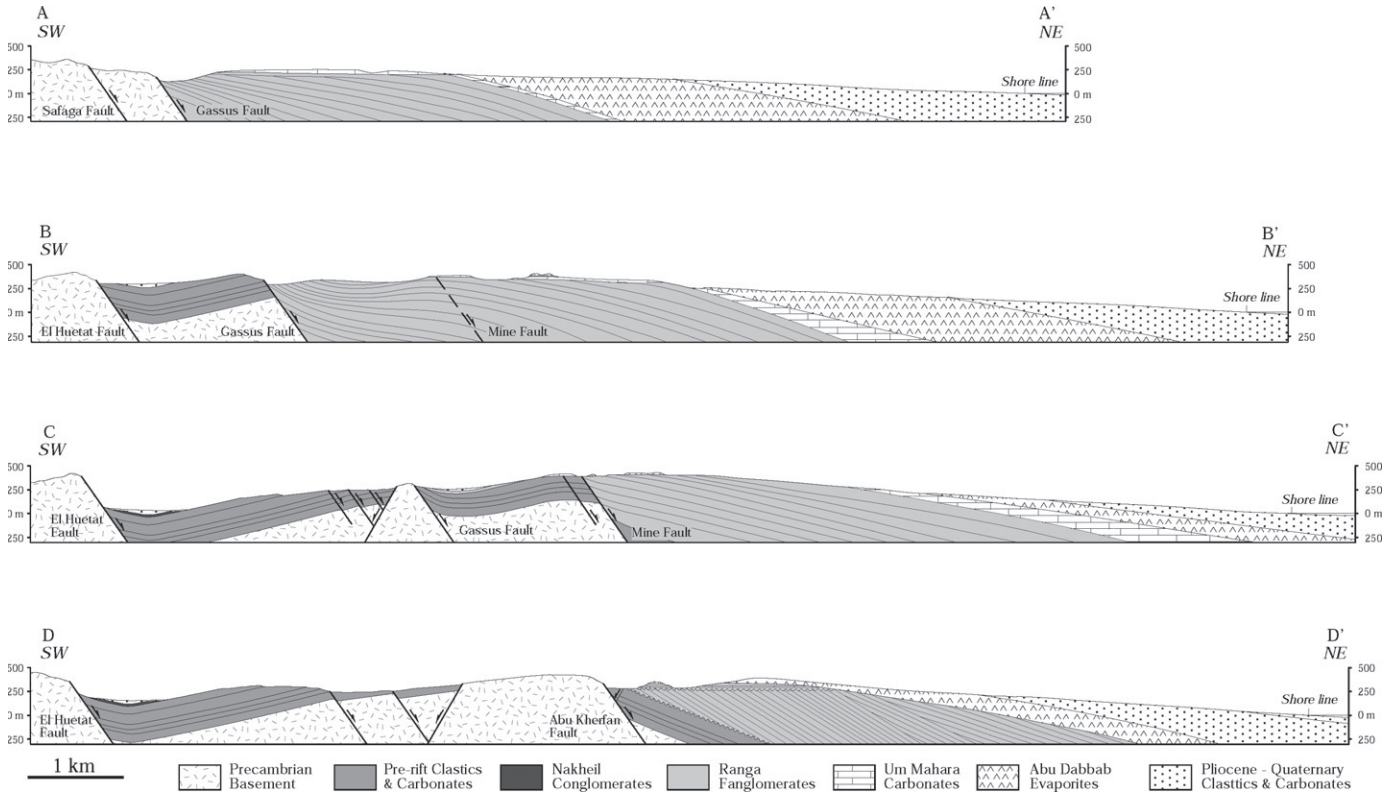

Figure 5.7 Cross-sections showing the Wadi Gassus (sections A, B and C) and Wadi Guesis (Section D) fan delta systems. Note wedge- to sheet-like geometries of the fans and the moderate to steep dip of the foreset beds. Locations of cross-sections are shown in Fig. 5.5.

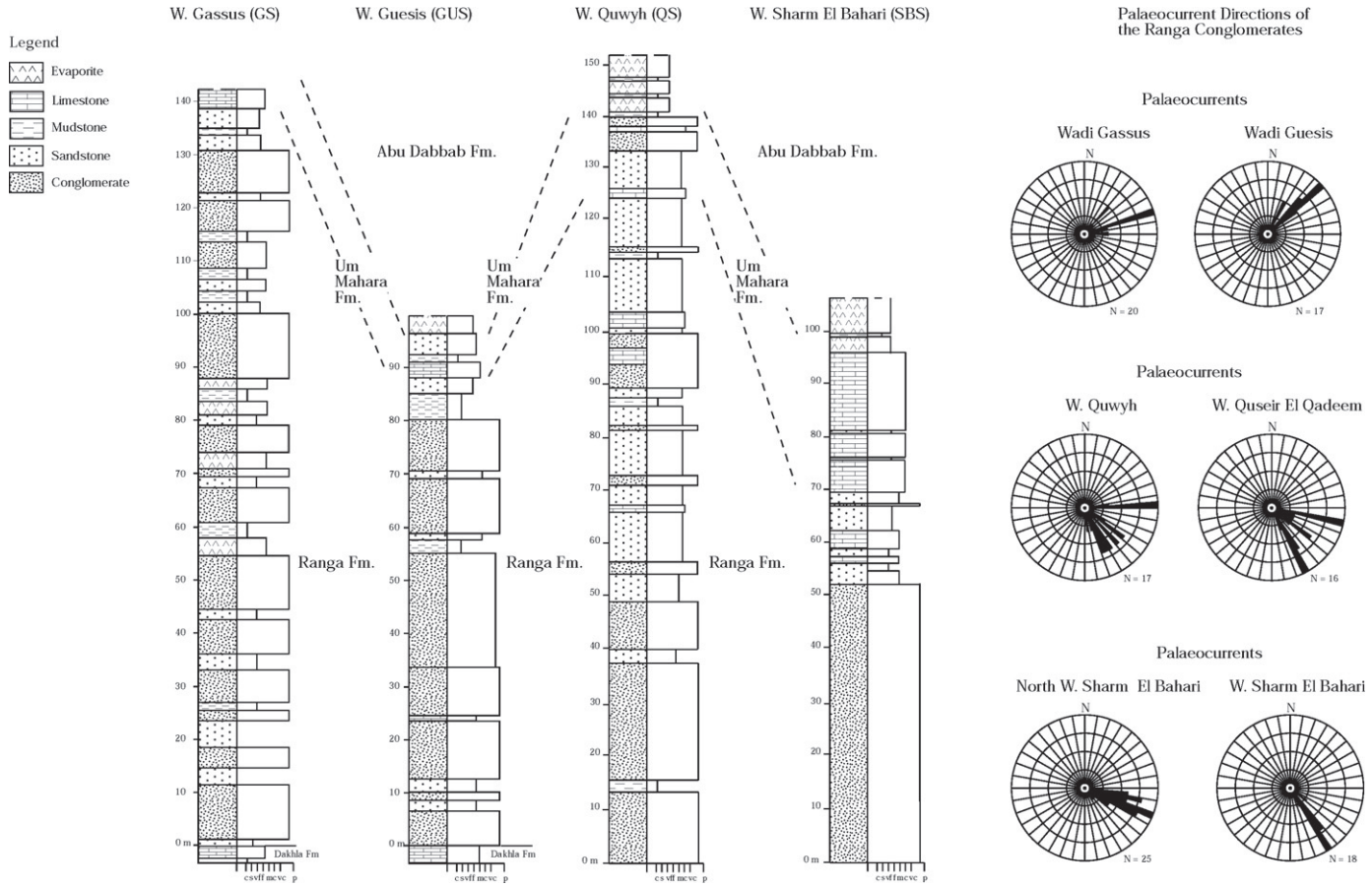

Figure 5.8 Lithostratigraphic logs of the Ranga Formation in Wadis Gassus, Guesis, Quwyh and Sharm El Bahari. Locations of logged sections are shown on the geological maps of Figs. 5.5, 5.10 and 5.12. Rose diagrams show the fanglomerates palaeocurrent directions at the localities cited in the text.

beds (Lower Miocene Rosa Member) whose average thickness is 4 m (Fig. 5.8; also Fig. 5.4A). In places, these evaporaite beds overlie thin algal laminite and shale units which, together with the evaporite beds, represent the restricted transitional facies that mark the Early Miocene marine transgression (Phillobbos et al., 1993; Purser and Philobbos, 1993). The basement clasts are dominantly granitic but they also include metavolcanic and metasedimentary components. They are subrounded to rounded and vary in size from 3 to 25 cm. Palaeocurrent data (based on conglomerate imbrications and the dip directions of foreset beds) indicate NE to ENE palaeoflow directions (Fig.5.8). The clastic section in Wadi Gassus is unconformably overlain by the Middle Miocene carbonates of the Um Mahara Formation and the Middle–Upper Miocene evaporites of the Abu Dabbab Formation. The thickness of the clastic section decreases from 140 m at the central part of Wadi Gassus to about 100 m in Wadi Safaga in the north and 65 m in the southern flank of Wadi Gassus.

The Wadi Guesis fan delta is about 4 km^2 in outcrop area (Fig. 5.5) and it has a sheet-like geometry, with longitudinal and strike lengths of about 2 km and a vertical height of 120 m above the floor of Wadi Gassus (Figs. 5.7 and 5.9). The fan geometry is well exposed in a cliff exposure, which runs near parallel to the progradation direction of the fan (Fig. 5.9). Along this cliff, the fan sequence is composed of a 95-m-thick conglomerate section of the Ranga Formation, which is unconformably overlain by the Um Mahara and Abu Dabbab Formations (Fig. 5.9). The thickness/progradation ratio of the fan is $\sim$0.06, similar to that of the Gassus fan delta. The Ranga conglomerates consist dominantly of granitic and metavolcanic clasts and are interbedded with a few pebbly sandstone, mudstone and limestone beds, which are 2–3 m in thickness (section GUS, Fig. 5.8). Chert and limestone clasts derived from the pre-rift sedimentary sequence are also present. These form a minor fraction ($<$15%) of the clast component, and are localised in the lower part of the conglomerate section. This reflects the progressive unroofing history of the uplifted footwall blocks in the rift margin. Adjacent to the Coastal fault, the basement clasts are 0.5 to 1 m in diameter, the clast size generally decreases eastwards towards the distal areas, and upwards within the conglomerate section.

The topset beds of the fan are subhorizontal, and they form an 8- to 10-m-thick unit that can be traced for hundreds of metres (Fig. 5.9). These beds are thinly stratified, composed of pebble and cobble conglomerates set in sandy matrix and locally show fining-upward units. The contact between the topsets and foresets is characterised by toplap of the foresets against the topset beds, creating typical oblique clinoform geometry similar to that described from other fan delta systems with comparable extensional setting (cf. Dart et al., 1994; Gawthorpe et al., 1990). This geometry may be interpreted to indicate stillstand conditions where erosion occurred above sea level, and the sediments bypassed the break in slope and were deposited basinward on the foreset slope (Gawthorpe et al., 1990).

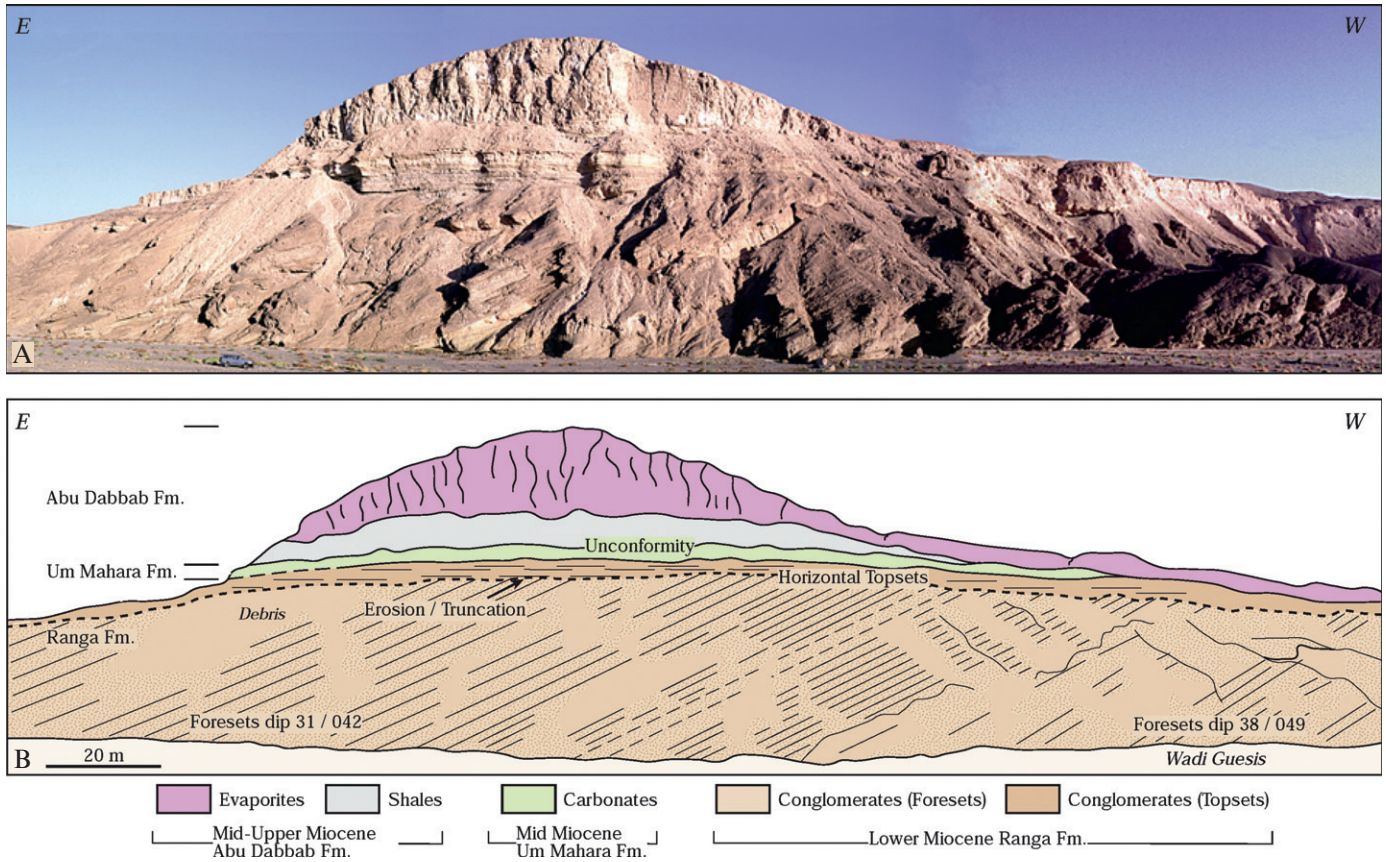

Figure 5.9 Field photo (A) and perspective sketch (B) showing the Wadi Guesis fan delta. The fan is characterised by sheet-like geometry, steeply dipping, planar foresets and horizontal topsets. The coastal fault system is about 1 km to the east of the photo and sketch.

The foreset beds are planar, about 60 m high, and have a depositional dip of 31–38°ENE (Fig. 5.9), decreasing eastwards to ~20° towards the distal part of the fan. The beds are 0.5–1 m in thickness, composed of highly organised, matrix-supported, pebble and cobble conglomerates which in places show normal grading into medium- to coarse-grained sandstones. The conglomerate clasts are subrounded and show an imbricated fabric which, together with the eastward dip of the foreset beds, indicates a dominant N50°E palaeocurrent direction (Fig.5.8). Marine oyster fragments and patch reef debris are found to occur in some of the conglomerate and sandstone beds, indicating probable deposition of the conglomerates in a shallow marine environment.

Although the bottomset beds are not well exposed along the cliff exposure of the fan, because of the foreset-bottomset transition zone below the wadi floor level, shallowing of the dip of the foresets in the down-dip direction is locally present, probably inferring a gentler dip for the bottomset units.

The overall characteristics of the conglomerate sequence in Wadi Guesis as described above suggest that the depositional system may be interpreted as a 'Gilbert-type' fan delta (e.g., Ethridge and Wescott, 1984; Gilbert, 1885; Holmes, 1965; Mcpherson et al., 1987). This interpretation is similar to that for the syn-rift coarse-grained fan delta systems described from the eastern margin of the Gulf of Suez (cf. Gawthorpe et al., 1990; Gupta et al., 1999) and from the Gulf of Corinth (Dart et al., 1994). The fanglomerate sequence in Wadi Guesis (the Lower Miocene Ranga Formation) is separated from the overlying evaporates of the Middle–Upper Abu Dabbab Formation by an unconformity characterised irregular erosional surface. This is interpreted to indicate emergence and erosion of much of the fanglomerate topsets prior to the deposition of the overlying evaporites during the Middle Miocene.

Structural control on Miocene sedimentation in the Gassus and Guesis areas

Detailed structural mapping of the Gassus-Guesis area revealed that the two fan systems are formed in the hanging-wall of a number of linked fault segments (Fig. 5.5). Between Wadi Safaga in the north and Wadi Abu Shiqlli in the south, the Coastal Fault system consists of four main segments – from north to south, these are the Safaga, Gassus, Abu Kherfan and Abu Shiqlli faults, respectively (Fig. 5.5).

The Safaga fault is oriented N12°W, and it juxtaposes Miocene clastics and carbonates against the Precambrian basement in the north and against Cretaceous strata in the south (Fig. 5.5). The maximum throw of this fault is ~1000 m. The Gassus fault consists of two segments oriented N45°W and has a maximum throw of ~800 m. It juxtaposes Miocene conglomerates down to the east with the Precambrian basement and Cretaceous strata in the footwall (Fig. 5.5). The Abu Kherfan Fault is oriented N35−40°W and has a maximum throw of ~850 m. It throws the Eocene Thebes Formation and Miocene conglomerates down to the

east against the basement of Gebel Abu Kherfan (Fig. 5.5). The Abu Shiqlli fault is oriented N50°W and its maximum throw is 870 m. Another fault cuts across the Wadi Gassus (the Mine fault, Fig. 5.5) and is oriented N10°W. The throw of this fault changes along its strike as it juxtaposes Cretaceous–Paleocene strata against Lower Miocene strata. The throw of this fault is a few hundreds of metres towards the east–northeast.

Calculation of the stratigraphic and topographic offsets shows that the throw of the fault segments decreases along-strike as these faults are traced both to the north and to the south. In the map and cross-sections (Figs. 5.5 and 5.7), the change of fault displacement is indicated by the variable juxtaposition of the basement against the pre-rift and syn-rift sediments along the strike of faults. This along-strike change in fault displacements produced relay ramps that link the fault segments where the fault tips approach and overlap each other (cf. Childs et al., 1995). The deposition of Miocene conglomerates in the Wadi Gassus fan delta was controlled by two relay ramps which served as pathways for clastic discharge and accumulation at the Wadi Gassus sediment-input point. The northern relay ramp (R1) is formed between the Safaga and Gassus fault segments and dips 31–42°SE, whereas the southern relay ramp (R2) (Fig. 5.5) is formed between Gassus fault and Abu Kherfan fault and dips 36–42°NE (Fig. 5.5). The southern relay (R2) is breached in the footwall (Gebel Abu Kherfan) via a small cross-fault, which strikes approximately parallel to Wadi Guesis (Fig. 5.5). The area between the two relays is a structural low, located opposite to the central part of the Gassus fault and it forms an open syncline that is filled with Miocene clastics (Fig. 5.5). This syncline has a structural relief of ~350 m.

Similar to the Wadi Gassus fan delta, the Wadi Guesis fan delta was controlled by relay structures formed between three fault segments – from north to south respectively, the Abu Shiqlli, Abu Kherfan and Mine faults (Fig. 5.5). The throws of these faults decrease as they approach each other as indicated by the juxtaposition of Cretaceous strata against basement, and the Lower Miocene conglomerates against Cretaceous strata at the fault terminations (Fig. 5.5). The northern relay (R3) (Fig. 5.5) occurs between the Abu Kherfan and the Mine faults, and it dips 17–25°ESE; the southern relay (R4) occurs between the Abu Shiqlli and Abu Kherfan faults, and it dips 11–18°NE (Fig. 5.5). The two relay ramps (R3 and R4) served as conduits for the clastic discharge to enter the basin and hence form the Guesis fan delta system.

Despite the fact that both the Gassus and Guesis fan deltas are formed in the hanging-wall segments of the Coastal Fault system and appear to have been similarly controlled by relay structures, the thickness and outcrop area of the coarse clastics in the proximal part of the Gassus fan system is 10 km^2 as compared with 4 km^2 in the Guesis fan system. This difference in fan size is interpreted to reflect the fact that the Gassus fan was formed almost opposite to the central part of the Gassus fault where this fault had its maximum displacement and, as a consequence, the

hanging-wall accommodation space was greater than in the Guesis fan, which was localised close to the tips of the fault segments.

Wadi Quwyh area

In Wadi Quwyh, the Lower Miocene sediments of the Ranga Formation form a fan delta, which is about 4 km^2 in outcrop area (Fig. 5.10). The geological map, perspective sketch and cross-section (Figs. 5.10 and 5.11) summarise the structural setting and geometry of this fan delta. The fan delta has a sheet-like geometry, with 2 km of average longitudinal and strike lengths (Figs. 5.10 and 5.11). The fan sequence is 145 m in thickness, which decreases gradually to <50 m in both the longitudinal and strike directions, resulting in a thickness/progradation ratio of 0.25–0.07. It is composed of conglomerates and sandstones interbedded with 3–5 ledge-forming reef limestone units whose average thickness is 2.5 m (Fig. 5.8; log section QS).

Topset beds are generally horizontal to gently dipping, with the dip increasing gradually in the progradation direction to ~8° at the distal areas. They are crudely stratified and composed of basement-clast-dominated conglomerates and pebbly sandstones. The conglomerate clasts are subrounded and moderately sorted. The sandstones are medium- to coarse-grained and locally show wave ripple cross-laminations. The limestone interbeds are pink-coloured, locally bioturbated and laminated and contain reef corals.

Within the fan system, the foreset beds are 20–40 m high and dip 15–20°SE and ESE. They are characterised by oblique to slightly sigmoid clinoforms

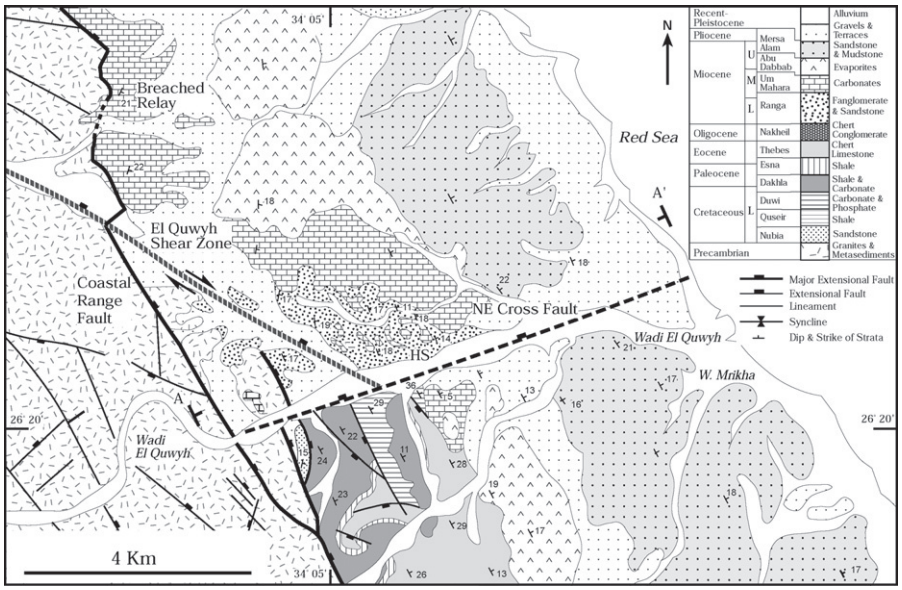

Figure 5.10 Detailed geologic map of the Wadi Quwyh area showing the structural setting of the Quwyh fan delta. QS indicates the location of the measured log section.

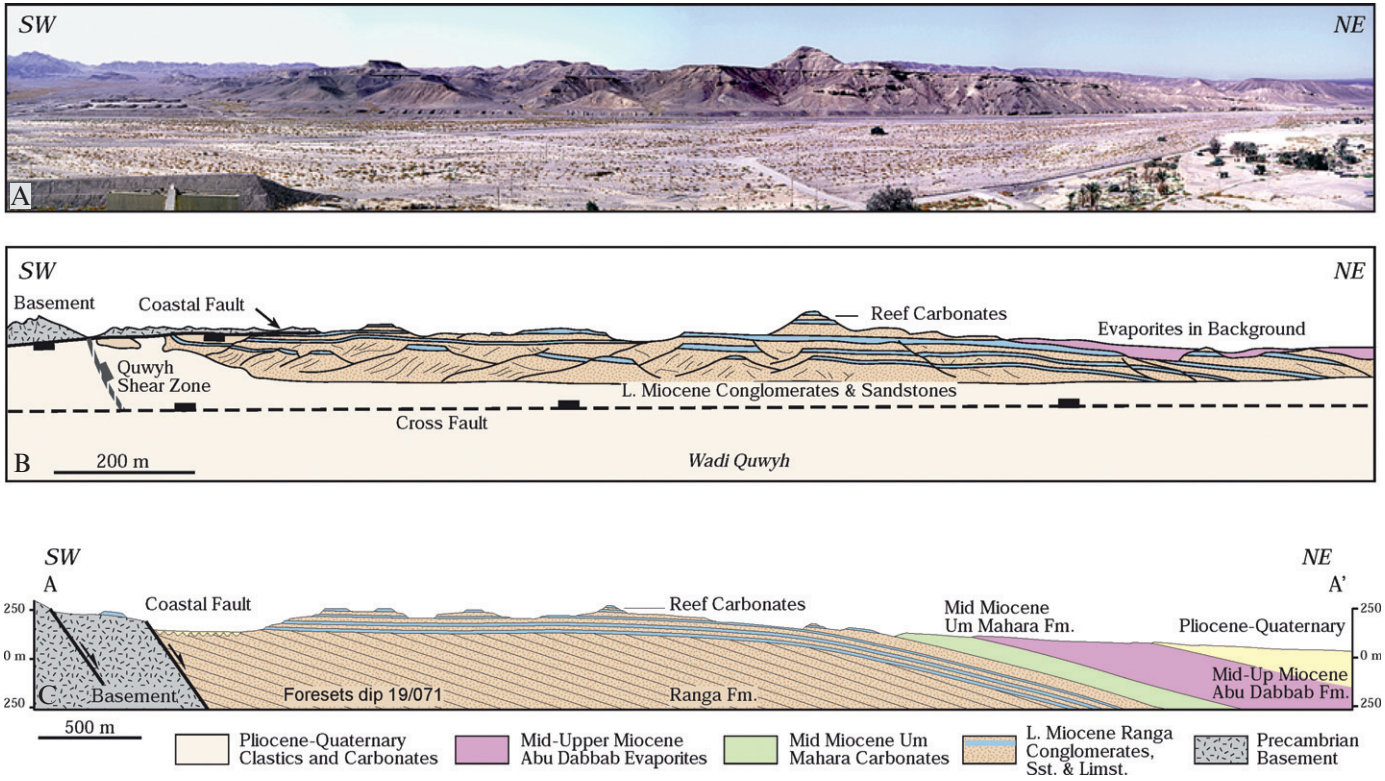

Figure 5.11 Field photo (A), perspective sketch (B) and cross-section (C) showing the geometry of the Wadi Quwyh fan delta. See Fig. 5.10 for location of cross-section.

(Fig. 5.11). The beds are 0.5–2 m thick, and are composed of crudely stratified polymict conglomerates dominated by basement clasts and minor chert and limestone clasts (~90% and 10%, respectively). The clasts are 4–10 cm in diameter, rounded to subrounded with crude imbrications, and in places show normal or inverse grading. The conglomerates in some locations contain patch reefs at higher levels close to the topset-foreset transition.

The conglomerate and sandstone foresets may be interpreted to indicate deposition by fluvial processes, with the coarse sediments transported to the foresets by sheetfloods (Gawthorpe et al., 1990). The dip direction of the foresets and the imbricated clast fabric indicate east and south east paleocurrent directions (Fig.5.8). The sandstones within the foresets are interpreted to have been deposited during periods of reduced fluvial input, with the sediment processes mainly dominated by reworking by wave activity (Gawthorpe et al., 1990). The presence of reef limestone and sandstone alternations within the topsets indicates episodic, generally low, fluvial input, allowing coral growth and reef buildup.

Structural control on Miocene sedimentation in the Wadi Quwyh area

The map, perspective sketch and cross-section of the Quwyh fan delta (Figs. 5.10 and 5.11) show that the deposition of the conglomerates was restricted to the northern flank of the Wadi Quwyh rather than along the southern flank. Here, the Coastal Fault system is oriented N25°W and juxtaposes pre-rift strata (in the southern flank of the wadi) and Miocene strata (in the northern flank of the wadi) against the Precambrian basement in the footwall (Fig. 5.10). Within Wadi Quwyh, a N70°E oriented cross-fault displaces the Miocene conglomerates down to the north against the Cretaceous strata to the south (Fig. 5.10). The cross-fault interacts with the Quwyh shear zone, which strikes N60°W (Fig. 5.10). This intersection produced a trapdoor structure, which controlled the localisation of the conglomerate units (Figs. 5.10 and 5.11). The east and southeastward transportation (as indicated by the palaeocurrents) of the coarse clastics derived from the basement footwall block was controlled by a relay ramp and the Quwyh shear zone. The relay ramp is formed between the coastal fault segments to the north of Wadi Quwyh, and the ramp dips 20–22°ESE (Fig. 5.10). This relay, together with the Quwyh shear zone, which strikes parallel to the down-dip direction of the relay, provided a pathway for the coarse clastics to enter the basin (Fig. 5.10).

The influence of cross-faults that controlled the location of Miocene clastics along the rift margin is also seen in Wadi Quseir El Qadeem, about 30 km to the south of Wadi Quwyh (Fig. 5.1). In this Wadi, the Lower Miocene sandstones and conglomerates (90 m thick) develop a local, ENE-trending channel localised by a cross-rift fault that appears to have interacted with the coastal, rift-parallel fault segments. The palaeocurrent data from this channel indicate east and southeast sediment transport directions (Rose diagrams, Fig. 5.8), similar to the palaeocurrent directions of the Wadi Quwyh fan delta.

Wadi Sharm El Bahari area

Wadi Sharm El Bahari is located about 30 km south of Quseir (Figs. 5.1 and 5.12). In this Wadi, the conglomerates of the Ranga Formation form a fan delta, which has a wedge-like to a sheet-like geometry and an east to southeastwards progradation direction (Fig. 5.13). The length of the fan in the progradation

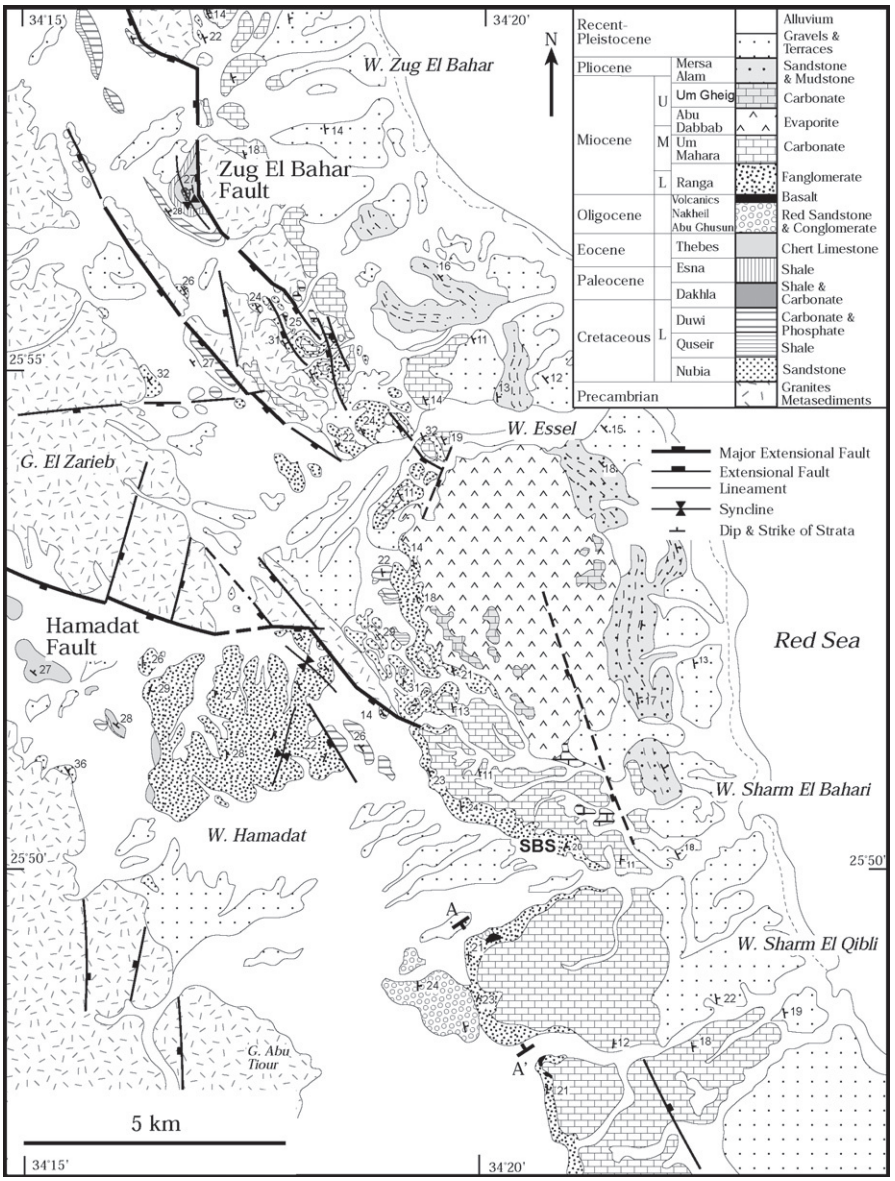

Figure 5.12
Detailed geologic map showing the structural setting of the Wadi Sharm El Bahari and Sharm El Qibli area. Note the localisation of the Ranga Formation conglomerates at the southern termination of the Hamadat and Zug El Bahar fault segments. At this locality, the basement blocks plunge southeastwards and have low structural relief. SBS indicates the location of the measured section.

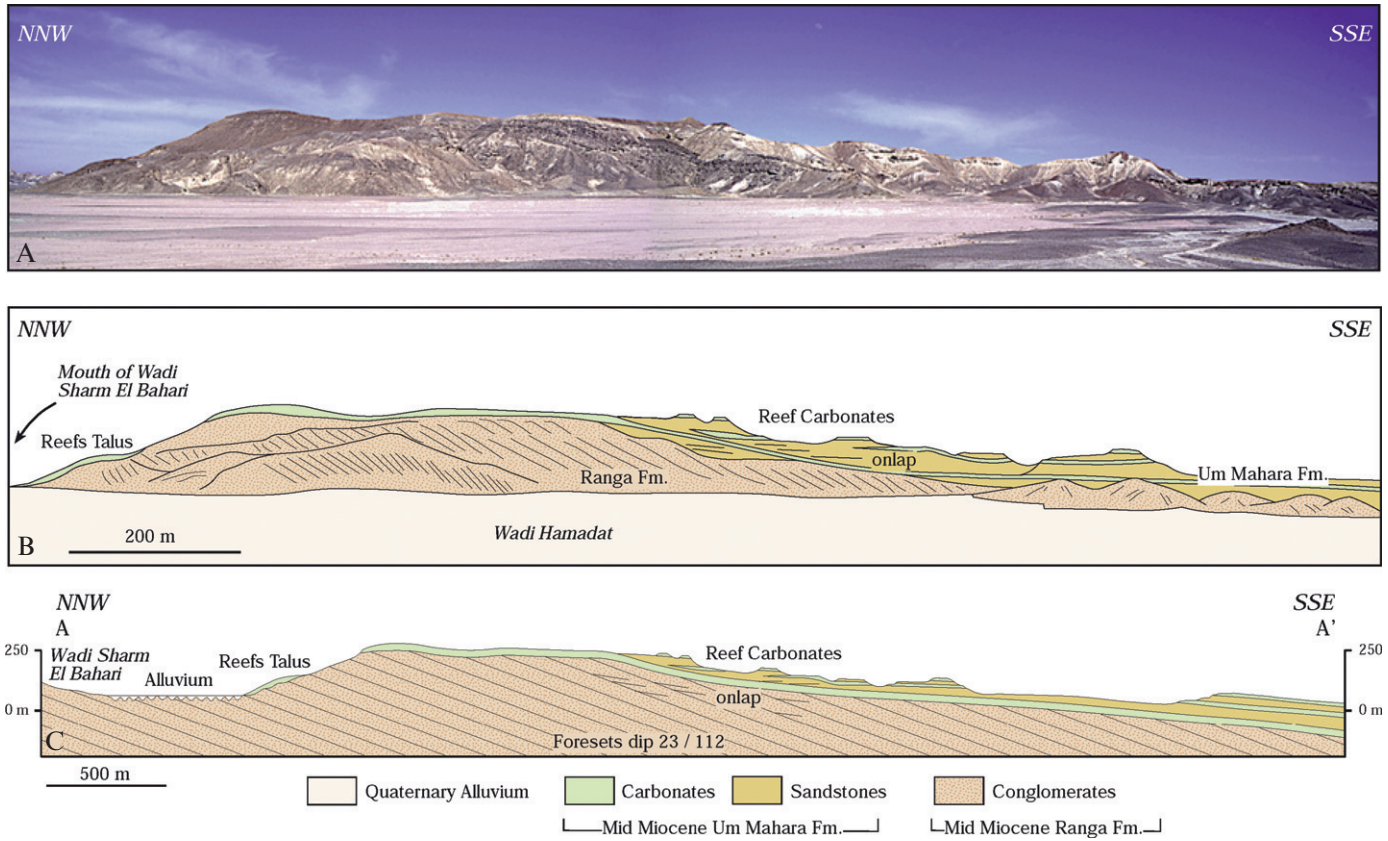

Figure 5.13 Field photo (A), perspective sketch (B) and cross-section (C) showing the geometry of the Wadi Sharm El Bahari fan delta. See location of cross-section in Fig. 5.12.

direction is 3 km and its average strike length is 2 km. The maximum height of the fan is about 200 m above the wadi floor and it decreases eastwards (at distal areas) to <50 m (Fig. 5.13). This fan sequence is dominated by lower Miocene coarse clastics of the Ranga Formation, which is 60–100 m in thickness (cf. Fig. 5.8; log section SBS). The average sequence thickness/progradation ratio of the fan is 0.025.

In the northern flank of Wadi Sharm El Bahari, the contact between the Ranga Formation and the older strata is covered by the wadi deposits, whereas in the southern flank, it unconformably overlies the red sandstone and conglomerates of the early syn-rift Oligocene strata, which locally contain basalt flows. The conglomerate sequence is characterised by large-scale foresets, which are 20–40 m high (Fig. 5.13). The average dip of these foresets is 22°, but this decreases gradually in both updip and downdip directions to <10°, producing sigmoidal to gently oblique clinoforms (Fig. 5.13). The foreset beds are moderately stratified, with bed thickness ranging from 0.5 to 3 m. These units are composed of chert-dominated conglomerates, which are both clast supported and sand-matrix supported. Clasts are 2–10 cm in diameter, rounded to subrounded, and in places have an imbricated fabric. When tracing the foreset updip, the beds become sandier, the dipping shallow, and there are shell fragments and patch reefs. These are onlapped in many places by gently dipping to horizontal shallow marine sands and reef (coral and algal) carbonates developed on the emergent topography that extends southeastwards to Wadi Sharm El Qibli (Figs. 5.12 and 5.13). The coarse clastic facies of the Wadi Sharm El Bahari fan delta also continues southeastwards to Wadi Sharm El Qibli, where these fanglomerates unite and probably coalesce into a larger fan system.

The conglomerate facies of the fan sequence in Wadi Sharm El Bahari is interpreted to indicate the dominance of fluvial processes, with the coarse sediments transported to the foreset slopes by sheet flows. Foreset bed dips and imbricated clast fabrics indicate ESE to SE palaeoflow directions (Fig.5.8). The finer and sandier facies were deposited when the clastic discharge was low and the siliciclastic input was reduced enough to permit reef growth and colonisation of large areas of the delta topsets.

Structural control on Miocene sedimentation in the Wadi Sharm El Bahari area

The Wadi Sharm El Bahari sediment-input site is located at the southeast corner of the Gebel El Zarieb and Zug El Bahar basement ridges (Fig. 5.12). The localisation of the fan delta in Sharm El Bahari appears to have been controlled by the WNW- and NW-trending, WSW-dipping faults (Hamadat and Zug El Bahar faults) that bound the Hamadat and Zug El Bahar half grabens (Figs. 5.1 and 5.12). The basement footwall blocks of these faults (Gebel El Zarieb and Zug El Bahar ridges) are interpreted to have formed barriers against the eastward

transportation of the clastics supplied by the basement of the rift shoulder in the west (Figs. 5.1 and 5.12). The Hamadat and Zug El Bahar faults offset and lose displacement as they are traced southeastward (towards the Sharm El Bahari and Sharm El Qibli area). This is indicated by juxtaposition of the Cretaceous Nubia and Duwi Formations against the basement at the southern termination of the faults (Fig. 5.12) and by the southeastward plunge of the footwall blocks (Zug El Bahar and El Zarieb basement blocks; Philobbos and Purser, 1993; Purser et al., 1987). These basement blocks have their lowermost structural relief at the locality of Sharm El Bahari (Fig. 5.12). Because of these combined structural and morphologic elements, the Miocene clastics, instead of being transported eastward towards Zug El Bahar in the coastal area, are considered to have been carried southeastward, towards the Wadi Sharm El Bahari sediment input-point, and farther south to Wadi Sharm El Qibli. In addition, the relay structures that occur between the offset fault segments (e.g., at the southern corner of the Gebel El Zarieb, Fig. 5.12) probably augmented this southeastward transportation of the clastics towards these sediment-input points. The chert-dominated conglomerates of the Wadi Sharm El Bahari fan are interpreted to have been derived from the pre-rift Cretaceous–Eocene stripped from the fault blocks in Wadi Hamadat and probably also from the pre-rift strata stripped from the basement highlands farther to the west (Fig. 5.12).

5.4 Discussion: Models for the structural control on the Miocene fan delta systems

The key areas studied in this chapter indicate that, in the northwestern Red Sea margin, Lower Miocene coarse-grained fan delta systems were developed in a number of structurally controlled sediment-input points (Figs. 5.14 and 5.15). Fault intersections, pre-rift (basement) fabrics, transfer zones and plunge directions of fault blocks are interpreted to have strongly influenced the Early Miocene sedimentation in the northwestern the Red Sea. Three conceptual models are proposed in this paper to illustrate the varieties of structural styles that controlled these sediment-input sites (Fig. 5.14). The locations of these sediment-input sites and their relation to the overall structural architecture of the northwestern Red Sea margin, together with the inferred drainage systems, sediment dispersal and palaeocurrent directions, are summarised in Fig. 5.15.

Model 1 proposes that both the Wadi Gassus and Wadi Guesis fan deltas were controlled by two oppositely dipping relay ramps that formed near the tips of individual fault segments of the Coastal fault system (Fig. 5.14A). These relay ramps formed topographic lows with inferred drainage systems that issued from the footwall of the fault segments of the Coastal Fault system, and hence provided pathways for the footwall-derived clastic sediments to enter the basin

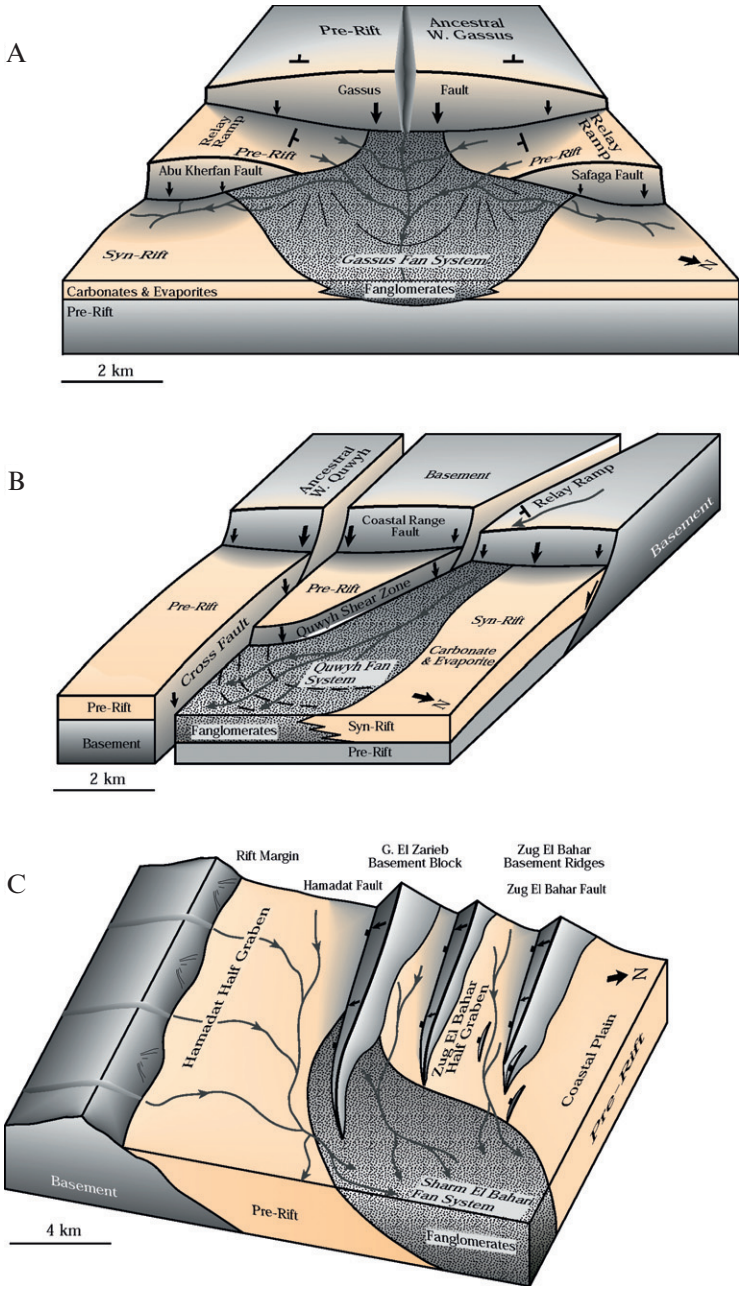

Figure 5.14 Summary schematic models illustrating the structural controls on sedimentation of Miocene coarse clastics in the northwestern Red Sea. (A) Wadi Gassus and Wadi Guesis fan deltas, (B) Wadi Quwyh fan delta and (C) Wadi Sharm El Bahari fan delta.

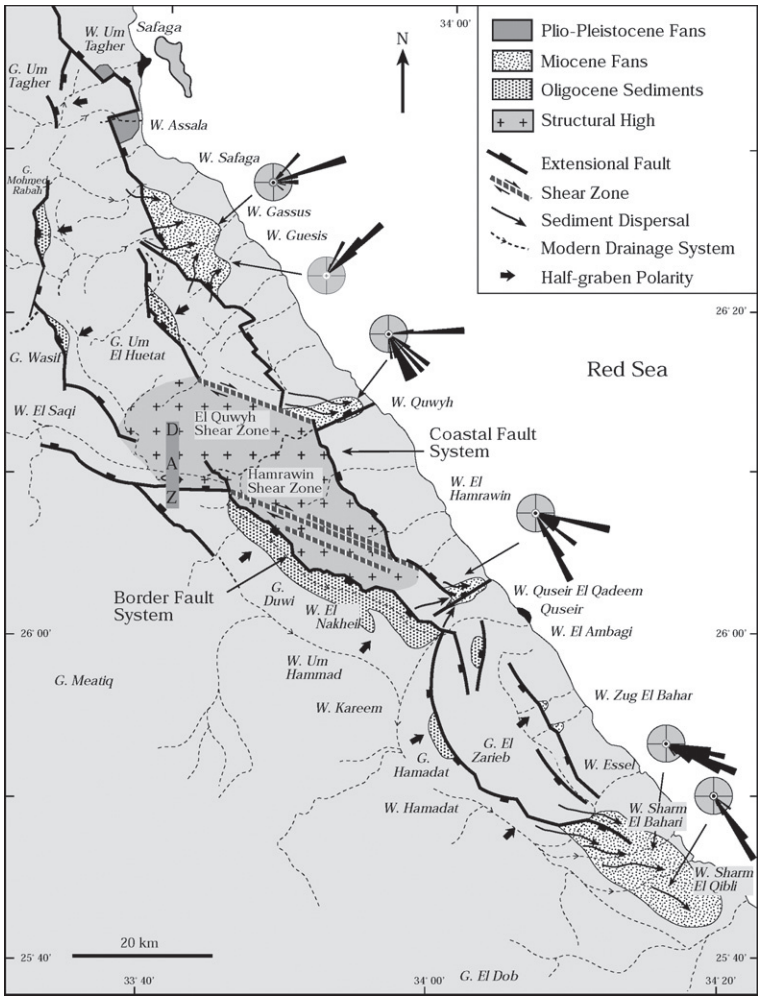

Figure 5.15 Summary map showing the major structures, sediment input sites, drainage systems and palaeocurrents of the lower Miocene coarse clastics of the Ranga Formation in the northwestern Red Sea.

(Fig. 5.14A). Between these two oppositely dipping relays, a local hanging-wall syncline formed adjacent to the central part of the Gassus fault segment, where the fault throw was maximum (Fig. 5.14A), and this provided accommodation space for the accumulation of the conglomerates and development of the fan delta in this locality.

In addition to the structural control exerted by the relay system as proposed above, the Gassus fan was probably also fed by the long-lived ancestral drainage system of Wadi Gassus (Figs. 5.14A and 5.15), which ran transversely across the Gassus and Um El Huetat fault system in the west (Fig. 5.15). The large size of the Gassus fan (~10 km^2) and the boulder-sized basement clasts probably were

derived from the exhumed basement in the footwall of the Gassus and Um El Huetat faults. The role of long-lived antecedent drainage systems in deposition of coarse-grained sediments is also well known from similar rift basins, for example, Gulf of Corinth (Seger and Alexander, 1993) and Gulf of Suez (Gawthorpe et al., 1990; Gupta et al., 1999; Leppard and Gawthorpe 2006; McClay et al., 1998). In these examples, drainage incision kept pace with footwall uplift and sediment transport was maintained into the basins in the hanging-walls of the extensional faults (Leppard and Gawthorpe, 2006).

Model 2 for the Wadi Quwyh sediment-input point is shown in Fig. 5.14B. This is interpreted to have been controlled by the intersection of the WNW-trending Quwyh shear zone and an ENE-trending cross-fault, together with a relay ramp formed between the NNW-trending segments of the Coastal Fault system (Fig. 5.14B). The shear zone formed a weak basement region that was subjected to severe erosion and as a consequence coarse-grained clastics were shed into the Quwyh input point. The shear zone, together with the relay ramp between the coastal fault segments, formed a pathway for the sediment influx. In addition, the interaction of the shear zone with the cross-fault formed a 'trapdoor' accommodation structure for these footwall-derived clastic sediments (Fig. 5.14B). The cross-fault is also interpreted to have controlled the course of the ancestral Wadi Quwyh, which overprinted the cross-fault and ran perpendicular to the Coastal Fault system (Figs. 5.14A and 5.15). It is interpreted that the ancestral Wadi Quwyh therefore equally sourced the footwall-derived basement conglomerates of the Wadi Quwyh fan delta system. NE-trending cross-faults are also interpreted to have controlled the NE-trending drainage systems and the location of syn-rift sediments in other parts of the Northwestern Red Sea margin, particularly in the Wadi Quseir El Qadeem and Wadi Assala areas (Fig. 5.15). The role of these cross-fault systems appears to have been similar to that exerted by the transfer faults described by Lambiase and Bosworth (1995) from the Sugata basin of the Gregory rift in East Africa and from Gebel Zeit in the western margin of the Suez rift in Egypt.

Model 3 for the Sharm El Bahari sediment-input point (Fig. 5.14C) proposes that the southeastward decrease of displacement on the border fault system strongly influenced the deposition of the Miocene sediments at this location (Fig. 5.14C and 5.15). The southeastward decrease of displacement of the Hamadat and Zug El Bahar faults resulted in the development of fault blocks that had a southeastward plunge direction (Fig. 5.14C). The plunge of the southern corner of the fault blocks and the associated low structural/topographic relief are thus interpreted to have provided a pathway for the clastic sediments derived from the uplifted rift margin to the northwest. The present day drainage shows that the ancestral Wadi Hamadat splayed into the easterly trending Wadis Sharm El Bahari and Wadi Sharm El Qibli at the southeast plunging corner of these fault blocks (Figs. 5.14C and 5.15).

Palaeocurrent indicators show that the flow directions varied from NE in the north (Gassus and Guesis fan deltas) to E and SE in the south (Quwyh and Sharm

El Bahari fan deltas and farther south at Wadi Sharm El Qibli (Fig. 5.15). This change in palaeocurrent direction occurs across the DAZ. This is inferred to have formed a topographic high compared to the oppositely dipping half grabens located both to the north and the south (Fig. 5.15). In addition, it is interpreted that the change of fault polarities across the DAZ resulted in the development of a horst to the east of the DAZ (Fig. 5.15). This horst (dominated by Precambrian basement at the present day) stands up to 600 m above sea level and plunges to about 400 m elevation in the northwest and 250 m elevation in the southeast. The DAZ and its strong palaeo-topographic expression are interpreted to have strongly influenced the drainage system and sediment dispersal during the structural evolution of this part of the Red Sea rift in the Lower Miocene. The longitudinal drainage systems (with drainage parallel to the border faults) in the south of the DAZ (Wadis Um Hammad, El Nakheil and Hamadat, Fig. 5.15) flowed southwestwards. The Wadi Hamadat drainage splays in the south to Wadis Sharm El Bahari and Sharm El Qibli, where the Bahari fan delta was located at the southern plunge of the G. Zarieb and Zug El Bahar fault blocks (Fig. 5.14C and 5.15).

5.5 Conclusions

Detailed field mapping of rift structures and the stratigraphy in the northwestern Red Sea has indicated that Lower Miocene syn-rift sediments developed coarse-grained fan delta systems with their locations strongly influenced by the rift fault geometries.

Relay ramps, interactions between rift-parallel faults, cross-rift faults and shear zones, as well as the DAZ, combined with plunge variations of the basement blocks, are interpreted to have been the main factors that controlled the development and localisation of the Lower Miocene syn-rift fan systems (Figs. 5.14 and 5.15).

The thickness/longitudinal length ratios of the Miocene fan delta systems vary from 0.025 to 0.07, indicating that these fans were progradational (Gawthorpe et al., 1990). The coarse-grained nature of the clastics, mud-poor character and large-scale moderately to steeply dipping foresets indicate that these fans may be interpreted as typical 'Gilbert-type' fan systems (e.g., Ethridge and Wescott, 1984; Gilbert, 1885; Holmes, 1965; Mcpherson et al., 1987).

The clast compositions of the conglomerates are interpreted to reflect variations in the lithologies of the source areas along the exhumed rift margin. In the Wadi Gassus and Guesis fan systems, the conglomerates are dominated by granitic clasts, which were derived from north of Wadi Safaga and Gebel Abu Kherfan (Fig. 5.1). In Wadi Quwyh, the conglomerates are polymict (dominantly granitic and metavolcanic clasts with subordinate chert and carbonate clasts), indicating different sources of clastic supply (i.e., probably derived from the basement rocks in the rift margin as well as from the pre-rift sediments that

occur on the intra-rift tilted fault blocks, Fig. 5.1). In Wadis Sharm El Bahari and farther south, in Wadi Sharm El Qibli, the conglomerates are dominantly chert clasts, indicating that the Miocene fan systems in this locality were sourced from the pre-rift Eocene strata that formed the tilted blocks in Wadi Hamadat and Wadi Zug El Bahar half grabens (Fig. 5.1).

The changes in palaeocurrent directions from NE to E and ESE directions across the DAZ clearly demonstrate that the DAZ played an important role in controlling the drainage system and sediment dispersal on the northwestern Red Sea margin. Synoptic models for these geometric relationships of fault systems, drainage and fan delta systems are shown in Figs. 5.14 and 5.15. The models proposed in this chapter for the structural control on Lower Miocene syn-rift fan systems and sediment-input points compare well with the results of similar studies in the Gulf of Suez to the north (e.g., Gawthorpe et al., 1990; Leppard and Gawthorpe, 2006). These models might also be applied to other rift basins where preexisting basement structures have exerted a strong control on rift fault geometries and patterns.

Acknowledgments

The research presented in this paper was supported by the Natural Environment Research Council (NERC) ROPA Grant GR3/R9529 to Ken McClay. Samir Khalil was supported by a Research Grant from BG International to Ken McClay. Additional support was received from the Fault Dynamics Project, Royal Holloway University of London (sponsored by ARCO British Limited, PETROBRAS U.K. Ltd., BP Exploration, Conoco (U.K.) Ltd., Mobil North Sea Limited, and Sun Oil Britain). The authors also gratefully acknowledge support from ARCO British Limited (now BP Exploration). Bill Bosworth and Marathon Petroleum Egypt are thanked for logistical support and for many fruitful discussions on the Northwestern Red Sea geology. BG Egypt and Maher Ayyad kindly sponsored with additional fieldwork in the northwestern Red Sea.

References

Abdel Khalek, M.L., Abdel Wahed, M., Sehim, A., 1993. Wrenching deformation and tectonic setting of the northwestern part of the Gulf of Aqaba. Geodynamics and sedimentation of the Red Sea-Gulf of Aden Rift system. Geol. Surv. Egypt Spec. Publ. 1, 409–445.

Abd El-Razik, T.M., 1967. Stratigraphy of the sedimentary cover of the Anz-Atshan-south Duwi district. Bull. Faculty Sci. Cairo Univ. 431, 135–179.

Akaad, M.K., Noweir, A.M., 1980. Geology and lithostratigraphy of the Arabian desert orogenic belt between latitudes 25° 35′ and 26°30′. In: Cooray, P.A.T.S. (Eds.), Evolution and Mineralization of the Arabian–Nubian shield. Permagon Press, New York, pp. 127–135.

Akkad, S., Dardir, A.A., 1966. Geology and phosphate deposits of Wasif, Safaga area. Geol. Surv. Egypt Pap. 36, 35.

Bosworth, W., Huchon, P., McClay, K., 2005. The Red Sea and Gulf of Aden Basins. J. Afr. Earth Sci. 43, 334–378.

Childs, C., Watterson, J., Walash, J.J., 1995. Fault overlap zones within developing normal fault systems. J. Geol. Soc. Lond. 152, 535–549.

Cochran, J.R., 1983. A model for development of the Red Sea. AAPG Bull. 67, 41–69.

Coleman, R.G., 1993. Geologic Evolution of the Red Sea. Oxford Monographs on Geology and Geophysics 24, Oxford University Press, Oxford, 186 pp.

Crossley, R., 1984. Controls on sedimentation in Lake Malawi Rift Valley, Central Africa. Sed. Geol. 40, 33–40.

Dart, C.J., Collier, R.E.L., Gawthorp, R.L., Keller, J.V., Nichols, G., 1994. Sequence stratigraphy of (?) Pliocene–Quaternary syn-rift Gilbert type deltas, northern Peloponnesos, Greece. Mar. Petrol. Geol. 11, 545–560.

Dawers, N.H., Underhill, J.R., 2000. The role of fault interaction and linkage in controlling syn-rift stratigraphic sequences: Statfjord East area, Northern North Sea. AAPG Bull. 84, 45–64.

El Gezeery, M.N., Marzouk, I.M. (Eds.), 1974. Miocene rock stratigraphy of Egypt. The Stratigraphic Sub-Committee of the National Committee of Geological Sciences of Egypt, Egypt. J. Geol. 18, pp. 1–59.

El Bassyony, A.A., 1982. Stratigraphical studies on Miocene and younger exposures between Quseir and Berenice, Red Sea coast, Egypt. Ph.D. Thesis, Ain Shams University, Cairo.

El Haddad, A.A., 1984. Sedimentological and geological studies on the Neogene sediments of the Egyptian part of the Red Sea. Ph.D. Thesis, Assiut University.

Ethridge, F.G., Wescott, W.A., 1984. Tectonic setting, recognition and hydrocarbon reservoir potential of fan-delta deposits. In: Koster, E.H., Steel, R.J. (Eds.), Sedimentology of Gravels and Conglomerates, Canadian Society of Petroleum Geologists Memoir, vol. 10, pp. 217–234.

Freund, R., 1970. Plate tectonics of the Red Sea and Africa. Nature 228, 453.

Gawthorpe, R.L., Hurst, J.M., 1993. Transfer zones in extensional basins: their structural style and influence on draining development and stratigraphy. J. Geol. Soc. Lond. 150, 1137–1152.

Gawthorpe, R.L., Hurst, J.M., Sladen, C.P., 1990. Evolution of Miocene footwall-derived coarse-grained deltas, Gulf of Suez, Egypt: implications for exploration. AAPG Bull. 74, 1077–1086.

Gawthorpe, R.L., Leeder, M.R., 2000. Tectono-sedimentary evolution of active extensional basins. Basin Res. 12, 195–218.

Gawthorpe, R.L., Sharp, I., Underhill, J.R., Gupta, S., 1997. Linked sequence stratigraphic and structural evolution of propagating normal faults. Geology 25, 795–798.

Gilbert, G.K., 1885. The topographic features of lake shores. USGS Annu. Rep. 5, 69–123.

Girdler, R.W., Southren, T.C., 1987. Structure and evolution of the northern Red Sea. Nature 330, 716–721.

Gupta, S., Underhill, J.R., Sharp, I.R., Gawthorpe, R.L., 1999. Role of fault interactions in controlling synrift sediment dispersal patterns: Miocene Abu Alaqa Group, Suez Rift, Sinai, Egypt. Basin Res. 11, 167–189.

Hardy, S., Dart, C.J., Waltham, D., 1994. Computer modelling of the influence of tectonics on sequence architecture of coarse-grained fan deltas. Mar. Petrol. Geol. 11, 561–574.

Heath, R., Vanstone, S., Swallow, J., Ayyad, M., Amin, M., Huggins, P., Swift, R., Warburton, I., McClay, K., Younnis, A., 1998. Renewed exploration in the offshore north Red Sea Region – Egypt. Proceedings of the 14th Petroleum Conference, Egyptian General Petroleum Corporation, Cairo, Egypt, pp. 16–34.

Hempton, M., 1987. Constraints on Arabian plate motion and extensional history of the Red Sea. Tectonics 6, 687–705.

Holmes, A., 1965. Principles of Physical Geology, second ed. Thomas Nelson, London, pp. 1288.

Issawi, B., Francis, M., El-Hinnawi, M., Mehanna, A., 1969. Contribution to the structure and phosphate deposits of Quseir area. Geological Survey of Egypt Paper 50.

Joffe, S., Garfunkel, Z., 1987. Plate kinematics of the circum Red Sea – a re-evaluation. Tectonophysics 141, 5–22.

Khalil, S., McClay, K., 2001. Tectonic evolution of the northwestern Red Sea-Gulf of Suez rift system. Geol. Soc. London Spec. Publ. 187, 453–473.

Khalil, S.M., McClay, K.R., 2002. Extensional fault-related folding, northwestern Red Sea, Egypt. J. Struct. Geol. 24 (Special Volume), 743–762.

Kröner, A., 1984. Late Precambrian plate tectonics and orogeny: a need to redefine the term Pan-African. In: Klerkx, J., Michot, J. (Eds.), African Geology. Tervuren, Musée R. l'Afrique Centrale, pp. 23–28.

Kröner, A., 1993. The Pan African belt of northeastern and Eastern Africa, Madagascar, southern India, Sri Lanka and East Antarctica: terrane amalgamation during the formation of the Gondwana supercontinent. In: Thorweihe, U., Schandelmeier, H. (Eds.), Geoscientific Research in Northeast Africa. Balkema, Rotterdam, pp. 3–9.

Lambiase, J.J., Bosworth, W., 1995. Structural controls on sedimentation in continental rifts. In: Lambiase, J.J. (Ed.), Hydrocarbon Habitat in Rift Basins, Geological Society of London, Special Publication vol. 80, pp. 117–144.

Leeder, M.R., Collier, R.E.L.I., Aziz, A.L.H., Trout, M., Ferentinos, G., Papatheodorou, G., Lyberis, E., 2002. Tectono-sedimentary processes along an active marine/lacustrine half-graben margin: Alkyonides gulf. E. Gulf of Corinth, Greece. Basin Res. 14, 25–41.

Le Pichon, X., Francheteau, J., 1978. A plate tectonic analysis of the Red Sea-Gulf of Aden area. Tectonophysics 46, 369–406.

Leppard, C.W., Gawthorpe, R.L., 2006. Sedimentology of rift climax deep water systems; Lower Rudeis Formation, Hammam Faraun Fault Block, Suez Rift, Egypt. Sed. Geol. 191, 67–87.

Lezzar, K.E., Tiercelin, J.J., Le Turdu, C., Cohen, A.S., Reynolds, D.J., Le Gall, B., Scholz, C.A., 2002. Control of normal fault interaction on distribution of minor Neogene sedimentary depocentres, Lake Tanganyika, East Africa. AAPG Bull. 86, 1027–1059.

McClay, K.R., Nicols, G.J., Khalil, S.M., Darwish, M., Bosworth, W., 1998. Extensional tectonics and sedimentation, eastern Gulf of Suez, Egypt. In: Purser, B.H., Bosence, D.W.J. (Eds.), Sedimentation and Tectonics of Rift Basins: Red Sea–Gulf of Aden. Chapman and Hall, London, pp. 223–238.

Mckenzie, D.P., Davies, D., Molnar, P., 1970. Plate tectonics of the Red Sea and east Africa. Nature 226, 243–248.

Mcpherson, J.G., Shanumugam, G., Moiola, R.J., 1987. Fan-deltas and braided deltas: varieties of coarse-grained deltas. Geol. Soc. Am. Bull. 99, 331–340.

Morgan, P., 1990. Egypt in the tectonic framework of global tectonics. In: Said, R. (Ed.), The Geology of Egypt. Balkema, Rotterdam, pp. 91–111, Chapter 7.

Moustafa, A.R., 1997. Controls on the development and evolution of transfer zones: the influence of basement structure and sedimentary thickness in the Suez rift and Red Sea. J. Struct. Geol. 19 (6), 755–768.

Orszag-Sperber, F., Purser, B.H., Rioual, M., Plaziat, J.C., 1998. Post Miocene sedimentation and rift dynamics in the southern Gulf of Suez and northern Red Sea. In: Purser, B.H., Bosence, D.W.J. (Eds.), Sedimentation and Tectonics of Rift Basins: Red Sea-Gulf of Aden. Chapman and Hall, London, pp. 427–447.

Phillobbos, E.R., El Haddad, A.A., Mahran, T.M., 1988. Comparison between Miocene and Pliocene facies distribution related to syn-rift tectonics along the Egyptian Red Sea coastal area. Egyptian General Petroleum Corporation, 9th Petroleum Exploration and Production Conference. vol. 1, pp. 246–254.

Philobbos, E.R., El Haddad, A.A., Luger, P., Bekir, R., Mahran, T., 1993. Syn-rift Miocen sedimentation arround fault blocks in the Abu Ghusun–Wadi el Gemal area, Red Sea, Egypt. In: Philobbos, E.R., Purser, B.H. (Eds.), Geodynamics and Sedimentation of the Red Sea–Gulf of Aden Rift system, Geological Society of Egypt, Special Publication, vol. 1, pp. 115–142.

Philobbos, E.R., Purser, B.H. (Eds.), 1993. Geodynamics and sedimentation of the Red Sea–Gulf of Aden rift system, Geological Society of Egypt, Special Publication.

Purser, B.H., Bosence, D.W.J. (Eds.), 1998. Sedimentation and Tectonics of Rift Basins: Red Sea–Gulf of Aden. Chapman and Hall, London, 680p.

Purser, B.H., Orszag-Sperber, F., Plaziat, J.C., 1987. Sedimentation et rifting: les series neogenes de la marge nord-occidental de la Mer Rouge (Egypte). Notes et Memoires, Compagnie Francaise de Petroles, Paris, 21, 111–114.

Purser, B.H., Philobbos, E.R., 1993. The sedimentary expressions of rifting in the NW Red Sea, Egypt. In: Philobbos, E.R., Purser, B.H. (Eds.), Geodynamics and sedimentation of the Red Sea–Gulf of Aden rift system, Geological Society of Egypt, Special Publication, vol. 1, pp. 1–45.

Quennell, A.M., 1984. The western Arabian rift system. In: Dixon, J.E., Robertson, A.H.F. (Eds.), The Geological Evolution of the Eastern Mediterranean. Blackwell Scientific, Oxford, pp. 775–788.
Ravnås, R., Steel, R., 1998. Architecture of marine rift-basin successions. AAPG Bull. 82, 110–146.
Roussel, N., Purser, B.H., Orszag-Sperber, F., Plaziat, J.C., Soliman, M., El Haddad, E.A., 1986. Geologie de la region de Quseir. Documents et Travaux, Institut Geologique Albert de lapparent. Paris, 10, 129–144.
Scholz, C.A., Rosendahl, B.R., Scott, D.L., 1990. Development of coarse-grained facies in lacustrain rift basins: examples from East Africa. Geology 18, 140–144.
Scholz, C.A., Johnson, T.C., McGill, J.W., 1993. Deltaic sedimentation in a rift valley lake: new seismic reflection data from Lake Malawi (Nyasa), East Africa. Geology 21, 395–398.
Said, R. (Ed.), 1990. The Geology of Egypt. Balkema, Rotterdam, 734 pp.
Stern, R.J., 1981. Petrogenesis and tectonic setting of Late Precambrian ensimatic volcanic rocks, Central Eastern Desert of Egypt. Precambrian Res. 16, 195–230.
Seger, M.J., Alexander, J., 1993. Distribution of Plio-Pleistocene and Modern coarse-grained deltas south of the Gulf of Corinth, Greece. In: Frostick, L., Steel, R. (Eds.), Tectonic Controls and Signatures in Sedimentary Successions, International Association of Sedimentologists, Special Publication, vol. 20, pp. 37–48.
Stern, R.J., 1994. Arc assembly and continental collision in the Neoproterozoic East African orogen: implications for the consolidation of Gondwanaland. Annu. Rev. Earth Planet. Sci. 22, 319–351.
Steckler, M.S., Berthelot, F., Lyberis, N., Le Pichon, X., 1988. Subsidence in the Gulf of Suez: implications for rifting and plate kinematics. Tectonophysics 153, 249–270.
Stoeser, D.B., Camp, V.E., 1985. Pan African microplate accretion of the Arabian shield. Geol. Soc. Am. Bull. 96, 817–826.
Tewfik, N., Ayyad, M., 1982. Petroleum Exploration in the Red Sea Shelf of Egypt. 6th Exploration Seminar, Egyptian General Petroleum Corporation, Cairo.
Versfelt, J., Rosendahl, B.R., 1989. Relationships between pre-rift structure and rift architecture in Lakes Tanganyika and Malawi, East Africa. Nature 337, 354–357.
Younes, A., McClay, K.R., 2002. Role of basement fabric on rift architecture: Gulf of Suez – Red Sea, Egypt. Am. Assoc. Pet. Geol. Bull. 86, 1003–1102.
Young, M.J., Gawthorpe, R.L., Sharp, I.R., 2000. Sedimentology and sequence stratigraphy of a transfer zone coarse-grained delta, Miocene Suez Rift, Egypt. Sedimentology 47, 1081–1104.
Youssef, M.I., 1957. Upper Cretaceous rocks in Kosseir area. Bull. Inst. Desert Egypt 7, 35–53.

In this chapter

6

Carbonate-dominated marine rifts

Dan Bosence
Department of Earth Sciences, Royal Holloway University of London, Egham, Surrey, United Kingdom

6.1 Introduction

Basin evolution from continental to marine flooding

Examination of ancient rift basins indicates that rifting commonly occurs initially in a continental environment. Subsequently, as a consequence of crustal thinning, driven by fault-related extension, the basin subsides and eventually may connect through to the world's seas and oceans. As a consequence of this, carbonate-dominated rifts occur late in the evolution of rift basins and they are often linked to the rift to drift phase when denser oceanic crust is emplaced. The processes behind this commonly observed pattern would appear to be that rifting, by whatever model, increases local relief and may also be linked to regional updoming. Both of these processes will increase rates of clastic supply during the early stages of rifting and lead to an initial clastic fill; initially continental and then marine (Fig. 6.1). Later stages (e.g., late syn-rift) appear to be characterised by marine flooding. However, the timing of this will be determined by individual rift basin history as controlled by pre-rift topography, subsidence, global/regional sea-level changes and location of the rift with respect to adjacent marine basins. End member examples could be taken from the Lake Baikal rift basin with an entirely non-marine fill to the North Sea with a dominantly marine, clastic rift stratigraphy to parts of the Gulf of Aden which have an entirely marine carbonate fill (Fig. 6.1). There do not appear to be any rift basins filled with high latitude (i.e., cold-water) carbonate deposits. Possibly the rate of carbonate production in such climates is too low to compete with rates of clastic sediment supply in rift basin settings.

A pattern of basin fill from early syn-rift clastics to late- and post-rift carbonates is commonly observed in passive or mature extensional margins today in low latitude areas (Fig. 6.1). Well known are the extensive carbonate shelves of

Phanerozoic Rift Systems and Sedimentary Basins DOI:10.1016/B978-0-444-56356-9.00005-5

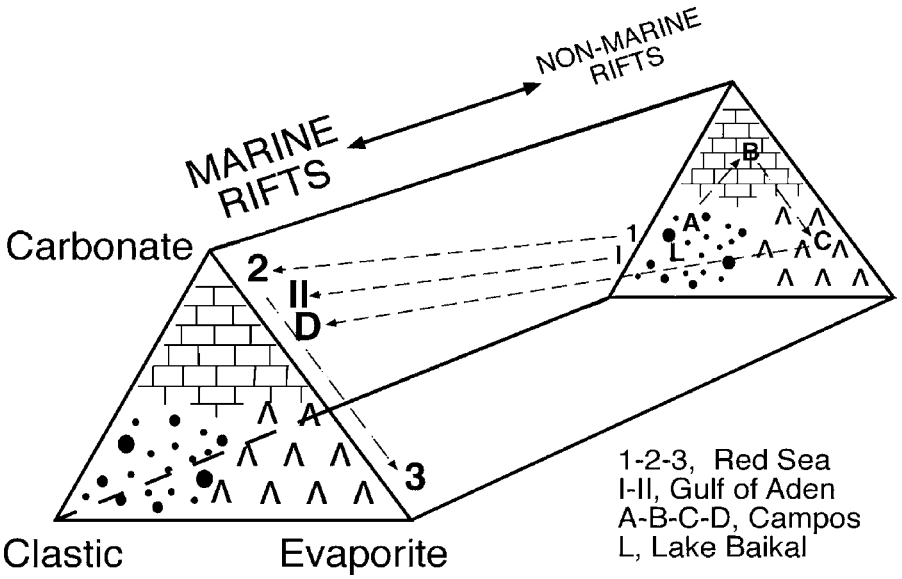

Figure 6.1 Variations in stratigraphic fill of marine and non-marine rift basins. Arrows, numbers and letters give geological succession of the three major lithotypes: carbonate, clastic and evaporite.

Mesozoic age of the Atlantic and Tethyan margins which have their foundations on rifted early Mesozoic clastics/volcaniclastics (Bernoulli and Jenkyns, 1974). Similarly, the syn- to post-rift carbonate shelves of the Red Sea overlie earlier syn-rift siliciclastics. Both of these settings are examined in this chapter.

Within marine, carbonate-dominated rifts, there are certain sites that favour carbonate platform development after the rift basin has been flooded by marine waters. During marine flooding, clastic systems will be pushed landwards so that deposition is focussed in the coastal zone and in structural lows. Examination of carbonate successions in rift basin fills indicates three main sites where carbonate platforms develop:

1. Offshore sites such as the highs on footwall blocks are isolated from clastic supply, and in low-latitude settings, photozoan carbonates will be produced and will accumulate. Carbonate platforms developed over rotating fault blocks during the syn-rift phase are common in rift basins, have a distinctive stratigraphy and sedimentology and have been labelled fault-block carbonate platforms (Bosence, 2005; Bosence et al., 1998a,b; Cross and Bosence, 2008).
2. During the marine flooding phase and in arid climate settings, deltas and fan deltas that protrude out into more open water sites are also sites of reef and carbonate platform growth. Such platforms (labelled delta-top platforms by Bosence, 2005) are common in the Cenozoic Gulf of Suez–Red Sea–Gulf of Aden rift basins.
3. Offshore, shallow-marine areas that are isolated from clastic supply are also formed in low-latitude rift basins over salt diapirs. As young marine rifts are narrow and tectonically active, they commonly have intermittent connections through to oceans and are prone to isolation and evaporite

accumulation. Later diapiric structures form submarine highs that will develop into carbonate platforms if they spend a significant amount of time in the shallow-water carbonate production zone. Such is the case in the Red Sea and earlier in the history of the Atlantic margin. Such platforms are labelled salt-diapir platforms (Bosence, 2005).

The nature and occurrence of these different platform types are discussed in the two case study basins below. These are chosen as representing particularly good examples of marine, carbonate-dominated rifts; the Gulf of Suez–Red Sea–Gulf of Aden rifts are particularly well-exposed examples of Cenozoic carbonate stratigraphies in the rift margins and coastal plain areas. For Mesozoic marine carbonate rifts, subsurface examples of Early Cretaceous carbonate platforms are taken from the early stages of the rifted South Atlantic margins.

From these two relatively well-studied regions, general patterns and processes within marine, carbonate-dominated rifts are discussed and models for the different types of carbonate platforms found within marine rifts presented.

6.2 Cenozoic of Gulf of Suez–Red Sea–Gulf of Aden case study

Setting of marine carbonates within rift basins

These rift basins show considerable heterogeneities along their 3500 km length. The northern Red Sea and Gulf of Suez have similar histories from the origins of the rift in the late Oligocene to the inception of left lateral shear of the Aqaba–Dead Sea fault in the middle Miocene. During this time, the syn-rift phase was first dominated by clastic sediments and then by carbonate sediments in the middle Miocene (Langhian), and finally by evaporite deposits in the mid- to late Miocene. Rift margin coastal areas have mixed carbonate–siliciclastic deposits in the Pliocene and Quaternary. These younger strata show features of syn-rift (local extensional faults and unconformities) and also features of post-rift strata (basal onlap and downlap and a regional seaward dip of strata), and this part of the basin is considered to be at a transitional syn- to post-rift stage (Bosence, 1998). Deposition and subsequent deformation of these strata are commonly affected by diapiric structures generated from the mid- to late Miocene salts. The southernmost Red Sea by contrast is a volcanic margin and is discussed elsewhere in this volume (Chapter 9.3.1).

The Gulf of Aden is a longer lived and more mature rift that has evolved into a young oceanic basin that has accumulated a mixed carbonate–siliciclastic stratigraphy since early Oligocene times. Post-rift sediments of late Miocene age lie unconformably on tilted syn-rift in offshore areas and these correspond to the emplacement of ocean floor at around 20 Ma. Having never been isolated from the Indian Ocean, the basin does not have thick evaporite deposits, or diapiric structures, effecting the syn- and post-rift successions. Offshore records

indicate rift development entirely in the marine, and mainly carbonate accumulating environment. Late Mesozoic and early Cenozoic marine (pre-rift) carbonates are unconformably overlain by syn-rift marine carbonates in southeastern Yemen (Brannan et al., 1997). In this case, the rift-related uplift could not have been great enough to outpace rift-related subsidence within this sub-basin.

Within the syn- to post-rift fills of the Gulf of Suez–Red Sea–Gulf of Aden rift basins, carbonate platforms develop in three main situations where shallow marine areas occur that can be isolated, either spatially or temporally (or both) from clastic supply: on top of rotated fault blocks, on top of deltas and on top of salt-diapirs.

Miocene to Recent fault-block platforms

Carbonate platforms that develop on subsiding and/or rotating fault blocks have been described from mid-Miocene carbonate platforms in the northwest Red Sea and Gulf of Suez (Fig. 6.2; Bosence, 1998; Bosence et al., 1998a; Burchette, 1988; Cross and Bosence, 2008; Cross et al., 1998; James et al., 1988; Purser et al., 1998). Early stages of rifting are largely dominated by clastic sedimentation with sediment transport mainly controlled by the evolving extensional fault systems and their oblique transfer zones (Purser et al., 1998). Transfer zones and hanging-wall sub-basins generally persist as sites of clastic sediment accumulation, whereas footwall areas, horsts and proximal areas of transfer zones isolated from clastic supply accumulate subtropical, photozoan carbonates (see Chapter 6.4.4, this volume). The platforms are often fault bounded, are rectilinear to trapezoidal in plan shape with maximum stratigraphic thicknesses of 130 m in outcrops in the Red Sea–Gulf of Suez margins. Within the platforms, rimmed-shelf margins or fault-truncated margins characterise the footwalls of fault blocks while hanging-wall dip-slopes are ramps and generally pass down-dip into hanging-wall basin clastics (Fig. 6.2). Fault accommodation zones, such as that preserved on the southern margin of Abu Shaar (Cross et al., 1998), have low relief and show progradational platform margin geometries, or are dominated by through-flowing fan-deltas or submarine fans (Bosworth et al., 1998; Purser et al., 1998). These platforms may be attached to the rift margin, detached from the margin but influenced by marginal clastic supply or unattached and in an axial location. In the latter case (e.g., Gebel Zeit; Fig. 6.2B), the platform drowns and is overlain by deeper water marls (Purser et al., 1998). Platform margins are commonly rimmed by coralgal reefs and these occur preferentially on faulted margins and shallow (inner) ramp sites (Fig. 6.2D). Ooid shoals less commonly form platform margins. Footwall platform slopes in these Egyptian examples are only exposed in their upper parts and comprise reef and platform-top bioclastic and intraclastic talus, with a composition reflecting the coeval platform-top stratigraphy. Shallow slope sediments are commonly cemented, fractured and slumped, and Miocene erosion may remove 100m to kilometre-sized blocks leaving lunate scars (Purser and Plaziat, 1998) and a truncated footwall stratigraphy (Fig. 6.2; Cross et al., 1998). Platform-top facies are bedded bioclastic and

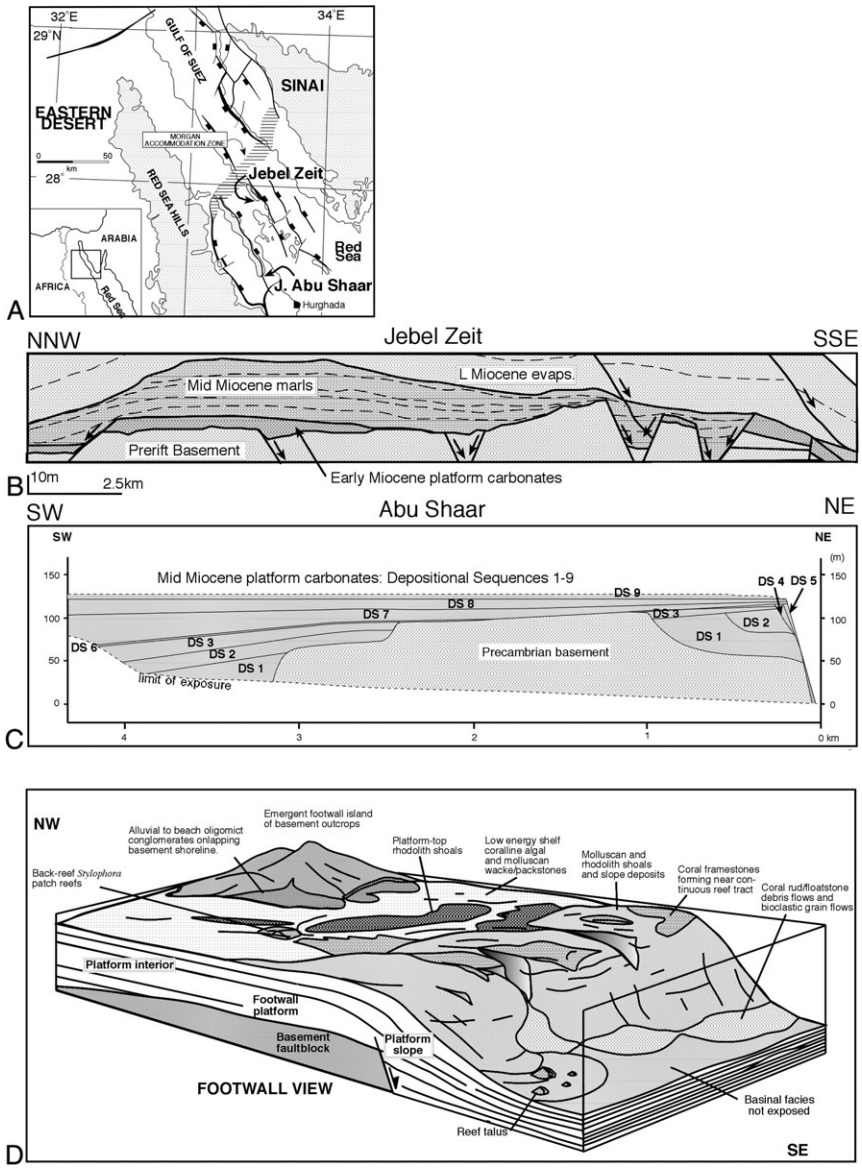

Figure 6.2 Fault-block platforms of the Gulf of Suez–NW Red Sea. (A) Location map of fault-block platforms, Jebel Zeit and Jebel Abu Shaar described in text and illustrated in (B)–(D) below *(after Cross et al., 1998)*. (B) Cross-section of Jebel Zeit, a thin platform that is detached from the rift margin. This syn-rift carbonate platform is drowned by mid Miocene marls and subsequently buried by late Miocene evaporites *(after Purser et al., 1998)*. (C) Reconstructed footwall to hanging-wall section through Abu Shaar illustrating syn-rift depositional sequences (mapped out by Cross et al., 1998). (D) Facies model for the Abu Shaar fault-block carbonate platform as viewed from the footwall *(after Cross et al., 1998)*.

peloidal wackestones, packstones and rudstones with scattered patch reefs. These are arranged in unconformity-bound depositional sequences, some of which can be demonstrated to be of tectonic origin (Cross et al., 1998). Such sequences thicken down hanging-wall dip-slopes and thin onto footwall sites where sequence boundaries converge (Fig. 6.2C). They consequently have wedge-shaped geometries with stacked reefal facies cut by sequence boundaries

in footwall sites and coeval shallowing-upward sequences separated by flooding surfaces on hanging-wall dip-slopes. The shallower slopes in hanging-wall dip-slopes and accommodation zones result in more progradational geometries, but these may not develop in footwall margins because of the steep, fault-related slopes and adjacent deepwater sub-basins.

Holocene examples include the abundant reef-rimmed platforms of the Red Sea and Gulf of Suez (e.g., Sanganeb Atoll, offshore platforms north of Jeddah, Shoab Ali) as reviewed by Dullo and Montaggioni (1998).

Subsurface examples from the early Neogene of the Gulf of Aden (Brannan et al., 1997) imaged in seismic sections (Fig. 6.3B) show overall platform morphologies and internal stratigraphic geometries that are consistent with the Gulf of Suez outcrop data. In the Qamar Basin (NE Gulf of Aden), the early Cenozoic pre-rift succession comprises shallow-marine, limestones and shales (Hadramaut Group) with marginal evaporites of the Russ Fm (Brannan et al., 1997). These are cut by the syn-rift unconformity (middle Eocene), a major tectono-stratigraphic break throughout the offshore (Bott et al., 1992; Brannan et al., 1997) and onshore stratigraphies (Fig. 6.3; Bosence et al., 1996; Watchorn et al., 1998). In the offshore Qamar Basin, the syn-rift (Shihr Group) is entirely marine but onshore outcrops in Yemen show fluvial clastics and evaporites passing into shallow-marine carbonates and clastics in outcrops along the present day coastal plain to the west and east of Mukalla (Fig. 6.3; Bosence et al., 1996; Watchorn et al., 1998). Onshore, the carbonate stratigraphy is not clearly separated into footwall carbonate platforms and hanging-wall clastics as is the case in the Gulf of Suez. Southwest of Mukalla, point-sourced, rift-shoulder-derived clastics interfinger with fault-related and delta-top shallow-marine carbonates (see below) in a complex three-dimensional pattern (Fig. 6.4; Bosence et al., 1996). Depositional sequences are separated by tectonically driven erosional sequence boundaries overlain by lowstand, alluvial fan conglomerates and sandstones. During transgression, carbonate platforms aggrade, interfingering with land-derived clastics, and then prograde during the highstand. Clastics and carbonates are then eroded by the following, fault- related, fall in sea level (Fig. 6.4E).

The extensive coastal plain to the northeast of Mukalla exposes the earlier syn-rift stratigraphy (Fig. 6.3B). Oligo-Miocene (Shihr Gp) sediments indicate an extensive low relief, rift margin coastal area dominated by fine grained marls and evaporites, and small, reefal platforms (Watchorn et al., 1998). Rift shoulder uplift appears to have diverted most of the clastic supply inland to the Hadramaut drainage basin. The stratigraphy appears to be a passive fill of a continuously subsiding basin margin (Fig. 6.3B). Classic, syn-rift depositional models (e.g., Leeder and Gawthorpe, 1987) and those described from the Gulf of Suez (above) do not apply to this section of the rift basin.

Offshore, seismic sections from the Qamar Basin indicate a pre- to syn-rift stratigraphy dominated by carbonates. The oblique setting of the rift basin at Qamar means that east-west extensional faults are essentially normal to main onshore-

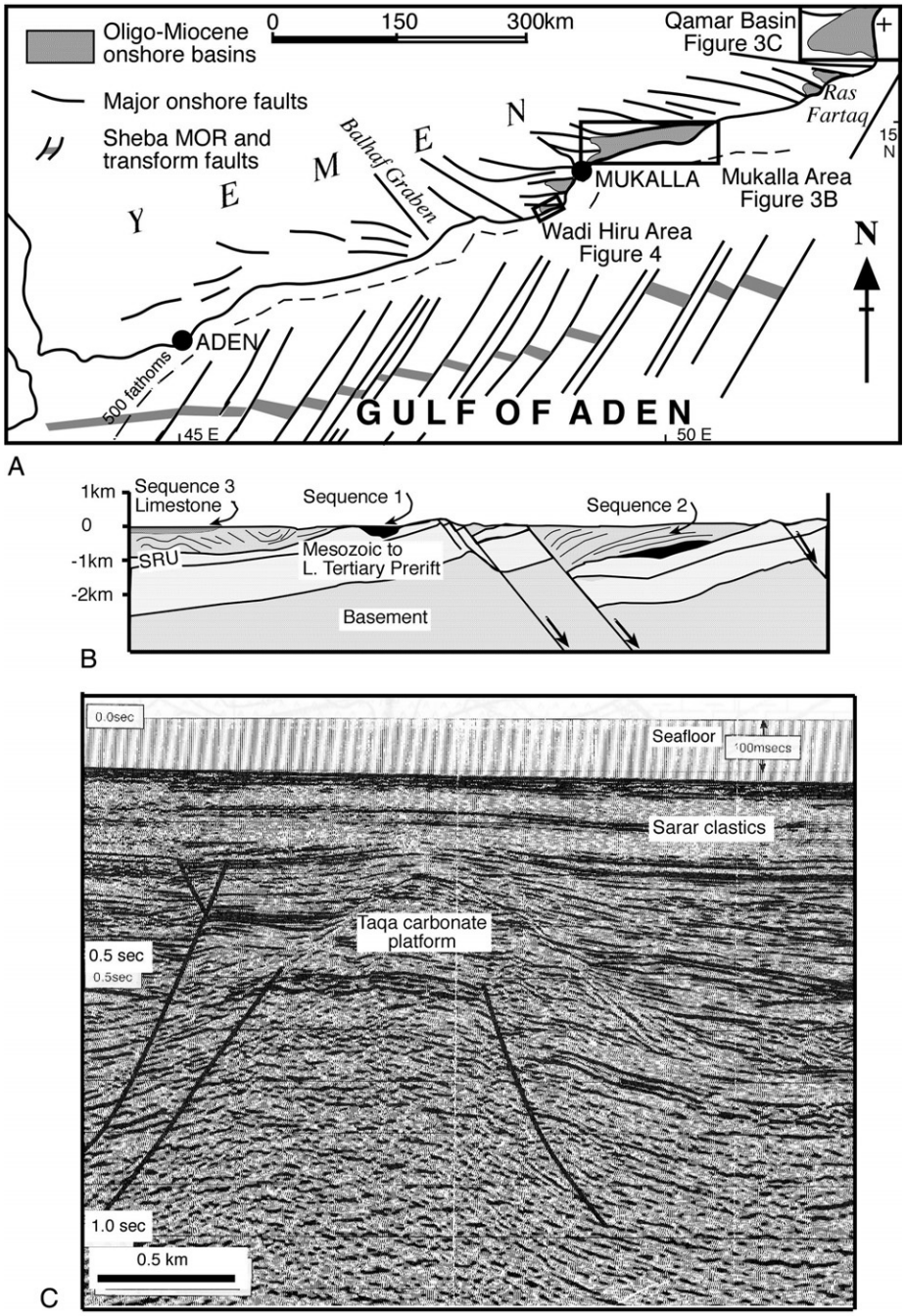

Figure 6.3 Fault-block platforms of the Yemen margin of the Gulf of Aden. (A) Location of onshore, syn-rift basins to northern Gulf of Aden and sections in this figure and Fig. 6.4 *(from Bosence et al., 1996)*. (B) North–south section through rift basin east of Mukalla indicating landward tilted fault blocks of prerift Mesozoic and early Tertiary strata. The syn-rift, Shihr Group (Oligocene to Recent) is divided into three unconformity bound depositional sequences *(after Watchorn et al., 1998)*. (C) North–south seismic section (location marked with + in box in (A)) illustrating tilted, fault-block carbonate platform, bounded by two syndepositional faults. Platform morphology of Taqa Formation carbonates in centre of section is onlapped by clastics of the Sarar Formation *(from Brannan et al., 1997)*.

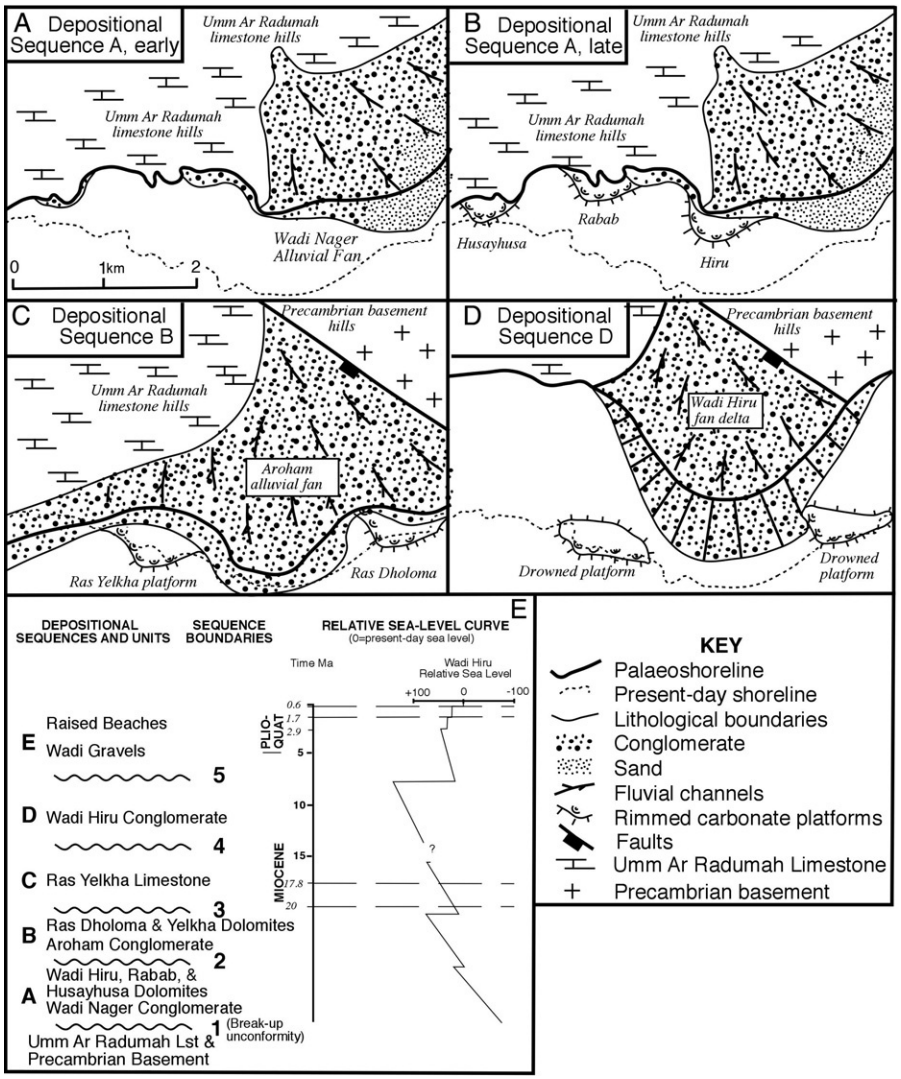

Figure 6.4 Delta-top platforms from Miocene-Pliocene of northern margin of Wadi Hiru area, Gulf of Aden (for location see Fig. 6.3A). Five depositional sequences (A–E) have been mapped out that illustrate the complex interplay of fluvial and fan-delta clastics with shallow-marine carbonate platforms in response to sea-level changes. Note small carbonate platforms built preferentially on fan delta front and adjacent rocky shorelines of prerift Umm Ar Radumah limestone *(after Bosence et al., 1996).*

offshore facies belts and the palaeo-coastline. Clastics from the Hadramaut drainage basin pass eastwards through hanging-wall basins within the carbonate province. Fault-block platforms, oriented normal to the coastline, with up to 200 ms relief in footwall areas, pass downslope to presumed fine-grained and turbiditic limestones (Fig. 6.3C; Brannan et al., 1997). Cores from the platforms indicate porous, shallow-marine bioclastic and reefal limestones, and seismic sections indicate aggradational and progradational geometries on the platform margins (Fig. 6.3C; Brannan et al., 1997). The platforms are onlapped by post-rift shales and pelagic marls.

Miocene to Recent delta-top platforms

In spite of the observation that rates of siliciclastic supply appear to be an overriding control on the global occurrence of shelf carbonates (e.g., Hay et al., 1988), deltas building out into shallow-marine areas are recurring sites of carbonate platform and reef development in the late Cenozoic of the Gulf of Suez, Red Sea and Gulf of Aden (Bosence et al., 1996; Purser et al., 1998; Roberts and Murray, 1983). In this semi-arid climate setting, river flow is rare, short-lived and generally carries a coarse load, all factors that are considered to permit colonisation by carbonate-producing communities.

In the Oligo-Miocene syn-rift of the Gulf of Aden west of Mukalla, carbonate platforms establish themselves on the seaward margins of alluvial fans, fan-deltas and adjacent sea-cliffs twice during the accumulation of the Shihr Group (Fig. 6.4; Bosence et al., 1996). In depositional sequence B, small platforms of bioclastic rudstones and grainstones and patch reefs interfinger or pass gradationally, but laterally, over a few metres, into boulder-sized, fluvial conglomerates. The carbonates subsequently aggrade and then prograde to form a 70 m thick and 1.5 km wide arcuate-shaped platform in plan view. Subsequent sea-level fall erodes the platform and a lowstand fan delta erodes into the earlier platform (Fig. 6.4C and D).

At Sharm el Behari (northwest Red Sea), a long lived (late Oligocene to Recent) fluvial system deposited continental and then marine fluvio-deltaic sediments which formed the substrate for later platform growth. A mid-Miocene fan delta, with 30 m foresets, progrades southeastwards through a half-graben towards the NW Red Sea. These foresets comprise coarse conglomerates passing downslope to marls. Coralgal patch reefs ($<$10 m thick) colonise the upper part of the delta cone which subsequently forms the substrate for a larger (8 km $\times$ 3 km) onlapping carbonate platform with up to 40 m of shallow peritidal marine facies. These are overlain by up to 30 m of microbialites and subaqueous clastics (Purser et al., 1998). They (*op cit.*), along with Roberts and Murray (1983) working in the Gulf of Suez, consider that the intermittent coarse, clastic supply from these semi-arid drainage systems is an important feature that allows carbonates to accumulate in such settings.

In a review of modern reefs developing around fluvial sources in the Red Sea and Gulf of Aqaba, Dullo and Montaggioni (1998) describe how the morphology of a delta and its distributary channels control the pattern of reef growth as corals preferentially colonise channel and delta margins. However, active channels prevent reef growth and instead provide down-slope pathways for the export of reef and clastic debris to deeper-water sites. They consider that because of the intermittent nature of clastic supply, reefs, temporarily destroyed by flash floods, are able to recolonise or continue to grow elsewhere. In addition, these authors consider that periods of turbid flood-waters are too brief to influence reef growth (Dullo and Montaggioni, 1998).

A common observation is that along a shoreline, reefs occur in an arcuate band on a fan delta but that either side of the delta are reef-free beaches (Dullo and Montaggioni, 1988; Roberts and Murray, 1983; authors' observations in Gulf of Suez). One explanation for this is that wave energy will be higher as wave orthogonals converge on the fan delta, thereby winnowing away fine-grained sediment. Adjacent embayments will have lower energy regimes where finer grained sediment will accumulate, or be reworked and both these processes are unfavourable for reef growth.

Pliocene to Recent salt-diapir carbonate platforms

Salt diapirism can result in shallow-water sites that may be isolated from high rates of clastic supply, thus providing suitable substrate for platform growth. The rise of diapirs relative to base level results in sea-floor highs that develop into domes, islands and intervening minibasins. If the domes enter into the photozoan carbonate factory (i.e., the photic zone) they develop carbonate platforms that are circular or ring-shaped reflecting the morphology of the top salt surface. Where salt movement is related to extensional faults in the Red Sea, salt walls and more elongate platforms are developed with associated horst and graben. The stratigraphy and sedimentology of platforms developing over salt diapirs have been studied in outcrops along the northwestern Red Sea and Gulf of Suez (Fig. 6.5; Orszag-Sperber et al., 1998), northern coast of Yemen (Bosence et al., 1998b; Davison et al., 1996) and the Farasan Islands offshore southwestern Saudi Arabia (Bantan, 1999). These are complemented by outcrops of salt-diapir platforms from the opposing margin of the southern Red Sea in the Dahlak Islands offshore Eritrea (Carbone et al., 1998; Fig. 6.5A).

These archipelagos comprise low relief, reef-fringed, late Cenozoic limestone islands. Morphologically, the islands and the surrounding submarine topography comprise carbonate platforms that, in plan view, have arcuate to sub-circular bays, re-entrants and promontories. The platforms vary in horizontal section from 1 km across at Salif (Bosence et al., 1998b) to Dahlak Kebir which is 140 km across (Carbone et al., 1998). The margins to the platforms are largely steep-sided and coral-reef rimmed (Fig. 6.5C; Bantan, 1999; Carbone et al., 1998). The internal lagoons are commonly seagrass meadows and fine-grained carbonates, or bioclastic sands and gravels on exposed shelves. Outcrops at Salif in northwest Yemen indicate colonisation of the irregular dissolved upper surface of the salt diapir by reef corals and molluscs (Fig. 6.5B and D; Bosence et al., 1998b) indicating that the diapir has moved up into the zone of shallow-water, photozoan carbonate production. Carbonate stratigraphies are up to 450 m thick and most exposed successions commonly shallow upwards (Bantan, 1999). To achieve this stratigraphic thickness on a substrate that is rising in relation to regional base level, the platforms must subside as well as rise and unconformities over circular diapirs are described from Farasan and from Salif (Bantan, 1999; Bosence et al., 1998b). Seismic sections illustrate multiple onlap and

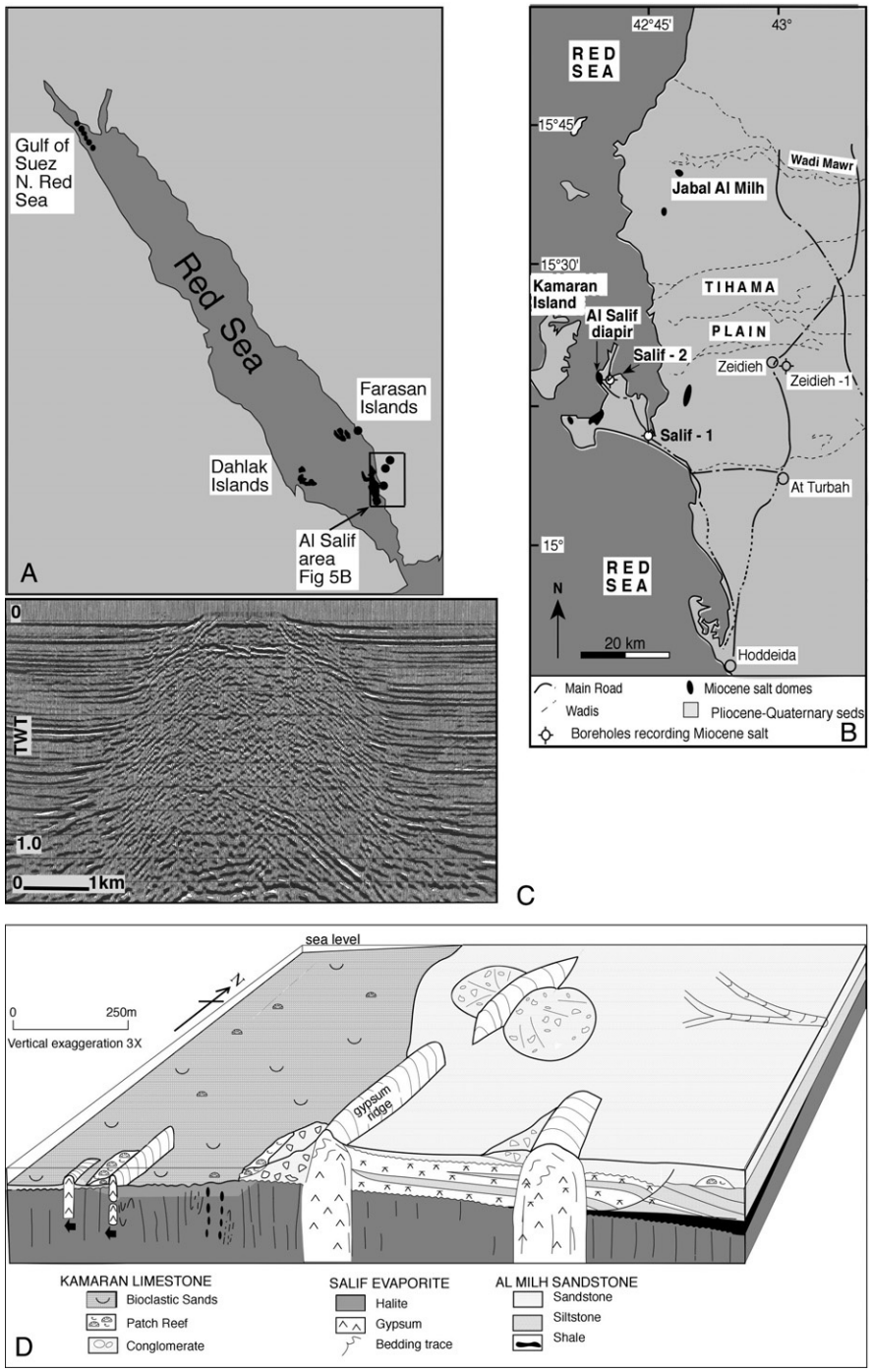

Figure 6.5 Salt-diapir carbonate platforms of the Red Sea. (A) Location map of late Miocene salt diapirs described in text. The real distribution is likely to be much more extensive than that shown here. (B) Location map of Salif area, northwest Yemen indicating outcrops of salt diapirs and boreholes penetrating Miocene salt described in text and illustrated (D) below. (C) Seismic section from southern Gulf of Suez indicating Miocene salt diapir overlain by carbonate platform. Note platform top and slope morphologies on sea floor and imaged in underlying reflectors (between 0.1 and 0.2 ms) *(from Orszag-Sperber et al., 1998).* (D) Block diagram to illustrate Quaternary facies developed on top of halite and gypsum diapir at Al Salif, Yemen *(after Bosence et al., 1998a,b).*

surfaces adjacent to diapirs indicate the balance between diapir growth, subsidence and platform production (Bosence et al., 1998b; Heaton et al., 1996). The stratigraphy of the platforms is complex with rapid lateral and vertical facies changes in the shallow-water, biogenic carbonates reflecting the complex morphology of the islands. Similarly depositional sequences have complex 3D geometries with thickening and thinning and convergence of sequence boundaries over positive diapirs, eroded vertical strata on diapir walls and their divergence into minibasins. Vertical movements are rapid (3–5 m/ky; Bosence et al., 1998b). Extensional faulting (Fig. 6.5D), horst and graben occur over areas of salt movement and many outcrops are blistered and brecciated.

The occurrence of this platform type within the Gulf of Suez and Red Sea is a direct consequence of the isolation of these basins from the Mediterranean Sea and Indian Ocean in the mid- to late Miocene and the formation of deep basin evaporites. This stratigraphic control is reflected in the early history of the Atlantic Ocean (see below) but not the Gulf of Aden, which, with its wedge-like morphology opening into the Indian Ocean, was never an isolated basin. Thin coastal evaporites are, however, common within the basin, reflecting its arid setting (Watchorn et al., 1998).

6.3 Cretaceous South Atlantic margins subsurface case study

American margin carbonate platforms

The Brazilian margin shows both similarities and differences when compared with the development of the Red Sea area in the Cenozoic. Similarities include the local areas of pre-rift volcanics, the high-angle synthetic normal faults of the rift phase and the phase of thick evaporite accumulation near the end of the syn-rift stage followed by the establishment of marine, mainly post-rift deposits. The presence of Cretaceous evaporites in the South Atlantic means that the syn- and post-rift basin evolution differs significantly from that of the Gulf of Aden where thick basinal evaporites are absent.

In the Santos and Campos basins, the syn-rift is largely non-marine, accumulating in a Neocomian rift valley setting (Fig. 6.6; Guardado et al., 1990). However fault-bound highs isolate areas from siliciclastic supply and these accumulate unusually thick (up to 200 m) non-marine carbonates composed of bivalve-rich rudstones, grainstones and packstones (or “coquinas” of the Brazilian literature; Fig. 6.6). These carbonates represent the principal hydrocarbon-producing syn-rift reservoirs in the Campos Basin (Cainelli and Mohriak, 1999; Guardado et al., 1990). More recently, large hydrocarbon discoveries have been made in deep water areas (2000 m) of the Santos Basin within pre-salt, syn-rift, non-marine carbonates (Fig. 6.7; Durham, 2009; Henry et al., 2009; Smith, 2008). Fault-block carbonate platforms with a lower unit of coquinas, interfingering with

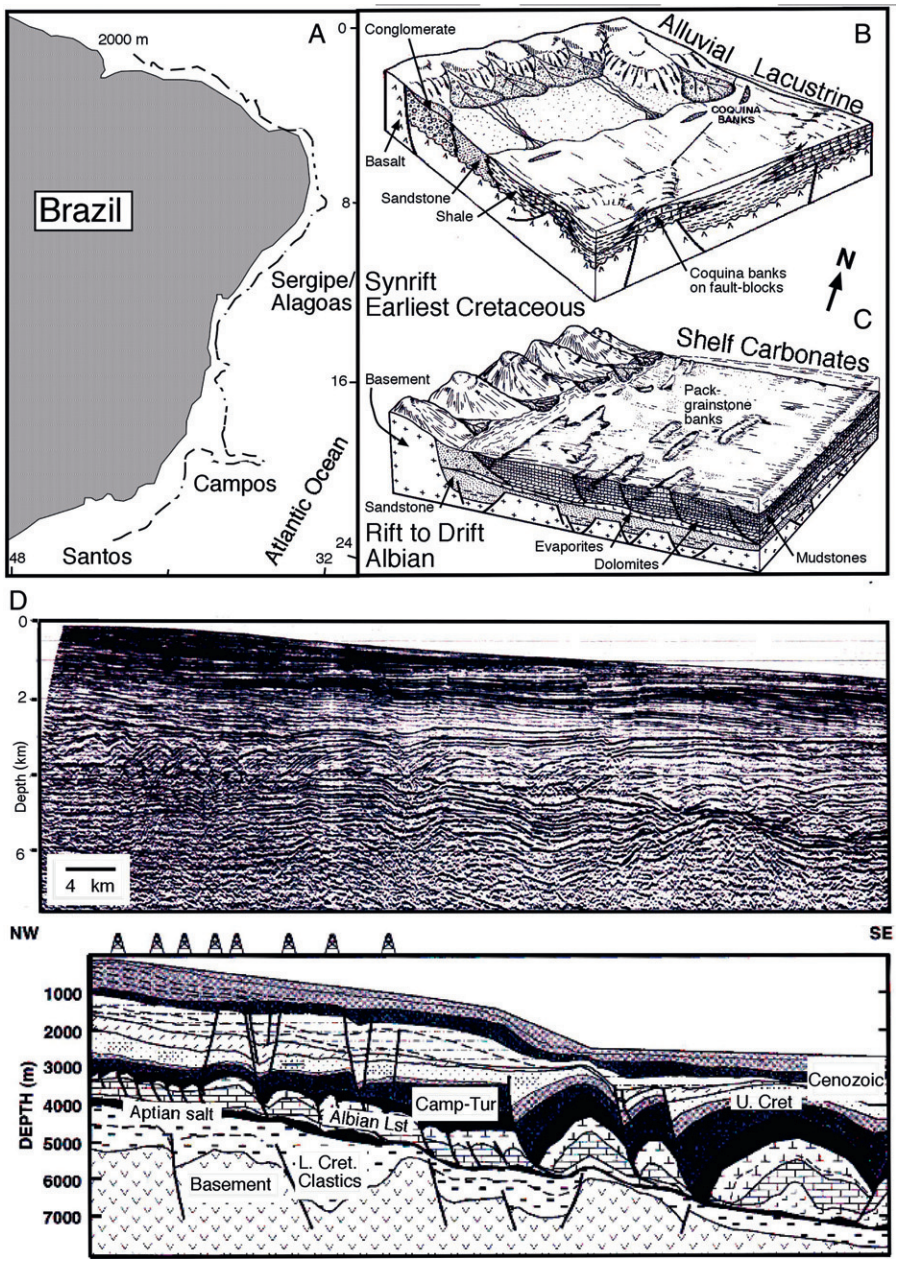

Figure 6.6
Albian carbonate platforms, offshore Brazil. (A) Location map of Brazilian basins discussed in text. (B, C) Block diagrams *(after Guardado et al., 1990)* illustrating siting of carbonate platforms over extensional fault-blocks in rift and rift to drift megasequences. (D) NW to SE seismic section through shelf to slope margin of Campos Basin *(after Cainelli and Mohriak, 1999)*. Syn-rift Early Cretaceous clastics are overlain by Aptian salt and then Albian shelf carbonates. These are drowned by Campanian to Turonian mudstones and marls.

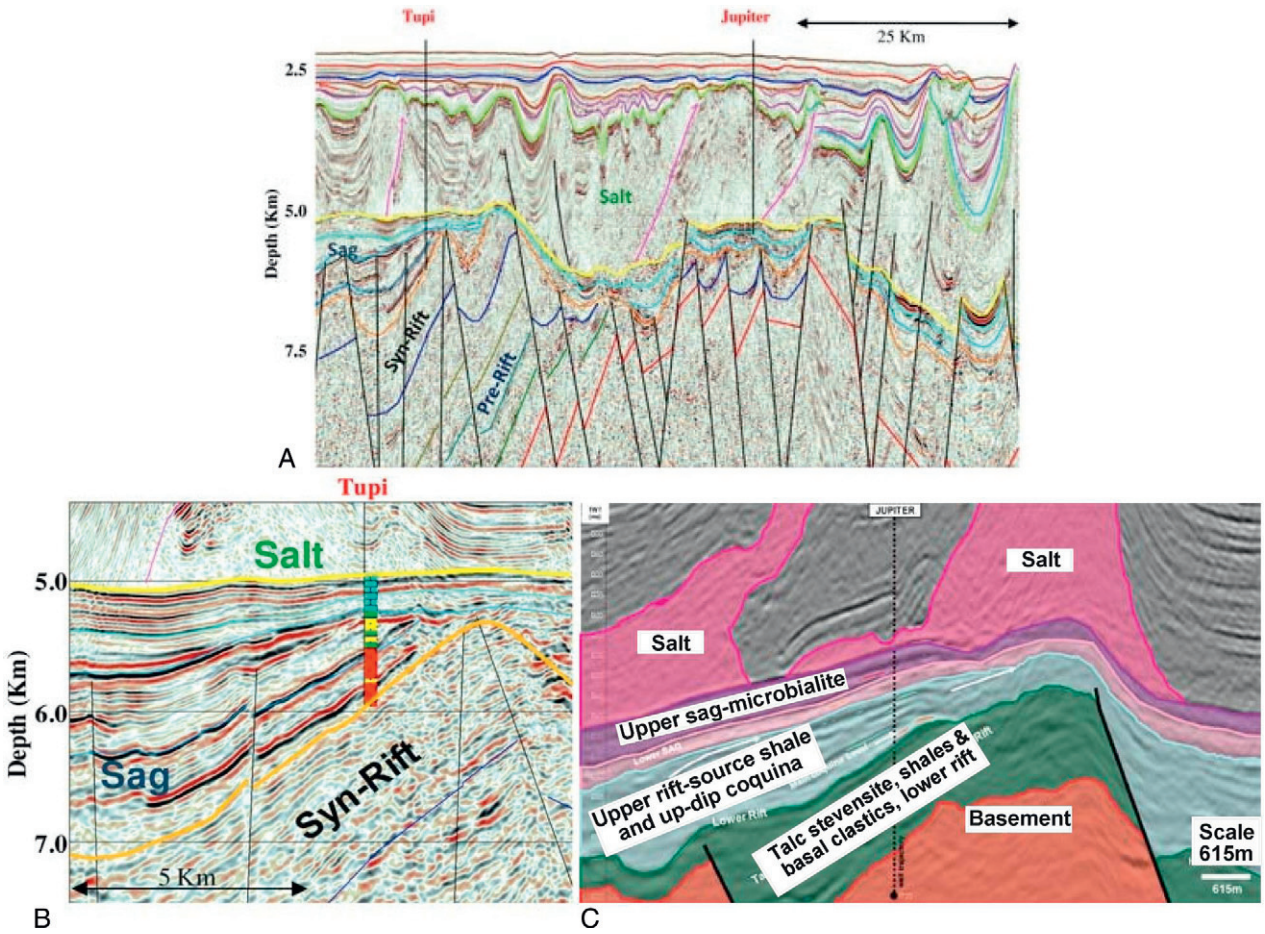

Figure 6.7 Seismic lines through Santos Basin, Brazil, to illustrate syn-rift, pre-salt carbonate platforms overlying early rift clastics. (A) West to east section showing deformed Prerift overlain by syn-rift clastics then pre-salt (Sag phase) carbonates. Note thickness changes and rotation in syn-rift and sag over rotated fault-blocks. Location of Tupi and Jupiter Fields of (B) and (C) below (B). Section through pre-salt Jupiter Field in Santos Basin with syn-rift to sag basin deposits thickening into hanging-wall basin. Non-marine clastics and evaporates onlap the basement and pass up into pre-salt coquina and microbialite non-marine carbonates *((A) and (B) from Henry et al., 2009; (C) from Smith, 2008).*

shale source rocks down hanging-wall dip-slopes, are overlain by microbialite carbonate reservoir facies (Fig. 6.7; Smith, 2008). Similar stratigraphic units and structural relations within syn-rift, pre-salt, fault-block platforms are known to the south in the Campos Basin (Muniz and Bosence, 2009).

With continued rifting, erosion of fault-block highs and subsidence, a major unconformity (post-rift or break-up unconformity) developed on the margin. This separates underlying non-marine megasequence from the transitional (or rift to drift) megasequence of Aptian to Albian age (Figs. 6.6 and 6.7). Initially, thick (<600 m) alluvial clastics are deposited with relatively minor extensional fault movement. This unit is followed by Aptian evaporites that occur on both margins of the South Atlantic but appear to be isolated from ocean waters by the Rio Grande fracture zone in the south and the Pernambuco Lineament in the north. Cainelli and Mohriak (1999) show that these deposits thicken up to 2 km in basinward diapiric structures (Figs. 6.6 and 6.7). Exposed or drilled successions in economically important deposits in Brazil and the Congo indicate halite, carnalite and tachyhydrite (Warren, 1999), some of which have been shown by Wardlow (1972) to be primary deposits. Hardie (1990) has argued that such $MgSO_4$-free primary evaporites cannot be sourced directly from evaporation of marine waters and that accumulation of these salts was from a hydrothermal source in rift valley lakes.

With thermal cooling and rifting, subsidence dissipated the barriers through to the Tethys and Pacific oceans and restricted marine carbonates of the marine megasequence accumulated during early to mid-Albian times. These are known as the neritic sequence (Cainelli and Mohriak, 1999; Guardado et al., 1990; Modica and Brush, 2004) and comprise up to a kilometre of aggrading shelf carbonates (Fig. 6.6). Packstones and grainstones are localised into carbonate platforms over fault-block and salt diapir highs with intervening lime mudstone basins as has already been demonstrated for the late Cenozoic of the Red Sea (cf. Figs. 6.2 and 6.6). The proximal and basal parts of this sequence comprise fan-delta clastics that pass offshore (eastwards) into mixed carbonate-clastic platform deposits. Surface analogues of these relations have been described in detail (above) from the Red Sea, Gulf of Suez and northern margin of the Gulf of Aden (e.g., Fig. 6.4). Overlying fan-delta clastics are beach-bar and lagoonal facies that pass upsection and offshore to platform carbonates. The Brazilian platforms are elongate northeast-southwest along the margin concordant with underlying extensional faults and salt walls and pillows. Development of the platforms is considered to have been influenced by salt movements by Guardado et al. (1990) and by Cainelli and Mohriak (1999). Three-dimensional visualisation of the top Albian (ca. top carbonate platform) surface in the Santos, Campos and Espirito Santos basins is used by Fainstein (2003) to map out salt walls and interspersed minibasins. However, published seismic sections (e.g., Fig., 6.6D) do not demonstrate stratigraphic geometries indicating platform growth synchronous with diapir movement. In the Red Sea and Gulf of Suez, carbonate platforms

are seen to thicken and aggrade into flat-topped and rimmed margins with marginal onlap surfaces (e.g., Fig. 6.5C; Bosence et al., 1998b) indicating a diapiric control on accommodation space for platform growth.

These carbonate platform facies are characterised by non-skeletal carbonates arranged in thick (hundreds of metres) packages interpreted as shoaling-upward cycles (Guardado et al., 1990). Cycle bases are typically oncolitic packstones and rudstones passing up to bioturbated, peloidal skeletal packstones (with echinoids, forams and bivalves). Cycle tops are massive to cross-bedded ooid grainstones (with minor peloids and aggregate ooids) which represent the best reservoir facies within these neritic carbonates. These platforms contrast with those from the Caribbean and southern USA in that they do not have margins with rudist reefs or biostromes (e.g., Scott and Warzeski, 1993; Yerewicz et al., 1993). Elevated salinities for these marine waters were also proposed by Guardado et al. (1990) from low diversity biotic data. Interplatform basins (minibasins) are characterised by lower energy, deeper water facies of bioturbated peloidal mudstones with up to 5% echinoderm fragments, planktonic forams and calcispheres. The platform carbonates are overlain in the late Albian by deeper-water, pelagic mudstones. This platform drowning marks the transition through to the drift phase of basin evolution with evidence of progressive deepening through to the Early Paleocene.

Farther north in the Sergipe Basin, the syn-rift and rift to drift carbonate accumulation is also controlled by seaward dipping extensional faults and an array of landward tilted half-graben (Koutsoukos et al., 1993). The Aptian to Albian platform carbonates of the Riachuelo Formation are exposed onshore while offshore areas are deeper-water, organic–rich shales and carbonate mudstones.

In the late Aptian to early Albian, proximal areas near siliciclastic supply routes accumulate dominantly conglomerates and sandstones in hanging-wall subbasins. Mixed carbonate siliciclastic facies include mollusc, coral, solenoporoid algal, echnoid bioclastic wackestones to grainstones. Carbonates accumulate on footwall highs and hanging-wall rollovers. These shallow-water carbonates are organised into metre-scale, shallowing-upward cycles comprising open marine oncolitic and bioclastic packstones and grainstones, with localised solenoporacean patch reefs, and dolomitised, lagoonal mud-rich facies. Note that these facies have more diverse and open-marine grain associations than the non-skeletal facies found farther south in Brazil, possibly reflecting the closer proximity of the open-ocean waters of the more structurally evolved central Atlantic area.

During early to mid-Albian times, the platforms expanded as a result of progradation into hanging-wall basins and more extensive salt-related highs (Koutsoukos et al., 1993). Progradation leads to shallowing-upward successions infilling hanging-wall dip-slopes as has been modelled by Bosence et al. (1998a). Through

the mid- to late Albian, fault movement died down and carbonate sedimentation expanded to create extensive (tens of kilometres wide) carbonate platforms accumulating high energy ooid, oncoid and bioclastic grainstones and packstones and solenoporacean patch reefs (Koutsoukos et al., 1993). The shelf margin is defined by a major fault zone; this is close to today's coastline. The rapid thermal and fault-induced subsidence of the offshore area prevented more extensive basinward progradation and pelagic facies accumulated throughout the Early Cretaceous. The platform drowns in the Cenomanian (i.e., substantially later than the platforms to the south) and pelagic chalks and marls of the Cotinguiba Formation accumulate. Tectonic activity still continued intermittently, giving rise to debris flows and submarine slides and local unconformities.

African margin carbonate platforms

The opposing African margin, while showing broadly similar phases of tectonic evolution, shows dissimilar styles of carbonate platform development. Syn-rift, continental fluvial and lacustrine rocks formed during the Early Cretaceous (Fig. 6.8; Neocomian to Barremian) (Eichenseer et al., 1999; Spathopoulos, 1996). During the early to mid-Aptian, subsidence-related rifting led to intermittent marine connections and accumulation of halite and anhydrite evaporites of the Loeme Formation (Fig. 6.8). Farther north, offshore Gabon, the Aptian evaporites are more K-rich salts (see above) and are known as Ezanga Fm (Teisserenc and Villemin, 1990). Both of these evaporite units are labelled as transitional phase (Spathopoulos, 1996; Teisserenc and Villemin, 1990) and have direct equivalence with this phase on the Brazilian margin. Ocean floor spreading at the Aptian–Albian boundary marks the rift to drift transition and accommodation space was generated continuously through to the end of the Albian that permitted the accumulation of the Pinda Group. To the north in the Congo Basin, siliciclastics dominate but to the south, in offshore Angola, the margin comprises Albian carbonate platforms made up of the Tuenza, Catumbela and Quissonde Formations (Fig. 6.8; Eichenseer et al., 1999). In Gabon, the Albian carbonate platform is known as the Madiela Fm (Fig. 6.7C). These Albian deposits reach up to 600 m in thickness and form major oil reservoirs in offshore Congo and Angola in carbonates to mixed carbonate-siliciclastics and pure siliciclastics sealed by offshore mudrocks (Eichenseer et al., 1999). The Pinda Group is overlain by proximal sands and distal shales during the Cenomanian. In Congo, the carbonates are prospective but no economic reservoirs have yet been found (Teisserenc and Villemin, 1990).

Salt-induced tectonism involving differential loading and basinward tilting of the Angolan margin began in the Albian and intensified during the Cenomanian and Turonian (Spathopoulos, 1999). Deformation took place largely along basinward-dipping, listric faults soling out on the Aptian salt (Fig. 6.8). The resultant gravitational sliding broke the Albian carbonate platform into a mosaic of variously labelled fault-blocks, rafts or turtle-backs that today form reservoir

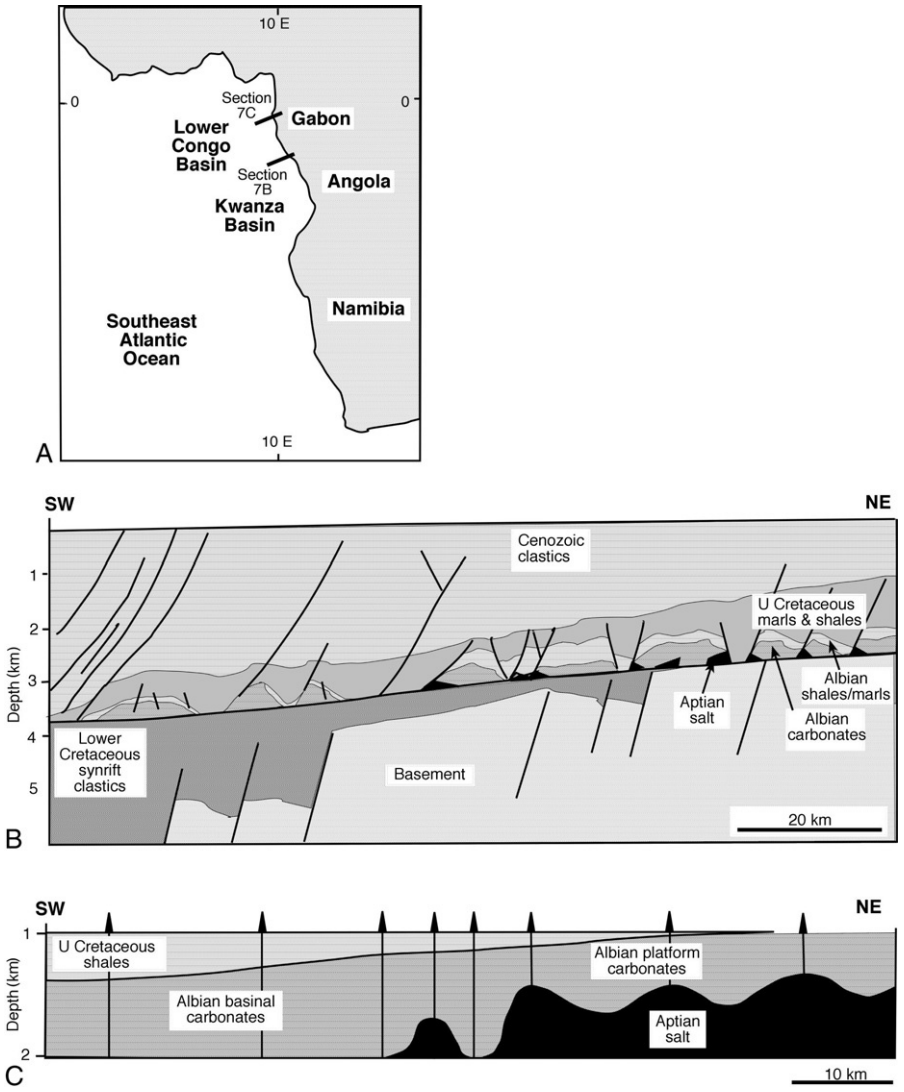

Figure 6.8
Albian carbonate platforms, offshore southwest Africa. (A) Location of shelf to slope cross-sections in Fig. 6.7B and C. (B) NE to SW section through offshore Kwanza Basin (Angola) illustrating fault-dissected Albian carbonate platform with underlying Aptian salts *(after Eichenseer et al., 1999)*. (C) NE to SW section through onshore to offshore Gabon. Note stratigraphic thinning of Albian platform carbonates over Aptian salt and thickening of offshore, basinal Aptian in response to salt withdrawal. The Upper Cretaceous shales onlap the Lower Cretaceous carbonates *(after Teisserenc and Villemin, 1990)*.

targets. The critical question with respect to facies distribution within these carbonates is whether the platforms were dissected into fault-block platforms and salt-diapir platforms in the Albian or whether this occurred later and faults dissected a more extensive subsiding-margin platform. This problem does not appear to have been addressed in the literature and is complicated by the carbonates occurring at the rift to drift transition. The most detailed published study of these Albian carbonates is that of Eichenseer et al. (1999) based on 150

exploration wells and some 4500 m of core. In their study, there are two lines of evidence that suggest that the platform segments originated from one large seaward-sloping carbonate, or mixed carbonate-siliciclastic, ramp that was dissected during the Cretaceous. The first argument for this is that many of the platform segments can be restored back to their original neighbouring segments along pathways of gravitational displacement. The second argument is that they are able to erect a consistent second to third order sequence stratigraphy for the ramp succession for many of the platform rafts. The second order sequence includes the entire Pinda Group starting with the basal one-third of the stratigraphy dominated by coastal sandstones of the Bufalo Fm. The upper two-thirds are mainly oolitic, pisolitic and oncoidal dolomites reflecting the marine flooding of the basin margin that pushes the clastics shoreward. Maximum flooding is represented by dolomitic siltstones and shales of the Punja Fm in the north and hemipelagic mudstones (Quissonde Fm) in the south that eventually overlie the entire platform succession (Eichenseer et al., 1999). Third order sequences are on average 10 m thick and in the Lower Congo Basin are characterised by a lower transgressive arkosic sandstone that thins basinward. These are erosively overlain by oolitic, pisolitic dolograinstones to rudstones that thicken shoreward but pass downramp into organic rich silty dolomudstones. Highstands comprise prograding oolite shoals capped with intermixed clastics. In the Kwanza Basin to the south, carbonate-evaporite sequences are found with basal, transgressive lagoonal shales, erosively overlain by sheets of bioclastic, peloidal grainstones that fine upwards muddy peloidal facies at maximum flooding. Highstand regressive facies are prograding bioclastic oolitic sand belts capped by lagoonal to salina stromatolites and anhydrite.

These consistent, regional, second and third order sequence stratigraphies imply the existence of a ramp profile shelf over the entire margin, or subsiding margin platform. Locally, there are some thickness variations identifying areas of greater subsidence which are interpreted by Eichenseer et al. (1999) to be likely fault-bound sub-basins on the ramp. However, this appears to be a minor control on this carbonate platform. Segmentation of the platform therefore appears to have happened after the main phase of platform growth rather than during platform growth, as is the case on the Brazilian margin.

Farther north (0–4°S) offshore Gabon, the late Aptian to Albian platform shows some broad trends from eastern (onshore) lagoonal and continental facies to varied nonskeletal and skeletal platform facies to western offshore basinal shales (Fig. 6.8C; Teisserenc and Villemin, 1990). Differential movement of the underlying Aptian Ezanga salt took place during platform growth as evidenced by thickness changes from 90 to 1500 m in the middle Madiela unit. A reconstructed shoreline to basin section (Fig. 6.8C; Teisserenc and Villemin, 1990) indicates that the relatively thin (400–800 m) carbonate platform is underlain by a 1200 m thick pillow of salt, whereas the thicker (1500 m) offshore basinal facies are underlain by 0–600 m of salt. These stratigraphic differences suggest

that the platform to basin configuration was controlled by syndepositional salt movement. If this is the case, then smaller scale platform morphology and facies would be expected to have been controlled by salt diapirism as is the case with the examples from the Red Sea (above) and in contrast to the Albian platform to the south in offshore Angola. The Gabon platform is drowned in the Cenomanian with shales of the Cap Lopez, Ekouata and Ndougou Fms.

6.4 Synthesis and discussion

The two case studies discussed above are chosen as they provide relatively well-documented examples of marine-dominated rifts, one from the Mesozoic and the other from the Cenozoic. The outcrop examples from the Gulf of Suez–Red Sea–Gulf of Aden provide probably the best examples we have today of the diversity found within rift basin carbonate platforms. The post-Miocene uplift of the rift margins in an arid climate setting provides outcrops that display the details of facies, facies relations and sequence stratigraphies where surfaces and systems tracts can be mapped out. However, the basin is young and not all stages of the rift to drift transition are preserved. The subsurface Cretaceous examples from the South Atlantic, while not providing much detail on fine-scale stratigraphy and facies, give a good view of the overall morphologies of rift basin carbonate platforms and their stratigraphic and tectonic context within the evolving Atlantic margins.

Cenozoic of the Gulf of Suez–Red Sea–Gulf of Aden

Carbonate platforms within this rift system develop from the Miocene through to the present day. The platforms occur in three main shallow-marine sites; on top of rotating and subsiding fault-blocks, on top of rising and subsiding salt diapirs and on top of coarse grained fan-deltas (Fig. 6.9). Examples are found along the present-day shelves and in the Miocene to Pliocene outcrops along the basin margins. Each platform type has a distinctive morphology, facies models and sequence stratigraphy (Fig. 6.9; Bosence, 2005). In addition, large areas of the more evolved Gulf of Aden show a Miocene stratigraphy with more margin-wide stratigraphy rather than platforms developing in response to more localised controls (i.e., fault-block, salt diapir etc.).

Although the concept of early, mid- and late syn-rift has been used to categorise rift basin fill, these phases should not be used as a prescriptive template. In this, one of the best studied marine rifts in the world, considerable variation is found along its margins. Its northern parts represent a sedimentary basin whose margins are concordant with either basinward or landward dipping faults. Carbonates are concentrated on footwall highs to fault blocks while clastics either pass axially through the carbonates in fault accommodation zones of cut across fault blocks, or laterally along hanging-wall basins. This pattern of sediment accumulation conforms to earlier tectonostratigraphic models for rift basins

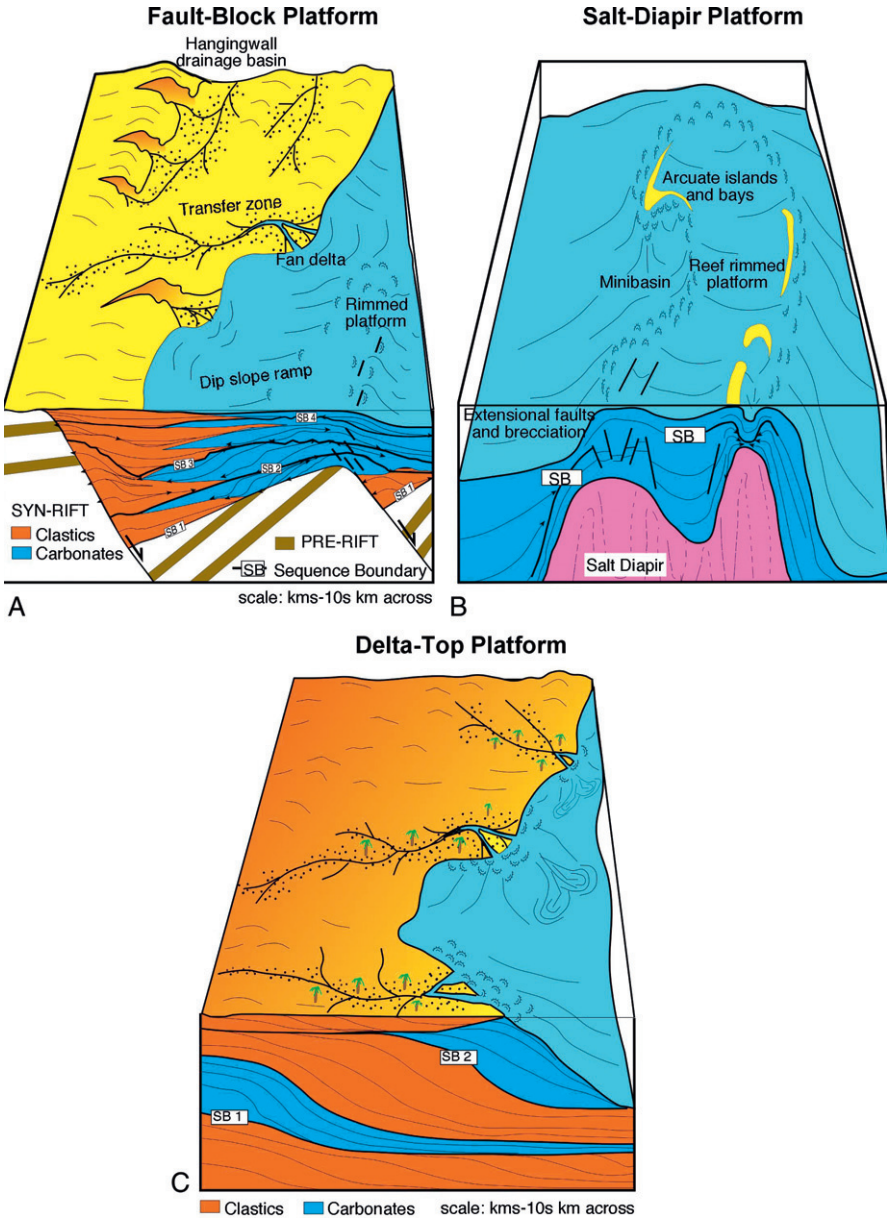

Figure 6.9 Facies and sequence stratigraphic models for carbonate platforms developing in rift and rift to drift settings. (A) Fault-block carbonate platform based on outcrop studies from Gulf of Suez and seismic sections from the Gulf of Aden. Note dipslope ramp and footwall rimmed shelf and wedge-shaped depositional sequences. (B) Salt-diapir carbonate platform based on outcrop studies in Yemen and Saudi Arabia and seismic sections from the Gulf of Suez and southern Red Sea. Note arcuate shaped platform with minibasin re-entrants and irregular shaped depositional sequences generated by salt piercement and withdrawal. (C) Delta-top carbonate platform based on outcrop studies in the Red Sea, Spain and the Gulfs of Aden, Suez and Aqaba. Note predominant lowstand clastic deltas, and transgressive and highstand carbonate platforms *(from Bosence, 2005)*.

(Bosence, 1998; Leeder and Gawthorpe, 1987) but it is not seen in the Gulf of Aden section of the rift basin. Here, on the northern margin, large areas have little active faulting, are of low relief and have little supply of course clastics from the rift shoulder. This section of the margin, although within the syn-rift phase, with active extensional faulting to the east, the west and the south, has more similarities to a passive margin fill than a rift basin. Strata appear to passively fill the accommodation space generated from regional subsidence of the margin. In addition, farther to the east in this oblique rift, the coastline is parallel to the direction of extension so that the major facies belts (deep-water carbonates, shelf carbonates and continental deposits) are normal to the extensional fault blocks. However, locally the fault blocks control the occurrence of platform and slope carbonates, as fault-block platforms, with clastics funnelled axially, through intervening hanging-wall basins (Fig. 6.9A). While the difference between the concordant and the oblique rift organisation might be predicted from regional data, the different sections of the rift are in different stages of structural evolution.

Another, sometimes overriding, control on carbonate platforms in marine rift basins is the occurrence of precurser, thick evaporite deposits. This is demonstrated by the comparison between coeval platforms in the Red Sea (with thick evaporites) where salt-diapir platforms (Fig. 6.9B) are as common as fault-block platforms, and the Gulf of Aden (without thick evaporites) where fault-block and subsiding margin platforms dominate. The importance of syn- to post-rift salt on carbonate platform development is also demonstrated in the South Atlantic.

Cretaceous of the South Atlantic

The syn-rift comprises continental clastic, local volcanics and apparently non-marine carbonate platforms. Despite their palaeoenvironmental setting, the platforms show characteristic morphologies of fault-block platforms. Platform development also occurs after evaporite accumulation during the transitional phase from rift to drift that coincides with marine flooding of the margin. This history is common to both the western and eastern Atlantic margins but the platforms that develop on these opposing margins are significantly different. The western margin develops syntectonic fault-block and salt-diapir carbonate platforms in the Albian, and the latter are also seen offshore Gabon on the eastern margin. These platforms would be expected to develop their own margins, slopes and platform top facies as have been described from the Cenozoic outcrops of the Gulf of Suez–Red Sea–Gulf of Aden rifts and presented in Fig. 6.9B. Subsequently, the Albian platforms are seen to evolve up section into laterally extensive and thick subsiding margin platforms that are typical of the central Atlantic today (e.g., Florida Shelf; Belize Shelf; see Chapter 9.10, this volume). However, the southeastern Atlantic margin develops an extensive, subsiding margin ramp over the Aptian salts. Extensional faulting and diapirism seem to have been only minor during this phase of basin evolution allowing one large

carbonate platform to build out over the entire margin. Rates of carbonate production must have exceeded rates of subsidence from fault or salt withdrawal so that accommodation space was continuously filled. Subsequently, during emplacement of oceanic crust, subsidence rates increased and along with tilting of the margin caused the dissection of the platform by listric faults soling out on the underlying salt. Both eastern and western margins have segmented platforms; superficially these may appear similar but those on the west are small individual platforms within intervening basins while those on the east are reported as segments or rafts of one larger platform with a margin-wide distribution of facies and no coeval margins, slopes and basins (cf. Figs. 6.6 and 6.8). The establishment of facies models of the post-salt platforms awaits more detailed subsurface examination or suitable post-salt outcrop analogues. The critical question is whether the platforms are extensive, margin-wide structures, or segmented, salt diapir platforms.

6.5 Conclusions

Carbonate-dominated marine rifts are common in the geological record as rift basins provide many shallow-water sites for the establishment of carbonate platforms. However, these are only known from low-latitude regions and can vary from marine to non-marine settings. The commonest site for platform growth in rift basins is on footwall or horst highs and intervening slopes. Many examples of such platforms are known from the syn-rift to post-rift transition. Post-rift to the thermal subsidence phase of basin evolution can result in extensive margin-wide platforms as seen in Mesozoic Atlantic margins.

Isolation of a low latitude rift basin in an arid setting may result in basin-wide evaporite accumulation and this has implications for subsequent basin evolution, carbonate platform development and hydrocarbon prospectivity. Pre-salt carbonate platforms may be sealed by evaporites as in the Gulf of Suez and Santos Basin. Salt diapirism may provide shallow-water sites for post-salt carbonate platforms to accumulate as in the southern Red Sea and Campos Basin. Large-scale, shelf-wide, post-salt platforms may be dissected into salt rafts as in the Kwanza Basin, Angola.

About the Author

Professor Dan Bosence obtained his Ph.D. on modern temperate carbonates from the University of Reading in 1976. Since then, he has of held academic posts in the University of London; initially at Goldsmiths' College and then at Royal Holloway (RHUL) during which time he has supervised 25 Ph.D. students. He currently holds an Emeritus Chair in Carbonate Sedimentology at RHUL as well as being a consultant carbonate sedimentologist to the hydrocarbon industry. He has published over 90 papers on modern and ancient carbonate sediments and has authored/coauthored/edited six books in this field and on rift basin sedimentology and stratigraphy.

References

Bantan, R.A., 1999. Geology and sedimentary environments of Farasan Bank (Saudi Arabia) southern Red Sea: A combined remote sensing and field study. University of London. Ph.D. thesis, 297.

Bernoulli, D.L., Jenkyns, H.C., 1974. Alpine, Mediterranean, and Central Atlantic Mesozoic facies in relation to the early evolution of the Tethys: Geosynclinal Sedimentation, Modern and Ancient, A symposium In: Dott, R.H., Shaver, R.W. (Eds.), Geosynclinal Sedimentation, Modern and Ancient, A Symposium, SEPM, Special Publication 19, pp. 129–160.

Bosence, D.W.J., 1998. Stratigraphic and sedimentological models of rift basins. In: Purser, B.H., Bosence, D.W.J. (Eds.), Sedimentary and Tectonic Evolution of Rift Basins – The Red Sea-Gulf of Aden. Kluwer, pp. 9–25.

Bosence, D.W.J., 2005. A genetic classification of carbonate platforms based on their basinal and tectonic settings in the Cenozoic. Sediment. Geol. 175, 49–72.

Bosence, D.W.J., Nichols, G.J., Al-Subbary, A.K., Al-Thour, K.A., Reeder, M., 1996. Synrift continental to marine depositional sequences, Tertiary, Gulf of Aden, Yemen. J. Sediment. Res. 66, 766–777.

Bosence, D.W.J., Cross, N.E., Hardy, S., 1998b. Architecture and depositional sequences of Tertiary fault-block carbonate platforms; an analysis from outcrop and computer modelling. Marine Pet. Geol. 15, 203–221.

Bosence, D.W.J., Al-Aawah, M.H., Davison, I., Rosen, B.R., Vita Finzi, C., Whitaker, E., 1998a. Salt domes and their control on basin margin sedimentation: a case study from the Tihama Plain, Yemen. In: Purser, B.H., Bosence, D.W.J. (Eds.), Sedimentary and Tectonic Evolution of Rift Basins – The Red Sea-Gulf of Aden. Kluwer, pp. 448–464.

Bosworth, W., Crevello, P., Winn, R.D., Steinmetz, J., 1998. Structure, sedimentation and basin dynamics during rifting of the Gulf of Suez and northwestern Red Sea. In: Purser, B.H., Bosence, D.W.J. (Eds.), Sedimentary and Tectonic Evolution of Rift Basins – The Red Sea-Gulf of Aden. Kluwer, pp. 77–96.

Bott, W.F., Smith, B.A., Oakes, G., Sikander, A.H., Ibrahim, A.I., 1992. The tectonic framework and regional hydrocarbon prospectivity of the Gulf of Aden. J. Pet. Geol. 15, 211–243.

Brannan, J., Gerdes, K.D., Newth, I.R., 1997. Tectono-stratigraphic development of the Qamar basin, eastern Yemen. Marine Pet. Geol. 14, 701–730.

Burchette, T.P., 1988. Tectonic control on carbonate platform facies distribution and sequence development: Miocene, Gulf of Suez. Sediment. Geol. 59, 179–204.

Cainelli, C., Mohriak, W.U., 1999. Some remarks on the evolution of sedimentary basins along the eastern Brazilian continental margin. Episodes 22, 206–212.

Carbone, F., Matteucci, R., Angelucci, A., 1998. Present day sedimentation on the carbonate platform of the Dahlak Islands, Eritrea. In: Purser, B.H., Bosence, D.W.J. (Eds.), Sedimentary and Tectonic Evolution of Rift Basins – The Red Sea-Gulf of Aden. Kluwer, pp. 523–536.

Cross, N., Bosence, D.W.J., 2008. 3D tectono-sedimentary models for marine, rift-margin, carbonate systems. In: Lukasik, J., Simo, T. (Eds.), Controls on Carbonate Platform and Reef Development. Society of Economic Paleontologists and Mineralogists, Special Publication, pp. 83–106.

Cross, N.E., Purser, B.H., Bosence, D.W.J., 1998. The tectono-sedimentary evolution of a rift margin carbonate platform: Abu Shaar, Gulf of Suez, Egypt. In: Purser, B.H., Bosence, D.W.J. (Eds.), Sedimentary and Tectonic Evolution of Rift Basins – The Red Sea – Gulf of Aden. Kluwer, pp. 271–295.

Davison, I., Bosence, D.W.J., Alsop, I., Al-Aawah, M.H., 1966. Deformation and sedimentation around active Miocene salt diapirs on the Tihama Plain, northwest Yemen. In: Alsop, I., Blundell, D.J., Davison, I. (Eds.), Salt Tectonics, vol. 100. Special Publication, Geological Society of London, pp. 23–39.

Dullo, W.C., Montaggioni, L., 1998. Modern Red Sea coral reefs: a review of their morphologies and zonation. In: Purser, B.H., Bosence, D.W.J. (Eds.), Sedimentary and Tectonic Evolution of Rift Basins – The Red Sea – Gulf of Aden. Kluwer, pp. 583–594.

Durham, L.S., 2009. Brazil dancing the 'Pre-Salt Salsa'. Am. Assoc. Pet. Geol. Explorer, 30, November, 4–8.

Eichenseer, H.T., Walgenwitz, F.R., Biondi, P.J., 1999. Stratigraphic control on facies and diagenesis of dolomitised oolitic and siliciclastic ramp sequences (Pinda Group, Albian, offshore Angola). Am. Assoc. Pet. Geol. Bull. 83, 1729–1758.

Fainstein, R., 2003. Mapping turtle structures. Brazilian Technology and Business Magazine of Petroleum, Gas Petrochemical and Plastic Industries 15, 32–34.

Guardado, L.R., Gamboa, L.A.P., Lucchesi, C.F., 1990. Petroleum geology of the Campos Basin, Brazil, a model for a producing Atlantic type basin. In: Edwards, J.D., Santogrossi, P.A. (Eds.), Divergent/Passive Margin Basins, American of Association of Petroleum Geologists Memoir 48, pp. 3–80.

Hardie, L.A., 1990. The roles of rifting and hydrothermal $CaCl_2$ brines in the origin of potash evaporates; an hypothesis. Am. J. Sci. 290, 43–106.

Hay, W.W., Rosol, M.J., Sloan, J.L., 1988. Plate tectonic control of global patterns of detrital and carbonate sedimentation. In: Doyle, L.J., Roberts, H.H. (Eds.), Carbonate-Clastic Transitions. Elsevier, pp. 1–34.

Heaton, R.C., Jackson, M.P.A., Bamahmoud, M., Nani, A.S.O., 1996. Superposed Neogene extension, contraction and salt canopy emplacement in the Yemneni Red Sea. In: Jackson, M.P.A., Roberts, D.G., Snelson, S. (Eds.), Salt Tectonics: A Global Perspective, American Association of Petroleum Geologists Memoir 65, pp. 333–352.

Henry, S.G., Kumar, N., Sujata, V., 2009. Geo Expro. www.geoexpro.com/brazil/beneathsalt/ (accessed on 29.10.2009).

James, N.P., Coniglio, M., Aissaoui, D.M., Purser, B.H., 1988. Facies and geological history of an exposed Miocene rift margin carbonate platform, Gulf of Suez, Egypt. Am. Assoc. Pet. Geol. Bull. 72, 555–572.

Koutsoukos, E.A.M., Destro, N., Fiulho, N.C.de A., Spadini, A.R., 1993. Upper Aptian-Lower Coniacian carbonate sequences in the Sergipe Basin, Northeastern Brazil. In: Simo, J.A.T., Scott, R.W., Masse, J.-P. (Eds.), Cretaceous Carbonate Platforms. American Association Petroleum Geologists Memoir 56, pp. 127–144.

Leeder, M., Gawthorpe, R.L., 1987. Sedimentary models for extensional tilt-block/half-graben basins. In: Coward, M.P., Dewey, J.F., Hancock, P.L. (Eds.), Continental Extensional Tectonics. Geological Society London, Special Publication 28, pp. 139–152.

Modica, C.J., Brush, E.R., 2004. Postrift sequence stratigraphy, palaeogeography and fill history of the deep-water Santos Basin, Brazil. Am. Assoc. Pet. Geol. Bull. 88, 923–946.

Muniz, M., Bosence, D.W.J., 2009. Sedimentological and stratigraphic analysis of Aptian non-marine carbonates of the southern Campos Basin, Brazil. American Association Petroleum Geologists Annual Convention, Denver, June 2–10. www.searchanddiscovery.net/abstracts/html/2009/annual/abstracts/muniz.htm.

Orszag-Sperber, F., Harwood, G., Kendall, A.C., Purser, B.H., 1998. A review of the evaporites of the Red Sea – Gulf of Suez rift. In: Purser, B.H., Bosence, D.W.J. (Eds.), Sedimentary and Tectonic Evolution of Rift Basins – The Red Sea – Gulf of Aden. Kluwer, pp. 409–426.

Purser, B.H., Plaziat, J.C., 1998. Miocene periplatform slope sedimentation in the northwestern Red Sea rift, Egypt. In: Purser, B.H., Bosence, D.W.J. (Eds.), Sedimentation and Tectonics of Rift Basins: Red Sea – Gulf of Aden. Kluwer, pp. 320–346.

Purser, B.H., Barrier, P., Montenat, C., Orszag-Sperber, F., Ott d'Estevou, P., Plaziat, J.C., et al., 1998. Carbonate and siliciclastic sedimentation in an active tectonic setting: Miocene of the Northwest Red Sea rift Egypt. In: Purser, B.H., Bosence, D.W.J. (Eds.), Sedimentation and Tectonics of Rift Basins: Red Sea – Gulf of Aden. Kluwer, pp. 239–270.

Roberts, H.H., Murray, S.P., 1983. Gulfs of the northern Red Sea: depositional settings of abrupt siliciclastic-carbonate transitions. In: Doyle, L.J., Roberts, H.H. (Eds.), Carbonate-Clastic Transitions. Elsevier, pp. 99–142.

Scott, R.W., Warzeski, E.R., 1993. An Aptian to Albian shelf ramp, Arizona and Sonoroa. In: Simo, J.A.T., Scott, R.W., Masse, J.-P. (Eds.), Cretaceous Carbonate Platforms, American Association Petroleum Geologists Memoir 56, pp. 71–80.

Smith, T., 2008. Monsters of the Deep. Geo Expro. www.geoexpro.com/brazil/monsters_o/ (accessed on 11.11.2008).

Spathopoulos, F., 1996. An insight on salt tectonics in the Angola Basin, South Atlantic. In: Alsop, G.I., Blundell, D.J., Davison, I. (Eds.), Salt Tectonics, Geological Society of London. Special Publication 100, pp. 153–174.

Teisserenc, P., Villemin, J., 1990. Sedimentary basin of Gabon – geology and oil systems. In: Edwards, J.D., Santogrossi, P.A. (Eds.), Divergent/Passive Margin Basins, American Association Petroleum Geologists Memoir 48, pp. 117–200.

Wardlow, N.C., 1972. Unusual marine evaporites with salts of calcium and magnesium chloride in Cretaceous basins of Sergipe, Brazil. Econ. Geol. 67, 156–168.

Warren, J., 1999. Evaporites: Their Evolution and Economics. Blackwell Science, Oxford, 438.

Watchorn, F., Nichols, G.J., Bosence, D.W.J., 1998. Rift related sedimentation and stratigraphy in southern Yemen. In: Purser, B.H., Bosence, D.W.J. (Eds.), Sedimentation and Tectonics of Rift Basins: Red Sea – Gulf of Aden. Kluwer, pp. 165–189.

Yerewicz, D.A., Marler, T.B., Meyerholtz, K.A., Siroky, F.X., 1993. Early Cretaceous carbonate platform, north rim of the Gulf of Mexico, Mississippi and Louisiana. In: Simo, J.A.T., Scott, R.W., Masse, J.-P. (Eds.), Cretaceous Carbonate Platforms, American Association of Petroleum Geologists Memoir 56, pp. 81–96.

In this chapter

7

Evolution of the Cenozoic East African rift system: Cratons, plumes, and continental breakup

Cynthia Ebinger
Department of Earth and Environmental Sciences, University of Rochester, Rochester, NY USA

7.1 Introduction

The broad, fault-bounded rift valleys of East Africa were the natural amphitheatre for man's early evolution, and they remain corridors for animal and human migration. For earth scientists, they provide first-order insights into the mechanics and dynamics of plate tectonic processes. Despite the long-term interest in the East African rift system, the extremes of topographic relief coupled with political instability have hindered attempts to determine the spatial extent and continuity of several rift sectors. Until the Space Radar Terrain Mission digital elevation models became available, even mountain ranges in East Africa were "missing" in our global images, leading to confusion and unnecessary controversy.

This chapter is intended to review current constraints on the structure and kinematics of the East African rift system, and then to link these findings to lithospheric deformation and deep mantle processes. I first review current models for the development of continental rift basins leading to continental breakup, pointing out model sensitivities and critical constraints required to differentiate between models. It is these critical observations from representative parts of the East African rift system that are presented, rather than an exhaustive review of the East African rift system. The $>$3000-km length of the rift system in East Africa comprises $<$1 My fault systems as well as nascent seafloor spreading centers in the Afar depression. Thus, the East African rift laboratory encompasses the birth to breakup history of a rift within one geodynamic setting.

Phanerozoic Rift Systems and Sedimentary Basins DOI:10.1016/B978-0-444-56356-9.00006-7

7.2 Continental breakup models

Extension leading to continental breakup and the creation of new oceanic lithosphere will occur if tensional stresses generated by far-field plate motions, pressure, and stress gradients induced by asthenospheric upwellings, and/or tractions at the base of the lithosphere produced by the convecting mantle are sufficient to thin and then rupture the initially 150–250-km-thick continental plates. Rupture requires a drastic reduction in thickness and loss of strength, given the available plate boundary forces of $<$0.5 GPa (e.g., Bott, 1991; Buck, 2004). The geological record reveals that only some continental rifts undergo stretching and strain localization to the point of rupture; "failed rifts" become inactive at various stages of their evolution, leaving long scarps and broad valleys. For rifts that achieve rupture, the new seafloor spreading center becomes the plate boundary, and the now inactive rift zone becomes a "passive margin." The passive margin subsides below sea level as the heat transferred to the plate from the active or passive asthenospheric upwelling during rifting dissipates.

Continental lithospheric strength. The average continental lithosphere comprises a quartz- and feldspar-rich, $\sim$40-km-thick crust above 100–200 km of the olivine-rich mantle that is colder than $\sim$1600 K (e.g., Turcotte and Schubert, 2002). The long-term rigidity of the rheologically layered lithosphere remains disputed, although the persistence of deep-keeled Archaean cratons attests to long-term strength (e.g., Sleep, 2003). Theory and observations show that extensional deformation within the crust is taken up by a combination of faulting, dyke intrusion, and aseismic ductile creep (e.g., Buck, 2004). Faulting, or brittle failure, requires relatively high stresses, roughly comparable to a half of the confining pressure (Byerlee, 1978). Brittle failure is restricted to upper crustal levels (15–25 km) because tectonic stresses are usually much less than 0.5 GPa. The lower crust is generally dominated by aseismic ductile creep, excepting regions of unusually low geothermal gradients (e.g., Déverchère et al., 1993; Foster and Jackson, 1998). Dyke intrusion needs a supply of magma, and ductile creep is promoted by higher temperatures. There is less agreement, and far fewer data, on deformation processes in the mantle lithosphere. Earthquakes and gravity-topography relationships provide constraints on the strength of the plate over periods of 10^0 to 10^4 years, respectively; differences between the two estimates are expected because different deformation mechanisms are likely to be activated at different time scales and strain rates (e.g., Ebinger et al., 1999; Watts and Burov, 2003). The depth extent of earthquakes within a rift provides an estimate of the background stress level of tectonically pre-stressed zones in the lithosphere (Watts and Burov, 2003). Locally high strain rates may result in brittle failure within the "ductile" mantle layer as the ductile creep cannot be physically activated at seismic time scales, and the entire lithosphere behaves as an elastic or brittle-elastic medium. Most earthquakes occur in the crust, and few, if any, earthquakes occur in the upper mantle of rift zones, leading to suggestions that the upper mantle

beneath continents is weak, or "ductile." However, taking a minimum bound on mantle viscosity of 10^{19} Pa s, the mantle is rigid at short time scales, at which it would rather break than flow. The aseismicity of the mantle thus reflects its great strength, rather than its weakness (e.g., Burov et al., 1998). Gravity-topography relations provide a much longer-term perspective on plate strength. Because the continental lithosphere flexes in response to loads applied to the top of the plate (e.g., volcano) or within the plate (e.g., crustal thinning), density contrasts within the plate will be displaced, producing measurable gravity anomalies. The wavelength of these topographic and gravity anomaly deflections can be described by an integrated yield strength of the plate, or, an effective elastic plate thickness that represents contributions from all brittle, elastic, and ductile layers. The effective elastic thickness does not correspond to a geological boundary, but it provides a comparative measure of the longer term mechanical response of the lithosphere. Estimates of effective elastic thickness from forward and inverse models of continental data are usually greater than the seismogenic layer thickness, indicating strength in the mantle lithosphere (e.g., Petit and Ebinger, 2000; Watts and Burov, 2003), although there is no universal agreement (e.g., Jackson and McKenzie, 2008).

Theory and numerical models show that continental breakup may be achieved through mechanical weakening of the lithosphere by stretching, intrusive heating, and interactions with a dynamic asthenosphere (e.g., Dunbar and Sawyer, 1998; McKenzie, 1978). At the scale of the zone of extensional deformation, Buck (1991) showed that >300-km-wide rift zones with many parallel basins (e.g., Basin and Range, Aegean) and <150-km-wide single rift zones could be reproduced by differences in plate strength at the onset of rifting, without requiring differences in mantle driving processes (i.e., active vs. passive). Weak or very weak plates with high geotherms developed "wide rifts" or core complexes; cold, strong plates are marked by a single extensional basin. New modeling techniques now allow one to simulate a rheologically layered lithosphere to examine the localization of strain with progressive extension (e.g., Frederiksen and Braun, 2001) as well as to examine the relative strength contribution from crust and mantle lithosphere (e.g., Burov and Poliakov, 2001; Huismans et al., 2001). Although still debated (e.g., Jackson and McKenzie, 2008), a narrow zone of extensional deformation with a broad, deep basin flanked by broad uplifts requires a strong upper mantle (e.g., Bassi, 1995; Frederiksen and Braun, 2001).

Continental rifts worldwide show consistent patterns that are independent of geodynamic setting, indicating that the thermal and mechanical properties of the lithosphere largely determine the distribution of strain during the early rifting stages (e.g., Bassi, 1995; Buck, 1991; Dunbar and Sawyer, 1989). Within any plate boundary zone lie a series of discrete, but kinematically linked basins whose dimensions, the flanking uplifts, and the maximum length and depth extent of faults largely depend upon the integrated yield strength of the lithosphere

(e.g., Hayward and Ebinger, 1996; Weissel and Karner, 1989). Thus, there is a strong signal in the along-axis segmentation pattern of continental rifts, which is clearly fault-controlled during the early rifting stages.

There is also a strong segmentation signal in mid-ocean ridges, the end result of continental rifting. The along-axis segmentation of mid-ocean ridges is a consequence of magma supply; thicker crust is produced above higher melt production zones in the upwelling asthenosphere (e.g., Batiza, 1996). With true seafloor spreading, we can expect the supply of melt from decompression melting of asthenosphere rising to fill the space created by lithospheric thinning to dominate. Thus, mantle dynamics and magmatic processes will increase in importance as the continental lithosphere is stretched to the point of rupture, but there are few models and even fewer data to constrain the magmatic processes during lithospheric stretching.

Continental breakup models can be divided into two classes: (A) purely kinematic (e.g., McKenzie, 1978), mechanical (e.g., Dunbar and Sawyer, 1989), or thermo-mechanical stretching (e.g., Huismans et al., 2001; Frederiksen and Braun, 2001) and (B) coupled mechanical or kinematic asthenosphere–lithosphere models that include magmatism in some way (e.g., Buck, 2004; d'Acremont et al., 2003; White and McKenzie, 1989). Because melt is buoyant to at least mid-crustal levels, the buoyancy forces effectively sum with the plate driving forces, whereas friction along fault surfaces competes with plate driving forces (e.g., Rubin, 1992). Thus, magma injection can accommodate strain at lower plate driving stresses than faulting, facilitating breakup. Class B models have yet to include feedback between melt and rheology.

Figure 7.1 shows two simplified cartoons that illustrate the major differences between magma-assisted and fault-controlled stretching models. The major difference between Class A and B is in the localization of strain as rifting progresses to seafloor spreading: Class A models accommodate strain by large offset faults in brittle layers, and ductile deformation in weaker layers. Depending on lithospheric rheology assumed, strain may be distributed across a broad zone, or localized along one large displacement zone fault (e.g., Burov and Poliakov, 2001; Frederiksen and Braun, 2001). Class B models accommodate extensional strain by magma injection, with small offset faults above the zone of magma injection. Magma intrudes the more ductile lower lithosphere, feeding dykes that intrude the stronger lithospheric layers (Fig. 7.1B). As stretching leads to more thinning, the heat transfer from magmatism also reduces the plate strength, and the level of magma intrusion rises to shallower levels that are now deforming in a ductile manner. Clearly, these cartoons were drawn to isolate process, and hybrid models may be more realistic.

A final consideration is the role of asthenospheric upwellings in continental rifting processes. A review of current ideas is well beyond the scope of this chapter; I present only the points directly relevant to rifting and continental

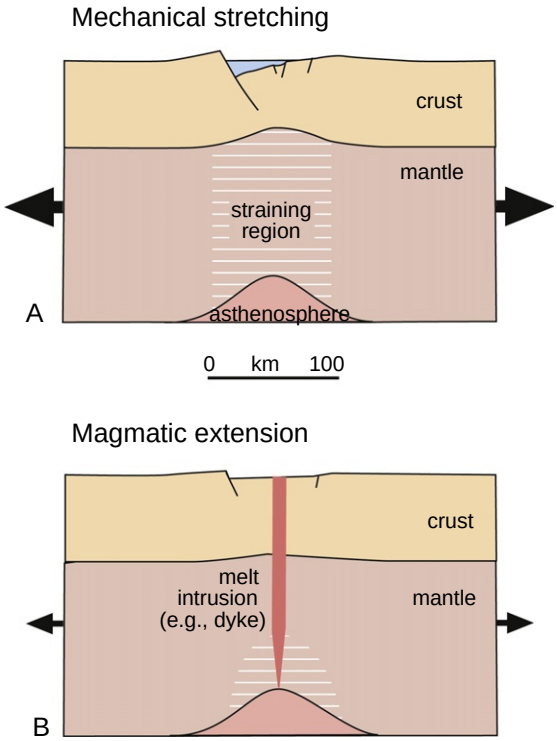

Figure 7.1
Cartoons of two general classes of conceptual models for extension of rheologically layered continental lithosphere. (A) Mechanical stretching models accommodate strain by large offset faults (e.g., detachments) in brittle layers, and by ductile deformation in weaker layers. (B) Magmatic extension models include effects of magma intrusion and accompanying heating. The strain localization and strength reduction are enhanced with melt intrusion. *(After Buck, 2004.)*

breakup. Zones of anomalously hot asthenosphere are susceptible to adiabatic decompression melting, but only small melt volumes (e.g., lamproites, kimberlites) will be produced beneath a thick continental lithosphere (e.g., Fischer et al., 2009; Harte et al., 1983). Although the continuity of shallow and deep mantle upwellings has been disputed, there is little controversy regarding the interactions of a variable thickness lithosphere with a convecting mantle. Regardless of the depth extent of the upwelling, numerical simulations demonstrate the focusing effects of preexisting variations in lithospheric thickness (e.g., King and Anderson, 1998; Sleep, 1996). Cratonic roots may deflect normal asthenospheric flow (Fouch et al., 2000); enhanced flow from a mantle plume concentrates stresses and melting at the craton margins (e.g., Sleep et al., 2002). Preexisting thin zones (e.g., failed rifts) pond and channel hot asthenospheric material, which is susceptible to adiabatic decompression melting. The spatial distribution of melting and strain is also sensitive to the initial lithospheric thickness and rheology (e.g., Burov and Guillou-Frottier, 2005).

Most of our observational record of rupture processes is derived from seismic profiles of ancient passive margins where the rupture zone is buried under thick post-rift sedimentary sequences and/or overprinted by secondary or later

tectonic processes. These data from passive margins provide fuzzy 2D images of the distribution of strain as rifting progresses to seafloor spreading, and we cannot discriminate between the increasingly more complex models for rupture of rheologically layered continental lithosphere (e.g., Burov and Poliakov, 2001; Huismans et al., 2005). The academic database is biased to margins with little or no volcanism, because relatively high-velocity basaltic lavas limit the depth penetration of sound waves. Yet, most passive margins worldwide show evidence of magmatic modification of the plate prior to or during continental breakup. Volcanic margins comprise thick, seaward-dipping wedges of basaltic lavas that mask the pattern of faults near the ocean-continent transition, as well as high-velocity lower crust interpreted as melt intruded at the crust–mantle interface (e.g., Hinz, 1981; Holbrook and Kelemen, 1993).

As outlined below, observations from youthful rifts with small amounts of extension as well as rifts approaching continental breakup allow us to test and refine current models for continental rupture in areas with a ready supply of magma, providing first-order constraints on the evolution of magmatic passive continental margins. The seismically and volcanically active East African rift system offers a viewpoint of breakup processes before the patterns of strain and magmatism are covered by oceans and sediments. I showcase results from the UK-led Project EAGLE in the northern Main Ethiopian rift (MER), one of the few areas worldwide that captures, on land, the ongoing transition from continental to oceanic rifting (e.g., Maguire et al., 2006). The East African rift system encompasses sectors in each stage of development, and with and without magmatism, providing an ideal laboratory to test current models.

7.3 Geodynamical and plate kinematic setting

Geophysical and geochemical data from the African continent provide compelling evidence for rifting above one or more Cenozoic mantle plumes, with controversy concerning the location, depth extent, and continuity of the hot asthenospheric material (e.g., Courtillot et al., 1999; Ebinger and Sleep, 1998; George et al., 1998; Nyblade et al., 2002). This controversy stems from gaps in data across this vast region, particularly in the region of the Western Rift System, as well as limitations in the resolution of global tomographic models (e.g., Montelli et al., 2004). The Afar triple junction, Ethiopian, Eastern, and Western rift systems transect the broad Ethiopia-Yemen and East African plateaus. The Turkana depression between the two plateaus marks a failed Mesozoic rift system, allowing the possibility that the plateaus are actually part of one large zone of uplift extending from southern Africa to the Red Sea, termed the "African superplume province" (e.g., Gurnis et al., 2000; Lithgow-Bertelloni and Silver, 1998; Nyblade and Robinson, 1994) (Fig. 7.3). Given the immense extent of the rift system, it is not surprising that local or regional studies have pointed to local or regional upwellings.

Seismic data derived from analyses of global and local earthquakes recorded on permanent stations and from temporary arrays in East Africa reveal the broad structure of both lithosphere and upper asthenosphere. Geophysical and geochemical data from the African continent provide compelling evidence that the uplifts and voluminous volcanic outpourings developed above anomalously hot asthenosphere, with controversy concerning the location, depth extent, and continuity of the hot asthenospheric material (e.g., Ebinger and Sleep, 1998; Furman et al., 2006; George et al., 1998; Nyblade et al., 2000; Rogers, 2006). This controversy stems from gaps in geochemical and geophysical data sets, as outlined below.

Global tomographic models and waveform modeling reveal a large-scale ridge-shaped low-velocity zone (e.g., Ni et al., 2005; Ritsema et al., 1999), beneath the anomalously high topography of southern Africa, termed the "African superplume" (Lithgow-Bertelloni and Silver, 1998; Nyblade and Robinson, 1994). The global mantle tomographic images of Ritsema et al. (1999) suggest that the large low velocity zone at the core-mantle boundary beneath southern Africa rises northeastward through the mantle to the upper mantle beneath East Africa, but critical gaps in data coverage prevent a direct link to the hot shallow asthenosphere beneath the East African region (e.g., Montelli et al., 2004; Ritsema et al., 1999).

Existing seismic data and tomographic models show hot asthenosphere beneath the East African rift system from southern Saudi Arabia (Benoit et al., 2003) through Ethiopia (Bastow et al., 2005; Knox et al., 1999) to central Tanzania (Ritsema et al., 1998; Venkataraman et al., 2004), with gaps along most of the length of the Western rift system. The lithospheric thin zone beneath the Afar depression is underlain by anomalously low velocity mantle that may persist to the 660-km discontinuity (Debayle et al., 2000; Montelli et al., 2004), although Benoit et al. (2003) argue that the hot asthenosphere probably is confined to depths shallower than 410 km beneath Arabia. Nyblade et al. (2000) note a depression of the 410-km discontinuity beneath the eastern side of the Tanzania craton and the Eastern Rift, and suggest that a >200-km-thick plume head underlies this area (Fig. 7.3). Weeraratne et al. (2003) examined the structure of the upper mantle beneath parts of the Western and Eastern rifts and the intervening Tanzania craton using Rayleigh wave tomography and found evidence for both a thick cratonic keel and a strong thermal perturbation that extends to 660 km, and perhaps even deeper locally. This deep-seated anomaly is interpreted as a plume stem centered around 4°S, 34°E, thus within the plume head province proposed by Nyblade et al. (2000) (Fig. 7.3). Heat flow data and estimates of lithospheric rigidity indicate that the lithosphere beneath the uplifted East African plateau away from the narrow rift valleys is relatively thick (>120 km) and cold (e.g., Ebinger et al., 1989; Nolet and Mueller, 1982; Nyblade and Pollack, 1992).

The geochemistry of Eocene-Recent eruptive products points to a mantle plume origin for the Ethiopia-Yemen flood basalt sequences, but the signal is less clear within the East African plateau region. Pik et al. (2006) compiled He^3/He^4 data from throughout Africa, and found clear evidence for a plume signature only in the Afar depression. The overlapping trace element and isotopic compositions of Ethiopian rift basalts (Bryce et al., 2003; Furman et al., 2006) with samples from the western Gulf of Aden (Deniel et al., 1994) and southern Red Sea rift (Barrat et al., 1998) support the presence of deep asthenospheric material as a source component in the Afar triple junction zone. Trace element and radiogenic isotopic data indicate melting of metasomatized lithospheric mantle in both the Western rift (e.g., Furman, 1995; Lloyd et al., 1985; Rogers et al., 1998) and the Eastern rifts (e.g., Macdonald et al., 2001; Paslick et al., 1996; Späth et al., 2001).

Tomographic models and wide angle seismic data from the Main Ethiopian and Kenya rift zones reveal mantle lithospheric thinning beneath the rift valleys, as well as anomalously hot asthenosphere beneath the regions. Tomographic models of Bastow et al. (2005) image a 75-km-wide, tabular low-velocity zone rising from depths of ~250 km to the base of the mantle lithosphere at about 65 km subsurface. This low-velocity zone broadens northeastward into the Afar depression where it merges with the regional low-velocity zone beneath the Afar depression (Bastow et al., 2005; Benoit et al., 2006). Green et al. (1991) image a zone of lithospheric thinning centered beneath the southern Kenya rift, but document an ~90-km-thick lithosphere thickness beneath the Eastern rift in southern Kenya. KRISP seismic studies show anomalously low velocities for seismic waves traveling through the uppermost mantle beneath the Eastern rift, as well as the Chyulu Hills Quaternary volcanic field, suggesting the presence of melt (e.g., Green et al., 1991; Prodehl et al., 1997; Ritter and Achauer, 1994). There are, as yet, few data to constrain upper mantle beneath the Western rift system (e.g., Nyblade et al., 2000; Ritsema et al., 1998).

7.4 Cenozoic rift systems of East Africa

The East African rift system comprises several discrete and diachronous rift sectors, with and without the surface expression of magmatism (Fig. 7.2). Rifting has progressed to seafloor spreading in parts of the Red Sea rift, and along the length of the Gulf of Aden rift, with incipient seafloor spreading in the northern and eastern Afar depression (e.g., Courtillot et al., 1999; Hebert et al., 1985; Wright et al., 2006) (Fig. 7.2). The Red Sea, Gulf of Aden, and MERs are superposed on the ~2500-m-high Ethiopia–Yemen plateau, and the Eastern and Western rift valleys are superposed on the ~1200-m-high East African plateau (Fig. 7.3). In contrast to the widespread volcanism observed in the Eastern Gregory (Kenyan) Rift System, volcanic provinces in the Western rift are areally and volumetrically small, leaving the vast majority of the Western rift devoid of magmatism (Fig. 7.2).

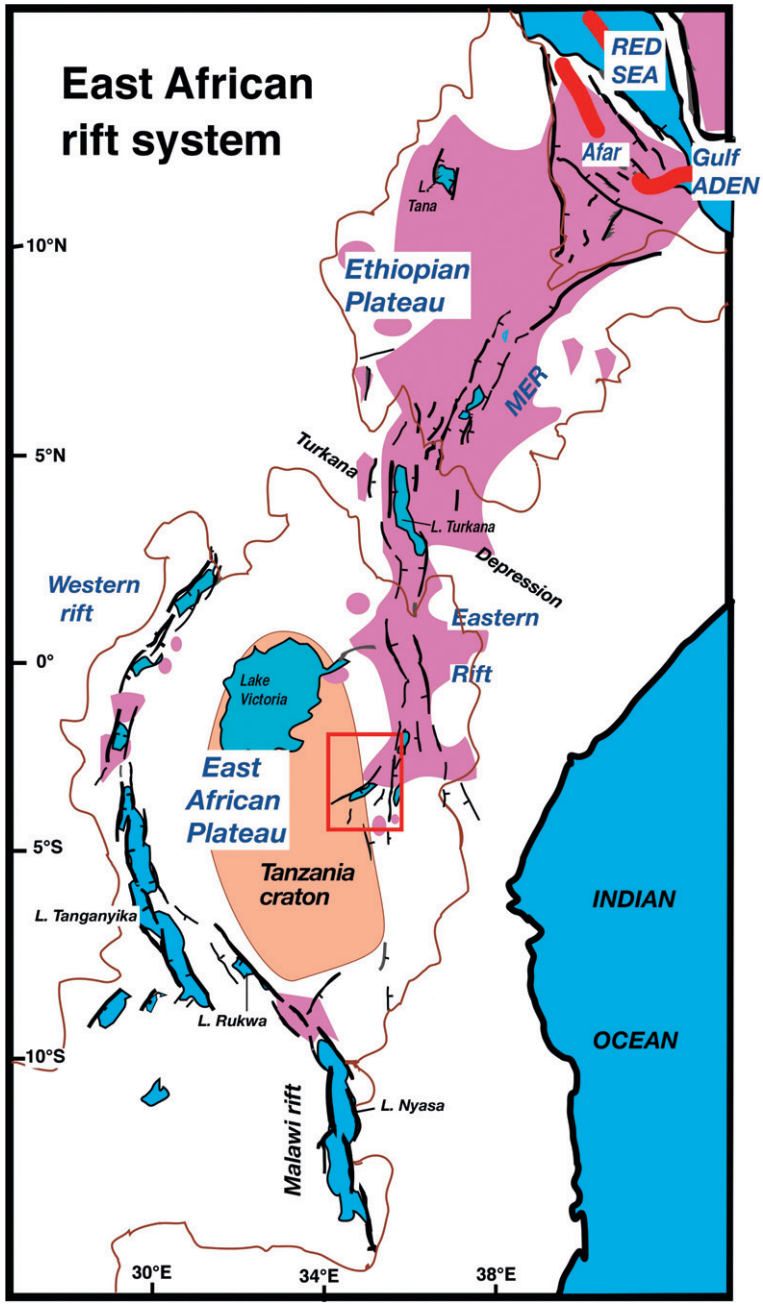

Figure 7.2
Major structures of the East African rift system, which extends from the Red Sea south to the Mozambique–South Africa border. The Tanzania craton is deeply rooted; the ~250-km-thick plate is stronger and colder than the adjacent lithosphere where the Western and Eastern rifts formed. The northern and eastern sides are characterized by much more voluminous magmatism. Red box encloses area of Fig. 7.4.

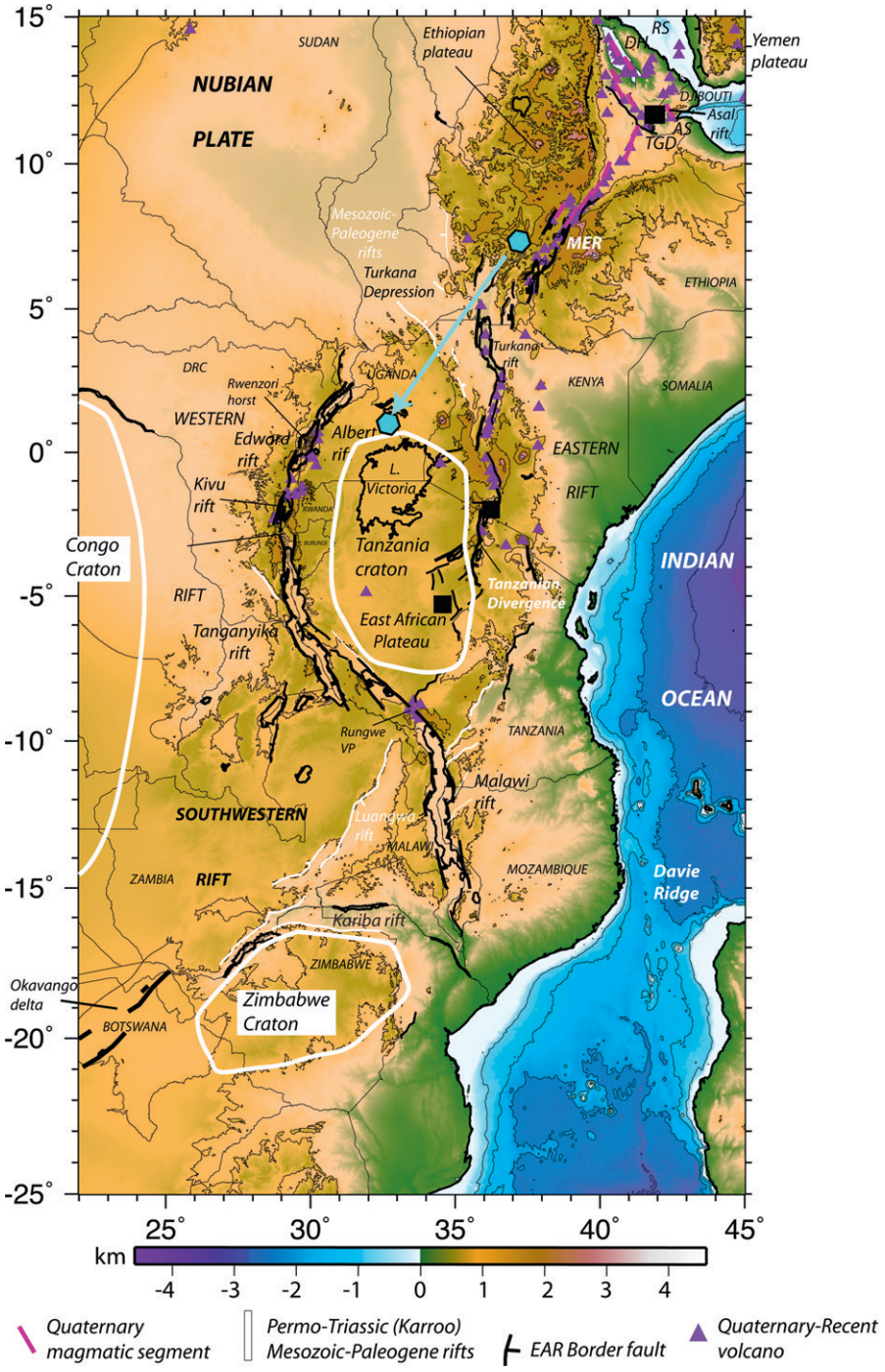

Figure 7.3 SRTM 1-km digital elevation model of the East African rift system region. Squares indicate the approximate central positions of plume heads and/stems proposed by Weeraratne et al. (2003); Nyblade et al. (2000); Courtillot et al. (1999); and Schilling et al. (1992). Octagons connected by arrows show predicted movement of Africa over the past 45 My relative to a fixed hotspot, as proposed by George et al. (1998) and modeled by Sleep et al. (2002).

The location of the East African rift system was influenced by the preexisting lithospheric structure (e.g., McConnell, 1972). The Western, Eastern, and Main Ethiopian, and Afar rifts developed in Archaean to late Proterozoic continental lithosphere, and largely within the Pan-African orogenic belt (Fig. 7.2). The age and structure of crystalline basement beneath the Ethiopian, southern Red Sea, and western Gulf of Aden rifts remain enigmatic; it is buried beneath 1–2 km of Cenozoic flood basalts and Mesozoic passive margin sequences. The Eastern and Western Rift formed near the eastern and western boundaries of the mechanically strong (e.g., Petit and Ebinger, 2000), cold (Nyblade and Pollack, 1992), and thick (e.g., Ritsema et al., 1998; Weeraratne et al., 2003) Archaean Tanzania craton, which is largely undeformed (Fig. 7.2). Although East African rift structures commonly cross-cut Permo-Triassic, Jurassic-Eocene rift systems associated with the breakup of Gondwana, they may have preferentially formed in these mechanically weaker zones (e.g., Petit and Ebinger, 2000; Morley, 1988).

7.5 Chronology of volcanism, uplift, and rifting

Radiometric age determinations of volcanic and volcaniclastic strata reveal consistent patterns in the spatial development of the rift systems. Earliest volcanism in the East African rift system (EARS) occurred in southwestern Ethiopia and northernmost Kenya between 45 and 37 Ma, based on $^{40}Ar/^{39}Ar$ dates (e.g., Ebinger et al., 2000; Knight et al., 2003) (Fig. 7.2). Although this Eocene phase of basaltic magmatism was accompanied by only localized warping, the flows lie near the eastern margin of a Palaeogene rift system extending through southern Sudan and reactivating parts of the Mesozoic Anza graben in northern Kenya (e.g., Hendrie et al., 1994; Vetel and LeGall, 2006). In contrast, the majority of the present-day EARS was magmatically quiet until the end of the Oligocene.

Between ~31 and 29 Ma, volcanism was widespread throughout the future sites of the Red Sea, easternmost Gulf of Aden, and the central Ethiopian Plateau, on the basis of a synthesis of $^{40}Ar/^{39}Ar$ data (Baker et al., 1996; Hofmann et al., 1997) (Fig. 7.2). During this period, up to 2 km of flood basalts and rhyolites were erupted throughout the southernmost Red Sea region. Flood basaltic magmatism occurred immediately after rift initiation in the Gulf of Aden at ~35 Ma (e.g., Watchorn et al., 1998), and just before rift initiation in the southern Red Sea at 28 Ma (e.g., Ukstins et al., 2002; Wolfenden et al., 2005). Volcanism continued outside the developing rifts until around 11 Ma (Kieffer et al., 2004). This Oligocene extension within the Red Sea and Aden rifts began separating Arabia from Africa, and is linked to the complex geometry of collision along the developing Alpine-Himalayan chain (e.g., Bellahsen et al., 2003). Thermochronology studies indicate that uplift of the Ethiopian plateau occurred at 30–25 Ma (Pik et al., 2004). The volcanic units overlying uplifted Mesozoic marine sequences now form a ~2500-m-high plateau on both sides of the southern Red Sea and western

Gulf of Aden (Fig. 7.3). Thus, the long-lived volcanism throughout the 1000-km-radius region suggests that the asthenospheric hot zone is also long-lived.

The connection between the Red Sea and Aden spreading centers and the MER is located within the complex Afar depression west of the Danakil microplate (e.g., Acton et al., 2000; Eagles et al., 2002) (Fig. 7.3). Although plate kinematic models of the Afar depression have assumed synchronous development of the Red Sea–Aden–East African rift systems in the Afar triple junction, new data from the MER indicate that the triple junction formed after 11 Ma (Wolfenden et al., 2004, 2005). As outlined below, the opening of the East African rift system occurred considerably after, and spatially distinct from, the Ethiopia–Yemen flood basaltic province and separation of Arabia from Africa.

The earliest extension documented in the EARS occurred in inactive basins west of present-day Lake Turkana at ~25 Ma, within lithosphere stretched during a Mesozoic rifting episode (Morley et al., 1992; Vetel and LeGall, 2006). This preexisting lithospheric "thin zone" may have ponded rising plume material, allowing small volumes of decompression melting at small stretching factors (e.g., Ebinger and Sleep, 1998; Hendrie et al., 1994). Mafic volcanism and faulting then propagated southward as the Eastern rift system formed, reaching central Tanzania by ~1 Ma (e.g., Baker, 1986; Foster et al., 1997). Rifting also propagated northward into Ethiopia, although not in a simple fashion: extension commenced at ~18 Ma in SW Ethiopia (e.g., Ebinger et al., 2002), but the central and northernmost sector of the MER, and therefore the Afar triple junction, developed after 11 Ma (Chernet et al., 1998; WoldeGabriel et al., 1999; Wolfenden et al., 2004).

The absence of datable material along large sections of the commonly water-filled Western Rift leads to more ambiguity, although a subtle north to south propagation of volcanism, and probably faulting, can be inferred. New exploration data from the Albert rift show that initial faulting and subsidence occurred at 18–20 Ma (Abeinomugisha and Mugisha, 2004). K–Ar dates from the Virunga province show that initial volcanism commenced at ~11 Ma, with initial volcanism in the nearby Kivu province becoming established by ~10 Ma (Kampunzu et al., 1998). $^{40}Ar/^{39}Ar$ dates from the Rungwe volcanic province at the southern margin of the Tanzania craton show that initial volcanism had begun by 8.6 Ma (Ebinger et al., 1989).

7.6 Kinematics of rifting

Active deformation within the Red Sea, Gulf of Aden, Ethiopian, Eastern, and Western rift systems splits the African plate into the Nubia and Somalia plates, as well as the Danakil microplate, but geodetic data are too unevenly distributed to constrain deformation within much of the uplifted region (e.g., Calais et al., 2006). Gripp and Gordon (2002) report an absolute plate motion vector for Africa of 285 ± 45° with rotation about a pole in the South Atlantic. Africa's slow NNW motion coincides with a regional north to south propagation of volcanism and extension along the Eastern and Western rift systems. There are, however, few

constraints on Africa's motion prior to 5 Ma (e.g., Jestin et al., 1994; Sella et al., 2002). Paleomagnetic data indicate that Africa has moved 700–1000 km in a northerly direction since 30 Ma (Rochette et al., 1998) (Fig. 7.3). Time-averaged patterns of seafloor-spreading anomalies in the Indian Ocean (Horner Johnson et al., 2005), and present-day sparse GPS data (Calais et al., 2006) both determine a Nubia-Somalia rotation pole located offshore South Africa and slow rotation rates of 0.09 to 0.07°/Myr, respectively.

The Afar depression hosts the Afar triple junction, an archetypal rift–rift–rift triple junction: the Red Sea, Gulf of Aden, and East Africa (Main Ethiopian) rift zones. Two parallel NNW-trending rifts, the broad subaerial Afar depression and southern Red Sea, had formed by Early Miocene time as Arabia separated from Africa (Fig. 7.2). Plate reconstructions and geodetic data show a NE–SW opening direction in the Red Sea and Gulf of Aden parts of the Afar depression. The NNE-trending MER is extending in a direction N108°E at 4 mm a^{-1} (Bilham et al., 1999) consistent with predictions of global plate motion data (e.g., Chu and Gordon, 1999). The NW-striking Tendaho (Manda)-Goba'ad fault zone acts as an incipient plate boundary connecting the southern and northern parts of the rift system in Afar which have been approximated to East African and Red Sea rifting, respectively (e.g., Hayward and Ebinger, 1996; Manighetti et al., 1998).

The structurally complex triple junction zone comprises a discontinuous system of seismically and volcanically active zones, with an apparent jump of seafloor spreading from the central Red Sea into the Afar depression at ~14N. The Danakil horst is a narrow, NW-trending ridge of Precambrian basement partly covered by Oligocene–Recent lavas of the Afar flood basalt province (e.g., Hofmann et al., 1997; Mohr, 1967).

The Danakil horst was first suspected as part of a microplate when reconstructions of the Red Sea in which it remains fixed with respect to Nubia caused it to overlap with Arabia (e.g., Le Pichon and Francheteau, 1978; Mohr, 1967). Courtillot et al. (1984) suggested that this overlap is the result of the variable stretching in continental crust of variable rheology by propagating rifts. Sichler's model for the opening of the Afar depression proposes that Danakil moved like a crank-arm between Euler poles at its northwestern and southeastern extremities, as though somehow "pinned" there to the separating Nubia and Arabia plates, respectively. The restricted geographical focus of later studies and their consideration of only Pliocene–Recent faults have given rise to conflicting assessments of the crank-arm model. Souriot and Brun (1992) found the crank-arm model to be consistent with fault patterns in southeastern Afar. Neogene fault kinematic data in the MER, however, do not show the strike-slip or highly oblique-slip motions predicted by the crank-arm model (e.g., Keir et al., 2006; Kidane et al., 2006). Acton et al. (2000) present paleomagnetic results from the Afar triple junction zone that do not support the crank-arm model. Eagles et al. (2002) suggest that independent movement of Danakil relative to Nubia, Arabia, and Somalia has become significant since ~5 Ma. The most recent,

statistically significant, independent movement of the Danakil microplate can be related to the onset of oceanic-type accretion in Afar that promoted the ongoing propagation of the neighboring plate boundaries (Eagles et al., 2002).

The lone geodetic profile constraining Nubia-Somalia opening is from the MER where differences in opening direction between models are very small (Bendick et al., 2006; Bilham et al., 1999). Direct measurements of Nubia-Somalia plate motion were made using a limited number of permanent Global Positioning System (GPS) stations on both plates (Fernandes et al., 2004; Sella et al., 2002). Again, these two GPS estimates differ significantly from each other, as well as from previous results derived from oceanic data (Fig. 7.3). Calais et al. (2006) jointly inverted earthquake slip vectors and continuous GPS data to estimate a new Nubia-Somalia Euler pole, and proposed that the Tanzania craton forms a CCW-rotating microplate (Victoria) between the Western and Eastern rift systems in response to plume-lithosphere interactions (e.g., Sleep et al., 2002).

Set within this regional framework, we can isolate parts of the East African rift system in different stages of development to trace the distribution of strain and magmatism as rifting progresses to seafloor spreading.

7.7 Rift structure

High-angle, 70–120-km-long border faults bounding commonly asymmetric basins up to 7 km deep have developed in Archaean to Pan-African lithosphere in East Africa (e.g., Ebinger et al., 1999; Karner et al., 2000). These fault systems show predominantly dip-slip movements, as supported by focal mechanism solutions of teleseismic events (e.g., Foster and Jackson, 1998; Nyblade and Langston, 1995). Intrabasinal faults are relatively widely spaced and accommodate a much smaller fraction of the displacement than do the border faults (e.g., Ebinger, 1989; Morley, 1988). In the Western Rift, all four volcanic provinces are found within accommodation zones where, presumably, deep faulting taps magmatic reservoirs.

There remains only sparse information on crustal thickness beneath the Western rift system. Receiver function estimates of crustal thickness are 30–35 km, indicating only minor crustal thinning has occurred (e.g., Last et al., 1997). Nolet and Mueller (1982) analyzed teleseismic arrivals at old WWSN stations in the Kivu-Virunga region to estimate an average crust and upper mantle structure beneath the northern Western rift system (1–10°N). They found crustal thickness of 35 km overlying upper mantle with low P- and S-wave velocities (4.5 and 7.7 km/s, respectively), consistent with surface wave tomography studies of Weeraratne et al. (2003) for the Tanganyika-Rukwa sectors.

In the Eastern rift system in Kenya, crustal stretching factors range from 1.8 beneath the multi-phase Turkana rift to 1.2 beneath the central Kenya rift (e.g., Ebinger et al., 1999; Keller et al., 1992). Reconstructions of basement-involved faults in Western rift basins where no seismic refraction data are available show small amounts of stretching (e.g., Ebinger, 1989; Morley, 1988). Karner

et al. (2000) model basin subsidence and gravity data from the Albert rift basin to the north, and predict 12–16 km of extension, or stretching factors <1.2. There are virtually no data, however, to constrain crustal thickness or stretching factors within the Virunga volcanic province.

Continental rift evolution

Below, I use specific examples from the East African rift system to trace the birth to breakup history of cratonic lithosphere interacting with a dynamically upwelling mantle. Clearly, these examples are chosen to illustrate the role of magmatic modification of continental lithosphere during progressive stages of continental breakup.

Birth

Figure 7.4 summarizes the birth sequence of a rift that forms in cold, strong continental lithosphere, exemplified by the <5 million-year-old Eastern rift system in Tanzania. Plate driving forces exert a horizontal pull on the thick plate, and cracks and extensional faults develop at the surface. The initial location of the fractures may be guided by preexisting weak zones in the lithosphere, such as the suture zone

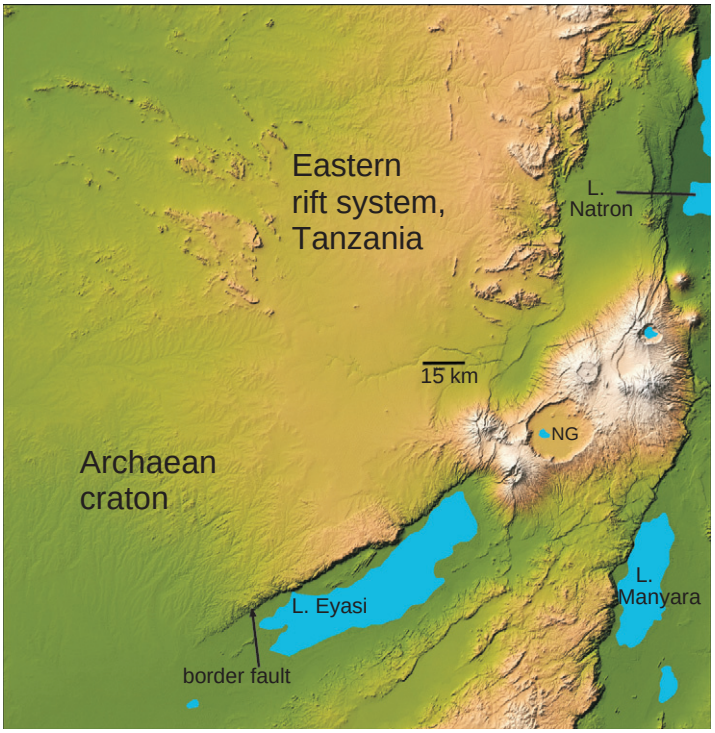

Figure 7.4 Shaded relief and colored height image of Space Radar Topography Mission data displayed as shaded relief and colored height. (Courtesy NASA/JPL-Caltech (PIA04959.) Location shown in Fig. 7.2.

between one of the oldest continental fragments on earth, the ~3-Ga Tanzania craton, and thinner, weaker 0.5-Ga lithosphere to the east (e.g., Foster et al., 1997). At the scale of individual faults, we can see a parallelism between NE-striking ancient shear zones and NE-striking normal faults on the craton, as well as the N–S-striking faults that are normal to the plate opening direction (e.g., image cover). The Eastern rift system bifurcates where it encounters and is probably deflected by the cold, thick, strong lithosphere of the ~3-Ga Tanzania craton (Fig. 7.4).

Geophysical data along a profile of the Magadi basin just north of the cover image reveal a few kilometers of crustal thinning beneath the 3.6-km-deep, asymmetric rift basin (Birt et al., 1997), and a narrow zone of thinned mantle lithosphere directly beneath the rift zone (Green et al., 1991). Seismic velocity information from both refraction and tomography experiments shows low-velocity mantle lithosphere beneath the rift, indicating the presence of a small melt fraction in the mantle (Birt et al., 1997; Green et al., 1991), and narrow high-velocity zones in the upper crust interpreted as cooled melt intrusions beneath the central rift (Ibs-von Seht et al., 2001).

The observed fault systems have grown from shorter fault segments that propagated along their length and linked with nearby faults, with the jagged but continuous pattern of N–S-striking faults bounding the Manyara and Natron basins forming only during the past 1 My (Foster et al., 1997). These N–S-striking faults clearly cross-cut the ancient NE-striking basement fabric, which is reutilized along some short linkage zones. Low relief and lack of seismic activity indicate that unfavorably orientated faults have been abandoned, like the ~5 million-year-old Oldonyo Ogol escarpment west of the Natron border fault system (Fig. 7.4). The rift immediately south of the area in Figure 7.4 is marked by diffuse seismicity and many parallel, small offset faults that are growing at the expense of other faults.

Studies along the length of the rift system in East Africa and worldwide have demonstrated that the dimensions of the basin and the flanking uplifts depend on the strength of the plate. With the growth and linkage of normal faults, their displacement increases, and one long fault system, the border fault, accommodates most of the extension across the basin, with small faults forming to accommodate bending of the plate into the depression created by the fault (Fig. 7.5A). The radius of curvature is a measure of plate strength; basin width is greater for stronger plates, which have border faults that penetrate to deeper crustal levels. There also will be an isostatic rebound of the plate to the changes in density across the deforming zone, and this slow rebound will occur across an area proportional to the strength of the plate. Broad flanks rising several kilometers above the surrounding region form in response to the mechanical denudation of the crust along the dipping fault surface, with the density of the material infilling the depression and erosion moderating the uplift response. This pattern commonly leads to the formation of long, narrow, and initially isolated lake basins

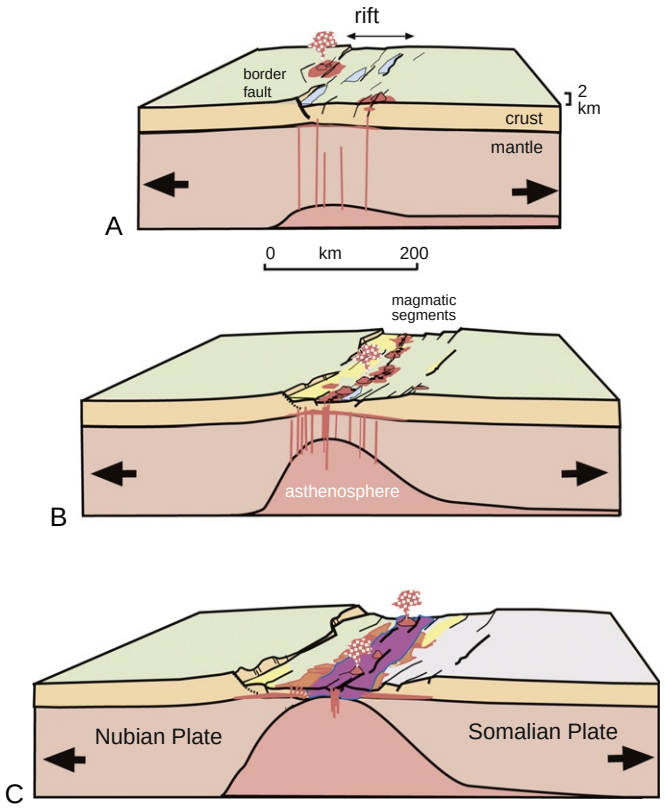

Figure 7.5 Three-stage model for continental breakup leading to the formation of a volcanic passive margin. The continental lithosphere beneath the region was initially heterogeneous, as represented by the greater thickness beneath the LHS. (A) 0–5 My after onset of rifting at the surface, the layered lithosphere has begun to thin through brittle and ductile deformation. The rise of asthenosphere to replace the thinning lithosphere transfers heat, and some decompression melting may occur. A small volume may reach shallow crustal levels (volcanoes) and some may be accreted at the compositional boundary between the crust and mantle lithosphere. Magmatic fluids modify and melt rocks at the base of the plate. Deformation in the brittle crust occurs by slip along the large offset border, or detachment, faults; the opposite side of the basin bends to accommodate the displacement. The changes in thickness of different density layers will lead to isostatic rebound of the basin and flanks, enhancing the asymmetry. (B) 10–15 My. With increasing time and strain, the lithosphere will continue to thin by faulting and ductile deformation. The asthenosphere beneath will rise to shallower levels, leading to more melting. This melt rises through the heated and weakened mantle lithosphere in cracks parallel to the faults at the surface. Strain localizes to a narrow zone marked by magmatic intrusions into the crust, a magmatic segment. The magma injection accommodates strain at lower tectonic stresses than faulting; the detachment faults are inactive. (C) Seafloor spreading. The tectonically and magmatically thinned lithosphere then ruptures in the heavily intruded zones, and new oceanic lithosphere is created. The thick piles of lavas in the magmatic segments load the weak plate, flexing it toward the new ocean basin to form seaward-dipping lavas. The passive margin subsides as heat transferred from the asthenosphere dissipates *(after Ebinger, 2005).*

whose faunal speciation patterns record the isolation and linkage patterns of the faults (Fig. 7.5A).

Gravity-topography relations indicate that the Tanzania craton is underlain by stronger lithosphere than beneath the younger belts surrounding the craton, with the weakest lithosphere beneath the only slightly stretched rift valleys (Petit and Ebinger, 2000). Earthquakes are distributed throughout the entire 35-km-thick crust, indicating that crustal heating is minimal (e.g., Foster and Jackson, 1998). The earthquakes are distributed along the 100–120-km-long fault systems bounding the ~50-km-wide sedimentary basins, and their focal mechanisms confirm that the plates are slowly opening across this zone in a direction normal to the faults.

Faulting and magmatism were coeval, with the earliest eruptive centers located on or near long, high-angle fault systems (Foster et al., 1997). Large shield volcanoes mark the intersection of discrete border fault systems, such as the 20-km-wide Ngorongoro crater. Fragments of deep lithosphere brought up in the lavas erupted from these volcanoes provide important clues on the pressure-temperature conditions and composition of the lithosphere beneath these volcanoes, and confirm the seismic tomography images of ~250-km-thick lithosphere beneath the center of the East African plateau (e.g., Chesley et al., 1999; Ritsema et al., 1998). The composition of the lavas and the mantle rock fragments indicates that lavas were generated by small volumes of melt beneath a ~140-km-thick lithosphere, and that the base of the lithosphere has been fundamentally altered by interaction with high-temperature fluids (e.g., Chesley et al., 1999).

Thus, geochemical, seismic, gravity, geodetic, structural, and earthquake data show that strain and magmatism are restricted to the fault-bounded rift valley within a few million years of rift initiation, with no detectable deformation in the broad uplifted plateau region outside the two rift arms. We can see the clear influence of preexisting heterogeneities in lithospheric structure on rift location. Strain has already localized to a few long faults that are oriented perpendicular to the plate opening direction, and many early stage, unfavorably oriented or located faults are abandoned. Erosion and deposition patterns will mask their presence as rifting progresses. The cross-sectional geometry of the youthful rift valley is asymmetric, with the highest flank adjacent to the deep side of the tilted basin. The along-axis segmentation pattern of the rift is largely controlled by the strength of the plate: strong plates have a narrow deformation zone comprising a long, wide basin; weak plates have a very broad deformation zone comprising many subparallel, short, narrow basins. Thus, the deep, narrow zone of deformation requires a strong upper mantle over the long time scales of geologic process. Small volumes of melt are generated beneath the rift by a combination of decompression melting of anomalously hot asthenosphere rising to fill the void created by stretching, and entrainment of rocks from the base of the plate that have been altered by high-temperature fluids.

Adolescence

The ~15 million-year-old basins of the central Eastern rift, or Kenya rift, represent the adolescence and early maturity of a rift system; here, crustal stretching approaches 10 km and the lithosphere has been thinned to about 90 km (e.g., Mechie et al., 1997). The rift basins show the classic asymmetry seen in the "Birth" stage, but new faults have initiated in the central basin cutting the <2 million-year-old central volcanoes. Most basins retain their asymmetric shape as the border faults bounding one side of the rift still accommodate strain, but new faults may form to link border faults, reversing the sense of basin asymmetry. Seismic and gravity data show a central zone of high-velocity, high-density material interpreted as solidified melt intruded to upper crustal levels, and reflective lower crust that indicates melt frozen at the crust-mantle interface (e.g., Mechie et al., 1997). Not only are the <2 million-year-old lavas derived from a shallower source, but they also show evidence for limited melting of the silica-rich crust (e.g., Macdonald, 1994). Small magnitude earthquakes located in the upper 15 km of the crust reveal a thinner brittle layer than that located to the south (e.g., Ibs-von Seht et al., 2001), and effective elastic thickness is less than in northern Tanzania.

Integrating these data, as the plate continues to stretch, the lithosphere–asthenosphere boundary rises, and the volume of decompression melting increases. Strain is accommodated both along the border faults, and by magmatic intrusion into the central rift valley above the zone of maximum lithospheric stretching. This magmatic intrusion transfers heat to the crust, and plate strength decreases still further.

Maturity to breakup

With increasing strain and decreasing lithospheric thickness, more melt should be generated as the asthenosphere rises and is decompressed. Melt will rise to shallower levels with time and heating, which then weakens the lithosphere, enhancing strain localization (Buck, 2004). All of these elements are evident in results of Project EAGLE; magmatic processes have fundamentally altered the crust and mantle lithosphere beneath the MER, which shows elements of both continental and oceanic rifting processes.

The MER is the northernmost sector of the East African rift system, which meets the NE-spreading Red Sea and Gulf of Aden rifts in the Afar depression (Fig. 7.2). The plate beneath the uplifted plateau was fundamentally modified at its top and internally by voluminous volcanic eruptions. Models of seismic refraction and wide-angle reflection data show a 10-km-thick, reflective, high-velocity layer at the base of the crust beneath the uplifted northern plateau, which Mackenzie et al. (2005) interpret as cooled basaltic melts that accumulated prior to extension across the MER. The thickness of the extruded and intruded lavas is much less on the southern side of the MER where upper mantle velocities are higher, suggesting that the location of the MER coincides with an ancient lithospheric-scale heterogeneity (e.g., Bastow et al., 2005).

Extension in the MER started at ~11 Ma with the initiation of high-angle border faults commonly marked by eruptive volcanic centers, with a progressive narrowing in the zone of deformation. Since 1.8 Ma, magmatism and faulting have become even more localized to ~20-km-wide, 60-km-long "magmatic segments" marked by aligned eruptive centers, fissures, and short faults in the central rift (e.g., Ebinger and Casey, 2001) (Fig. 7.3). At this point in rift evolution, the MER contains elements of strong plate and weak plate deformation: a new, shorter, narrower, and magmatic along-axis segmentation has developed within the broad basin defined by old, long border faults and broad flanks. Thus, spectral gravity-topography analysis techniques will provide an unrepresentative average of old and new effective elastic thicknesses.

The structure of the rift zone shown in Fig. 7.5B is on the basis of new geophysical data from the MER. Seismic and structural data show a 5-km-deep asymmetric basin tilted toward the large offset border fault system, as in the Eastern rift examples (Mackenzie et al., 2005). Velocity variations evident in refraction and 3D seismic tomography and gravity models show that the magmatic segments are underlain by high-velocity, high-density elongate bodies that rise to ~10 km subsurface, interpreted as cooled melt intrusions (Keranen et al., 2004; Tiberi et al., 2005). Upper crustal thinning beneath the rift is ~8 km, but the usually strong velocity contrast at the base of the crust is lacking beneath the magmatic segments (e.g., Mackenzie et al., 2005).

Seismic waves from distant earthquakes that sample the lithosphere and asthenosphere beneath the rift reveal strong evidence for melt directly beneath the surface expression of the rift. Low P- and S-wave upper mantle velocities are localized beneath a 150-km-wide zone centered on the MER (e.g., Bastow et al., 2005). Patterns of seismic velocity anisotropy determined from shear wave splitting studies constrain the distribution of melt in the mantle beneath the rift. The magnitude of anisotropy and its parallelism with aligned chains of volcanoes and fissures suggest the presence of melt-filled cracks throughout the lithosphere. The amount of splitting is highest beneath the rift flanks where gradients at the lithosphere–asthenosphere boundary are steepest, leading to enhanced melt extraction (Kendall et al., 2005), and the lithosphere is comparatively thicker, allowing a greater thickness over which to acquire anisotropy (Bastow et al., 2005).

The long record of volcanism in this region provides invaluable constraints on past and present processes, as well as the various depth levels of magma generation and storage. Major element compositions of some <2 My-old lavas indicate that they were derived from melting at 60–75-km depth subsurface (Rooney et al., 2005), consistent with the lithosphere–asthenosphere boundary interpreted in tomographic images (Bastow et al., 2005). Ayalew et al. (2006) demonstrate the increasing importance of crustal melting in the chemistry of quartz-rich lavas explosively erupted in alternation with the basaltic lavas. Shalllow magma reservoirs feeding volcanoes were not imaged in EAGLE data.

Geodetic data along a profile of the MER indicate that 80% of the present-day strain across the incipient plate boundary is accommodated across the magmatic segment (Bilham et al., 1999). Yet, the measured extensional velocity is about half that predicted by plate kinematic models. Analyses of earthquake data reveal the same strain deficit: earthquakes are too few and of too small a magnitude, indicating strain is accommodated aseismically (Hofstetter and Beyth, 2003). Most events occur in rift-parallel clusters concentrated around volcanoes and fissures at depths $<$10 km, and above the segmented magma intrusions (magmatic segments). Historic to recent seismicity shows that the border faults are largely aseismic. These patterns led Keir et al. (2006) to propose that present-day strain is accommodated by repeated episodes of aseismic magma injection into the crust. Short, small offset faults and dykes accommodate strain in the $\sim$10-km-thick seismogenic crust above the intrusions.

Seismic, geochemical, gravity, magneto-telluric, and structural data document melt and frozen melt in the asthenosphere, mantle lithosphere, crust, and surface of the MER (Fig. 7.5B). The ready supply of hot, weak magma reduces the thickness of competent layers and allows strain accommodation by magma intrusion and dyking at lower stress levels than are needed to activate the large displacement faults of the rift zone. As a result, border faults become inactive, and magma intrusion accommodates 50% or more of the strain. Small offset, short faults, and dykes develop in a narrow belt above the ever shallowing zone of magma intrusion, distributing strain across the brittle uppermost layer of the crust. Repeated eruptions from the volcanoes, aligned vents, and fissures in the narrow magmatic segments pile onto one another, effectively loading the weakened plate across a narrow zone. With time, the older lava flows will bend toward the rift axis, creating the base of the seaward-dipping wedge of lavas seen on passive margins worldwide (Fig. 7.6).

The combined interpretation of seismicity, structural, and magmatic patterns shows a clear riftward migration of strain away from the border faults to the progressively shallowing zone of melt intrusion in the central rift. A new along-axis segmentation accompanies the temporal decrease in lithospheric strength; this is a magmatic segmentation evident at all lithospheric levels, as predicted by Buck (2004). At this stage, the rift is functioning as a slow-spreading mid-ocean ridge, albeit sandwiched by continental lithosphere. With larger melt supply and/or increase in strain rate, new oceanic lithosphere will be formed in the magmatic segments, and the now heavily intruded, relatively thick crust and underlying mantle lithosphere will begin to subside below sea level (Fig. 7.5C).

Dynamical models

As described above, existing data from East Africa indicate that the Archaean Tanzania craton has acted as a mechanical obstacle to crustal extension, and probably to mantle flow. Numerical models of plume interactions with a variable thickness lithosphere indicate that this cratonic root may have deflected asthenospheric flow (Sleep et al., 2002), concentrating stresses and melting at the craton

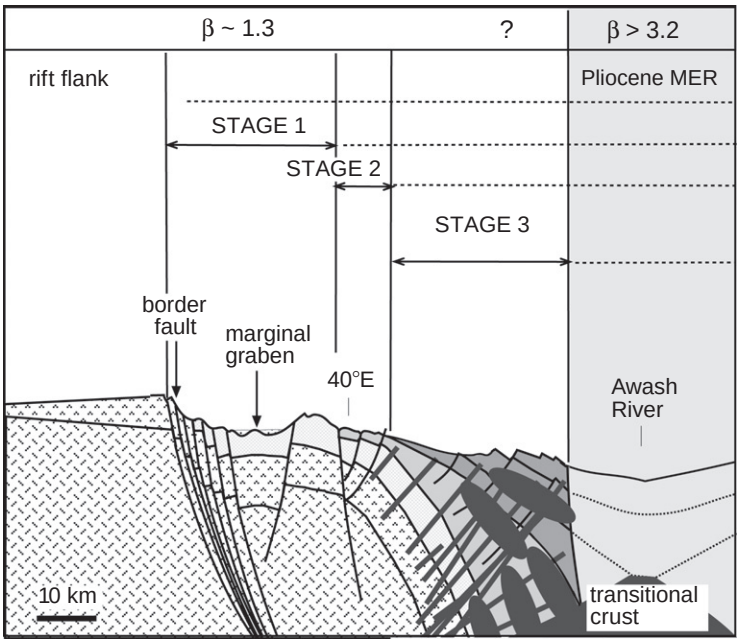

Figure 7.6 Summary schematic cross-section illustrating magmatic margin development of the southern Red Sea rift on the basis of topography at 10°50′N. Vertical exaggeration is 4:1. Stage 1 border faults developed between 29 and 26 Ma. By 15 Ma the locus of extension stepped eastward from the Stage 1 border fault system to localized zones of magmatic construction (Stage 2). By 7–8 Ma (Stage 3), another eastward jump in strain and magmatism occurred. Stage 3 comprises riftward-dipping successions, inferred to have evolved to Icelandic–type magmatic accretion. Stage 3 sequences are cut by numerous dikes, some of which have been rotated eastward. Riftward-dipping and offlapping flows of Stages 2 and 3 form a riftward-dipping wedge analogous to seaward-dipping reflector sequences imaged on volcanic margins worldwide. This pattern of strain migration from the border faults to localized dike injection zones argues against detachment fault models of breakup, and suggests that magma production drives strain localization, as predicted in numerical models (Buck, 2004). *(From Wolfenden et al., 2005.)*

margins (Nyblade and Brazier, 2002; Petit and Ebinger, 2000). The persistence of this thick cratonic keel leads to laterally variable chemistry of erupted lavas.

The fundamental ambiguity about East African rift magmatism is that the earliest volcanism occurred ~45 Ma in southwestern Ethiopia and northern Kenya, but the thickest and most rapidly extruded flows were erupted ~30 Ma along the margins of the Red Sea and Aden rifts. Given the ambiguity of existing plate kinematic constraints and critical data gaps, there are two classes of plume models for the development of the East African rift system. Ebinger and Sleep (1998) suggested that one large plume spread beneath the African plate near the Turkana rift at ~45 Ma, but that only small melt volumes were produced until lithospheric

thinning commenced in the Red Sea and Gulf of Aden. Preexisting zones of thinning channeled melt up to 1000 km from the plume's center into the evolving Red Sea rift, as well as beneath Mesozoic rift zones throughout eastern and central Africa. As Africa moved north over the plume stem and the plume head dispersed, smaller volumes and different compositions of melt were produced south of the original plume's center. The plume stem material would have been deflected west and east as the plume stem encountered the deep keel of the Tanzania craton (Sleep et al., 2002).

George et al. (1998) and Rogers et al. (2000) noted differences in the chemistry of rocks in southern Ethiopia, the Kenya rift, and the Afar region, and suggested that two distinct plumes had formed beneath Africa in Cenozoic time. Plume 1 rose and dispersed beneath southern Ethiopia at ~45 Ma, and the northern Plume 2 arose beneath the Afar depression, equivalent to the Afar plume of Schilling et al. (1992). Subsequent northeastward movement of Africa over the southern plume would place Plume 1's stem presently beneath the central Tanzania craton (Fig. 7.3), but there is no further discussion of the Plume 1 track. Other authors favoring a two-plume scenario have different interpretations as to the age and location of individual plumes. Nyblade et al. (2000) cite the deflection of the 410-km discontinuity as evidence for a modern spreading plume head beneath the central Tanzania craton, with hot material spilling up along the steep margins of the cratonic keel. The volume of warm material required to produce this deflection is interpreted as evidence for a young "Tanzanian plume" distinct from the Oligocene "Afar plume" or Plume 1, as the plume head for the ~30 Ma flood basalts would have dispersed by present day. Beneath the Afar region, recent detailed tomographic analyses (Benoit et al., 2003; Debayle et al., 2001; Montelli et al., 2004) indicate a narrow slow seismic anomaly that extends to depths of at least 300–500 km, suggesting that it may penetrate to the deep mantle. This apparently discrete "Afar plume" has either stayed fixed relative to the African plate since ~31 Ma (e.g., Courtillot et al., 1999), or it has left no clear plume track (e.g., George et al., 1998). Alternatively, it represents a complex interaction between lateral flow of plume material and newly formed spreading ridges in the Red Sea and Gulf of Aden (e.g., Sleep et al., 2002).

Information on mantle structures in East Africa comes from estimates of anisotropy from SKS-wave splitting data (Walker et al., 2004) that show fast directions organized in a pattern compatible with (1) asthenospheric flow around cratonic keels as Africa moves to the NNW in a hot-spot frame (Gripp and Gordon, 2002), and/or (2) lateral asthenospheric flow from a mantle plume located north of central Kenya (Ebinger and Sleep, 1998; Sleep et al., 2002). At a larger scale, Behn et al. (2004) model asthenospheric flow under Africa and propose that anisotropy could be generated in large part by density heterogeneities associated with the African superplume, a large-scale mantle upwelling rooted in the lower mantle beneath southern Africa (e.g., Ritsema et al., 1999). The deep-seated asthenospheric velocity anomaly of Ritsema et al. (1999) may be the deeper

continuation of the one large plume of Ebinger and Sleep (1998), or the second "Tanzanian" spreading plume head proposed by Nyblade et al. (2000), or the plume stem of Weeraratne et al. (2003) (Fig. 7.3).

Acknowledgments

I thank Eric Calais, Evgene Burov, Tanya Furman, Norm Sleep, Mike Kendall, Dave Waltham, and Derek Keir for thoughtful discussions of lithospheric deformation and mantle dynamics. CE acknowledges support from the Royal Society and NERC grants NER/A/S/2000/00563 and NER/.

References

Abeinomugisha, D., Mugisha, F., 2004. Structural analysis of the Albertine graben, Western Uganda, abstract, East African Rift System. Evolution, Resources, and Environment Conference, Addis Ababa, June, 2004.

Acton, G., Tessema, A., Jackson, M., Bilham, R., 2000. The tectonic and geomagnetic significance of paleomagnetic observations from volcanic rocks from central Afar. Earth Planet. Sci. Lett. 180, 225–241. doi:10.1016/S0012-821X(00)00173-4.

Ayalew, D., Bourdon, E., Ebinger, C., Wolfenden, E., Yirgu, G., 2006. Temporal compositional variation of early syn-rift rhyolites along the western Red Sea margin and northern Main Ethiopian rift. In: Yirgu, G., Ebinger, C., Maguire, P. (Eds.), The Afar Volcanic Province within the East African Rift System. Geol. Soc. Lond. Spec. Publ. 259, 121–130.

Baker, B., 1986. Tectonics and volcanism of the southern Kenya rift valley and its influence on rift sedimentation. In: Frostick, L.E. et al., (Eds.), Sedimentation in the African Rifts. Geol. Soc. Spec. Pub. 25, 45–57.

Baker, J., Snee, L., Menzies, M., 1996. A brief Oligocene period of flood volcanism in Yemen: implications for the duration and rate of continental flood volcanism at the Afro-Arabian triple junction. Earth. Planet. Sci. Lett. 138, 39–55.

Barrat, J.A., Fourcade, S., Jahn, B.M., Cheminée, J.L., Capdevila, R., 1998. Isotope (Sr, Nd, Pb, O) and trace element geochemistry of volcanics from the Erta' Ale range (Ethiopia). J. Volcan. Geotherm. Res. 80, 85–100.

Bassi, G., 1995. Relative importance of strain rate and rheology for the mode of continental extension. Geophys. J. Int. 122, 195–210.

Bastow, I., Stuart, G.W., Kendall, J.-M., Ebinger, C., 2005. Upper mantle seismic structure in a region of incipient continental breakup: northern Ethiopian rift. Geophys. J. Int. 162, 479–493.

Batiza, R., 1996. Magmatic segmentation of mid-ocean ridges: a review. Geol. Soc. Lond. Spec. Publ. 118, 103–130. doi:10.1144/GSL.SP.1996.118.01.06.

Behn, M.D., Conrad, C.P., Silver, P.G., 2004. Detection of upper mantle flow associated with the African Superplume. Earth Planet. Sci. Lett. 224, 259–274.

Bellahsen, N., Faccenna, C., Funiciello, F., Daniel, J.M., Jolivet, L., 2003. Why did Arabia separate from Africa? Earth Planet. Sci. Lett. 216, 365–381.

Bendick, R., McClusky, S., Bilham, R., Asfaw, L., Klemperer, S., 2006. Distributed Nubia–Somalia relative motion and dike intrusion in the Main Ethiopian Rift. Geophys. J. Int. 165, 303–310.

Benoit, M.H., Nyblade, A.A., VanDecar, J.C., Gurrola, H., 2003. Upper mantle P wave velocity structure and transition zone thickness beneath the Arabian Shield. Geophys. Res. Lett. 30 (10), 1531. doi:10.1029/2002GL016436.

Benoit, M., Nyblade, A.A., vanDecar, J.C., 2006. Upper mantle P-wave speed variations beneath Ethiopia and the origin of the Afar hotspot. Geology 34, 329–332. doi:10.1130/G22281.1.

Bilham, R., Bendick, R., Larson, K., Mohr, P., Braun, J., Tesfaye, S., et al., 1999. Secular and tidal strain across the Main Ethiopian Rift. Geophys. Res. Lett. 26 (18), 2789–2792.

Birt, C., Maguire, P.K.H., Khan, M.A., Thybo, H., Keller, G., Patel, J., 1997. The influence of pre-existing structures on the evolution of the southern Kenya rift valley: evidence from seismic and gravity studies. Tectonophysics 278, 211–242.

Bott, M.H.P., 1991. Sublithospheric loading and plate-boundary forces. Philos. Transact. A Math. Phys. Sci. Eng. 337 (1645), 83–92.

Bryce, J.G., Furman, T., Hanan, B., Ayalew, D., Yirgu, G., 2003. Magma genesis during continental rifting: isotopic constraints from Quaternary lavas of the Main Ethiopian Rift, Abstract. Trans. Am. Geophys. Union S52G-04.

Buck, W.R., 1991. Modes of continental extension. J. Geophys. Res. 96, 20161–20178.

Buck, W.R., 2004. Consequences of asthenospheric variability on continental rifting. In: Karner, G., Taylor, B., Driscoll, N., Kohlstedt, B. (Eds.), Rheology and Deformation of the Lithosphere at Continental Margins. Columbia University Press, New York, pp. 92–137.

Burov, E., Jaupart, C., Mareschal, J.C., 1998. Large-scale crustal heterogeneities and lithospheric strength in cratons. Earth Planet. Sci. Lett. 164, 205–219. doi:10.1016/S0012-821X(98)00205-2.

Burov, E., Guillou-Frottier, L., 2005. The plume head-continental lithosphere interaction using a tectonically realistic formulation for the lithosphere. Geophys. J. Int. 161, 469–490.

Burov, E., Poliakov, A.N.B., 2001. Erosion and rheology controls on synrift and postrift evolution, Verifying old and new ideas using a fully coupled numerical model. J. Geophys. Res. 106, 16461–16481. doi:0.1029/2001JB000433.

Byerlee, J., 1978. Friction of rocks. Pure Appl. Geophys. 116, 615–626.

Calais, E., Ebinger, C., Hartnady, C., Nocquet, J.M., 2006. Mantle-driven plate motions in the East African rift? In: Yirgu, G., Ebinger, C., Maguire, P. (Eds.), The Afar Volcanic Province within the East African Rift System. Geol. Soc. Lond. Spec. Publ. 259, 9–22.

Chernet, T., Hart, W.K., Aronson, J.L., Walter, R.C., 1998. New age constraints on the timing of volcanism and tectonism in the northern Main Ethiopian Rift-southern Afar transition zone (Ethiopia). J. Volcan. Geotherm. Res. 80, 267–280.

Chesley, J.T., Rudnick, R.L., Lee, C.T., 1999. Re-Os systematics of mantle xenoliths from the East African Rift; age, structure, and history of the Tanzanian Craton. Geochim. Cosmochim. Acta 63, 1203–1217.

Chu, D., Gordon, R.G., 1998. Current plate motions across the Red Sea. Geophys. J. Int. 135, 313–328.

Chu, C., Gordon, R., 1999. Evidence for motion between Nubia and Somalia along the Southwest Indian Ridge. Nature 398, 64–67.

Courtillot, V., Jaupart, C., Manighetti, I., Tapponnier, P., Besse, J., 1999. On causal links between flood basalts and continental breakup. Earth Planet. Sci. Lett. 166, 177–195.

d'Acremont, E., Leroy, S., Burov, E.B., 2003. Numerical modelling of a mantle plume: the plume-head lithosphere interaction in the formation of oceanic lithosphere. Earth Planet. Sci. Lett. 206, 379–396.

Debayle, E., Leveque, J.J., Cara, M., 2001. Seismic evidence for deeply rooted low-velocity anomaly in the upper mantle beneath the northeastern Afro/Arabian continent. Earth Planet. Sci. Lett. 193, 423–436. doi:10.1016/S0012-821X(01)00509-X.

Deniel, C., Vidal, P., Coulon, C., Vellutini, P.J., Piguet, P., 1994. Temporal evolution of mantle sources during continental rifting: the volcanism of Djibouti. J. Geophys. Res. 99, 2853–2869.

Déverchère, J., Houdry, F., Solonenko, F., Solonenko, A., Sankov, V., 1993. Seismicity, active faults, and stress field of the north Muya region, Baikal rift: new insights on the rheology of extended continental lithosphere. J. Geophys. Res. 98, 19895–19912.

Dunbar, J., Sawyer, D.S., 1989. Continental rifting at pre-existing lithospheric weaknesses. Nature 333, 450–452 (2 June 1988). doi:10.1038/333450a0.
Eagles, G., Gloaguen, R., Ebinger, C., 2002. Kinematics of the Danakil microplate. Earth Planet. Sci. Lett. 203 (2), 607–620.
Ebinger, C., 1989. Tectonic development of the western branch of the East African rift system. Geol. Soc. Am. Bull. 101, 885–903.
Ebinger, C.J., Deino, A.L., Drake, R.E., Tesha, A.L., 1989. Chronology of volcanism and rift basin propagation; Rungwe volcanic province, East Africa. J. Geophys. Res. 94, 15785–15803.
Ebinger, C., Sleep, N.H., 1998. Cenozoic magmatism in central and east Africa resulting from impact of one large plume. Nature 395, 788–791.
Ebinger, C.J., Jackson, J.A., Foster, A.N., Hayward, N.J., 1999. Extensional basin geometry and the elastic lithosphere. Philos. Trans. R. Soc. Lond. A 357, 741–765.
Ebinger, C., Yemane, T., Harding, D., Tesfaye, S., Rex, D., Kelley, S., 2000. Rift deflection, migration, and propagation: linkage of the Ethiopian and Eastern rifts. Afr. Geol. Soc. Am. Bull. 102, 163–176.
Ebinger, C.J., Casey, M., 2001. Continental break-up in magmatic provinces: an Ethiopian example. Geology 29, 527–530.
Ebinger, C.J., 2005. Continental breakup: the East African perspective. Astron. Geophys. 46, 2.16–2.21.
Fernandes, R.M.S., Ambrosius, R.A.C., Noomen, R., Bastus, L., Combrinck, L., Miranda, J.M., et al., 2004. Angular velocity of Nubia and Somalia from continuous GPS data: implications on present-day relative kinematics. Earth Planet. Sci. Lett. 222, 197–208.
Fischer, T.P., Burnard, P., Marty, B., Hilton, D.R., Furi, E., Palhol, F., et al., 2009. Upper-mantle volatile chemistry at Oldoinyo Lengai volcano and the origin of carbonatites. Nature 459, 77–80. doi:10.1038/nature 07977.
Foster, A., Ebinger, C., Mbede, E., Rex, D., 1997. Tectonic development of the N. Tanzania sector of the East African rift. J. Geol. Soc. Lond. 154, 689–700.
Foster, A.N., Jackson, J.A., 1998. Source parameters of large African earthquakes: implications for crustal rheology and regional kinematics. Geophys. J. Int. 134, 422–448.
Fouch, M.J., Fischer, K.M., Parmentier, E.M., Wysession, M.E., Clarke, T.J., 2000. Shear wave splitting, continental keels, and patterns of mantle flow. J. Geophys. Res. 105 (B3), 6255–6275. doi:10.1029/1999JB900372.
Frederiksen, S., Braun, J., 2001. Numerical modelling of strain localisation in the mantle lithosphere. Earth Planet. Sci. Lett. 188, 241–251.
Furman, T., 1995. Melting of metasomatized subcontinental lithosphere: undersaturated mafic lavas from Rungwe, Tanzania. Contrib. Mineral. Petrol. 122, 97–115.
Furman, T., Bryce, J.G., Rooney, T., Hanan, B.B., Ayalew, D., Yirgu, G.G., 2006. Plume heads and tails: 30 My of the Afar plume. In: Yirgu, G., Ebinger, C., Maguire, P. (Eds.), The East African Rift System Within the Afar Plume Province. Geol. Soc. London Spec. Pub. 259, 95–119. doi:10.1144/GSL.SP.2006.259.01.09.
George, R., Rogers, N., Kelley, S., 1998. Earliest magmatism in Ethiopia: evidence for two mantle plumes in one flood basalt province. Geology 26, 923–926.
Green, V., Achauer, U., Meyer, R.P., 1991. A 3D seismic image of the crust and upper mantle beneath the Kenya rift. Nature 354, 199–203.
Gripp, A.E., Gordon, R.G., 2002. Young tracks of hotspots and current plate velocities. Geophys. J. Int. 150, 321–361.
Gurnis, M., Mitrovica, J.X., Ritsema, J., van Heijst, H.J., 2000. Constraining mantle density structure using geological evidence of surface uplift rates; the case of the African Superplume. Geochem. Geophys. Geosyst. G3 (1) 1999GC000035.
Hayward, N., Ebinger, C.J., 1996. Variations in the along-axis segmentation of the Afar rift system. Tectonics 15, 244–257.

Hebert, L., Langston, C.A., 1985. Crustal thickness estimate at AAE (Addis-Ababa, Ethiopia) and NAI (Nairobi, Kenya) using teleseismic P-wave conversions. Tectonophysics 111, 299–327.

Hébert, H., Deplus, C., Huchon, P., Khanbari, K., Audin, L., 2001. Lithospheric structure of a nascent spreading ridge inferred from gravity data: the western Gulf of Aden. J. Geophys. Res. 106, 26345–26363. doi:10.1029/2000JB900391.

Hendrie, D.B., Kusznir, N.J., Morley, C.K., Ebinger, C.J., 1994. Cenozoic extension in northern Kenya; a quantitative model of rift basin development in the Turkana region. Tectonophysics 236, 409–438.

Hinz, K., 1981. A hypothesis on terrestrial catastrophes: wedges of very thick oceanward dipping layers beneath passive continental margins–their origin and paleoenvironmental significance. Geol. Jahrb. E22, 3–28.

Hofmann, C., Courtillot, V., Féraud, G., Rochette, P., Yirgu, G., Ketefo, E., et al., 1997. Timing of the Ethiopian flood basalt event and implications for plume birth and global change. Nature 389, 838–841. doi:10.1038/39853.

Hofstetter, R., Beyth, M., 2003. The Afar depression: interpretation of the 1960–2000 earthquakes. Geophys. J. Int. 155, 715–732. doi:10.1046/j.1365-246X.2003.02080.x.

Holbrook, W.S., Kelemen, P.B., 1993. Large igneous province on the US Atlantic margin and implications for magmatism during continental breakup. Nature 364, 433–436.

Horner-Johnson, B.C., Gordon, R.G., Cowles, S.M., Argus, D.F., 2005. The angular velocity of Nubia relative to Somalia and the location of the Nubia–Somalia–Antarctica triple junction. Geophys. J. Int. 162, 221–238. doi:10.1111/j.1365-246X.2005.02608.x.

Huismans, R.S., Podladchikov, Y.Y., Cloetingh, S.A.P.L., 2001. Transition from passive to active rifting: relative importance of asthenospheric doming and passive extension of the lithosphere. J. Geophys. Res. 106, 11271–11292.

Huismans, R., Buiter, S., Beaumont, C., 2005. Effect of plastic-viscous layering and strain softening on mode selection during lithospheric extension. J. Geophys. Res. 110, doi:10.1029/2004JB003114.

Ibs-von Seht, M., Blumenstein, S., Wagner, R., Hollnack, D., Wohlenberg, J., 2001. Seismicity, seismotectonics, and crustal structure of the southern Kenya rift-new data from the Lake Magadi area. Geophys. J. Int. 146, 439–453.

Jackson, J., McKenzie, D.P., 2008. New views on the structure and rheology of the lithosphere. J. Geol. Soc. 165 (2), 453–465.

Jestin, F., Huchon, P., Gaulier, J.M., 1994. The Somalia plate and the East-African Rift system – present-day kinematics. Geophys. J. Int. 116, 637–654.

Kampunzu, A.B., Bonhomme, M.G., Kanika, M., 1998. Geochronology of volcanic rocks and evolution of the Cenozoic Western Branch of the East African rift system. J. Afr. Earth Sci. 26 (3), 441–461.

Karner, G., Byamungu, B., Ebinger, C., Kampunzu, A., Mukasa, R., Nyakaana, J., et al., 2000. Distribution of crustal extension and regional basin architecture of the Albertine rift system. East Afr. Mar. Petrol. Geol. 17, 1131–1150.

Keir, D., Ebinger, C., Stuart, G., Daly, E., Ayele, A., 2006. Strain accommodation by magmatism and faulting at continental breakup: seismicity of the northern Ethiopian rift. J. Geophys. Res. 111, B05314, doi:10.1029/2005JB003748.

Keller, R., Braile, L.W., Davis, P.M., Meyer, R.P., Mooney, W., the KRISP Working Group, 1992. Kenya Rift International Seismic Project, 1989–90 experiment. EOS Trans. AGU 73, 345–347.

Kendall, M., Stuart, G., Ebinger, C., Bastow, I., Keir, D., 2005. Magma assisted rifting in Ethiopia. Nature 433, 146–148.

Keranen, K., Klemperer, S.L., Gloaguen, R., EAGLE Working Group, 2004. Three-dimensional seismic imaging of a protoridge axis in the Main Ethiopian rift. Geology 32, 949–952.

Kidane, T., Ebinger, C., Abebe, B., Platzman, E., Keir, D., Lahitte, P., et al., 2006. Palaeomagnetic constraints on continental breakup processes: observations from the Main Ethiopian rift. In:

Yirgu, G., Ebinger, C., Maguire, P. (Eds.), The Afar Volcanic Province within the East African Rift System. Geol. Soc. London Spec. Pub. 259, 165–184.
Kieffer, B., Arndt, N., Lapierre, H., Bastien, F., Bosch, D., Pecher, A., et al., 2004. Flood and shield basalts from Ethiopia: magmas from the African Superswell. J. Petrol. 45, 793–834.
King, S., Anderson, D.L., 1998. Edge-driven convection. Earth Planet. Sci. Lett. 160, 289–296. doi:10.1016/S0012-821X(98)00089-2.
Knight, K., Furman, T., Bryce, J., 2003. 40 million years of mafic volcanism in Turkana, Kenya: geochemical insights. EOS Trans. AGU 84 (46), Fall Meet. Suppl. Abstract S52J–04.
Knox, R., Nyblade, A., Langston, C., 1999. Upper mantle S velocities beneath Afar and western Saudi Arabia from Rayleigh wave dispersion. Geophys. Res. Lett. 25, 4233–4236.
Le Pichon, X., Francheteau, J., 1978. A plate-tectonic analysis of the Red Sea–Gulf of Aden area. Tectonophysics 46, 369–406.
Lithgow-Bertelloni, C., Silver, P., 1998. Dynamic topography, plate driving forces, and the African superswell. Nature 395, 269–272.
Lloyd, F.E., Arima, M., Edgar, A.D., 1985. Partial melting of a phlogopite-clinopyroxenite nodule from south-west Uganda: an experimental study bearing on the origin of highly potassic continental rift volcanics. Contrib. Mineral. Petrol. 91, 321–329.
Macdonald, R., 1994. Petrological evidence regarding evolution of the Kenya Rift Valley. Tectonophysics 236, 373–390.
Macdonald, R., Rogers, N.W., Fitton, J.G., Black, S., Smith, M., 2001. Plume-lithosphere interactions in the generation of the basalts of the Kenya Rift, East Africa. J. Petrol. 42, 877–900.
Mackenzie, G.D., Thybo, H., Maguire, P.K.H., 2005. Crustal velocity structure across the Main Ethiopian Rift: results from two-dimensional wide-angle seismic modelling. Geophys. J. Int. 162, 994–1006. doi:10.1111/j.1365-246X.2005.02710.x.
Maguire, P.K.H., Keller, G.R., Klemperer, S.L., Mackenzie, G.D., Keranen, K., Harder, S., et al., 2006. Crustal structure of the Northern Main Ethiopian Rift from the EAGLE controlled source survey; a snapshot of incipient lithospheric break-up. In: Yirgu, G., Ebinger, C., Maguire, P.K.H. (Eds.), The Afar volcanic province within the East African Rift System. Geol. Soc. London Spec. Pub. 259, 269–291.
Manighetti, I., Tapponnier, P., Gillot, P.Y., Jacques, E., Courtillot, V., Armijo, B., et al., 1998. Propagation of rifting along the Arabia-Somalia plate boundary; into Afar. J. Geophys. Res. 103, 4947–4974.
McConnell, R.B., 1972. Geological development of the East African rift system. GSA Bull. 83 (9), 2549–2572.
McKenzie, D., 1978. Some remarks on the formation of sedimentary basins. Earth Planet. Sci. Lett. 40, 25–32.
Mechie, J., Keller, G.R., Prodehl, C., Khan, M.A., Gaciri, S.J., 1997. A model for the structure, composition and evolution of the Kenya rift. Tectonophysics 278, 95–119. doi:10.1016/S0040-1951(97)00097-8.
Mohr, P.A., 1967. Major volcano-tectonic lineament in the Ethiopian rift system. Nature 213 (5077), 664–665.
Montelli, R., Nolet, G., Dahlen, F.A., Masters, G., Engdahl, E.R., Hung, S.H., 2004. Finite-frequency tomography reveals a variety of plumes in the mantle. Science 303, 338–343. doi:10.1126/science.1092485.
Morley, C.K., 1988. Variable extension in Lake Tanganyika. Tectonics 7, 785–801.
Morley, C.K., Wescott, W.A., Stone, D.M., Harper, R.M., Wigger, S.T., Karanja, F.M., 1992. Tectonic evolution of the northern Kenyan Rift. J. Geol. Soc. Lond. 149, 333–348.
Ni, S., Helmberger, D., Tromp, J., 2005. Three-dimensional structure of the African superplume from waveform modelling. Geophys. J. Int. 161, 283–294.
Nolet, G., Mueller, S., 1982. A model for the deep structure of the East African rift system from simultaneous inversion of teleseismic data. Tectonophysics 84, 151–178.
Nyblade, A.A., Owens, T.J., Gurrola, H., Ritsema, J., Langston, C., 2000. Seismic evidence for a deep upper mantle thermal anomaly beneath east Africa. Geology 28, 599–602.

Nyblade, A., 2002. Crust and upper mantle structure in East Africa: implications for the origin of Cenozoic rifting and volcanism and the formation of magmatic rifted margins. In: Menzies, M., Klemperer, S., Ebinger, D., Baker, J. (Eds.), Volcanic Rifted Margins. Geol. Soc. Amer. Spec. Paper 362, 15–26.

Nyblade, A.A., Brazier, R.A., 2002. Precambrian lithospheric controls on the development of the east African rift system. Geology 30, 755–758.

Nyblade, A., Robinson, S., 1994. The African superswell. Geophys. Res. Lett. 21, 765–768.

Nyblade, A.A., Langston, C.A., 1995. East African earthquakes below 20 km and their implications for crustal structure. Geophys. J. Int. 121, 49–62.

Nyblade, A.A., Pollack, H.N., 1992. A gravity model for the lithosphere in western Kenya and northeastern Tanzania. Tectonophysics 212, 257–267.

Nyblade, A.A., Knox, R.P., Gurrola, H., 2000. Mantle transition zone thickness beneath Afar; implications for the origin of the Afar Hotspot. Geophys. J. Int. 615–619.

Paslick, C., Halliday, A., Lange, R.A., James, D., Dawson, J.B., 1996. Indirect crustal contamination: evidence from isotopic and chemical disequilibria in minerals from alkali basalts and nephelenites from northern Tanzania. Contrib. Mineral. Petrol. 125, 277–292.

Petit, C., Ebinger, C., 2000. Flexure and mechanical behaviour of cratonic lithosphere: gravity models of the East African and Baikal rifts. J. Geophys. Res. 105, 19151–19162.

Pik, R., Marty, B., Carignan, J., Lave, J., 2004. Stability of the Upper Nile drainage network (Ethiopia) deduced from (U-Th)/He thermochronometry: implications for uplift and erosion of the Afar plume dome. Earth Planet. Sci. Lett. 215, 73–88.

Pik, R., Marty, B., Hilton, D.R., 2006. How many plumes in Africa? The geochemical point of view. Chem. Geol. 226, 100–114.

Prodehl, C., Ritter, J.R.R., Mechie, J., Keller, G.R., Khan, M.A., Jacob, B., et al., 1997. The KRISP 94 lithospheric investigation of southern Kenya – the experiments and their main results. Tectonophysics 278, 121–147. doi:10.1016/S0040-1951(97)00098-X.

Ritter, J.R.R., Achauer, U., 1994. Crustal tomography of the central Kenya rift. Tectonophysics 236, 291–304. doi:10.1016/0040-1951(94)90181-3.

Ritsema, J., Nyblade, A., Owens, T., Langston, C., Van Decar, J., 1998. Upper mantle seismic velocity structure beneath Tanzania: implications for the stability of cratonic roots. J. Geophys. Res. 103, 21200–21214.

Ritsema, J., van Heijst, H., Woodhouse, J., 1999. Complex shear wave velocity structure imaged beneath Africa and Iceland. Science 286, 1925–1928.

Rochette, P., Tamrat, E., Feraud, G., Pik, R., Courtillot, V., Ketefo, E., et al., 1998. Magnetostratigraphy and timing of the Oligocene Ethiopian traps. Earth Planet. Sci. Lett. 164, 497–510.

Rogers, N., Macdonald, R., Fitton, J.G., George, R., Smith, M., Barreiro, B., 2000. Two mantle plumes beneath the East African rift system: Sr, Nd and Pb isotope evidence from Kenya Rift basalts. Earth Planet. Sci. Lett. 176, 387–400.

Rogers, N.W., James, D., Kelley, S.P., DeMulder, M., 1998. The generation of potassic lavas from the eastern Virunga province, Rwanda. J. Petrol. 39, 1223–1247.

Rogers, N.W., 2006. Basaltic magmatism and the geodynamics of the East African rift system. Geol. Soc. Lond. Spec. Publ. 259, 77–93.

Rooney, T.O., Furman, T., Yirgu, G., Ayalew, D., 2005. Structure of the Ethiopian lithosphere: Xenolith evidence in the Main Ethiopian Rift. Geochim. Cosmochim. Acta 69 (15), 3889–3910. ISSN 0016-7037. doi:10.1016/j.gca.2005.03.043.

Rubin, A.M., 1992. Dike-induced faulting and graben subsidence in volcanic rift zones. J. Geophys. Res. 97 (B2), 1839–1858 doi:10.1029/91JB02170.

Schilling, J.G., Kingsley, R., Hanan, B., McCully, B., 1992. Nd-Sr-Pb isotopic variations along the Gulf of Aden: evidence for the Afar mantle plume-lithosphere interaction. J. Geophys. Res. 97, 10927–10966.

Sella, G.F., Dixon, T.H., Mao, A., 2002. REVEL: a model for recent plate velocities from space geodesy. J. Geophys. Res. 107 (B4), 2081. doi:10.1029/2000JB000033.

Sleep, N.H., 1996. Lateral flow of hot plume material ponded at sublithospheric depths. J. Geophys. Res. 101 (B12), 28065–28083. doi:10.1029/96JB02463.
Sleep, N., Ebinger, C., Kendall, M., 2002. Deflection of mantle plume material by cratonic keels. In: Fowler, C.M., Ebinger, C.J., Hawkesworth, C.J. (Eds.), Early Earth. Geol. Soc. Lond. Spec. Pub. 199, 135–150.
Sleep, N.H., 2003. Geodynamic implications of xenolith geotherms. Geochem. Geophys. Geosyst. 4 (9), 1079. doi:10.1029/2003GC000511.
Souriot, T., Brun, J.P., 1992. Faulting and block rotation in the Afar triangle, East Africa: the Danakil "crank-arm" model. Geology 20, 911–914.
Späth, A., Le Roex, A.P., Opiyo-Akech, N., 2001. Plume-lithosphere interaction and the origin of continental rift-related alkali volcanism – the Chyulu Hills volcanic province, southern Kenya. J. Petrol. 42, 765–787.
Tiberi, C., Ebinger, C., Ballu, V., Stuart, G., Oluma, B., 2005. Inverse models of gravity data from the Red Sea-Gulf of Aden-Ethiopian rift triple junction zone. Geophys J. Int. 163, 775–787.
Turcotte, D., Schubert, G., 2002. Geodynamics, second ed. Cambridge University Press, New York, 441 pp.
Ukstins, I.A., Renne, P.R., Wolfenden, E., Baker, J., Ayalew, D., Menzies, M., 2002. Matching conjugate volcanic rifted margins: 40Ar/39Ar chrono-stratigraphy of pre- and syn-rift bimodal flood volcanism in Ethiopia and Yemen. Earth Planet. Sci. Lett. 198, 289–306. doi:10.1016/S0012-821X(02)00525-3.
Venkataraman, A., Nyblade, A., Ritsema, J., 2004. Upper mantle Q and thermal structure beneath eastern Tanzania, East Africa, from teleseismic P wave spectra. Geophys. Res. Lett. 31, L15611 doi:10.1029/2004GL020351.
Vetel, W., LeGall, B., 2006. Dynamics of prolonged continental extension in magmatic rifts: the Turkana rift case study (N. Kenya). Geol. Soc. Lond. Spec. Publ. 259, 209–233. doi:10.1144/GSL.SP.2006.259.01.17.
Walker, K.T., Nyblade, A.A., Klemperer, S.L., Bokelmann, G.H.R., Owens, T.J., 2004. On the relationship between extension and anisotropy: constraints from shear wave splitting across the East African Plateau. J. Geophys. Res. 109, B08302, doi:10.1029/2003JB002866.
Watchorn, F., Nichols, G.J., Bosence, D.W.J., 1998. Rift related sedimentation and stratigraphy, southern Yemen (Gulf of Aden). In: Purser, B.H., Bosence, D.W.J. (Eds.), Sedimentation and Tectonics of Rift Basins: Red Sea–Gulf of Aden. Chapman and Hall, London, 663 pp.
Watts, A.B., Burov, E.B., 2003. Lithospheric strength and its relationship to the elastic and seismogenic layer thickness. Earth Planet. Sci. Lett. 213, 113–131. doi:10.1016/S0012-821X(03)00289-9.
Weeraratne, D., Forsyth, D., Fischer, K., Nyblade, A.A., 2003. Evidence for an upper mantle plume beneath the Tanzanian craton from Rayleigh wave tomography. J. Geophys. Res. 108.
Weissel, J.K., Karner, G.D., 1989. Flexural uplift of rift flanks due to mechanical unloading of the lithosphere under extension. J. Geophys. Res. 94, 13919–13950.
White, R., McKenzie, D., 1989. Magmatism at rift zones: the generation of volcanic passive continental margins and flood basalts. J. Geophys. Res. 94, 7685–7729.
WoldeGabriel, G., Walter, R.C., Hart, W.K., Mertzman, S., Aronson, J.L., 1999. Temporal relations and geochemical features of felsic volcanism in the central sector of the Main Ethiopian rift. Acta Vulcanol. 11, 53–67.
Wolfenden, E., Ebinger, C., Yirgu, G., Deino, A., Ayalew, D., 2004. Evolution of the northern Main Ethiopian rift: birth of a triple junction. Earth Planet. Sci. Letts. 224, 213–228.
Wolfenden, E., Ebinger, C., Yirgu, G., Renne, P., Kelley, S.P., 2005. Evolution of the southern Red Sea rift: birth of a magmatic margin. Geol. Soc. Amer. Bull. 117, 846–864.
Wright, T.J., Ebinger, C., Biggs, J., Ayele, A., Yirgu, G., Keir, D., et al., 2005. Magma-maintained rift segmentation at continental rupture in the 2005 Afar dyking episode. Nature 442, 291–294.

In this chapter

8

The Gulf of Suez rift basin

J.A.M.M. Peijs, T.G. Bevan,† J.T. Piombino‡*
*BP Exploration Operating Co. Ltd., Sunbury-on-Thames, Middlesex, United Kingdom
†BP Exploration Libya Ltd., Sunbury-on-Thames, Middlesex, United Kingdom
‡BP Egypt, Digla, Maadi, Cairo, Egypt

8.1 Introduction

The Gulf of Suez is one of the best studied examples of a continental rift in the world. It has been the subject of many excellent reviews of rift basins (e.g., Bosworth and McClay, 2001; Garfunkel and Bartov, 1977; Moustafa, 2002; Patton et al., 1994; Schutz, 1994). Superb rift margin exposures provided by outcrop on both sides of the modern gulf in the Eastern Desert and Sinai, in desert conditions, have enabled numerous studies of the rift geometry (Angelier, 1985; Bosence, 1998; Bosworth, 1994, 1995; Gawthorpe et al., 1997; Moustafa, 1976, 1995, 2002), rift tectono-stratigraphy (Gawthorpe and Hurst, 1993; Gawthorpe et al., 1994; Lambaise and Bosworth, 1995; Gupta et al., 1999; Jackson et al., 2002), pre-rift control on fault linkage (McClay and Khalil, 1998; McClay et al., 1998; Younes and McClay, 1998, 2002), and carbonate platform development (Burchette, 1988; Cross et al., 1998; James et al., 1988).

The Oligo-Miocene Gulf of Suez is the northern termination of the Gulf of Aden-Red Sea rift (Fig. 8.1) which developed as a result of the northeastward separation of the Arabian plate from the African plate (Bosworth and McClay, 2001; Cochran, 1983; Coleman, 1993, 1974; Girder and Southren, 1987; Hempton, 1987; Joffe and Garfunkel, 1987; McKenzie et al., 1970). Several authors (Bosworth and McClay, 2001; Evans, 1988; Moretti and Colletta, 1987; Patton et al., 1994; Richardson and Arthur, 1988; Steckler et al., 1988) have suggested that by the late middle Miocene, rifting became subdued in the Gulf of Suez as the opening of the Red Sea became linked to sinistral strike-slip displacement along the Gulf of Aqaba-Dead Sea transform fault system (Fig. 8.1). However, seismic and well data from the Gulf of Suez show that subsidence in the rift remained active through the Late Miocene to Pliocene. With the onset of movement on the Aqaba-Levant transform, a rotation in the stress field took place and extension in the Gulf of Suez rotated from northeast to northerly extension.

Phanerozoic Rift Systems and Sedimentary Basins DOI:10.1016/B978-0-444-56356-9.00007-9

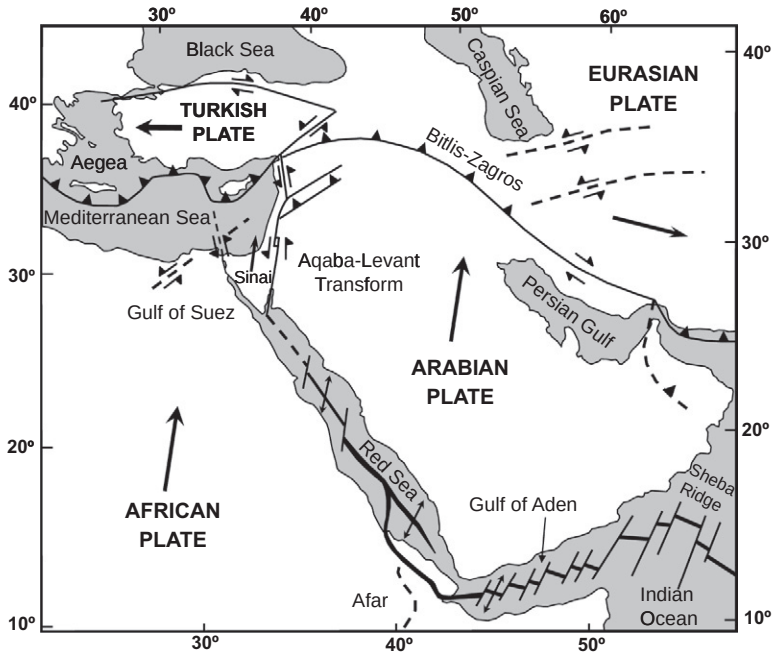

Figure 8.1 Plate tectonic setting of the Gulf of Suez *(modified after Bosworth and McClay, 2001).*

Since the mid-1960s, the Gulf of Suez Petroleum Company (GUPCO) has been one of the largest acreage holders and producers of hydrocarbons in the basin. As a result, GUPCO has a vast database from approximately 2000 wells drilled both onshore and offshore (cuttings, core, paleontological, petrographic, wire-line log, and production data), a regionally extensive two-dimensional and three-dimensional seismic database, gravity and aeromagnetic data, satellite imagery, and geological data from the outcrops on the rift margins. These data have been incorporated with those published to interpret the structural and stratigraphic development of the basin. The interpretations build from the details from the offshore well and seismic data to establish a regional framework. A series of new structural cross-sections have been constructed across the rift, which are constrained by two- and three-dimensional seismic data. Offshore well data have also enabled focus on the detailed syn-rift sedimentary facies distribution for the whole rift basin. Integrated use of all available data, especially from a subsurface, provides a modern view on this classic rift basin.

8.2 Megasequence description

The stratigraphic record of the Suez rift basin and its onshore continuation can be divided into five distinct tectonic megasequences: Paleozoic passive margin, Mesozoic rift to passive margin, Syrian Arc inversion, latest Oligocene to middle Miocene rift, and late Miocene to recent rift (Fig. 8.2). Each

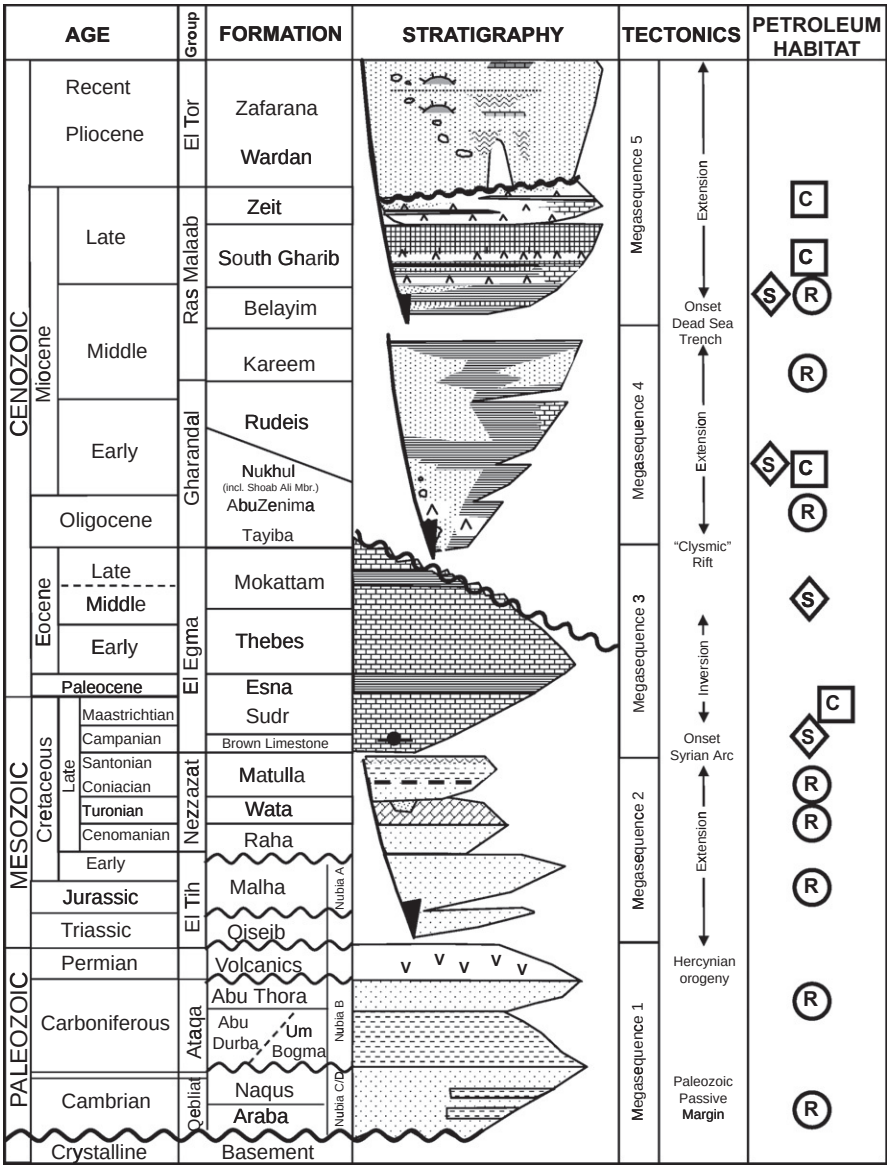

Figure 8.2 Tectono-stratigraphic section for the Gulf of Suez. For petroleum habitat, S, source; R, reservoir; C, seal.

megasequence is deposited during a complete and major phase of basin formation. They are bounded at the top and bottom by regional unconformities that mark the onset and end of the basin forming process. The megasequence is a single basin entity and its geometry defines the gross basin margins and depocenter.

Megasequence 1: Paleozoic (Cambrian to Permian)

In the Gulf of Suez, the Paleozoic is represented by the predominantly fluvial and shallow-marine "Nubian Sandstone" Group (Klitzsch and Squyres, 1990). Because of a lack of biostratigraphic markers, this sedimentary package is generally poorly age constrained, except for the presence of a Lower Carboniferous marine shale sequence in the central and southern Gulf of Suez region. This has been termed the Nubia B in the subsurface. In offshore petroleum industry data, the Paleozoic Nubia formations are generally termed the Nubia B, C, and D (Fig. 8.2), which have onshore equivalents in the Abu Durba, Naqus, and Araba Formations, respectively (Klitzsch, 1990). However, because of the lack of biostratigraphic control, the "Nubia" or "Nubian" term is broadly applied to an undifferentiated group of clastic sediments ranging in age from Cambrian to Early Cretaceous.

The Paleozoic Nubia extends across most of the Gulf of Suez area, but with two exceptions. First on the margins of the rift, in the Red Sea Hills and Sinai, the Paleozoic has been removed because of Cenozoic rift-related thermal uplift which has exposed basement at the present-day surface. Second, the Paleozoic is absent in the surface and subsurface in the southernmost part of the Gulf of Suez. A combined isopach of the Nubia Group (Fig. 8.3) illustrates the assumed edge of the sequence in the south and a gradual northward thickening to a sequence of over 1000 m in the north. It is unknown whether the absence of the Nubia in the south is due to non-deposition or erosion; the speculative basement feature termed the Ras Mohammed Arch might indicate removal of the Nubia through uplift. Figure 8.4 is a NNW–SSE cross-section along the present rift basin, demonstrating the stratigraphic relationships in the pre-rift sequences. The broad northward thickening of the Paleozoic would suggest that this is caused by regional northward tilting associated with Neo-Tethyan margin development (Patton et al., 1994, their Fig. 8.2). Patton et al. (1994) also suggested that a Hercynian event uplifted the Kharga Arch (their Fig. 8.4), lying to the southwest of the Ras Mohammed Arch. A Hercynian event is also a plausible explanation for the thinning of the Paleozoic section in the south of the Gulf of Suez as is widely observed throughout North Africa.

Megasequence 2: Jurassic to Coniacian

Jurassic age sediments present in the Gulf of Suez were deposited in a broad passive margin setting during the opening of the Neo-Tethys Ocean (Kerdany and Cherif, 1990). In addition, somewhat isolated growth-fault controlled depocenters are scattered across the Western Desert (see Bevan and Moustafa, 2012), the modern Nile delta, and across the Northern Gulf of Suez.

Jurassic marine sediments are only known in the northern Gulf of Suez from outcrops south of Ain Sukhna and from wells in the Darag basin, for example, Ayun Musa-2 (Schutz, 1994). The Jurassic stratigraphy is similar to that in the Western Desert (Bevan and Moustafa, 2012), where the predominantly carbonate

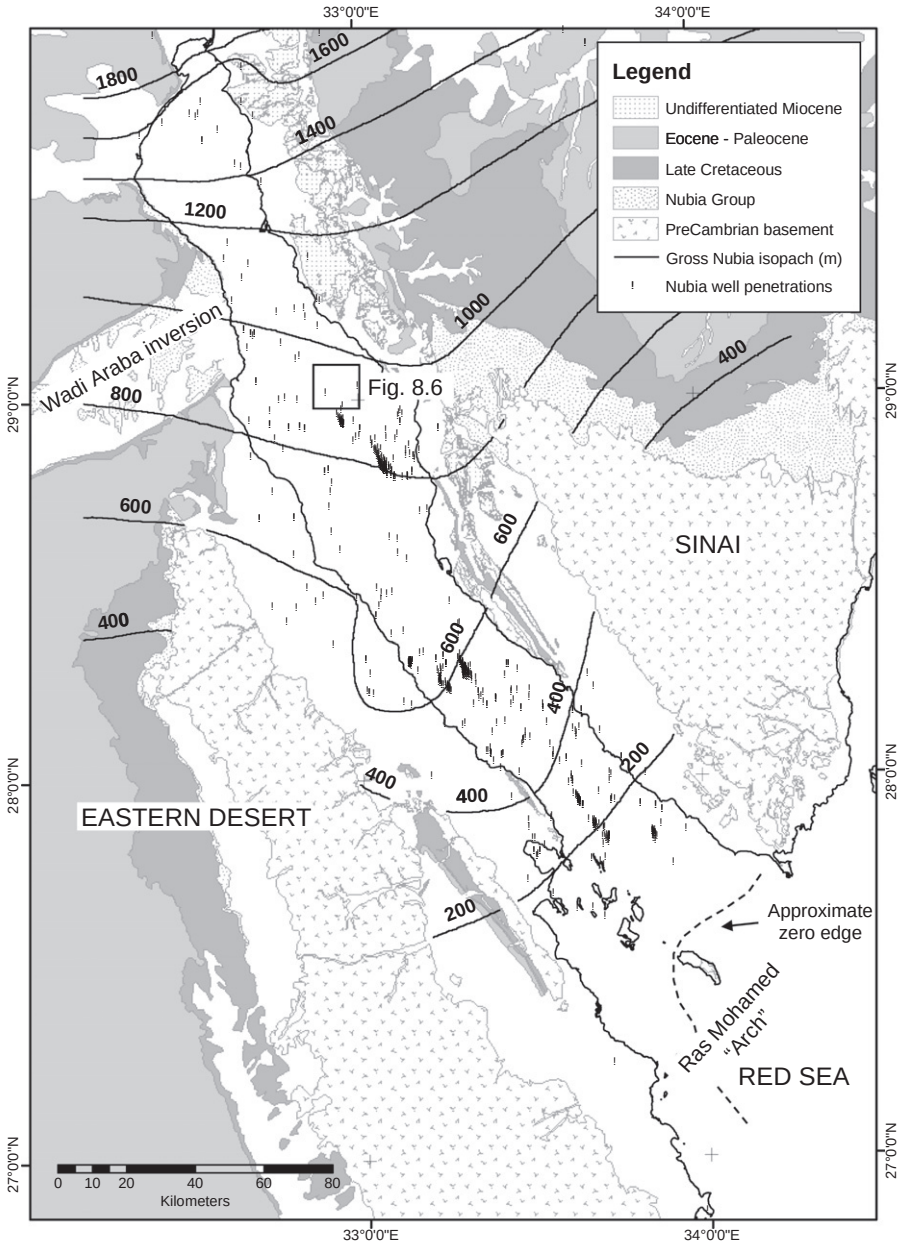

Figure 8.3
Nubia isopach map (CI = 200 m), based on offshore well penetrations.

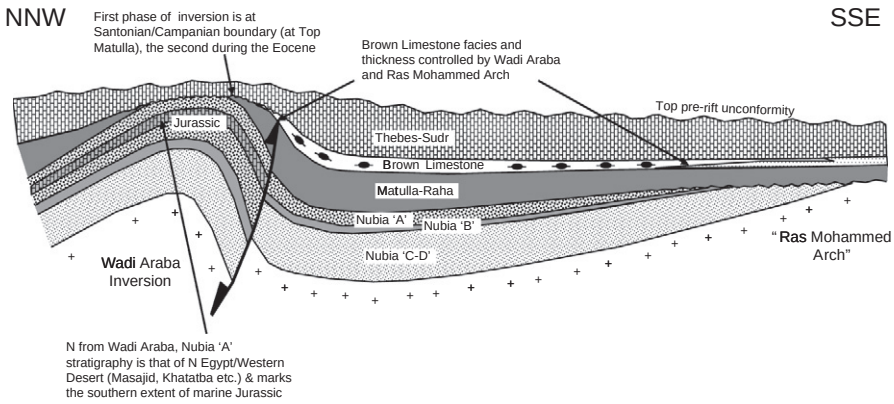

Figure 8.4 NNW–SSE schematic strike cross-section along the Gulf of Suez illustrating pre-rift stratigraphic relationships (not to scale). See Fig. 8.3 for locations of the Wadi Araba inversion and Ras Mohammed Arch.

Masajid Formation, of Upper Jurassic (Callovian-Bathonian) age, overlies the Middle Jurassic (Bajocian) Khatatba and Lower Jurassic Bahrain Formations. The Masajid Formation is a widespread unit recognizable along the northern African shelf of the Western Desert to Northern Sinai and far into Arabia and represents uniform sedimentation and transgression on the southern margin of the Tethys (Schutz, 1994). As documented by Bevan and Moustafa (2012), the Jurassic half-graben bounding faults were later inverted by the Santonian "Syrian Arc" event. In the Gulf of Suez, the Wadi Araba structure is a Jurassic to Late Cretaceous half-graben which has been subsequently inverted (Fig. 8.4), and is one of a series of WNW–ENE trending of half-graben which developed across northern Egypt (Bevan and Moustafa, 2012).

At the onset of the Cretaceous, the Gulf of Suez remained in a proximal passive margin setting. During this period, five formations were deposited: the Malha Formation (Nubia A in the subsurface terminology) and the Nezzazat group consisting of the Raha, the Abu Qada, the Wata, and the Matulla formations (Fig. 8.2). The Early Cretaceous age Malha Formation unconformably overlies the Abu Durba Formation, and oversteps, from south to north, pre-Carboniferous, Carboniferous, Permian, and Jurassic sediments (Fig. 8.4). It is mainly composed of medium to coarse, cross-bedded red sandstones deposited in a braided-river environment, with occasional shale and rare limestone layers (Schutz, 1994). The overlying Nezzazat Group consists of varying sandstones, carbonates, and shales, and is age equivalent to the Abu Roash Group of the Western Desert (Bevan and Moustafa, 2012). It represents an overall transgressive sequence on the passive margin of the Tethys Ocean.

Megasequence 3: Santonian to Late Eocene (syn-Syrian arc)

Megasequence 3 comprises the carbonate-dominated interval represented by the Sudr, Esna, Thebes, Darat, Khaboba, Tanka, and Mokattam Formations (see Said, 1990a,b). Following deposition of the Nezzazat Group, the first

Syrian-Arc inversion event occurred which resulted in folding, faulting, and uplift. The Santonian and older formations are eroded in the cores of the inversion anticlines, as at Wadi Araba on the western side of the Gulf of Suez (Moustafa and Khalil, 1995). The base of the megasequence is marked by a major angular unconformity between the Campanian Brown Limestone Member and Matulla Formation, indicating that the first major phase of inversion occurred at the end of Matulla deposition in the Late Santonian (Fig. 8.4).

The impact of the Santonian inversion on the thickness of formations and subsequent growth of the structures during the Late Senonian to Eocene can be seen from isopachs around the Wadi Araba anticline on the northern Gulf of Suez. Bevan and Moustafa (2012; Fig. 4, this volume) illustrate a series of isopach maps, on the basis of well data, of the Santonian-Coniacian age Matulla Formation, the Maastrichtian-Campanian Sudr Formation, and the Paleocene and Eocene age Esna and Thebes Formations. The Matulla and Sudr Formation isopachs are regionally uniform to the south and east of the Wadi Araba structure. However, toward this structure the isopach thins to zero, as the formation has been removed because of erosion over its crest. By contrast, the Esna and Thebes Formation isopachs increase in thickness toward the inversion structure before thinning over the crest. Here, local depocenters developed in front of the inversion structure. The growth of the Wadi Araba structure significantly impacted on facies distributions; well data show that the Brown Limestone, the major oil-prone carbonate source rock for the Gulf of Suez, is absent north of a line defined by the southern edge of the inversion structure. This suggests that the structure provided topographic relief which controlled the distribution of organic matter and resulting source facies.

During deposition of the Sudr Formation, the open-marine conditions of the brown-limestone continued, resulting in the deposition of uniform massive white chalk beds. The Esna Formation is a relatively thin shale unit. The absence of several fossil zones suggests that sedimentation was discontinuous across the Cretaceous–Tertiary boundary. The interbedded limestones and chert of the Lower Eocene Thebes formation reveal the beginning of a major flooding event. These carbonates are deposited over wide areas across Egypt and essentially infill any remaining Syrian-Arc topography. Although several limestone-shale formations of Middle Eocene age overlie the Thebes formation (Darat, Khaboba, Tanka, and Mokattam), they are frequently absent in the Gulf of Suez because of erosion on the crests of the tilted fault blocks developed in the later rift phase.

Megasequence 4: Latest Oligocene to Middle Miocene (rift phase)

This megasequence defines the modern rift basin of the Gulf of Suez. Basaltic dikes, sills, and flows along the margins of the rift have commonly been cited as evidence for initiation of rifting. Absolute ages of flows range from

between ±22 and ±24 Ma (Montenat et al., 1986; Moussa, 1987; Steen, 1984). Montenat et al. (1988) reported basalt pebbles with radiometric dates of 25–26 Ma at the base of the red beds in Wadi Nukhul. Bosworth and Burke (2004) suggested that Tertiary magmatism occurred as a regional dyke event in Sinai and Arabia between 24 and 20 Ma, propagating 2000 km from Eritrea to Egypt, possibly in less than 1 Ma. Syn-tectonic strata associated with the dikes are the Abu Zenima and Nukhul Formations in the Gulf of Suez, of early Miocene age. Extension during this phase was rift-normal, perpendicular to the dike system. At about 20 Ma, the rift shoulders were exhumed (Omar et al., 1989), synchronous with rapid subsidence and the main phase of syn-sedimentary deposition. Marginal marine to marine sediments of the Rudeis and Kareem Formations were deposited through to approximately 14 Ma (Richardson and Arthur, 1988; Wescott et al., 1997). The syn-rift sedimentary sequence is subdivided into four main formations; the Nukhul, Lower Rudeis, Upper Rudeis, and Kareem Formations (Fig. 8.2). The detailed tectono-stratigraphic evolution of these formations is described in the next section with the aid of subsurface data from the entire basin.

Megasequence 5: Late Miocene to Recent

The onset of the youngest syn-rift megasequence is contemporaneous with the onset of the Dead Sea/Levant transform boundary at approximately 14 Ma (Serravalian). It is distinct from the Oligo-Miocene phase of rifting in both extent and later, stress field orientation. Extension during the later stages of rifting is confined to the major linked coastal fault system, which defines the present marine gulf, and has an extension direction approximately NNE–SSW to N–S. This extension direction is parallel to movement along the Aqaba-Levant transform and hence rifting became oblique to the main rift-parallel faults.

A subsidence history plot (Fig. 8.5) from the rift shows that there is a dramatic increase in the subsidence rate from approximately 10 Ma. Many workers (Bosworth et al., 1988; Evans, 1988; Garfunkel and Bartov, 1977; Richardson and Arthur; 1988; Steckler et al., 1988) interpret a dramatic decrease in tectonic subsidence during the Serravalian as resulting from a shift of the Sinai-Africa plate boundary to the Gulf of Aqaba-Dead Sea Transform. Major evaporite deposition due to marine basin evaporation began during the Serravalian and continued into the Pliocene. This was possibly because of a rotation of the Sinai microplate and compression between Sinai and Africa (Bosworth and McClay, 2001; Patton et al., 1994), associated with drag along the Aqaba-Levant transform, leading to restriction of the marine connection of the Gulf of Suez with the Mediterranean (in addition to globally falling sea level, Haq et al., 1987). Thick Pliocene clastics and evaporites were then rapidly deposited in the main basin depocenters, and in the southern Gulf of Suez halite became mobilized by subsequent sediment loading to form salt diapirs and salt walls (Orszag-Sperber et al., 1998) that are focused along the crests of pre-rift fault block footwall highs.

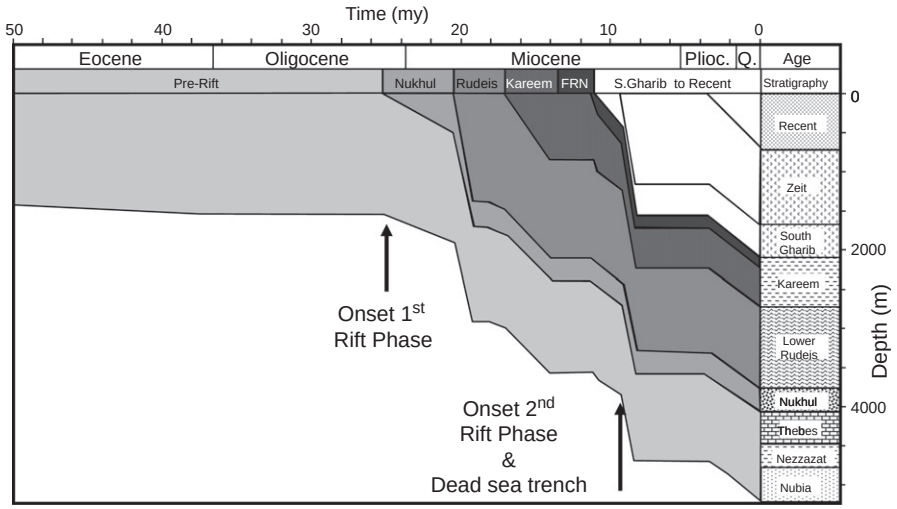

Figure 8.5
Subsidence history plot of a North October area well *(source: GUPCO).*

During very latest rift extension in the Quaternary, Bosworth and McClay (2001), Bosworth and Steckler (1997), and Bosworth and Taviani (1996) note that the extension direction in the Gulf of Suez had rotated from N60°E to N15°E, from paleostress indicators in raised Pleistocene reefs in the southern Gulf of Suez, and to N–S from wellbore breakout data from the central gulf. In the northern gulf, around the Abu Zenima area, we also see evidence of the influence of stress rotation on fault patterns in the subsurface. Figure 8.6 is an amplitude extraction of the shallow section just below the water bottom. The gray scale is chosen to give an image, similar to coherency, to display a clearer recent fault

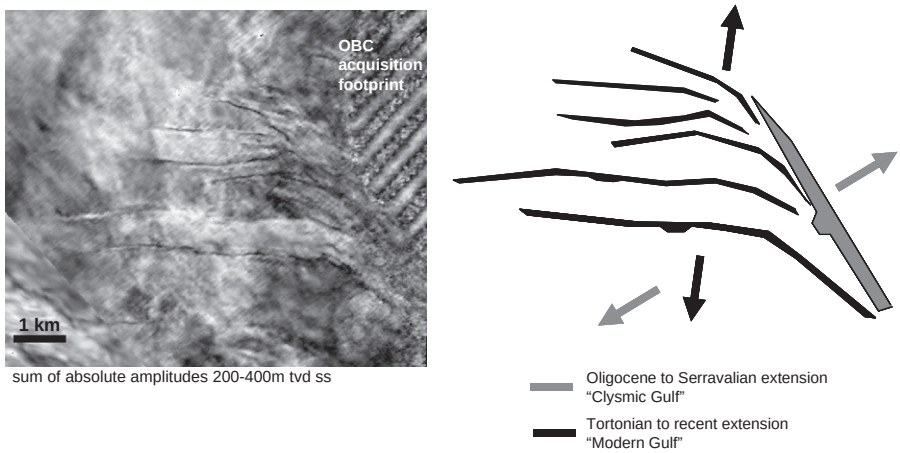

Figure 8.6
Simplified Pliocene structure map in the North October area. Location shows in Fig. 8.3.

pattern. At the northern tip of a NW–SE "Clysmic trend" fault, there is a splay of a series of younger, E–W trending faults. This could be interpreted as a transfer zone. The development of the E–W trending faults, however, is not contemporaneous with the opening of the Oligo-Miocene gulf. The fact that these E–W faults are much younger could also be indicative of a rotation of the stress field from N60°E to more N–S extension. The present-day stress field within the modern Gulf of Suez and Sinai is shown in Fig. 8.7, from the World Stress map (Reinecker et al., 2004). This shows that the maximum in-situ stress direction from southern Sinai to Jordan on the western side of the Levant-Aqaba transform

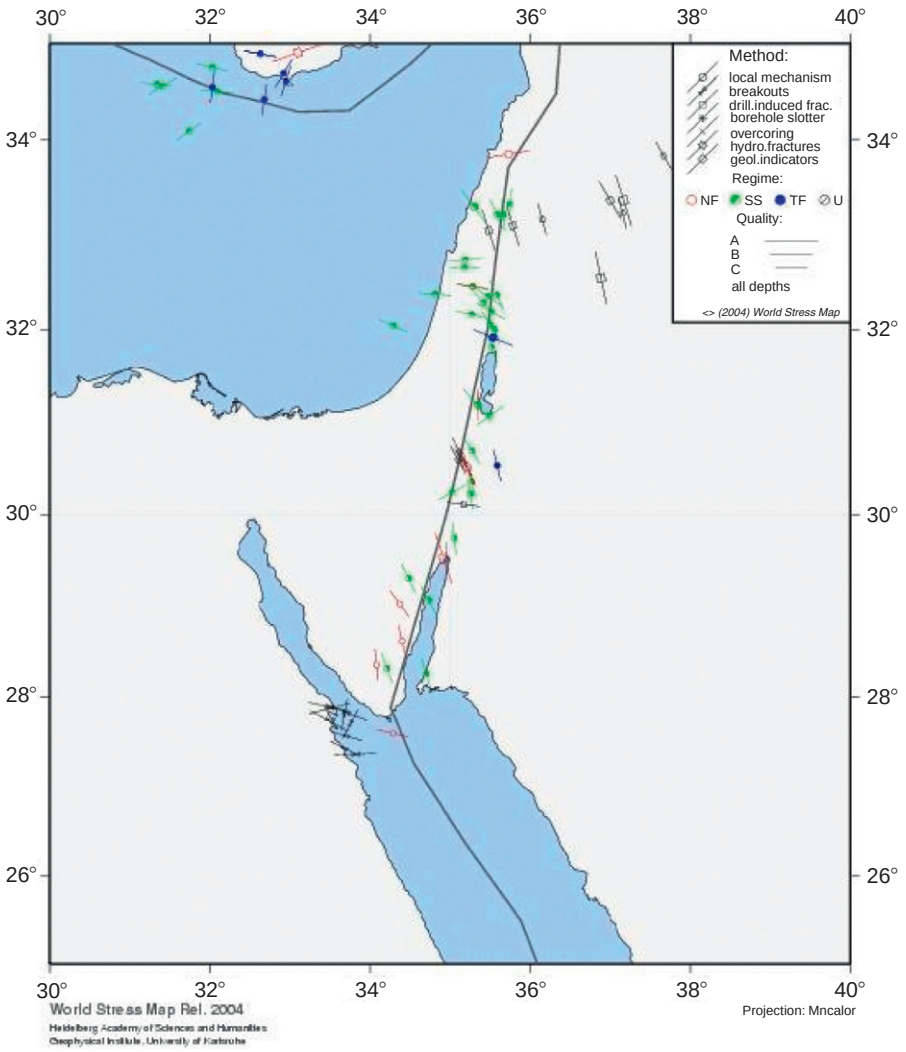

Figure 8.7
Present-day maximum compressive stress directions in Sinai and the Arabian plate *(from the World Stress Map Project, Reinecker et al., 2004)*.

is the same orientation as that on the Arabian plate side (in eastern Jordan). The similarity in direction suggests that stress is being transmitted from the Arabian plate through to the Sinai micro-plate. Thus, the rotation of the extensional stress field in the Gulf of Suez through the Plio-Pleistocene may be due, in part, to the northward drag of the Sinai micro-plate caused by continued movement of the Arabian plate.

The presence of uplifted Pleistocene reefs along the coastal faults, the Plio-Pleistocene depocenter thicks, thermal reconstruction, and current seismicity data demonstrates that the Gulf of Suez rift is active present day. Recognition of this neotectonic phase is critical as it is superimposed on all the earlier tectonic events and provides a controlling factor to some of the hydrocarbon traps in the basin.

8.3 Depositional patterns in megasequence 4 (Middle Miocene)

Within each megasequence, palaeontologically defined stratigraphic sequences have been mapped over the entire rift basin, using approximately 1000 wells. The sequences are broadly correlative to the main lithostratigraphic formations of the Gulf of Suez, shown in Fig. 8.2. The presence of sands has been petrophysically controlled, using stringent Vshale, porosity, and caliper criteria. This approach is well suited for economic evaluation of net sand, but misses the potential for identifying poorer quality calc–arenites, which are common in certain portions of the basin.

Gross depositional environment (GDE) maps for the four syn-rift packages of megasequence 4 have been constructed showing the generalized sedimentary facies. It is recognized that for any single location, numerous environments can be present; however, these highly generalized maps portray the representative facies distributions that characterize the overall period of sedimentation, with the focus of highlighting reservoir distributions. In areas with limited well control, especially in undrilled deep basinal hanging-wall blocks, facies and sand isopachs are heavily model driven.

Syn-rift sedimentation was greatest in six sub-basins, each of which exhibits its own local character, yet still retains common elements. These sub-basins are named the Darag, Lagia, October, South Belayim, Zeit Bay, and South-Central basins. The structural elements isolating these sub-basins result in highly variable input points and in turn, sand and evaporite depositional patterns.

Nukhul formation (Aquitanian)

Though lacking robust internal time constraints, lithostratigraphic relationships suggest that the Nukhul is comprised of several diverse unconformity-bounded packages, which are not time equivalent. Nukhul sediments are also the thinnest

of the four syn-rift sequences, with few areas exhibiting a gross interval greater than 150 m (Fig. 8.8A), which is in stark contrast to the overlying Lower and Upper Rudeis sequences.

The earliest syn-rift sequences were deposited on an unconformity, which is a regional subaerial erosion surface (Patton et al., 1994, Fig. 16). The Eocene age Thebes limestone is the most common sub-cropping horizon to this unconformity; however, locally complex sub-crop and super-crop relationships illustrate pre-rift structuring (Syrian Arc inversion). For example, because of the Senonian to Eocene inversion at Wadi Araba, sediments as old as the Carboniferous age Nubia Group sub-crop unconformably below the Nukhul sequence. The earliest Nukhul sediments, on the basis of stratigraphic position alone, are located in the southern areas of the rift, and are comprised of fluvial to estuarine sandstones of the Shoab Ali Member. Rifting may have therefore initiated in the south, as suggested by Patton et al. (1994). However, from the dispersed pattern of the gross isopach for the Nukhul sequence (Fig. 8.8A), it is evident that the Gulf of Suez did not simply propagate northward, but rather initiated coevally along its present length through the development of isolated small sub-basins.

Subsequent to the rift onset unconformity, rising sea level initiated sand deposition in the erosional and structural lows. Detailed mapping in the densely drilled Shoab Ali field (southern Gulf of Suez) strongly illustrates that Nukhul sands were deposited in a series of north oblique oriented, fault bounded half-graben (Fig. 8.9A). Similarly Nukhul sediments thicken dramatically across a north oblique fault in the southern "B trend," south of Sidki field. Quartz rich, clean Shoab Ali sands in-filled the preexisting fluvial drainage network which linked these earliest depressions.

Deposition of the Shoab Ali member sandstones in the southern Gulf of Suez was terminated by continued rising sea level, initiating the deposition of shallow water carbonates and anhydrites over the majority of the Gulf of Suez. In the southern Gulf of Suez, up to four distinctly mappable anhydrites are present locally, representing periods of marine basin restriction and intervening open marine circulation. These massive, pure anhydrites are interpreted to have been deposited in restricted silled basins, not sabkhas. The anhydrites are distinctly mappable around the entire southern Gulf of Suez basin and do not show any kind of shingled relationship. Their purity and absence of any interbeds, as shown by the fine resolution gamma (GR), neutron (NPHI), and density (RHOB) logs, would not be expected in a sabkha where one would expect some occasional wind-blown/storm clastic interbeds. Anhydrites are present intermittently as far north as the October sub-basin. Where the Shoab Ali sands are not present, the anhydrites lie immediately above the rift onset unconformity. Basin-wide above the anhydrites, limestone, shale, and rare sands are present, which, as suggested by lithostratigraphic correlations, are all younger than the Shoab Ali Member. Thick

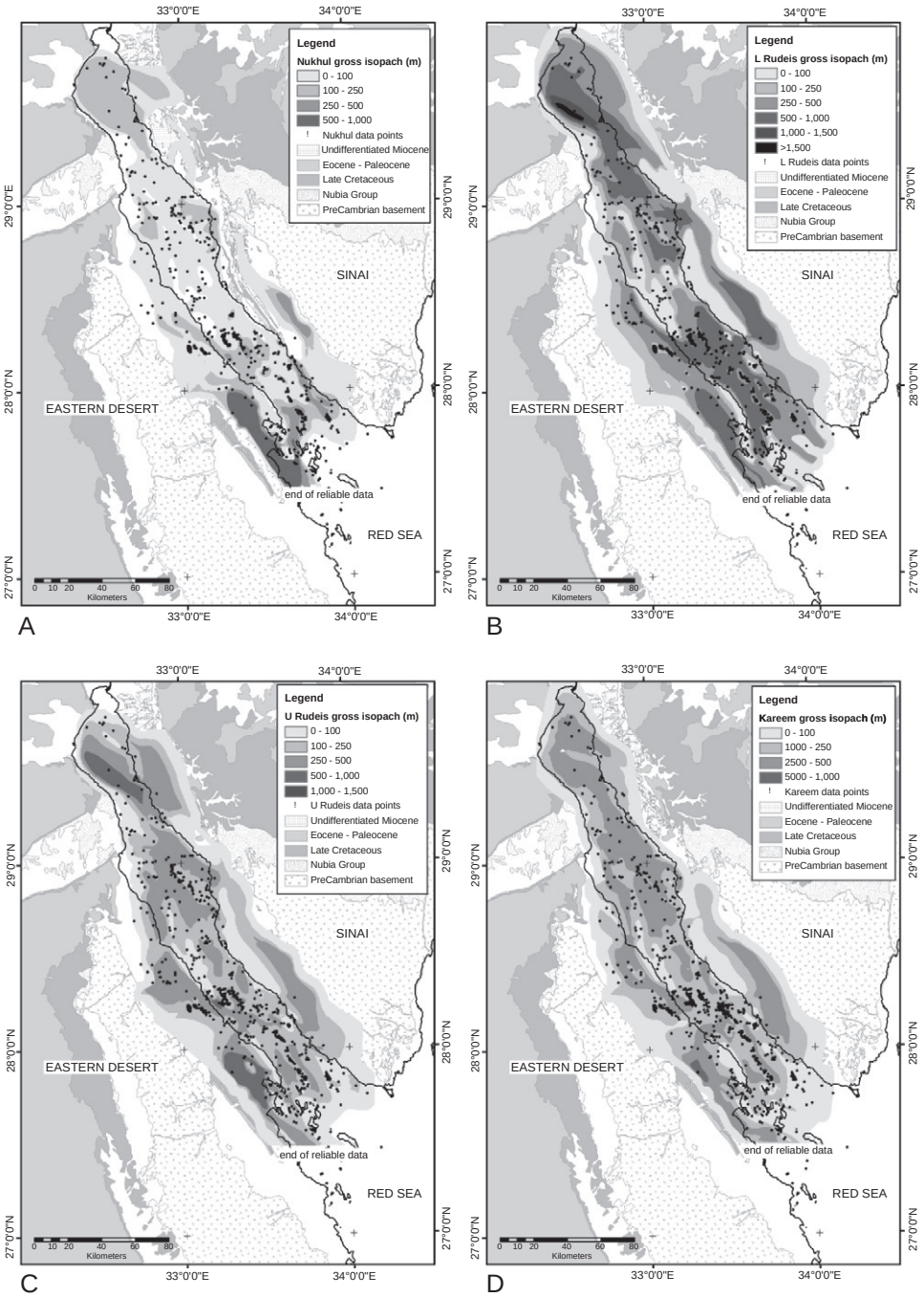

Figure 8.8
Miocene gross isopach maps: (A) Nukhul Formation, (B) Lower Rudeis Formation, (C) Upper Rudeis Formation, (D) Kareem Formation.

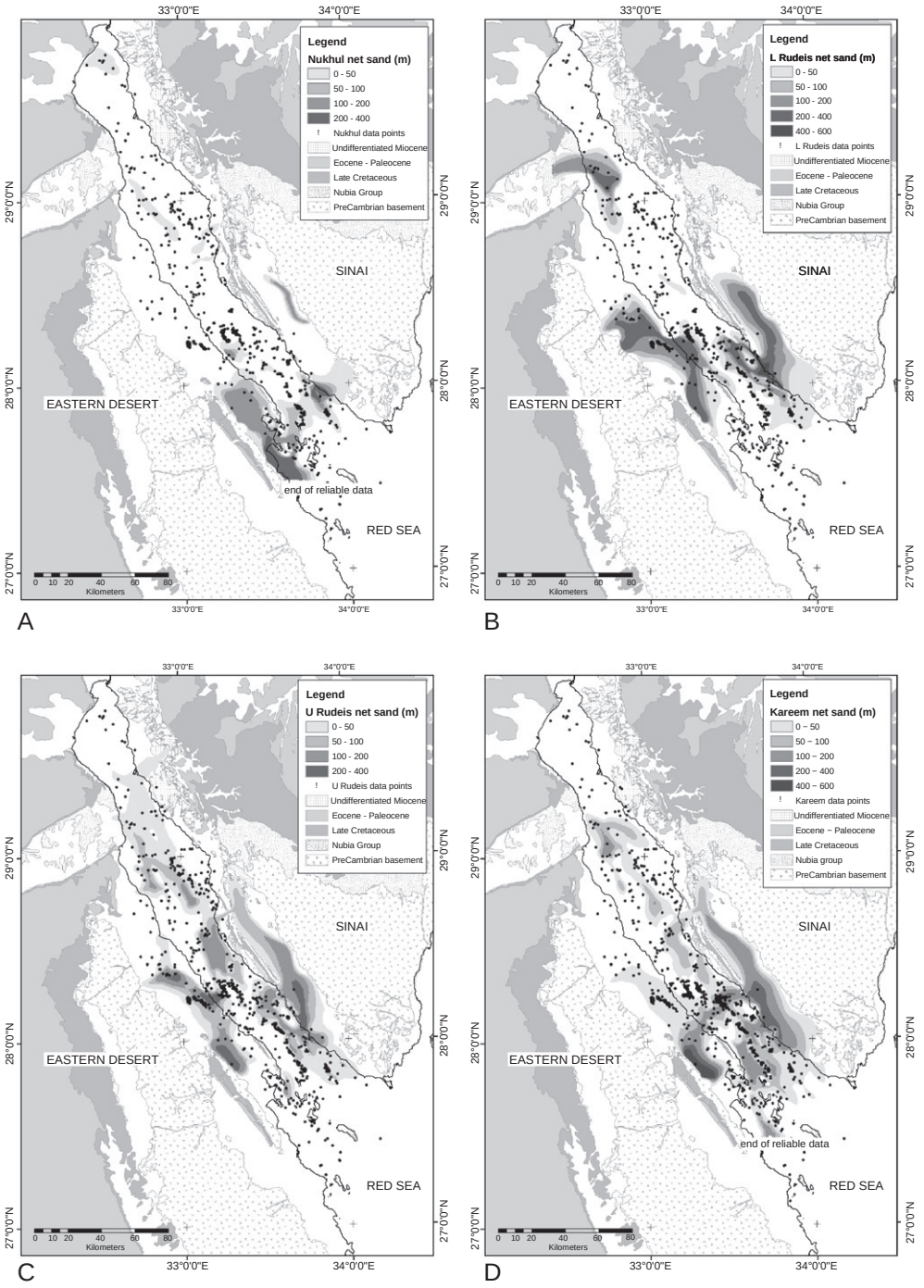

Figure 8.9 Miocene net sand maps: (A) Nukhul Formation, (B) Lower Rudeis Formation, (C) Upper Rudeis Formation, (D) Kareem Formation.

Nukhul aged sediments are also present in the Zeit Bay basin. Field studies by Winn et al. (2001), on outcrops high on the Gebel Zeit footwall on the southwest coast of the gulf, report these poorly sorted chert and calc-clastic rich Nukhul strata as being deposited by below storm wave base gravity flows. Winn et al. (2001) also cite the influence of small north oblique faults exerting control over facies, isopachs, and reservoir characteristics. Wells distal from the outcrops in the Zeit Bay sub-basin also penetrate a low-maturity lithic-arenite that differs from the Shoab Ali sandstone. Clean Nukhul quartz sands occur locally in the Darag basin, where the Nubia sub-crops immediately below the unconformity. Lacking any paleontology data and evaporite markers, the age relationships of these Nukhul sands relative to the Shoab Ali member are unknown.

The gross depositional environment (GDE) map (Fig. 8.10A) illustrates the generalized paleogeography during Nukhul time. The preponderance of bio-stratigraphic data suggests deposition in marginal-marine to shelfal environments, with little direct palaeontological evidence for deep water Nukhul deposition. Major sand input point sources appear to be the Red Sea Hills and the southern Qaa Basin, with minor input from Wadi Araba. Petrophysical and petrographic analyses reveal the Shoab Ali sands to be highly mature quartz arenites probably derived from local erosion of the Nubia sandstone. This supports provenance from the Red Sea Hills/Ras Mohamed Arch source hypothesis for the sediments, which is an area of thin post-Nubia, pre-rift stratigraphy.

Lower Rudeis formation (Burdigalian)

Numerous authors (e.g., Bosworth and McClay, 2001) have recognized the Lower Rudeis Formation (also known as the Mheiherrat Formation) as being deposited during the main period of rifting, when substantial movement along NW–SE oriented Clysmic faults created the Gulf of Suez basin. This regional well study illustrates the thousands of feet of accommodation space created in all of the sub-basins and that accommodation space creation significantly outpaced sedimentation over much of the Gulf of Suez basin (Fig. 8.8B). Sands are mainly restricted to rift shoulder sub-basins such as the Qaa and the Zeit Bay basins; sands were able to prograde into the main Gulf of Suez basins via entry points from the southern Qaa basin near El Tor and a relay zone south of the Younis Field (Fig. 8.9B). A significant drainage entry point was also established at Wadi Abu Had/Wadi Gharib on the west flank of the Gulf of Suez; however, detritus from this source had only limited penetration beyond the coastal fault during Lower Rudeis time. The previously established Wadi Arabia Syrian Arc inversion anticline minor point source was now established as a major sediment source, with sands prograding up to 40 km to the south into the Lagia sub-basin. These sands enter the basin at Zaafarana and then immediately are diverted by Clysmic oriented faults into a longitudinal hanging-wall basin. Lower Rudeis sands are notably missing from all hanging-wall penetrations in the North Darag, October, and South Belayim sub-basins (Fig. 8.9B).

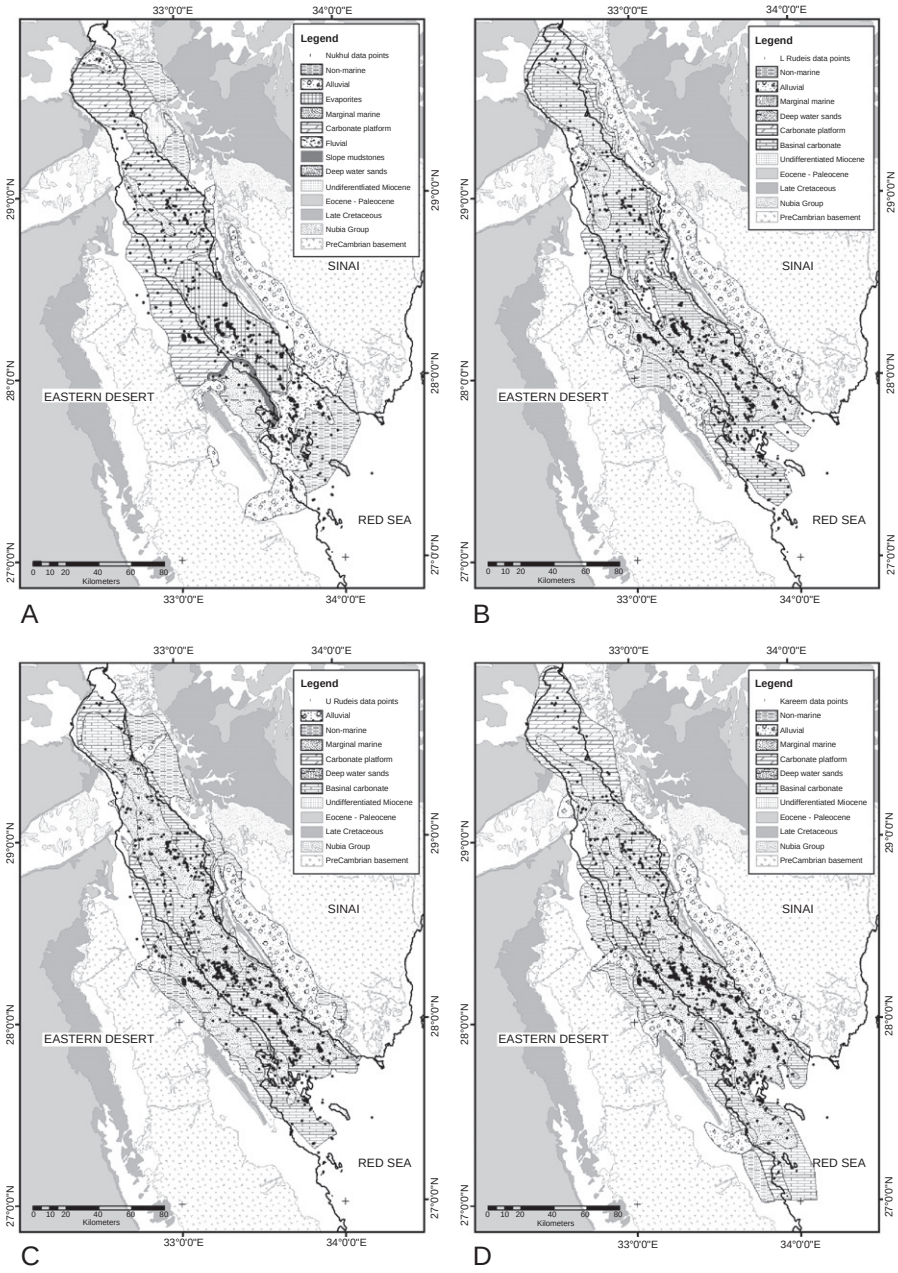

Figure 8.10
Miocene gross depositional environment (GDE) maps: (A) Nukhul Formation, (B) Lower Rudeis Formation, (C) Upper Rudeis Formation, (D) Kareem Formation.

Highly calcareous marls are the predominant rock type identified in wells. These sediments also include calc-arenites, calc-lutites, and bioclastic debris. Well penetrations in the deepest portions of each sub-basin show that the Lower Rudeis gross interval isopach is greater than 600 m. Seismic profiles suggest that the undrilled hanging-walls proximal to major faults contain significantly thicker Lower Rudeis gross intervals than the footwall biased well control offers. With the massive volume of accommodation space created during Lower Rudeis time, basinal restriction did not occur and there are no evaporites in the Mheiherrat sequence.

All major footwall high blocks, such as October, July, Ramadan, El Morgan, and the B trend, exhibit isopach thinning of the Lower Rudeis interval. Additionally, July, Morgan, and the B trend highs were major impediments to gravity flow sands spreading into deeper portions of the Gulf of Suez basin. The overwhelming majority of paleobathymetric interpretation from well cuttings suggests that outer neritic to bathyal environments prevailed over the entire Gulf of Suez with the exception of shelfal conditions in the extreme North Darag basin. Thick sands are interpreted to be deposited as deep water submarine fan systems (Figs. 8.8B and 8.9B). Proximal environments are interpreted to occur in the Qaa basin and landward portions of the mirror image Zeit Bay basin; however, we have no direct paleontological data to support this thesis. Outcrop studies by Young et al. (2000) document that proximal environments were in the Hammam Faraun area, landward of the main coastal fault.

Upper Rudeis formation (Langhian)

Relative to those of the Lower Rudeis Formation, sands in the Upper Rudeis travelled much farther into the Gulf of Suez basin. With the exception of the North Darag basin, thick Upper Rudeis sands were deposited in all the major axial hanging-wall drainages of all Gulf of Suez sub-basins. This pattern reflects decreasing rate of accommodation space creation, allowing coarse clastic progradation. The Upper Rudeis gross interval isopach is also thinner than the Lower Rudeis in all sub-basins (Fig. 8.8C). The same point sources active during Lower Rudeis deposition were also active during this time, with the significant addition of the quartz rich Wadi Feiran source, providing sand to the South Belayim sub-basin, an area previously devoid of siliciclastics (Fig. 8.9C). Wadi Wardan/Wadi Baba also acted as a point source to the Lagia sub-basin during this time although this provenance area contains mainly limestones. The resulting mix of calcareous and siliceous sediments adversely impacted on the Upper Rudeis Asl and Hawara Member sandstone reservoir quality in portions of the Lagia and October sub-basins. The central and southern basins were supplied with mainly siliciclastics and generally exhibit better reservoir characteristics. Wadi Abu Had/Wadi Gharib derived sediments also prograded into the South Belayim sub-basin, in contrast to their restriction to the Zeit sub-basin during Lower Rudeis time.

Paleobathymetric interpretations suggest that like the Lower Rudeis, the bulk of the Upper Rudeis sediments were deposited in outer neritic to bathyal water depths, with the exception of some proximal environments landward of the coastal faults (Fig. 8.10C). The Upper Rudeis gross interval isopach (Fig. 8.8C) also thins over all the major structural culminations cited previously. The October high focused all the Upper Rudeis sands to the west of that structure, and over the July and Ramadan structures, the sands thin, and the B trend blocked all sands emanating from the Qaa basin from entering the East Zeit basin (Fig. 8.9C). A detailed analysis of the depositional patterns of the Upper Rudeis around the July fault block is given by Pivnik et al. (2003). Upper Rudeis sands show some thinning but were not blocked by either the Morgan or the Belayim Marine culminations. Like the Lower Rudeis interval, there are no evaporites in the Upper Rudeis sequence, suggesting that a relative rise in sea level permitted open marine circulation across the intervening basinal sills.

Kareem formation, including the Lagia Member (Serravallian)

Following Upper Rudeis deposition, a relative fall in sea level occurred forming a widespread unconformity. Immediately following this period of erosion, restricted marine conditions occurred locally as documented by the variable occurrence of the Lagia and Markha anhydrites. The thickest anhydrites occur in the Lagia and October sub-basins where 30–45 m of clean massive anhydrite was deposited. These sub-basins were the most isolated from the marine waters of the Gulf of Suez. In contrast, Lagia anhydrites are absent to extremely thin in the North Darag basin, suggesting open marine conditions at that time. Similarly, Lagia and Markha anhydrites are thin in the South Central sub-basin, becoming absent from the majority of the south Gulf of Suez. Rising relative sea levels ended marine restriction for the remainder of Kareem and Lagia time.

Similar to the Upper Rudeis, fidelity to specific point sources for quartz rich detritus is apparent on the Kareem sand isopach map (Fig. 8.9D), and as before, sand is absent in the North Darag basin. Kareem and Lagia sands are present but thinner in the October and South Belayim sub-basins. The Central-Southern basin is the main site of Kareem/Lagia sand deposition, with the primary entry points at the Morgan transfer zone (from both sides of the basin and the southern Qaa basin). The Kareem progradation into the southern Gulf of Suez represents the culmination of the progressive sand infilling of the Gulf of Suez syn-rift basin. The Kareem gross isopach and sand maps (Figs. 8.8D and 8.9D) illustrate that the October, July, Ramadan, and the southern B trend were clearly in place, with sands onlapping these impressive footwall structures. The northern B trend was unable to block Kareem sands from entering the East Zeit sub-basin. Kareem sands also prograde and thicken impressively across the El Morgan and Badri structures with near impunity. Paleobathymetry data from wells suggest that bathyal conditions were present over the majority of the Gulf of Suez during

Kareem time. Empirical observations suggest that major footwall structures such as the B trend were subaerial during late Kareem time, as the Kareem section onlaps these highs (Fig. 8.10D). It should be noted that reservoir quality sand presence is primarily linked to granite and Nubia outcrop at the time of synrift deposition (see all net sand maps, Fig. 8.9). Detailed understanding of syn-rift provenance is therefore fundamental to accurately predicting reservoir quality.

8.4 Structure of the Gulf of Suez

In 2003, BP acquired a high-resolution aeromagnetic (HRAM) survey of the entire Gulf of Suez. Proprietary analysis of the HRAM data has resulted in a new structure map of the basement surface (Fig. 8.11). This is the first image of the structure of the whole basin and has been achieved independently of current seismic data, which has highly variable quality and does not cover the entire basin. A slope analysis of the basement surface was used to derive a new regional fault pattern (Fig. 8.11), with which previous maps compare well (e.g., Bosworth and McClay, 2001; Colletta et al., 1988; Moustafa, 2002; Patton et al., 1994) but lack the degree of complexity that has been achieved from a complete surface analysis. In addition to the basement structure map, a new series of cross-sections has been constructed (Fig. 8.13), utilizing both the basement surface and GUPCO's extensive three-dimensional and two-dimensional seismic maps. These have also utilized previously published work and unpublished GUPCO work to extend the sections to the rift shoulders and where there is no seismic coverage.

The Gulf of Suez is characterized by three distinct dip domains; in the northern Darag basin, the dominant faults dip to the NE and stratal dip is predominantly to the SE, whereas the Lagia to Belayim basins have opposite SW-dipping main faults and regional stratal dip to the NE; and in the southern Gulf, the dip domains are reversed back to predominantly NE-dipping faults and regional stratal dips to the SW (Fig. 8.12). The areas of major change in structural dip domain have been termed accommodation zones, twist zones, and transfer zones by previous workers. Younes and McClay (2002) have termed the northern zone the Zaafarana accommodation zone (ZAZ) and the southern Morgan accommodation zone (MAZ), whereas Moustafa (2002) uses the terms Gharandal and Surf El Dara transfer zones. As examination of seismic data and the HRAM basement map (Figs. 8.10 and 8.12) shows, no clear cross-fault connection (i.e., hard-linked transfer) between the tips of the dip domains, and the term accommodation zone is the most appropriate description.

Fault displacements and basin depocenters are largest toward the centers of each dip-domain province and therefore tip toward the accommodation zones. The presence of the accommodation zones suggests that the rift basin initially developed in three distinct sub-basins, partitioned by the accommodation zones. The positions of the accommodation zones are potentially related to the preexisting basement structure and in particular, the presence of Syrian Arc inversion structures. The Zaafarana accommodation zone overlies the main

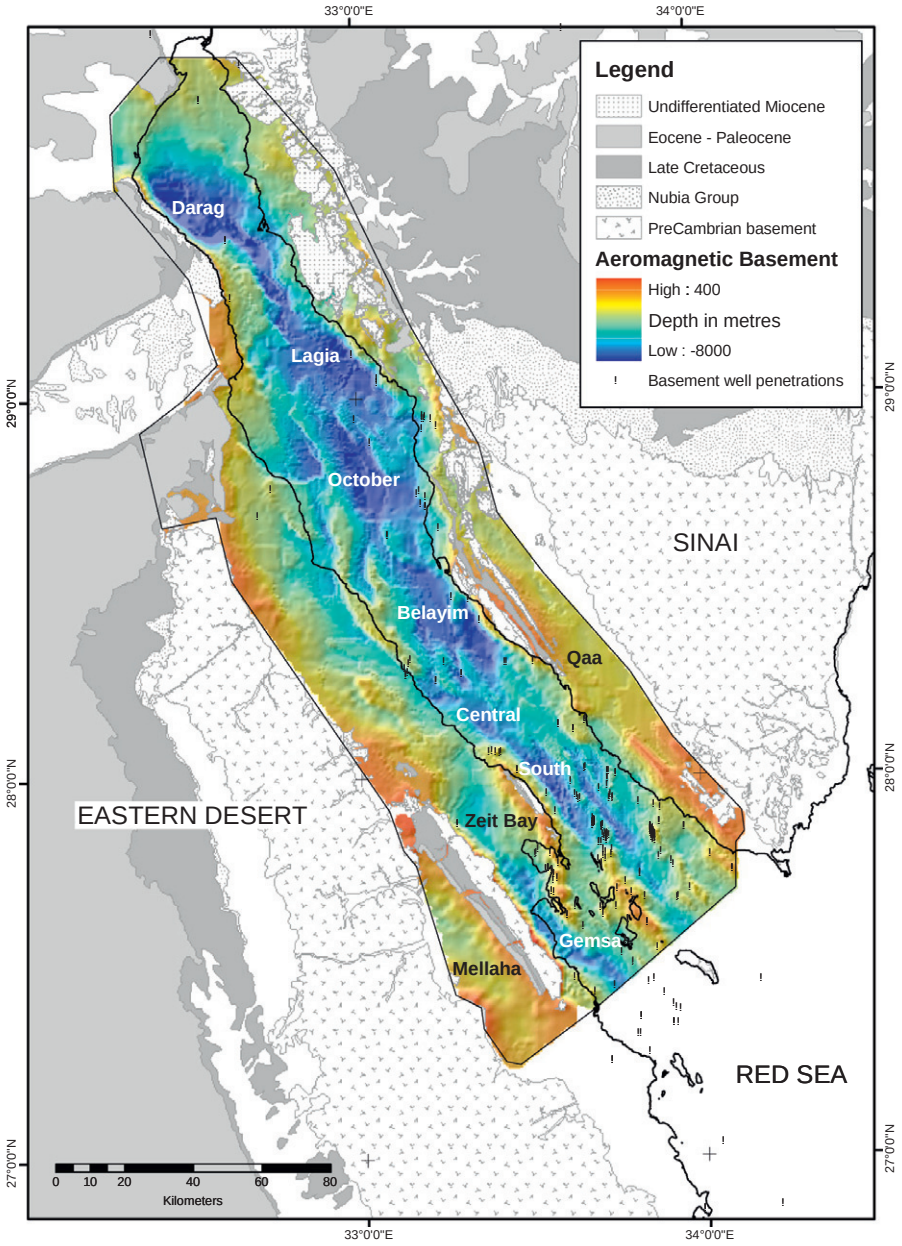

Figure 8.11 Basement depth structure map of the Gulf of Suez derived from High Resolution Aeromagnetic Data.

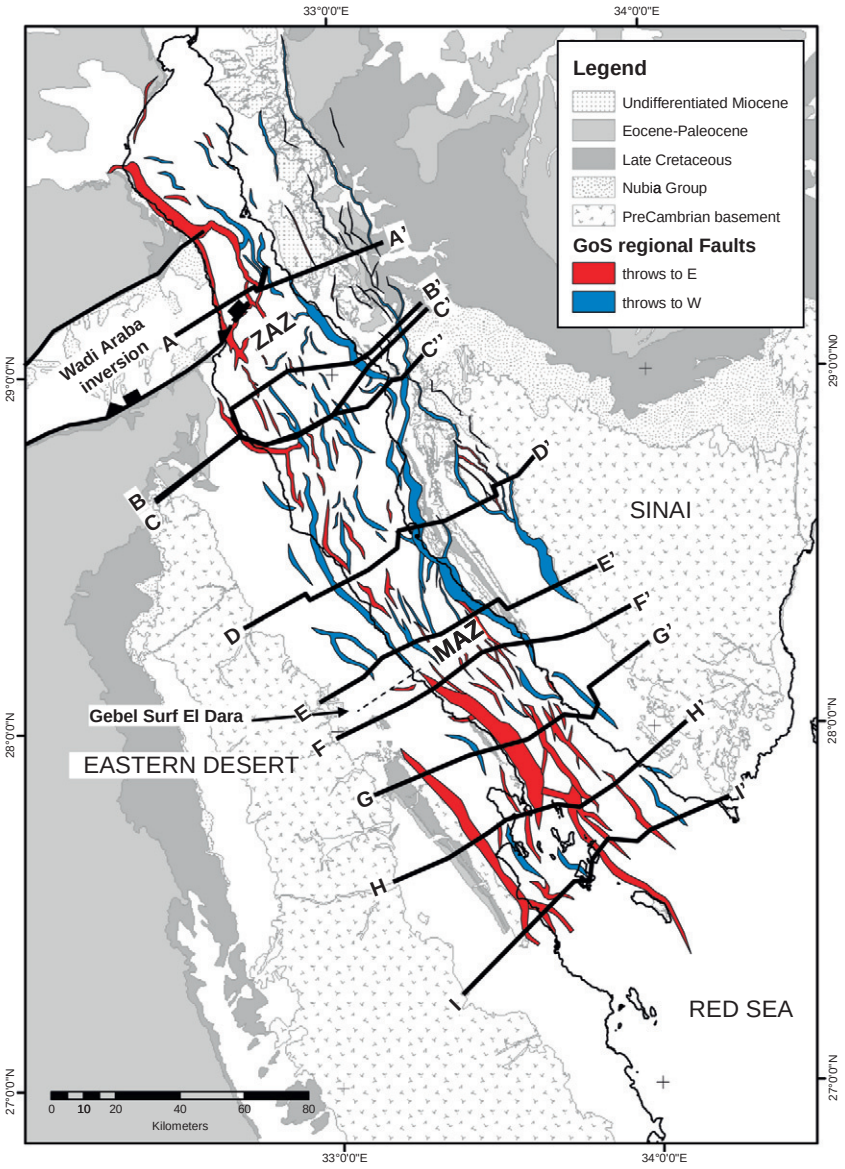

Figure 8.12 Regional fault pattern derived from aeromagnetic basement structure map, showing major fault dip trends, accommodation zones, and the location of inversion folds. ZAZ, Zaafarana Accommodation Zone; MAZ, Morgan Accommodation Zone. Onshore Sinai fault pattern *(after Moustafa, 2003)*.

southern fault of the Wadi Araba inversion anticline, which will have had significant structural relief at the basement level. The Morgan accommodation zone (MAZ) in the central-south Gulf of Suez does not, in contrast, have a clear pre-existing inversion structure to develop over. Like the ZAZ, the MAZ represents an area of relatively low fault displacement, and is characterized by fault tips of the two opposing fault dip-domains. However, onshore to the west of the

accommodation zone is the complex outcrop pattern at Gebel Surf El Dara where pre-rift rocks outcrop and which Moustafa (2002) has interpreted as a strike-slip transfer zone. Moustafa (2002, Figs. 19 and 20) shows that the pre-rift stratigraphy at outcrop is deformed by ENE–WSW trending folds and small thrusts which strike NW–SE. It is not inconceivable that this complex structural zone, which is quite unique in an extensional basin, originates from the compressional event that produced the Syrian Arc folds. The Cretaceous outcrop pattern to the west of Gebel Surf El Dara at its boundary with the Eocene shows a marked curve, suggestive of a broad fold. If so, this could mark a southern inversion structure which, like the Wadi Araba anticline, imparted a distinct geometrical character on the Gulf of Suez rift. Bosworth and McClay (2001) argue that the northern extent of the Gulf of Suez rift is limited by an E–W oriented structural boundary of Late Eocene age, possibly a Syrian Arc feature. To the north of this boundary, the extension is more diffuse.

The basement structure has therefore influenced the development of the geometry of the rift faults. Basement topography, created through late Cretaceous to Eocene inversion, appears to have controlled the sites of the accommodation zones developed during Oligo-Miocene rifting, either side of which the largest fault displacements and basins occur. The accommodation zones are sites of the tips of each domain and the fault geometry within the accommodation zones is more symmetric compared to the dominant dips in the basins. Progressive fault development has been described in the Gulf of Suez (e.g., McClay and Khalil, 1998), showing that the present-day fault pattern has evolved from the growth of faults that were initially concentrated in the main extensional sub-basins. These faults have merged and grown such that the present gulf is defined by a series of major faults, which control much of the present coastline.

The nine regional cross-sections are shown in Fig. 8.13. They extend from the Wadi Araba inversion structure in the north, to Esh El Mellaha and the tip of the Sinai Peninsula in the south. The sections utilize the onshore cross-sections of Moustafa (2003), Patton et al. (1994), and numerous unpublished works from GUPCO. Cross-section A–A′ crosses from the outcrop in the Wadi Araba inversion and cuts obliquely through the southern inversion fault to the east. The section is a strike line relative to the inversion structure. The rift has a fairly symmetrical fault pattern as it lies in the ZAZ, in contrast to the strong SW-dipping dip panel to the north in the Darag Basin (e.g., Patton et al., 1994, their Fig. 20A). Well control clearly shows how the inversion has resulted in a complex sub-crop to the overlying syn-rift strata, as they onlap the eastward-plunging fold. Paleozoic Nubia outcrops in the inversion structure and the Miocene rests unconformably on the Nubia in the west. Late Cretaceous to Eocene pre-rift stratigraphy is progressively preserved down plunge until an almost complete, but greatly thinned, section is preserved in the immediate hanging-wall of the inversion. In the footwall, onshore to the east of the present-day gulf, a full Late Cretaceous to Eocene section is preserved, which is over three times thicker than that recorded in the hanging-wall. To the south,

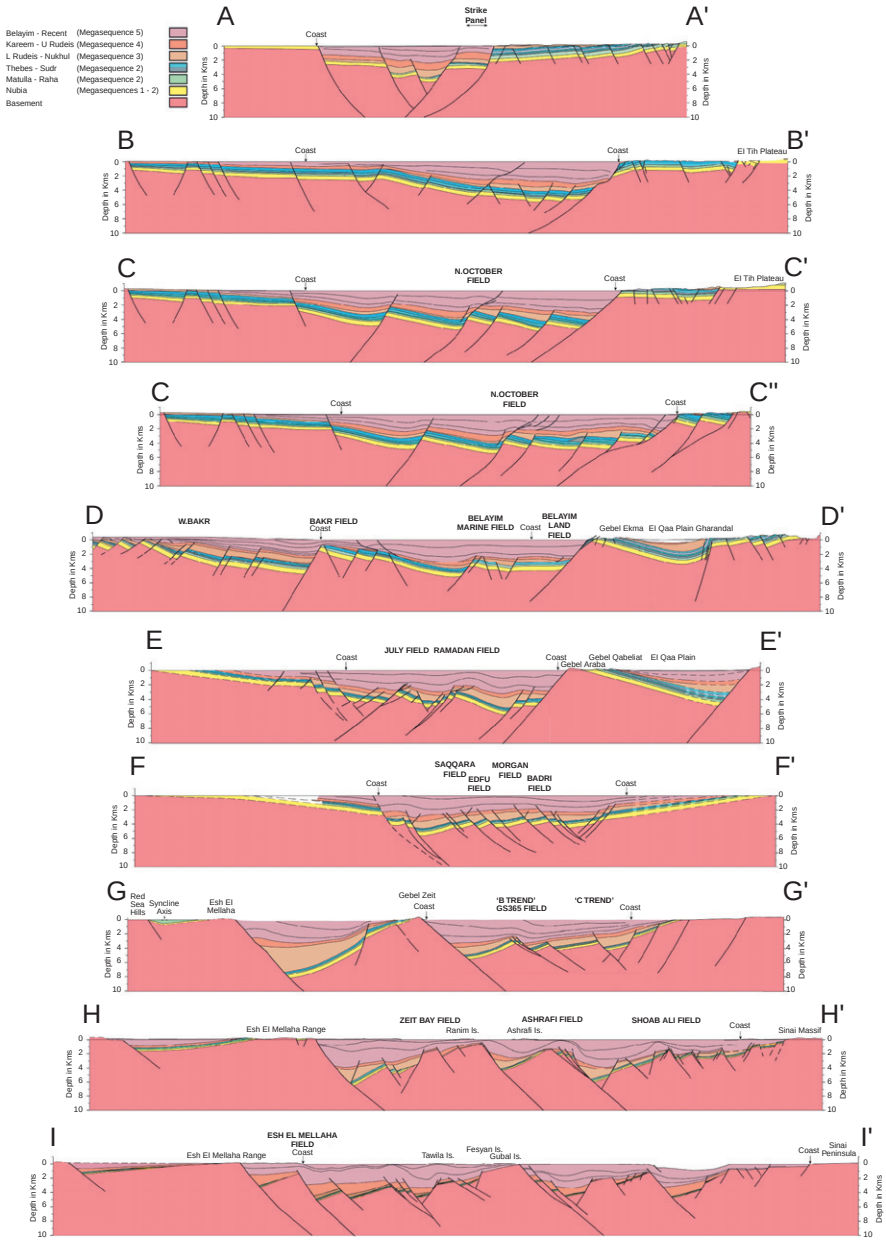

Figure 8.13 Gulf of Suez structural cross-sections. For location, see Fig. 8.12.

cross-sections B–B′ to E–E′ lie in the NE-stratal dip domain and clearly show dominant dip and rotation toward the eastern coastal and rift bounding faults. Well control on section B–B′ (AZ-1 and DD84-1) shows that the coastal fault can display a listric to ramp/flat geometry, which creates hanging-wall rollovers. Similarly at Ras Budran (section C–C″), the geometry of the hanging-wall indicates a major listric nature to the coastal fault. Major faults also frequently show an upward decrease in dip and the development of hanging-wall rollovers in the younger, evaporite-dominant syn-rift sediments. Sections B–B′, C–C′, and C–C″ show how the central fault, which contains the October field complex in the pre-rift strata in the footwall, changes dip in the evaporite interval (Feiran-younger). This is possibly because of the refraction of the fault as it propagated up section into the evaporite-rich stratigraphy. Major shallow listric faults extend almost to the surface, with rollover anticlines developed in the hanging-walls. Shallow detachments are also present, which have an opposite sense of dip to the east; detachments are created toward the base of the evaporite section and gravitationally induced slip occurs down the dip slope of a major fault block (e.g., east of the Bakr Field on section D–D′). In contrast to the listric coastal fault style to the north, in the central gulf, the main east-bounding coastal fault of Gebel Araba is far more planar and no significant hanging-wall rollover is developed (sections D–D′ and E–E′). Footwall blocks in the center of the basin are often cut by break-back extensional faults (e.g., July and Ramadan fields, section E–E′).

Cross-section F–F′ lies to the south of the central MAZ, but the influence of the accommodation zone can be seen by the nature of the low elevation of the footwalls on either side of the basin. The section is located between two main basement outcrops; it is down plunge of both the Gebel Araba footwall high to the north on the east coast, and the Gebel Zeit footwall high to the south on the west coast. The largest field in the Gulf of Suez, the Morgan field, lies on section F–F′, and is a major anticline in the syn-rift section located over the highest point of the tilted fault blocks beneath. There is also an element of halokinesis to the structure, whereby structural elevation and down building on the flanks have led to the flow of halite to form broad salt domes over tilted fault block crests. This becomes significant farther south to the east of the Gebel Zeit fault and over the "B trend" tilted fault blocks (section G–G′), where the salt has developed into a diapiric salt wall. Section G–G′ also illustrates the significant Esh El Mellaha basin, which contains the thickest onshore syn-rift section. The high degree of dip on the Gebel Zeit fault block has previously been interpreted as listric (e.g., Bosworth, 1995; Colletta et al., 1988). Cross-sections H–H′ and I–I′ show rotation into the east-dipping coastal and rift bounding faults, as well as the gradual southward attenuation of the Nubia Formation and younger Cretaceous pre-rift stratigraphy. In the southernmost Gulf of Suez, the crests of many fault blocks have had the pre-rift strata removed, so that the syn-rift sediments lie directly on basement. The fault block rotation and elevation of the fault block footwalls were far greater in the south of the rift basin, such that the crests of the fault blocks were exposed at sea level

and eroded before being covered by the younger, Late Miocene to Pliocene-age syn-rift sediments. The elevation of basement in the southern Gulf of Suez, shown by erosion both over footwall crests in the basin and in the exposed basement in the rift shoulders, may be a result of thermal doming at the triple junction of the Red Sea, Gulf of Suez, and Gulf of Aqaba rifts.

8.5 Petroleum habitat

The stratigraphic and structural history that has been described via tectonic sequences has set up ideal petroleum systems in the Gulf of Suez. Known source rocks are the Campanian Brown Limestone and the Eocene Thebes Formation, with localized contributions from the Cenomanian Raha Formation, and the Miocene Lower Rudeis and Belayim Formations (Fig. 8.2). The distribution of Brown Limestone source rock facies is controlled by the Wadi Araba inversion structure; the source facies is not present north of this structure in the Darag Basin. Here, in the north of the rift, the main source rock is the Thebes Formation, charging overlying Nukhul sands. The main reservoir sands are found in the Kareem and Lower Rudeis Formations of the syn-rift section, and in the Nubia Formation in the pre-rift section. Secondary reservoirs are the Zeit, Upper Rudeis, and Nukhul in the syn-rift section, and the Thebes, Nezzazat Group, and Precambrian basement in the pre-rift section. Deepwater shales of the Lower Rudeis Formation, carbonates of the Sudr and Thebes formations, and the evaporites of the South Gharib Formation provide the main top seals.

Figure 8.14 shows the location of the major oil fields and Fig. 8.15 shows the main Gulf of Suez play styles. Pre-rift footwall blocks in Nezzazat and Nubia

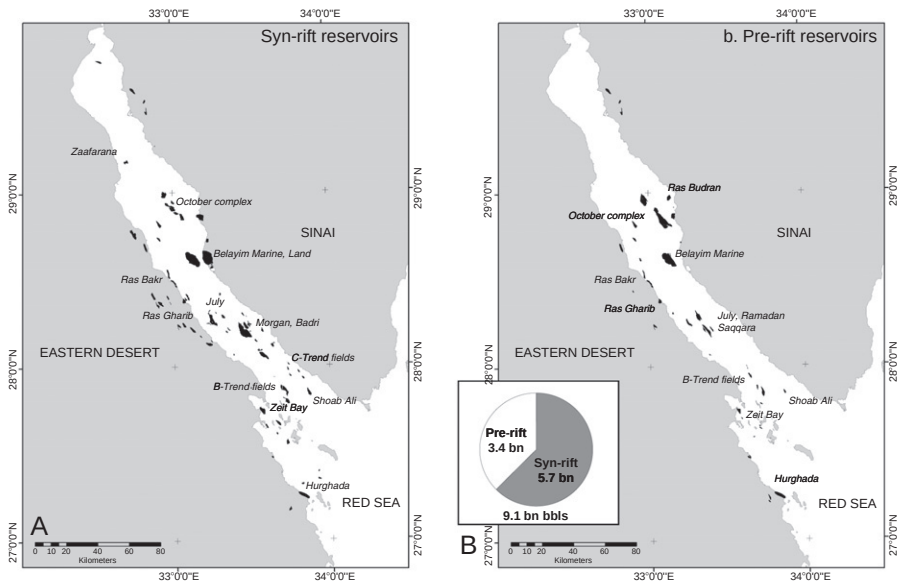

Figure 8.14
Location map of the major oil fields in (A) syn-rift and (B) pre-rift plays; major fields labeled. Inset: cumulative reserves discovered by play.

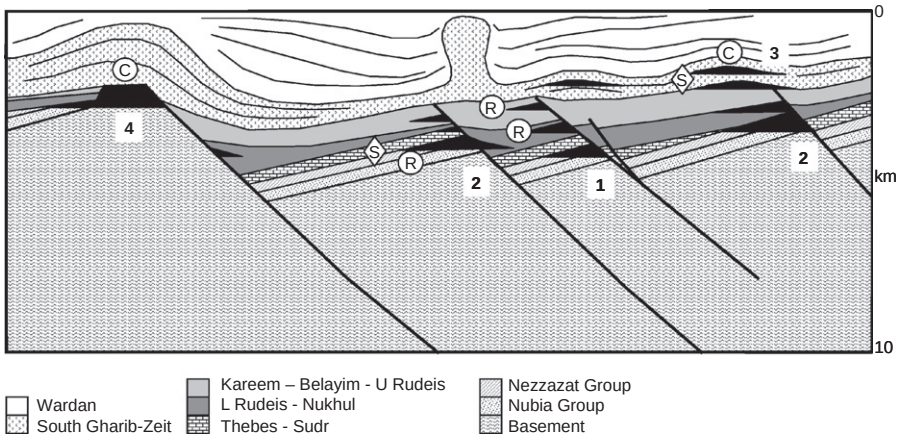

Figure 8.15 Gulf of Suez plays. 1. Pre-rift footwall blocks in Nezzazat and Nubia, charged from overlying Brown Limestone (e.g., Ramadan, Saqqara, B-trend). 2. Combination with hanging-wall syn-rift reservoirs (four-way combination, e.g., October), or shallower three-way in syn-rift (e.g., July). 3. Four-way closures in syn-rift section sealed by evaporites (e.g., Morgan, Belayim). 4. Shallow basement footwall with syn-rift reef development (e.g., Ras Gharib), or combination eroded pre-rift and basement footwall (e.g., Zeit Bay, Hurghada, and Shaob Ali).

are charged from the overlying Brown Limestone source rock (e.g., Ramadan, 625 mmboe; Saqqara, 80 mmboe). Some pre-rift footwall traps form combination traps with hanging-wall syn-rift reservoirs (e.g., October, 1 billion boe; July, 465 mmboe). There are also simple four-way traps in the syn-rift section sealed by evaporites (e.g., Morgan, 1.5 billion boe; Belayim, 1.6 billion boe). The Ras Gharib field is a combination of shallow basement and Nubia footwall with a Miocene syn-rift reef development above the crest, into which hydrocarbons have migrated. Accumulations also exist in eroded pre-rift and basement footwall blocks (e.g., Zeit Bay, Hurghada, and Shaob Ali). Since first oil was discovered in the Gemsa block in the Eastern Desert in 1886, over 9 billion barrels of oil equivalent have been discovered in the Gulf of Suez, and in excess of 5 billion barrels have been produced. The syn-rift, Miocene sands contain approximately 60% of these reserves. The remaining is mostly reservoired in the Nubia Formations. Even after 40 years of offshore exploration, significant discoveries are still being made, such as the 80 mmboe Saqqara Field, found by GUPCO in 2003. Dolson et al. (2000) estimated that there are between 1.5–3.3 billion barrels of oil equivalent (boe) yet to be found in the Gulf of Suez, although most of the fields are predicted to be less than 100 million barrels.

8.6 Conclusions

Inherited structures play a key role in the structural and stratigraphic evolution of the Gulf of Suez rift. Jurassic normal faults that were reactivated and inverted during Late Cretaceous to Eocene, for example, at Wadi Araba and possibly farther south at Gebel Surf El Dara, controlled the partitioning of the rift and the location of future accommodation zones. Syrian Arc inversion folds also controlled the deposition of the Campanian Brown Limestone; the primary source rock for the basin. Syrian Arc inversion and folding brought the Nubia Formation

to outcrop at Wadi Araba and provided a major clastic source for the syn-rift reservoirs. The accommodation zones set up in the basin also had a major impact on syn-rift sediment transport patterns into the sub-basins during the Miocene.

Extension due to the separation of Arabia from Africa has had two distinct phases during the Miocene to Pliocene because of the change in plate vector movement from N60°E rift-perpendicular extension to N15°E oblique rifting as the Aqaba-Levant transform fault boundary developed, as Arabia converged with the Bitlis-Zagros boundary. During this phase of oblique rifting, substantial thicknesses of Pliocene to recent sediments were deposited in half-graben basins that were controlled by the major linked coastal fault system. Deposition in the rift stepped inward, away from the Miocene-age rift shoulders and to the extent of the modern rift, which is still experiencing extension at the present day.

Understanding provenance is fundamental to syn-rift exploration. GDE, gross interval, and net sand maps over the entire gulf demonstrate that the presence of good quality reservoir is directly related to the presence of granitic basement and/or Nubia outcrops, fed through well-established sediment input points. Critically, although subsurface well data imply lateral edges to fan-delta systems, current seismic data do not permit the identification of sediment dispersal patterns in the subsurface; stratigraphic plays in the syn-rift section have therefore, to date, eluded exploration.

With only 30% of the Gulf of Suez covered by three-dimensional seismic data, there are large areas not covered adequately by seismic. However, even with seismic data, the presence of interbedded evaporites in the Zeit, South Gharib, and Belayim Formations have a profound effect on data quality with the introduction of severe multiples. Data can be so poor that dips interpreted on seismic data can be completely opposite to that known to exist in wells from dipmeter data. Seismic and non-seismic technologies need to progress in order to tap the remaining potential of the Gulf of Suez. Because of the current poor imaging, understanding the structural history of the basin is paramount; as concepts change with new data and improved imaging, integrating structural and depositional models across the whole rift basin should provide the basis for the next generation of exploration discoveries.

Acknowledgments

We acknowledge all current and past geoscientists at the Gulf of Suez Petroleum Company (GUPCO), whose work has greatly enhanced the understanding of the Gulf of Suez rift. Dave Pivnik (now at Apache Egypt) pioneered much of the detailed syn-rift work on the central Gulf of Suez and Steve Matthews (BP Sunbury) collaborated on the construction of the regional cross-sections. Jennifer Villinski (BP Egypt) provided the subsidence curve. Our thanks go to Keith Greenwood and Patrick Randell of BP Sunbury for drafting the regional cross-sections.

We also thank the management of BP, GUPCO and the Egyptian General Petroleum Corporation for permission to publish this paper, and in particular Howard Leach (BP) and Dr. Moataz Hassouba (GUPCO) for their support.

References

Angelier, J., 1985. Extension and rifting: the Zeit region, Gulf of Suez. J. Struct. Geol. 7, 605–612.

Bevan, T.G., Moustafa, A.R., 2012. Inverted rift basins of northern Egypt. In: Roberts, D.G., Bally, B.W. (Eds.), Phanerozoic Regional Geology of the World. Vol. 2, 479–502.

Bosence, D.W.J., 1998. Stratigraphic and sedimentological models of rift basins. In: Purser, B.H., Bosence, D.W.J. (Eds.), Sedimentation and Tectonics in Rift Basins: Red Sea – Gulf of Aden. Chapman Hall, London, pp. 9–25.

Bosworth, W., 1994. A model for the three-dimensional evolution of continental rift basins, north-east Africa. Geology of Northeast Africa (Part 2), Geologische Rundschau, Springer, vol. 83. pp. 671–688.

Bosworth, W., 1995. A high-strain rift model for the southern Gulf of Suez (Egypt). In: Lambaise, J.J. (Ed.), Hydrocarbon Habitat in Rift Basins. Geological Society of London. Special Publication No. 80, pp. 75–112.

Bosworth, W., Burke, K., 2004. Tectonic evolution of the Red Sea: a synthesis. Abstract. PESGB/HGS Third International Conference on Africa, London, September 2004.

Bosworth, W., McClay, K.R., 2001. Structural and stratigraphic evolution of the Gulf of Suez Rift, Egypt: a synthesis. In: Zeigler, P.A., Cavazza, W., Robertson, A.H.F., Crasquin-Soleau, S. (Eds.), Peri-Tethyan Rift-Wrench Basins and Passive Margins. Musee Nationale Hist. Nat., pp. 567–606.

Bosworth, W., Steckler, M.R., 1997. Stress field changes in the Afro-Arabian rift system during the Miocene to recent period. Tectonophysics 278, 47–62.

Bosworth, W., Taviani, M., 1996. Late Quaternary reorientation of stress field and extension direction in the southern Gulf of Suez, Egypt: Evidence from uplifted coral terraces, mesoscopic fault arrays and borehole breakouts. Tectonics 15, 791–802.

Bosworth, W., Crevello, P., Winn Jr., R.D., Steinmetz, J., 1998. Structure, sedimentation, and basin dynamics during rifting of the Gulf of Suez and north-western Red Sea. In: Purser, B.H., Bosence, D.W.J. (Eds.), Sedimentation and Tectonics in Rift Basins: Red Sea – Gulf of Aden. Chapman Hall, London, pp. 77–96.

Burchette, T., 1988. Tectonic control on carbonate platform facies distribution and sequence development: Miocene, Gulf of Suez. Sediment. Geol. 59, 179–204.

Cochran, J.R., 1983. A model for the development of the Red Sea. Am. Assoc. Pet. Geol. Bull. 67, 41–69.

Coleman, R.G., 1974. Geologic background of the Red Sea. The Geology of Continental Margins. Springer, Berlin, pp. 743–751.

Coleman, R.G., 1993. Geologic Evolution of the Red Sea. Oxford University Press, Oxford, 186.

Colletta, B., Le Quellec, P., Letouzy, J., Moretti, I., 1988. Longitudinal evolution of the Suez rift structure (Egypt). Tectonophysics 153, 221–233.

Cross, N.E., Purser, B.H., Bosence, D.W.J., 1988. The tectono-sedimentary evolution of a rift margin carbonate platform: Abu Shaar, Gulf of Suez, Egypt. In: Purser, B.H., Bosence, D. W.J. (Eds.), Sedimentation and Tectonics in Rift Basins: Red Sea – Gulf of Aden. Chapman Hall, London, pp. 271–295.

Dolson, J.C., Shann, M.V., Matbouly, S.I., Hammouda, H., Rashed, R.M., 2000. Egypt in the twenty-first century: petroleum potential in offshore trends. GeoArabia 6, 221–230.

Evans, A.L., 1988. Neogene tectonic and stratigraphic events in the Gulf of Suez rift area, Egypt. Tectonophysics 153, 235–247.

Garfunkel, Z., Bartov, Y., 1977. The tectonics of the Suez Rift. Geol. Surv. Israel Bull. 71, 44.
Gawthorpe, R.L., Hurst, J.M., 1993. Transfer zones in extensional basins: their structural style and influence on drainage development and stratigraphy. J. Geol. Soc. Lond. 150, 1137–1152.
Gawthorpe, R.L., Fraser, A., Collier, R.E., 1994. Sequence stratigraphy in active extensional basins: implications for the interpretation of ancient basin-fills. Marine Pet. Geol. 11, 642–658.
Gawthorpe, R.L., Sharp, I.R., Underhill, J.R., Gupta, S., 1997. Linked sequence stratigraphic and structural evolution of propagating normal faults. Geology 25, 795–798.
Girder, R.W., Southren, T.C., 1987. Structure and evolution of the northern Red Sea. Nature 330, 716–721.
Gupta, S., Underhill, J.R., Sharp, I.R., Gawthorpe, R.L., 1999. Role of fault interactions in controlling synrift sediment dispersal patterns: Miocene, Abu Alaqa Group, Suez Rift, Sinai, Egypt. Basin Res. 11, 167–189.
Haq, B.U., Hardenbol, J., Vail, P.R., 1987. Chronology of fluctuating sea levels since the Triassic. Science 235, 1156–1167.
Hempton, M., 1987. Constraints on Arabian plate motion and extensional history of the Red Sea. Tectonics 6, 687–705.
Jackson, C.A.L., Gawthorpe, R.L., Sharp, I.R., 2002. Growth and linkage of the East Tanka fault zone, Suez rift: structural style and syn-rift stratigraphic response. J. Geol. Soc. Lond. 159, 175–187.
James, N.P., Coniglio, M., Aissaoui, D.M., Purser, B.H., 1988. Facies and geologic history of an exposed Miocene rift-margin carbonate platform: Gulf of Suez, Egypt. Am. Assoc. Pet. Geol. Bull. 72, 555–572.
Joffe, S., Garfunkel, Z., 1987. Plate kinematics of the circum Red Sea – a re-evaluation. Tectonophysics 141, 5–22.
Kerdany, M.T., Cherif, O.H., 1990. Mesozoic. In: Said, R. (Ed.), The Geology of Egypt. Balkema, Rotterdam, pp. 407–438.
Klitzsch, E.H., 1990. Paleozoic. In: Said, R. (Ed.), The Geology of Egypt. Balkema, Rotterdam, pp. 393–406.
Klitzsch, E.H., Squyres, C.H., 1990. Paleozoic and Mesozoic geological history of northeastern Africa based upon new interpretation of Nubian strata. Am. Assoc. Pet. Geol. Bull. 74, 1203–1261.
Lambaise, J.J., Bosworth, W., 1995. Structural controls on sedimentation in continental rifts. In: Lambaise, J.J. (Ed.), Hydrocarbon Habitat in Rift Basins. Geological Society of London, pp. 117–144.
McClay, K.R., Khalil, S.M., 1998. Extensional hard linkages, eastern Gulf of Suez, Egypt. Geology 26, 563–566.
McClay, K.R., Nichols, G.J., Khalil, S.M., Darwish, M., Bosworth, W., 1998. Extensional tectonics and sedimentation, eastern Gulf of Suez, Egypt. In: Purser, B.H., Bosence, D.W.J. (Eds.), Sedimentation and Tectonics in Rift Basins: Red Sea – Gulf of Aden. Chapman Hall, London, pp. 211–238.
McKenzie, D.P., Davies, D., Molnar, P., 1970. Plate tectonics of the Red Sea and east Africa. Nature 226, 243–248.
Montenat, C., Ott D'Estevou, P., Purser, B.H., 1986. Tectonic and sedimentary evolution of the Gulf of Suez and northwestern Red Sea: a review. In: Montenat, C. (Ed.), Ecological Studies on the Gulf of Suez, the Northwestern Red Sea Coasts, Tectonic and Sedimentary Evolution of a Neogene Rift, Documents et Travaux, Institut geologique Albert de Lapparent, vol. 10, pp. 7–18.
Montenat, C., Ott D'Estevou, P., Purser, B.H., Burollet, P., Jarrige, J., Sperber, F., et al., 1988. Tectonic and sedimentary evolution of the Gulf of Suez and the northwestern Red Sea. Tectonophysics 153, 166–177.
Moretti, I., Colletta, B., 1987. Spatial and temporal evolution of the Suez Rift subsidence. J. Geodyn. 7, 151–168.

Moustafa, A.R., 1976. Block faulting in the Gulf of Suez. Abstracts of Papers from the 5th Exploration Seminar, Cairo. Egypt. Gen. Pet. Corp. 19, 36p.
Moustafa, A.R., 1995. Internal structure and deformation of an accommodation zone in the northern part of the Suez Rift. J. Struct. Geol. 18, 93–107.
Moustafa, A.R., 2002. Controls on the geometry of transfer zones in the Suez rift and northwest Red Sea: Implications for the structural geometry of rift systems. Am. Assoc. Pet. Geol. Bull. 86, 979–1002.
Moustafa, A.R., 2003. Geological map the eastern side of the Suez rift. Am. Assoc. Pet. Geol. Bull.
Moustafa, A.R., Khalil, M.H., 1995. Superposed deformation in the northern Suez rift, Egypt: relevance to hydrocarbon exploration. J. Pet. Geol. 18, 245–266.
Moussa, H.E., 1987. Geologic studies and genetic correlation of basaltic rocks in west central Sinai. PhD dissertation, Aim Shams University, Cairo, 308p.
Omar, G.I., Steckler, M.S., Buck, W.R., Kohn, B.P., 1989. Fission-track analysis of basement apatites at the western margin of the Gulf of Suez rift, Egypt: evidence for synchroneity of uplift and subsidence. Earth Planet. Sci. Lett. 94, 316–328.
Orszag-Sperber, F., Harwood, G., Kendall, A., Purser, B.H., 1998. A review of the evaporites of the Red Sea-Gulf of Suez rift. In: Purser, B.H., Bosence, D.W.J. (Eds.), Sedimentation and Tectonics in Rift Basins: Red Sea – Gulf of Aden. Chapman Hall, London, pp. 409–426.
Patton, T.L., Moustafa, A.R., Nelson, R.A., Abdine, S.A., 1994. Tectonic evolution and structural setting of the Suez rift. In: Landon, S.M. (Ed.), Interior Rift Basins. Am. Assoc. Pet. Geol., Tulsa, pp. 9–55.
Pivnik, D.A., Ramzy, M., Steer, B.L., Thorseth, J., El Sisi, Z., Gaafar, I., et al., 2003. Episodic growth of normal faults as recorded by syntectonic sediments, July oil field, Suez Rift, Egypt. Am. Assoc. Pet. Geol. Bull. 87 (6), 1015–1030.
Reinecker, J., Heidbach, O., Tingay, M., Connolly, P., Müller, B., 2004. The 2004 release of the World Stress Map (available online at www.world-stress-map.org).
Richardson, M., Arthur, M.A., 1988. The Gulf of Suez-northern Red Sea Neogene rift: a quantitative basin analysis. Marine Pet. Geol. 5, 247–270.
Said, R., 1990a. Cretaceous paleogeographic maps. In: Said, R. (Ed.), The Geology of Egypt. Balkema, Rotterdam, pp. 439–449.
Said, R., 1990b. Cenozoic. In: Said, R. (Ed.), The Geology of Egypt. Balkema, Rotterdam, pp. 451–486.
Schutz, K.I., 1994. Structure and stratigraphy of the Gulf of Suez, Egypt. In: Landon, S.M. (Ed.), Interior Rift Basins. American Association of Petroleum Geologists, Tulsa, pp. 57–96.
Steckler, M.S., Bertholot, F., Lyberis, N., Le Pichon, X., 1988. Subsidence in the Gulf of Suez: implications for rifting and plate kinematics. Tectonophysics 153, 249–270.
Steen, G., 1984. Radiometric age dating of some Gulf of Suez igneous rocks. Proceedings of the 6th Exploration Seminar, vol. 1. Egyptian Petroleum Exploration Society, Cairo, pp. 199–211.
Wescott, W.A., Krebs, W.N., Dolson, J.C., Ramzy, M., Karamat, S.A., Moustafa, T., 1997. Chronostratigraphy, sedimentary facies, and architecture of tectono-stratigraphic sequences: an integrated approach of rift basin exploration, Gulf of Suez, Egypt. In: Shanley, K.W., Perkins, B.F. (Eds.), Shallow marine and non-marine reservoirs, Gulf Coast SEPM Foundation 18th Annual Research Conference, December 1997, pp. 377–399.
Winn Jr., R.D., Crevello, P.D., Bosworth, W., 2001. Lower Miocene Nukhul Formation, Gebel el Zeit, Egypt: Model for structural control on early synrift strata and reservoirs, Gulf of Suez. Am. Assoc. Pet. Geol. Bull. 85, 1871–1890.
Younes, A.I., McClay, K.R., 1998. Role of basement fabric on Miocene rifting in the Gulf of Suez-Red Sea. Proceedings of the 14th EGPC Exploration, vol. 1. Production Conference, Cairo, pp. 35–50.
Younes, A.I., McClay, K.R., 2002. Development of accommodation zones in the Gulf of Suez – Red Sea rift, Egypt. Am. Assoc. Pet. Geol. Bull. 86, 1003–1026.
Young, M.J., Gawthorpe, R.L., Sharp, I.R., 2000. Sedimentology and sequence stratigraphy of a transfer zone coarse-grained delta, Miocene Suez Rift, Egypt. Sedimentology 47, 1081–1104.

In this chapter

9

Cenozoic rifts of eastern China

Li Desheng
Chinese Academy of Geosciences 20, Institution Road, P.O. Box 910, Beijing, China

9.1 Introduction and overview

Of the 9.6 million km^2 of land area in China, 4.2 million km^2 is covered by unmetamorphosed sedimentary strata. The offshore extension of up to 200 m depth of water is about 1.3 million km^2, giving a total area of 5.5 million km^2 of explorable sedimentary basins.

The continent and continental shelf of China underwent a period of complex geologic evolution from the Proterozoic to the Cenozoic (Fig. 9.1).

The following review emphasizes the overall structural and stratigraphic setting with selected emphasis on hydrocarbon source rocks.

Proterozoic

China's Precambrian cratons include the Huabei (North China), Jiaoliao, Yangtze (South China), and Tarim blocks. These were subject to a period of profound metamorphic evolution during the Lüliang phase of Early Proterozoic age. Specifically for the North China block Zhai, M. (2004), Kusky et al. (2007) offer a recent overview of its Precambrian-Paleozoic evolution. A subsequent Middle Proterozoic transgression resulted in the deposition of a sequence of strata dominated by siliceous marine dolomites, up to 9400 m thick (about 1900–800 Ma), in North China. This sequence is rich in algal fossils, characteristic of a typical source rock. Oil seepages and asphalts have been found in dolomite and shale outcrops in the Yanshan region. High-yielding oil pools have been discovered in Middle Proterozoic and Paleozoic tilted fault block buried hills underlying the pre-Tertiary in the Jizhong (Central Hebei) depression.

In South China, plutonic metamorphism persisted up to the Middle Proterozoic. A sequence of blue-green algae and green algae fossil-bearing siliceous marine dolomites, about 500–700 m in thickness, was deposited during the Sinian (800–600 Ma) subsequent to the Jinning Phase. These Sinian dolomitic strata are an important gas-bearing reservoir sequence in the Sichuan basin.

Phanerozoic Rift Systems and Sedimentary Basins DOI:10.1016/B978-0-444-56356-9.00008-0

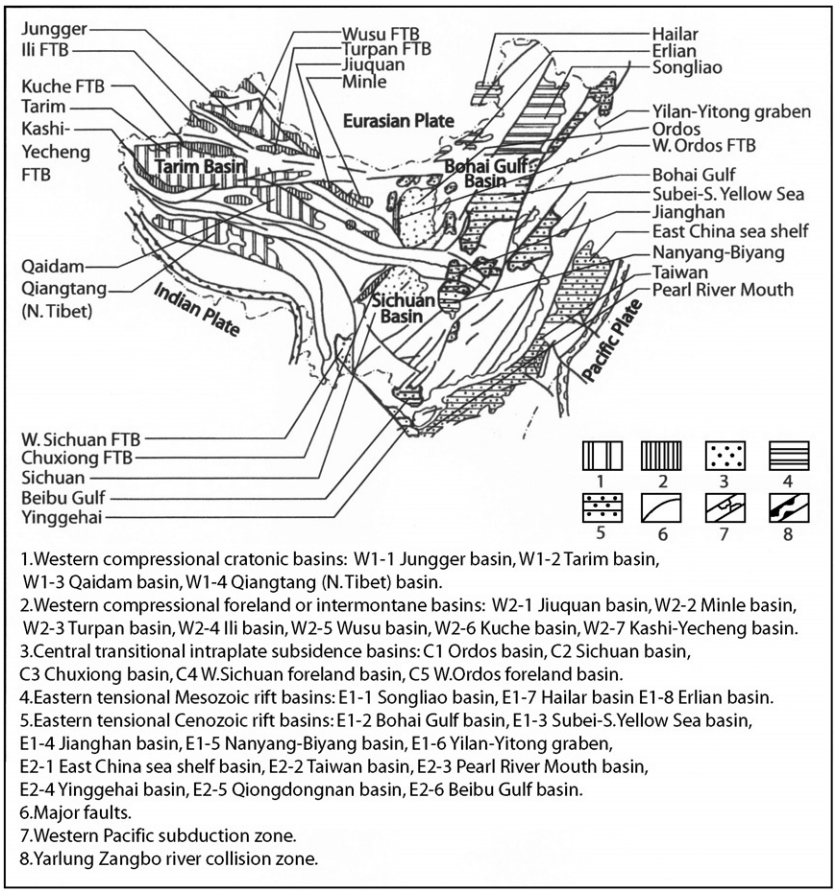

1.Western compressional cratonic basins: W1-1 Jungger basin, W1-2 Tarim basin, W1-3 Qaidam basin, W1-4 Qiangtang (N.Tibet) basin.
2.Western compressional foreland or intermontane basins: W2-1 Jiuquan basin, W2-2 Minle basin, W2-3 Turpan basin, W2-4 Ili basin, W2-5 Wusu basin, W2-6 Kuche basin, W2-7 Kashi-Yecheng basin.
3.Central transitional intraplate subsidence basins: C1 Ordos basin, C2 Sichuan basin, C3 Chuxiong basin, C4 W.Sichuan foreland basin, C5 W.Ordos foreland basin.
4.Eastern tensional Mesozoic rift basins: E1-1 Songliao basin, E1-7 Hailar basin E1-8 Erlian basin.
5.Eastern tensional Cenozoic rift basins: E1-2 Bohai Gulf basin, E1-3 Subei-S.Yellow Sea basin, E1-4 Jianghan basin, E1-5 Nanyang-Biyang basin, E1-6 Yilan-Yitong graben, E2-1 East China sea shelf basin, E2-2 Taiwan basin, E2-3 Pearl River Mouth basin, E2-4 Yinggehai basin, E2-5 Qiongdongnan basin, E2-6 Beibu Gulf basin.
6.Major faults.
7.Western Pacific subduction zone.
8.Yarlung Zangbo river collision zone.

Figure 9.1
Sketch map of tectonic basin systems of China.

Paleozoic

At the end of the Middle Proterozoic, the Jixian deformation (about 800 Ma) in the northern part of China resulted in the emergence of the area covering the Xinjiang–Mongolia–Heilongjiang and the Jiaoliao–Korea trends. From the Early Cambrian to the Middle Ordovician, shallow water marine sediments deposited include primarily carbonates, intercalated with thin beds of mudstones and evaporites, whose total thickness is 1000–1500 m. Following the Middle Ordovician, associated with mantle upwelling in Mongolia, the Asian continental crust was rifted and very thick marine sediments were deposited in the "Mongolian geosyncline" located between Siberia and North China. Extensive orogenic activity and plutonic metamorphism, associated with the "Caledonian" orogeny, created new continental crust that accreted around the old continent. The Huabei (North China) platform was uplifted and was then subjected to a long period of erosion

and peneplanation lasting until the Early Carboniferous. In southern China, the 3000–5000 m of sediments deposited throughout the entire Paleozoic consist mostly of carbonates intercalated with thick marine shales. The "Caledonian orogeny" also resulted in plutonic metamorphism in the southern part of China. At that time, the basement of the Japanese islands was connected with mainland Asia and shallow marine deposition was taking place off the Chinese continent.

During the Permo-Carboniferous period, the Mongolian geosyncline continued to develop. Plutonic metamorphism along the continental margin became even more intense during the Hercynian orogeny. Alternating continental and marine environments were particularly frequent. During the Middle–Late Carboniferous, except for some areas, the Huabei (North China) platform subsided overall, with the deposition of alternating continental and marine facies including some 200–400 m of coal beds that are the coal-related hydrocarbon source rocks of the Ordos basin.

During the Permian, the Huabei platform evolved into an intraplatformal basin, depositing a suite of 300–1500 m of red beds.

A widespread transgression occurred on the Yangtze (South China) platform during the Permo-Carboniferous period which persisted to the Middle Triassic in some areas. Carboniferous dolomites and Permian limestones are important gas-bearing reservoir rocks in the Sichuan basin.

Mesozoic

During the Triassic, the E–W trending Kunlun–Qinling–Dabie fold belt was formed by the collision of the North and South China Cratonic Platforms. Subduction of Pacific Ocean crust may have begun at the end of the Hercynian movements during the Late Permian. Compression of the Mongolian geosynclines resulted in the emergence of a large area extending from the Qinling Mountains northward to Siberia. This tectonism also caused the formation of many intraplatformal depressions, such as the Junggar, Ordos, and Qinshui basins. During the Triassic, a significant transgression from the ancient Tethys invaded the Yangtze Platform of southern China.

Pacific subduction processes intensified by the end of the Triassic. The whole of southern China was affected by the Indo-Sinian orogeny which led to the retreat of the Jurassic Sea to Tibet and western Yunnan. During the Cretaceous, the sea further retreated toward southern Tibet and the southwestern part of the Tarim basin.

During the Jurassic and Cretaceous, the whole of China was under the influence of the Yanshan tectonic phase. Several basins in the middle and western parts of China formed in the Triassic, such as the Songliao, Erlian, Hailar, Junggar, Tarim, Turpan, Ordos, Sichuan, and Chuxiong basins, all inheriting earlier geologic characteristics. Intense folding, faulting, and intermediate-acidic volcanism occurred in eastern China. The Paleozoic platforms were rifted, accompanied by the rise of the upper mantle, forming a series of intraplate rift basins.

Cenozoic

During the Paleogene, eastern China was entirely dominated by extensional block faulting. The Paleogene depressions of the Bohai Gulf, Subei–South Yellow Sea, Nanyang–Biyang, Jianghan, Beibu Gulf, and Pearl River Mouth basins are mostly rifted half-grabens or graben infilled by lacustrine sediments that include important source and reservoir rocks. In southwestern China, due to the collision between the Indian and Eurasian plates, the northern branch of the Tibetan Sea became closed. The Songpan-Ganzi and the Sanjiang fold belt formed a land mass, while the Tibet–Dianxi (western Yunnan) subplate collided with the Eurasian plate to become a part of the latter. A narrow, elongated trench zone in the Himalayan area was the only remnant of the Tethys Sea during the Tertiary. The other branch extended to the Kashi and Yecheng areas of the southwestern Tarim basin.

During the Himalayan period, active tectonism resulted in the development of the rift basins of Eastern China and the formation of the Pacific trench-island arc-marginal basin. A major depression first formed in the East China Sea basin due to the initial back-arc extension and was later closed as a result of subsequent folding. The other depression, the Okinawa trough, was formed to the east of the East China Sea basin at a later time. Therefore, the East China Sea basin went through a rifting and subsidence stage, while the Okinawa trough was again a rifted basin undergoing subsidence during the Pleistocene. The central high between the two depressions is probably a remnant island formed before the Pliocene. The island arc has since migrated eastward to form the present Japanese and Ryukyu Islands. The South China Sea basin is a back-arc basin of the Philippine arc and the Pearl River Mouth basin is the northern margin of this back-arc basin. The Pearl River Mouth, Yinggehai, and Qiongdongnan basins were rifted during the Paleogene to passively subside after the Late Oligocene: depositional environments changed from lacustrine during the rift phase to semienclosed sea and finally to open marine in the Neogene (Fig. 9.2).

9.2 The geodynamic development of rifts in eastern China

The subduction of the Pacific Plate led to a back-arc-related extension of the eastern China cratonic platform. Cenozoic rifts formed in the Bohai Gulf basin, the Subei and Southern Yellow Sea basin, the Jianghan Basin, the Nanyang–Biyang basins, and the Yilan–Yitong graben. Much of the extension is thought to be associated with an elevated Moho (Li Desheng, 1980a & 1980b; Zhu Xia,1983). Griffin et al.,1998, Menzies and Xu (1998), Wilde et al., 2003, Menzies et al., 2007 review the geophysical and geochemical observations and processes that during the Mesozoic-Cenozoic have led to the formation of an attenuated, relatively thin continental lithosphere ($<$50Km) and continental crust ($>$ 32km). The East China Sea and Taiwan basins are the marginal basins

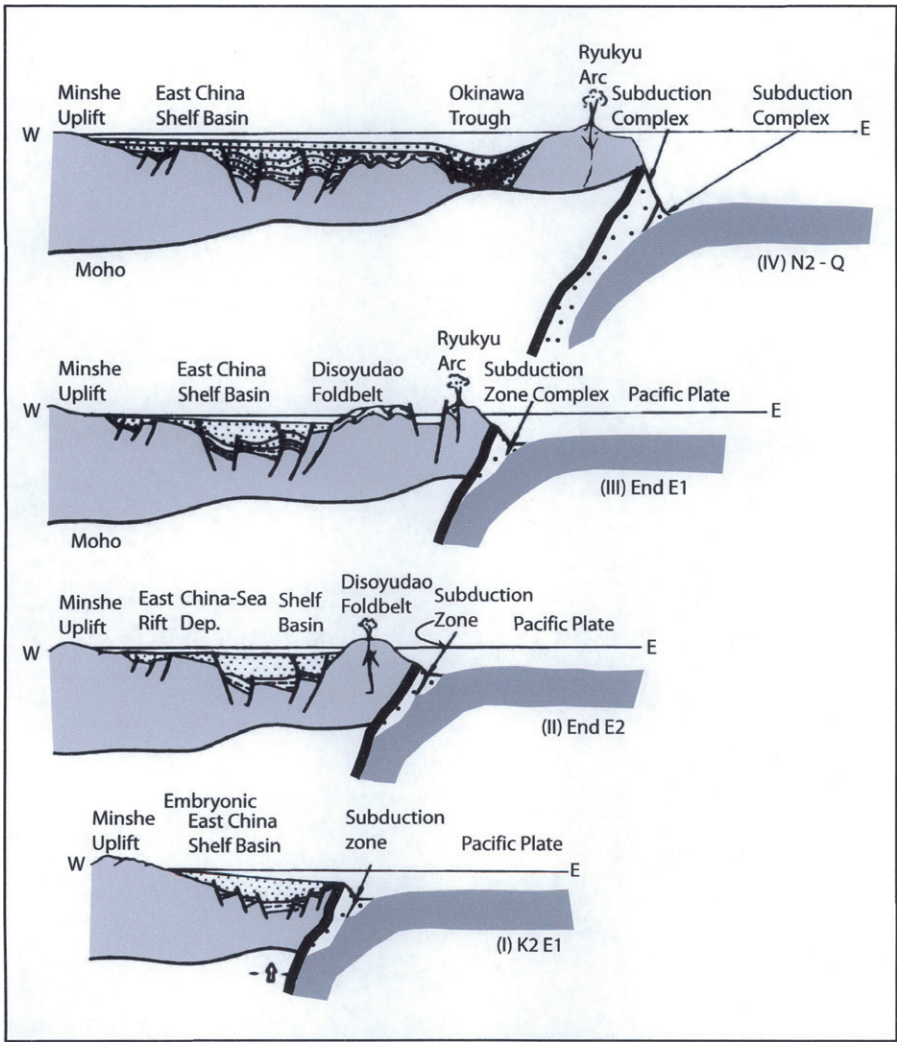

Figure 9.2
Diagrammatic cross-sections of Cenozoic rift basins in East China Sea basins showing subduction of Pacific Plate and mantle rise of Eurasia Plate.

of the western Pacific trench-arc-basin system Hilde, T et al., 1977, Howell et al., 1983. In contrast, the Pearl River Mouth, Qiongdongnan, and the Yinggehai basins are located along the northern divergent margins of the South China Sea oceanic plate (Figs. 9.3 and 9.4).

Major plate tectonic movements occurred during the Indosinian and Yenshanian Orogenies. In eastern China, the movement of structural blocks can be related to two generalized extensional zones active at different times and places from the Early Cretaceous to the Late Tertiary. The rift zone trending from the Songliao basin through the Bohai Gulf basin and, farther on, the Jianghan basin to its

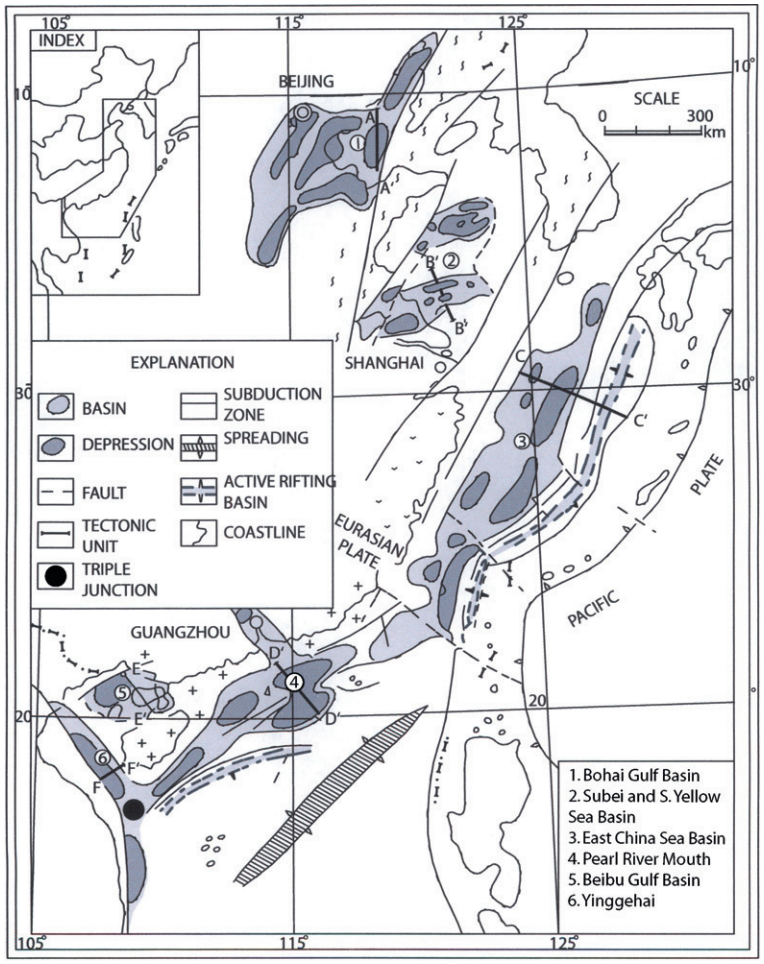

Figure 9.3
Cenozoic rifts on continental shelf of China.

end in the Beibu Gulf basin is the most pronounced feature of onshore eastern China (Tong Chongguang, 1980). Another extensional zone passing through the South Yellow Sea basin, the East China Sea basin, the Taiwan basin, the Pearl River Mouth basin, the Qiongdongnan basin, and the Yinggehai basin has exerted a major influence on the active tectonic history of the system of basins offshore eastern China.

From recent geophysical data and petroleum exploration in the petroliferous basins of eastern China and data available from adjacent areas, it is clear that the regional geology and tectonic regime of these basins can be explained as follows.

The location of the major eastern China rift basins in intraplate or in epicontinental positions can be explained by crustal extension and thinning, which resulted

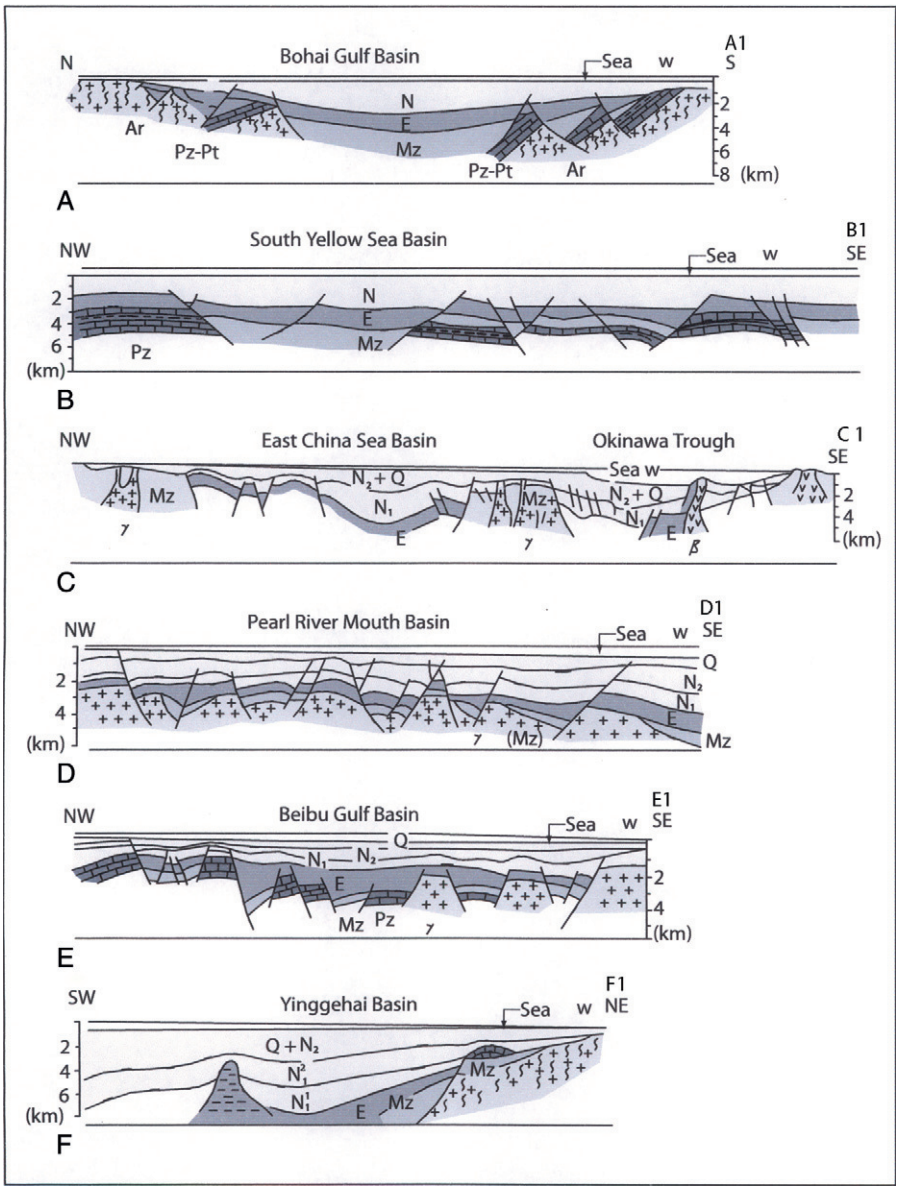

Figure 9.4
Schematic cross-sections of Cenozoic rifts on Continental Shelf of China. For location of cross-sections see Fig. 9.3.

in elevation of the Mohorovicic discontinuity and the upper mantle. Basin outlines are nearly coincident with the underlying upper mantle elevation which is several hundred kilometers wide and about 2–8 km in relief. The crustal extension formed a series of Cenozoic rift basins whose development was episodic, resulting in deposition of many favorable hydrocarbon-bearing sequences in the polycyclic rift basins.

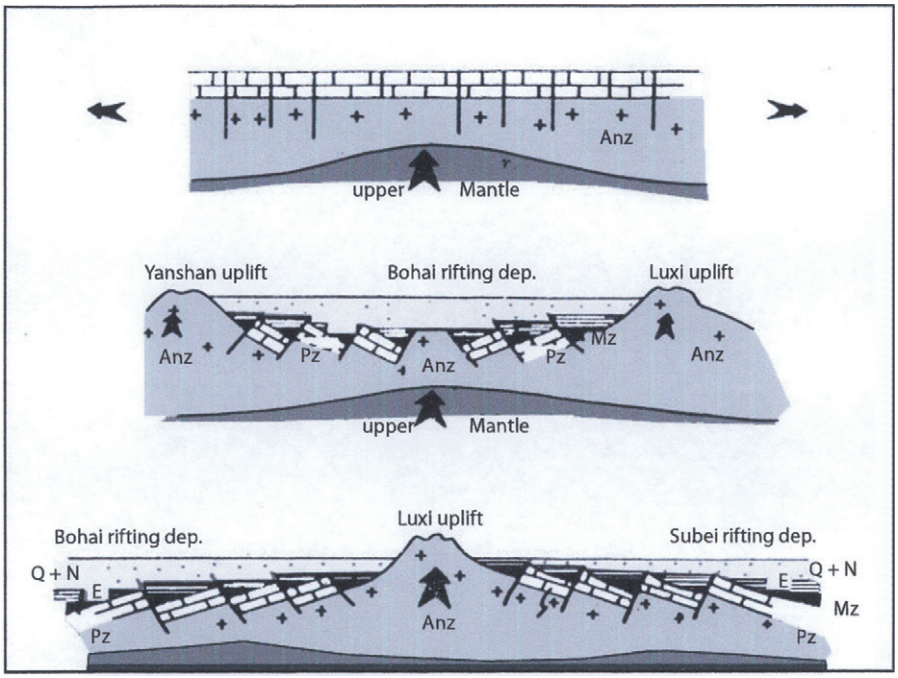

Figure 9.5
N-S oriented diagrammatic cross-sections of Cenozoic basins in eastern China showing crustal thinning, block faulting, and the relationship to the development of a series of rifting half-grabens. For location see Fig. 9.6A.

The rift grabens and half-grabens are believed to be of extensional origin in association with crustal thinning and block faulting (Fig. 9.5). Based on seismic reflection profiles and exploration drilling, the major basins are considered to be controlled by a series of low-angle normal faults, dipping mostly at 30–50°. A large number of contemporaneous normal faults are steeper in their upper part with a gradual change in dip to lower angles and are sometimes nearly horizontal and thus listric in nature (Li Desheng, 1980a). The rifts between the Paleozoic, Upper Proterozoic, or Pre-Upper Proterozoic blocks appear to have widths of 2–15 km, and the thickness of bounding sediments in the half-graben varies depending on the amount of vertical subsidence and the average subsidence rate associated with each rifting stage.

The back-arc extension of the Okinawa Trough and the East Taiwan Rift depression during the period of Himalayan orogeny induced westward compressional forces. A series of en echelon anticlinal folds with westward thrusts developed on the western East China Sea Shelf and the Western Taiwan basins.

9.3 Eastern China Cenozoic rifts

Bohai Gulf basin

The Bohai Gulf basin covers an area of 20×10^4 km^2. The onshore part of the basin extends over the provinces of Hebei, North and West Shandong, South Liaoning, and North Henan, as well as the cities of Beijing and Tianjing, covering

an area of 12.7×10^4 km^2. The Bohai Gulf Sea covers an area of 7.3×10^4 km^2 with an average water depth of 18 m. The first discovery, the Shengtuo oil field, was made in 1964 and, to date, more than 199 oil fields including 16 giant oil fields have been discovered and developed. Thus, it is an important oil and gas province of China. In 2000, the annual oil production was 56 million t/yr (or 1.12 million bopd), and natural gas production was 4.6 billion cu m/yr. Cumulative oil production was 1.4 billion t (or 10 billion bbl) and cumulative natural gas production was 72 billon cu m. Oil and gas exploration is still active in this prolific basin.

Basin history

The Bohai Gulf basin (Figs. 5 and 9.6A) is a Mesozoic–Cenozoic rift developed on the North China Platform whose crust is 29–37 km in thickness. The Archean Taishan crystalline complex series constitutes the basement of the basin. The Changcheng, Jixian, and Qingbaikou Middle and Late Proterozoic megasequences consist mainly of marine carbonates reaching a thickness of up to about 9400 m. The Cambrian, Early, and Middle Ordovician sediments are mainly carbonates intercalated with thin shales and evaporites and between 1000 and 1500 m in thickness. The North China Platform was regionally uplifted after the Middle Ordovician. In the Middle and Late Carboniferous, deposition of alternating transgressive and regressive coal-bearing sequences 200–400 m in thickness took place. The Permian intracratonic formations are 300–1500 m thick in various depressions. Regional uplift took place in the Late Permian Hercynian tectonic phase. This phase of widespread uplifts caused by the Indosinian orogeny resulted in folding of formations from Proterozoic to Permian age throughout the whole of northern China.

The Mentoukou formation of Lower Jurassic age is composed of 1750 m of sandstones, mudstones, and conglomerates intercalated with coal seams, with basalt at its base. The Middle and Late Jurassic is composed of volcanic agglomerates, sandstones, mudstones, conglomerates, and volcanic tuffs intercalated with oil shales and coal seams: their maximum thickness is 8000–10,000 m. The Qingshan formation of Lower Cretaceous age is composed of tuffs, andesitic agglomerates, andesites, basalts, tuffaceous conglomeratic sandstones, and siltstones with variable thicknesses of up to 1200–5400 m. The Wangsi formation of Upper Cretaceous age is composed of sandstones, conglomerates, siltstones, and mudstones with a thickness of 2000–4360 m.

The Kongdian formation of Paleocene–Eocene age and the Shahejie and Dongying formations of Eocene–Oligocene age, composed of sandstones, mudstones, oil shales, fossiliferous limestones, and conglomerates, were deposited in the rift basins with thicknesses of 2000–5000 m. The Miocene Guantao, Pliocene Minhunzhen, and the Pingyuan formations of Quaternary age are composed of conglomerates, sandstones, and mudstones whose total thickness is 1400–5000 m.

Because of the strong effects of the Yanshan orogeny, the Paleozoic and Pre-Paleozoic Erathem formations were highly deformed and eroded in several

stages. The Jurassic–Cretaceous rift basins were uplifted and subjected to intensive erosion. Only the Paleogene rift basins and their Neogene–Quaternary cover have been well preserved in the Bohai Gulf basin.

Fig. 9.8 is a pre-Cenozoic subcrop (i.e., "paleogeologic map") that shows the preserved residual distribution of Paleozoic and Proterozoic megasequences and their underlying Precambrian basement all involved the Jurassic/Cretaceous rifting progress, and also in subsequent Cenozoic rifting.

Tectonic framework

In the Bohai Gulf basin, under strong regional tensional stress, the North China Platform was extended and separated into blocks. Rifting and volcanic activity possibly started during the Upper Triassic Indosinian orogeny and the Lower Jurassic Yanshan orogeny. The main zones of rifting were the NNE-striking Tanlu, Cangxian–Dongming, and East Taihang fault zones and the east–west striking Beitang–Leting, Qihe-Quangyao, and Huanghe fault zones.

In the Paleocene–Eocene–Oligocene Huabei phase, the basin was subjected to the most important phase of strong differential block-faulting movements.

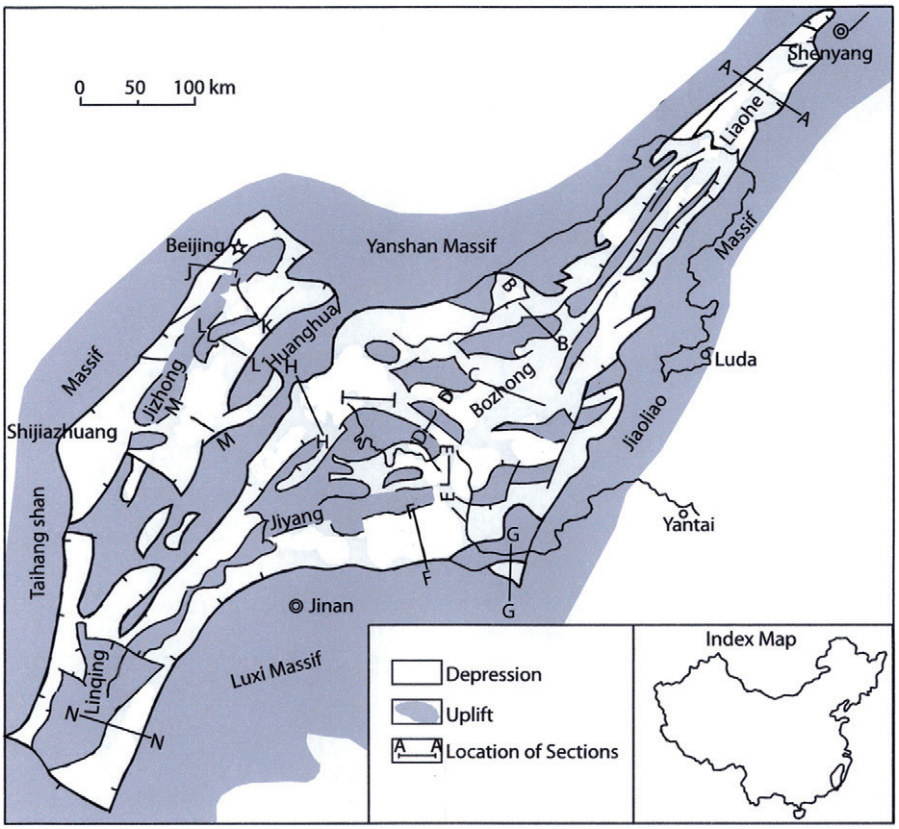

Figure 9.6 (A) General map showing depressions and uplifts of Paleogene in Bohai Gulf Basin, China (with location of schematic cross-sections Fig. 9.7A and B).

(Continued)

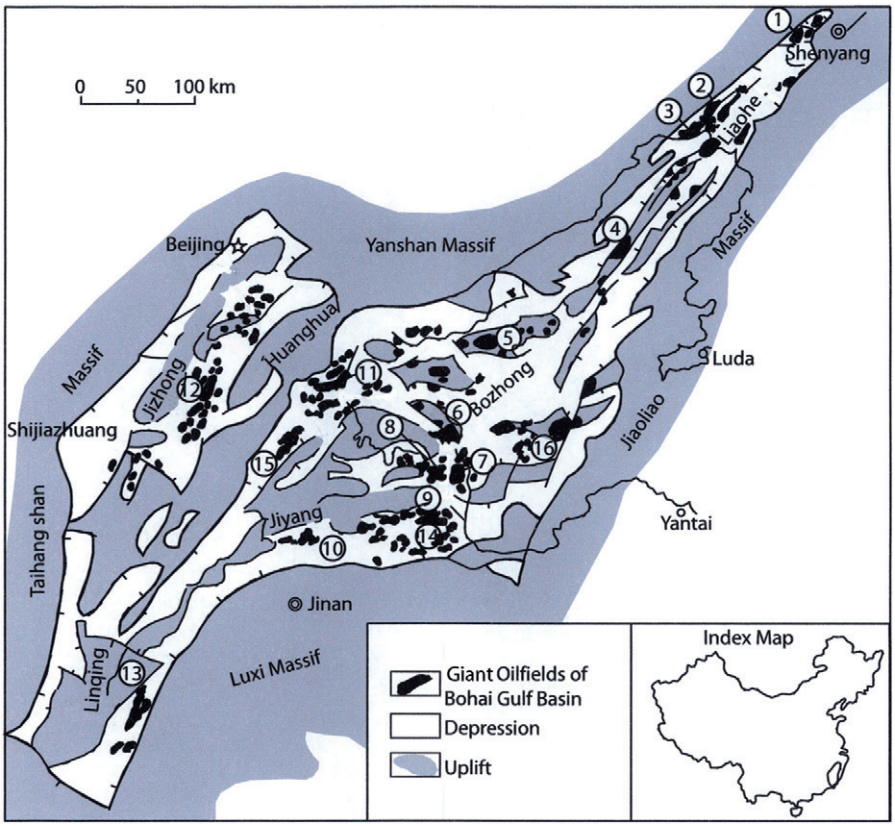

Figure 9.6 Cont'd (B) Oilfields:
1. Dongshenpu–Jinganpu;
2. Shuguang;
3. Huanxiling;
4. SZ36-1;
5. QHD32-6;
6. Chengdao;
7. Gudong;
8. Gudao;
9. Shengtuo;
10. Linpan;
11. Beidagang;
12. Renqiu;
13. Dongpu;
14. Dongxin;
15. Wangguantun–Zaoyuan;
16. Pl19-3.

Under the general tensional stress during successive periods of extensions, synrift subsidence coupled with rapid deposition in the old zones of rifting resulted in a new fragmentation of the basin floor. The margins of the grabens or half-grabens were uplifted and subjected to erosion. Along the elevated flanks, erosion cut deeply into Paleozoic and Upper Proterozoic strata and locally even into the Archaeozoic metamorphic complex.

The Paleogene depression systems of the Bohai basin are distributed along the following rifting zones (Fig 9.6A and Fig. 7):

a. *Tanlu rift zone*. It is a composite fault zone with four NNE-striking faults and consists of a central horst (Gongdanshan horst) situated between the Luxian and Yihe grabens. It extends from the central Shandong region northward to the Liaodongwan and Lower Liaohe depressions, which appear in the same structural framework with a central horst situated between the Liaohe west and east depressions. The central horst bifurcates and leads to the formation of three Paleogene depressions in the Liaodongwan area.

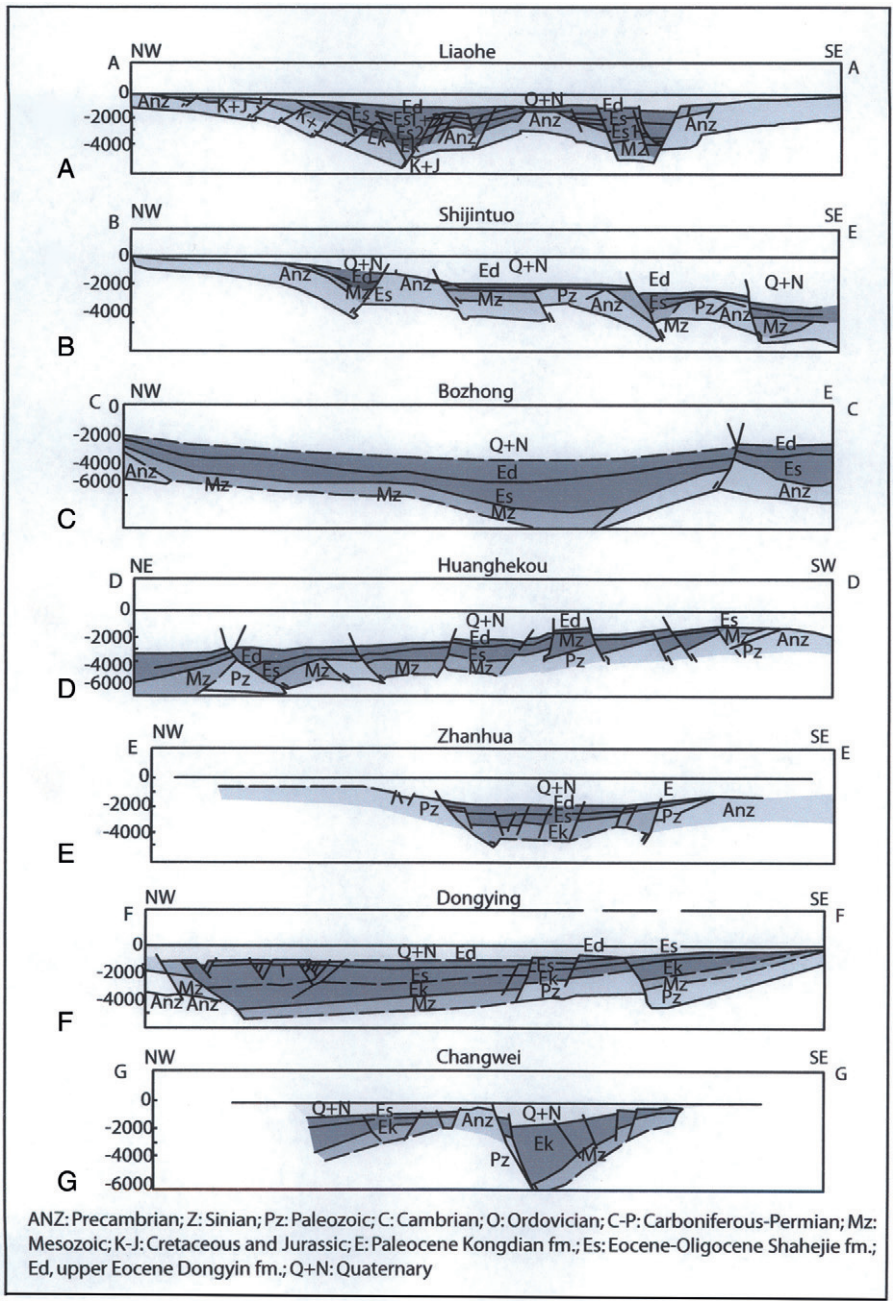

Figure 9.7 (A) Schematic cross-sections A-G across the major depression of the Bohai Gulf basin (for locations see Fig. 9.6A).

(Continued)

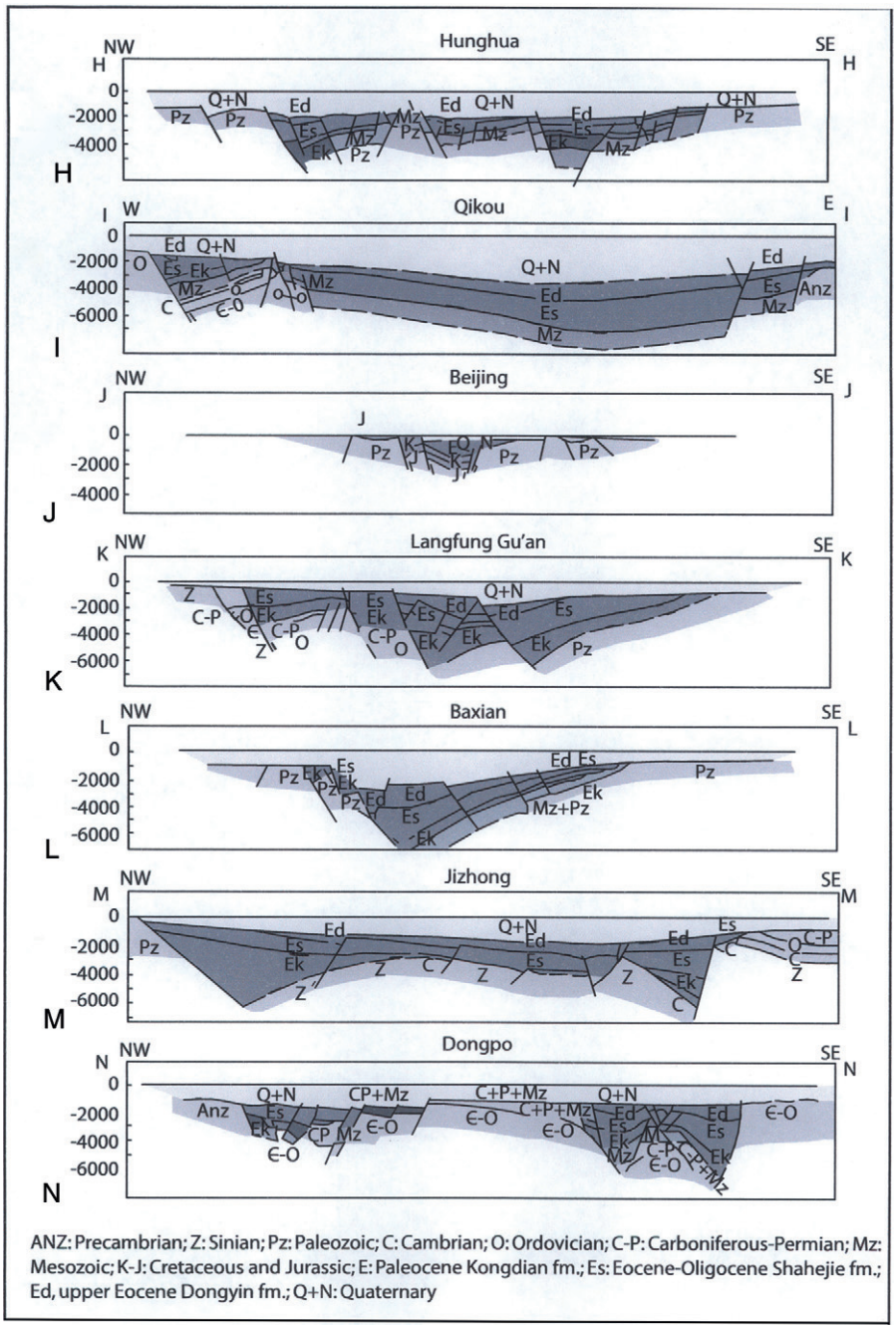

Figure 9.7 Cont'd (B) Schematic cross-sections H-N across the major depression of the Bohai Gulf basin (for locations see Fig. 9.6A).

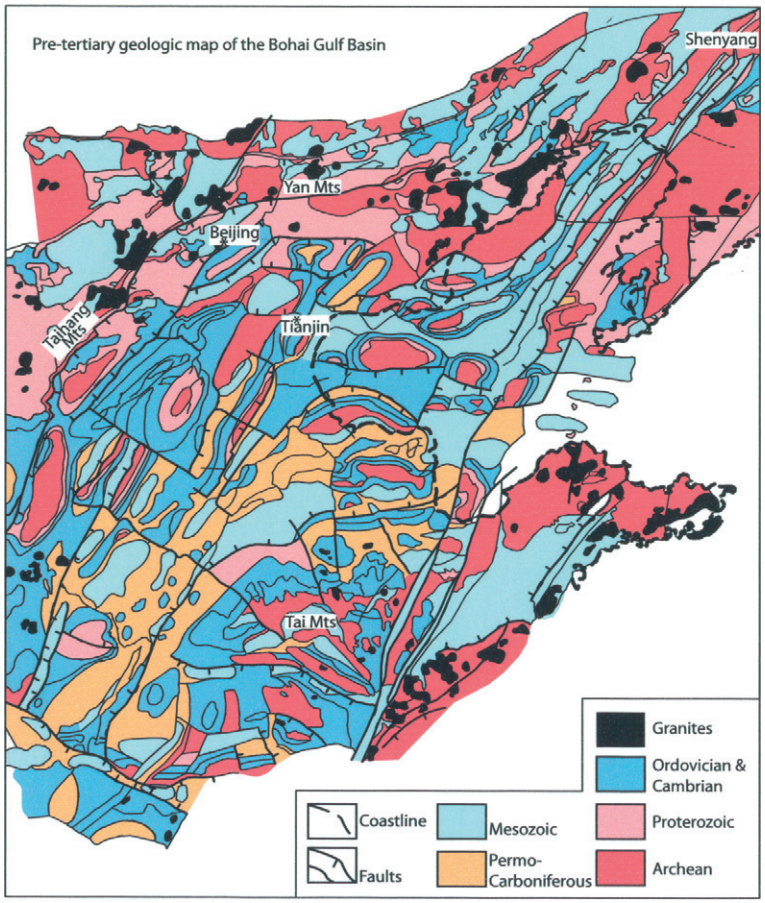

Figure 9.8
Pre-tertiary geologic map of the Bohai Gulf Basin and adjacent areas.

b. *Beitang–Leting rift zone*. It divides into the Laowangzhuang–Matouying–Shijiutao south rift zone, the Shijiutao south rift zone, the Shijiutao north rift zone, and the Haizhong north rift zone. The associated depression system, including the Qinnan, Nanpo, and Bozhong depressions, roughly follows the above-mentioned rift zones.

c. *Qihe–Quangyao rift zone*. It divides into the Pingfangwang and Chengjiazhuang–Binxian south rift zones and the Chengdong rift zone. The associated half-graben system, including the Dongying, Linnan, Zhanhua, Chezhen, Yangjiaogou, Chengbei, and Shanan depressions, roughly follows the above-mentioned rift zones.

d. *Cangxian–Dongming rift zone*. The margins are faults and monoclinal flexures. The associated depression system, including the Beitang, Banjiao, Qikou, Candong, Nanpi, Wujiao, Dezhou, Guanxian, Xinxian, and Dongpo depressions, roughly follows the above-mentioned rift zones.

e. *East Taihang rift zones*. There are two parallel rift zones. The first is the Handan–Shulu–Baxian rift zone with its associated depression system, including the Julu, Shulu, Yanyang, Baxian, and Wuging depressions, which roughly follow the rift zone. The second is the Shijiazhuang–Zhuoxian–Daxing rift zone with its associated depression system including the Shijiazhuang, Jixian, Baoding Xushui, Guan, and Daichang depressions, which roughly follow the rift zone.

f. Owing to renewed activity on the Nankou–Linshan rift zone, the Beijing and Linshan depressions were formed.

g. Owing to the activity on the Feicheng, Taian–Dongyandiian, Yangliudian–Xintai, Mengshan, Wenshan–Linyi, Peixian, and Changwu rift zones in the Luxi massif and southwestern Shandong region, the Feicheng, Dawenkou, Laiwu, Xintai, Mengying, Sishui, Wensheng, Jingxiang, and Chengwu depressions were formed (Fig. 9.7).

Information obtained from recent geophysical exploration and drilling in the Bohai Gulf basin and additional data available from adjacent areas show that the basin is controlled by a series of low-angle normal faults (dips mostly 35–50°). The tilted fault blocks whose basement is of Paleozoic, Upper Proterozoic, or pre-Upper Proterozoic age appear to have widths of 2–15 km and bounding fault throws of 1–10 km, due to the active extension of the rift zone along low-angle normal faults. Many of the depressions are fault-bounded on one side and monoclinally bounded on the other, forming a half-graben and adjacent rollover; a few depressions are fault-bounded on both sides, forming grabens (Fig. 9.7).

The Bohai Gulf basin is therefore characterized by differential block-fault movement. It is a complex geological entity comprising a series of half-graben and graben in which various combinations of source beds and reservoirs were deposited with various types of structural and stratigraphic oil and gas traps (Fig. 9.9).

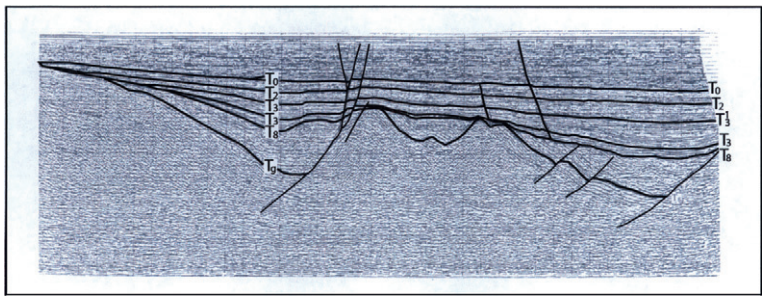

Figure 9.9
Regional seismic profile of Bohai Gulf Basin *(after Lin Dianzhong et al., 2001).* T_0, bottom reflector of Pliocene Minhuazheng Fm.; T_2, bottom reflector of Miocene Guantao Fm.; T_3, bottom reflector of Oligocene Dongying Fm.; T_8, bottom reflector of Paleogene Fm.; T_9, bottom reflector of Cretaceous.

Subsidence history

The Bohai Gulf basin, with a length of 1080 km from northeast to southwest, and a width of 65–530 km from west to east, includes six major depressions and three major uplifts: the Liaohe depression in the northeastern part, the Bozhong depression in the eastern part, the Jiyang depression, the Huanghua and Jizhong depressions in the central part, and the Linqing depression in the southwestern part. The Chengning uplift is situated between the Jiyang depression and Huanghua depression; the Cangxian uplift between the Huanghua depression and Jizhong depression; and the Neihuang uplift is located in the central part of Linqing depression. Secondary normal faults controlled 55 sags and 44 minor swells within the 6 depressions. Each sag is controlled by one major normal fault and they are usually half-graben or graben.

The Cenozoic subsidence history of the Bohai Gulf basin is divided into a Paleogene synrift phase and Neogene postrift phase (Fig. 9.10).

Synrift phase

The Paleogene synrift phase comprises two rift phases. During the first phase of rifting, the Paleocene–Eocene Kongdian formation and the fourth Member of the Shahejie formation were deposited. During the second rift phase, the Eocene–Oligocene third + second + first Members of the Shahejie formation and Dongying formation were deposited (Ren et al., 2002; Qiu Yinan et al., 1997).

There are three important unconformities in the Paleogene synrift phase; they lie between the Kongdian formation and the fourth Member of the Shahejie formation, between the third Member and second Member of the Shahejie formation, and between the Dongying formation and the Neogene Guantao formation, respectively.

The sediments of the Paleogene–Eocene Kongdian formation and the fourth Member Shahejie formation were mainly distributed along the major fault zones, for example, the Langgu, Baoding, and Shijiazhuang sags, along the east fault zone of the Taihang Mountains; the Cangdong, Nanpi, and Dongpu sags, along the Cangdong and Liaolan fault zones; the Dongying and Huimin sags, along Jihe-Guangrao fault zone; and the Changwei sag, along the Tanlu fault zone (Fig. 9.11).

As one of the distinctive characteristics of Bohai rift basin, Paleocene–Eocene basalts are widespread in the Liaohe, Huanghua, and Jiyang depressions. Thick basalt sequences are intercalated with thin-bedded dark gray, black mudstone, carbonaceous mudstone, and thin-bedded coal seams. Volcanism took place in lacustrine and swampy environments.

The sediments of the Eocene–Oligocene 1–3 Member Shahejie formation and Dongying formation represent deposition during the second rifting phase. The sedimentary area of the Bohai Gulf basin subsided greatly in the Shahejie-3 phase: paleoclimatic conditions were far more humid than in Paleocene–Eocene

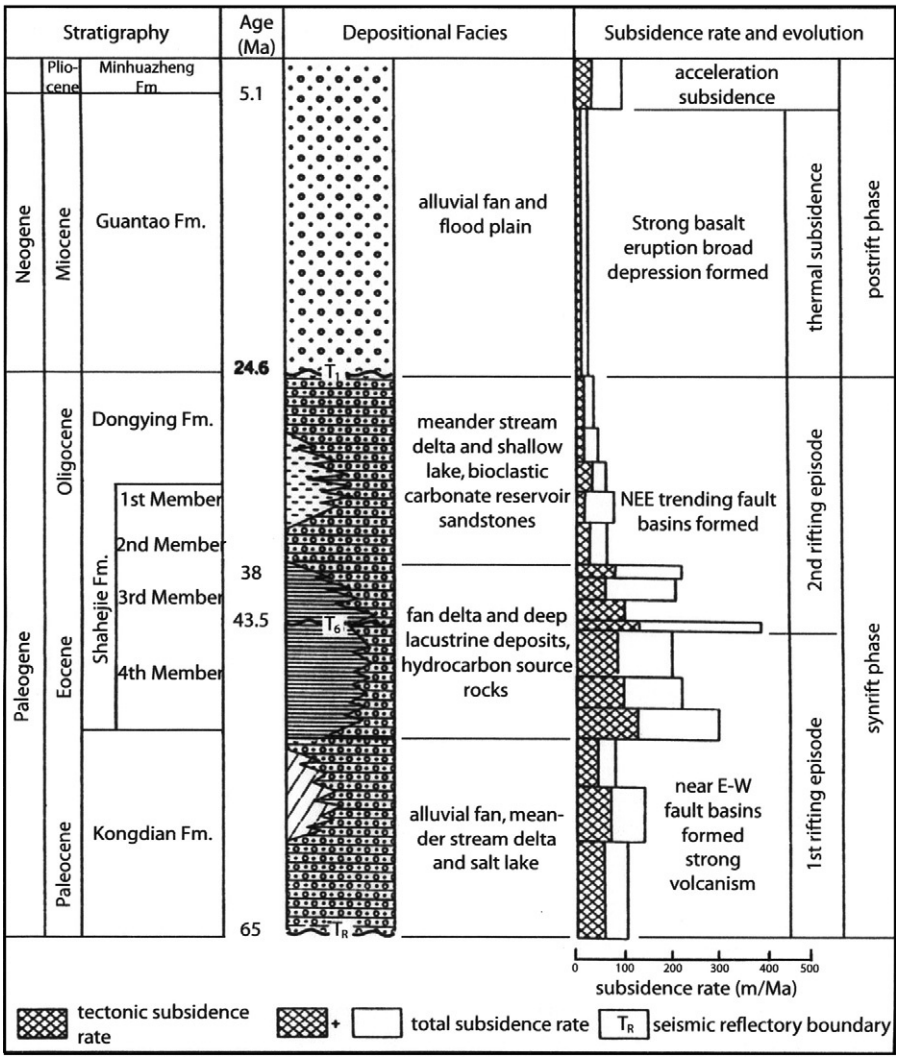

Figure 9.10
Filling sequences and subsidence history of Bohai Gulf basin *(after Ren Jianye et al., 2002)*.

time. The basin rapidly changed into deep lake environments. Sediments of this phase are characterized by large suites of dark gray mudstone which are the major source rocks whose presence determines the hydrocarbon potential in each prospective sag (Fig. 9.12).

A general uplift took place between the Shahejie-3 and Shahejie-2 phases (about 38 Ma age between the Eocene and Oligocene). The lacustrine facies of the Shahejie-3 Member changed into the fluvial and shallow lake facies of

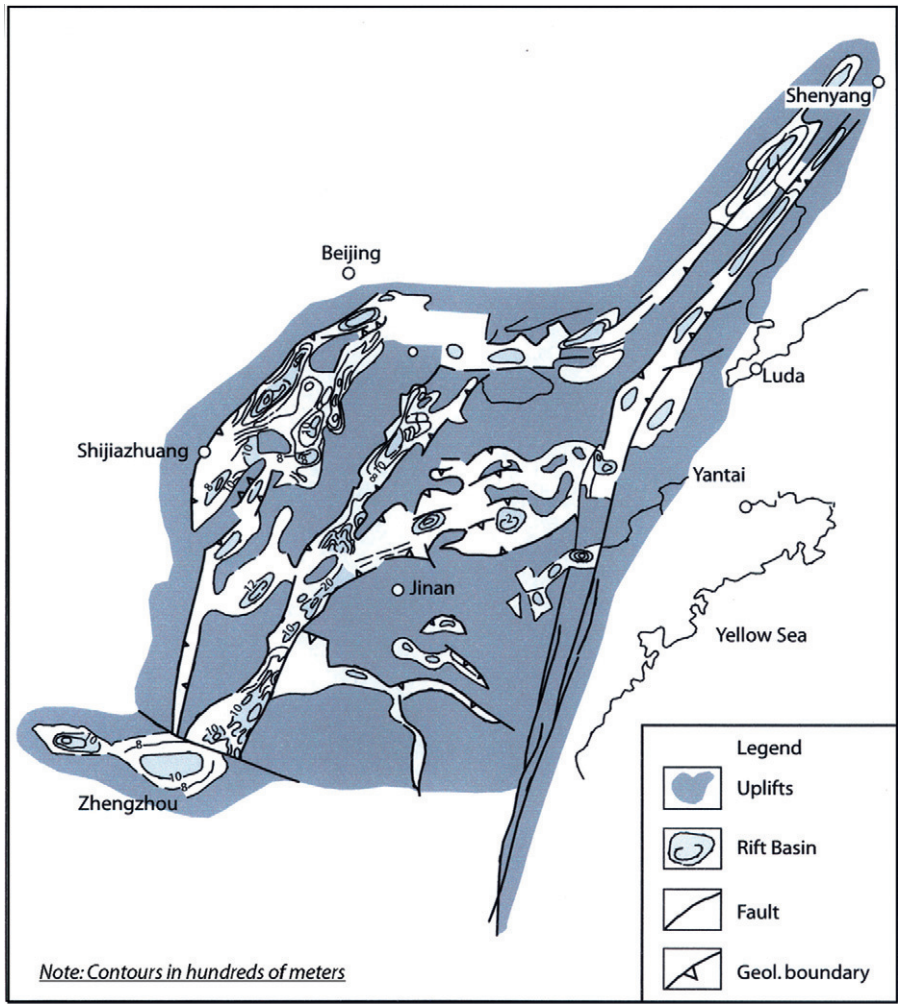

Figure 9.11 The sediments of the 1st rifting episode of the Paleocene–Eocene age Kongdian formation and fourth Member of Shahejie formation in Bohai Gulf Basin.

the Shahejie-2 Member represented by yellowish sandstones with grayish green, brownish red, and gray mudstones.

Following the Shahejie-2 phase, the basin continued to stably subside and expand into the Shahejie-1 phase. The climate became humid and lake waters saline. Sediments comprise gray, grayish green mudstone with biolimestone and dolomite.

The Donying formation represents the last phase of rifting. The depocenter shifted toward the Bozhong depression. Drainage, developed in marginal source areas, transported large amounts of clastic rocks into the lake basin. Fluviodeltaic deposits were widespread. The Dongying formation, over 2000 m thick in the Bozhong area, is composed of gray, dark gray, grayish brown mudstone with a few thin-bedded sandstones with abundant shallow lake environment fossils.

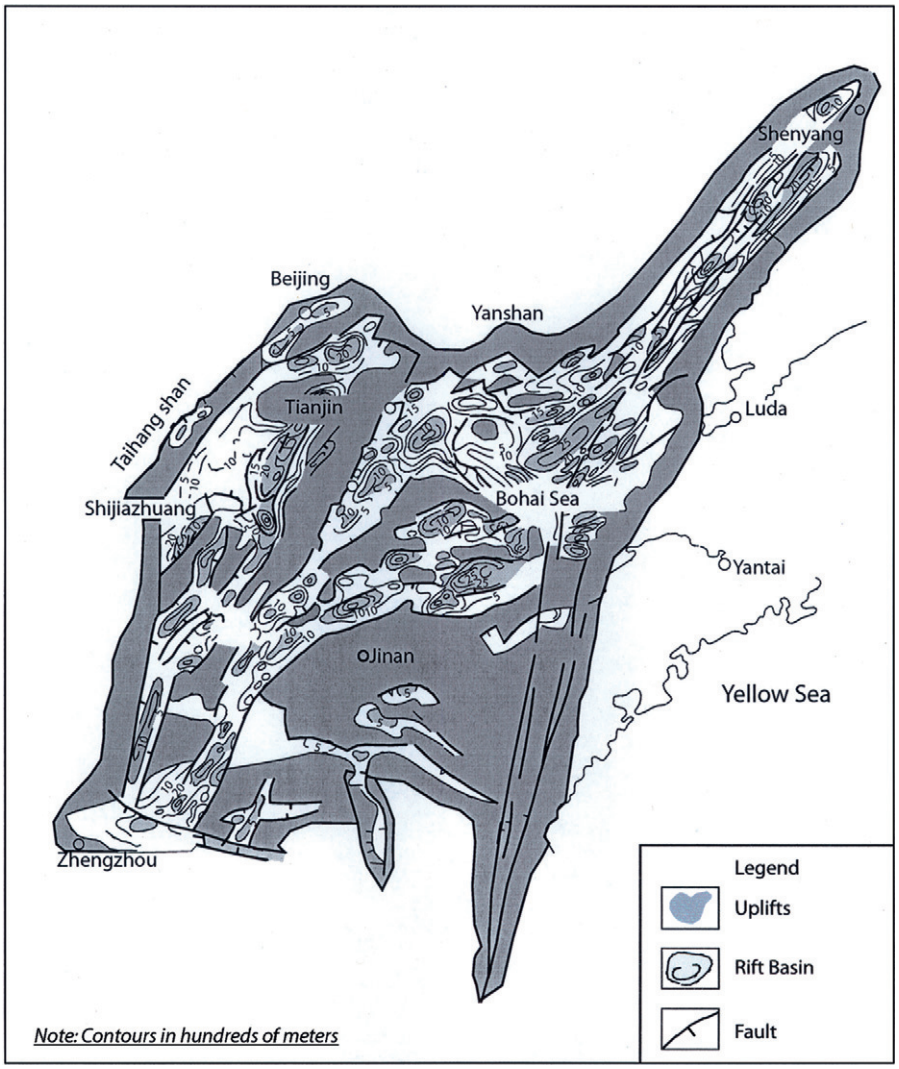

Figure 9.12 The sedimentary areas of the second rifting episode of the Eocene–Oligocene Shahejie 1–3 Members and Dongying formations in Bohai Gulf basin.

Postrift phase

During the Neogene stage, the Bohai Gulf basin was involved in postrift regional subsidence, forming a broad depression over the whole basin area. The fluvio-deltaic Miocene Guantao formation and the Pliocene Minhuazheng formation covered both uplifts and sags and are composed of conglomerates, conglomeratic sandstones, sandstones, and mudstones with a thickness of 800–3000 m.

The Quaternary age Pingyuan formation is composed of conglomerates, sandstones, mudstones, and aeolian loess deposited as horizontal strata with thickness of 400–1000 m (Fig. 9.13).

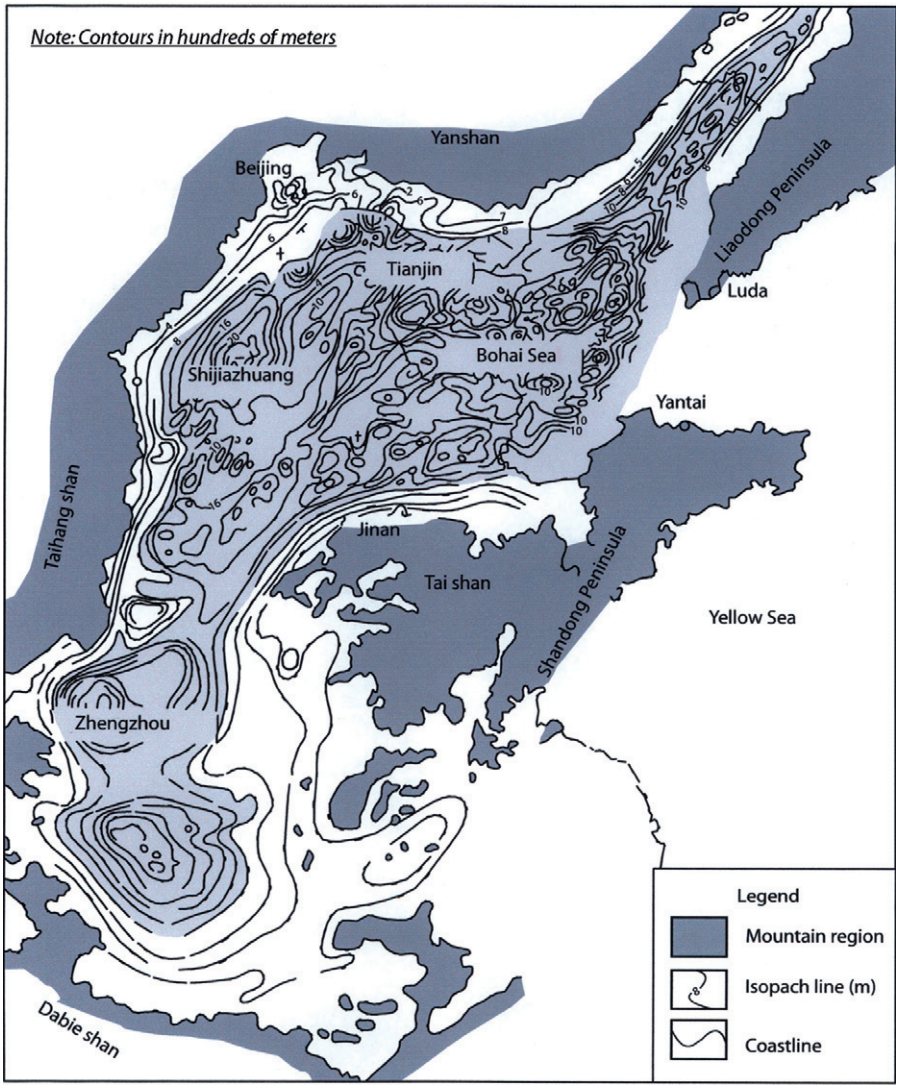

Figure 9.13 Sedimentary areas and isopachs of the postrift phase of Neogene–Quaternary formations in Bohai Gulf basin.

Hydrocarbon trap types

The tectonic fabric of the Bohai Gulf, comprising multiple uplifts and depressions, was developed by major block fault movements predominantly during the Yanshan and Himalayan orogenies. The abundant oil and gas resources of the basin have accumulated in relatively complex traps of various origins. There are hundreds of megastructural belts in which oil and gas have accumulated in many highly productive blocks. Due to block faulting, unconformities, and facies changes, the petroliferous traps include different pay horizons and different trap styles, which combined

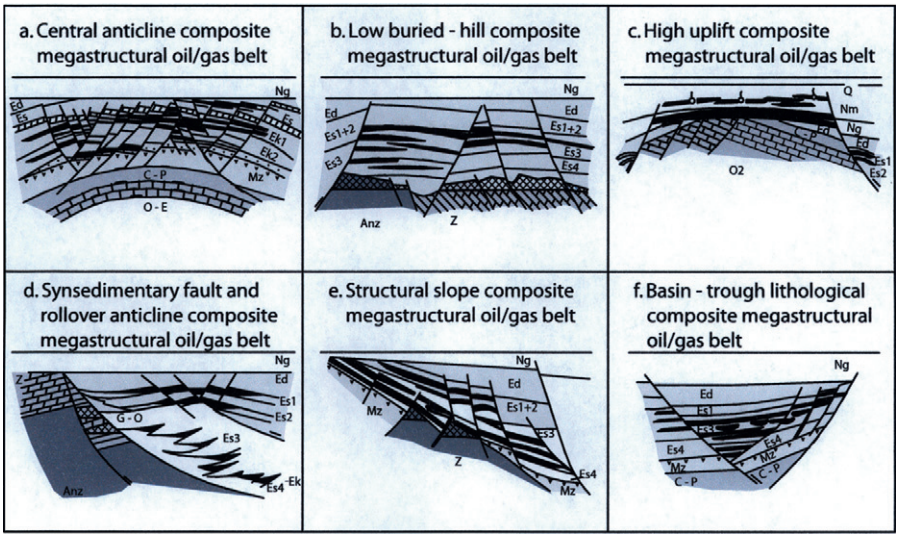

Figure 9.14 The composite megastructural hydrocarbon trap types of Bohai Gulf basin.

with one another to form megastructural oil fields. Six conceptual models for composite megastructural oil fields are described as follows (Fig. 9.14):

a. *The central anticline belts* (Fig. 9.14) include the faulted anticline belt formed in the central part of the sag. Therefore, each central anticline constitutes a rich belt of hydrocarbon reserves. The central anticline belts were distributed in large scale and controlled by major fault systems. Some large anticlinal closures are 50–100 km in axial length and 5–10 km in width. The structure belts are often complicated by a series of secondary faults. The secondary structural belt controls the accumulation of oil and gas. The main fault blocks have always been found with the greatest hydrocarbon columns. Lithological traps may be distributed on favorable paleoerosional surfaces. The central anticline belt consists of fault block oil pools and lithological oil pools in the composite megastructural oil and gas fields, such as the Dongxin central anticline belt of the Dongying sag (Fig. 9.15) and the Wenliu central anticline belt of Dongpu sag (Fig. 9.16).

b. *Low buried-hill composite megastructural oil/gas belt* (Fig. 9.14). The known buried-hill structures can be divided into the tilted fault block hills with monoclinal stratigraphic traps and the paleogeomorphic hills with massive basement traps. There are many types of reservoir rocks such as Mesozoic clastics and volcanics, Permo-Carboniferous sandstones, Cambro-Ordovician carbonates, Middle and Upper Proterozoic carbonates, and Archaeozoic gneiss and metamorphic crystalline rocks. The oil has migrated from the depressions and from Tertiary source rocks above the unconformity but may also derive

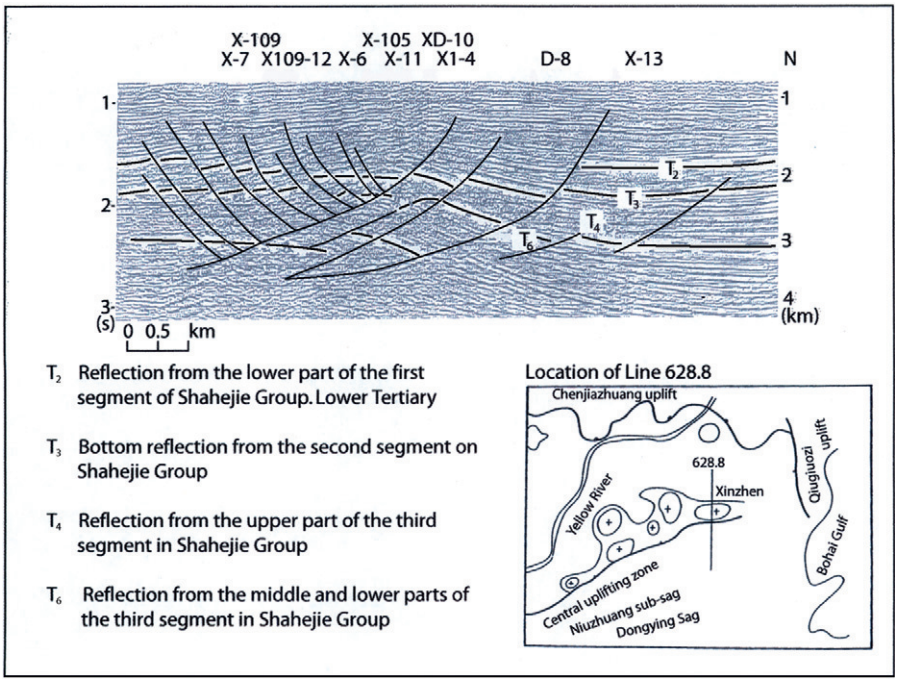

Figure 9.15
Seismic profile Line 628.8 showing the Dongxin central anticline belt of the Dongying sag, Ji yang depression.

from the Paleozoic. The hydrocarbon accumulations and column heights in the tilted fault block traps depend upon the relative displacements between the upthrown and downthrown blocks and the high production depends on cavities, pores, and fissures. Neogene sediments on buried hills generally drape the anticlinal structure with the characteristic that the traps are charged by large-scale vertical migration. Before the Paleogene onlapped the buried hills, a set of sandstones was deposited followed by bioclastic and reefal limestones on the top of buried hills in shallow water with associated sediments pinching out updip such as alluvial fans and bars distributed along the flank. Rollover anticline traps are developed on the downthrown side of growth faults. The low buried-hill structural belt is situated at the central part of a half-graben or graben. It has always been found near the oil-generating area with the shortest migration distance, with greater structural amplitude, multiple-pay horizons, and multiple trap types. Such types of oil and gas megastructural belts are more likely to develop into good exploration targets in the Bohai Gulf basin, for example, the Renqiu low buried-hill oil field of the Jizhong depression (Fig. 9.17).

c. *High uplift composite megastructural oil/gas belt* (Fig. 9.14). No Paleogene formations on the top of high uplift buried hill were deposited or are absent by

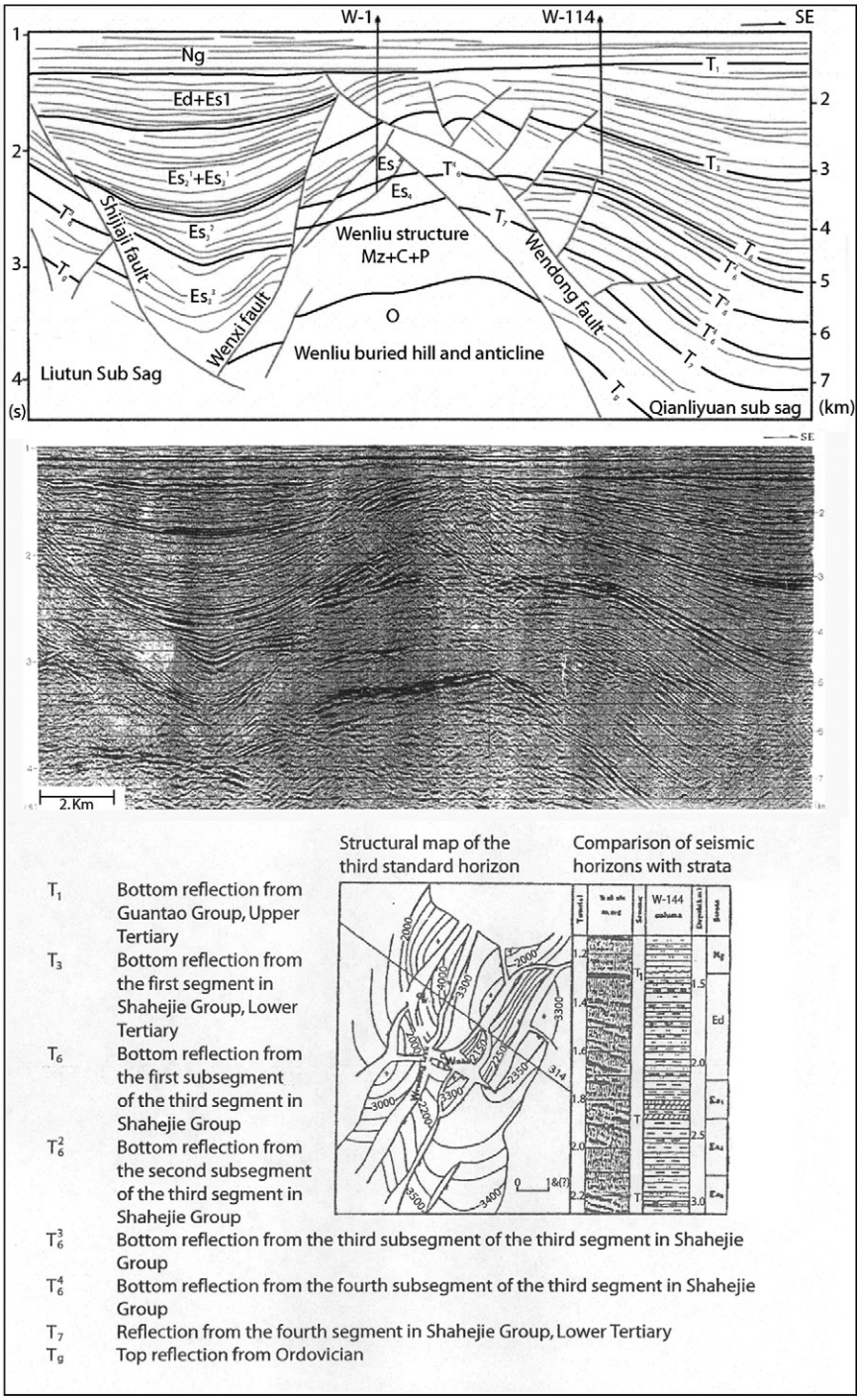

Figure 9.16
Seismic profile Line 314 showing the Wenliu central anticline belt of the Dongpu sag, Linqing depression.

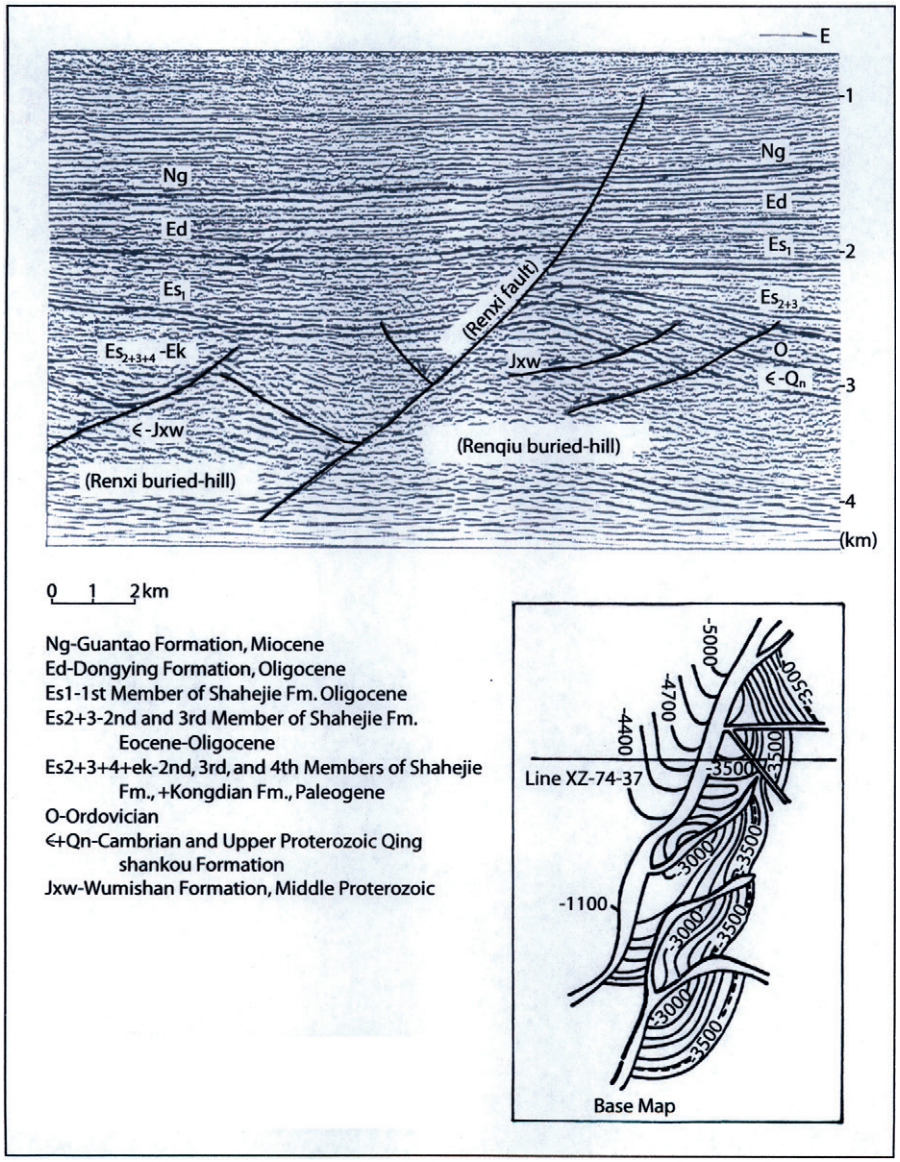

Figure 9.17
Seismic profile Line XZ-74-37 showing Renqiu low buried-hill oil/gas belt in Jizhong depression.

erosion. The paleo-oil pools were destroyed in the tilted fault block-buried-hill traps. Oil and gas migrated through unconformities to accumulate in Neogene formations as secondary oil and gas pools. Various types of traps are distributed around the flanks of a high uplift structural belt, such as step-faulted-type buried-hill traps; Paleogene rollover anticline traps may have

been formed on the downthrown side of synsedimentary faults. Several lines of small buried-hill traps may have been formed on the upthrown side of antithetic normal faults. Paleogene lacustrine fans, diluvial clastics, and bioherm buildups may constitute stratigraphic traps. The overlapping lines surrounded with the uplift were formed during deposition of Paleogene formations due to gradual expansion of lakes. The overlapping lines at different horizons followed the gullies and ridges of the ancient landform surface below the unconformity, forming many stratigraphically overlapping oil and gas fields. The high uplift structural belt is situated at the edge of a graben or half-graben. It is associated with large heavy oil reservoirs or composite oil and gas composite megastructural fields with heavy and light oil in different horizons, such as the Gudong high megastructural oil/gas belt in the Jiyang depression (Fig. 9.18).

d. *Synsedimentary fault and rollover anticline composite megastructural oil/gas belt* (Fig. 9.14). The belt is situated on the downthrown side of the synsedimentary border fault. Giant rollover anticlines located on the downthrown side of the border fault are common; fault blocks with some lithological conglomeratic traps constitute the composite megastructural oil/gas traps, such as the Langgu sag, northwest of the Jizhong depression (Fig. 9.19B).

e. *Structural slope composite megastructural oil/gas belt* (Fig. 9.14). This belt is distributed on the slope of the depression. Reservoir formations are eroded at their updip ends, with the remaining oil sealed by bitumen or tars, and are covered unconformably by younger formations. Downward on the monocline, Paleogene producing formations are well developed with the crude quality becoming better with richer gas combined with multiple-pay horizons and multiple trap types. Under the Tertiary unconformities, a series of counternormal faults of affecting Paleozoic to Proterozoic or Archaeozoic basement may constitute one or several lines of buried-hill traps along their strikes. Known oil accumulations are considered to be of high-yielding rates. The Paleogene dark-clay oil-generating source beds were deposited above the unconformity. Turbidities derived from the clastic materials of fault scarps, within the canyon fill generally containing thick pay horizons and good physical properties, combine with each other as the upper series of a composite of megastructural oil field, e.g. along the western slope of the Liaohe depression (Fig. 9.20).

f. *Basin-trough lithological composite megastructural oil/gas belt* (Fig. 9.14). The continental Paleogene rift basin provides favorable conditions for deposition of various types of sandstones in deltaic, alluvial fans, diluvial fan settings, etc. Along the delta slope, in the saddles between the paleogeomorphologic nose structures or the deeper parts of troughs around nearby buried hills, turbidities, channel fill sand bodies, deep lacustrine turbidities, and delta-front lenticular sand bodies were deposited by flood, landslide, and gravity

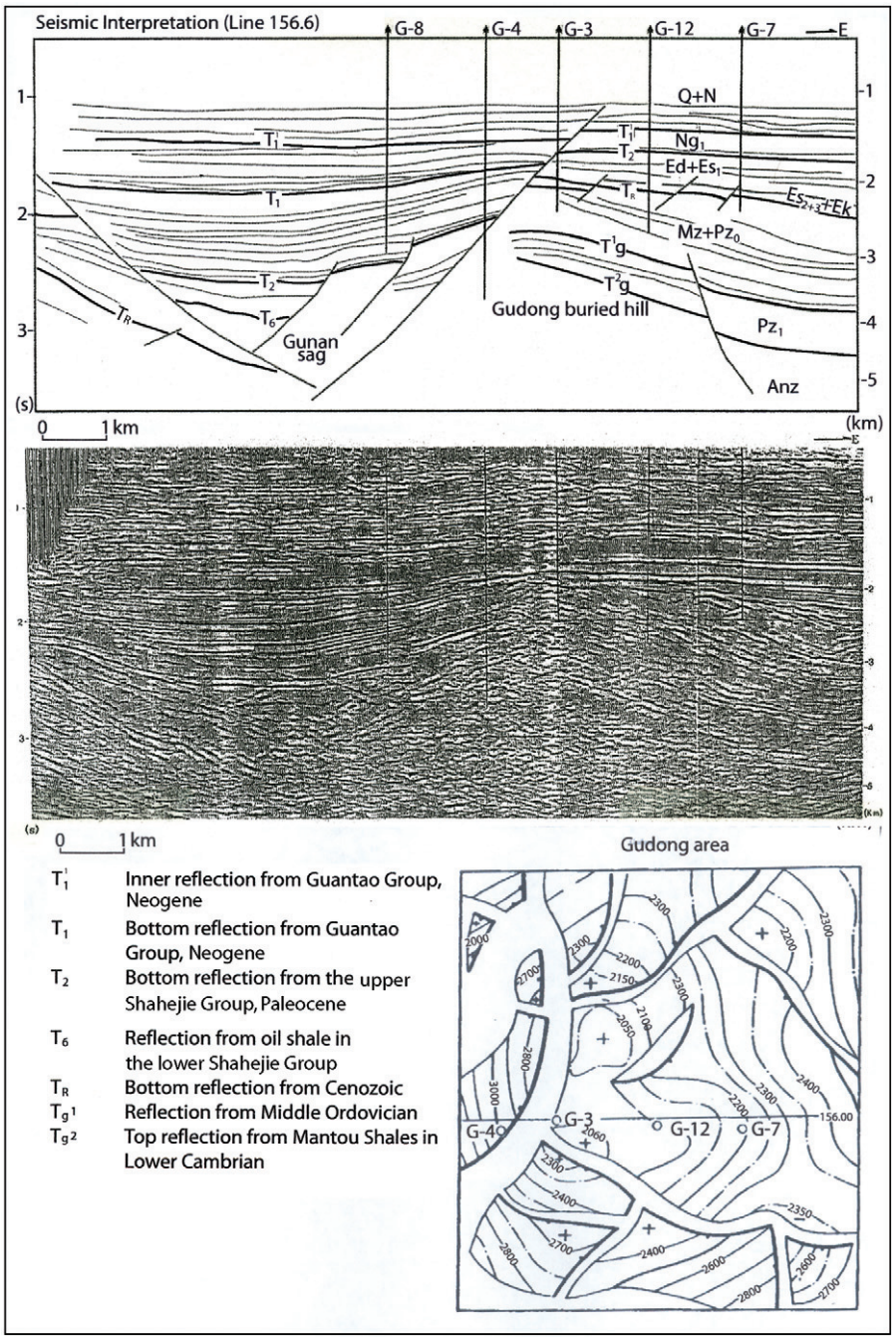

Figure 9.18
Seismic profile Line 156.6 showing Gudong high uplifted draping the anticlinal oil/gas belt in Jiyang depression.

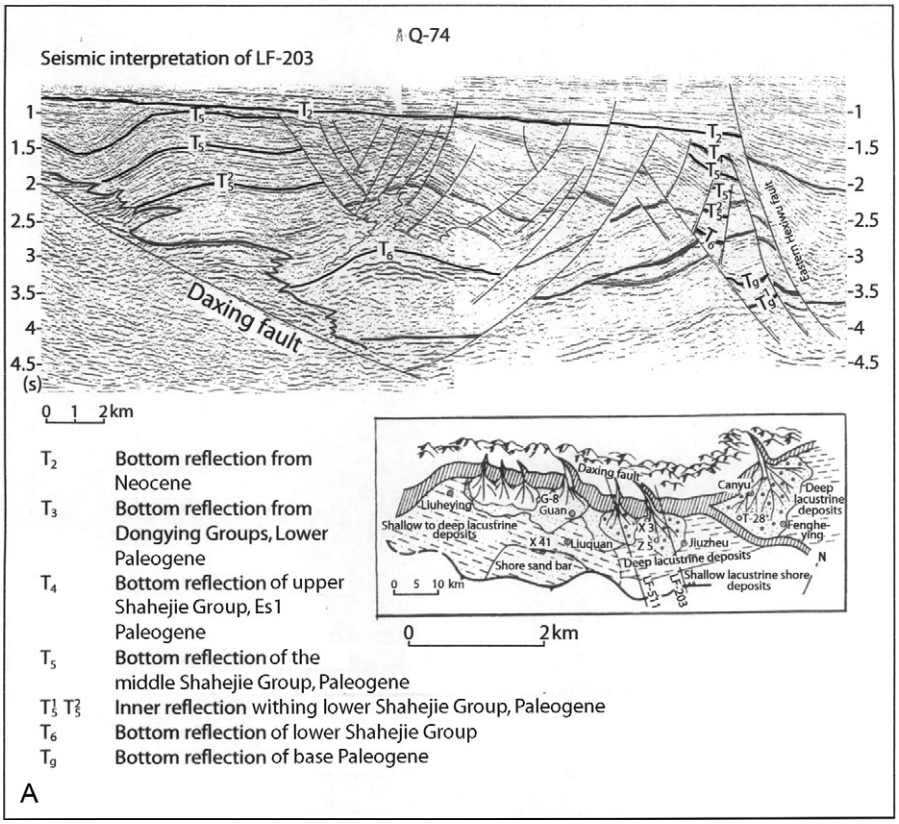

Figure 9.19 A Seismic profile Line LF-203 showing the synsedimentary fault and rollover anticline composite megastructural oil/gas belt in Langgu sag, northwest of the Jizhong depression.

processes. Various prograding turbidites flowed downward to the deep basin axis. Thus, there is an abundance of lenticular sandy zones flowing down the dip slope. The various turbidites and channel sand bodies were surrounded by thick source rock sequences to comprise source, reservoir cap rock combinations. Favorable oil traps may exist at the updip direction of sand bodies when the displacement of transverse normal or antithetic faults is greater than the thickness of the sand bodies.

Many oil and gas field have been discovered in the composite turbidites and channel sand bodies in the Oligocene Shahejie-3 Member. Mature source rocks in the Liaohe, Zizhong (Fig. 9.19A), and Huanghua depressions charge the Liangjialou deep water fan oil pools in the Jiyang depression (Fig. 9.21).

It has been previously described that the six types of composite megastructural oil and gas belts are situated at certain positions in a half-graben: on the steeper, faulted flank of the basin, there may occur high uplift composite megastructure oil and gas fields; on the downthrown side of large growth faults there may be developed fault terraces or rollover anticlines capable of trapping oil and gas.

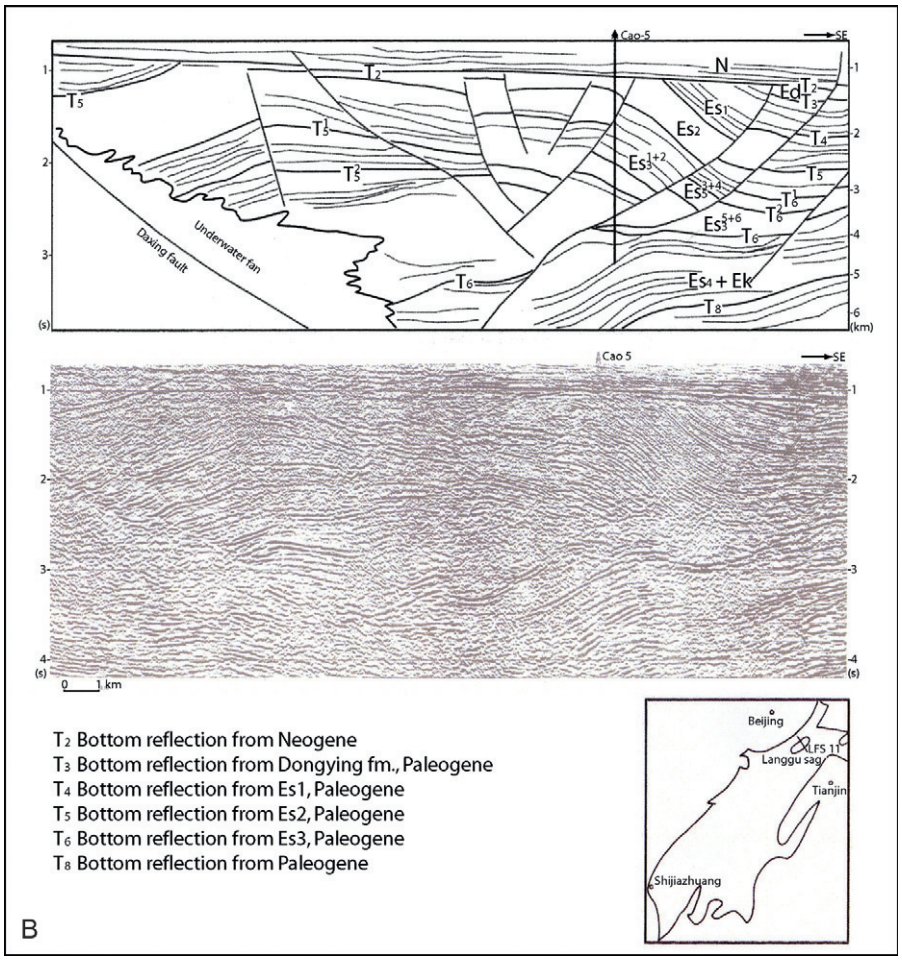

Figure 9.19 B Seismic profile Line LF-203 of Langfung Guan sag, Jizhong.

On the gentler flank of the basin, owing to the successive overlap of Paleogene sequences, slope composite megastructure oil and gas fields may be formed; however, due to the smaller amplitude of the synsedimentary faults, only small-scale rollover anticlines or structural noses can be formed on the Tertiary gentler flank. In contrast, a series of antithetic faults in basement may constitute one or several lines of small buried-hill traps along their strikes. In the deeper part of the basin, there may exist composite oil and gas fields constituted by channel sand bodies and turbidities. Due to the differential block-faulting movements, very prospective low buried-hill composite megastructural oil and gas fields may be formed, while the central anticline composite megastructural oil and gas field trend may also occur due to uplift.

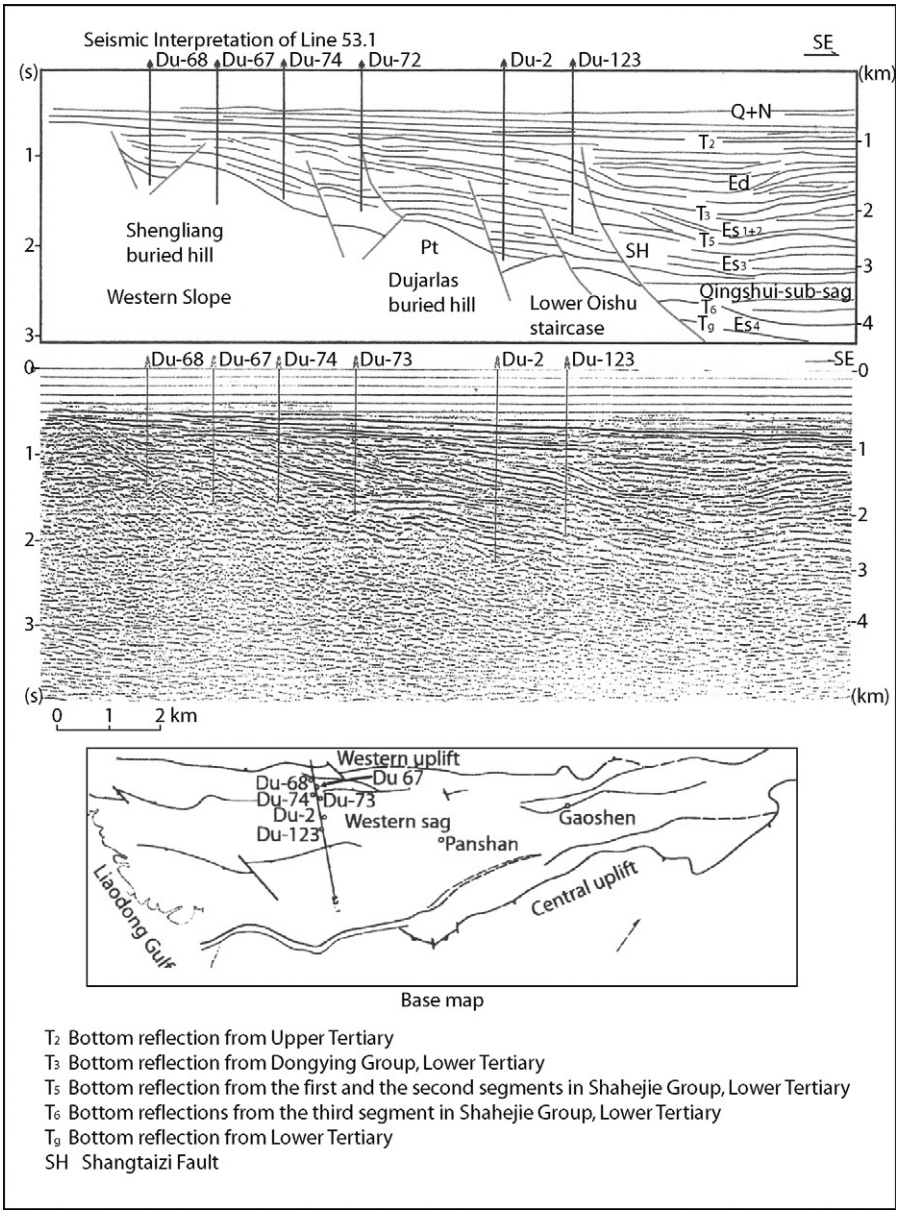

Figure 9.20
Seismic profile Line 53-1 showing the western slope composite megastructural oil/gas belt in the Liaohe depression.

In the graben depression, both sides of the steeper flanks may localize rollover anticlines or step-faulted structures. In the central portion of broad graben, low buried-hill composite megastructural oil and gas fields or central anticline composite megastructural oil and gas fields may be formed. In the deeper part

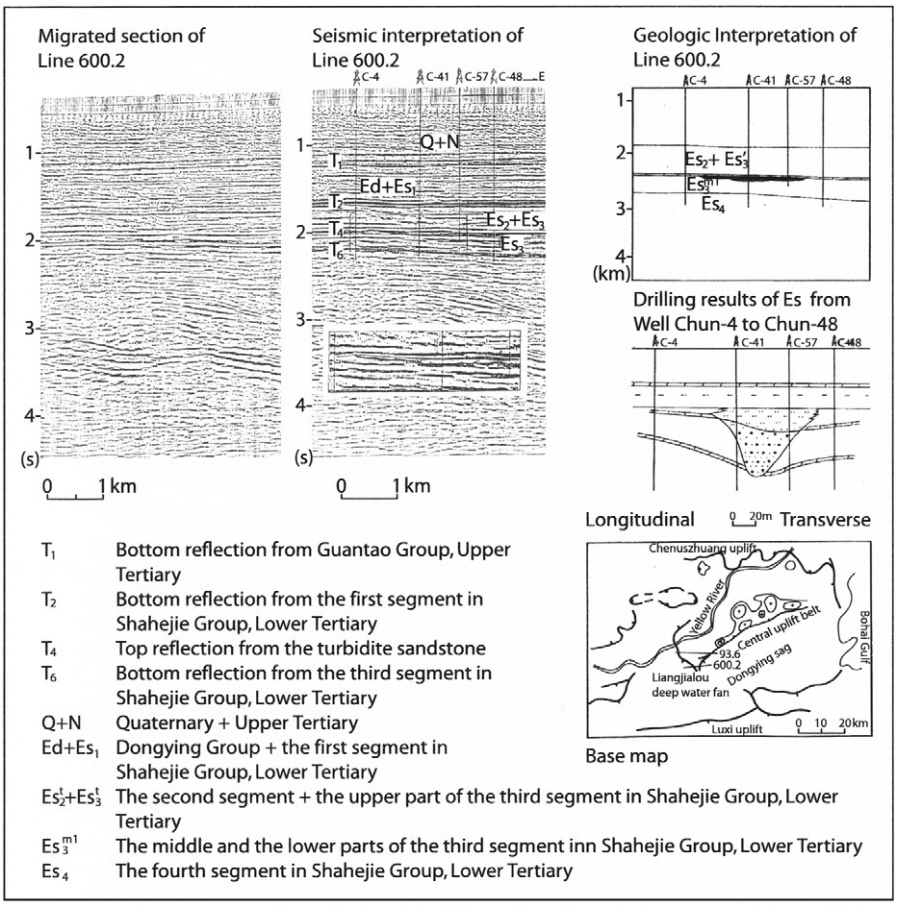

Figure 9.21 Seismic profile Line 600.2 showing the migrated section, seismic interpretation, geologic interpretation, and drilling results of Es_3 sand pools in the Liangjialou region, Jiyang depression.

of the faulted trough, a series of lithological composite oil and gas fields may exist (Fig. 9.22).

Therefore, each half-graben and graben with oil generation can be considered as a composite megastructural oil and gas field formed by various types of composite oil and gas accumulation belts. As exploration work continues and the accuracy of digital seismic techniques increases, more and more composite megastructural oil and gas fields including giant oil and gas fields and high production oil fields will certainly be found in the Bohai Gulf Basin.

The Subei basin

The Subei basin with an area of 35,000 km^2 is developed in the eastern part of the Yangtze Paleozoic Platform. According to the distribution and development of the Lower Tertiary succession, the Subei basin is divided into two depressions

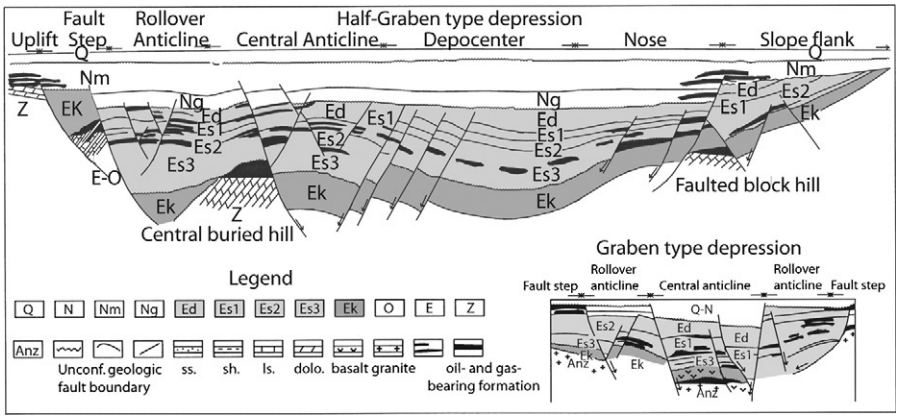

Figure 9.22 Structural models related to hydrocarbon occurrences in the half-graben-type or graben-type depressions of the Bohai Gulf basin.

(Dongtai and Yanfu) and two uplifts (Jianhu and Binhai), including 12 sags and 14 swells. Its western boundary is the famous Tanlu deep fault and the eastern offshore part is called the South Yellow Sea basin (Fig. 9.23).

The main formations in this area include the Taizhou formation (Et) of Paleocene age, the Funing formation (Ef) of Eocene–Paleocene age, the Dainan (Ed), and Sanduo (Es) formations of Oligocene–Eocene age, the Upper Tertiary Yancheng formation (Ny), and the Dongtai formation (Qd) of Quaternary age. The maximum thickness of these Cenozoic formations is over 7000 m.

There are six source rock intervals in the Lower Tertiary of the Subei basin, Et2, Ef1, Ef2, Ef3, Ef4, and Ed1. All of them are of subdeep lacustrine facies, with the main lithology of gray-dark mudstones. The total thickness of these source rocks is more than 400 m. Their evolution was controlled by tectonic subsidence; only 30% of the source rocks are mature in the deep parts of some sags.

The reservoirs in Subei basin include Et1, Ef1, Ef2, Ef3, Ed, Es, and Nf. Apart from some organic bank and ooid deposits in Ef2, the others are all sandstones. The physical properties in Et, Ef, and Ed1 are worse, with average porosities of 10–18% and permeabilities of 8×10^{-3}–700×10^{-3} μm^2, but those of Ed2, Es, and Ny are better, with average porosities of 21–26% and permeabilities of 209–2327 $\times 10^3$ μm^2.

The mudstones in Et2, Ef2, Ef4, Ed1, Es1, Es2, and Ny are well developed and are potential seals in the Subei basin.

After about 50 years of exploration from 1955 in Subei basin, about 680 wells have been drilled and commercial oil and gas was found in 261 wells with discovery of more than 50 small-scale oil and gas fields. Total proved oil reserves in place are about 1.85×10^8 t, with total oil and gas potential resources of about 6.8×10^8 t. The annual oil production of Subei oil fields in 2002 was 157×10^4 t, and annual natural gas production was 24×10^6 m^3.

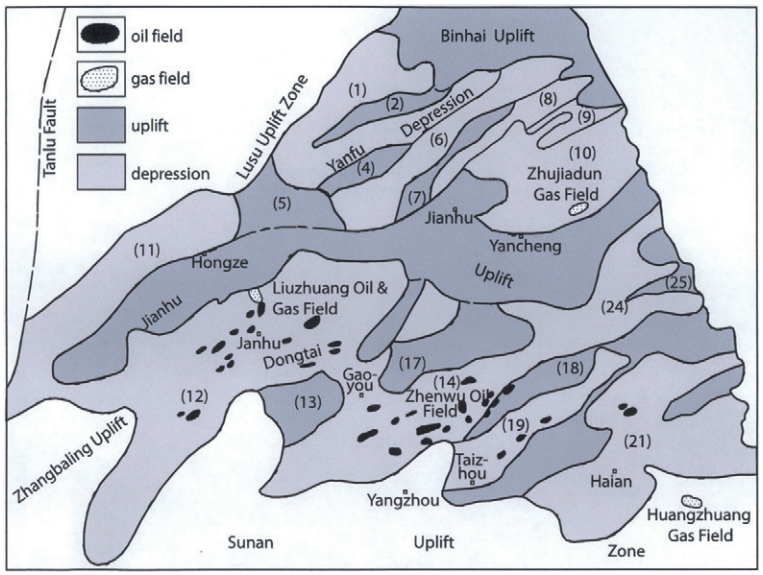

Figure 9.23
Tectonic units and oil and gas fields of the Subei basin.
1. Lianbei sag,
2. Dadong swell;
3. Liannan sag;
4. Sujiazui swell;
5. Huaiyin swell;
6. Funing sag;
7. Haligang swell;
8. Tongyanggang sag;
9. Xiawanggang;
10. Yangcheng sag;
11. Hongze sag;
12. Jinhu sag;
13. Lingtangqiao low swell;
14. Gaoyou sag;
15. Liubao low swell; 16. Linze sag;
17. Zheduo low swell; 18. Wubao low swell;
19. Qintong sag;
20. Taizhou low swell; 21. Haian sag; 22. Sancang low swell;
23. Xiaohai swell;
24. Baiju sag;
25. Yuhua swell.

The East China Sea Shelf basin

The East China Sea, facing the western Pacific Ocean, is one of the marginal seas of China. In the west, it is adjacent to the Shanghai, Zhejiang, and Fujian coastal areas, and in the east, it extends to the Ryukyu Islands. The East China Sea Shelf basin covers an area of 26×10^4 km^2 and in the west water depths are less than 120–150 m. It is divided into three zones: the eastern depression zone, the central uplift zone, and the western depression zone (Fig. 9.24).

The East China Sea Shelf basin is a major Cenozoic active marginal rift basin with sedimentary fill exceeding 10,000 m. Its basement comprises mainly older metamorphic rocks and Mesozoic igneous rocks. The overlying sediments are of Tertiary age, including the Shimentan, Lingfeng, and Mingyuefeng formations of Paleocene age, the Oujiang, Wenzhou, and Pinghu formations of Eocene age, the Huagang formation of Oligocene age, the Longjing, Yuquan, and Liulang formations of Miocene age, the Santan formation of Pliocene age, and the Quaternary Donghai formation; the major lithologies are clastic rocks.

Subordinate tectonic units are controlled by NE longitudinal faults, displaying an alternating distribution of three basinal and uplift belts. Basin evolution can be divided into five stages: (1) the Late Jurassic to Early Cretaceous thermal uplift stage; (2) the Paleocene–Eocene rifting stage; (3) the Oligocene depression stage; (4) the Miocene inversion depression stage; and (5) the Pliocene–Quaternary draping stage (Lee et al., 2006 ; Yang et al., 2008).

The source rocks in the East China Sea Shelf basin are of Paleocene, Eocene, Oligocene, and probably Lower Miocene age. The organic matter is mainly

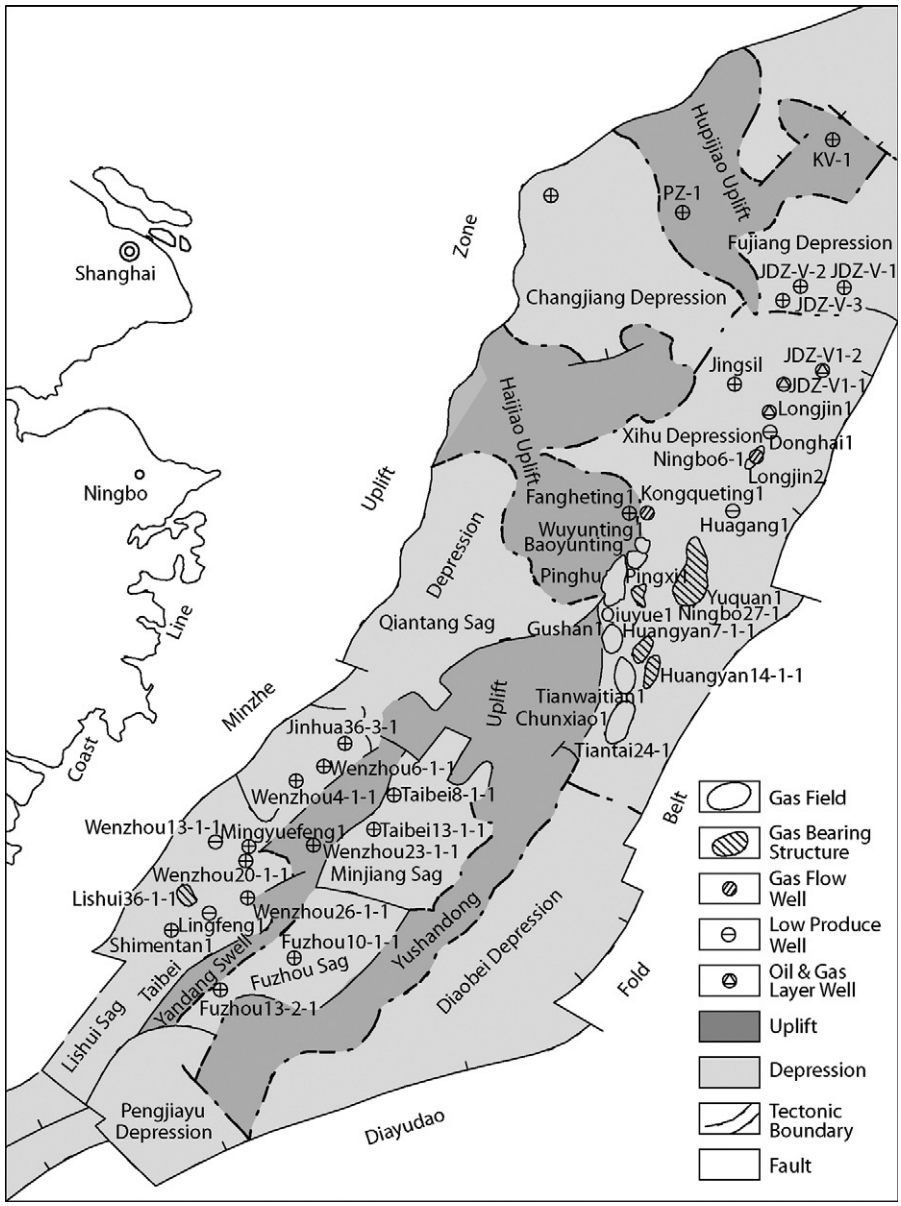

Figure 9.24
Tectonic units and oil and gas fields of East China Sea Shelf basin.

humic. The stratigraphic section of clastic rocks is often intercalated with coal beds and carbonaceous mudstones and shale.

In the Xihu depression, the major reservoirs are clastics. Reservoir depths are about 2500–3800 m with porosities of 15–25% and permeabilities of 10–400 $\times$ 10^{-3} μm^2. The mudstones in Paleocene, Eocene, Oligocene, and Miocene comprise the better seals.

The principal trap types are large anticlines, with areas of about 50–100 km^2. The main oil is light and or condensate. The gas is mainly CH_4, without H_2S.

Since 1974, a total of about 20×10^4 km 2D and 3500 km^2 3D digital seismic profiles have been completed and 59 exploration wells were drilled in the Xihu and Taibei depressions. Seven gas/oil fields have been proven in the Xihu depression. They are the Pinghu, Chunxiao, Baoyunting, Wuyunting, Duanqiao, Canxue, and Tianwaitian fields. Six gas/oil-bearing structures have been discovered and are Huanyan 7-1, Huangyan 14-1, Kongquanting, Yuquan, Ningbo 6-1, and Gushan. Total natural gas proven reserves (in place) are 100×10^9 m^3.

The Pinghu gas/oil field, located about 400 km east of Shanghai on the west slope of the Xihu depression, was discovered in 1983, and was put on production in 1998. There are seven oil wells and eight gas wells on the production platform. Reservoirs are the Oligocene Huagang and Eocene Pinghu formations. The proven area is 12.1 km^2, with proven gas reserves in place of 170×10^8 m^3, condensate oil 306×10^4 t, and light crude oil reserves 597×10^4 t. Annual oil and gas production in 2001 was 60×10^4 t and 4×10^8 m^3. Natural gas is transported by a 14″ subsea pipeline 385 km to Shanghai; crude oil and condensate are transported by a 10″ subsea pipeline 306 km to Ningbo, Zhejiang province.

One gas field (Lishui 36-1) was discovered in 1997 in the southern part of this basin, the Lishui sag in the Taibei depression. Its source rocks and reservoirs are the Paleocene.

The oil and gas resources assessment of the East China Sea Shelf basin were 34.3×10^8 t and 3.76×10^{12} m^3, respectively, in 2002.

The Pearl River Mouth basin

The Pearl River Mouth basin (Fig. 9.25) is located beneath the northern shelf of the South China Sea and covers an area of about 175,000 km^2. It is a rifted Cenozoic passive continental margin. It is one of the main offshore oil-bearing basins in China. It consists of five tectonic units: the north uplift and fault step belt, the north depression belt (including the Zhu-1 depression and Zhu-3 depression), the central uplift belt (consisting of the Dongsha uplift, the Panyu low uplift, and the Shenhu Ansha uplift), the south depression belt (consisting of the Zhu-2 depression and Chaoshan depression), and the south uplift belt. It is further divided into 30 subtectonic units (sags and swells; Fig. 9.21). For additional background see Yu 1990. 1994 ; Xie et al. 2006 ; Xu et al. 2008.

The formations include the Upper and Lower Tertiary sequences separated by a major unconformity. The main formations are the Quaternary; the Pliocene Wanshan formation; the Miocene Yuehai, Hanjiang, and Zhujiang formations; the Oligocene Zhuhai and Enping formations; the Eocene Wenchang formation; and the Paleocene Shenhu. The maximum thickness of the Cenozoic is over 10,000 m.

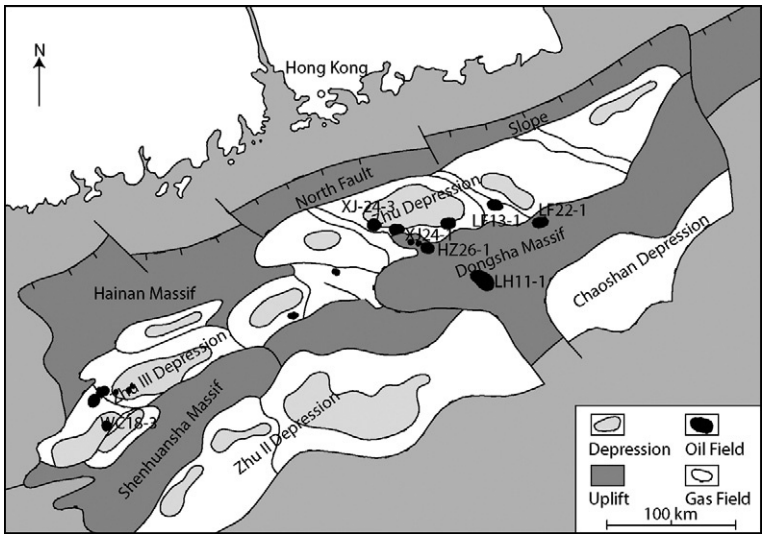

Figure 9.25
Tectonic units and oil/gas fields of the Pearl River Mouth basin.

The Pearl River Mouth basin evolved by major rifting in Early Tertiary times from several smaller basins of Mesozoic age. In the Late Oligocene, it formed a large lagoonal area that was part of the proto South China Sea. During the postrift phase in the early Miocene, it continued to subside and formed a partly barred marine basin. In the Middle Miocene to Pliocene, this basin expanded and became an open marine passive margin.

The source rocks of Pearl River Mouth basin are the Wenchang formation of Eocene age, the Oligocene Enping and Zhuhai formations, and the Lower Miocene Zhujiang formation. The organic carbon content of the best source rocks in the Wenchang, Enping-Zhuhai, and Zhujiang formations is 2.43%, 1.43%, and 0.67%, respectively.

The main reservoirs are the Oligocene Zhuhai formation, the Lower Miocene Zhujiang formation, and the Middle Miocene Hanjiang formation. The main lithologies of these reservoirs are sandstones and limestones in biohermal facies. The average porosities and permeabilities of the sandstones and limestones are about 18–25% and 15–23%, 800×10^{-3}–2500×10^{-3} μm^2, and 150×10^{-3}–400×10^{-3} μm^2, respectively.

The main local seals are Oligocene mudstones with average thicknesses of 10–20 m. The major regional seals are the Lower Miocene Zhujiang formation with average thicknesses of 500 m.

Traps in the Pearl River Mouth basin include anticlines, fault traps, and bioherm traps.

Oil exploration in the Pearl River Mouth basin began in 1974, and industry found oil first in the Zhu-5 well in 1979. To date, 33 oil fields and oil-bearing structures have been discovered, with total proved oil reserves in place of about 5×10^8 t and gas reserves of 41×10^8 m^3. Since the first oil field put on production in 1990, 12 oil fields (such as LH11-1, HZ26-1, HZ26-2, HZ21-1, XJ24-3, XJ24-1, HZ32-2, HZ32-3, HZ32-5, LF13-1, and LF22-1) have been put on stream. The annual oil production in 2002 was 936×10^4 t. The cumulative oil production is over 9600×10^4 t and the Pearl River Mouth has become one of the important oil basins in China.

The oil and gas resources assessment of Pearl River Mouth basin were 53.9×10^8 t and 2.13×10^{12} m^3, respectively, in 2002.

References

Griffin, W.L., Zhang, A.D., O'Reilly, S.Y., Ryan, C.G., 1998. Phanerozoic evolution of the lithosphere beneath the Sino-Korean Craton. In: Flower, M.F.J., Chung, S.-L., Lo, C.-H., Lee, T.-Y (Eds.), Mantle Dynamics and Plate Interactions in East Asia. A.G.U. Geodynamics Series , vol. 27., pp. 107–126.

Hilde, T.W.C., Uyeda, S., Kroenke, L., 1977. Evolution of the western Pacific and its margins. Tectonophysics 38, 145–165.

Howell, D.G., et al., 1983. Tectonostratigraphic terrains of the frontier Circum-Pacific region. AAPG BulletinBull. 67, 485–486.

Kusky , T.M., Windley, B.F., and Zhai, M.-G., 2007. Tectonic evolution of the North China Block: from orogen to craton to orogen. In: Zhai, M.G., Windley, B.F., Kusky, T.M., Meng, Q.R (Eds.), 2007. Mesozoic Sub-Continental Lithospheric Thinning Under Eastern Asia. Geol. Soc. Spec. Publ.280, pp. 1–34.

Li, D., 1980a. Geology and structural characteristics of the Bohai. China. Acta Petrol. Sin. 1, 6–20.

Menzies, M.A., Xu, Y., 1998. Geodynamics of North China Craton. Flower, M.F.J., Chung, S.-L., Lo, C.-H., Lee, T.-Y. (Eds.), Mantle Dynamics and Plate Interactions in East Asia. A.G.U. Geodynamics Series, vol. 27. pp. 155–165.

Menzies, M., Xu, Y., Zhang, H., Fan, W., 2007. Integration of geology, geophysics and geochemistry: a key to understanding the North China Craton. Lithos 96, 1–21.

Qiu, Y., Tang, X., Tong, Z., Wang, X., Wu, S., 1997. Petroleum Geology of China. 342 pp.

Ren, J.Y., Tamaki, K., Li, S.T., Zhang, J.X., 2002. Late Mesozoic and Cenozoic rifting and its dynamic setting in Eastern China and adjacent areas. Tectonophysics 344, 175–205.

Tong, C., 1980. Geological characteristics of rift valley systems in Eastern China. Acta Petrol. Sin. 19–26.

Wilde, A.S., Zhou, X.H., Nemchin, A.A., Sun, M., 2003. Mesozoic crust-mantle interaction beneath the N. China craton: a consequence of the dispersal of Gondwanaland and accretion of Asia. Geol. Soc. Am. Bull. 31, 817–820.

Xie, X., Muller, R.D., Li, S., Gong, Z., Steinberger, B., 2006. Origin of anomalous subsidence along the northern South China Sea margin. Mar. Pet. Geology. 23, 745–765.

Yu, H.-S., 1990. The Pearl River Mouth basin: a rift basin and its geodynamic relationship with the southeastern Eurasian margin. Tectonophysics 183, 177–186.

Yu, H.-S., 1994. Structure, stratigraphy and basin subsidence of Tertiary basins along the Chinese southeastern continental margin. Tectonophysics 235, 63–76.

Zhai, M., 2004. Precambrian tectonic evolution of the North China Craton. In: Malpas, J., Fletcher, C.J.N., Ali, J.R., Atchinson, J.C. (Eds.), Aspects of the Tectonic Evolution of China, Geol. Soc. Spec. Publ. 226, 57–72.

Further reading

Allen, M.B., Macdonald, D.I.M., Xun, Z., Vincent, S.J., Brouet Menzies, C., 1997. Early Cenozoic two phase extension and later Cenozoic thermal subsidence and inversion in the Bohai basin, northern China. Mar. Pet. Geol. 14, 951–972.

Allen, M.B., Macdonald, D.I.M., Xun, Z., Vincent, S.J., Brouet Menzies, C., 1998. Transtensional deformation in the evolution of the Bohai basin. Northern China. Geol. Soc. London Spec. Publ. 135, 215–229.

Dong, Y., Xiao, L., Zou, H., Wang, C., et al., 2010. The Tertiary evolution of the prolific Nanpu Sag of Bohai basin, China: constraints from volcanic records and tectono-stratigraphic sequences. Geol. Soc. Am. Bull. 122, 609–626.

Gao, S., Rudnick, R-.L., Xu, W-.L., Yuan, H-.L., Liu, Y., Walker, J., Puchtel, L.S., Liu, X., Huang, H., Wang, X-.R., 2008. Recycling deep cratonic lithosphere and generation of intraplate magmatism in the North China Craton. Earth Planet. Sci. Lett. 270, 41–53.

Lee, G.H., Kim, B., Shin, K.S., Sunwoo, D., 2006. Geologic evolution and aspects of the petroleum geology of the northern East China Sea Shelf Basin. AAPG Bull. 90, 237–260.

Letouzey, J., Sage, L., Muller, C., 1988. Geological and Structural Map of Eastern Asia.. 1: 2 500 000. Introductory Notes,. AAPG, Tulsa, OK, 52 pp. 3 maps sheets, 3 Cross section sheets (1:1250 000 horizontal scale).

Li, D., 1980b. Geological structure and hydrocarbon occurrence of the Bohai Gulf Oil and Gas Basin (China). In: Mason, J. (Ed.), Petroleum Geology in China. PennWell Books, Tulsa, OK, pp. 180–192.

Li, D., 1982. Tectonic types of oil and gas basins in China. Acta Petrol. Sin. 3, 1–12 (in Chinese).

Li, D., 1984. Geologic evolution of petroliferous basins on continental shelf of China. AAPG Bull. 68, 993–1003.

Li, Desheng, Li, Dawei, 2003. Tectonic Types of Oil and Gas Basins in China, second ed. Petroleum Industry Press, Beijing, China pp. 1–188.

Li, S., Lu, F., Lu, C., et al. (Eds.), 1997. Evolution of Mesozoic and Cenozoic Basins in Eastern China and Their Geodynamic Background. China University Geosciences Press, Wuhan, China 239 pp (in Chinese).

Li, S.Z., Kusky, T.M., Zhao, G., Wu, F., Liu, J.Z., Sun, M., Wang, L., 2007. Mesozoic tectonics in the eastern block of the North China Craton: implications for subduction of the Pacific plate beneath the Eurasian plate. In: Zhai, M.G., Windley, B.F., Kusky, T.M., Meng, Q.R. (Eds.), Mesozoic Sub-Continental Lithospheric Thinning Under Eastern Asia, Geol. Soc. Spec. Publ.280, pp. 171–188.

Lin, W., Faure, M., Monie, P., Wang, Q.C., 2007. Polyphase Mesozoic tectonics in the eastern block of the North China Block. In: Zhai, M.G., Windley, B.F., Kusky, T.M., Meng, Q.R. (Eds.), Mesozoic Sub-Continental Lithospheric Thinning Under Eastern Asia, Geol. Soc. Spec. Publ.280, pp. 153–169.

Lin, J.-Y., Sibuet, J.C., Hsu, S.K., 2005. Distribution of the East China Sea continental shelf basins and depths of magnetic sources. Earth Planet. Space Sci. 57, 1063–1072.

Liu, H., 1986. Geodynamic scenario and structural styles of Mesozoic and Cenozoic basins in China. AAPG Bull. 70, 327–395.

Ma, L-.F., Qiao, X.-F., Min, L.-R., Fan, B-.X., Ding, X-.Z., Liu, N-.L., 2002. Geological Atlas of China. China Geological Press, 348 pp, 59 map sheets.

Meng, Q-.R., Li, S-.Y., Li, R.-W., 2007. Mesozoic evolution of Hefei basin eastern China: sedimentary response to deformations in the adjacent Dabieshan and along Tanlu fault. Geol. Soc. Am. Bull. 119, 897–916.

Miyashiro, A., 1986. Hot regions and the origins of marginal basins in the western Pacific. Tectonophysics 122, 122–216.

Northtrup, C.J., Royden, L.H., Burchfiel, B.C., 1995. Motion of the Pacific plate, relative to Eurasia and its potential relation to Cenozoic extension along the eastern margin of Eurasia. Geology 23, 719–722.

Pigot, J.D., Ru, K., 1994. Basin superposition on the northern margin of the South China Sea. Tectonophysics 235, 27–50.

Pubellier, M., Chamot-Rooke, N., et al., 2008. Structural map of Eastern Eurasia. 1: 1 2500000. Com. Geol. Map of the World (CCGM-CGMW).

Shinn, Y.J., Chough, S.K., Hwang, I.G., 2009. Structural development and tectonic evolution of Gunsan basin (Cretaceous to Tertiary) in the central Yellow Sea. Mar. Pet. Geol. 27, 500–514.

Xu, Y., Hao, T., Li, Z., Liu, J., 2008. Analysis of lithosphere structures and tectonics of marginal seas and adjacent regions. Earth Sci. Front. 15, 55–63.

Yang, M.H., Zhou, X.H., Liu, L., Li, C.X., Zheng, X.F., Liu, X.J., Gao, L.B., 2008. Segment linkage, and extensional fault-related folds in Western Liaodong Bay Subbasin, Northeastern Bohai Sea. China. J. Chin. Univ. Geosci. 19, 602–610.

Zhu, X., 1983. On the geodynamic background of Meso-Cenozoic petroliferous basins in China. In: Zhu, X. (Ed.), Tectonics and Evolution in Mesozoic and Cenozoic Basins of China. Science Press, Beijing, China, pp. 1–10 (in Chinese).

Zhu, X. (Ed.), 1989. Chinese Sedimentary Basins. In: Hsu, K. (Series Ed.), Sedimentary Basins of the World Series, second ed., vol. 1. p. 283.

Zhu, W., 2002. The tectonic evolution and structural characteristics of offshore petroliferous basins in China. In: Li, Desheng, Li, Dawai (Eds.), Tectonics of Petroliferous Basins in China. Petroleum Industry Press, Beijing, China, pp. 292–305 (in Chinese).

Zhu, W., Xia, Q., Zhou, X., 2011. Recent significant discoveries in mature basins–take offshore Bohai Basin as an example. AAPG Search and Discovery Article # 10342. 35 pp.

In this chapter

10

Xialiao, North China Basin

Li-Yuan Hsiao, Stephan Graham†*

*Department of Geological and Environmental Sciences, Stanford University, Stanford, California, USA

†Department of Geological and Environmental Sciences, Stanford University, Stanford, California, USA

10.1 Introduction

A broad area of northeastern China was extended from Paleocene to Oligocene time, forming an intricate system of rifts and grabens known as the North China basin (hereafter NCB, Ye et al., 1985; also known as Bohai basin, Allen et al., 1997, 1998; Bohai Bay basin, Chang, 1991; Bohaiwan basin, Ren et al., 2002) (Fig. 10.1). The rifting involved faulting, differential tectonic subsidence, and voluminous volcanism (Chang, 1991), followed by diminished faulting, post-rift thermal subsidence, and reduced volcanism in Neogene and Quaternary time. Terrestrial sediments more than 12 km thick accumulated in the North China basin (NCB) throughout the Cenozoic era (Liu, 1987).

The NCB figures importantly in the long-standing debate about the origins of extensional basins, because it has variously been cited as a classic example of a passive rift, an active rift, and a transtensional basin. The passive rifting model of Ye et al. (1985) proposed that this basin was formed by uniform lithospheric stretching. Alternatively, Liu's (1987) active rifting model suggested that the basin formed as a result of asthenospheric upwelling, based on the observation of thinned crust and elevated heat flow/asthenospheric conductivity/gravity beneath the basin center. This interpretation is consistent with that deduced from subsidence analysis by Shedlock et al. (1985). However, in view of the prominence of the Tan-Lu strike-slip fault along the eastern margin of the basin (Fig. 10.1), a composite pull-apart basin model was subsequently proposed by Allen et al. (1997, 1998) to explain the formation of the NCB. This model suggests that the NCB was initially formed by E–W extension, and was later pulled apart by the dextral movement of two basin-bounding strike-slip faults. This model thus represented the NCB as a classic example of a composite pull-apart basin (cf. Nilsen and Sylvester, 1995). The correctness of this model remains uncertain, although it can be easily assessed from structural maps of the basin; that is, the model requires a particular pattern of the rift-related faulting (Fig. 11 in Allen et al., 1998). However, evaluation of this and

Phanerozoic Rift Systems and Sedimentary Basins DOI:10.1016/B978-0-444-56356-9.00009-2

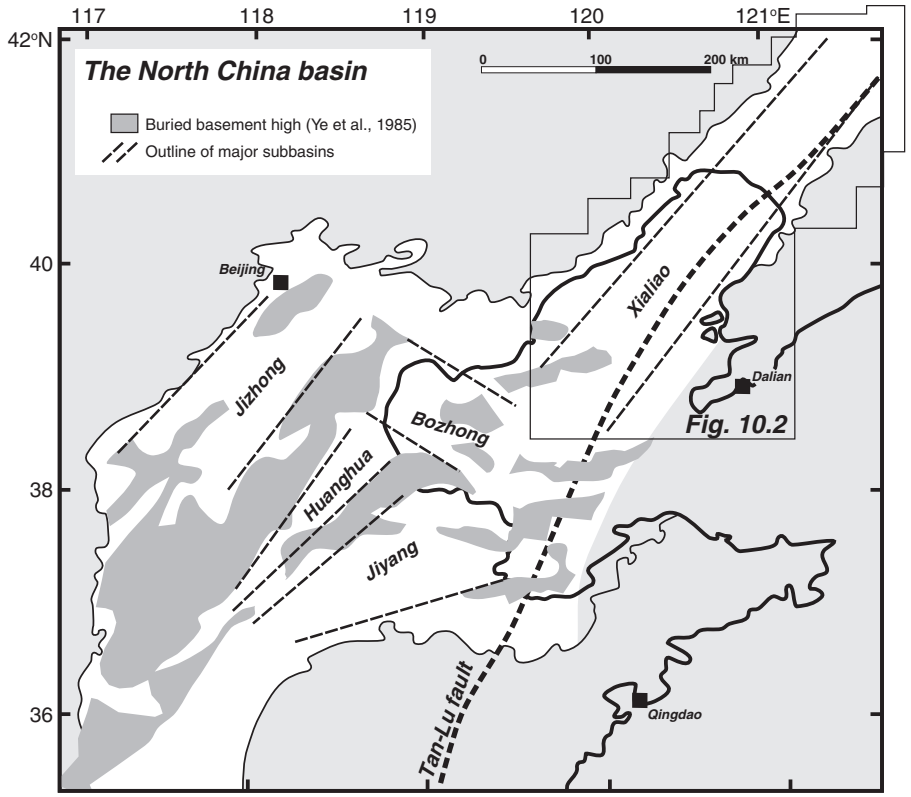

Figure 10.1
Tectonic setting of the North China basin *(modified from Ye et al., 1985)*.

other models of the NCB has been difficult, because of limited descriptions and documentation in the literature (e.g., Liu et al., 1987; Xu et al., 1983).

This chapter presents a summary of (1) basement geology; (2) rift stratigraphy and structural features, including the Tan-Lu strike-slip fault, as mapped from 2D and 3D seismic data sets; (3) igneous activities; and (4) extension of the Xialiao basin, which forms the NE rift arm of the NCB. We then discuss the origins and lithospheric dynamics of the Xialiao basin, as well as the larger NCB, on the basis of direct structural observations, subsidence analysis, crustal thinning, heat flow, and post-rift thermal subsidence.

10.2 Geologic setting

North China basin

Extending across 200,000 km^2 of NE China, the NCB is defined by rift structures (Fig. 10.1), post-rift sediments, thinned continental crust, and high heat flow (Liu, 1987). The NCB consists mainly of five depressions (major subbasins;

Fig. 10.1), composed of over 50 Paleogene half-graben and graben subbasins. These subbasins are mostly asymmetrical sedimentary troughs bounded by high-angle normal or strike-slip faults sub-parallel to the trend of depressions (Chang, 1991; Hsiao et al., 2004).

The Bozhong depression, along with the Xialiao and Jiyang depressions, forms a three-armed geometry (Fig. 10.1), reminiscent of basins of rift origins (Burke and Dewey, 1973). The Paleogene troughs and highs are buried by less-deformed Neogene/Quaternary strata of relatively uniform thickness, suggesting that the Paleogene rifting was followed in the Neogene by post-rifting regional subsidence (Liu, 1987). Although post-rift strata are less deformed, their distribution is also clearly controlled by the three-armed rift geometry.

Localization of Cenozoic NCB rifting might have been influenced by preexisting lithospheric heterogeneity; for example, the Xialiao basin is elongate along the Tan-Lu fault, which had a Mesozoic history of major strike-slip (e.g., Xu and Zhu, 1994; Yin and Nie, 1993). Two other major depressions are superposed on pre-rift structural systems: a Cretaceous rift and older Mesozoic Yanshan orogen, along which the Jizhong (Tang et al., 1988) and Huanghua depressions (Wang et al., 1998) were developed, respectively. However, the detailed relation between Cenozoic and Mesozoic structures remains undocumented.

Tan-Lu fault

The Tan-Lu fault system (TLF) trends along the length of the Xialiao basin and parallel to the east margin of the NCB. As a major tectonic feature of East Asia (Fig. 10.1), this fault zone extends NNE for ca. 3500 km within China, is tens to 200 km wide, and has been depicted repeatedly in regional tectonic maps (e.g., Molnar and Tapponier, 1977; Tapponnier and Molnar, 1977). The TLF is a lithospheric-scale structure, because it corresponds to earthquakes up to nearly 100 km deep (http://ciei.colorado.edu/~nshapirco/MODEL/); magnetic, gravity, and heat flow anomalies; and sudden changes in crustal thickness and lithospheric velocity structure (Huo et al., 2000). The TLF was active as a major left-lateral strike-slip fault between Late Triassic and Early Cretaceous when it accrued an estimated 740 km of slip, on the basis of correlation of potential piercing points (Xu, 1980). Slip sense reversed in the Cenozoic, when an estimated 35 km of right-slip occurred in the Xialiao basin sector (Hsiao et al., 2004).

10.3 Xialiao basin

The Xialiao basin (Fig. 10.2; Shedlock et al., 1985) forms the northeastern arm of the composite North China basin (Fig. 10.1). It extends NNE for nearly 400 km and is 80–120 km wide. Liaodong Bay and Liaohe basin comprise its offshore

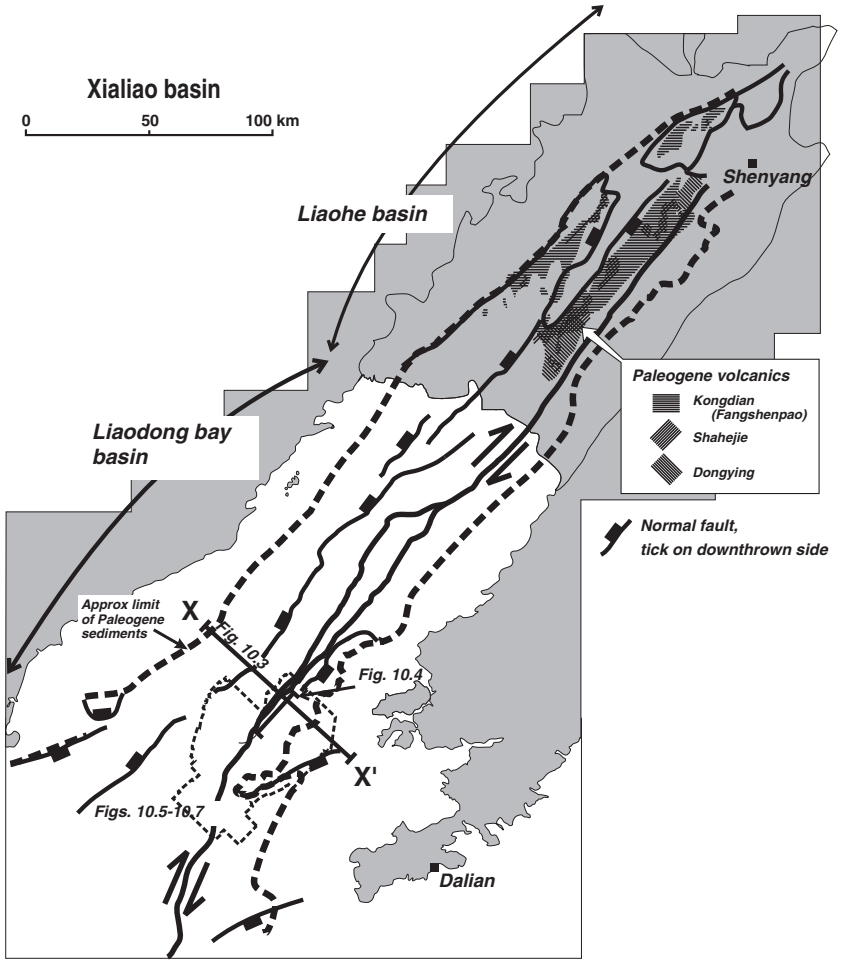

Figure 10.2 Structural framework of the Xialiao basin. For location see Fig. 10.1.

(southern) and onshore (northern) portions. The present-day rift deepens southward, and southerly axial drainage has been the primary sedimentary system since the late Oligocene (Liu et al., 1987).

Regional cross-sections demonstrate that the rift valley has a classic continental rift, steer's head configuration: faulted pre-rift basement is overlain by Cenozoic rift-associated strata (Fig. 10.3; cf. White and McKenzie, 1988). Divergent-configured syn-rift strata overlie the pre-rift basement and are covered by less-tectonized post-rift strata. Syn-rift strata were deposited in isolated half-grabens, whereas post-rift strata are regionally extensive, less-tectonized, and

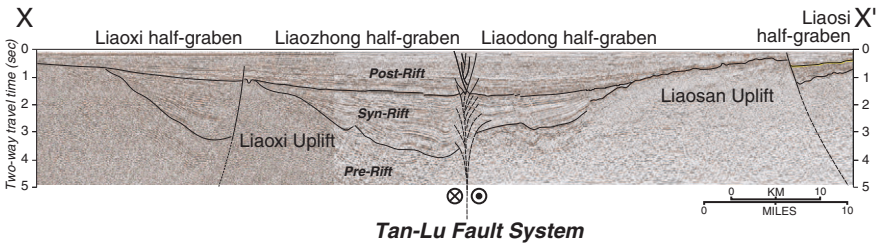

Figure 10.3 Regional cross-section of the Xialiao basin. For location see Fig. 10.2. Interpreted seismic reflection profile (above) and depth-converted geologic profile using interval velocity of data processing (below). Circle with dot indicates motion toward viewer; circle with x is away from viewer. *(From Hsiao et al. AAPG©, 2004, reprinted by permission of the AAPG whose permission is required for further use.)*

thicken toward the basin center. The otherwise typical rift cross-section is modified by the Tan-Lu strike-slip fault system, which bisects the basin (Fig. 10.3).

Pre-rift basement

The onshore geology of Liaoning Province provides the best constraint on the nature of the basement under the Xialiao basin. The pre-rift basement records a long and complex geologic history, as described by the Bureau of Geology and Mineral Resources of Liaoning Province (1989) and summarized below.

Liaoning Province is generally bisected by the Xialiao basin into two geologic terranes (Liaoxi and Liaodong, west and east of Liaoning, respectively). The two terranes share common features as well as notable differences. Precambrian metamorphic rocks and granite are covered by metamorphosed Ordovician/Silurian shallow-marine carbonate strata, which are overlain by Carboniferous/Permian terrestrial sandstone and metasandstone formations. The thickness of the carbonate section changes significantly on opposite sides of the Xialiao basin (Liu et al., 1987).

During Mesozoic time, terrestrial basins developed, possibly related to the Yanshan orogeny. Triassic to Cretaceous strata, up to thousands of meters thick, include terrestrial sandstone, conglomerate, and shale. In addition to sedimentary rocks, Jurassic and Lower Cretaceous volcanic rocks, consisting of andesite and basalt, are interlayered in this sedimentary sequence.

The stratigraphy in the Liaodong area differs from that of the Liaoxi area in terms of thickness and rock type. The thickness of Paleozoic carbonate strata changes abruptly across the Liaodong Bay. One thousand meters of Cambrian shallow-marine carbonate strata are present, overlain by unmetamorphosed Ordovician carbonate. Devonian to Permian shallow-marine to terrestrial sandstone, shale, and conglomerate formations lie on the Silurian unconformity. Mesozoic terrestrial deposits also occur in Liaodong, but the thickness is significantly less than in Liaoxi. Another significant difference is that Jurassic andesitic magmatism is missing in Liaodong.

Mesozoic activity of the TLF likely accounts for contrasts on opposite sides of the rift. Strata in Liaodong apparently were tectonically transported northward for hundreds of kilometers along the TLF, accounting for the abrupt change in thickness of the Paleozoic carbonate and differences in Mesozoic stratigraphy (Bureau of Geology and Mineral Resources of Liaoning Province, 1989).

Rift stratigraphy

Faulted pre-rift basement is overlain by divergently configured strata deposited during basement tilting. The divergent strata are covered by a regional stratigraphic package, which is less tectonized and becomes thinner toward the basin margin. These two stratigraphic packages are regarded as syn- and post-rift megasequences separated by a megasequence boundary (Figs. 10.3 and 10.4). The ages of the three megasequences are pre-Cenozoic, Paleogene, and Neogene/Quaternary, respectively (Fig. 10.4; Hsiao, 2003; Hsiao et al., 2004).

The Cenozoic stratigraphy is revealed by regional seismic stratigraphic studies, whereas pre-rift strata are constrained by outcrops in onshore Liaoning areas, as discussed above. In the unexposed basement, the pre-rift megasequence is commonly free of seismic reflections, but locally well-developed seismic reflections indicate that basement lithologies vary significantly.

The distribution of the syn-rift megasequence reflects rift structure. Strata thicken toward the major faults but are thin toward or pinch out on the ramp side of each half-graben (Fig. 10.3). This divergent configuration suggests that the basement tilted during deposition. The syn-rift megasequence consists of three sequences of tectonic systems tracts that reflect the mode of continental rifting (Fig. 10.4), as suggested by their stratal geometry and dominant environmental facies (Hsiao, 2003; cf. Lambiase, 1990; Prosser, 1993).

Kongdian sequence (initial rift tectonic systems tract)

The lowest Kongdian sequence (Fig. 10.4) displays a wide variety of seismic reflection features, including high to variable amplitude/continuity concordant, chaotic, and clinoform reflections, indicating its highly variable environment of

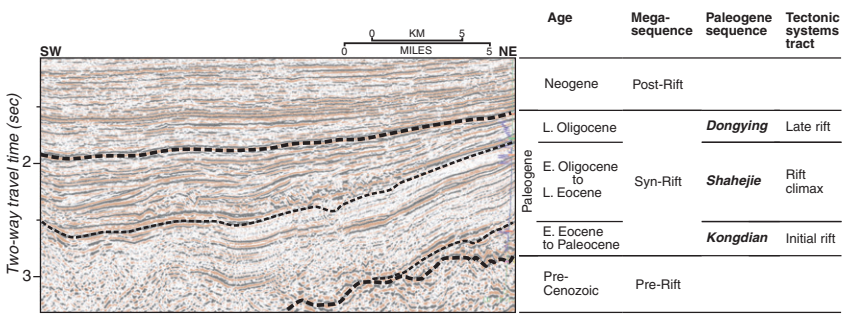

Figure 10.4 Seismic section longitudinal to the basin illustrating character of stratigraphic sequences. Well log is a shale-volume log, increasing sand plotted to the left. See Fig. 10.2 for location. *(From Hsiao et al. AAPG©, 2004, reprinted by permission of the AAPG whose permission is required for further use.)*

deposition (cf. Mitchum et al., 1977). Reported rock types include alluvial conglomerate, lacustrine sandstone and siltstone, and volcaniclastics. In the Liaohe basin to the north, voluminous volcanic layers (flood basalt of Zhou et al., 1988) occur at the bottom of the Cenozoic strata. Their thickness is generally hundreds of meters and locally more than 1200 m (Zhao et al., 1999).

Shahejie sequence (rift climax tectonic systems tract)

The Shahejie sequence (Fig. 10.4) is characterized by parallel, continuous, and consistent amplitude reflections, possibly representing profundal lacustrine environment near the basin center. Toward the basin margin, these reflections may increase in amplitude, lose continuity, or change shape from concordant to clinoform, suggesting transitions to turbidite-dominated lacustrine fans and exposed islands.

Dongying sequence (late rift tectonic systems tract)

The Dongying sequence (Fig. 10.4) is represented by a set of clinoforms and associated topset and bottomset units. The clinoforms are in complex sigmoidal-oblique configuration, representing deltaic sedimentation in variable lithology related to high-frequency base-level fluctuations Hsiao (2003). These base-level changes also influenced the abundance of fluvial channels developed on the topsets, characterized by parallel reflections with variable amplitude (Hsiao, 2003). Bottomsets are parallel reflections with fairly consistent amplitude, possibly indicating lacustrine hemipelagic sedimentation (cf. profundal lacustrine facies of Carroll and Bohacs, 1999) of and/or turbidite-dominated facies of hyperpycnal flow (cf. Parsons et al., 2001).

Post-rift megasequence

The post- and syn-rift megasequences are separated by a high-amplitude and continuous seismic reflection mappable throughout the NCB. The post-rift megasequence is relatively uniform in distribution and untectonized. It is thickest near the basin center and thinner toward the basin margin (Figs. 10.3 and 10.4). It also thickens toward SSW along the basin axis (Fig. 10.2), although there is another depocenter in northern Liaodong Bay as the result of local transtensional tectonics of the TLF (Hsiao et al., 2004).

The post-rift megasequence is characterized by continuous and discontinuous seismic reflections in parallel configuration. The discontinuous reflections are regionally widespread, whereas continuous reflections are better developed to the south. Extending to the north, they die out or laterally become discontinuous reflections. The discontinuous reflections often correspond to sand and gravel deposited in fluvial environments (Liu et al., 1987). The continuous reflections, in contrast, often correlate with mud layers, the deposits of swamp and/or shallow lacustrine environments.

The basin filled during post-rift time (Neogene and Quaternary). Because of limited accommodation, coarse-grained sediments were distributed throughout the basin. Around the center of Bohai to the south of the Xialiao basin, a shallow lake developed in the area of greatest subsidence (Liu et al., 1987). This depression likely connected with the open marine environment in late Neogene time, as suggested by the fact that upper Neogene strata overlie the structural high to the east of Bozhong depression that bounded the Bohai and the Yellow Sea (Jiaoliao uplift; N. Tilander, oral communication, 2001).

Rift structures

The Xialiao basin is characterized by three NNE-orienting fault systems: Liaoxi and Liaodong normal fault and Tan-Lu strike-slip fault systems (Fig. 10.2), all of which are high-angle and cut into the basement sub-vertically. The Liaoxi fault system extends throughout the Xialiao basin sub-parallel to the coastline. The Liaodong normal faults trend NE, and one of those may extend onshore to the Liaodong Peninsula and die out near the bay center.

The normal faults are the boundaries between areas of subsidence and uplift on the hanging-wall and foot-wall sides of the fault, respectively. The magnitude of subsidence is commonly 4+ km toward the hanging-wall and becomes zero or uplift toward the footwall. The magnitude of the uplift is uncertain, but erosional features on the Liaosi fault block suggest that the uplift may have been at a scale of hundreds of meters (Hsiao, 2003; Hsiao et al., 2004).

The timing and intensity of the rifting is directly suggested by stratal geometry. The Paleogene strata are in divergent configuration in each half-graben bounded by faults, whereas the Neogene/Quaternary strata are relatively uniform; that is, their thickness does not significantly change across the faults (Fig. 10.3). The tectono-stratigraphic relation suggests that the faults were mostly active during the Paleogene time, particularly the period during which the Shahejie sequence was deposited, because this sequence has the most significantly divergent geometry.

Tan-Lu fault

In the Xialiao basin, the Tan-Lu fault zone is a through-going feature that bisects the rift system. In the southern basin, it is characterized by a flower structure in cross-section (Fig. 10.3) and en echelon folds and faults in plan view (Figs. 10.5 and 9.6), but northward it divides into multiple strands characterized by flower structures (Fig. 10.7). The strands merge again beneath the northern limit of Liaodong Bay, and a single major strand cuts Liaohe basin (Fig. 10.2). Regionally distributed focal solutions demonstrate that the fault is a right-slip fault (Chen and Nabelek, 1987; Yang et al., 1989), consistent with the stepping sense of en echelon folds related to the fault in Xialiao basin (Fig. 10.5). Hsiao et al. (2004) inferred 30–40 km of post-Eocene right slip on the basis of the separation

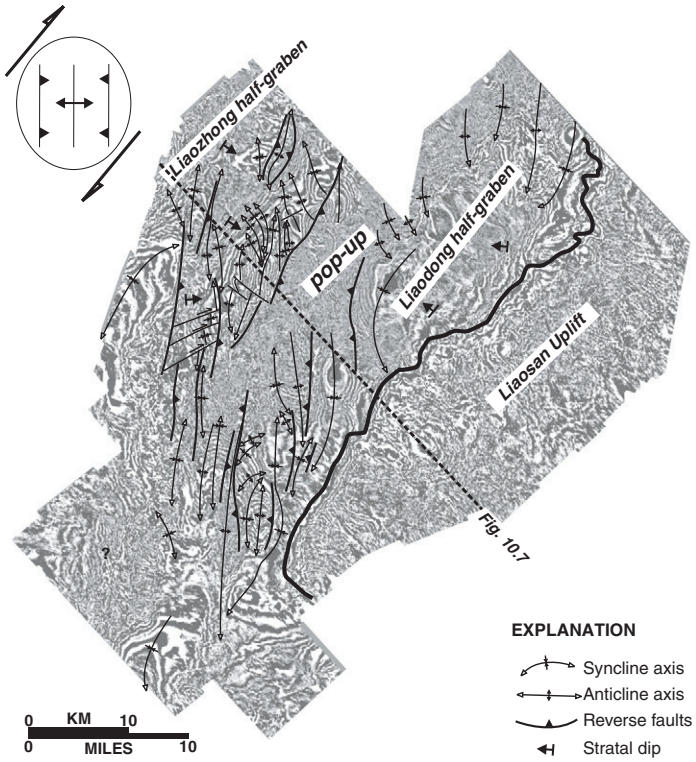

Figure 10.5 Interpreted time slice (2864 ms, amplitude display) from 3D seismic volume near the middle of the Shahejie sequence showing the distribution of shortening features at lower structural levels of the basin. See Fig. 10.7 for position of time slice in vertical section. Strain ellipse is from Wilcox et al. (1973). See Fig. 10.2 for location. *(From Hsiao et al. AAPG©, 2004, reprinted by permission of the AAPG whose permission is required for further use.)*

of deformation zones and depocenters. The distribution of basement blocks related to rift-fault geometry forced a major restraining bend in the TLF early in its Cenozoic history of activity. This created a positive flower structure during Shahejie time, causing deformed growth strata (Fig. 10.7), influencing Shahejie facies patterns in the center of the rift, and ultimately deforming Shahejie strata in a pattern of en echelon folds (Fig. 10.5). By Donying time, transtension dominated the Tan-Lu fault zone, all flower structures became negative, subsidiary normal faults were widespread along the fault zone (Fig. 10.6), and the earlier axial transpressional welt subsided (Fig. 10.7). Strike-slip continues to the present day, judging from stratal disruption upward all the way to the sea floor (Figs. 10.3 and 10.7).

Igneous activity

Cenozoic igneous activity was widespread throughout the Xialiao basin. In the onshore Liaohe basin, volcanism occurred throughout the Paleogene, as revealed by the extensive distribution of volcanic rocks (Fig. 10.2). In the lower Kongdian sequence, basaltic sections are generally 100–200 m in thickness, and

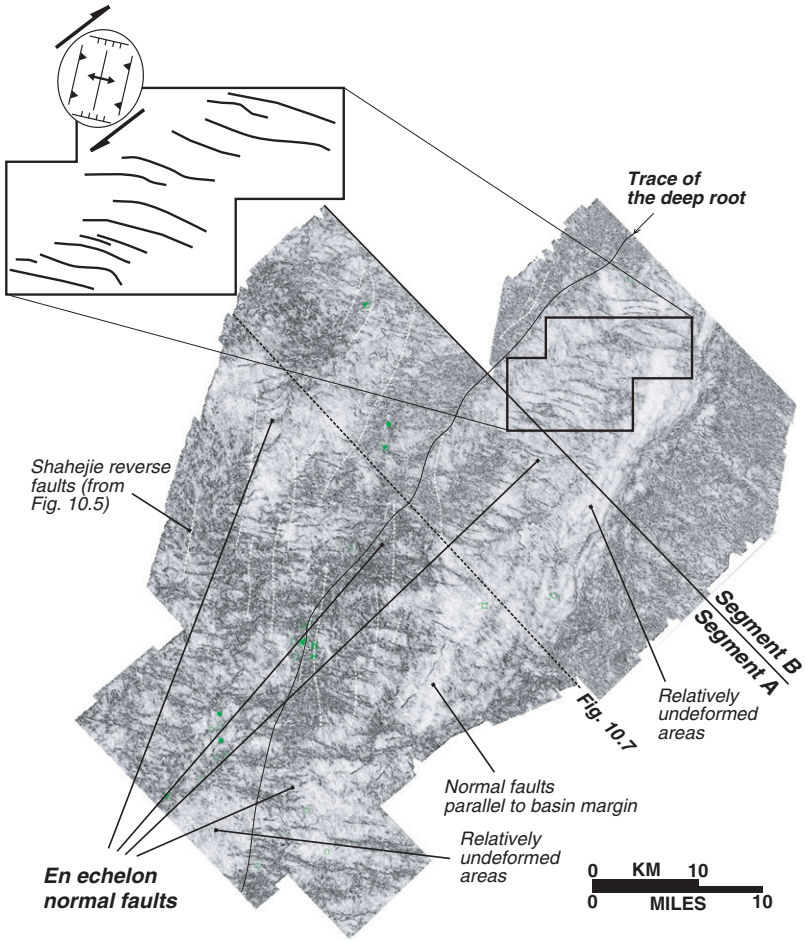

Figure 10.6 Time slice (1904 ms, coherency display) from 3D seismic volume near the top of the Dongying sequence showing the distribution of normal faults at upper structural levels of the basin. The left-stepping en echelon pattern of normal faults typical of the area is highlighted in the inset map. The traces of reverse faults at depth are shown as white lines. See Fig. 10.7 for position of time slice in vertical section. Strain ellipse is from Wilcox et al. (1973). See Fig. 10.2 for location. *(From Hsiao et al. AAPG©, 2004, reprinted by permission of the AAPG whose permission is required for further use.)*

locally exceed 1200 m (Zhao et al., 1999). This thickness is comparable in scale to that of other basins in similar settings, such as Red Sea rift (Chazot et al., 1998). In the Shahejie sequence, basaltic layers are about 10–30 m thick. In the Dongying sequence, volcanism was localized to the north and south of the Liaohe basin, where the basaltic sequence thickness locally exceeds 800 m. The basalt is distributed along major faults and hence possibly originated from fissure eruptions.

Basaltic rocks from the Kongdian sequence yield K/Ar ages ranging from 45 to 65 Ma (Liang et al., 1992), and the geochemical signatures are fairly similar to that of basalt in other continental rift settings. The alkaline-dominated basaltic rocks consist mainly of basalt and trachybasalt and some basaltic trachybasalt and basanite (Hongde Liang, personal communication, 2001) as per the TAS

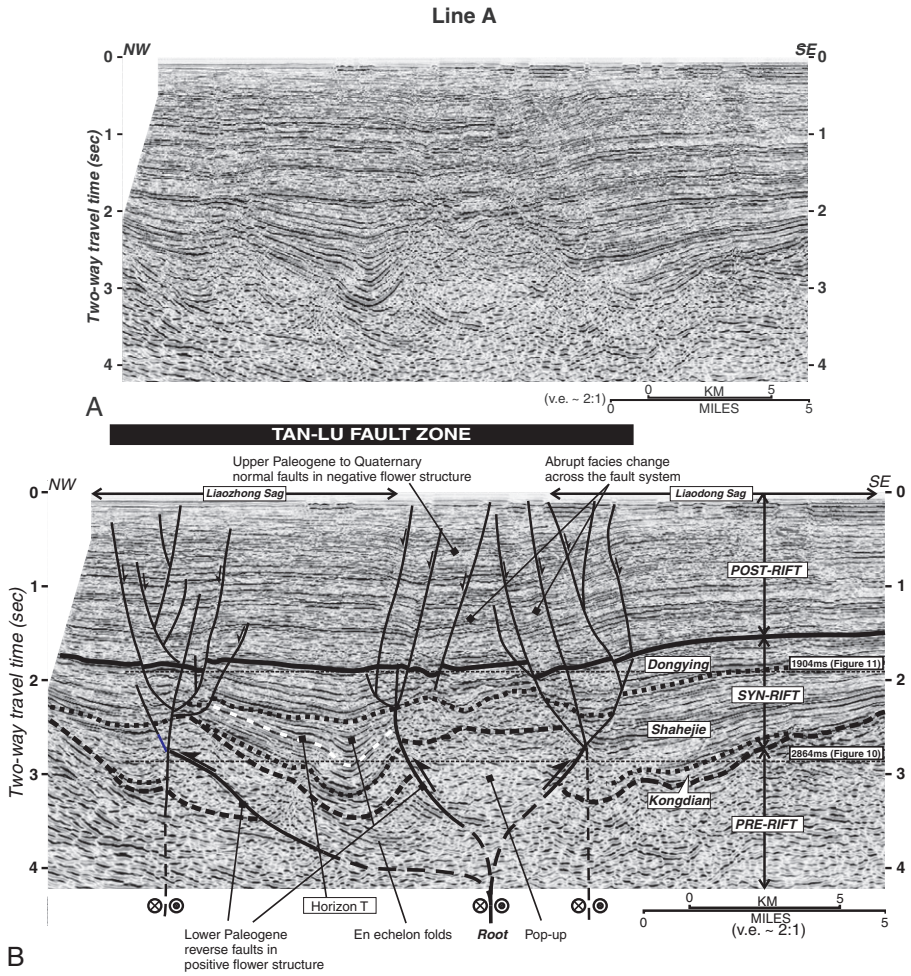

Figure 10.7
(A) Uninterpreted and (B) interpreted 2D seismic line illustrating detailed structure in transverse section of flower structures of the Tan-Lu fault zone. The TLF strand in the center of the basin (and center of the seismic line) features a positive flower structure at Shahejjie levels, characterized by a central pop-up structure and flanking compressional growth syncline (especially on its left flank). In contrast, from the Dongying level to the sea floor, both flower structures imaged on this section are negative. Positions of time slices of Figs. 10.5 and 10.6 are indicated at the right edge of the section. See Fig. 10.2 for location of seismic line. *(From Hsiao et al. AAPG©, 2004, reprinted by permission of the AAPG whose permission is required for further use.)*

classification scheme (Le Maitre et al., 1989). They mostly contain olivine, hypersthene, plagioclase, and augite (Zhao et al., 1999). The Nd-Sr isotopic field from lower Shahejie basalt (Hongde Liang, 2001, personal communication) indicates near standard mantle values (PREMA and HIMU zones of Zindler and Hart, 1986), whereas those from younger sequences suggest more lithospheric influences (Hongde Liang, 2001, personal communication). Such a trend is also observed in the Huanghua depression, where the alkalinity of the basalt decreases from the Paleogene to the Neogene systems (Gao, 1986). Paleogene tholeiitic basalt has been reported in Jizhong (Zhou et al., 1988). In the Huanghua depression, voluminous magmatism has been imaged by seismic reflection profiling and confirmed by wells (Lu, 1990). In general, Liaohe volcanism was fed by the asthenosphere (cf. Fitton et al., 1998).

Lower Cenozoic basalt also exists in other northeastern areas of China, including Hannuoba (Song and Frey, 1989; Zhi et al., 1990), Wangqing (Xu et al., 2001), and the Jiyang and Huanghua depressions (Zhou et al., 1988) in the North China basin. These rocks consist mostly of tholeiitic and subalkalic basalt, and minor alkalic basalt. In Hannuoba and Wangqing areas, the basalt includes mantle xenoliths that involve spinel peridotite with minor garnet peridotite, suggesting that the depth of the magmatic source exceeded 75 km. The whole-rock Nd–Sr isotope ratios scatter between zones of standard mantle and lithosphere (e.g., Rollinson, 1993; Smith, 1998; Tatsumoto et al., 1992; Zartman et al., 1991). These data suggest an asthenospheric source for the magma, an interpretation that is consistent with results from the Liaohe basin.

Extension

The amount of basin extension (i.e., extension factor β) can be estimated from direct measurement of heaves along basement faults (βf). By assuming that this basin was formed by lithospheric stretching, the extensional factors can also be evaluated by subsidence analysis (βs), crustal stretching (βc), amount of post-rifting thermal subsidence (βt), and heat flux (βh) (Jarvis and McKenzie, 1980; McKenzie, 1978; White, 1988; Ziegler, 1983; Table 10.1). The extension factor βf from Fig. 10.3 is 6%, giving rise to βf 1.06, by directly measuring the heave of the two normal faults. This is probably an overestimation because the effect of block rotation (cf. Sclater and Célérier, 1989) has not been considered. This low amount of extension is in good agreement with the Liaohe basin, where Chen and Li (1998) analyzed six sections throughout the basin and obtained an average βf of 1.08.

The observed extension, βf, is far less than the βs, βc, βt, and βh values (Table 10.1). In the Liaohe basin, Shedlock et al. (1985) derived average βs values of 1.3. Subsidence analysis in the same area yielded βs values ranging from 1.1 to 2.0 (Chen and Li, 1998). The βc is approximately 1.5–2 for the Xialiao basin. The βt and βh are estimated as near 2 and >4, respectively, using the heat flux-time and sediment thickness-time plots provided by McKenzie (1978). The cause for the discrepancy between the βf and other measures of extension is best viewed in the context of the rest of the NCB and other rift systems, as discussed hereafter.

10.4 Discussion

Lithospheric dynamics

Beyond the Xialiao rift, unexpectedly high βs, βc, βt, and βh values have also been derived from other parts of the NCB. The subsidence analysis of Hellinger et al. (1985) throughout the NCB derived βs values ranging from 1.26 to 1.72. The βt and βh are both estimated as >4. The mismatch between

Table 10.1 Extension factors of the Xialiao and North China basins

Subbasins		Extensional factors									
		βf	βs	Thermal subsidence (km)[a]	βt[b]	Moho depth (km)[c]	Total subsidence (km)[d]	Upper crustal thickness (km)[e]	βc[f]	Present heat flow (HFU)[c]	βh[b]
Xialiao basin	Liaohe basin	1.08[g]	1.3[h]	0.5–1.2	<1.25	29–33	5–9[g]	20–24	1.5–1.8	1.6–2.0	~4–∞
	Liaodong bay basin	1.06[d]	N/A	1.2–2.5	<1.25–1.5~2	~28	6–10[d]	18–22	1.64–2	1.8–2.0	∞
East Bozhong depression		N/A	>1.3[a]	3.7+	2–4	<28	>10[c]	~18	~2	2.36	∞

[a]Ye et al. (1985).
[b]Using plots of McKenzie (1978).
[c]Liu (1987).
[d]This study.
[e]Moho depth − total subsidence.
[f]Pre-rift crustal thickness (36 km; Liu, 1987)/upper crustal thickness.
[g]Chen and Li (1998).
[h]Shedlock et al. (1985).

measurable fault extension and magnitude of extension predicted from other criteria is by no means unique to the NCB, as documented by others in various rift settings (e.g., Chenet et al., 1982; Karner et al., 1987; Moretti and Pinet, 1987). Nor can the discrepancy in extension estimates from NCB be explained by errors from estimation (cf. White, 1990); instead, it probably suggests that the lithospheric stretching of McKenzie (1978) is not the (only) mechanism contributing to basin formation, because the basin subsided without sufficient upper crustal extension.

It is possible that asthenosphere upwelling accompanied or caused the basin rifting (Liu, 1987; Shedlock et al., 1985), accounting for the discrepancy among extension indicators. The process of mantle penetration through the crust is unclear in detail, but a preexisting zone of anomalously low-viscosity asthenosphere is required (Olsen et al., 1988). In the case of the NCB, the zones of lithospheric weakness could have been provided by the TLF, Mesozoic orogenic belts, and Cretaceous rifting, as mentioned earlier.

We are uncertain about the origin of asthenospheric upwelling and its relation to modest crustal extension in the NCB. Asthenospheric upwelling may result in continental extension; crustal fractures created by extension and preexisting zones of weakness may release mantle pressure and trigger the melting and upwelling of the upper mantle (Saunders et al., 1992). The former mechanism is similar to that of active rifting (e.g., Burke and Dewey, 1973), except that it is driven by the asthenosphere instead of a mantle plume. Under the active rifting model, the base of the lithosphere would be ponded by rising magma for long periods of time. The ponding results in conductive heating of the overlying lithosphere and production of large amounts of melt (flood basalt; Farnetani and Richards, 1994). This scenario could account for the present high heat flow (Ye et al., 1985) and the low P-wave velocity under the NCB area (Zhang, 1998). Hence, either passive or active rifting processes remain possible causes for NCB formation, as in other well-studied cases of rift basins such as the East Africa, Baikal, Rio Grande, and Rhine rifts, which have many similar geological features (e.g., magmatism, lithospheric thinning, asthenospheric upwarping, etc.; Ruppel, 1995).

In either the passive or active rifting scenario, pre-rift lithospheric heterogeneity may have played an important role in basin formation. Thinned continental crust is preferred for mantle upwelling, decompressional melting, magmatism, and/or crustal underplating (e.g., Huang et al., 1996; McKenzie and Bickle, 1988). In the NCB case, the TLF changes orientation ca. 10 degrees near the NCB center (Fig. 10.1), which should have created great structural complexity. The resulting extension may have promoted mantle melting. At the upper crust level, preexisting fabrics can control the geometry and location of rifts by initiating, diverting, or inhibiting fracture propagation (cf. Lezzar et al., 2002). On a smaller scale, the Xialiao, Huanghua, and Jizhong depressions might correspond to preexisting zones of weakness.

Evolution of the Xialiao basin

We infer the following evolution of the Xialiao basin:

Stage 1: Paleocene to Eocene: Rift initiation

As a result of either lithospheric extension or asthenospheric upwelling, abnormal mantle occurred under and along the present-day Xialiao basin area. Hot upper mantle material heated the lithosphere and reduced its thickness and density. Driven by isostatic buoyancy, lithospheric uplift produced a tensile stress field that triggered normal faulting and basin formation. Voluminous basaltic magma flooded the Liaohe basin to the north and may also have extruded along the major faults of the Liaodong Bay basin. Basin accommodation was limited and mostly distributed along the faults. Deposited sediments include alluvial conglomerate and sandstone, lacustrine mudstone, and possible volcaniclastics.

Stage 2: Eocene to Oligocene: Rift climax

Asthenosphere upwelling persisted and reached its climax. The lithosphere was hottest and had lowest density, and therefore the maximum magnitude of uplift, normal faulting, and basin accommodation occurred. In addition, the TLF was reactivated as a right-slip fault soon after the onset of rifting. Rift-related normal faults are high angle. Between the faults, blocks were rotating, producing uplift and subsidence of the hanging and foot wall sides, respectively. Like the normal faults related to rifting, the TLF formed an uplift zone because of the transpressional bending in southern Liaodong Bay and was subject to erosion (e.g., erosion on the order of 10^2 m occurred on the Liaosi uplift in the southeast bay, Hsiao, 2003). Sub-lacustrine fans or exposed platform facies developed along uplifted basin margins, whereas fine-grained lacustrine sediments dominated the basin center.

Stage 3: Upper Oligocene to present: Rift fading and post-rifting thermal subsidence

Asthenosphere upwelling ceased and the lithosphere began cooling, but the TLF remained active as a transtensional system. Melt may have underplated the NCB, as suggested by minor later Tertiary magmatism, relatively high heat flow, and intense thermal subsidence. The magnitude of normal faulting decreased. The region subsided and sediments filled the basin through deltaic progradation along the axis of the rift basin.

Evolution of the North China basin

We propose that asthenospheric upwelling may have played a key role in forming the North China basin, and the upwelling may or may not have been triggered by lithospheric extension (e.g., active and passive rifting, respectively).

The asthenospheric upwelling was probably located near the center of Bohai on the basis of the geometry of three rift arms: Xialiao (NNE), Jiyang (SSW), and Bozhong (E–W) depressions. The upwelled asthenosphere heated the lithosphere along these rift arms and caused localized extension in the crust above. In each rift valley, Paleogene rift-related normal faults are parallel to sub-parallel to the rift valley, as well as Neogene to Quaternary pattern of sediments distribution. The Paleogene normal faulting reflects localized extension, and post-rift sedimentation controlled by basin accommodation created by thermal subsidence, the amount of which is directly related to the distribution of heated continental lithosphere. The three-arm geometry of asthenospheric upwelling corresponds to regional geophysical measurements, including thickness of crust and lithosphere, high heat flow, residual gravity anomaly, and low p-wave velocity (Liu, 1987).

The three-arm geometry still controls modern depositional patterns and coastline geomorphology. Relatively intense thermal subsidence localized the axis of subsidence along the center of the rift valleys. Each rift valley therefore corresponds to a major fluvial input system: Liaohe, Huanghe (Yellow), and Haihe rivers for Xialiao, Jiyang, and Bozhong depressions, respectively. As a result of the limited amount of sediment input, the coastlines of the Xialiao and Bozhong depressions have concave-landward shapes, whereas the Jiyang rift has concave-seaward geometry; the latter probably reflects sediment input from the Huanghe River so voluminous that it exceeds basin accommodation from thermal subsidence.

Failure of the composite pull-apart basin model and the role of TLF in the NCB formation

Allen et al. (1997, 1998) proposed a composite pull-apart basin model for the formation of the NCB, based on the recognition of the right-lateral strike-slip movement of the TLF, and the overall "lazy z" shape in map view of the NCB (Fig. 10.1). If this 300 km wide (N–S direction) portion had been pulled apart by right-slip, the following would be required: (1) Paleogene rift-related normal faults in the Xialiao basin should be arranged in an en echelon pattern, (2) TLF slip would have ceased near the Oligocene-Miocene boundary time, and (3) the TLF would have accrued 67–133 km of slip throughout the Paleogene (on the basis of β ranging from 1.3 to 1.8 (Allen et al., 1997).

However, these requirements are not met by the regional geologic relations derived from a structural analysis of Hsiao et al. (2004) and summarized below. The Paleogene rift-related major normal faults in Liaodong Bay are mostly long and straight rather than en echelon (Fig. 10.2). The TLF has been active from Paleogene through Quaternary: stratal wedging signals Paleogene fault actively, yet most allied faults cut through the entire Cenozoic strata rather than terminate at the top-Oligocene horizon. Finally, total Cenozoic slip along the TLF is

30–40 km (Hsiao et al., 2004). We therefore conclude that although the TLF was active during rifting of the NCB, the magnitude of strike-slip is insufficient to account for the NCB. Instead of pulling apart the entire basin, the Cenozoic and Mesozoic movement of the TLF may have contributed to the subsidence of the NCB by weakening the lithosphere, as discussed above.

10.5 Conclusions

The Xialiao basin displays a classic continental rift, a symmetric "steer's head" configuration that consists of pre-, syn-, and post-rift megasequences. The pre-rift basement consists of metamorphic, carbonate, sedimentary, and volcanic strata. The thickness and types of pre-rift rocks change abruptly across the Liaodong Bay, a change that is related to major Mesozoic strike-slip along the Tan-Lu fault. The syn-rift megasequences consist of tracts from three tectonic systems, characterized by alluvial/fluvial/lacustrine, profundal lacustrine, and deltaic settings; the post-rift megasequence consists of fluvial and shallow lacustrine deposits. Volcanic rocks are particularly abundant within the initial rift sequence, and mainly consist of alkaline basalt, probably reflecting asthenospheric upwelling. The strata were cut by high-angle normal faults that accommodated initial basin rifting and extension. These basement-involved structures trend NNE subparallel to the basinal axis. The observed amount of extension is about 6%, which is markedly lower than anticipated by subsidence analysis, crustal thinning, thermal subsidence, and heat flow.

Abnormally high values of heat flow, thermal/initial subsidence, and crustal thinning of the NCB are probably the consequences of asthenospheric upwelling. This mantle event occurred along the major depressions of the NCB, among which the Xialiao, Bozhong, and Jiyang depressions comprise a three-armed geometry of continental rifting. The Huanghua, Jizhong, and Xialiao depressions correspond to preexisting zones of lithospheric weakness. The asthenospheric upwelling may have elevated the crust and provided tensile stress that rifted the continent, and extensional fractures by extension and TLF activity may have triggered the asthenospheric upwelling. The TLF was active as a right-lateral strikes-slip fault system during basin formation, and it served as a weak zone for intense asthenosphere upwelling instead of directly causing NCB rifting.

Acknowledgments

We acknowledge support by the member companies of the Stanford-China Industrial Affiliates Program. We thank Dennis Astilla, Attila Aydin, Edmund Chang, Tim Cope, Kuan Hsu, Yu Jin, Chuck Kluth, Hongde Liang, Nat Tilander, Maoshan Wang, Yongjun Yue, and Lori Zhang for discussions and/or assistance in preparing this chapter. ChevronTexaco, Petronas, and the China National Offshore Oil Company granted permission to publish the seismic data presented in this chapter, and the American Association of Petroleum Geologists Bulletin granted permission to reproduce Figs. 10.3–9.7 from Hsiao et al. (2004).

References

Allen, M.B., McDonald, D.I.M., Zhao, X., Vincent, S.J., Brouet-Menzies, C., 1997. Early Cenozoic two-phase thermal subsidence and inversion of the Bohai basin, northern China. Mar. Petrol. Geol. 14, 951–972.

Allen, M.B., McDonald, D.I.M., Zhao, X., Vincent, S.J., Brouet-Menzies, C., 1998. Transtensional deformation in the evolution of the Bohai basin, Northern China. In: Holdsworth, R.E., Strachan, R.A., Dewey, J.F. (Eds.), Continental Transpressional and Transtensional Tectonics, vol. 135. Geological Society Special Publication, London, pp. 215–229.

Bureau of Geology and Mineral Resources of Liaoning Province, 1989. Regional Geology of Liaoning Province. Geology Press, Beijing, 856.

Burke, K., Dewey, J., 1973. Plume generated triple-junctions: key indicators in applying plate tectonics to old rocks. J. Geol. 81, 406–433.

Carroll, A.R., Bohacs, K.M., 1999. Stratigraphic classification of ancient lakes: balancing tectonic and climatic controls. Geology 27, 99–102.

Chang, C.Y., 1991. Geological characteristics and distribution patterns of hydrocarbon deposits in the Bohai Bay basin, east China. Mar. Pet. Geol. 8, 98–106.

Chazot, G., Menzies, M.A., Baker, J., 1998. Pre-, syn-, and post-rift volcanism on the south western margin of the Arabian plate. In: Purser, B.H., Bosence, D.W.J. (Eds.), Sedimentation and Tectonics of Rift Basin – Gulf of Aden. Chapman and Hall, London, pp. 50–55.

Chen, W.P., Nabelek, N., 1987. Seismogenic strike-slip faulting and the development of the North China Basin: Tectonics, 7 (5), 975–989.

Chen, Q., Li, Z. (Eds.), 1998. Structures of Eastern Depression, Liaohe basin and hydrocarbon potential analyses. Geology Press, Beijing, 156.

Chenet, P.Y., Montadert, L., Gairaud, H., Roberts, D., 1982. Extensional ratio measurements on the Galicia, Portugal and northern Biscay continental margins. In: Watkins, J.S., Drake, C.L. (Eds.), Studies in Continental Margin Geology, American Association of Petroleum Geologists Memoir 34, Tulsa, pp. 703–715.

Farnetani, C.G., Richards, M.A., 1994. Numerical investigations of the mantle plume initiation model for flood basalt events. J. Geophys. Res. 99, 13813–13833.

Fitton, J.G., James, D., Kempton, P.D., Ormerod, D.S., Leeman, W.P., 1998. The role of lithospheric mantle in the generation of late Cenozoic basic magmas in the western United States. J. Petrol. Spec. Lithospheric Issue, vol. 1988, 331–349.

Gao, Z., 1986. The Tertiary blind volcanic rocks in Huanghua Depression and their tectonic setting. Acta Petrol. Sin. 1986, 14–30.

Hellinger, S.J., Shedlock, K.M., Sclater, J.G., Hong, Y., 1985. The Cenozoic evolution of the North China basin. Tectonics 4, 343–358.

Hsiao, L.Y., 2003. Sequence stratigraphy and structure of the south Xialiao basin, Bohai, offshore China (Ph.D. Dissertation). Stanford University, Stanford, 281.

Hsiao, L., Graham, S.A., Tilander, N., 2004. Reflection seismic imaging of a major strike-slip fault zone within a rift system: Paleogene structure and evolution of the Tan-Lu Fault system, Liaodong Bay, Bohai, offshore China. Am. Assoc. Pet. Geol. Bull. 88, 71–98.

Huang, W., Gao, W., Ding, G., 1996. Neogene volcanism and Holocene earthquakes in the Tanlu fault zone, eastern China. Tectonophysics 260, 259–270.

Huo, G., Wang, X., Bai, J., Li, R., 2000. Geophysical features of the Tan-Lu fault zone. In: Wang, X. (Ed.), Tan-Lu Fault Zone. Geology Press, Beijing, pp. 74–107.

Jarvis, G.T., McKenzie, D.P., 1980. Sedimentary basin formation with finite extension rates. Earth Planet. Sci. Lett. 48, 42–52.

Karner, G.D., Lake, S.K., Dewey, J.F., 1987. The thermal and mechanical development of the Wessex basin. In: Coward, M.P., Dewey, J.F., Hancock, P.L. (Eds.), Continental Extensional Tectonics. Geological Society Special Publication 28, London, pp. 517–536.

Lambiase, J.J., 1990. A model for tectonic control of lacustrine stratigraphic sequences in continental rift basin. In: Katz, B.J. (Ed.), Lacustrine Basin Exploration; Case Studies and Modern Analogs, American Association of Petroleum Geologists Memoir 50, Tulsa, pp. 265–276.

Le Maitre, R.W., Bateman, P., Dudek, A., Keller, J., Lameyre Le Bas, M.J., Sabine, P.A., et al., 1989. A Classification of Igneous Rocks and Glossary of Terms. Blackwell, Oxford, Boston, 193.

Lezzar, K.E., Tiercelin, J.J., Le Turdu, C., Cohen, A.S., Reynolds, D.J., Le Gall, B., et al., 2002. Control of normal fault interaction on the distribution of major Neogene sedimentary depocenters, Lake Tanganyika, East Africa rift. Am. Assoc. Pet. Geol. Bull. 86, 1027–1059.

Liang, H., Shen, S., Liu, X., Chen, W., Li, D., 1992. The age of the volcanic rocks and their geological time in Liaohe Depression. Acta Pet. Sin. 13, 35–41.

Liu, G., 1987. The Cenozoic rift system of the North China Plain and the deep internal processes. Tectonophysics 133, 277–285.

Liu, X., Wang, X., Wang, Y., Ho, B., Wang, L., Chen, H., 1987. Sedimentary basins in Bohai region. In: Wang, S., Zhao, L. (Eds.), Sedimentary Basins on Continental Shelf of North Offshore China. Vol. 16, Petroleum Geology of ChinaPetroleum Industry Press. Beijing, pp. 3–262.

Lu, B., 1990. Typical Seismic Sections in China. Petroleum Industry Press, Beijing, 260.

McKenzie, D., 1978. Some remarks on the development of sedimentary basins. Earth Planet. Sci. Lett. 40, 25–32.

McKenzie, D., Bickle, M.J., 1988. The volume and composition of melt generated by extension of the lithosphere. J. Petrol 29, 625–679.

Mitchum Jr., R.M., Vail, P.R., Thompson III, S., 1977. Seismic stratigraphy and global changes of sea level, Part 2: the depositional sequence as a basic unit for stratigraphic analysis. In: Payton, C.E. (Ed.), Seismic Stratigraphy – Applications to Hydrocarbon Exploration, American Association of Petroleum Geologists Memoir 26, Tulsa, pp. pp. 53–62.

Molnar, P., Tapponier, P., 1977. Relation of the tectonics of Eastern China to the India-Eurasia collision: application of slip line field theory to large scale continental tectonics. Geology 5, 212–216.

Moretti, I., Pinet, B., 1987. Discrepancy between lower and upper crustal thinning. In: Beaumont, C., Tankard, A.J. (Eds.), Sedimentary Basins and Basin Forming Mechanisms, Canadian Society of Petroleum Geology Memoir 12, pp. 233–239.

Nilsen, T.H., Sylvester, A.G., 1995. Strike-slip basins. In: Busby, C.J., Ingersoll, R.V. (Eds.), Tectonics of Sedimentary Basins. Blackwell Science, Malden, pp. 425–458.

Olsen, P., Shubert, F., Anderson, C., Goldman, P., 1988. Plume formation and lithospheric erosion: a comparison of laboratory and numerical experiments. J. Geophys. Res. 93, 15065–15084.

Parsons, J.D., Bush, J.W.M., Syvitski, J.P.M., 2001. Hyperpycnal plume formation from riverine outflows with small sediment concentrations. Sedimentology 48, 465–478.

Prosser, S., 1993. Rift-related linked depositional systems and their seismic expression. In: Williams, G.D., Dobb, A. (Eds.), Tectonics and Seismic Sequence Stratigraphy, Geological Society Special Publication 71, London, pp. 35–66.

Ren, J., Tamaki, K., Li, S., Zhang, J., 2002. Late Mesozoic and Cenozoic rifting and its dynamic setting in Eastern China and adjacent areas. Tectonophysics 344, 175–205.

Rollinson, H.R., 1993. Using Geochemical Data: Evaluation, Presentation, Interpretation. Longman, Singapore, 352.

Ruppel, C., 1995. Extensional processes in continental lithosphere. J. Geophys. Res. 100, 24187–24215.

Saunders, A.D., Storey, M., Kent, R.W., Norry, M.J., 1992. Consequences of plume-lithosphere interactions. In: Storey, B.C., Alabaster, T., Pankhurst, R.J. (Eds.), Magmatism and the Causes of Continental Break-Up. Geological Society Special Publication 68, London, pp. 41–60.

Sclater, J.G., Célérier, P.A.F., 1989. Errors in extension measurements from planar faults observed on seismic reflection lines. Basin Res. 1, 217–221.

Shedlock, K.M., Hellinger, S.J., Hong, Y., 1985. Evolution of the Xialiao basin. Tectonics 4, 171–185.

Smith, A.D., 1998. The geodynamics significance of the DUPAL anomaly in Asia. In: Flower, M.F.J., Chung, S.L., Lo, C.H., Lee, T.Y. (Eds.), Mantle Dynamics and Plate Interactions in East Asia. American Geophysical Union Geodynamics Series 27, pp. 89–106.

Song, Y., Frey, F.A., 1989. Geochemistry of peridotite xenoliths in basalt from Hannuoba, Eastern China: implications for subcontinental mantle heterogeneity. Geochim. Cosmochim. Acta 53, 97–113.

Tang, Z., Wu, H., Gao, W., Qin, K., Liu, Y. (Eds.), 1988. Huabei Oilfields. Petroleum Geology of China 5. Petroleum Industry Press, Beijing, 569.

Tapponnier, P., Molnar, P., 1977. Active faulting and tectonics in China. J. Geophys. Res. 82, 2905–2930.

Tatsumoto, M., Basu, A.R., Huang, W., Wang, J., Xie, G., 1992. Sr, Nd, and Pb isotopes of ultramafic xenoliths in volcanic rocks of Eastern China: enriched components EMI and EMII in subcontinental lithosphere. Earth Planet. Sci. Lett. 113, 107–128.

Wang, Z., Liu, H., Duan, Z., Wang, H., 1998. Analysis of Meso-Cenozoic tectonic inversion of Huanghua Depression, Hebei, China. J. China Univ. Geosci. 23, 289–293.

White, N., 1988. Extension and subsidence of the continental lithosphere (Ph.D. dissert.) University of Cambridge, Cambridge (as quoted in White, 1990).

White, N., 1990. Does the uniform stretching model work in the North Sea? In: Blundell, D.J., Gibbs, A.D. (Eds.), Tectonic Evolution of the North Sea Rifts. Clarendon Press, Oxford, pp. 217–240.

White, N., McKenzie, D.P., 1988. Formation of the "steer's head" geometry of sedimentary basins by differential stretching of the crust and mantle. Geology 16, 250–253.

Wilcox, R.E., Harding, T.P., Seely, D.R., 1973. Basic wrench tectonics: American Association of Petroleum Geologists Bulletin 57 (4), 74–96.

Xu, H., Lu, W., Wang, S., Wan, J., 1983. Paleogene sedimentary facies systems and direction of searching for oil and gas in Bohaiwan basin. Acta Geol. Sin. 3, 243–253.

Xu, J., 1980. The horizontal displacement of the Tancheng-Lujiang fault zone and its geologic significance. Scientific Papers on Geology for International Exchange, No. 1. Geological Publish House, Beijing, pp. 129–142.

Xu, J., Zhu, G., 1994. Tectonic models of the Tan-Lu Fault Zone, Eastern China: International Geology Review, 36 (8), 771–784.

Xu, Y.G., Menzies, M.A., Ross, J.V., 2001. Thermo-tectonic destruction o fthe Archaean lithospheric keel beneath the Sino-Korean craton in China: evidence, timing and mechanism. Phys. Chem. Earth (A) 26, 747–757.

Ye, H., Shedlock, K.M., Hellinger, S.J., Sclater, J.G., 1985. The North China Basin: an example of a Cenozoic rifted intraplate basin: Tectonics 4 (2), 153–169.

Yin, A., Nie, S., 1993. An indentation model for the North and South China collision and the development of Tanlu and Honam fault systems, eastern Asia. Tectonics 12, 801–813.

Yang, M., Lu, P., Hua, X., Song, R., 1989. Focal mechanism solutions of earthquakes. In: Ma, X., Ding, G., Gao, W., Zhang, H., Zhang, B., Ma, Z. (Eds.), Lithospheric dynamics atlas of China: Beijing, China Cartographic Publishing House, p. 26.

Zartman, R.E., Futa, K., Peng, Z.C., 1991. A comparison of Sr-Nd-Pb isotopes in young and old continental lithospheric mantle: Patagonia and eastern China. Aust. J. Earth Sci. 38, 545–557.

Zhang, Y.S., 1998. Three-dimensional upper mantle structure beneath east Asia and its tectonic implications. In: Flower, M.F.J., Chung, S.L., Lo, C.H., Lee, T.Y. (Eds.), Mantle Dynamics and Plate Interactions in East Asia. American Geodynamics Union Geodynamics Series 27, pp. 11–23.

Zhao, C., Meng, W., Jin, C., Cai, G., Zhao, S., Ji, H., 1999. Volcanic Rocks and Oil and Gas in Liaohe Basin. Petroleum Industry Press, Beijing, 101.

Zhi, X., Song, Y., Frey, F.A., Feng, J., Zhai, M., 1990. Geochemistry of Hannuoba basalts, Eastern China; constraints on the origin of continental alkalic and tholeiitic basalt. Chem. Geol. 88, 1–33.

Zhou, X., Zhu, B., Liu, R., Chen, W., 1988. Cenozoic basaltic rocks in eastern China. In: Macdougall, J.D. (Ed.), Continental Flood Basalt. Kluwer Academic Publishers, Dordrecht, pp. 311–330.

Ziegler, P.A., 1983. Crustal thinning and subsidence in the North Sea: matters arising. Nature 304, 561.

Zindler, A., Hart, S.R., 1986. Chemical geodynamics. Annu. Rev. Earth Planet. Sci. 14, 493–571.

In this chapter

11

Lake Baikal

Hus R., [*,†] *Poort J.*, [*,**] *Charlet F.*, [*,‡] *Naudts L.*, [*,§]
Khlystov O., [§,§§] *Klerkx J.*, [¶] *De Batist M.* [*]

*Renard Centre of Marine Geology (RCMG), Universiteit Gent, Gent, Belgium
†BHP Billiton, Newman, Australia
**ISTeP, Université Pierre et Marie Curie, Paris, France
‡Dredging International, Scheldedijk, Zwijndrecht, Belgium
§Management Unit of the North Sea Mathematical Models and the Scheldt Estuary (MUMM), Brussels, Belgium
§§Limnological Institute of the Siberian Branch of the Russian Academy of Sciences, Irkutsk, Russia
¶International Bureau of Environmental Studies (IBES), Brussels, Belgium

11.1 Introduction

Lake Baikal is the largest lake in the world. It contains 23,615 km^3 of water, or 20% of all fresh liquid surface water on Earth. With water depths up to 1642 m (INTAS Project 99–1669 Team, 2002) and a sedimentary infill up to 9 km (ten Brink and Taylor, 2002), it forms the central and most strongly subsiding part of the largest tectonically active rift system in Eurasia: the Baikal Rift Zone. The Baikal Rift Zone consists of a series of fault-bounded basins, arranged in a ~1800-km-long S-shaped strip that rims the wedge of the Siberian Platform (Fig. 11.1; e.g., Logatchev, 1993). This chapter, which provides an overview of the subject, focuses on the central part of the rift: the three Lake Baikal basins.

11.2 General geological setting and evolution

The precise location and the typical S-shape of the Baikal Rift Zone are determined mainly by the strong rheological difference between the Archean craton, the Siberian Platform, in the northwest and the Sayan-Baikal Mobile Belt in the southeast (Zonenshain and Savostin, 1981). The structure of this complex fold-and-thrust belt results from several stages of compression and extension that have affected the region from Early Paleozoic to Mesozoic times (Delvaux et al., 1995). After the final closure of the Mongol-Okhotsk Ocean in the Late Jurassic to Early Cretaceous, a period of tectonic quiescence existed (Cretaceous to Paleogene) that resulted in a peneplanation of the newly formed orogen, and

Phanerozoic Rift Systems and Sedimentary Basins DOI:10.1016/B978-0-444-56356-9.00010-9

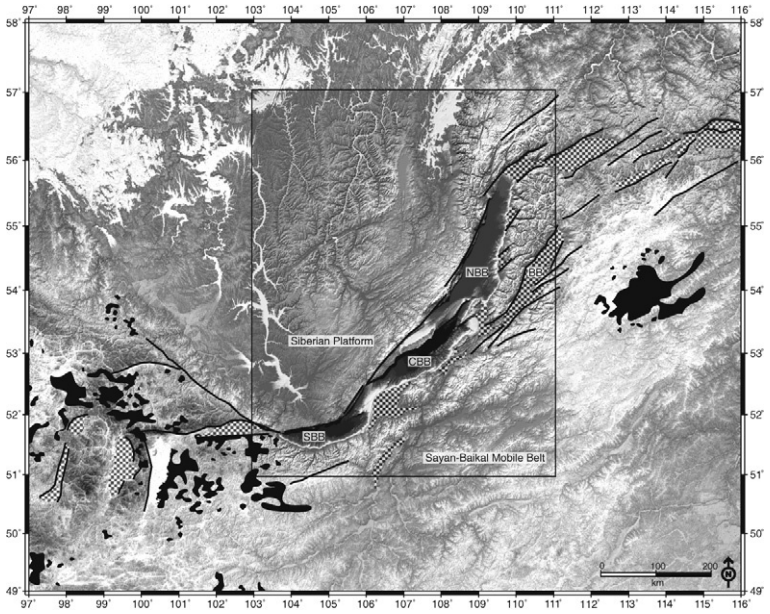

Figure 11.1 Shaded-relief digital terrain model (DTM) of the Baikal Rift Zone, constructed by compiling SRTM-derived topography data with bathymetry data from Lake Baikal (INTAS Project 99–1669 Team, 2002). The central part of the DTM (inside rectangle) is gridded in higher resolution. Indicated are the location of the Siberian Platform and the Sayan-Baikal Mobile Belt, the main rift-zone border faults (black lines), sediment-filled rift basins (chequered) and volcanic fields (black). SBB, South Baikal Basin; CBB, Central Baikal Basin; NBB, North Baikal Basin; BB, Barguzin Basin.

the formation of a vast laterite-kaolinite weathering crust (Delvaux et al., 1995; Mats, 1993).

After the Late-Oligocene, the present rift system began to develop. This resulted in the formation of 14 individual rift basins. The three central basins – the South, Central and North Baikal Basins – are occupied by Lake Baikal, and together with the Barguzin Basin they can be considered the "core" of the Baikal Rift Zone. Each of the basins has a different orientation, turning from ENE in the south to NNE in the north, and they are at present predominantly controlled by extensional tectonics. The other (smaller) basins of the Baikal Rift Zone have developed north and south of Lake Baikal in E-W oriented deformation zones defined mainly by strike-slip faulting.

On the basis of the analysis of the onshore geology around the lake – including deep boreholes – and of multi-channel reflection seismic profiles on the lake, it is generally assumed that Cenozoic rifting started by slow subsidence of the South and Central Baikal Basins sometime in the Late Oligocene (~30 Ma), and of the North Baikal Basin in the Late Miocene (~8 Ma) (Logatchev and Florensov, 1978; Mats et al., 2000; Fig. 11.2). For more than 20 Ma, a series of lacustrine and fluvial sediments up to 4–5 km thick accumulated in slowly subsiding basins surrounded by subdued uplands. This period is referred to as the "slow rifting stage" (Logatchev and Florensov, 1978) or the "early rifting stage" (Mats et al., 2000). From the Late Pliocene (~3.5 Ma) onward, a strong acceleration in basin subsidence and flank uplift took place. This "fast rifting stage" or "late rifting

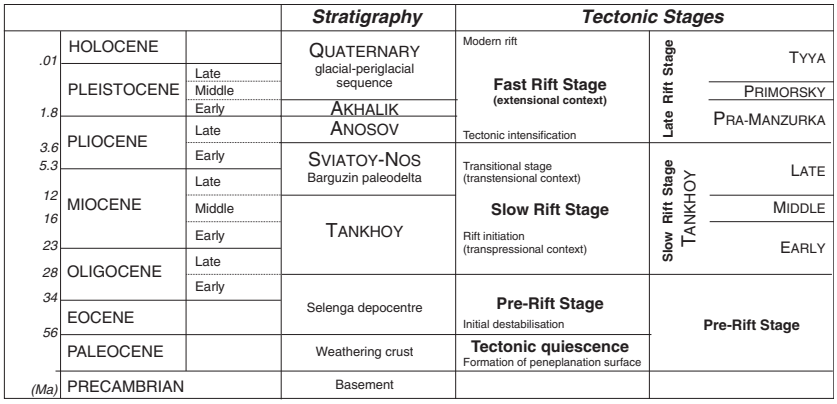

Figure 11.2 Schematic overview of the main stratigraphic units and tectonic stages in the central part of the Baikal Rift Zone *(based on Delvaux et al., 1997; Logatchev and Florensov, 1978; Mats et al., 2000)*.

stage" resulted in an additional sedimentary infill of more than 4 km, a Baikal water depth of more than 1 km and flank uplifts of 1–2 km. Ongoing present-day rift deformation is testified by numerous seismic events annually (e.g., Déverchère et al., 2001) and by a GPS-derived mean rate of extension of about 4 mm/yr (Calais et al., 2003).

11.3 Morpho-structural characteristics and architecture

The South, Central and North Baikal Basins have maximum water depths of 1461, 1642 and 904 m, respectively (INTAS Project 99–1669 Team, 2002). The steep western perimeter of the lake is bordered by the Primorsky and Baikalsky mountain ranges, while the Khamar-Daban, Ulan-Burgasy and Barguzin ranges border the coastal plains on the east side (Fig. 11.3). The height of the mountains increases from the south of the lake to the north, from about 1000 to 2500 m, except for the extreme south where the Khamar-Daban also rises to 2100 m. The lake itself is at 455.5 m above sea level.

The three Baikal basins show a clear asymmetrical shape with major large-displacement faults on the western side and a more gradual change in topography along their eastern margin (e.g., Hutchinson et al., 1992; Logatchev, 1993; Mats, 1993; Zonenshain and Savostin, 1981). The vertical displacement that took place along the western border faults in the central part of lake Baikal is estimated to be around 8000 m by Zonenshain et al. (1992), but when assuming a sediment thickness of 8–9 km for the central basin (ten Brink and Taylor, 2002), this value is more likely around 12 km (i.e., with rift shoulders reaching heights of 1500–2000 m above lake level and a water depth of 1500 m).

The orientation of the border faults along the western side of Lake Baikal changes from an ENE direction along the South Baikal Basin to an approximately

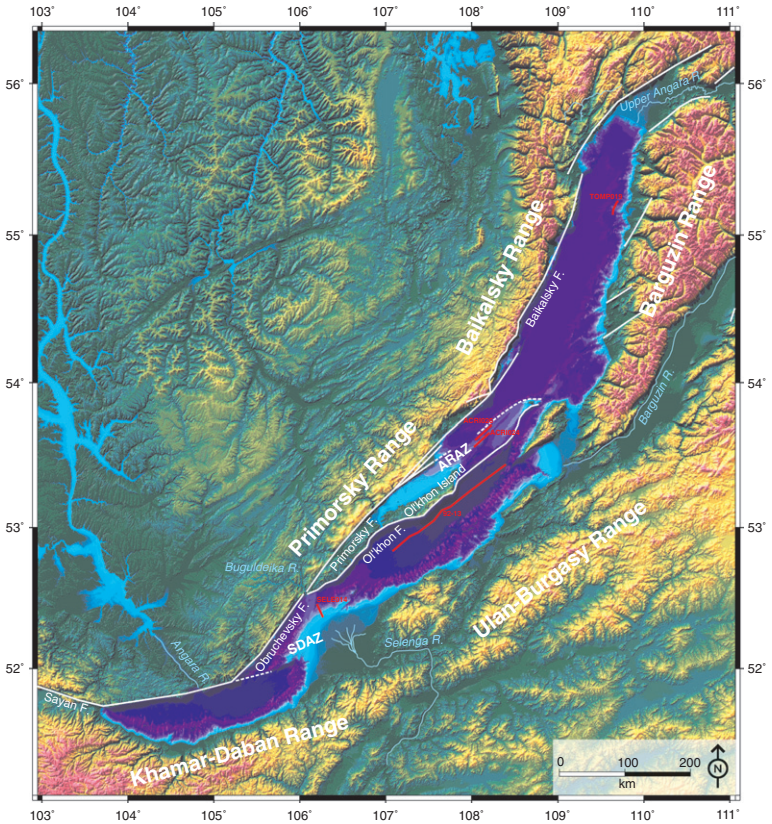

Figure 11.3 Shaded-relief, colour-coded DTM of the central part of the Baikal Rift Zone, constructed by compiling SRTM-derived topography data with bathymetry data from Lake Baikal (INTAS Project 99–1669 Team, 2002). Indicated are the main mountain ranges and rivers, the main border faults of the three Lake Baikal basins and the location of the seismic profiles shown in Figs. 11.4–11.8. SDAZ, Selenga Delta Accommodation Zone; ARAZ, Academician Ridge Accommodation Zone.

NNE orientation in the North Baikal Basin (Fig. 11.3). This results in a characteristic segmentation of the lake basin, a property that is also recognised in other rift basins, for example, the East African Rift System and the Basin and Range Province. As a result of this segmentation, two large structurally complex accommodation zones have formed, which are expressed as bathymetric sills separating the different Baikal basins: the Selenga Delta Accommodation Zone between the South and Central Baikal Basins (Scholz and Hutchinson, 2000), and the Academician Ridge Accommodation Zone between the Central and North Baikal Basins (Mats et al., 2000).

The Obruchevsky Fault scarp forms the northwestern border of the South Baikal Basin. At the mouth of the Buguldeika River, it splays into an eastern branch, the Ol'khon Fault, and a western branch, the Primorsky Fault, the main boundary of the Central Baikal Basin. The Ol'khon Fault cross-cuts Lake Baikal, delimiting the southern side of Ol'khon Island and the submerged Academician Ridge, two major blocks of the Academician Ridge Accommodation Zone (Mats et al.,

2000). Farther to the north, the Primorsky Fault dies out and is replaced by the Baikalsky Fault, which has a slightly different orientation and borders the North Baikal Basin. In between the different segments of the western border fault, several relay zones have developed (Agar and Klitgord, 1995; Delvaux et al., 2000; Hus et al., 2006).

11.4 Sedimentary infill

On the basis of multi-channel seismic reflection data, three first-order stratigraphic units have been identified in the lake's sedimentary infill (Hutchinson et al., 1992; Fig. 11.4). The first unit ("proto-rift deposits") directly overlies the basement and has a maximum thickness of 4–5 km. It is overlain by the second unit ("middle rift deposits"), which is 1–2 km thick. The boundary between these two units, a well-defined angular unconformity, has been interpreted by Hutchinson et al. (1992) as corresponding to the transition from the slow to the fast rifting stage (~3.5 Ma). On the basis of the thicknesses of these units, the sedimentation rate during the middle rift deposits is inferred to have been around 5–10 times higher than that during deposition of the lower rift deposits (Logatchev, 1993). This is attributed to larger topographic gradients in the surrounding mountains related to the tectonic intensification. On top, the third unit ("upper rift deposits") has accumulated with thicknesses that are in general less than 500 m. It includes Pleistocene and Holocene sediments, and likely represents a final tectonic pulse that affected the Baikal Rift Zone (Logatchev, 1993).

Not much is known about the composition of the older sediments in the deep Baikal basins because of the absence of deep boreholes. Logatchev (1993) believes that the proto-rift deposits consist mainly of fine-grained sediments that are intercalated by layers of coal and diatomaceous clay. He also infers that the middle-rift deposits at the margins of the Baikal basins are typically sandy gravels and pebble and boulder deposits of fluvial, fluvio-glacial and gravitational origin, whereas in the central part of the basins they have a more fine-grained composition.

Much more information is available concerning the lithology and distribution of the different sediment types that make up the upper part of the sedimentary infill, thanks to the interpretation of numerous high-resolution reflection seismic profiles, sediment cores and boreholes (e.g., Ceramicola et al., 2001; Charlet et al., 2005; Colman et al., 2003). Climate, as well as tectonic and physiographic setting, controls the clastic sediment supply to the lake and determines the distribution of the main sedimentary facies in the Quaternary deposits (Back et al., 1999; Nelson et al., 1999). By far, the most widespread depositional environment in Lake Baikal is made up of turbidite systems that characterise most of the margins and deep basin floors. Small, sand-rich aprons form at the base of the steep western border-fault slopes, while the more gentle eastern slopes adjacent to the highest mountain ranges are characterised by large glacio-lacustrine sub-aqueous fans (Fig. 11.5). Very large deltas (Fig. 11.6) and

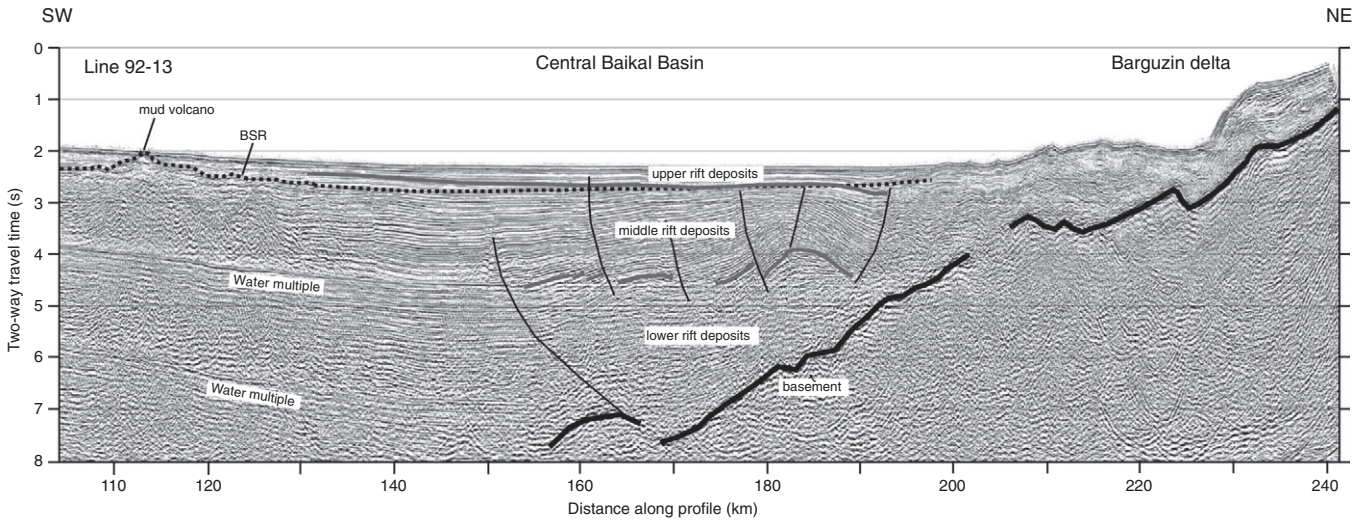

Figure 11.4 Multi-channel seismic profile 92–13 along the Central Baikal Basin *(modified from ten Brink and Taylor, 2002 seismic data courtesy of USGS),* with indication of the three first-order stratigraphic units. Intra-basin faults at the transition between the Central Baikal Basin and the Academician Ridge Accommodation Zone are indicative of a phase of oblique opening of the central part of the rift zone during the Late Miocene to Early Pliocene (Delvaux et al., 1997). Also indicated is the bottom-simulating reflector (BSR), which indicates that gas hydrates are present in the deep-water sediments of the Central Baikal Basin (Golmshtok et al., 1997, 2000; Vanneste et al., 2001). Location of the profile on Fig. 11.3.

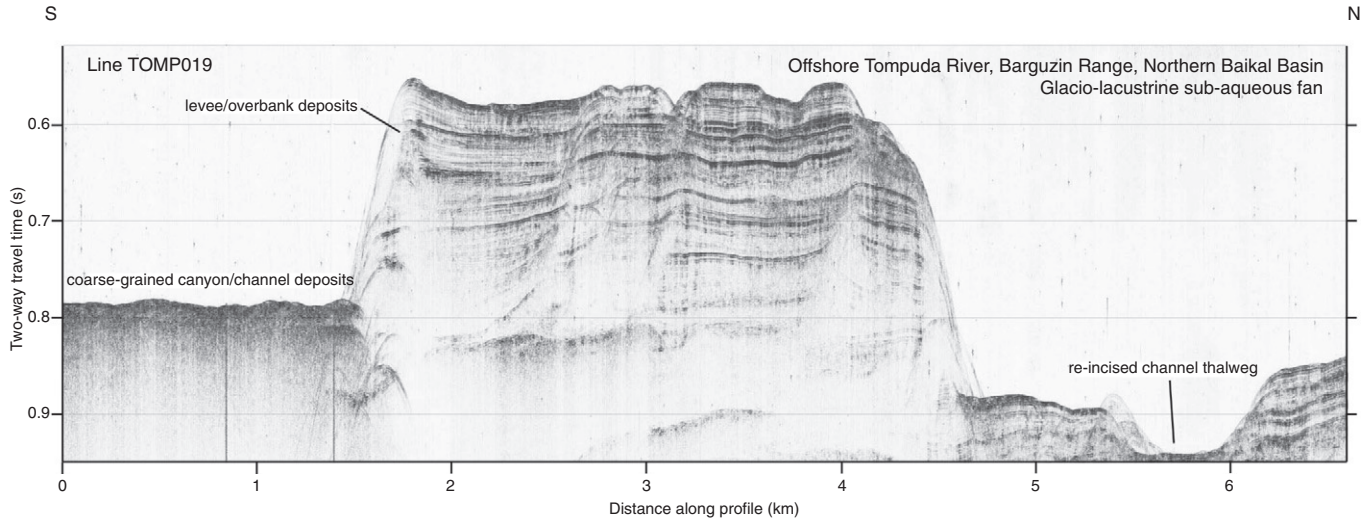

Figure 11.5 High-resolution seismic profile TOMP019 in the Northern Baikal Basin, offshore the Barguzin Range. The profile shows high-relief channel-levee systems associated with the large glacio-lacustrine sub-aqueous Tompuda fan, and illustrates one type of turbidite systems that characterise the margins and deep basin floors of Lake Baikal. Location of the profile on Fig. 11.3.

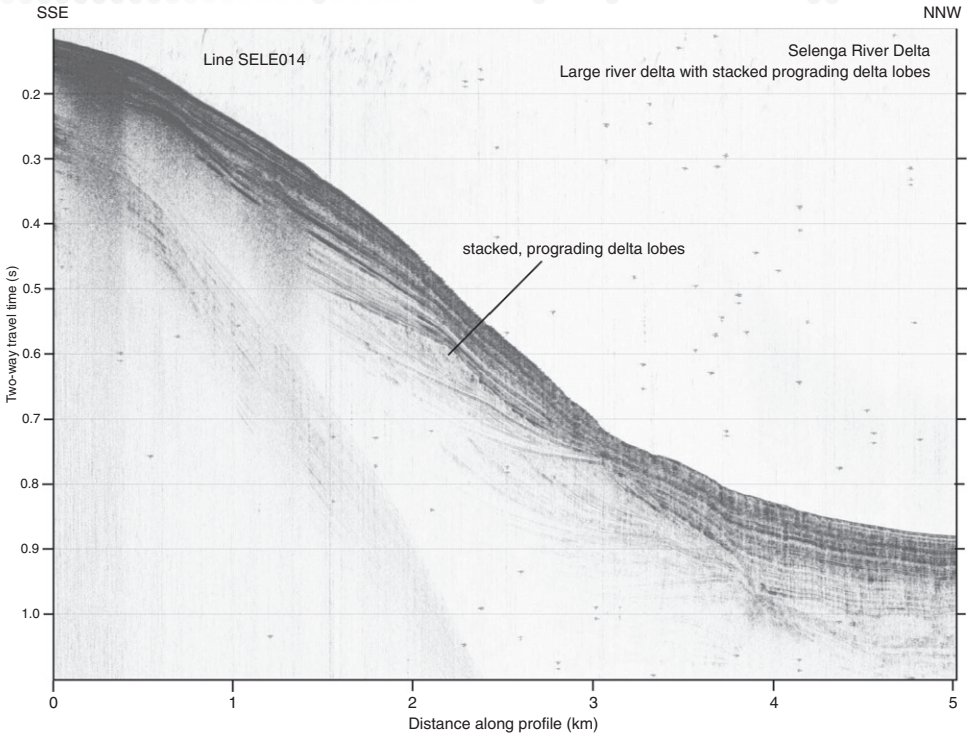

Figure 11.6
High-resolution seismic profile SELE014 across the Selenga River delta. The profile shows a series of stacked, prograding delta lobes. Location of the profile on Fig. 11.3.

associated mud-rich fans developed at the mouths of the major rivers, which typically enter the lake either axially (Upper Angara River) or near accommodation zones (Selenga and Barguzin rivers). A third depositional environment exists on top of tectonically or topographically isolated ridges or banks. These are characterised by the accumulation of fine hemipelagic sediments, with some contribution from ice-rafted debris. These sediments accumulate often in the form of lacustrine drifts (e.g., mounds, moats and sediment waves) that result from bottom-current reworking (Figs. 11.7 and 11.8). In all depositional environments, there is a distinct difference in sedimentary composition between sediments that accumulated under glacial or interglacial conditions, glacial sediments being characterised by much lower biogenic fraction and higher detrital fraction. This climate-controlled alternation is most pronounced in the hemipelagic environment on top of the ridges and banks, where interglacial sediments are composed of fine diatomaceous ooze (diatom content up to 80%) and glacial sediments of diatom-barren, terrigenous silty clay (e.g., Grachev et al., 1998; BDP-98 Members, 2001).

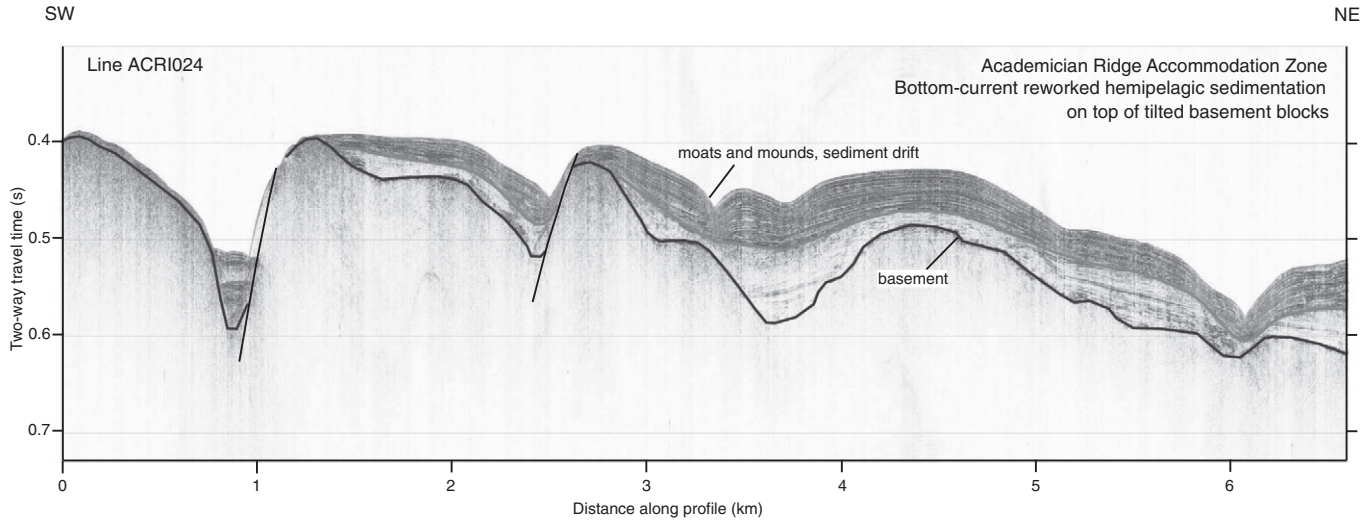

Figure 11.7 High-resolution seismic profile ACRI024 along the crest of the Academician Ridge Accommodation Zone. The profile shows the complex basement structure of the accommodation zone, with a series of tilted blocks, and the sedimentary cover composed of bottom-current reworked hemipelagic sedimentation. Typical indications for bottom-current reworking are the asymmetric sediment cover on basement knolls, and the presence of moats and sediment mound (Ceramicola et al., 2001). Location of the profile on Fig. 11.3.

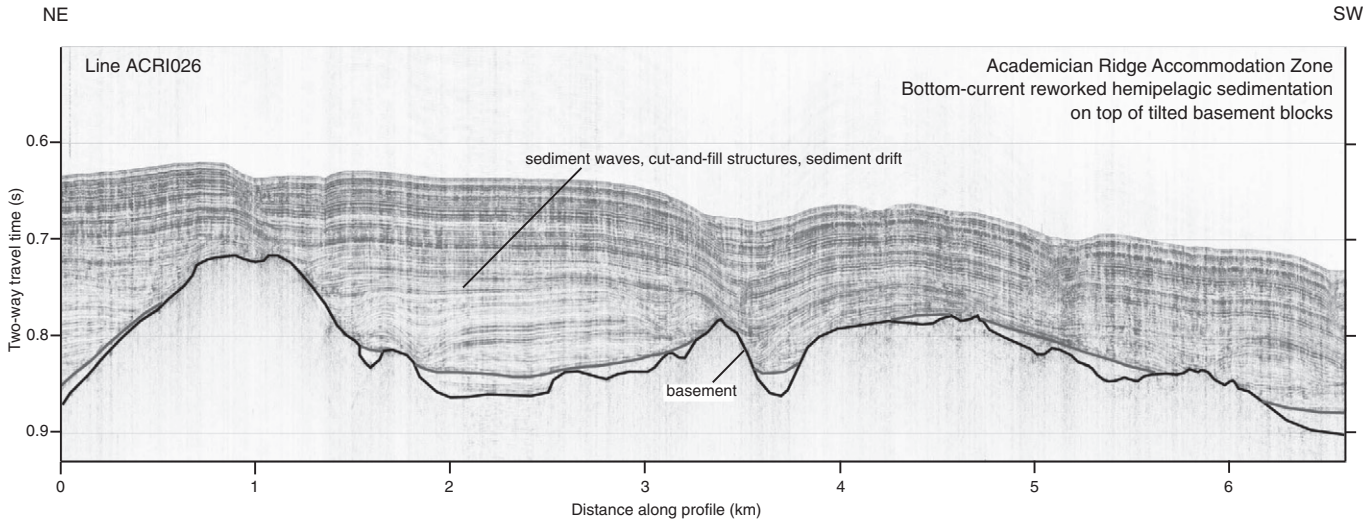

Figure 11.8 High-resolution seismic profile ACRI026 along the crest of the Academician Ridge Accommodation Zone. The profile shows the complex basement structure of the accommodation zone, and the sedimentary cover composed of bottom-current reworked hemipelagic sedimentation. Typical indications for bottom-current reworking are the presence of sediment waves and cut-and-fill structures (Ceramicola et al., 2001). Location of the profile on Fig. 11.3.

11.5 Volcanism

Rift-related volcanics are absent in Lake Baikal (Fig. 11.1). In the larger area of the Baikal Rift Zone, three basaltic fields have formed during rifting: the Sayan–Khamar-Daban, Vitim and Udokan fields (Logatchev, 1993). Peaks of magmatism occurred in the Middle to Late Miocene and in the Pliocene to Quaternary (Rasskazov, 1994). Unlike other rifts, the volcanism in the Baikal Rift Zone occurs independently from major rift faults or basins (Logatchev, 1993). Moreover, the total volume of volcanic rocks is very limited (5000–6000 km^3) compared to other rifts. For the Rio Grande Rift, for example, this volume is believed to be an order of magnitude larger (e.g., Lipman et al., 1989) and for the Kenya Rift even 20 times larger (e.g., Logatchev et al., 1983).

11.6 Deep structure

From long-wavelength gravity anomalies (Zorin et al., 1989) and deep seismic soundings (Puzyrev et al., 1973), the thickness of the lithosphere beneath the regions adjacent to the rift has been estimated to be 200 km for the Siberian Platform and 160–175 km in the Sayan-Baikal Mobile Belt; the crust is calculated to be 40 km thick below the craton and 45 km in the fold belt. These studies also indicate a decreased crustal thickness of 35–37 km below the rift axis. However, recent studies of P-wave velocities (ten Brink and Taylor, 2002) question this large crustal thinning and estimate a Moho uplift under the rift axis of $<$3 km. Gravity modelling by Petit et al. (1997) supports a thinning up to 7 km, but indicates that crustal thinning is limited to an area 160 km wide under the Central Baikal Basin and 50 km under the North Baikal Basin.

The upper-mantle structure below Lake Baikal is still a topic of debate. Two opposing models of interpretation exist: (1) a total replacement of the lithosphere up to crustal levels by warm asthenosphere underneath the rift (Gao et al., 1994; Zorin, 1981; and references therein), and (2) only limited lithospheric thinning and a hot, narrow mantle plume resulting in magmatic underplating (Kiselev and Popov, 1992; Krylov et al., 1981; Petit et al., 1998).

The presence of a low-velocity zone beneath the Moho (Puzyrev et al., 1973), an apparent regional domal uplifting, high heat-flow values and long-wavelength gravity anomalies (Zorin et al., 1989) seems to support the first hypothesis.

However, similar geophysical data have been used to reject the asthenospheric upwelling hypothesis, for example, teleseismic studies (Petit et al., 1998; Tiberi et al., 2003) and gravity modelling (Diament and Kogan, 1990; Poort et al., 1998; Ruppel et al., 1993). Mechanical models of the lithosphere, constrained by topography, gravity and heat-flow data, have confirmed that the lithosphere cannot be significantly thinned under the main part of Lake Baikal, but that a small amount of thinning could be present below the North Baikal

Basin. Burov et al. (1994) and Petit et al. (1997) explained the flank uplift surrounding the Baikal basins as caused by a downward flexure that results from dense mantle material at crustal levels (magmatic underplating) and not as a (thermo)isostatic rebound in response of extension. All these models indicate that the lithosphere has a relatively large flexural rigidity, on the order of 3–4 $\times$ 10^{23} Nm (effective elastic thickness Te $\approx$ 30–50 km). This is supported by the recordings of earthquakes up to unusual large depths of 25–30 km (Déverchère et al., 1991) and by detailed studies of the thermal regime revealing the absence of a large thermal anomaly in Lake Baikal (Lysak, 1992; Poort and Klerkx, 2004). The alternative hypothesis of mantle structure assumes a narrow mantle plume along the Siberian Craton and sub-crustal magmatic underplating, and underscores the importance of the Paleozoic suture zone as a major factor in rift evolution (Kiselev and Popov, 1992; Petit et al., 1998).

The absence or presence of an asthenospheric upwelling has been the main argument in the debate about whether rift onset and rift evolution occurred "actively" or "passively", as discussed in the next section.

11.7 Deformation mechanisms

Evolution models

The question whether the Lake Baikal basins have been actively or passively rifting has been the subject of a heated debate during the past decades. Believers of the active rifting hypothesis have argued that evidence can be found for a broad asthenospheric upwelling at the location of the rift zone (see above). According to the passive rift hypothesis, extension in the Baikal Rift is believed to result from far-field stresses and the absence of a largely disturbed deep-mantle structure (see discussion above) and the necessary stresses are believed to result from the indentation of India into Eurasia (Molnar and Tapponnier, 1975; Zonenshain and Savostin, 1981) and from the subduction of the Pacific plate along its western boundary (Calais et al., 1998). The passive rift hypothesis is supported by numerical models which have calculated that the presence of far-field stresses in combination with the favourably oriented zones of weakness in the Baikal rift could be responsible for the development of the extensional basins in Baikal (Lesne et al., 1998).

Kinematic evolution

From the reconstruction of paleostress tensors, it has been suggested that the initial evolution of Lake Baikal (i.e., before Late Miocene) took place in a transpressional regime (Delvaux et al., 1997). During the Late Miocene to Early Pliocene, this regime changed into one of transtension, resulting in an oblique opening of the central part of the rift zone. From the Late Pliocene onward – during the

fast rifting stage – the main faults of Lake Baikal evolved in predominantly dip-slip faults, with only minor lateral movements. This resulted in the approximately orthogonal opening of the North and Central Baikal Basins. The southern basin continued to open obliquely (Delvaux et al., 1997).

Present-day deformation

Based on GPS measurements, the present-day rate of extension in the southern part of the Baikal Rift Zone has been calculated to be 4.5 ± 1.2 (Calais et al., 1998) or 4 ± 1 mm/yr (Calais et al., 2003) in a WNW-ESE direction. This measured rate is considerably higher than the ones calculated on the basis of kinematic models of Central Asia, in which the convergence between India and Eurasia is the sole driving mechanism for the present deformation (e.g., England and Molnar, 1997). Such models predict extension rates in the Baikal Rift Zone of a maximum of 2 mm/yr. On the other hand, estimates based on the seismic moment release that resulted from the three large earthquakes ($M > 6.9$) on the Obruchevsky Fault during the past 300 years suggest an average slip along the fault of 5.6 mm/yr (Calais et al., 1998). This indicates that little or no aseismic slip is occurring along the fault (Calais et al., 1998). In the north of Lake Baikal, the average extension rate has been estimated to be 3.2 ± 0.5 mm/yr in a N140 ± 20E direction, based on summed Holocene displacements on major faults (San'kov et al., 2000). Zonenshain et al. (1992) reported a spreading rate of less than 0.1 cm/yr.

The present-day activity of the Baikal Rift Zone is evidenced by the 4000 seismic events occurring annually. Between 1961 and 1999, 30,000 earthquakes have been instrumentally recorded with magnitudes $2.5 \leq M \leq 7.6$ (Sherman et al., 2004). Since 1760, 27 events have been reported with magnitude $M > 6$ (Sherman et al., 2004). Déverchère et al. (2001) relocated 632 earthquakes that occurred between 1971 and 1997, and found a relatively high abundance of earthquakes at depths between 15 and 25 km (50%). Earthquake activity persists up to depths between 30 and 40 km (i.e., 7–13%), indicating that the lower crust and upper mantle are seismogenic at great depths (Déverchère et al., 1991, 2001).

11.8 Some topics of current research

The active rift-basin context of Lake Baikal produces a unique environment and a natural laboratory in which a variety of geological processes can be studied. Over the past few years, it has therefore attracted scientists studying topics such as active fluid-flow systems involving hydrothermalism, gas hydrates, mud volcanism and cold seeps, as well as the signals of past climates recorded in the sedimentary basin fill. Below, we give a short overview of some of the main topics of current research in Lake Baikal as they illustrate the variety of geological phenomena associated with an active rift basin and underscore the relevance to a wide scientific community today.

Reconstruction of paleoclimate

Because of its isolated, interior-continental setting, its relatively high-latitude location, its old age and the sensitivity of its biogenic and terrigenous sediment fractions to record changes in climate, Lake Baikal's sedimentary infill also represents an important paleoclimate archive. In the past decade, several attempts have been made to unravel the various paleoclimate signals enclosed in the sediments accumulated on the tectonically and topographically isolated ridges and banks (e.g., BDP-93 Members, 1997; BDP-98 Members, 2001; BDP-99 Members, 2005; Oberhäensli and Mackay, 2005). Sediment coring and deep drilling have yielded several continuous records, some of them up to 10 Ma long. They indicate that a major shift towards glacial climate conditions affected the region at 2.8–2.5 Ma, most likely in response to regional uplift due to tectonic intensification (i.e., the "fast rifting stage" at ~3.5 Ma). This initial glacial event was followed by a return to warm, stable climate conditions between 2.4 and 1.8 Ma and therefore does not represent a permanent change in the regional climate mode as often hypothesised. It was only the next climatic deterioration at 1.8–1.5 Ma that resulted in the beginning of the typical eccentricity-paced glacial-interglacial oscillations that are particularly well expressed in the Lake Baikal diatom-abundance records (Prokopenko et al., 2001a).

Other studies have also addressed higher-resolution, millennial-scale climate signals (e.g., Heinrich events, Bond Cycles; Prokopenko et al., 2001b) and, in particular, their timing relative to similar events recorded in the North Atlantic or North Pacific realms. These studies were often confronted by the fact that Lake Baikal sediments are notoriously difficult to date (Colman et al., 1996). Many of the age models that have been used were constructed by "tuning" diatom-abundance records (or a proxy thereof), calibrated by a limited number of tie-points (e.g., derived by $^{210}Pb/^{137}Cs$, AMS ^{14}C, paleomagnetic reversals), to the oceanic oxygen isotope records, obviously involving a certain degree of circular reasoning. Recently, breakthroughs towards an independent dating method have been achieved on the basis of the analysis of geomagnetic paleo-intensity variations (Demory et al., 2005).

Gas hydrates, mud volcanism and gas seeps

Gas escape in Lake Baikal has long been known but the historical records result from observations at the lake surface and mainly concern seeps in shallow waters (Granin and Granina, 2002). During recent years, extensive hydro-acoustic, high-resolution reflection seismic and side-scan sonar surveys have proved that gas escape on the lake floor is widespread and also occurs at great water depths. These seeps mainly involve methane and pore-fluid venting into the lake water, but some also expel remobilised sub-surface sediments (i.e., mud volcanism; Van Rensbergen et al., 2002). In all cases, methane venting occurs along well-constrained segments of active, first-order rift-basin faults (De Batist et al., 2002). Deep-water seeps and mud volcanoes appear to be

unique environments, in which methane hydrates occur at or just below the lake floor (Klerkx et al., 2003; Matveeva et al., 2003).

The presence of gas hydrates in the deeper Baikal sediments was first inferred by Golmshtok et al. (1997) from the observation of a bottom-simulating reflection (BSR) on multi-channel seismic reflection profiles (Fig. 11.4). The BSR can be traced over an area of >4000 km^2 on the slope of the Selenga River delta and the basin floors of the adjacent South and Central Baikal Basins (Golmshtok et al., 2000; Vanneste et al., 2001). In 1997, hydrate samples were retrieved during deep drilling in the South Baikal Basin from 120 and 161 m below the lake floor (Kuzmin et al., 1998, 2000). The Baikal hydrates consist essentially of methane ($>99\%$ of the total gas volume) of biogenic origin (Kuzmin et al., 1998).

Acknowledgments

The high-resolution seismic profiles in Figs. 11.5–11.8 have been acquired in the framework of a series of joint Belgian-Russian seismic expeditions onboard the R.V. Vereshchagin and R.V. Titov, which were financed topics such as by the Belgian Science Policy Office, INTAS, the Russian Foundation for Basic Research and the Integration Program of the Siberian Branch of the Russian Academy of Science. The Limnological Institute (Irkutsk) provided all logistic support. We thank U. ten Brink (USGS) for granting permission to publish the multi-channel seismic profile in Fig. 11.4.

R. Hus was funded through an IWT-grant; J. Poort was funded through a Postdoctoral Fellowship of the Research Foundation – Flanders (FWO).

References

Agar, S.M., Klitgord, K.K., 1995. Rift flank segmentation, basin initiation and propagation: a neotectonic example of Lake Baikal. J. Geol. Soc. Lon. 152, 849–860.

Back, S., De Batist, M., Vanhauwaert, P., Strecker, M., 1999. Quaternary depositional systems in Northern Lake Baikal, Siberia. J. Geol. 107, 1–12.

BDP-93 Members, 1997. Preliminary results of the first drilling on Lake Baikal, Buguldeika site, southeastern Siberia. Quat. Int. 37, 3–17.

BDP-98 Members, 2001. The new BDP-98 600-m drill core from Lake Baikal: a key late Cenozoic sedimentary section in continental Asia. Quat. Int. 81–82, 19–36.

BDP-99 Members, 2005. A new Quaternary record of regional tectonic, sedimentation and paleoclimate changes from drill core BDP-99 at Posolskaya Bank, Lake Baikal. Quat. Int. 136, 105–121.

Burov, E.B., Houdry, F., Diament, M., Déverchère, J., 1994. A broken plate beneath the North Baikal rift zone revealed by gravity modelling. Geophys. Res. Lett. 21, 129–132.

Calais, E., Lesne, O., Déverchère, J., San'kov, V., Lukhnev, A., Miroshnitchenko, A., et al., 1998. Crustal deformation in the Baikal rift from GPS measurements. Geophys. Res. Lett. 25, 4003–4006.

Calais, E., Vergnolle, M., San'kov, V., Lukhnev, A., Miroshnitchenko, A., Amarjargal, S., et al., 2003. GPS measurements of crustal deformation in the Baikal-Mongolia area (1994–2002): implications for current kinematics of Asia. J. Geophys. Res. 108, doi:10.1029/2002JB002373.

Ceramicola, S., Rebesco, M., De Batist, M., Khlystov, O., 2001. Seismic evidence of small-scale lacustrine drifts in Lake Baikal (Russia). Mar. Geophys. Res. 22, 445–464.

Charlet, F., Fagel, N., De Batist, M., Hauregard, F., Minnebo, B., Meischner, D., SONIC Team. 2005. Sedimentary dynamics on isolated highs in Lake Baikal: evidence from detailed high-resolution geophysical data and sediment cores. Glob. Planet. Change 56, 125–144.

Colman, S.M., Jones, G.A., Rubin, M., King, J.W., Peck, J.A., Orem, W.H., 1996. AMS radiocarbon analyses from Lake Baikal, Siberia: challenges of dating sediments from a large oligotrophic lake. Quat. Sci. Rev. 15, 669–684.

Colman, S.M., Karabanov, E.B., Nelson, C.H., 2003. Quaternary sedimentation and subsidence history of Lake Baikal, Siberia, based on seismic stratigraphy and coring. J. Sed. Res. 73, 941–956.

De Batist, M., Klerkx, J., Van Rensbergen, P., Vanneste, M., Poort, J., Golmshtok, A., et al., 2002. Active hydrate destabilization in Lake Baikal, Siberia? Terra. Nova 14, 436–442.

Delvaux, D., Moeys, R., Stapel, G., Melnikov, A., Ermikov, V., 1995. Palaeostress reconstructions and geodynamics of the Baikal region, Central Asia, Part I. Palaeozoic and Mesozoic pre-rift evolution. Tectonophysics 252, 61–101.

Delvaux, D., Moeys, R., Stapel, G., Petit, C., Levi, K., Miroshnichenko, A., et al., 1997. Paleostress reconstructions and geodynamics of the Baikal region, Central Asia, Part 2. Cenozoic rifting. Tectonophysics 282, 1–38.

Delvaux, D., Fronhoffs, A., Hus, R., Poort, J., 2000. Normal fault splays, relay ramps and transfer zones in the central part of the Baikal Rift Basin: insight from digital topography and bathymetry. Bull. Centr. Rech. Expl. 22, 341–358.

Demory, F., Nowaczyk, N.R., Witt, A., Oberhänsli, H., 2005. High-resolution magnetostratigraphy of late quaternary sediments from Lake Baikal, Siberia: timing of intracontinental paleoclimatic responses. Glob. Planet. Change 46, 167–186.

Déverchère, J., Houdry, F., Diament, M., Solonenko, N.V., Solonenko, A.V., 1991. Evidence for a seismogenic upper mantle and lower crust in the Baikal Rift. Geophys. Res. Lett. 18, 1099–1102.

Déverchère, J., Petit, C., Gileva, N., Radziminovitch, N., Melnikova, V., San'kov, V., 2001. Depth distribution of earthquakes in the Baikal rift system and its implications for the rheology of the lithosphere. Geophys. J. Int. 146, 714–730.

Diament, M., Kogan, M.G., 1990. Long-wavelength gravity-anomalies and the deep thermal structure of the Baikal Rift. Geophys. Res. Lett. 17, 1977–1980.

England, P., Molnar, P., 1997. The field of crustal velocity in Asia calculated from Quaternary rates of slip on faults. Geophys. J. Int. 130, 551–582.

Gao, S., Davis, P.M., Liu, H., Slack, P.D., Zorin, Y.A., Logatchev, N.A., et al., 1994. Asymmetric upwarp of the asthenosphere beneath the Baikal rift zone, Siberia. J. Geophys. Res. 99, 15319–15330.

Golmshtok, A.Y., Duchkov, A.D., Hutchinson, D.R., Khanukaev, S.B., Elnikov, A.I., 1997. Estimation of heat flow on Baikal from seismic data on the lower boundary of the gas hydrate layer. Russ. Geol. Geophys. 38, 1714–1727.

Golmshtok, A.Y., Duchkov, A.D., Hutchinson, D.R., Khanukaev, S.B., 2000. Heat flow and gas hydrates of the Baikal Rift Zone. Int. J. Earth Sci. (Geol. Rundsch.) 89, 193–211.

Grachev, M.A., Vorobyova, S.S., Likhoshway, Y.V., Goldberg, E.L., Ziborova, G.A., Levina, O.V., et al., 1998. A high-resolution diatom record of the palaeoclimates of East Siberia for the last 2.5 My from Lake Baikal. Quat. Sci. Rev. 17, 1101–1106.

Granin, N.G., Granina, L.Z., 2002. Gas hydrates and gas venting in Lake Baikal. Russ. Geol. Geophys. 43, 589–597.

Hus, R., De Batist, M., Klerkx, J., Matton, C., 2006. Fault linkage in continental rifts: structure and evolution of a large relay ramp in Zavarotny; Lake Baikal (Russia). J. Struct. Geol. 28, 1338–1351.

Hutchinson, D.R., Golmshtok, A.J., Zonenshain, L.P., Moore, T.C., Scholz, C.A., Klitgord, K.D., 1992. Depositional and tectonic framework of the rift basins of Lake Baikal from multichannel seismic data. Geology 20, 589–592.

INTAS Project 99–1669 Team, 2002. A New Bathymetric Map of Lake Baikal. Open-File Report on CD-ROM.

Kiselev, A.I., Popov, A.M., 1992. Asthenospheric diapir beneath the Baikal Rift – Petrological constraints. Tectonophysics 208, 287–295.

Klerkx, J., Zemskaya, T.I., Matveeva, T.V., Khlystov, O.M., Namsaraev, B.B., Dagurova, O.P., et al., 2003. Methane hydrates in deep bottom sediments of Lake Baikal. Dokl. Earth Sci. 393A, 1342–1346.

Krylov, S.V., Mandelbaum, M.M., Mishen'kin, B.P., Mishen'kina, Z.P., Petric, G.V., Seleznev, V.C., 1981. The Interior of Baikal from Seismic Data. Nauka, Novosibirsk, 105 pp. (in Russian).

Kuzmin, M.I., Kalmychkov, G.V., Geletij, V.F., Gnilusha, V.A., Goreglyad, A.V., Khakhaev, B.N., et al., 1998. First find of gas hydrates in sediments of Lake Baikal (in Russian). Dokl. Akad. Nauk. 362, 541–543.

Kuzmin, M.I., Geletiy, V.F., Kalmychkov, G., Kuznetsov, F.A., Larionov, E.G., Manakov, A.Y., et al., 2000. The first discovery of the gas hydrates in the sediments of the Lake Baikal. In: Holder, G.D., Bishnoi, P.R. (Eds.), Gas Hydrates – Challenges for the Future. Annals of the New York Academy of Sciences, New York, pp. 112–115.

Lesne, O., Calais, E., Déverchère, J., 1998. Finite element modelling of crustal deformation in the Baikal rift zone: New insights into the active-passive debate. Tectonophysics 289, 327–340.

Lipman, P.W., Logatchev, N.A., Zorin, Y.A., Chapin, E., Kovalenko, V., Morgan, P., 1989. Intracontinental rift comparisons: Baikal and Rio Grande Rift systems. Eos Trans. AGU 70, 578–579 586–587.

Logatchev, N.A., 1993. History and geodynamics of the Lake Baikal Rift in the context of the Eastern Rift System: a review. Bull. Centr. Rech. Expl. 17, 353–370.

Logatchev, N.A., Florensov, N.A., 1978. Baikal system of rift valleys. Tectonophysics 45, 1–13.

Logatchev, N.A., Zorin, Y.A., Rogozhina, V.A., 1983. Baikal Rift – active or passive – comparison of the Baikal and Kenya Rift zones. Tectonophysics 94, 223–240.

Lysak, S.V., 1992. Heat-flow variations in continental rifts. Tectonophysics 208, 309–323.

Mats, V., 1993. The structure and development of Baikal rift depression. Earth Sci. Rev. 34, 81–118.

Mats, V.D., Khlystov, O.M., De Batist, M., Ceramicola, S., Lomonosova, T.K., Klimansky, A., 2000. Evolution of the Academician Ridge Accommodation Zone in the central part of the Baikal Rift, from high-resolution reflection seismic profiling and geological field investigations. Int. J. Earth Sci. (Geol. Rundsch.) 89, 229–250.

Matveeva, T.V., Mazurenko, L.L., Soloviev, V.A., Klerkx, J., Kaulio, V.V., Prasolov, E.M., 2003. Gas hydrate accumulation in the subsurface sediments of Lake Baikal (Eastern Siberia). Geo. Mar. Lett. 23, 289–299.

Molnar, P., Tapponnier, P., 1975. Cenozoic tectonics of Asia – effects of a continental collision. Science 189 (4201), 419–426.

Nelson, C.H., Karabanov, E.B., Colman, S.M., Escutia, C., 1999. Tectonic and sediment supply control of deep rift lake turbidite systems: Lake Baikal, Russia. Geology 27, 163–166.

Oberhänsli, H., Mackay, A.W., 2005. Introduction to "Progress towards reconstructing past climate in Central Eurasia, with special emphasis on Lake Baikal." Glob. Planet. Change 46, 1–7.

Petit, C., Burov, E.B., Déverchère, J., 1997. On the structure and mechanical behavior of the extending lithosphere in the Baikal rift from gravity modelling. Earth Planet. Sci. Lett. 149, 29–42.

Petit, C., Koulakov, I., Déverchère, J., 1998. Velocity structure around the Baikal rift zone from teleseismic and local earthquake traveltimes and geodynamic implications. Tectonophysics 296, 125–144.

Poort, J., Klerkx, J., 2004. Absence of a regional surface thermal high in the Baikal Rift; New insights from detailed contouring of heat flow anomalies. Tectonophysics 383, 217–241.

Poort, J., van der Beek, P., ter Voorde, M., 1998. An integrated modelling study of the central and northern Baikal rift: Evidence for non-uniform lithospheric thinning. Tectonophysics 291, 101–122.

Prokopenko, A.A., Karabanov, E.B., Williams, D.F., Kuzmin, M.I., Khursevich, G.K., Gvozdkov, A.A., 2001a. The link between tectonic and paleoclimatic events at 2.8–2.5 Ma BP in the Lake Baikal region. Quat. Int. 80–81, 37–46.

Prokopenko, A.A., Williams, D.F., Karabanov, E.B., Khursevich, G.K., 2001b. Continental response to Heinrich events and Bond cycles in sedimentary record of Lake Baikal, Siberia. Glob. Planet. Change 28, 217–226.

Puzyrev, N.N., MandelBaum, M.M., Krylov, S.V., Mishenkin, B.P., Krupskaya, G.V., Petrick, G.V., 1973. Deep seismic investigations in Baikal rift zone. Tectonophysics 20, 85–95.

Rasskazov, S.V., 1994. Magmatism related to the eastern Siberia rift system and the geodynamis. Bull. Centr. Rech. Expl. 18, 437–452.

Ruppel, C., Kogan, M.G., McNutt, M.K., 1993. Implications of new gravity data for the Baikal rift zone structure. Geophys. Res. Lett. 20, 1635–1638.

San'kov, V., Déverchère, J., Gaudemer, Y., Houdry, F., Filippov, A., 2000. Geometry and rate of faulting in the north Baikal rift, Siberia. Tectonics 19, 707–722.

Scholz, C.A., Hutchinson, D.H., 2000. Stratigraphic and structural evolution of the Selenga Delta accommodation zone, Lake Baikal rift, Siberia. Int. J. Earth Sci. (Geol. Rundsch.) 89, 212–228.

Sherman, S.I., Dem'yanovich, V.M., Lysak, S.V., 2004. Active faults, seismicity and recent fracturing in the lithosphere of the Baikal rift system. Tectonophysics 380, 261–272.

ten Brink, U.S., Taylor, M.H., 2002. Crustal structure of central Lake Baikal: Insights into intracontinental rifting. J. Geophys. Res. 107 doi:10.1029/2001JB000300.

Tiberi, C., Diament, M., Déverchère, J., Petit-Mariani, C., Mikhailov, V., Tikhotsky, S., et al., 2003. Deep structure of the Baikal rift zone revealed by joint inversion of gravity and seismology. J. Geophys. Res. 108 doi:10.1029/2003JB002512.

Vanneste, M., De Batist, M., Versteeg, W., Golmshtok, A., Kremlev, A., 2001. Multi-frequency seismic study of the gas hydrate-bearing sediments in Lake Baikal, Siberia. Mar. Geology 171, 1–21.

Van Rensbergen, P., De Batist, M., Klerkx, J., Hus, R., Poort, J., Vanneste, M., et al., 2002. Sublacustrine mud volcanoes and methane seeps caused by dissociation of gas hydrates in Lake Baikal. Geology 30, 631–634.

Zonenshain, L.P., Savostin, L.A., 1981. Geodynamics of the Baikal rift zone and plate tectonics of Asia. Tectonophysics 76, 1–45.

Zonenshain, L.P., Golmshtok, A.Y., Hutchinson, D., 1992. Baikal rift structure. Geotectonics 26, 396–407.

Zorin, Y.A., 1981. The Baikal Rift – an example of the intrusion of asthenospheric material into the lithosphere as the cause of disruption of lithospheric plates. Tectonophysics 73, 91–104.

Zorin, Y.A., Kozhevnikov, V.M., Novoselova, M.R., Turutanov, E.K., 1989. Thickness of the lithosphere beneath the Baikal rift zone and adjacent regions. Tectonophysics 168, 327–337.

In this chapter

12

Geology of the shelves surrounding the New Siberian Islands from seismic images: Laptev Sea and East Siberian Sea, Russian Arctic

Dieter Franke, Karl Hinz
Bundesanstalt für Geowissenschaften und Rohstoffe (BGR), Hannover, Germany

12.1 Introduction

The vast and semi-permanent ice covered shelves around the New Siberian Islands are a unique region for studying the spatial and temporal variation and mechanics of lithospheric extension. The active spreading centre in the Arctic Ocean, the Gakkel Ridge, that also represents the plate boundary between the North America and Eurasia Plates, meets the adjacent continental margin of the Laptev Sea abruptly at a curvilinear slope. Total spreading rates along the Gakkel Ridge range from 12.7 near Greenland to 6 mm/a in the Eurasia Basin. On the adjacent Siberian continental shelf spreading is accommodated by continental rifting, resulting in the formation of a huge rift system, the Laptev Sea Rift (Fig. 12.1). In this chapter, we focus on the major sedimentary basins on the shelves of the Laptev and the western East Siberian Sea. We present several examples of seismic sections to illustrate the style of the basins and to make the interpretation comprehensible.

12.2 Data basis

The Bundesanstalt für Geowissenschaften und Rohstoffe (BGR, Germany), in co-operation with Sevmorneftegeofizika (SMNG, Russia), carried out three seismic cruises on the shelves around the New Siberian Islands. In 1993, a grid of multichannel seismic reflection lines (total 3189 km) was surveyed on the outer shelves of the Laptev and New Siberian Seas north of the New Siberian Islands (Roeser et al., 1995). In 1994, seismic reconnaissance data (total 3965 km) have been

Phanerozoic Rift Systems and Sedimentary Basins DOI:10.1016/B978-0-444-56356-9.00011-0

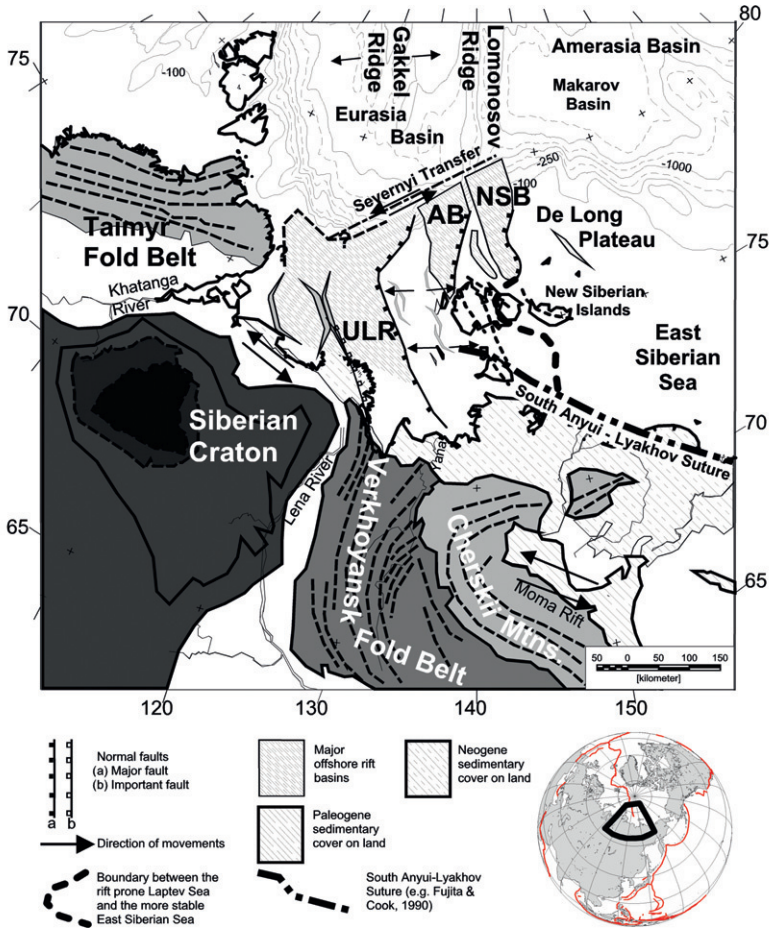

Figure 12.1 Main structural elements in the study area in polar-stereographic projection. URL denotes the Ust' Lena Rift, AB the Anisin Basin, NSB the New Siberian Basin. The onshore structures were adopted from the geological map (Nalivkin, 1983).

acquired primarily in the western Siberian Sea south of latitude 76°N (Franke et al., 2004), and in 1997 about 4623 km of MCS data were collected in the eastern Laptev Sea (Franke et al., 2001) with some additional lines across the East Siberian Sea and the western Laptev Sea. A detailed description of the seismic field parameters and processing of the three surveys is given in Franke et al. (2001, 2004).

12.3 Tectonic setting and structure of the shelves

The vast shelves of the Laptev and East Siberian Seas between the Taimyr Peninsula in the west, the New Siberian Islands in the centre and Wrangel Island to the east are among the least explored regions of the world. The shelves are bordered

on the North by the Arctic Ocean Basin and are surrounded by Phanerozoic fold belts: the Chukchi fold belt, which includes the mainland, Wrangel Island, and associated Chukchi Sea shelf, the New Siberian fold belt, which includes the New Siberian Islands and surrounding Laptev Sea–East Siberian Sea continental shelves, and the Taimyr, Verkhoyansk and Cherski fold belts (e.g., Drachev et al., 1998; Fujita and Newberry, 1982; Fujita et al., 1997; Khain, 1994; Parfenov, 1991; Zonenshain et al., 1990; Fig. 12.1).

The fold belts underwent intensive pervasive deformation and were intruded by granitic plutons during the Middle Jurassic and Lower Cretaceous. Following this regional deformation, the formation of large extensional basins named Blagoveshenk, New Siberian and North Chukchi/Vil'kitskii (e.g., Grantz et al., 1990; Kos'ko, 1984) has been postulated, which are believed to be filled primarily with Paleozoic to Mesozoic – and possibly some Cenozoic – sediments.

Knowledge of kinematics and the history of the pre-Tertiary opening of the Arctic Ocean Basin is still insufficient, despite the numerous models for the origin of the Amerasia Basin. Lawver and Scotese (1990) discuss a variety of proposed models for the origin of the Amerasia Basin. The Canada Basin evolved likely throughout the Late Jurassic/Early Cretaceous. A popular model involves the opening of the Amerasia Basin by in-situ seafloor spreading and counterclockwise rotation of the Arctic Alaska and Chukotka away from Arctic Canada about a pivot point situated in northern Yukon (Carey, 1955, and several authors in the following). Lane (1997) rejected the rotation model and introduced a multistage kinematic model with varying extinct spreading axes in the Amerasia Basin while Embry (2000) presented a modified rotation model with three main segments of spreading separated by transform faults. Lawver et al. (2002) reintroduced the "rotation hypothesis".

The Cenozoic development of the Arctic Ocean Basin is better constrained: There is general consensus that the opening of the Eurasia Basin initiated with the splitting of the North America–Eurasia lithospheric plates during the Late Cretaceous, and that at the time of magnetic anomaly #24/25 (52.4–55.9 Ma, according to Cande and Kent, 1995) the Eurasia Basin opened along the Gakkel Ridge (e.g., Jackson and Gunnarsson, 1990; Kristoffersen, 1990; Rowley and Lottes, 1988; Srivastava and Tapscott, 1986). It is assumed that the creation of rift basins on the Laptev Sea Shelf began at the same time (e.g., Franke et al., 2000, 2001; Fujita and Cook, 1990; Grachev, 1983).

From extrapolation of onshore geology, the shelves of the Laptev Sea and East Siberian Sea are subdivided into the following four domains (e.g., Fujita and Cook, 1990; Kos'ko and Trufanov, 2002; cf. Fig. 12.2) from east to west:

De Long Domain encompasses Bennett, Henrietta, Jeanette, Zhokov and Vil'kitkii Islands (Fig. 12.2). Moderately tilted Cambrian to Ordovician siliclastic rocks crop

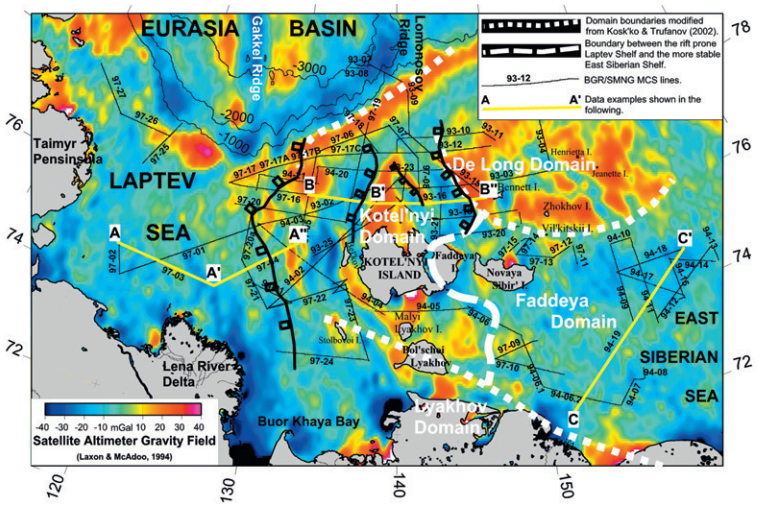

Figure 12.2 Altimeter derived gravity field (Laxon and McAdoo, 1994) and location of the reflection seismic lines acquired by BGR in co-operation with SMNG. The extensions of the different domains in the area were modified from Kos'ko and Trufanov (2002). The locations of the interpreted seismic line-drawings shown in Figs. 12.3 and 12.7 are highlighted in yellow.

out on Bennett Islands, and Paleozoic igneous rocks, volcaniclastics and siliclastic deposits are reported from Henrietta Island (Vinogradov, 1984). Paleozoic basic lavas, volcaniclastics and siliclastics have been reported from Henrietta Island; Neogene volcanism is reported to have affected the area of the De Long Islands from at least the Middle Miocene through Recent (e.g., Kos'ko and Trufanov, 2002).

Faddeya Domain, also called Novaya Sibir'Terrane by Fujita and Cook (1990), comprises the islands of Novaya Sibir' and Faddeya, and probably underlies a large portion of the East Siberian Shelf (Fujita and Cook, 1990). It is characterized by extensive Paleogene coal-bearing terrigenous formations, and it is separated from the Kotel'nyi Domain by a fault zone located between Kotel'nyi and Faddeya Islands. The oldest exposed rocks forming the Novosibirsk complex of the Late Cretaceous to Eocene age are extensively deformed into folds. The Faddeya Domain is thought to represent a region of early Paleogene subsidence which underwent deformation in Late Oligocene time (Fujita and Cook, 1990).

Lyakhov Domain comprises the Lyakhov Islands and Stolbovoi Island, including the South Anyui–Lyakhov Suture. It is characterized by thrusted sequences of Late Paleozoic/Mesozoic ophiolites, Permian to Triassic clastic turbidites, Upper Jurassic to Lower Createous basaltic rocks and intruded granites and granodiorites (Drachev and Savostin, 1993; Drachev et al., 1998; Fujita and Cook, 1990; Fujita and Newberry, 1982).

Kotel'nyi Domain comprises Kotel'nyi and the small Bel'kov Islands. It is characterized by a nearly continuous succession of thick Paleozoic carbonates and

pelitic to sandy deposits of Mesozoic to Cenozoic age. The Paleozoic and Mesozoic deposits are folded in northwest-striking anticlines and synclines (Vol'nov et al., 1970). Truncation, peneplanation and weathering at the transition from Mesozoic to Tertiary deposits are widespread.

12.4 Seismic stratigraphy of the acoustic basement and the superimposed sedimentary successions

Since no deep wells have been drilled so far on the shelves surrounding the New Siberian Islands, the proposed age and nature of the defined major seismic horizons are uncertain. We have tried to correlate these horizons throughout the survey area, assuming that these main reflectors are present in all basins within the Laptev and East Siberian Seas. However, this might not be the case, if the individual basins underwent different developments.

Laptev Sea Shelf

By extrapolation from known major unconformities and hiatuses on the New Siberian Islands (Kos'ko and Trufanov, 2002; Kos'ko et al., 1990), from the onshore area of Buor Khaya Bay (Drachev et al., 1998) and correlating regional seismic unconformities to major plate tectonic events, as well as to major paleoenvironmental changes observed in the northern oceans, three regional seismic marker horizons labeled LS1 (Laptev Sea 1), LS2 and LS3 have been defined, albeit some more but less distinct and less correlatable seismic horizons are present.

Horizon LS1 is the most prominent and extensive horizon. It is a distinct erosional unconformity that appears as a peneplain on several structural highs, and it forms the base of the sedimentary infill of the rift basins. Its depth ranges from more than 13 km (Franke et al., 2001) in the deepest rifts to less than 1 km in the most elevated basement area. We suggest that it developed prior to the major Cenozoic stretching episode following regional uplift and subsequent strong erosion and weathering during Late Cretaceous (?) and early Paleocene time in the Laptev Sea area (Kim, 1986; Patyk-Kara and Laukhin, 1986). We assign an age between 65 and 56 Ma to horizon LS1, because this interval represents several important tectonic episodes in the Arctic. Among these are initiation of seafloor spreading in the Eurasia Basin (Jackson and Gunnarsson, 1990; Kristoffersen, 1990), separation of Greenland from Eurasia during chron 24R (e.g., Eldholm et al., 1989) and the final separation of Greenland from North America in the Paleocene (Chalmers et al., 1993).

Unconformity LS2 is a distinct unconformity within the rift basins and is absent on the most elevated horsts. It marks the top of a high-reflective sequence. An Early Oligocene age (about 33 Ma) was assigned to horizon LS2, because of the documentation of an erosional event in the beginning of the Oligocene at several localities on the New Siberian Islands (Kos'ko and Trufanov, 2002), and a major global sea-level fall near the Rupelian/Chattian boundary (Haq et al., 1988).

Unconformity LS3 is manifested in the seismic data by a distinct change in the reflection pattern, from pronounced sub-parallel bedding to a less reflective sequence. LS3 probably represents a significant change in the depositional regime during the Neogene. We assign a Late Miocene age (between 5 and 10 Ma) to horizon LS3, because of a revival of tectonic activity in the Verkhoyansk-Chukchi region about the end of the Miocene (e.g., Khain, 1994), the initiation of large-scale Northern Hemisphere glaciations (e.g., Mangerud et al., 1996; Myhre and Thiede, 1995) and Late Miocene and Pliocene tectonic deformation associated with the Indo-Asian collision.

East Siberian Sea Shelf

The seismic reconnaissance lines show a well-layered succession representing sediments and resting on a smooth acoustic basement mostly lacking a coherent internal reflection pattern.

Horizon ESS1 (East Siberian Sea 1), manifested as the base of the layered succession in the seismic data, forms the surface of the acoustic basement and most probably represents the peneplained surface of the complex Paleozoic-Mesozoic New Siberian-Chukchi fold belt.

It must be stated that the stratigraphy of the East Siberian Shelf is even less well constrained with respect to the Laptev Sea because a well-dated event such as the initial opening of the Eurasia Basin is missing in that region. Albeit the entire sedimentary succession, or parts of it, may be of Cretaceous age, we tentatively infer a Late Cretaceous age for horizon ESS1, because subsequent to the halt of granitoid plutonism in the Verkhoyansk-Chukotka folded system in the Late Cretaceous (Drachev et al., 1998; Parfenov, 1991) followed a period of levelling evidenced by the formation of extensive surfaces of planation, as well as weathering horizons and thin coal-bearing limnic sediments.

The layered succession is subdivided by at least two distinct regional seismic marker horizons, labelled *ESS2* and *ESS3*, which show reflection characteristics similar to the seismic marker horizons *LS2* and *LS3* from the Laptev Shelf, as discussed before. Therefore, we tentatively propose the same ages to ESS2 and ESS3, that is, Early Oligocene and Late Miocene, respectively.

12.5 Major rift basins of the Laptev Shelf

Some line drawing interpretations of MCS profiles from the Laptev Shelf have been prepared for the following discussion of the major rift features. Lines BGR97-03 and BGR97-04 (Fig. 12.3, lower panel, and Fig. 12.4) traverse the Ust'Lena Rift and the North Laptev Horst in a west–northwest–east-southeast and southwest-northeast direction, respectively. Lines BGR97-16 and BGR93-16 (Fig. 12.3, upper panel, and Fig. 12.5) run across the Anisin Basin, the Kotel'nyi Horst, the Neben Basin and the New Siberian Basin in a west-east direction. The Bel'khov Svyatoi Nos Rift (e.g., Drachev et al., 1998) belongs to the category of smaller basins that developed in the region of the Laptev Horst. Figure 12.6 shows the total thickness of the primarily Cenozoic sedimentary cover in milliseconds (twt).

Ust'Lena Rift

The Ust'Lena Rift, with a minimum width of 380 km, covers the main part of the Laptev Shelf. Its western flank is not covered by our data set. Line BGR97-03 (Fig. 12.3, lower panel) starts in the area of the defined South Laptev Basin (e.g., Drachev et al., 1995) and runs with a general 98° orientation across the Ust'Lena Rift. Horizon LS1, interpreted to represent the rift-onset unconformity, forms the base of the sedimentary infill with thicknesses in the range between 4 and 5.5 s (twt). The major portion of the sedimentary infill is found between horizons LS1 and LS2, suggesting that the development of the Ust'Lena Rift was nearly completed prior to the forming of unconformity LS3.

Line BGR97-04 continues Line BGR97-03 to the east in a north 47° east direction (Fig. 12.3, lower panel). The sedimentary basin fill above horizon LS1 thins continuously from 5 (twt) in the eastern part of the basin to 2.5 s (twt) at the MV Lazarev Fault. This distinct westerly dipping listric fault bounds the Ust'Lena Rift in the east against the Laptev Horst. The MV Lazarev Fault penetrates the whole upper crust and flattens down at the top of a reflective lower crustal unit at a level of approximately 7–8 s (twt).

A high reflective crustal unit between 7 and 9 s (twt) extends westward from the MV Lazarev Fault for some 100 km toward the rift centre. Several listric faults penetrate most of the upper crust down to the band of sub-horizontal reflections. This zone of high crustal reflectivity thins to the west and merges finally with the interpreted crust-mantle boundary (MOHO). Beyond and west of this point (Line BGR97-03) the middle and lower crust shows no coherent reflection elements. We interpret the high-reflective band as the detachment plane of the MV Lazarev Fault (cf. Figs. 12.3 and 12.4). A band of high reflectivity at crustal levels between 8 and 9 s (twt), locally present along lines BGR97-03 and -04, is thought to image the crust-mantle transition.

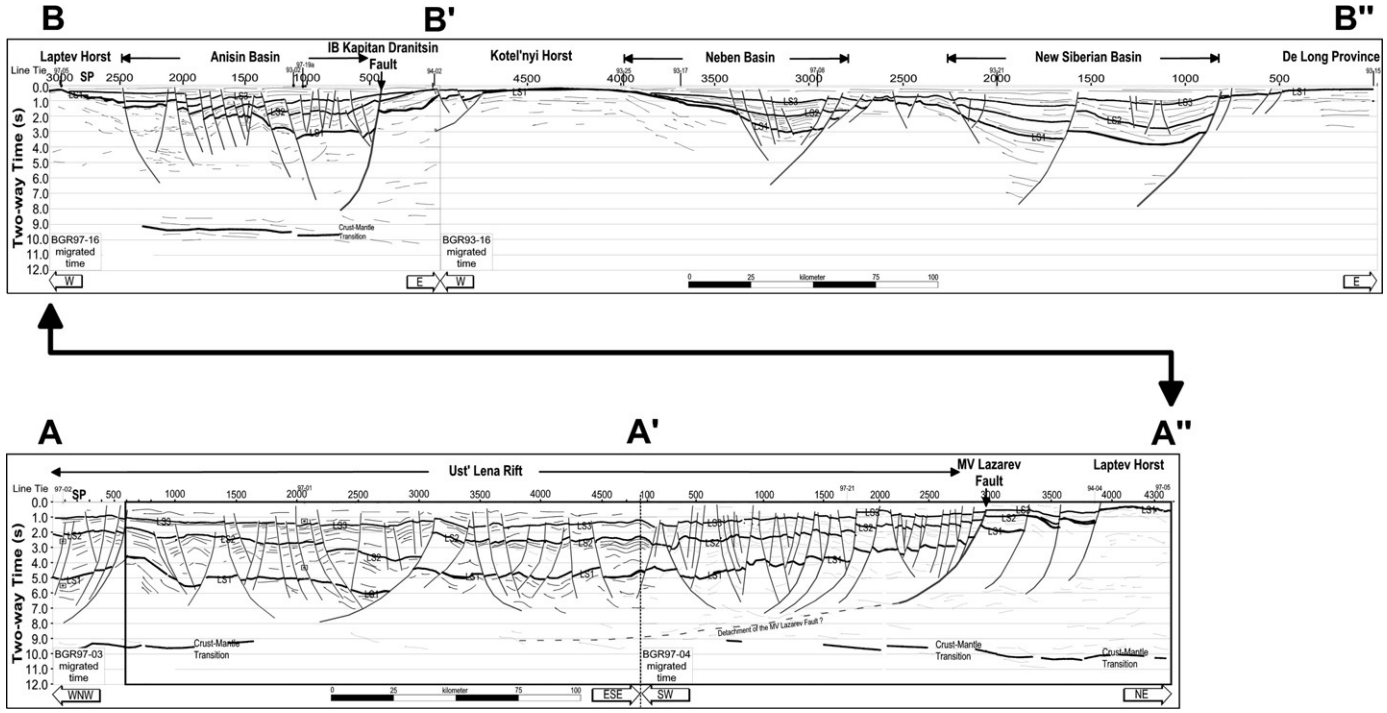

Figure 12.3 Line drawing interpretation of MCS lines BGR97-03/-04 (lower panel) across the Ust'Lena Rift and eastern part of BGR97-16 and BGR93-16 (upper panel) across the Anisin, the Neben, and the New Siberian Basins. LS1, LS2 and LS3 denote the individual marker horizons (see text). For location refer to Figs. 12.2 and 12.6.

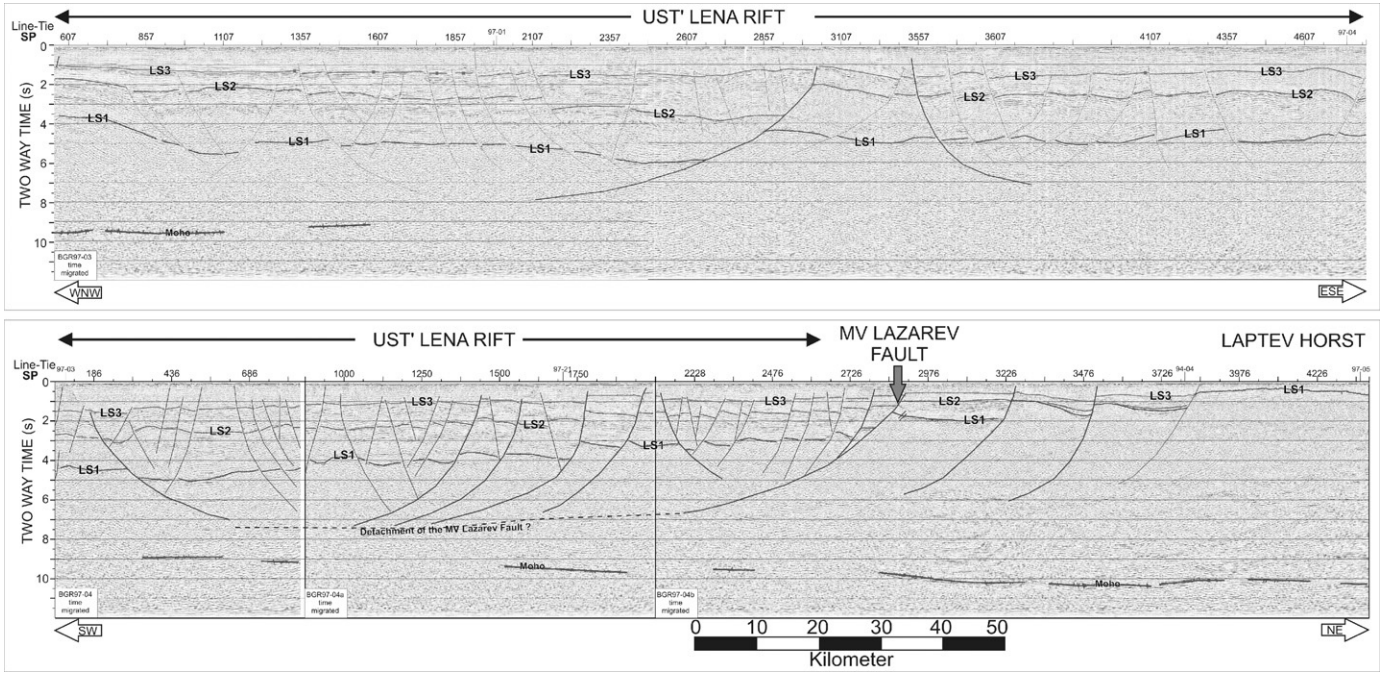

Figure 12.4 Time migrated sections of the eastern part of line BGR97-03 (top) and the lines BGR97-04, -04a, -04b (bottom) across the eastern Ust'Lena Rift onto the Laptev Horst. LS1, LS2 and LS3 denote the individual marker horizons (see text). For location refer to Figs. 12.2 and 12.3.

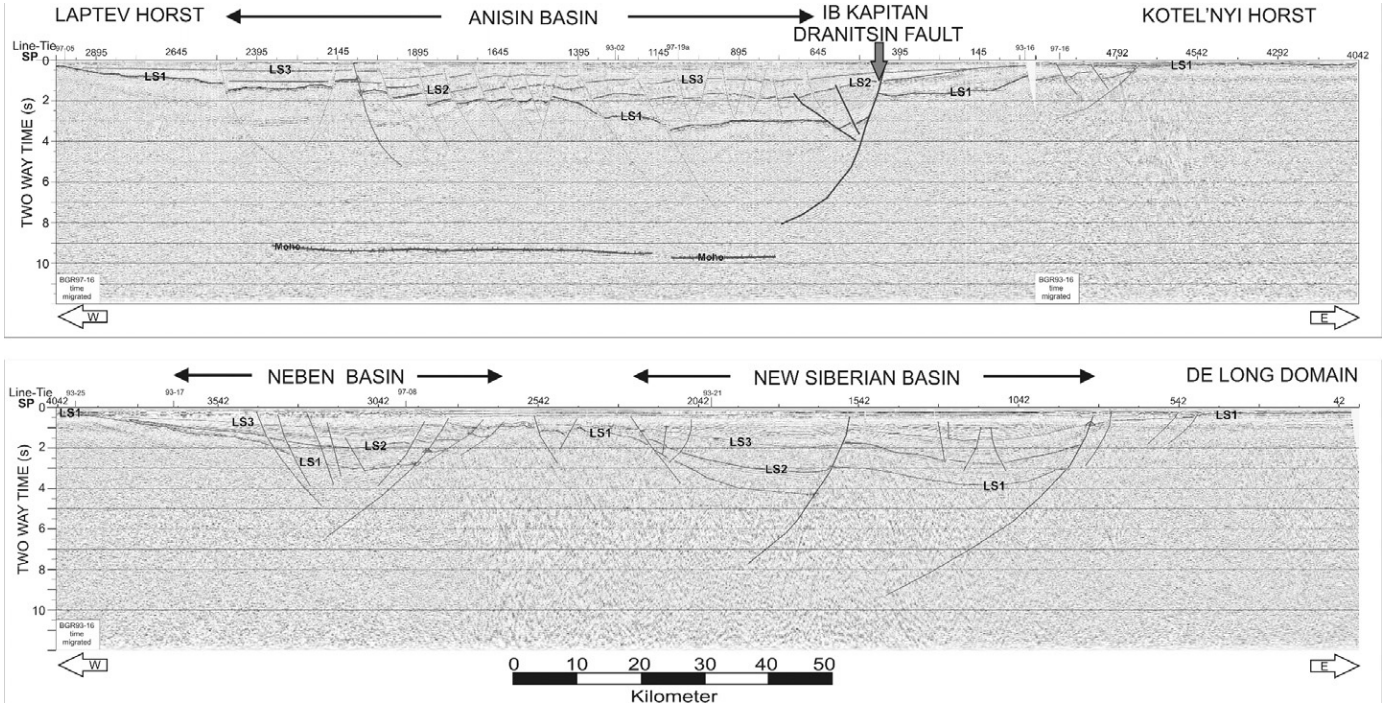

Figure 12.5 Time migrated sections of the eastern part of line BGR97-16 (top) and line BGR93-16 (bottom) across the Laptev Horst, the southern part of the Anisin Basin, the Kotel'nyi Horst, the Neben Basin, the New Siberian Basin, and the De Long Domain. LS1, LS2 and LS3 denote the individual marker horizons (see text). For location refer to Figs. 12.2 and 12.3.

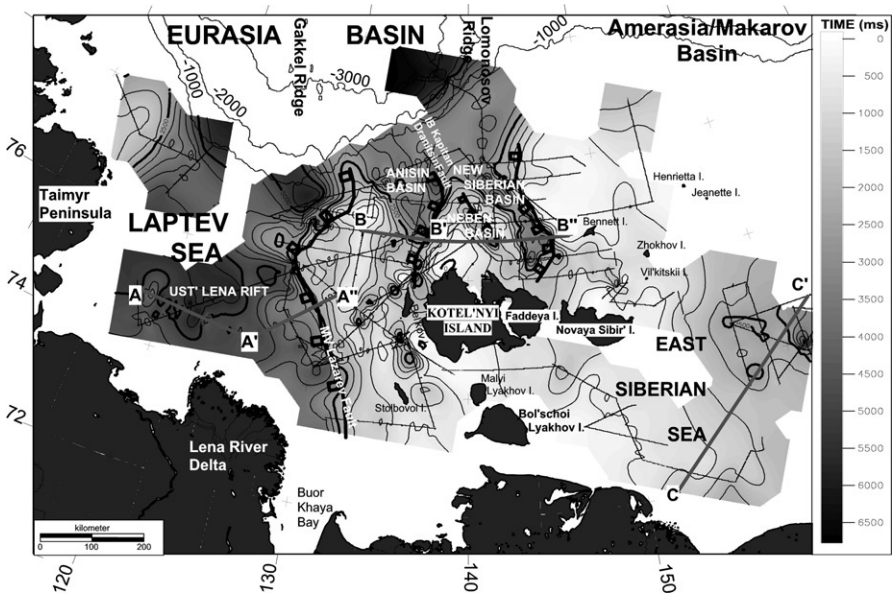

Figure 12.6 Sedimentary thickness map of the Laptev Rift system. Shown is the gridded depth to the acoustic basement (marker horizon LS1/ESS1) in milliseconds (twt). The main faults mentioned in the text are shown. The locations of the line-drawing interpretations shown in Figs. 12.3 and 12.7 are indicated.

Anisin Basin

This rift basin extends along longitude 136° E from latitudes 76°N to 78°N. It is about 40 km wide at the southern end but broadens to about 150 km at latitude 78°N (Fig. 12.3, upper panel, and Fig. 12.6). The basin is imaged in the satellite altimeter gravity map as a gravity low (Fig. 12.2). The eastern part of Line BGR97-16 (Fig. 12.3, upper panel, and Fig. 12.5) traverses from the Laptev Horst in the west across the Anisin Basin. A prominent north-northeast to south-southwest trending listric fault, the IB Kapitan Dranitsin Fault, bounds the basin against the Kotel'nyi Horst in the east. The acoustic basement dips to the east within the basin (Fig. 12.3, upper panel, and Fig. 12.5), resulting in an increase of the thickness of the presumably Cenozoic basin fill from about 1.5 s (twt) at the western flank to 3.5 s (twt) at shotpoint 480 near the eastern flank; however, thickness of the basin infill increases gradually towards the north to about 5 s (twt). There is some evidence that extension affected the western half of the Anisin Basin during the Neogene, resulting in basement partitioning associated with the formation of small-offset faults which penetrate unconformity LS3.

12.6 New Siberian Basin and Neben Basin

Line BGR93-16 (Fig. 12.3, upper panel, and Fig. 12.5, lower panel) traverses from the Kotel'nyi Horst in the west across the Neben Basin and the New Siberian Basin onto the De Long Plateau in the east. Both northwest trending basins,

the Neben Basin, about 35 km wide and the 40–75 km wide New Siberian Basin, are best described as half-grabens bounded at their eastern side by a deep reaching listric fault. Depressed and faulted basement blocks form the base of the sedimentary infill subdivided by the unconformities LS2 and LS3 into three depositional units. The sedimentary basin infill of the New Siberian Basin, increasing in thickness from the southern end of the basin to the north, has a maximum thickness of more than 4.5 s (twt). Our data show unequivocally that the New Siberian Basin disappears as a conclusive rift basin when approaching Faddeya and Novaya Sibir' Islands.

12.7 Structural features of the East Siberian Shelf

The De Long Plateau, located between 75.5°N and 78.5°N, 145°E and 157°E, covers a large area of the East Siberian Shelf. It is well imaged in compilations of potential field data (Drachev et al., 1999; Laxon and McAdoo, 1994; MacNab, 1993; Piskarev et al., 2001; Verhoef et al., 1996). Basaltic effusiva overlie Paleozoic rocks. Though the age of the volcanic flow units, each 40–100 m thick (Kos'ko and Trufanov, 2002), is still debated, most authors agree that they were emplaced in Cretaceous times in a subaerial environment (e.g., Fujita and Cook, 1990; Kos'ko, 1984; Kos'ko and Trufanov, 2002; Sekretov, 2002). However, there is also evidence for Pliocene and Quaternary volcanism from K–Ar rock age determination of basalts from Zhokov and Vil'kitskii Islands (Kos'ko and Trufanov, 2002; Vinogradov et al., 1977).

Only one narrow, less than 10 km wide, graben with a maximum sedimentary infill of only 1 s (twt) was recognised in our seismic data from the De Long region, whereas termination of the seismic marker horizons against the sea floor by toplap is manifested in the seismic data at several localities, indicating uplift and associated intensive erosion of the De Long region since at least the Late Miocene.

Line BGR94-19 (Figs. 12.7 and 12.8) has been chosen to show the structural style of that part of the East Siberian Shelf that is located to the south of the De long Plateau. The line runs from the Indigirka Bay in the south with a north-northeast orientation up to latitude 75°N. The well-layered sedimentary unit superimposing the surface of the acoustic basement, labelled ESS1, thickens from about 1 s (twt) in the south to more than 4 s (twt) in the north, near the southern front of the De Long Plateau.

Along the southern half of the line the surface of the acoustic basement dips gently towards the north, but along the northern half of the line, between shotpoints 1 and 4250, several listric faults displace the surface of the acoustic basement and the older sedimentary unit resting on horizon ESS1 and bounded by unconformity ESS2. Horizon ESS3, interpreted as the base of the Late Miocene

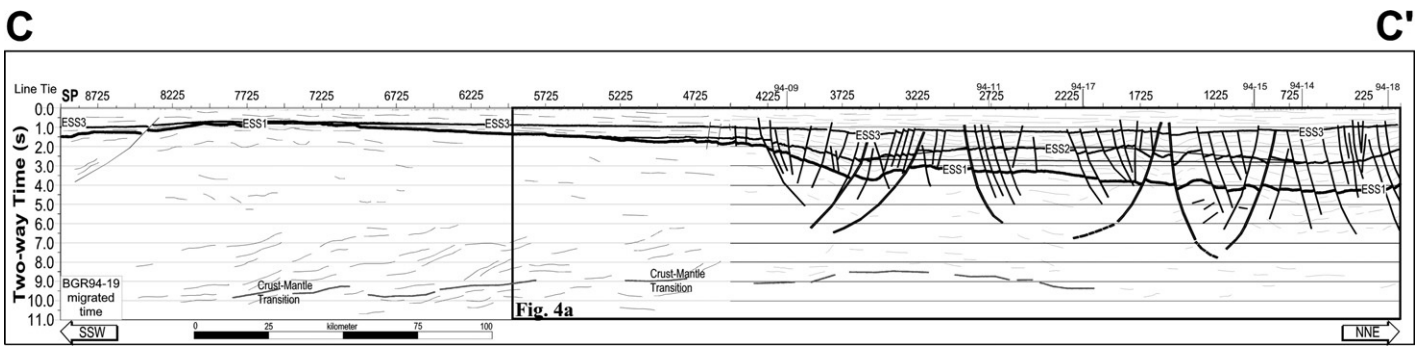

Figure 12.7 Line drawing interpretation of MCS lines BGR94-19 across the East Siberian Shelf. ESS1, ESS2 and ESS3 denote the individual marker horizons (see text). For location refer to Figs. 12.2 and 12.6.

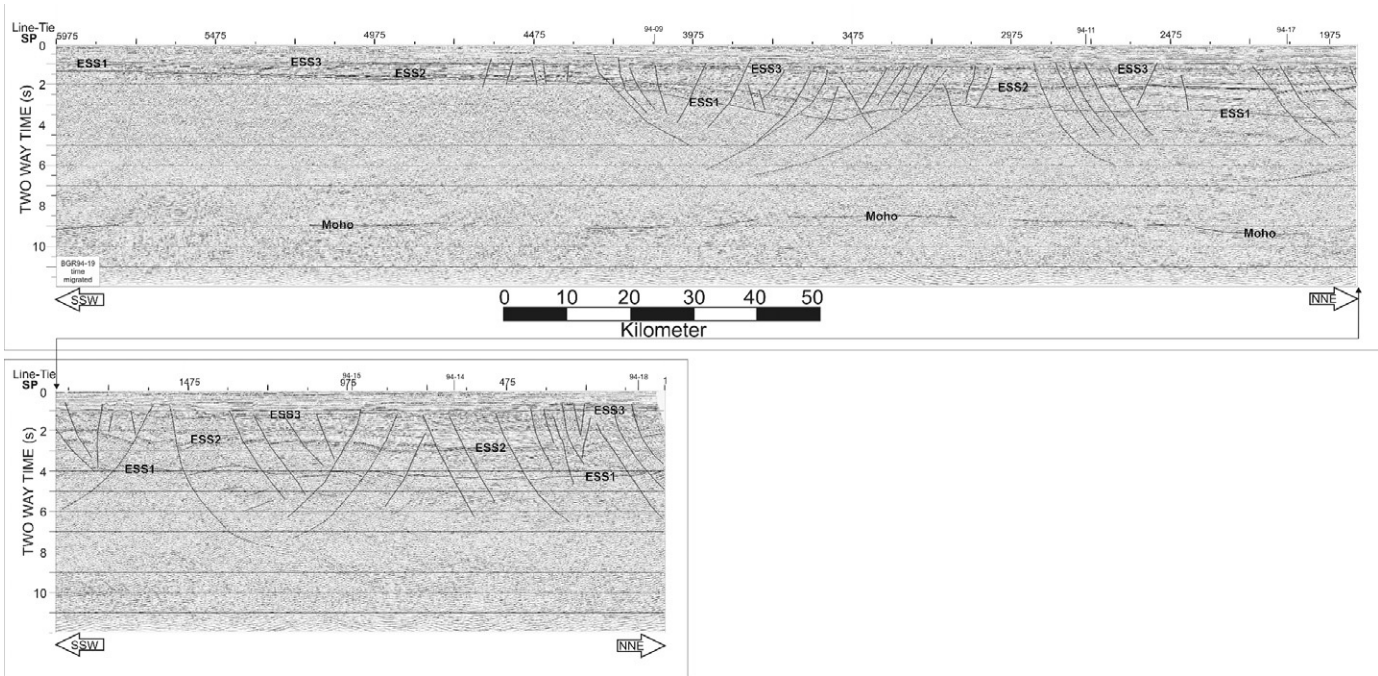

Figure 12.8 Time migrated section of the eastern part of line BGR94-19 across the East Siberian Shelf. ESS1, ESS2 and ESS3 denote the individual marker horizons (see text). For location refer to Figs. 12.2 and 12.7.

through Quaternary cover, is rarely affected by this faulting. It appears that the entire region traversed by the line is controlled mainly by subsidence. Although Franke et al. (2004) described the presence of some narrow sag basins, trending west-northwest, which developed after the formation of unconformity ESS2 but definitively prior to the formation of ESS3, they categorize the East Siberian Shelf surveyed by them as an epicontinental platform that gradually subsided and was filled up by sediments since the Late Cretaceous.

12.8 Discussion and conclusion

There is a wide variety of interpretations available for the sedimentary cover of the Laptev Shelf. The interpretations range from Proterozoic (e.g., Vinogradov, 1984; Sekretov, 2000) to Cenozoic (Drachev et al., 1998, 1999; Franke and Hinz, 2005; Franke et al., 2001).

As no deep wells have been drilled so far, the age and nature of the seismic horizons, which have been defined, remain uncertain. All interpretations are based on different evolution scenarios for the shelf areas and there are two fundamentally different concepts for the evolution of the area. The basement of the rift basins of the Laptev Shelf may have been formed either by the Siberian craton, or by the Mesozoic fold belts situated around the craton. If the Laptev Sea Shelf is underlain by the Siberian craton, there is a wide variety of possible scenarios explaining the formation of the basins at any pre-Cenozoic time. If the basins on the Laptev Shelf developed on a Mesozoic fold belt potential pre-Late Creatceous basins are unlikely preserved. In this case, the basins on the Laptev Shelf are likely to have developed in conjunction with the opening of the Eurasia Basin in the Arctic Ocean. Although most structures around the Laptev Sea Shelf are Mesozoic, Paleozoic, or even older and the transition to the proposed younger sequences is unclear, we propose for several reasons that the second scenario is more likely. The area that is affected by rifting fits well with theoretically expected values as derived from calculations of rotation poles for the splitting of Eurasia and North America during the Cenozoic. Until recent times earthquakes were spread over the entire Laptev Shelf. This indicates that the extension is likely linked to spreading in the Arctic Ocean, that is, movements along the Eurasia/North American plate boundary. The style and architecture of the rift basins are in accordance with the proposed Atlantic-type rifting. Modelling and plate reconstructions based on marine magnetic and gravity data confirm a period of compression in the Late Cretaceous (14 mm/yr in the Laptev Sea) that was followed by extension from 68 to 40 Ma (Gaina et al., 2002). Adding the width of all the major rift basins of the Laptev Shelf in the east-west direction, we get a value of about 580 km extension since the Paleocene. This value is close to the Gaina et al. (2002) model, which predicts (at about 72°N and 122°E) extension and transtension in the range of 452 $\pm$ 20 km from 68.7 Ma to the Middle Eocene and extension in the range of 186 km $\pm$ 28 km until the present.

By closing the grabens on the Laptev Shelf, the New Siberian Islands are shifted some 100–300 km west and fit well into an assumed continuation of the Verkhoyansk fold belt. According to Drachev et al. (1989), the western Anjou unit (mainly Stolbovoi Island) is part of the Late Paleozoic passive margin of the Siberian craton. If this is right, the northern boundary of the craton must be onshore, south of the Laptev Sea. Our major argument, however, is the style of the sedimentary units in the rift grabens. If the major part of the sedimentary cover were of Mesozoic or even Paleozoic age, the Cenozoic cover would be represented by the uppermost sedimentary succession (i.e., around and above LS3). However, this part of the cover is widely undisturbed by faulting, at least in the Ust'Lena Rift. It seems unlikely that a major rift phase resulting in seafloor spreading in the Arctic Ocean leaves a preexisting zone of weakness (an older basin) undisturbed that is located only some 100–200 km to the south.

We thus suggest that the described rift basins of the Laptev Shelf were primarily formed in interaction with the opening of the Eurasia Basin. This view is only partly shared by Drachev et al. (1998), who relate the opening of the New Siberian Basin with the opening of the Makarov Basin, a sub-basin of the Amerasia Basin, in Late Cretaceous (80–53 Ma). There is convincing evidence from geophysical data that the rift basins of the Laptev Shelf terminate to the north against a major northeast to southwest trending tectonic boundary defined by Fujita et al. (1990) as the Severnyi Transfer, also named the Northern Fracture by Drachev et al. (1998, 1999). Such lineament may explain the link between the opening by seafloor spreading of the Eurasia Basin and extension of the Laptev Shelf. Opening of the Eurasia Basin by seafloor spreading was accommodated by preferential thinning of the continental crust on the Laptev Shelf.

From distinct differences in size and architecture between the Anisin, Neben and New Siberian Basins, which are best described as half-grabens, and the Ust'Lena Rift, we propose an additional major tectonic boundary close to the location of the MV Lazarev Fault. The fact that the north-northwest to south-southeast trending rifted basins of the Laptev Shelf coincide with the general trend of the Anyui–Lyakhov Suture (Franke et al., 2008) suggest that these basins formed along a zone of weakness that presumably was created in association with the subduction of the proto-South Anyui Ocean.

Our seismic data from the East Siberia Shelf (Franke and Hinz, 2005; Franke et al., 2004) allow the statement that large Late Lower Cretaceous–Tertiary rift basins of the tectonic style of both, the Ust'Lena Rift and the Anisin, Neben and New Siberian Basins, do not exist on the surveyed part of the East Siberia Shelf. The East Siberia Shelf can be considered a relatively stable epicontinental platform, composed of a complex suite of Paleozoic and Mesozoic rocks that subsided, and sediments were deposited gradually since Late Cretaceous time with stronger subsidence toward the north.

Acknowledgment

Funding of the seismic surveys and this work was provided by the Federal Institute for Geosciences and Natural Resources (BGR), Hannover; Germany.

References

Cande, S.C., Kent, D.V., 1995. Revised calibration of the geomagnetic polarity timescale for the late Cretaceous and Cenozoic. J. Geophys. Res. 100, 6093–6095.

Carey, S.W., 1955. The orocline concept in geotectonics. R. Soc. Tasman. Proc. 89, 255–288.

Chalmers, J.A., Pulvertaft, T.C.R., Christiansen, F.G., Larsen, H.C., Laursen, K.H., Ottesen, T.G., 1993. The southern West Greenland continental margin: rifting history, basin development, and petroleum potential. In: Parker, J.R. (Ed.), Petroleum Geology of Northwest Europe, Proc. of the 4th Conference, Geological Society Publication, London, pp. 915–931.

Drachev, S.S., Savostin, L.A., 1993. Ophiolites of the Bol'shoi Lyakhov Island (Novosibirsk Islands). Geotektonika 6, 33–51.

Drachev, S.S., Savostin, L.A., Bruni, I.E., 1995. Structural pattern and tectonic history of the Laptev Sea Region. In: Kassens, H., et al. (Eds.), Reports on Polar Research, vol. 176, pp. 348–366.

Drachev, S.S., Savostin, L.A., Groshev, V.G., Bruni, I.E., 1998. Structure and geology of the continental shelf of the Laptev Sea, Eastern Russian Arctic. Tectonophysics 298, 357–393.

Drachev, S.S., Johnson, G.L., Laxon, S.W., McAdoo, D.C., Kassens, H., 1999. Main structural elements of Eastern Russian Arctic continental margin derived from satellite gravity and multichannel seismic reflection data. In: Kassens, H., Bauch, H.A., Dmitrenko, I.A., Eicken, H., Hubberten, H.W., Melles, M., et al., Land-Ocean Systems in the Siberian Arctic. Dynamics and History, Springer, pp. 667–692.

Eldholm, O., Thiede, J., Taylor, E., et al., 1989. Proceedings of ODP, Science Results, 104; College Station, TX (Ocean Drilling Programme).

Embry, A.F., 2000. Counterclockwise rotation of the Arctic Alaska Plate: Best available model or untenable hypothesis for the opening of the Amerasia Basin. In: Roland, N.W., Tessensohn, F. (Eds.), Polarforschung, vol. 68 (1998), Alfred-Wegener-Institute for Polar and Marine Research and the German Society of Polar Research, Bremerhaven, pp. 247–274.

Embry, A.F., Dixon, J., 1994. The age of the Amerasia Basini. In: Thurston, D.K., Fujita, K. (Eds.), Proceedings of 1992 International Conference on Arctic Margins, Anchorage, Alaska, pp. 289–295.

Franke, D., Hinz, K., 2005. The structural style of sedimentary basins on the shelves of the Laptev Sea and the western East Siberian Sea, Siberian Arctic. J. Pet. Geol. 28 (3), 269–286.

Franke, D., Hinz, K., Block, M., Drachev, S.S., Neben, S., Kos'ko, M.K., et al., 2000. Tectonics of the Laptev Sea region in north-eastern Siberia. In: Roland, N.W., Tessensohn, F. (Eds.), ICAM III: III, International Conference on Arctic Margins, Polarforschung, vol. 68 (1998), Alfred-Wegener-Institute for Polar and Marine Research and the German Society of Polar Research, Bremerhaven, pp. 51–58, ISSN 0032–2490.

Franke, D., Hinz, K., Oncken, O., 2001. The Laptev Sea Rift. Mar. Petrol. Geol. 18 (10), 1083–1127.

Franke, D., Hinz, K., Reichert, C., 2004. Geology of the Shelf of the East Siberian Sea south of the De Long Uplift/Russian Arctic from seismic images. J. Geophys. Res. 109, No. B7, B07106, 10.1029/2003JB002687, 1–19.

Franke, D., Reichert, C.h.r., Damm, V., Piepjohn, K., 2008. The South Anyui suture, northeast Arctic Russia reveald by offshore seismic data. Norw. J. Geol. 188 (4), 189–200.

Fujita, K., Cook, D.B., 1990. The Arctic continental margin of eastern Siberia. In: Grantz, A., Johnson, L., Sweeney, J.F. (Eds.), The Geology of North America: The Arctic Ocean Region, vol. L. Geological Society of America, pp. 289–304.

Fujita, K., Newberry, J.T., 1982. Tectonic evolution of Northeastern Siberia and adjacent regions. Tectonophysics 89, 337–357.

Fujita, K., Cambray, F.W., Velbel, M.A., 1990. Tectonics of the Laptev Sea and Moma Rift Systems, Northeastern USSR. Mar. Geol. 93, 95–118.

Fujita, K., Stone, D.B., Layer, P.W., Parfenov, L.M., Koz'min, B.M., 1997. Cooperative programme help decipher tectonics of Northeastern Russia. EOS 78 (245), 252–253.

Gaina, C., Roest, W.R., Müller, R.D., 2002. Late Cretaceous–Cenozoic deformation of northeast Asia. Earth Planet. Sci. Lett. 197, 273–286.

Grachev, A.F., 1983. Geodynamics of the transitional zone from the Moma Rift to the Gakkel Ridge. In: Watkins, J.S., Drake, C.L. (Eds.), Studies in Continental Margin Geology, American Association of Petroleum Geologists, Memoirs 34, pp. 103–113.

Grantz, A., May, S.D., Hart, P.E., 1990. Geology of the Arctic continental margin of Alaska. In: Grantz, A., Johnson, L., Sweeney, J.F. (Eds.), The Geology of North America: The Arctic Ocean Region, vol. L. Geological Society of America, pp. 257–288.

Haq, B.U., Hardenbrol, J., Vail, P.R., 1988. Mesozoic and Cenozoic Chronostratigraphy and Cycles of sea-level change. Sea-Level Changes – An Integrated Approach. SEPM Special Publication No. 42, pp. 71–108.

Hinz, K., Eldholm, O., Block, M., Skogseid, J., 1993. Evolution of the North Atlantic volcanic margins. In: Parker, J.R. (Ed.), Petroleum Geology of Northwest Europe. Proceedings of the 4th Conference. Geol. Soc. Pub., London, pp. 901–913.

Jackson, H.R., Gunnarsson, K., 1990. Reconstructions of the Arctic: Mesozoic to Present. Tectonophysics 172, 303–322.

Khain, V.E., 1994. Geology of Northern Eurasia (Ex USSR). 2. Phanerozoic Fold Belts and Young Platforms, Bornträger, Berlin, 404p., ISSN 3–443–11024-X.

Kim, B.I., 1986. Cenozoic history of the development of the East Arctic shelves and paleoshelves. In: Egiazarov, B.K.H., Kazmin, Y.B. (Eds.), Structure and history of development of the Arctic ocean. Sevmorgeologiya, Leningrad, pp. 105–119 (in Russian).

Kos'ko, M.K., 1984. East Siberian Sea. In: Gramberg, I.S., Pogrebitsky, Y.E. (Eds.), Geologic Structure of USSR and its Relationship to the Distribution of Mineral Resources. Seas of the Soviet Arctic, Vol. 9. Nedra, Leningrad, pp. 51–60.

Kos'ko, M.K., Trufanov, G.V., 2002. Middle Cretaceous to Eopleistocene sequences on the New Siberian Islands: an approach to interpret offshore seismic. Mar. Petrol. Geol. 19, 901–919.

Kos'ko, M.K., Lopatin, B.G., Ganelin, V.G., 1990. Major geological features of the islands of the East Siberian and Chukchi Seas and the northern coast of Chukotka. Mar. Geol. 93, 349–367.

Kristoffersen, Y., 1990. Eurasia Basin. In: Grantz, A., Johnson, L., Sweeney, J.F. (Eds.), The Arctic Ocean Region, The Geology of North America, vol. L, pp. 365–378.

Lane, L.S., 1997. Canada Basin, Arctic Ocean: evidence against a rotational origin. Tectonics 16, 363–387.

Lawver, L.A., Scotese, C.R., 1990. A review of tectonic models for the evolution of the Canada Basin. In: Grantz, A., Johnson, L., Sweeney, J.F. (Eds.), The Arctic Ocean Region. The Geology of North America, vol. L. Geological Society of America, Boulder, pp. 593–618.

Lawver, L.A., Grantz, A., Gahagan, L.M., 2002. Plate kinematic evolution of the present Arctic region since the Ordovician. In: Miller, E.L., Kemperer, S.L., Grantz, A.W. (Eds.), Geology and Tectonic Development of the Bering and Chukchi Shelves and Adjacent Arctic Margins, GSA Special Paper, vol. 360, pp. 337–362.

Laxon, S., McAdoo, D., 1994. Arctic ocean gravity field derived from ERS-1 satellite altimetry. Science 165, 621–624.

Mangerud, J., Jansen, E., Landvik, J.Y., 1996. Late Cenozoic history of the Scandinavian and Barents ice sheets. Glob. Planet. Change 12, 11–26.

Myhre, A.M., Thiede, J., 1995. North Atlantic – Arctic gateways. In: Myhre, A.M., Thiede, J., Firth, J.V. et al. (Eds.), Proceedings of the ODP, Inititial Reports, 151; College Station, TX (Ocean Drilling Programme).

Nalivkin, D.V. (Ed.), 1983. Geological map of the USSR: Moscow, Ministry of Geology of the USSR, 16 sheets, scale 1: 2,500,000.

Parfenov, L.M., 1991. Tectonics of the Verkhoyansk-Kolyma Mesozoides in context of plate tectonics. Tectonophysics 199, 319–342.

Patyk-Kara, N.G., Laukhin, S.A., 1986. Cenozoic evolution of the Arctic coastal relief of North-Eastern Asia. Sov. Geol. 1, 75–84 (in Russian).

Piskarev, A.L., Roeser, H.A., Hinz, K., Kos'ko, M.K., 2001. Potential field studies on the crustal structure of the Laptev Sea and the western East Siberian Sea. In: Roland, N.W., Tessensohn, F., ICAM, I.I.I. (Eds.), : III, International Conference on Arctic Margins. Polarforschung, vol. 69 (1999). Alfred-Wegener-Institute for Polar and Marine Research and the German Society of Polar Research, Bremerhaven, pp. 41–50, ISSN 0032–2490.

Roeser, H.A., Block, M., Hinz, K., Reichert, C., 1995. Marine geophysical investigations in the Laptev Sea and the western part of the East Siberian Sea. Reports on Polar Research (176): Russian-German Cooperation in the Siberian Shelf Seas: Geo-System Laptev Sea, Alfred Wegener Institute for Polar and Marine Research, Bremerhaven, Germany, pp. 367–377.

Rowley, D.B., Lottes, A.L., 1988. Plate-kinematic reconstructions of the North Atlantic and Arctic: Late Jurassic to Present. Tectonophysics 155, 73–120.

Sekretov, S.B., 2000. Petroleum Potential of the Laptev Sea Basins: Geological, Tectonic and Geodynamic Factors. In: Roland, N.W., Tessensohn, F. (Eds.), Polarforschung, Alfred-Wegener-Institute for Polar and Marine Research and the German Society of Polar Research, Bremerhaven, pp. 179–186.

Sekretov, S.B., 2002. Structure and tectonic evolution of the Southern Eurasia Basin, Arctic Ocean. Tectonophysics 351, 193–243.

Srivastava, S.P., Tapscott, C., 1986. Tucholke, B.E., Vogt, P.R. (Eds.), The Geology of North America, The Western Atlantic Region. (A Decade of North American Geology), vol. M. Geological Society of America, Boulder, Colorado, pp. 379–404.

Verhoef, J., Walter, R.R., Macnab, R., Arkani-Hamed, J., members of the project team, 1996. Magnetic anomalies of the Arctic and North Atlantic oceans and adjacent land areas. Geol. Surv. Can. Open File 3125a.

Vinogradov, V.A., 1984. Laptev Sea. In: Gramberg, I.S., Pogrebitskii, Y.E. (Eds.), Geologic Structure of the USSR and its Relationship to the Distribution of Mineral Resources. Seas of the Soviet Arctic, vol. 9. Nedra, Leningrad, pp. 51–60 (in Russian).

Vinogradov, V.A., Gaponenko, G.I., Gramberg, I.S., Shimarayev, V.N., 1977. Structural-associational complexes of the Arctic shelf of eastern Siberia. Int. Geol. Rev. 19, 1331–1343.

Vol'nov, D.A., Voitsekhovsky, V.N., Ivanov, O.A., Sorokov, D.S., Yashin, D.S., 1970. Novosibirskie ostrova. In: Tkachenko, B.V., Egiazarov, B.K. (Eds.), Geology SSSR. Ostrova Arktiki, vol. 26. Nedra, Moskva, pp. 224–274.

Zonenshain, L.P., Kuz'min, M.I., Natapov, L.M., 1990. Geology of the USSR: A Plate-Tectonic Synthesis. In: Page, B.M. (Ed.), Geodynamics Series, vol. 21. Am. Geophys. Union, Washington, D.C., p. 242.

In this chapter

13

Development of the passive margin of Eastern North America: Mesozoic rifting, igneous activity, and breakup

Martha Oliver Withjack, Roy W. Schlische,* Paul E. Olsen†*

*Department of Earth and Planetary Sciences, Rutgers University, Piscataway, New Jersey, USA
†Department of Earth and Environmental Sciences and Lamont-Doherty Earth Observatory of Columbia University, Palisades, New York, USA

13.1 Introduction

Eastern North America is a natural laboratory for studying passive-margin development. It hosts one of the world's largest rift systems (the eastern North American rift system), one of the world's oldest intact passive margins, and one of the world's largest igneous provinces (the Central Atlantic Magmatic Province, CAMP). Additionally, seismic-reflection profiles, field exposures, and drill-hole data provide a wealth of information about the tectonic and depositional processes associated with rifting, breakup, and the early stages of seafloor spreading. In this chapter, we review the geologic development of this passive margin. First, we present information on rifting, igneous activity, and postrift deformation for the region from northern Florida to the eastern Grand Banks of maritime Canada (Fig. 13.1). Then, we systematically describe the evolution of the passive margin from the onset of rifting to the early stages of drifting as eastern North America separated from northwestern Africa and Iberia.

13.2 Geologic overview

During early Mesozoic time, a massive rift zone developed within the Pangean supercontinent (insert, Fig. 13.1). The breakup of Pangea splintered this rift zone into extinct fragments, each now separated and preserved on the passive margins of eastern North America, northwestern Africa, and Europe. The fragment

Phanerozoic Rift Systems and Sedimentary Basins DOI:10.1016/B978-0-444-56356-9.00012-2

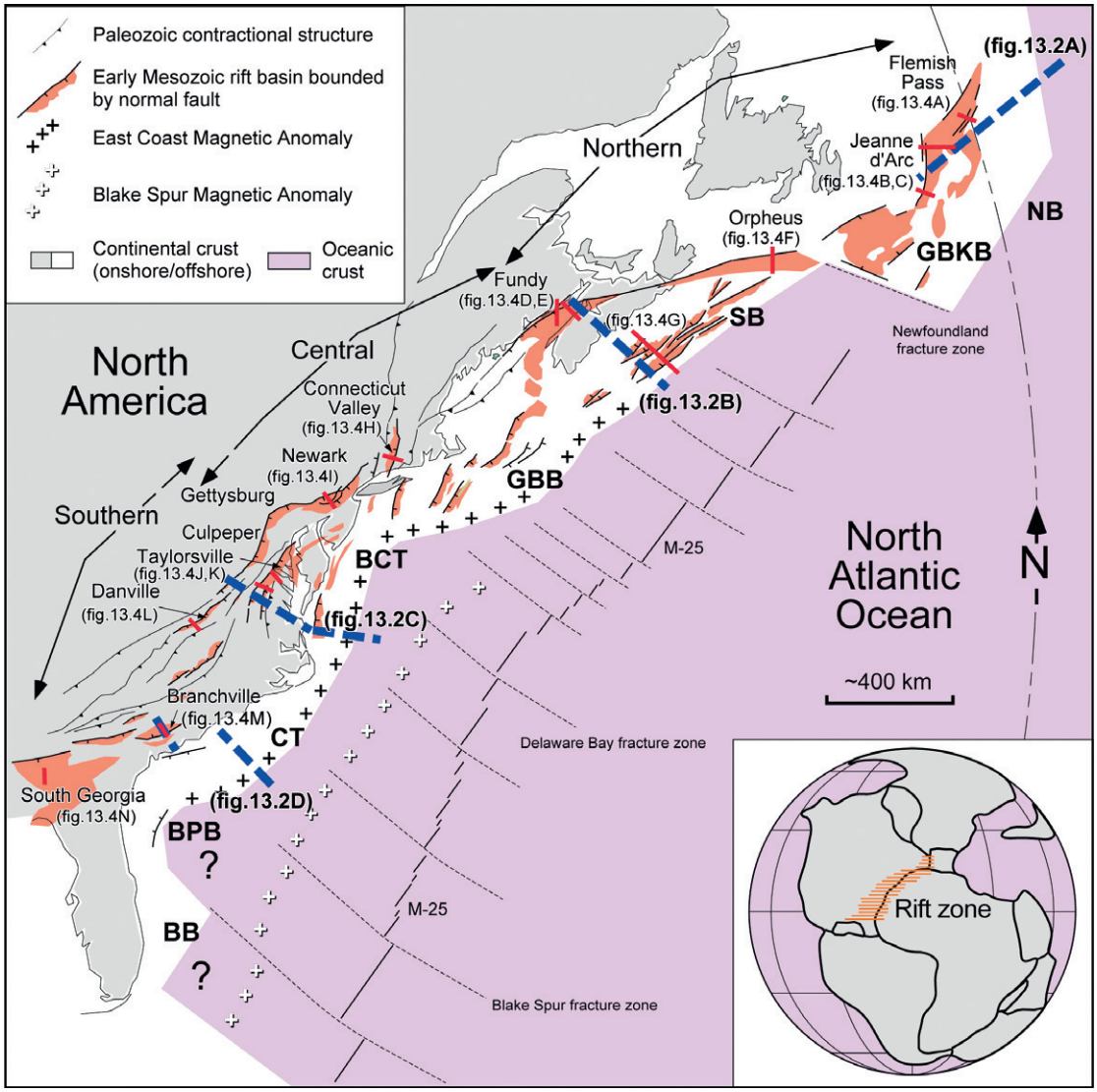

Figure 13.1 Major Paleozoic contractional structures and early Mesozoic rift basins of eastern North America, and key tectonic features of the eastern North Atlantic Ocean (Benson, 2003; Foster and Robinson, 1993; Klitgord et al., 1988; Olsen et al., 1989; Rankin, 1994; Welsink et al., 1989). Mesozoic/Cenozoic postrift basins near the continent/ocean boundary are NB, Newfoundland basin; GBKB, Grand Banks basin; SB, Scotian basin; GBB, Georges Bank basin; BCT, Baltimore Canyon trough; CT, Carolina trough; BPB, Blake Plateau basin; and BB, Bahamas basin. Thick dashed lines show locations of transects in Fig. 13.2. Thin solid lines show locations of sections in Fig. 13.4. The exact geometry of the buried rift basins in the southern and central segments of the eastern North American rift system, and the type of crust beneath the Newfoundland basin, the southern Blake Plateau basin, and the Bahamas basin is uncertain (e.g., Klitgord et al., 1988; Shipboard Scientific Party, 2003). The East Coast Magnetic Anomaly follows the continental/ocean boundary (light gray/white contact) and is associated with the presence of seaward-dipping reflectors (SDRs). Insert shows Pangaean supercontinent during Late Triassic time (Olsen, 1997) and highlights the rift zone between eastern North America and northwestern Africa and Iberia.

on the North American margin, called the "eastern North American rift system," consists of a series of exposed and buried rift basins extending from northern Florida to the eastern Grand Banks of Canada (e.g., Manspeizer and Cousminer, 1988; Olsen et al., 1989; Schlische, 1993, 2003; Withjack et al., 1998; Figs. 13.1–13.4). It is one of the world's largest rift systems, affecting a region of up to 500 km wide and 3000 km long.

We divide the eastern North American rift system into three geographic segments. The southern segment encompasses the southeastern United States, the central segment encompasses the northeastern United States and southeastern Canada, and the northern segment encompasses the eastern Grand Banks of Canada (Fig. 13.1). The boundary between the southern and central segments is a diffuse zone, passing through Virginia and Maryland. The boundary between the central and northern segments is a well-defined zone trending WNW-ENE and following the northern faulted margins of the Fundy and Orpheus basins (i.e., the Minas fault zone) and the Newfoundland fracture zone. As discussed below, each segment of the North American rift system has a distinct geologic history.

Rift-basin structure

The eastern North American rift system consists of a series of asymmetric rift basins (i.e., half-grabens) bounded, on at least one side, by a series of basement-involved border faults (Figs. 13.2–13.4). Field data and 3D seismic data show that, in most basins, these border faults are either right-stepping (e.g., Newark basin, Withjack et al., 1998) or left-stepping (e.g., Jeanne d'Arc basin, Sinclair et al., 1999) and linked by relay ramps. The border-fault zones dip either seaward (e.g., Fig. 13.4B–F and I–L) or landward (e.g., northwestern half of Fig. 13.4G, H, and M) and have gentle to moderate dips. Most border-fault zones strike NE-SW and have mostly normal displacement (e.g., Hutchinson and Klitgord, 1988; Schlische, 1993, 2003; Fig. 13.3). A few border-fault zones, however, have an anomalous strike and displacement. For example, the northern border-fault zone of the Fundy basin, the Minas fault zone (Fig. 13.3B), strikes ENE–WSW and has both normal and left-lateral strike-slip components of displacement (Olsen and Schlische, 1990; Withjack et al., 1995). The eastern North American rift system developed within Paleozoic and older orogenic belts. Generally, the attitudes of the border-fault zones of the rift basins mimic the attitudes of the fabric created during these orogenies (e.g., deVoogd et al., 1990; Lindholm, 1978; Olsen and Schlische, 1990; Ratcliffe and Burton, 1985; Ratcliffe et al., 1986; Swanson, 1986; Withjack et al., 1995; Fig. 13.1). Thus, the border-fault zones of many rift basins are reactivated, preexisting structures.

A great variety of smaller-scale extensional structures developed throughout the eastern North America rift system. Intrabasin faults are common in most rift basins. The strike of these intrabasin faults, with respect to the border-fault

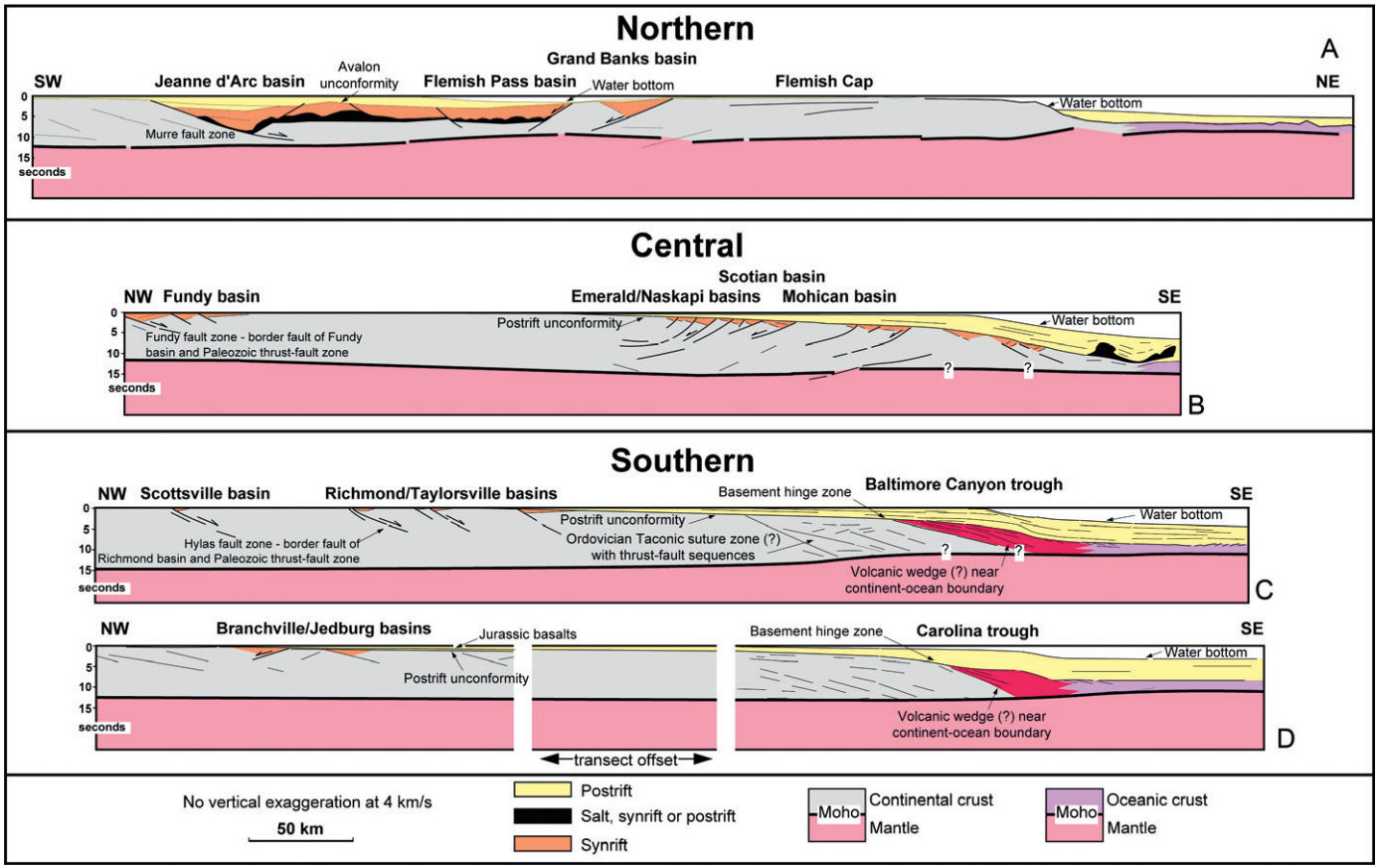

Figure 13.2 Transects through the northern, central, and southern segments of the passive margin of eastern North America. Transects show Paleozoic structures, Mesozoic rift basins and Mesozoic/Cenozoic postrift basins. Vertical axes are in two-way travel time. Transect locations are shown in Fig. 13.1. (A) Transect from offshore Newfoundland, Canada, based on seismic data from Keen et al. (1987). Rift-basin fill includes synrift strata and/or strata deposited during quiet period between rifting episodes. (B) Section from Nova Scotia, Canada, based on seismic data from Keen et al. (1991a, 1991b) and Withjack et al. (1995). (C) Section through the central United States based on geological and geophysical data from Letourneau (2003), Olsen et al. (1989), Shaler and Woodworth (1899), and Sheridan et al. (1993). Onshore geology was converted to two-way travel time by assuming a velocity of 4000 m/s. (D) Section through the southeastern United States based on seismic data from Austin et al. (1990), Behrendt (1986), and Oh et al. (1995).

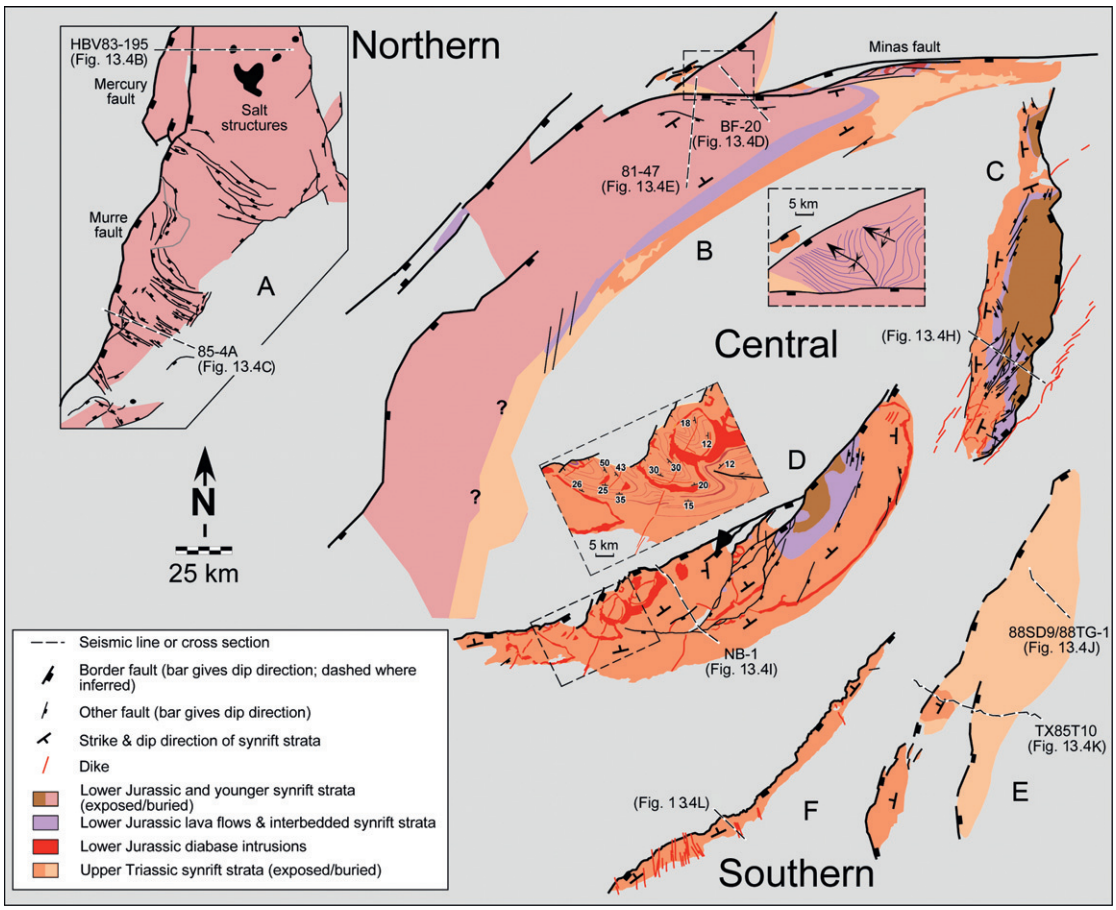

Figure 13.3 Maps of several rift basins from the northern, central, and southern segments of eastern North America. Basin locations are shown in Fig. 13.1. Dashed lines show sections in Fig. 13.4. (A) Jeanne d'Arc basin, Grand Banks, Canada. Southern half of map shows faults cutting prominent Middle Jurassic reflection (after Sinclair, 1995a), and northern half shows faults cutting Aptian/Albian sequence (after Sinclair, 1995b). (B) Fundy basin, Canada (after Baum, 2002; Wade et al., 1996; Withjack et al., 1995). Enlargement (dashed box) shows folds near northern end of basin. Dark lines are structure contours on the surface of synrift lava flows. (C) Connecticut Valley basin, northeastern United States (after Schlische, 1993). CAMP dykes trend NE–SW. (D) Newark basin, northeastern United States (after Schlische, 1992, 1995). Enlargement (dashed box) shows folds near southern end of basin. White lines follow stratigraphic markers. (E) Taylorsville/Richmond basin, southeastern United States (after LeTourneau, 2003). (F) Danville basin, southeastern United States (after Schlische, 1993). CAMP dykes trend NW–SE, cutting across the basin.

zones, varies considerably. Many intrabasin faults in the Newark basin are subparallel or oblique to the border-fault zone (Fig. 13.3D); nearly all intrabasin faults in the Connecticut Valley basin are oblique to the border-fault zone (Fig. 13.3C); and many intrabasin faults in the Jeanne d'Arc basin are orthogonal to the border-fault zone (Fig. 13.3A). Many intrabasin faults formed during

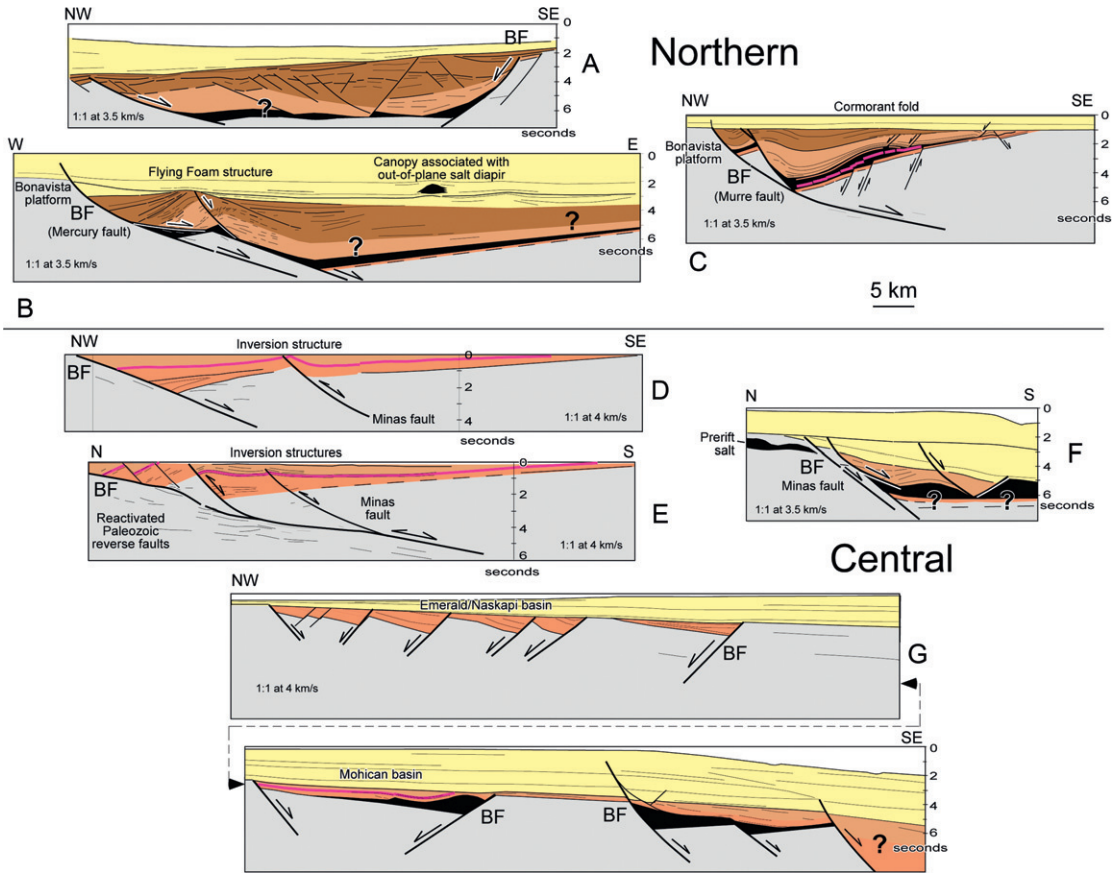

Figure 13.4 Sections through several rift basins from the northern, central, and southern segments of the eastern North American rift system. Section locations given in Figs. 13.1 and 13.3. Vertical axes of seismic lines are in two-way travel time. (A) Interpreted line drawing of time-migrated seismic line from Flemish Pass basin, Grand Banks, Canada. Deep events are poorly imaged. (B) Interpreted line drawing of time-migrated seismic line HBV83–195 from northern Jeanne d'Arc basin, Grand Banks, Canada (after Withjack and Callaway, 2000). The Flying Foam structure is a forced fold above an E-dipping normal fault. A detached normal fault formed near the Mercury fault at the western limit of the Triassic/Jurassic evaporite package. Deep events on the eastern part of the line are poorly imaged. (C) Interpreted line drawing of seismic line 85–4A from southern Jeanne d'Arc basin, Grand Banks, Canada (after Keen et al., 1987; Sinclair, 1995a; Withjack and Callaway, 2000). Cormorant fold developed above subsalt normal faults, antithetic to Murre border fault. Early to Middle Jurassic stratal packages thicken toward the Murre border fault. (D) Interpreted line drawing from northern Fundy basin, Canada, based on time-migrated seismic line BF-20 (inner box) and onshore geology (after Baum, 2002). Inversion structure developed near E-striking Minas fault. (E) Interpreted line drawing from northern Fundy basin, Canada, based on time-migrated seismic line 81–47 (inner box) and onshore geology (after Baum, 2002; Withjack et al., 1995). Border fault is a reactivated Paleozoic reverse fault. Inversion structures developed near E-striking Minas fault zone. (F) Interpreted line drawing of time-migrated seismic line from Orpheus graben, Scotian shelf, Canada. Many faults detach within Triassic/Jurassic evaporite package and possibly prerift evaporites. Deep events are poorly imaged. (G) Interpreted line drawing of time-migrated seismic data from Scotian shelf, Canada (after Welsink et al., 1989). Line crosses several rift basins. Jurassic strata, in addition to Triassic strata, may be present in the northwestern rift basins. Southeastern rift basins contain Triassic/Jurassic evaporites and detached faults.

(Continued)

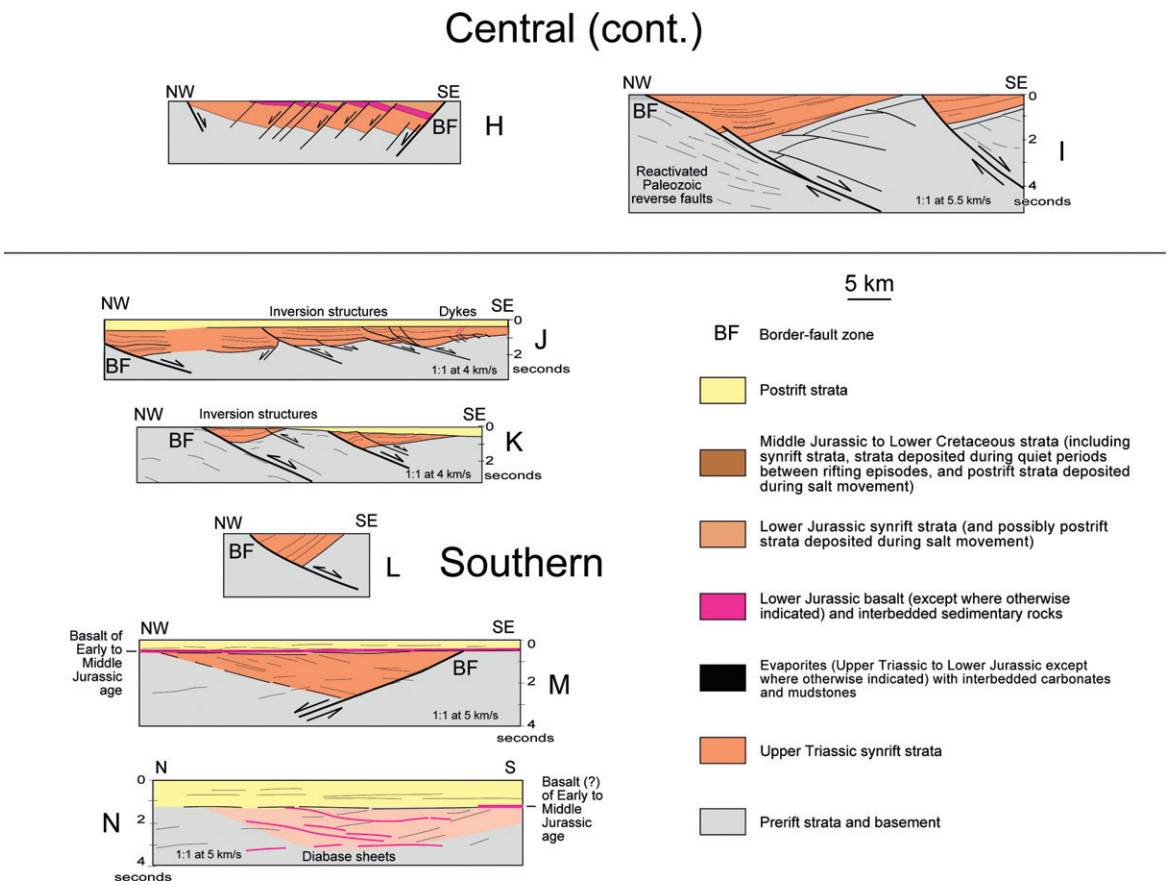

Figure 13.4 Cont'd (H) Cross section through Connecticut Valley basin, northeastern United States (after Schlische, 1993). (I) Interpreted line drawing of time-migrated seismic line NB-1 from Newark basin, northeastern United States. Border fault is a reactivated Paleozoic reverse fault. (J and K) Interpreted line drawings of time-migrated seismic lines 88SD9/88TG-1 and TX85T10, respectively, from Taylorsville basin, southeastern United States (after LeTourneau, 1999, 2003). Inversion structures affect the synrift strata. (L) Cross section through Danville basin, southeastern United States (after Schlische et al., 2003). Border fault may have undergone reverse movement after rifting. (M) Interpreted line drawing of seismic line S4 (unmigrated) through the Branchville basin, southeastern United States (after Behrendt, 1986). Flat-lying postrift basalts overlie dipping synrift strata. (N) Interpreted line drawing of COCORP Georgia line 11 (time-migrated) through the South Georgia basin (after McBride et al., 1989). High-amplitude events are probably diabase sills. Reflections from synrift strata are obscured by these events.

the early stages of rifting (e.g., the intrabasin faults in the Taylorsville basin, Plate 13.1), whereas others developed during the later stages of rifting (e.g., the intrabasin faults in the Newark basin, Plate 13.1). Fault-displacement folds, related to segmentation and/or undulations on the border faults or intrabasin faults, are common in the central segment of the rift system (Schlische, 1993, 1995; Wheeler, 1939; Withjack et al., 2002; inserts, Fig. 13.3B, D). The thinning and thickening of the synrift strata within the anticlines and synclines, respectively, and the preferential intrusion of diabase along the axial traces show that these folds formed, in part, during rifting.

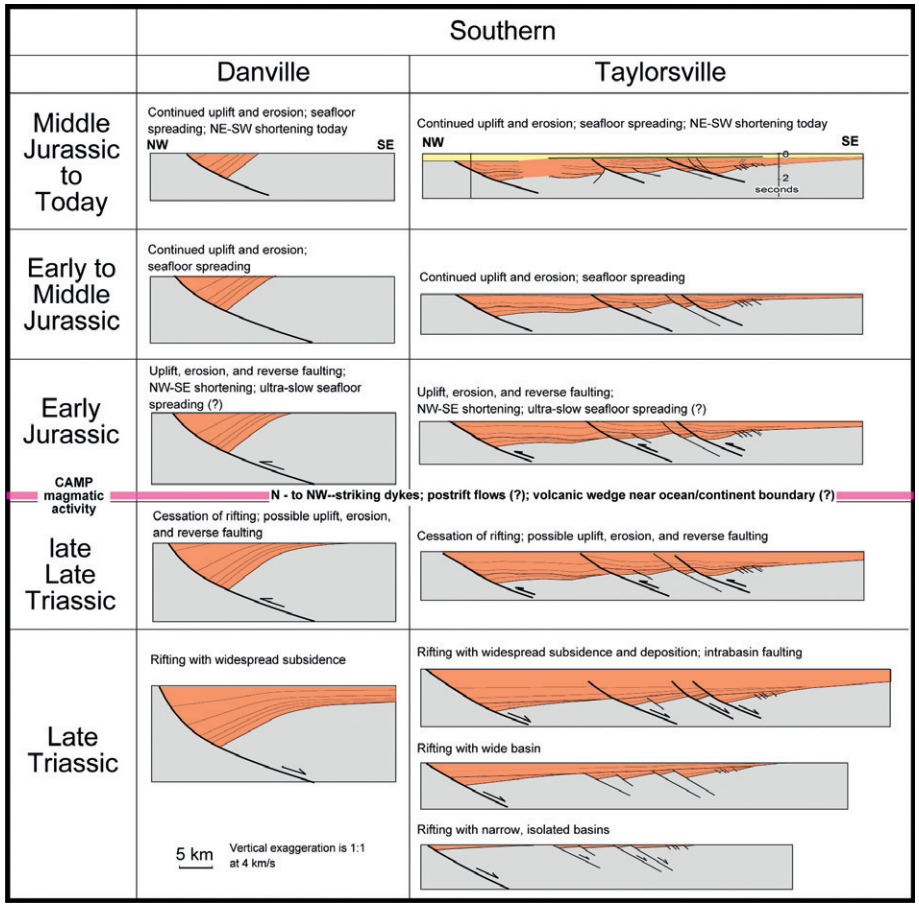

Plate 13.1 Evolution of rift basins from the northern, central, and southern segments of eastern North America. See Fig. 13.4 for description of the sections today. To estimate the amount of erosion for the Taylorsville and Newark basins, we used the results of thermal modeling studies and fission-track analyses (Malinconico, 1999, 2003; Pratt et al., 1988; Steckler et al., 1993; Tseng et al., 1996). To restore the sections from the Taylorsville, Fundy, and Jeanne d'Arc basins through time, we displayed the seismic sections with approximately no vertical exaggeration and divided each section into blocks with relatively constant bedding dip. We rotated and translated the blocks until the restored horizons became flat. We also assumed that the cross-sectional area remained constant during deformation. These restorations are approximations (i.e., we did not convert the seismic profiles to depth, and we did not decompact the sedimentary section). To restore the section through the Newark basin, we converted the seismic section to depth, we assumed that vertical shear was the hanging-wall deformation mechanism, and we decompacted the sedimentary section using the exponential decay formula, $\phi = 0.5e^{-0.5z}$, where ϕ is porosity and z is depth in kilometers.

(Continued)

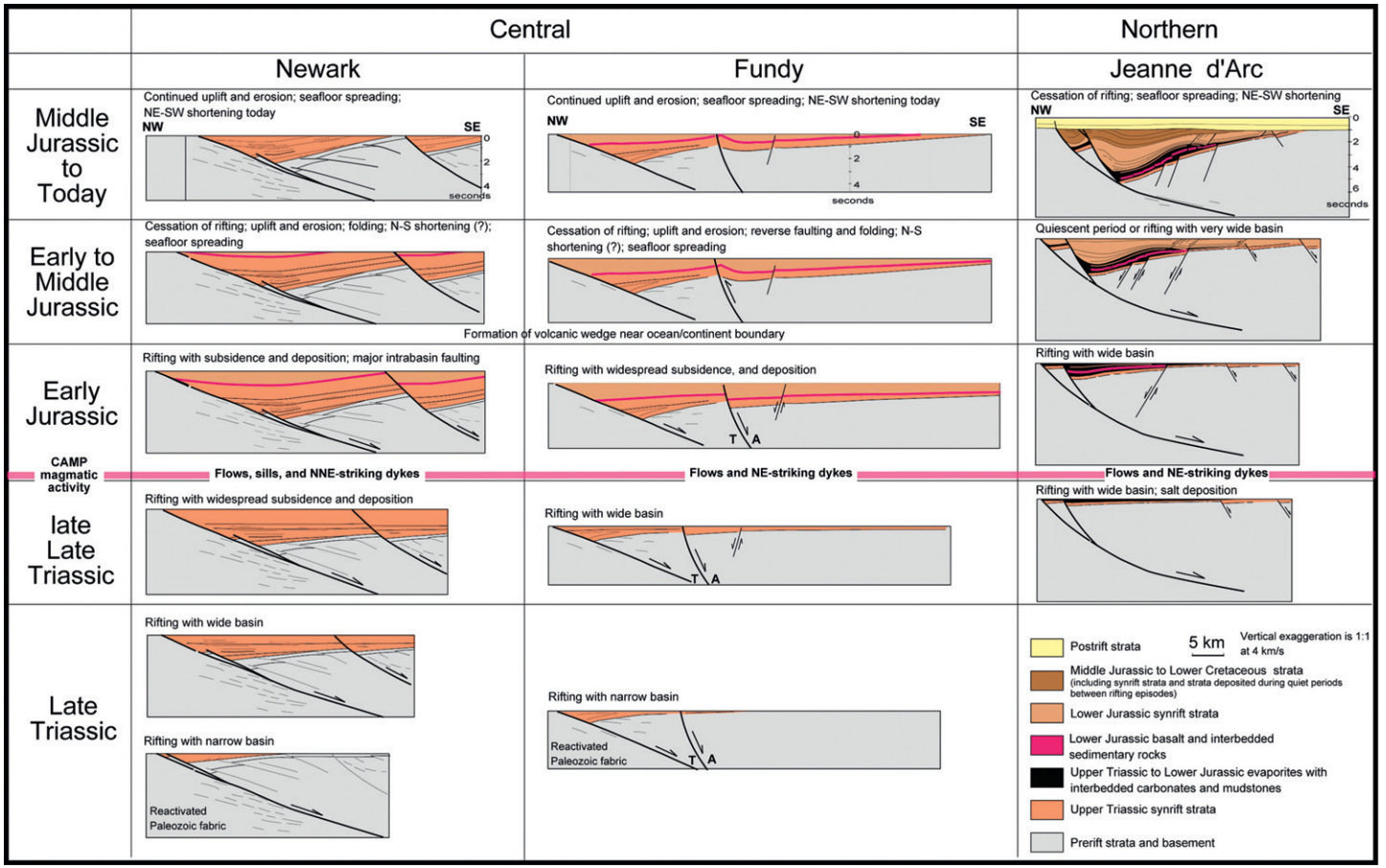

Plate 13.1 Cont'd

The presence of salt profoundly affected the structural development of many of the rift basins in the northern and central segments of the eastern North American rift system (Fig. 13.5). Tectonic activity, regional tilting, and/or differential sediment loading triggered salt flow, producing a variety of salt structures during and after rifting. For example, pillows, diapirs, and detached normal faults formed within the Jeanne d'Arc basin in the northern segment (Enachescu, 1987; Sinclair, 1995a; Tankard and Welsink, 1987; Figs. 13.3A and 13.4B, C) and the Orpheus basin in the central segment (MacLean and Wade, 1992; Fig. 13.4F) during and after rifting. The presence of salt also impeded the upward propagation of deep-seated faults through the overlying sedimentary cover. Scaled experiments and geologic examples from several salt basins (e.g., Vendeville et al., 1995; Withjack and Callaway, 2000) show that deep-seated normal faults cannot propagate upward through thick salt (i.e., subsalt and suprasalt faults cannot directly link). Instead, large fault-propagation folds (e.g., the Flying Foam structure in the Jeanne d'Arc basin; Fig. 13.4B) form in the sedimentary cover above the subsalt faults.

Timing of rifting

The timing of rifting is based principally on the presence of growth strata within the rift basins. Generally, strata of Late Triassic age coarsen abruptly near the border faults, showing that a local source of relief existed adjacent to the border faults during deposition. Furthermore, seismic, core, and outcrop data show that strata of Late Triassic age thicken and fan toward the border faults (e.g., Olsen et al., 1996a; Schlische and Withjack, 2005; Schlische, 1992, 1993; Withjack et al., 1998; Fig. 13.4, Plate 13.1). Near the base of the synrift section, wedge-shaped growth packages are narrow (<10 km), and thickness changes are pronounced. Higher in the section, wedge-shaped growth packages are wide (50–100 km), have subtle thickness changes, and have great lateral continuity. In fact, without ample core and outcrop data, it would be easy to mistake these latter growth packages, with their great width, subtle thickness variations, and lateral continuity, for prerift or postrift strata (e.g., Faill, 1973, 1988, 2003). The presence of growth strata indicates that rifting was under way throughout eastern North America by Late Triassic time (Fig. 13.5). Rifting may have begun earlier in some basins. Seismic data show that *undated* synrift strata underlie synrift strata of Late Triassic age in several rift basins (e.g., the Fundy and Newark basins; Fig. 13.4D, E, and I). Also, Permian (?) and Middle (?) Triassic strata crop out in the Fundy basin (Olsen, 1997). Coeval strata on the conjugate margin of Morocco display geometries consistent with rifting, suggesting that these older Fundy outcrops also may be synrift strata (Olsen et al., 2000).

The age range of dated, preserved synrift strata varies considerably among the three segments of the eastern North American rift system (Fig. 13.5). In the southern segment, only strata of Late Triassic age strata are present. In the central segment, strata of Late Triassic to Early Jurassic age are present. In the northern

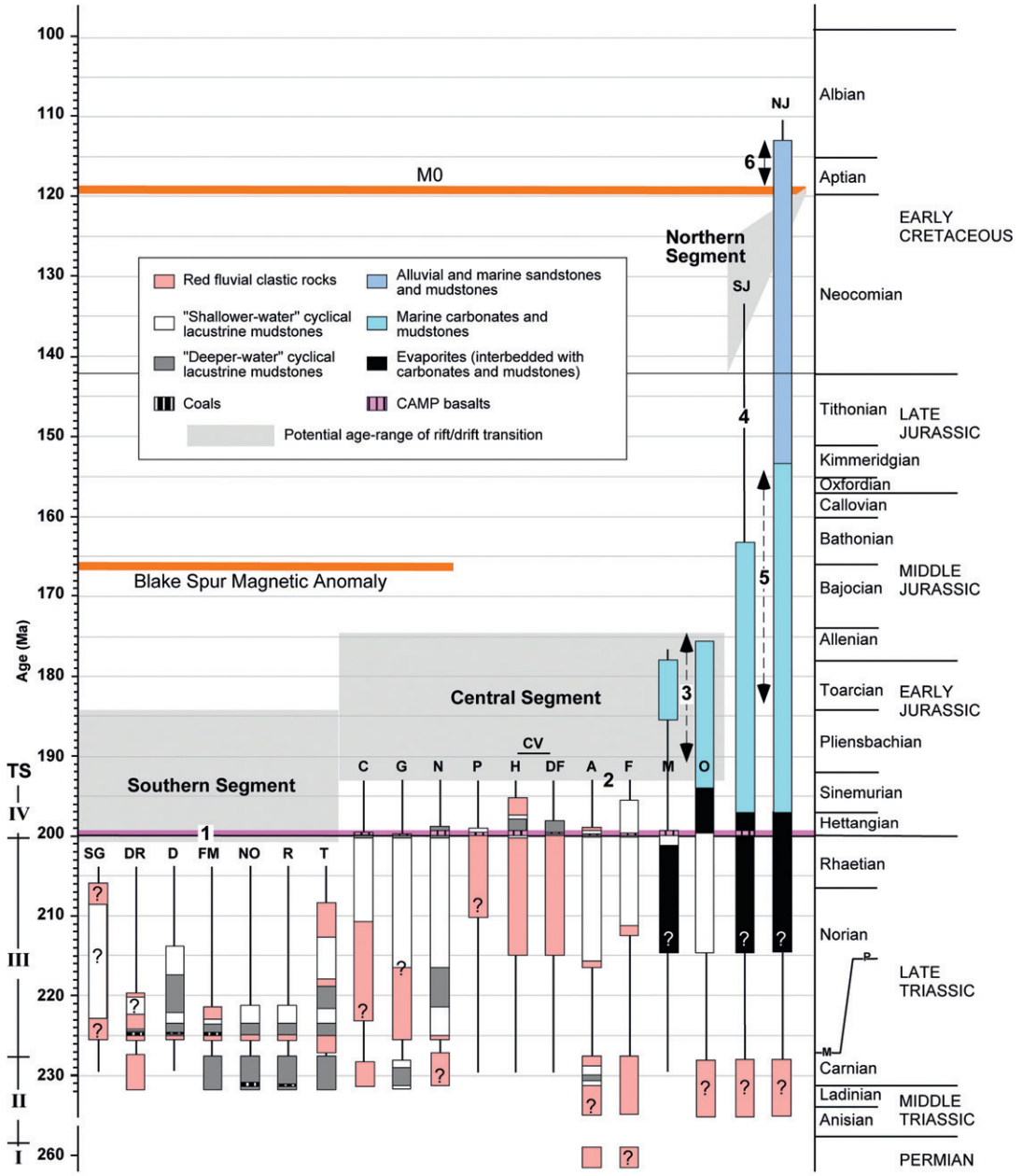

Figure 13.5 Ages, basic facies, and formations in the eastern North American rift system and Argana basin of Morocco. Jurassic time scale from Pálfy et al. (2000), and Cretaceous time scale from Palmer (1983). The M and P on the line dividing Norian from Carnian represents the new correlations to marine sections based on paleomagnetics (M; Channell et al., 2003; Krystyn et al., 2002; Muttoni et al., 2004) and the "conventional" palynological correlations (Olsen, 1997). Basins are: SG, South Georgia; DR, Deep River; D, Danville/Dan River; FM, Farmville and Briery Creek; NO, Norfolk; R, Richmond; T, Taylorsville; C, Culpeper; G, Gettysburg; N, Newark; P, Pomperaug; H, Hartford; DF, Deerfield; CV, Connecticut Valley (Hartford and Deerfield combined); A, Argana; F, Fundy; M, Mohican (Glooscap C-63 well: Pe-Piper et al., 1992); O, Orpheus (after Tanner and Brown, 2003); SJ, southern Jeanne d'Arc (after McAlpine, 1990); NJ, northern Jeanne d'Arc (after McAlpine, 1990). (1) CAMP activity (diabase sheets, NW-striking dykes, and possibly postrift basalt flows in southern segment; diabase sheets, NE-striking dykes, and synrift basalt flows in central and northern segments). (2) Oldest postrift strata in Morocco. (3) Synrift or postrift strata associated with salt movement. (4) Strata eroded during development of Avalon unconformity. (5) Strata associated with thermal subsidence or synrift strata. (6) Synrift strata associated with rifting between the northern Grand Banks and Greenland/Europe or postrift strata associated with salt movement.

segment, strata of Late Triassic to late Early Cretaceous age are present. Many researchers have proposed that rifting was episodic in the northern segment of the eastern North American rift system (e.g., Enachescu, 1987; Foster and Robinson, 1993; McAlpine, 1990; Sinclair, 1995a,b; Tankard and Welsink, 1987). With this interpretation, rifting occurred during Late Triassic to earliest Jurassic time and again during latest Jurassic to Early Cretaceous time. Thermal subsidence, not rift-related subsidence, occurred during the intervening Early to Late Jurassic time. The primary evidence for the cessation of rifting during this time interval is the broad distribution, subtle thickness variations, and monotonous character of the stratal packages of Early to Late Jurassic age. Several lines of evidence, however, suggest that some rifting occurred during Early to Late Jurassic time in the northern segment. (1) As discussed previously, proven synrift rocks in the southern and central segments of the eastern North American rift system have broad distributions and subtle thickness variations like the strata of Early to Late Jurassic age in the northern segment. Thus, the Early to Late Jurassic strata within the northern rift basins, with these same characteristics, *could* also be synrift rocks. (2) As suggested by Sinclair et al. (1999), the thick section of strata of Early to Late Jurassic age within the Jeanne d'Arc basin compared to the absence of these strata on the adjacent Bonavista platform suggests that the border faults were active during the Jurassic age (Figs. 13.4B, C). (3) Seismic sections from the southern Jeanne d'Arc basin, where the oldest strata are best imaged, clearly show that stratal packages of Early to Middle Jurassic age thicken toward the Murre border fault (Fig. 13.4C). Thus, we believe that some rifting, albeit subdued or intermittent, occurred during Early to Late Jurassic time in the northern segment of the eastern North American rift system.

Depositional patterns

Continental conditions prevailed throughout eastern North America during Late Triassic (Carnian) time (e.g., McAlpine, 1990; Olsen, 1997; Fig. 13.5). The exposed basins in the southern and central segments remained continental throughout their entire preserved depositional history. By latest Triassic (Norian) time, however, encroachment of the Tethys Sea from the north created marine conditions in the northern segment and the northeastern rift basins of the central segment. Evaporites (mostly halite) and carbonates filled these rift basins during Late Triassic and Early Jurassic time (Fig. 13.5). Sulfur isotopic evidence from the oldest evaporites suggests only a moderate marine contribution of highly evolved brines (Holser et al., 1988). Coeval basins on the conjugate Moroccan margin, however, have progressively more marine influence toward the east (Et-Touhami, 2000; Olsen et al., 2003), and in eastern Morocco, the sedimentary units interbedded with CAMP basalt flows are carbonates with abundant marine mollusks (Olsen et al., 2003). In the northern segment of eastern North America, marine conditions prevailed throughout Jurassic time leading to the deposition of marine carbonates and mudstones (McAlpine, 1990; Tankard and Welsink,

1987; Fig. 13.5). During the latest Jurassic and Early Cretaceous time, alluvial and shallow marine sandstones and mudstones filled the rift basins in the northern segment (McAlpine, 1990; Tankard and Welsink, 1987).

The evolving geometry of the rift basins also influenced depositional patterns in the eastern North American rift system. Tectonostratigraphic sequences bounded by unconformities in the southern and central segments and Morocco (Olsen, 1997) share a similar stratigraphic succession known as a "tripartite stratigraphy" (e.g., Schlische and Olsen, 1990; Fig. 13.5). Near the basin depocenter, each tectonostratigraphic sequence (TS) consists of a basal fluvial unit followed upward by lacustrine strata that rapidly reach maximum paleodepth and then slowly shallow upward, sometimes returning to fluvial deposits. The lacustrine strata tend to be cyclical, especially in the regions between 2° and 15° paleolatitude (Olsen and Kent, 2000), reflecting Milankovitch climate cycle control of lake depth (Olsen and Kent, 1996; Olsen, 1986). Exceptions include TS III in some rift basins, such as the Connecticut Valley basin, that consist only of fluvial strata, as well as the basal part of TS IV that can lack a basal fluvial unit in areas with a correlative conformity with TS III (Olsen, 1997). Facies patterns tend to be centripetal with fine-grained lacustrine strata at the basin depocenter. Asymmetrically distributed fluvial and marginal lacustrine strata are present along the basin margins – tending to be extensively developed along hinge margins and at the lateral ends of the basins, and restricted to much narrower, but commonly very coarse-grained, bands on the border-fault margins (Fig. 13.6; Olsen, 1997). Both the vertical sequence of facies and their asymmetric distribution suggest that each TS originated with a major extensional pulse that produced an asymmetrically subsiding basin that widened through time (Contreras et al., 1997; Olsen, 1997; Schlische and Olsen, 1990; Schlische, 1991).

Climate profoundly influenced the depositional patterns in the rift basins of eastern North America. The clearest climatic effect is the arrangement of facies relative to the paleoequator during Carnian time. Coals and deep-water lacustrine deposits were produced around the paleoequator (the southern basins in Figs. 13.5 and 13.6C), while cyclical perennial lacustrine and playa deposits and bioturbated red beds accumulated 10° to the north and south of the paleoequator (the Newark basin in Figs. 13.5 and 13.6A, B; Kent and Olsen, 1997; Kent et al., 1995; Olsen and Kent, 2000; Olsen, 1997). Broadly contemporaneous deposits at 30° N paleolatitude in Greenland (Clemmensen et al., 1998; Clemmensen, 1980) are comprised of red mudstones, eolian sand dunes, and evaporite beds, while farther north on the conjugate margin in the Barents Sea, deltaic coals and black mudstone again dominate (van Veen et al., 1992). This conforms to a simple zonal pattern, with a narrow equatorial humid zone and an arid belt mostly south of 30°, passing northward into hothouse humid temperate climates. Although non-zonal elements such as orography and an enhanced monsoon may have been important elements of the Earth's climate system during the Carnian, such are not required by the observations.

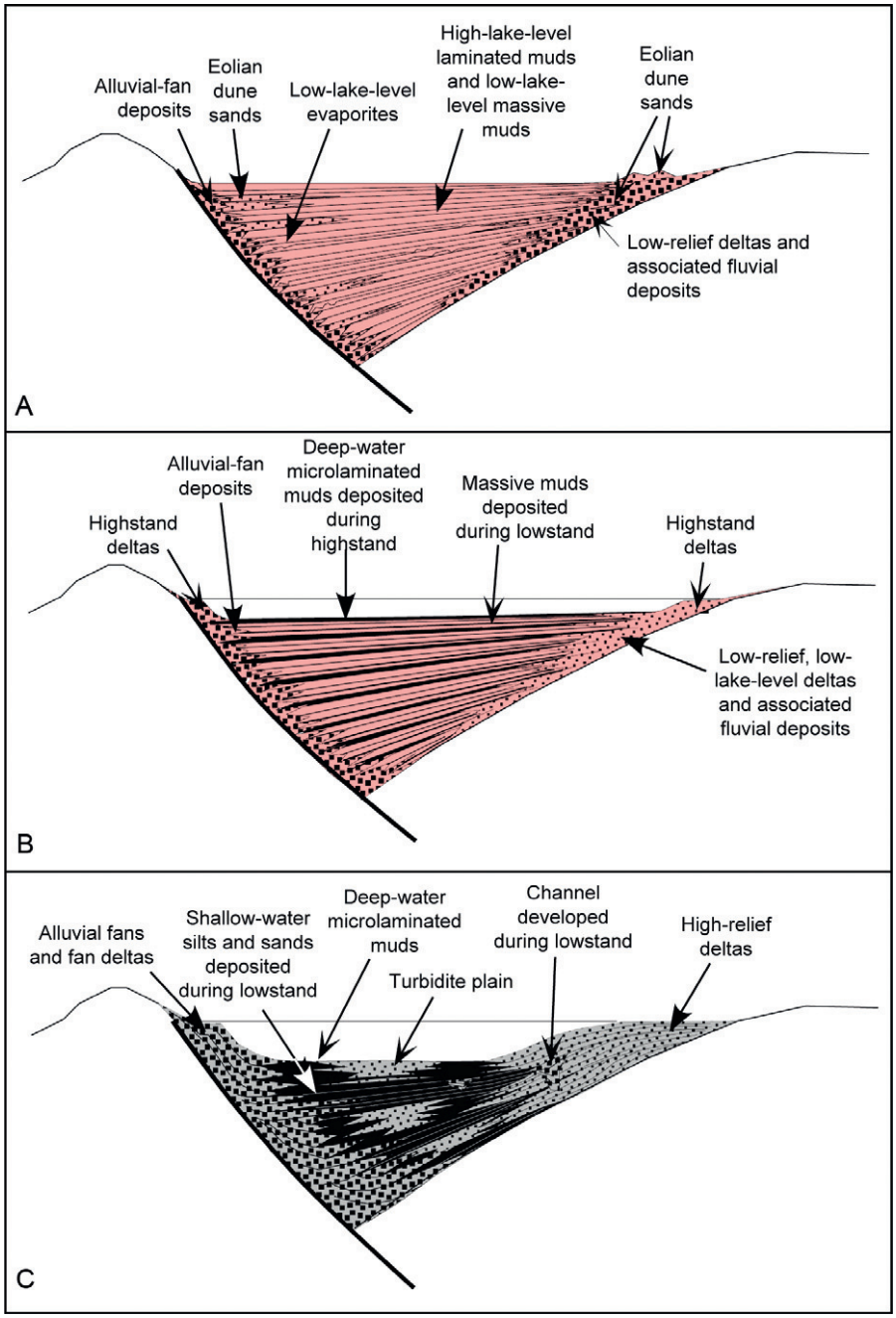

Figure 13.6 Cross-sectional diagrams showing rift-basin lacustrine architecture (*after Olsen, 1990).* (A) Arid type (e.g., Fundy basin during Norian time). (B) Intermediate type (e.g., Newark basin during Carnian time). (C) Humid type (e.g., Richmond basin during Carnian time).

As Pangea drifted northward, the vertical sequence of climate-sensitive facies within individual basins changed as the basins passed from one climate zone to another. Thus, in the rift basins of eastern North America (and Morocco), the transition from Carnian through Norian-age strata is characterized by apparent drying with shallow-water cyclical lacustrine strata predominating in the southern and central basins (Olsen and Kent, 2000; Olsen, 1997; Fig. 13.5). Conversely, in Greenland and offshore Norway, the vertical Late Triassic sequence within individual basins is from red beds and evaporites upward into black lacustrine, paludal, and paralic shales (Clemmensen, 1980; Jacobsen and van Veen, 1984). This vertical pattern within all of these basins fits the same basic geographic pattern consistent with a northward drift of central Pangea.

Rift-basin subsidence and uplift

Restorations based on seismic, field, and drill-hole data and modeling studies of thermal-maturation indices and fission-track analyses (Malinconico, 1999, 2003; Tseng et al., 1996) show that subsidence patterns in eastern North America varied spatially and temporally during rifting (Plate 13.1). The thickness of the Upper Triassic synrift rocks is much greater in the southern and central segments (5–10 km) than in the northern segment (<5 km) of the eastern North American rift system (Plate 13.1). Thus, subsidence rates (and extension rates) were greater in the south than in the north during the Late Triassic. Subsidence rates also varied through time. Unconformities separate the four Ts's in the southern and central rift basins (Fig. 13.5; Olsen, 1997). The TS II–TS III unconformity (Late Carnian) is well developed near the hinge margins of several southern and central rift basins, and the TS III–TS IV unconformity (latest Triassic to earliest Jurassic) is well developed near the hinge margins of some central basins (e.g., the Connecticut Valley and Fundy basins). Unconformities are also common in the northern rift basins (e.g., Driscoll et al., 1995; Foster and Robinson, 1993; McAlpine, 1990; Sinclair, 1995a,b). For example, at least four erosional events during Late Jurassic through Early Cretaceous time produced the Avalon unconformity in the northern segment (e.g., McAlpine, 1990; Fig. 13.5). Uplift and erosion of the southern Grand Banks exceeded that of the northern Grand Banks, producing a northward tilt of the basement during Late Jurassic through Early Cretaceous time. Generally, subsidence rates (and extension rates) increased during the final stages of rifting. In the central segment, subsidence rates during the earliest Jurassic were greater than those in the Late Triassic (Schlische and Anders, 1996). In the northern segment, sedimentation rates during the latest Jurassic to Early Cretaceous were greater than those in the Middle to latest Jurassic (McAlpine, 1990), reflecting renewed or accelerated extension prior to breakup.

Igneous activity

The CAMP includes flood basalts, dykes, and intrusive sheets. It is one of the world's largest igneous provinces (e.g., Hames et al., 2003; Marzolli et al., 1999; May, 1971; McHone, 1996, 2000; Olsen, 1999), affecting eastern North

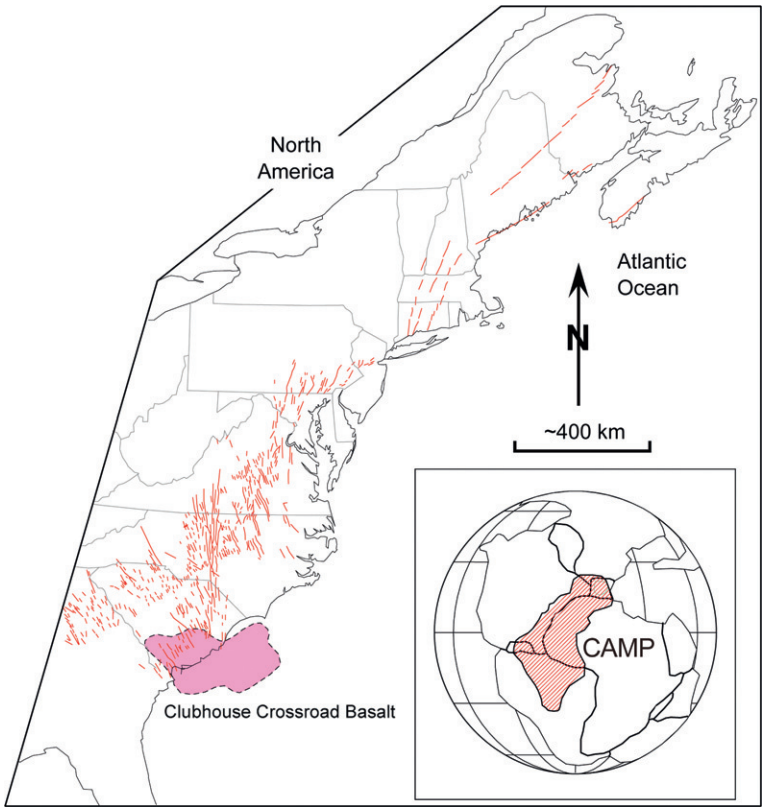

Figure 13.7
Early Jurassic-age diabase dykes (thin lines) in eastern North America and possible extent of Clubhouse Crossroads Basalt (Oh et al., 1995) (Modified from McHone, 2000, and McHone et al., (2004).

America, northern South America, northwestern Africa, and southwestern Europe (insert, Fig. 13.7). CAMP-related igneous activity occurred during the earliest Jurassic (~200 Ma; e.g., Dunning and Hodych, 1990; Hames et al., 2000; Hodych and Dunning, 1992; Olsen, 1999; Olsen et al., 1996b, 2003; Ragland et al., 1992; Schlische et al., 2003; Sutter, 1988; Turrin, 2000). The duration of this activity was short, less than 1 million years (Olsen et al., 1996b, 2003).

The expression of CAMP differs in the three segments of the eastern North American rift system. Generally, the intensity of CAMP magmatism (i.e., the number of dykes, sheets, and flows) increased from north to south (Figs. 13.3, 13.4, and 13.7). In the northern segment, CAMP rocks include lava-flow sequences found within the synrift section of the Jeanne d'Arc basin (Fig. 13.4C) and the NE-striking Avalon dyke of Newfoundland (Pe-Piper et al., 1992; Sinclair, 1995a). In the central segment, CAMP rocks include thick lava-flow sequences within the synrift section (Figs. 13.3B–D and 13.4D, E, G, and H), N- to NE-striking dykes (Figs. 13.3C, D, and 12.7), and intrusive sheets (Fig. 13.3C, D). In the southern segment, no CAMP lava-flow sequences are present within the synrift section (e.g., Olsen, 1997). Flows

are present in the postrift section (Behrendt et al., 1981; Hamilton et al., 1983; McBride et al., 1989). These postrift flows are flat-lying and locally overlie dipping synrift strata (Fig. 13.4M, N). The conventional interpretation is that these postrift basalts are about 185 Ma (Lanphere, 1983) and, thus, younger than CAMP-related flows of earliest Jurassic age (200 Ma). The data supporting this age, however, are suspect (e.g., Olsen et al., 2003; Ragland et al., 1992), and the postrift basalts may, in fact, be associated with CAMP. Intrusions (dykes and sheets) are abundant in the southern segment of the rift system (Figs. 13.3F and 13.4J, N). Most dykes are NW-striking, but some are NNW- to N-striking (e.g., King, 1971; Ragland, 1991; Ragland et al., 1983, 1992; Fig. 13.7). Dated dykes in the southern segment are ~200 Ma (e.g., Ganguli et al., 1995; Hames et al., 2000; Sachs et al., 1999; Stoddard et al., 1986). Igneous sheets intrude the synrift strata within many of the buried rift basins in the southern segment (Fig. 13.4N). Generally, these sheets are subhorizontal and cut across the dipping synrift strata, suggesting that they intruded at or near the end of rift-related tilting. Isotopic ages for these sheets are ~200 Ma (Olsen, 1998). Thus, in the southern segment of the rift system, igneous sheets and NW- and N-striking dykes are associated with CAMP. It is still uncertain, however, whether postrift flows, with their poorly constrained age, are associated with CAMP.

The passive margin of eastern North America, from the southern segment to the southern part of the central segment (i.e., from the Blake Plateau basin to the southern Scotian basin), is volcanic. A wedge of seaward-dipping reflectors (SDRs), presumably composed of volcanic and volcaniclastic rocks, is present near the continent-ocean boundary and is associated with the East Coast Magnetic Anomaly (Austin et al., 1990; Benson and Doyle, 1988; Hinz, 1981; Holbrook and Keleman, 1993; Keleman and Holbrook, 1995; Klitgord et al., 1988; Lizarralde and Holbrook, 1997; Oh et al., 1995; Sheridan et al., 1993; Figs. 13.1 and 13.2). The SDRs formed during the transition from rifting to drifting (e.g., Austin et al., 1990; Benson and Doyle, 1988; Hinz, 1981). The remainder of the passive margin of eastern North America, from the northern part of the central segment through the northern segment, lacks SDRs and, thus, is non-volcanic (Hopper et al., 2004; Keen and Potter, 1995; Shipboard Scientific Party, 2003).

In the central segment of the eastern North American rift system, CAMP-related basalt flows are *within* the synrift section (Fig. 13.5). Thus, CAMP activity occurred during rifting and before the rift/drift transition and the formation of the SDRs. In the southern segment, flat-lying basalt flows are roughly coeval with the formation of the SDRs (Oh et al., 1995). These postrift basalt flows reach the continent-ocean boundary (Fig. 13.7) and directly overlie SDRs in the Carolina trough (Fig. 13.2C) and directly underlie SDRs in the Blake Plateau basin. If these basalts are CAMP-related flows, then the rift/drift transition and the formation of the SDRs in the southern segment occurred during CAMP activity (earliest Jurassic). If the basalts are younger than CAMP activity, then the rift/drift transition and the formation of the SDRs in both the central *and* southern segments occurred after CAMP activity (Early Jurassic to early Middle Jurassic).

Strain state during rifting

Many faults in the eastern North American rift system are reactivated, preexisting zones of weakness. Thus, their orientations alone, without slip measurements, provide limited information about the strain state during rifting. Despite these limitations, structural analyses using fault/fracture orientations, slip measurements, dyke orientations (Fig. 13.7), subsidence patterns, and early seafloor-spreading directions (e.g., Klitgord and Schouten, 1986; Olsen and Schlische, 1990; Olsen et al., 1989; Ratcliffe and Burton, 1985; Schlische and Ackermann, 1995; Schlische, 1993; Srivastava et al., 2000; Withjack et al., 1995) suggest the following strain state during rifting. (1) During Late Triassic time, all three segments of the rift system were active, and the extension direction was approximately NW-SE. (2) During Early Jurassic time, only the central and northern segments were clearly active. In these segments, the extension direction was approximately NW–SE (as indicated, for example, by the NE-striking CAMP dykes in the central and northern segments). (3) During latest Jurassic and into Early Cretaceous time, only the northern segment was active, and the extension direction was roughly WNW–ESE (as indicated by the early seafloor-spreading directions between the eastern Grand Banks and Iberia).

Timing of rift/drift transition

The timing of the rift/drift transition for the three segments of the eastern North American rift system is poorly constrained. Marine magnetic data are limited (e.g., Klitgord and Schouten, 1986) or contested (e.g., Driscoll et al., 1995; Shipboard Scientific Party, 2003; Srivastava et al., 2000); no wells have penetrated the oldest postrift strata observed on seismic data near the continent-ocean boundary (e.g., Benson, 2003; Klitgord et al., 1988; Shipboard Scientific Party, 2003); and postrift erosion has removed the youngest synrift strata from most rift basins (Klitgord et al., 1988). In addition, postrift structures and deposition associated with salt flow can resemble synrift deformation and deposition. Despite these limitations, the available marine magnetic data and ages of the synrift and postrift rocks provide some constraints on the timing of the rift/drift transition and the onset of seafloor spreading in eastern North America.

The youngest *preserved* synrift rocks in the southern segment of the eastern North American rift system are Late Triassic (Norian) in age (e.g., Olsen et al., 1989; Olsen, 1997; Fig. 13.5). Modeling studies based on thermal-maturation indices (Malinconico, 2003) and fission-track analyses (Tseng et al., 1996) indicate that, if any strata were deposited in the southern rift basins during latest Triassic to Early Jurassic time, they were very thin. Thus, subsidence had slowed substantially or stopped by Early Jurassic time. As discussed above, NW-striking, CAMP-related dykes of earliest Jurassic age (Figs. 13.3F and 13.7) cut across the southern rift basins and provide additional evidence that the NW-SE extension associated with rifting had ceased in the southern segment of the eastern North American rift system by Early Jurassic time (Schlische et al., 2003; Withjack et al., 1998). Thus, available geological data indicate that widespread rifting had ceased in the southern segment of the eastern North

American rift system by latest Triassic to earliest Jurassic time. The age of the oldest postrift rocks in the southern segment of the eastern North American rift system is controversial. As noted above, the eruption of postrift basalt flows appears to be roughly coeval with the formation of the SDRs and, by inference, the rift/drift transition in the southern segment of the eastern North American rift system (Oh et al., 1995). If these postrift basalts are CAMP-related flows, then drifting commenced soon after the cessation of rifting in latest Triassic to earliest Jurassic time. If these postrift basalts are younger than CAMP flows (i.e., ~185 Ma; Lanphere, 1983), then drifting began during Early Jurassic time, ~15 million years after the cessation of widespread rifting in the southern segment. With this latter scenario, extension in the southern segment became focused near the eventual site of continental breakup during a prolonged transition from rifting to drifting.

The youngest *preserved and dated* synrift rocks in the exposed rift basins in the central segment of the eastern North American rift system are Early Jurassic (early Sinemurian) in age (Olsen, 1997; Fig. 13.5). Thus, rifting continued into Early Jurassic time in the central segment. The age of the oldest postrift strata is controversial. Researchers, using offshore seismic and well data, have identified the postrift unconformity at several different stratigraphic levels, ranging from Early Jurassic to early Middle Jurassic (e.g., Benson, 2003; Klitgord et al., 1988; MacLean and Wade, 1992; Olsen, 1997; Welsink et al., 1989). The presence of reworked palynomorphs, multiple unconformities, and synrift and postrift salt movement has contributed to this debate (Fig. 13.5). On the conjugate margin of northwest Morocco, seismic-reflection profiles and well data, provided by industry, suggest that the oldest postrift strata are Sinemurian/Pliensbachian in age (Hafid, 2000; Medina, 1995; Fig. 13.5). Thus, rifting in the central segment of the eastern North America rift system had ceased and drifting had commenced between late Sinemurian and early Middle Jurassic time. If the Moroccan seismic and well data are reliable, then drifting had commenced soon after the cessation of rifting in Early Jurassic time (Sinemurian/Pliensbachian).

Magnetic anomalies show that the rift/drift transition between the eastern Grand Banks and Iberia was diachronous, starting earlier in the south (as early as earliest Berriasian) and later in the north (Aptian; e.g., Dean et al., 2000; Driscoll et al., 1995; Shipboard Scientific Party, 2003; Srivastava et al., 2000; Fig. 13.5). In the northern Jeanne d'Arc and Flemish Pass basins, the youngest synrift strata are late Early Cretaceous (Aptian to Albian) in age (e.g., Driscoll et al., 1995; Foster and Robinson, 1993; Sinclair, 1995a,b). The youngest of these strata are, in fact, younger than the oceanic crust directly adjacent to the northeastern Grand Banks (magnetic anomaly M0; Fig. 13.5). Thus, it is likely that the youngest of these strata are associated with postrift salt movement (Tankard and Welsink, 1987) and/or the subsequent rifting and separation of the northern Grand Banks from Greenland/Europe (Foster and Robinson, 1993; Sinclair, 1995b; Tankard and Welsink, 1987). Thus, rifting had ceased and drifting between the eastern Grand Banks and Iberia had commenced during late Early Cretaceous time in the northern part of the northern segment.

Postrift deformation

Recent work (Schlische, 2003; Schlische et al., 2003; Withjack et al., 1995, 1998) shows that postrift contractional deformation, long recognized in eastern North America (e.g., deBoer and Clifton, 1988; Sanders, 1963; Shaler and Woodworth, 1899; Wise, 1992), is more pervasive and represents more shortening than previously reported. Many of these postrift contractional structures are inversion structures (i.e., extensional structures reactivated as contractional structures). No collision or subduction zones existed near eastern North America during Mesozoic time. Thus, the cause of the postrift shortening/inversion on the passive margin of central eastern North America is enigmatic. Incipient ridge-push forces and/or an initial continental resistance to plate motion may produce shortening and inversion on passive margins during the early stages of seafloor spreading (Boldreel and Andersen, 1993; Bott, 1992; Dewey, 1988; Schlische et al., 2003; Withjack et al., 1995).

Examples of postrift contractional structures in the southern segment of the eastern North American rift system include (1) NE-striking basement-involved reverse faults and associated folds in the Richmond basin (Shaler and Woodworth, 1899; Venkatakrishnan and Lutz, 1988); (2) NE-striking anticlines above NE-striking intrabasinal faults of the Taylorsville basin (LeTourneau, 1999, 2003; Fig. 13.4J, K); and (3) the Cooke fault, a NE-striking, basement-involved reverse fault in South Carolina with about 140 m of reverse displacement before the eruption of the postrift basalts (Behrendt et al., 1981; Hamilton et al., 1983). Inversion may also be responsible for some of the anomalously high stratal dips recorded in many of the exposed southern rift basins. For example, the Danville basin contains relatively steep dipping beds (~45°; Fig. 13.4L). Experimental clay models (Eisenstadt and Withjack, 1995) indicate that gentle stratal dips develop during low to moderate amounts of extension but steepen appreciably during inversion. Based on the orientation of the above structures and the NW-striking CAMP-related dykes, the shortening direction in the southern segment was NW–SE. This contractional episode occurred prior to and continued through CAMP activity. Considerable uplift and erosion occurred throughout the southern segment after rifting. The Danville basin is exceptionally narrow relative to its length (Fig. 13.3F). It acquired its unusual geometry by undergoing significant postrift erosion (Plate 13.1). The Taylorsville basin also experienced up to 3 km of postrift erosion, with the largest amount of erosion occurring over inversion-related anticlines (Malinconico, 2003).

Examples of postrift contractional deformation in the central segment of the eastern North American rift system include (1) broad NE-trending anticlines in the hanging walls of gently dipping, NE-striking border faults in the Fundy basin (Withjack et al., 1995); (2) tight ENE- to E-trending synclines and anticlines formed in proximity to the ENE- to E-striking Minas fault of the Fundy basin (Withjack et al., 1995; Fig. 13.4D, E); (3) tightening of the fault-displacement

folds that formed during rifting in the Fundy and Newark basins (inserts, Figs. 13.3B and 13.4D); and (4) WNW-striking axial planar cleavage in some WNW-trending folds in the Newark basin (e.g., Lucas et al., 1988). Small-scale faults (Elder Brady, 2003; deBoer, 1992; deBoer and Clifton, 1988; Elder Brady et al., 2003), calcite twins (Lomando and Engelder, 1984), axial-planar cleavage (Lucas et al., 1988), and folds not directly related to preexisting extensional faults (Baum, 2002; Baum et al., 2003) indicate a N–S to NE–SW shortening direction for the contractional episode in the central segment of the eastern North American rift system. Shortening began after CAMP time and after the deposition of the Jurassic (Hettangian and Sinemurian) synrift strata that overlie the CAMP extrusives (Withjack et al., 1995). Thus, this contractional episode started after the contractional episode in the southern segment. Withjack et al. (1995), using information from the offshore Orpheus basin, proposed that most shortening occurred before or during Early Cretaceous time. Considerable uplift and erosion occurred in the central segment after rifting. The Newark basin underwent 2 to 5+ km of postrift erosion (e.g., Malinconico, 1999; Pratt et al., 1988; Steckler et al., 1993).

As discussed previously, salt flow produced a variety of structures within the northeastern rift basins of the central segment of the eastern North American rift system. Many of these salt-related structures may be postrift structures. For example, MacLean and Wade (1992) report that a series of detached faults developed within the Orpheus basin during Early to Middle Jurassic time as salt flowed toward the east, down the basin axis. Depending on the exact timing of the rift/drift transition in the central segment, these detached faults of Early to Middle Jurassic age may be synrift and/or postrift structures (Fig. 13.5).

Postrift deformation also occurred in the northern segment of the eastern North American rift system. Foster and Robinson (1993), Sinclair (1995a,b), Sinclair et al. (1999), and Tankard and Welsink (1987) report the formation of NW-striking normal faults and the reactivation of preexisting, NE-striking normal faults as oblique-slip faults during Aptian to Albian time in the Jeanne d'Arc and Flemish Pass basins. The age of this deformation is younger than the age of the oceanic crust directly adjacent to the eastern Grand Banks (magnetic anomaly M0). Thus, these structures formed after the onset of drifting between the eastern Grand Banks and Iberia, and reflect a change from WNW–ESE extension during rifting to NE–SW extension during drifting. If these structures reflect the basement strain state, then the NE–SW extension is likely associated with the subsequent rifting and separation of the northern Grand Banks from Greenland/Europe (Foster and Robinson, 1993; Sinclair, 1995b; Sinclair et al., 1999). Alternatively, this deformation may reflect postrift salt movement induced by the northward tilting of the Grand Banks during the development of the Avalon unconformity (Tankard and Welsink, 1987).

13.3 Evolution of eastern North America

Paleozoic orogenic activity

Orogenic activity associated with subduction, accretion, and collision occurred throughout eastern North America during much of Paleozoic time (Plate 13.2A). Numerous gently to moderately dipping, basement-involved thrust faults formed during these Paleozoic orogenies (e.g., Hutchinson et al., 1988; Keen et al., 1991a). The final collisional event, the late Paleozoic Alleghanian–Variscan orogeny, welded the North American and African continents and created the Pangean supercontinent (e.g., Rankin, 1994; Rast, 1988). The collision probably elevated parts of eastern North America well above sea level, leading to significant erosion.

Late Triassic rifting

In response to NW–SE regional extension, rifting occurred throughout eastern North America by Late Triassic time (Plate 13.2B). Simultaneously, rifting occurred in western Europe (e.g., offshore Norway and Iberia), western Africa (e.g., Morocco), and northern South America as Pangea split apart. Many preexisting Paleozoic structures were reactivated as normal faults or oblique-slip faults, and asymmetric rift basins began to develop. Initially, the rift basins were narrow. As rifting progressed, the rift basins widened considerably as border faults lengthened and linked (e.g., Schlische, 1992). Although rifting occurred in all three segments of the rift system during Late Triassic time, subsidence was considerably greater in the southern and central segments than in the northern segment (e.g., Plate 13.1). Residual uplift associated with the late Paleozoic collision may have continued to produce erosion in eastern North America, except in the rift basins where subsidence exceeded erosion. Footwall uplift associated with the rift-basin border faults would have produced additional erosion on the rift-basin flanks. Fluvial and lacustrine deposits filled the rift basins.

Latest Triassic/earliest Jurassic

Rifting continued in the central and northern segments of the eastern North American rift system during latest Triassic/earliest Jurassic time (Plate 13.2C). The rift basins became much wider and deeper as rifting progressed. Continental (fluvial and lacustrine) deposits filled most rift basins. Marine encroachment from the north, however, led to the deposition of evaporites (mostly halite) in the northern segment and the northeastern basins of the central segment of the eastern North American rift system.

By latest Triassic/earliest Jurassic time, widespread rifting had significantly declined or ceased in the southern segment of the eastern North American rift system. Instead, extension became focused near the site of eventual continental breakup. The inactive rift basins began to erode and narrow. Several processes may have led to this erosion, including (1) residual uplift associated with the late Paleozoic

collision, (2) postrift shortening and inversion, and/or (3) high lithospheric temperatures associated with the impending CAMP magmatism and seafloor spreading.

Earliest Jurassic

Rifting continued in the central and northern segments of the eastern North American rift system during earliest Jurassic time (Plate 13.2D1 and D2). In the central segment, subsidence rates increased significantly, and major intrabasin faults formed in several rift basins. CAMP magmatism resulted in the emplacement of NE-trending dykes, diabase sills, and synrift basalt flows throughout the central and northern segments. Dyke trends suggest that extension was NW–SE during CAMP magmatic activity in the central and northern segments.

In the southern segment, the inactive rift basins continued to erode and narrow. CAMP magmatism resulted in the emplacement of NW-striking dykes and diabase sheets. These dyke trends indicate that the NW–SE extension associated with rifting had ceased before CAMP activity. In fact, NW–SE shortening replaced the NW–SE extension. In response, NE-striking reverse faults formed and many rift-related normal faults experienced reverse movement. If the postrift basalts in the southern segment are CAMP-related flows, then the rift/drift transition and the formation of a volcanic wedge occurred during earliest Jurassic time in the southern segment (Plate 13.2D1). If the postrift basalts in the southern segment are younger than CAMP activity, then extension shifted to the eventual site of continental breakup during a prolonged rift/drift transition (Plate 13.2D2).

Early to early Middle Jurassic

During Early to early Middle Jurassic time, the basins in the northern segment became wider and deeper in response to thermal subsidence or continued rifting (Plate 13.2E). Marine sediments filled the basins.

Rifting had ceased and drifting had commenced in the central segment during Early to early Middle Jurassic time. In the southern half of the central segment, a volcanic wedge formed near the continent-ocean boundary. In the northern half of the central segment, no volcanic wedge developed. During the rift/drift transition, the inactive rift basins in the central segment began to erode and narrow. Again, several processes may have led to this erosion, including (1) residual uplift associated with the late Paleozoic collision, (2) postrift shortening and inversion, and/or (3) high lithospheric temperatures associated with incipient seafloor spreading.

If the postrift basalts in the southern segment are CAMP-related flows, then drifting was under way in the southern segment of eastern North America during Early Jurassic time (Plate 13.2E1). If the postrift basalts in the southern segment are younger than CAMP activity, then the transition from rifting to drifting occurred during Early to early Middle Jurassic time (Plate 13.2E2) with the formation of the volcanic wedge near the continent-ocean boundary.

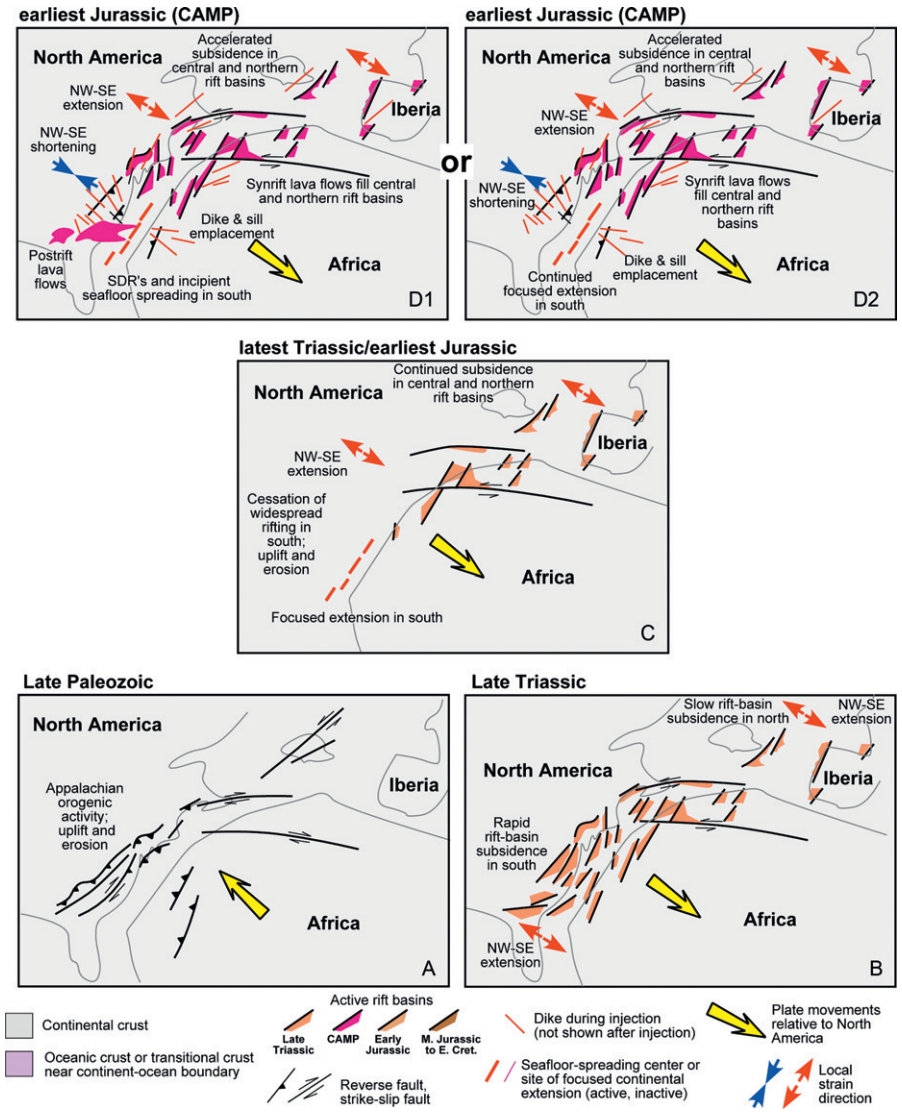

Plate 13.2 Cartoon showing tectonic evolution of the eastern North American rift system. (A) Late Paleozoic – orogenic activity creates preexisting zones of weakness and uplift. (B) Late Triassic – rifting under way throughout eastern North America. (C) Latest Triassic/earliest Jurassic – widespread rifting in southern segment replaced by focused extension near site of eventual continental breakup, and continued rifting in central and northern segments. (D1) Earliest Jurassic – CAMP igneous activity producing flows, intrusive sheets, and dykes throughout eastern North America and seaward-dipping reflectors (SDRs) in southern segment. (D2) Earliest Jurassic – CAMP igneous activity without postrift basalts and SDRs in southern segment.

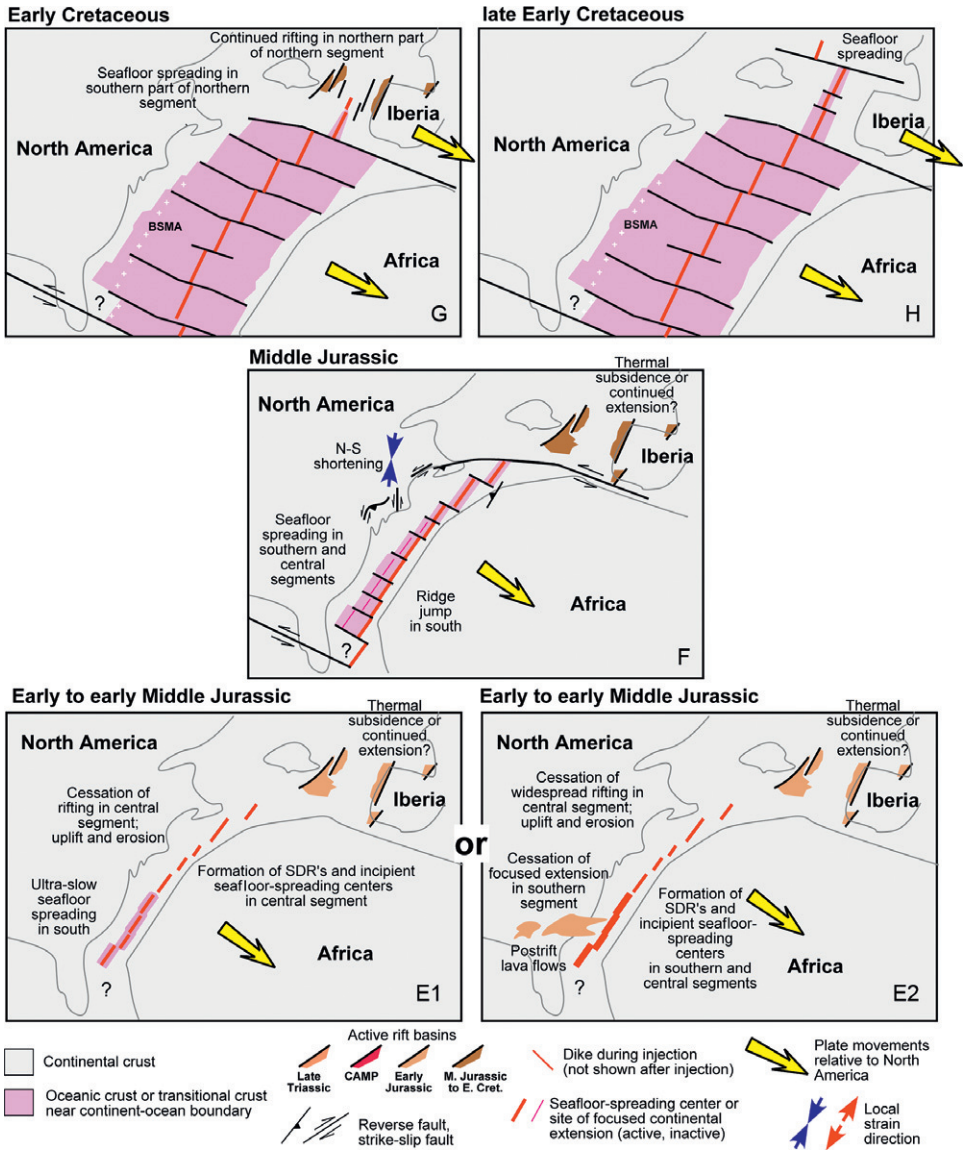

Plate 13.2 Cont'd (E1) Early Jurassic to early Middle Jurassic – drifting in southern segment, widespread rifting in central segment replaced by focused extension near site of eventual continental breakup, SDRs at southern end of central segment, and continued rifting in northern segment. (E2) Early Jurassic to early Middle Jurassic – eruption of postrift basalts in southern segment, SDRs in southern segment and southern part of central segment, and continued rifting in northern segment. (F) Middle Jurassic – drifting in southern and central segments with ridge jump, and continued rifting or quiet episode in northern segment. (G) Early Cretaceous – drifting in southern and central segments, cessation of rifting in southern part of northern segment, and continued rifting in northern part of northern segment. (H) Late Early Cretaceous – drifting in southern, central, and northern segments.

Middle Jurassic

During Middle Jurassic time, the basins in the northern segment continued to widen and deepen in response to thermal subsidence or continued rifting (Plate 13.2F). Marine sediments filled the basins.

Drifting was under way in the southern and central segments by Middle Jurassic time. The exposed rift basins continued to erode and narrow. The continental margin continued to subside, and postrift strata progressively onlapped the postrift unconformity. Contractional structures associated with N–S to NE–SW shortening may have developed in the central segment at this time.

At about 170 Ma, the southern part of the Mid-Atlantic ridge jumped to the east, producing the Blake Spur Magnetic Anomaly (Vogt, 1973). Seafloor-spreading rates were slow before the ridge jump. About 130 km of oceanic crust separates the East Coast Magnetic Anomaly from the Blake Spur Magnetic Anomaly offshore of the southern segment of the eastern North American rift system (Klitgord and Schouten, 1986). If seafloor spreading began during CAMP activity (200 Ma), then full spreading rates were about 4 mm/yr. If seafloor spreading began about 185 Ma, then full-spreading rates were about 8 mm/yr. These rates are similar to those of the ultra-slow spreading Gakkel ridge (Dick et al., 2003; Michael et al., 2003).

Late Jurassic to Early Cretaceous

During latest Jurassic and Early Cretaceous time, subsidence rates increased significantly in the northern segment of the eastern North American rift system, reflecting renewed or accelerated extension (Plate 13.2G, H). The southern end of the northern segment began to rise and erode, producing the Avalon unconformity.

Drifting, now with faster spreading rates (e.g., Benson, 2003; Klitgord and Schouten, 1986), continued in the southern and central segments during Late Jurassic through Early Cretaceous time. The exposed western rift basins continued to erode and narrow, and postrift strata continued to progressively onlap the postrift unconformity.

Rifting ceased in the northern segment of the eastern North American rift system by the end of Early Cretaceous time. The cessation of rifting and the onset of drifting between the eastern Grand Banks and Iberia were diachronous, progressing from south (as early as Berriasian) to north (Aptian). Seafloor-spreading rates were slow, about 14 mm/yr, during the early stages of drifting (Hopper et al., 2004; Srivastava et al., 2000).

13.4 Summary and discussion

1. The eastern North American rift system, extending from northern Florida to the eastern Grand Banks, consists of a series of asymmetric rift basins. The border faults of many rift basins are reactivated, preexisting contractional structures.

2. Widespread rifting in the three segments of the eastern North America rift system began by the Late Triassic.
3. In the southern segment, widespread rifting continued until the latest Triassic/earliest Jurassic. In the central segment, widespread rifting continued into the Early Jurassic (and possibly into the early Middle Jurassic). In the northern segment, the final stage of widespread rifting ended by the late Early Cretaceous. Thus, the cessation of widespread rifting was diachronous in eastern North America.
4. It is unclear how the cessation of widespread rifting relates to the rift/drift transition. If the rift/drift transition occurred immediately after the cessation of widespread rifting, then the rift/drift transition and the formation of oceanic crust were diachronous, occurring first in the southern segment, second in the central segment, and last in the northern segment. If the cessation of widespread rifting reflected a change from distributed extension to focussed extension near the eventual site of continental breakup, then it is unclear whether the rift/drift transition and the formation of oceanic crust were synchronous or diachronous for the southern and central segments.
5. The CAMP developed simultaneously (earliest Jurassic, $\sim$200 Ma) throughout eastern North America. This magmatic activity included the intrusion of diabase sheets and dykes and the eruption of tholeiitic basalts. It occurred after the cessation of widespread rifting in the southern segment and during widespread rifting in the central and northern segments.
6. The passive margin of eastern North America, from northern Florida to southern Nova Scotia, is volcanic, characterized by seaward-dipping reflectors (SDRs) near the continental-oceanic boundary. The remainder of the margin, from northern Nova Scotia to the eastern Grand Banks, lacks SDRs and is, thus, non-volcanic. It is unclear whether the SDRs in the southern segment are younger than or coeval with CAMP. The SDRs in the central segment are younger than CAMP.
7. The deformational regime changed substantially after rifting in the southern and central segments. In the southern segment, NW–SE shortening (inversion) replaced synrift extension. In the central segment, N–S to NE–SW shortening (inversion) replaced synrift extension. The cause of this postrift shortening/inversion is enigmatic. Detached structures associated with salt flow also developed in the central segment after the cessation of widespread rifting.
8. In the northern segment, structures associated with NE–SW extension developed after the rifting and breakup of the eastern Grand Banks from Iberia. If these structures involve the basement, then the NE–SW extension is likely associated with the subsequent rifting and breakup of the northern Grand Banks from Greenland/Europe. Alternatively, these structures may detach within salt, reflecting postrift salt flow, not basement-involved deformation.

Acknowledgments

We thank Albert Bally for his support during this research. We also thank Albert Bally, Mark Baum, Jennifer Elder Brady, Dave Roberts, Robert Sheridan, and Ian Sinclair for their thought-provoking comments and discussions. The Petroleum Research Fund of the American Chemical Society provided support for some of the research presented in this chapter.

References

Austin, J.A., et al., 1990. Crustal structure of the Southeast Georgia embayment-Carolina trough: preliminary results of a composite seismic image of a continental suture (?) and a volcanic passive margin. Geology 18, 1023–1027.

Baum, M., 2002. 3-D Geometry of Inversion Structures in the Mesozoic Fundy Rift Basin, M.S. Thesis, Rutgers University, p. 51.

Baum, M.S., Withjack, M.O., Schlische, R.W., 2003. Controls of structural geometries associated with rift-basin inversion. Am. Assoc. Pet. Geol., Program & Abstracts 12, A10.

Behrendt, J.C., 1986. Structural interpretation of multichannel seismic reflection profiles crossing the southeastern United States and the adjacent continental margin – decollements, faults, Triassic (?) basins and Moho reflections. In: Barszangi, M., Brown, L. (Eds.), Reflection Seismology, the Continental Crust, Geodynamic Series, vol. 14, American Geophysical Union, Washington, D.C., pp. 201–214.

Behrendt, J.C., Hamilton, R.M., Ackermann, H.D., Henry, V.J., 1981. Cenozoic faulting in the vicinity of the Charleston, South Carolina, 1886 earthquake. Geology 9, 117–122.

Benson, R.N., 2003. Age estimates of the seaward-dipping volcanic wedge, earliest oceanic crust, and earliest drift-stage sediments along the North Atlantic continental margin. In: Hanes, W.E., McHone, J.G., Renne, P.R., Ruppel, C. (Eds.), The Central Atlantic Magmatic Province, Insights from Fragments of Pangea, Geophysical Monograph, vol. 136. American Geophysical Union, Washington, D.C., pp. 61–75.

Benson, R.H., Doyle, R.G., 1988. Early Mesozoic rift basins and the development of the United States middle Atlantic continental margin. In: Manspeizer, W. (Ed.), Triassic-Jurassic Rifting, Continental Breakup and the Origin of the Atlantic Ocean Passive Margins, Part A. Elsevier, New York, pp. 99–127.

Boldreel, L.O., Andersen, M.S., 1993. Late Paleocene to Miocene compression in the Faero-Rockall area. In: Parker, J.R. (Ed.), Petroleum Geology of Northwest Europe. Geological Society of London, pp. 1025–1034.

Bott, M.H.P., 1992. The stress regime associated with continental break-up. In: Storey, B.C., Alabaster, T., Pankhurst, R.J. (Eds.), Magmatism and the Causes of Continental Break-up, Geological Society Special Publication, vol. 68, pp. 125–136.

Channell, J.E.T., Kozur, H.W., Sievers, T., Mock, R., Aubrecht, R., Sykora, M., 2003. Carnian-Norian bio-magnetostratigraphy at Silicka Brezova (Slovakia): correlation to other Tethyan sections and to the Newark Basin. Paleogeogr. Palaeoclimatol. Palaeoecol. 191, 65–109.

Clemmensen, L.B., 1980. Triassic rift sedimentation and palaeogeography of central East Greenland. Grøn geol Undersøg, 136p.

Clemmensen, L.B., Kent, D.V., Jenkins, F.A., 1998. A Late Triassic lake system in East Greenland; facies, depositional cycles and palaeoclimate. Palaeogeogr. Palaeoclimatol. Palaeoecol. 140, pp. 135–159.

Contreras, J., Scholz, C.H., King, G.C.P., 1997. A general model of rift basin evolution: constraints of first order stratigraphic observations. J. Geophys. Res. 102, 7673–7690.

Dean, S.M., Minshull, T.A., Whitmarsh, R.B., Louden, K.E., 2000. Deep structure of the ocean-continent transition in the southern Iberia Abyssal Plain from seismic refraction profiles: the IAM-9 transect at 40°20′ N. J. Geophys. Res. 105, 5859–5885.

deBoer, J.Z., 1992. Stress configurations during and following emplacement of ENA basalts in the northern Appalachians. In: Puffer, J.H., Ragland, P.C. (Eds.), Eastern North American Mesozoic Magmatism. Geological Society of America Special Paper, vol. 268, pp. 361–378.

deBoer, J.Z., Clifton, A.E., 1988. Mesozoic tectogenesis: development and deformation of "Newark" rift zones in the Appalachians (with special emphasis on the Hartford basin, Connecticut). In: Manspeizer, W. (Ed.), Triassic-Jurassic Rifting, Continental Breakup and the Origin of the Atlantic Ocean Passive Margins, Part A. Elsevier, New York, pp. 275–306. [Clifton was incorrectly published as Clifford.]

deVoogd, B., Keen, C.E., Kay, W.A., 1990. Fault reactivation during Mesozoic extension in eastern offshore Canada. Tectonophysics 173, pp. 567–580.

Dewey, J.F., 1988. Lithospheric stress, deformation, and tectonic cycles: the disruption of Pangaea and the closure of the Tethys. In: Audley-Charles, M.G., Hallam, A. (Eds.), Gondwana and Tethys, Geological Society Special Publication, vol. 37, pp. 23–40.

Dick, H.J.B., Lin, J., Schouten, H., 2003. An ultraslow-spreading class of ocean ridge. Nature 426, 405–412.

Driscoll, N.E., Hogg, J.R., Christie-Blick, N., Karner, G.D., 1995. Extensional tectonics in the Jeanne d'Arc basin, offshore Newfoundland: implications for the timing of break-up between Grand Banks and Iberia. In: Scrutton, R.A., Stoker, M.S., Shimmield, G.B., Tudhoope, A.W. (Eds.), The Tectonics, Sedimentation and Palaeoceanography of the North Atlantic Region, Geological Society Special Publication, vol. 90, pp. 1–28.

Dunning, G.R., Hodych, J.P., 1990. U-Pb zircon and baddeleyite age for the Palisade and Gettysburg sills of northeast United States: implications for the age of the Triassic-Jurassic boundary. Geology 18, 795–798.

Eisenstadt, G., Withjack, M.O., 1995. Estimating inversion: results from clay models. In: Buchanan, J.G., Buchanan, P.G. (Eds.), Basin Inversion, Geological Society Special Publication, vol. 88, pp. 119–136.

Elder Brady, J.A., 2003. Effectiveness of small-scale structures in deciphering the tectonic history of the Fundy rift basin. M.S. thesis, Rutgers University.

Elder Brady, J.A., Schlische, R.W., Withjack, M.O., 2003. Rift-basin inversion: evidence from small-scale structures. Am. Assoc. Pet. Geol., Program & Abstracts 12, A49.

Et-Touhami, M., 2000. Lithostratigraphy and depositional environments of Lower Mesozoic evaporites and associated red beds, Khemisset basin, northwestern Morocco. In: Bachmann, G., Lerche, I. (Eds.), Epicontinental Triassic, Volume 2. Zentralblatt fur Geologie und Palaontologie, VIII, pp. 1217–1241.

Enachescu, M.E., 1987. The tectonic and structural framework of the northwest Newfoundland continental margin. In: Beaumont, C., Tankard, A.J. (Eds.), Sedimentary Basins and Basin-Forming Mechanisms, Canadian Society of Petroleum Geologists Memoir, vol. 12, pp. 117–145.

Faill, R.T., 1973. Tectonic development of the Triassic Newark-Gettysburg basin in Pennsylvania. Geol. Soc. Am. Bull. 84, 725–740.

Faill, R.T., 1988. Mesozoic tectonics of the Newark basin, as viewed from the Delaware River. In: Husch, J.M., Hozik, M.J. (Eds.), Geology of the central Newark basin, field guide and proceedings, Fifth Meeting of the Geological Association of New Jersey, Rider College, Lawrenceville, pp. 19–41.

Faill, R.T., 2003. The early Mesozoic Birdsboro central Atlantic margin basin in the Mid-Atlantic region, eastern United States. Geol. Soc. Am. Bull. 115, 406–421.

Foster, D.G., Robinson, A.G., 1993. Geological history of the Flemish Pass basin, offshore Newfoundland. AAPG Bull. 77, 588–609.

Ganguli, P.M., Kunk, M.J., Wintsch, R.P., Dorais, M.J., Sacks, P.E., 1995. High precision sanidine $^{40}Ar/^{39}Ar$ results from Mesozoic rhyolite dikes near Lake Gaston, North Carolina and Virginia. Geol. Soc. Am., Abstract with Programs 27, 45.

Hafid, M., 2000. Triassic-Early Jurassic extensional systems and their Tertiary inversion, Essaouira basin (Morocco). Mar. Petrol. Geol. 17, 409–429.

Hames, W.E., Renne, P.R., Ruppel, C., 2000. New evidence for geologically instantaneous emplacement of earliest Jurassic Central Atlantic magmatic province basalts on the North American margin. Geology 28, 859–862.

Hames, W., McHone, J.G., Renne, P., Ruppell, C. (Eds.), 2003. The Central Atlantic Magmatic Province, Insights from Fragments of Pangea. In: Geophysical Monograph, vol. 136, Washington, D.C., American Geophysical Union, 267p.

Hamilton, R.M., Behrendt, J.C., Ackermann, H.D., 1983. Land multichannel seismic-reflection evidence for tectonic features near Charleston, South Carolina. In: Gohn, G.S. (Ed.), Studies Related to the Charleston, South Carolina, Earthquake of 1886 – Tectonics and Seismicity, Geological Survey Professional Paper, vol. 1313, pp. I1–I18.

Hinz, K., 1981. A hypothesis on terrestrial catastrophes; wedges of very thick, oceanward-dipping layers beneath passive continental margins: Geol. Jb. E22, 3–38.

Hodych, J.P., Dunning, G.R., 1992. Did the Manicouagan impact trigger end-of-Triassic mass extinction? Geology 20, 51–54.

Holbrook, W.S., Keleman, P.B., 1993. Large igneous province on the US Atlantic margin and implications for magmatism during breakup. Nature 364, 433–436.

Holser, W.T., Clement, G.P., Jansa, L.F., Wade, J.A., 1988. Evaporite deposits of the North Atlantic Rift. In: Manspeizer, W. (Ed.), Triassic-Jurassic Rifting: Continental Breakup and the Origin of the Atlantic Ocean and Passive Margins, Part A, Developments in Geotectonics, vol. 22. Elsevier, Amsterdam, pp. 525–556.

Hopper, J.R., et al., 2004. Continental breakup and the onset of ultraslow seafloor spreading off Flemish Cap on the Newfoundland rifted margin. Geology 32, 93–96.

Hutchinson, D.R., Klitgord, K.D., 1988. Evolution of rift basins on the continental margin off southern New England. In: Manspeizer, W. (Eds.), Triassic-Jurassic Rifting, Continental Breakup and the Origin of the Atlantic Ocean Passive Margins, Part A. Elsevier, New York, pp. 81–98.

Hutchinson, D.R., Klitgord, K.D., Lee, M.W., Trehu, A.M., 1988. U.S. Geological Survey deep seismic reflection profile across the Gulf of Maine. Geol. Soc. Am. Bull. 100, 172–184.

Jacobsen, V.W., van Veen, P., 1984. The Triassic offshore Norway north of 62N. In: Spencer, A.M. et al. (Eds.), Petroleum Geology of the North European Margin. Norwegian Petroleum Society, Graham & Trotman, London, pp. 317–327.

Keen, C.E., Potter, D.P., 1995. The transition from a volcanic to a nonvolcanic rifted margin off eastern Canada. Tectonics 14, 359–371.

Keen, C.E., Boutilier, R., deVoogd, B., Mudford, B., Enachescu, M.E., 1987. Crustal geometry and extensional models for the Grand Banks, eastern Canada: constraints from deep seismic reflection data. In: Beaumont, C., Tankard, A.J. (Eds.), Sedimentary Basins and Basin-Forming Mechanisms. Canadian Society of Petroleum Geologists, Memoir, vol. 12, pp. 101–115.

Keen, C.E., Kay, W.A., Keppie, J.D., Marillier, F., Pe-Piper, G., Waldron, J.W.F., 1991a. Deep seismic reflection data from the Bay of Fundy and Gulf of Maine: tectonic implications for the northern Appalachians. Can. J. Earth Sci. 28, 1096–1111.

Keen, C.E., Kay, W.A., MacLean, B.C., 1991b. A deep seismic reflection profile across the Nova Scotia continental margin, offshore eastern Canada. Can. J. Earth Sci. 28, 1112–1120.

Keleman, P.B., Holbrook, W.S., 1995. Origin of thick, high-velocity igneous crust along the U.S. east coast margin. J. Geophys. Res. 100, 10177–110094.

Kent, D.V., Olsen, P.E., 1997. Magnetostratigraphy and paleopoles from the Late Triassic Dan River-Danville basin: interbasin correlation of continental sediments and a test of the tectonic coherence of Newark rift basins in eastern North America. Geol. Soc. Am. Bull. 109 (3), 366–377.

Kent, D.V., Olsen, P.E., Witte, W.K., 1995. Late Triassic-earliest Jurassic geomagnetic polarity sequence and paleolatitudes from drill cores in the Newark rift basin, eastern North America. J. Geophys. Res. 100, 14965–14998.

King, P.B., 1971. Systematic pattern of Triassic dikes in the Appalachian region – second report: U.S. Geol. Surv. Prof. Pap. 750-D, D84–D88.

Klitgord, K.D., Schouten, H., 1986. Plate kinematics of the central Atlantic. In: Vogt, P.R., Tucholke, B.E. (Eds.), The Geology of North America, The Western North Atlantic Region, vol. M. Geological Society of America, pp. 351–378.

Klitgord, K.D., Hutchinson, D.R., Schouten, H., 1988. U.S. Atlantic continental margin; structural and tectonic framework. In: Sheridan, R.E., Grow, J.A. (Eds.), The Geology of North America, The Atlantic Continental Margin, vol. I-2, Geological Society of America, pp. 19–56.

Krystyn, L., Gallet, Y., Besse, J., Marcoux, J., 2002. Integrated Upper Carnian to Lower Norian biochronology and implications for the Upper Triassic magnetic polarity time scale. Earth Planet. Sci. Lett. 203, 343–351.

Lanphere, M.A., 1983. $^{40}Ar/^{39}Ar$ ages of basalt from Clubhouse Crossroads test hole #2, near Charleston, South Carolina. In: Gohn, G.S. (Eds.), Studies Related to the Charleston, South Carolina, Earthquake of 1886 – Tectonics and Seismicity, Geological Survey Professional Paper, vol. 1313, pp. B1–B8.

LeTourneau, P., 1999. Depositional history and tectonic evolution of Late Triassic rifts of the U.S. central Atlantic margin: results of an integrated stratigraphic, structural, and paleomagnetic analysis of the Taylorsville and Richmond basins. Ph.D. dissertation, Columbia University.

LeTourneau, P., 2003. Tectonic and climatic controls on the stratigraphic architecture of the Late Triassic Taylorsville basin, Virginia and Maryland. In: LeTourneau, P.M., Olsen, P.E. (Eds.), The Great Rift Valleys of Pangea in Eastern North America, Sedimentology, Stratigraphy, and Paleontology, vol. 2. Columbia University Press, New York, pp. 12–58.

Lindholm, R.C., 1978. Triassic-Jurassic faulting in eastern North America – a model based on pre-Triassic structures. Geology 6, 365–368.

Lizarralde, D., Holbrook, W.S., 1997. U.S. mid-Atlantic margin structure and early thermal evolution. J. Geophys. Res. 102, 22855–22875.

Lomando, A.J., Engelder, T., 1984. Strain indicated by calcite twinning: implications for deformation of the early Mesozoic northern Newark basin, New York. Northeast. Geol. 6, 192–195.

Lucas, M., Hull, J., Manspeizer, W., 1988. A foreland-type fold and related structures in the Newark rift basin. In: Manspeizer, W. (Eds.), Triassic-Jurassic Rifting, Continental Breakup and the Origin of the Atlantic Ocean Passive Margins, Part A. Elsevier, New York, pp. 307–332.

MacLean, B.C., Wade, J.A., 1992. Petroleum geology of the continental margin south of the islands of St. Pierre and Miquelon, offshore eastern Canada. Bull. Can. Pet. Geol. 40, pp. 222–253.

Malinconico, M.L., 1999. Thermal history of the Early Mesozoic Newark (NJ/PA) and Taylorsville (VA) basins using borehole vitrinite reflectance: conductive and advective effects. Geol. Soc. Am., Abstracts with Programs 31, A–31.

Malinconico, M.L., 2003. Paleo-maximum thermal structure of the Triassic Taylorsville (Virginia) basin: evidence for border fault convection and implications for duration of syn-rift sedimentation and long-term elevated heat flow. In: LeTourneau, P.M., Olsen, P.E. (Eds.), Aspects of Triassic-Jurassic Rift Basin Geoscience, State Geological and Natural History Survey of Connecticut Miscellaneous Reports, vol. 1, pp. 25–26.

Manspeizer, W., Cousminer, H.L., 1988. Late Triassic-Early Jurassic synrift basins of the U.S. Atlantic margin. In: Sheridan, R.E., Grow, J.A. (Eds.), The Geology of North America, The Atlantic Continental Margin, vol. I-2. Geological Society of America, U.S., pp. 197–216.

Marzolli, A., Renne, P.R., Piccirillo, E.M., Ernesto, M., Bellieni, G., deMin, A., 1999. Extensive 200-million-year-old continental flood basalts of the Central Atlantic Magmatic Province. Science 284, pp. 616–618.

May, P.R., 1971. Pattern of Triassic-Jurassic diabase dikes around the North Atlantic in the context of the predrift configuration of the continents. Geol. Soc. Am. Bull. 82, 1285–1292.
McAlpine, K.D., 1990. Mesozoic stratigraphy, sedimentary evolution, and petroleum potential of the Jeanne d'Arc basin, Grand Banks of Newfoundland. Geol. Surv. Can. Pap. 89–17, 50p.
McBride, J.H., Nelson, K.D., Brown, L.D., 1989. Evidence and implications of an extensive early Mesozoic rift basin and basalt/diabase sequence beneath the southeast coastal plain. Geol. Soc. Am. Bull. 101, 512–520.
McHone, J.G., 1996. Broad-terrane Jurassic flood basalts across northeastern North America. Geology 24, 319–322.
McHone, J.G., 2000. Non-plume magmatism and rifting during the opening of the central Atlantic Ocean. Tectonophysics 316, 287–296.
McHone, J.G., Anderson, D.L., Fialko, Y.A., 2004. Giant Dikes: Patterns and Plate Tectonics. http://www.mantleplumes.org/.
Medina, F., 1995. Syn- and postrift evolution of the El Jadida-Agadir basin (Morocco): Constraints for the rifting models of the central Atlantic. Can. J. Earth Sci. 32, 1273–1291.
Michael, P.J., et al., 2003. Magmatic and amagmatic seafloor generation at the ultraslow-spreading Gakkel ridge, Arctic Ocean. Nature 423, 956–961.
Muttoni, G., Kent, D.V., Olsen, P.E., DiStefano, P., Lowrie, W., Bernasconi, S., Hernandez, F.M., 2004. Tethyan magnetostratigraphy from Pizzi Mondello (Sicily) and correlation to the Late Triassic Newark astrochronological polarity time scale. Geol. Soc. Am. Bull. 116, 1043–1058.
Oh, J., Austin, J.A., Phillips, J.D., Coffin, M.F., Stoffa, P.L., 1995. Seaward-dipping reflectors offshore the southeastern United States: Seismic evidence for extensive volcanism accompanying sequential formation of the Carolina trough and Blake Plateau basin. Geology 23, 9–12.
Olsen, P.E., 1986. A 40-million-year lake record of early Mesozoic climatic forcing. Science 234, 842–848.
Olsen, P.E., 1990. Tectonic, climatic, and biotic modulation of lacustrine ecosystems: examples from the Newark Supergroup of eastern North America. In: Katz, B. (Eds.), Lacustrine Basin Exploration: Case Studies and Modern Analogs, American Association of Petroleum Geologists Memoir, vol. 50, pp. 209–224.
Olsen, P.E., 1997. Stratigraphic record of the early Mesozoic breakup of Pangea in the Laurasia-Gondwana rift system. Ann. Rev. Earth Planet. Sci. 25, 337–401.
Olsen, P.E., 1998. Geological interpretation of the Rattlesnake Ridge Project – McNair et al. # 1 well. Project report to Rattlesnake Ridge Joint Venture 1986, +21.
Olsen, P.E., 1999. Giant lava flows, mass extinctions, and mantle plumes. Science 284, 604–605.
Olsen, P.E., Kent, D.V., 1996. Milankovitch climate forcing in the tropics of Pangea during the Late Triassic. Palaeogeogr. Palaeoclimatol. Palaeoecol. 122, 1–26.
Olsen, P.E., Kent, D.V., 2000. High resolution early Mesozoic Pangean climatic transect in lacustrine environments. In: Bachmann, G., Lerche, I. (Eds.), Epicontinental Triassic, Zentralblatt fur Geologie und Palaontologie, vol. 3, VIII, pp. 1475–1496.
Olsen, P.E., Schlische, R.W., 1990. Transtensional arm of the early Mesozoic Fundy rift basin: penecontemporaneous faulting and sedimentation. Geology 18, 695–698.
Olsen, P.E., Schlische, R.W., Gore, P.J.W. (Eds.), 1989. Tectonic, depositional, and paleoecological history of early Mesozoic rift basins, eastern North America: International Geological Congress Field Trip T351. American Geophysical Union, Washington, D.C., 174.
Olsen, P.E., Kent, D.V., Cornet, B., Witte, W.K., Schlische, R.W., 1996a. High-resolution stratigraphy of the Newark rift basin (early Mesozoic, eastern North America). Geol. Soc. Am. Bull. 108, 40–77.
Olsen, P.E., Schlische, R.W., Fedosh, M.S., 1996b. 580 kyr duration of the Early Jurassic flood basalt event in eastern North America estimated using Milankovitch cyclostratigraphy. In: Morales, M. (Ed.), The Continental Jurassic: Museum of Northern Arizona Bulletin, vol. 60, pp. 11–22.

Olsen, P.E., Kent, D.V., Fowell, S.J., Schlische, R.W., Withjack, M.O., LeTourneau, P.M., 2000. Implications of a comparison of the stratigraphy and depositional environments of the Argana (Morocco) and Fundy (Nova Scotia, Canada) Permian-Jurassic basins. In: Oujidi, M., Et-Touhami, M. (Eds.), Le Permien et le Trias du Maroc, Actes de la Premièr Réunion su Groupe Marocain du Permien et du Trias, Oujda, Hilal Impression, pp. 165–183.

Olsen, P.E., Kent, D.V., Et-Touhami, M., Puffer, J., 2003. Cyclo-, magneto-, and bio-stratigraphic constraints on the duration of the CAMP event and its relationship to the Triassic-Jurassic boundary. In: Hanes, W.E., McHone, J.G., Renne, P.R., Ruppel, C. (Eds.), The Central Atlantic Magmatic Province, Insights from Fragments of Pangea, Geophysical Monograph, vol. 136. American Geophysical Union, Washington, D.C., pp. 7–32.

Pálfy, J., Jansa, L.F., Lambert, R.S.J., 2000. A U-Pb and $^{40}Ar/^{39}Ar$ time scale for the Jurassic. Can. J. Earth Sci. 37, 923–944.

Palmer, A.R., 1983. The decade of North American Geology, geologic time scale. Geology 11, 503–504.

Pe-Piper, G., Jansa, L.F., Lambert, R.S.J., 1992. Early Mesozoic magmatism of the Eastern Canadian margin; petrogenetic and tectonic significance. In: Puffer, J.H., Ragland, P.C. (Eds.), Eastern North American Mesozoic Magmatism, Geological Society of America Special Paper, vol. 268, pp. 13–36.

Pratt, L.M., Shaw, C.A., Burruss, R.C., 1988. Thermal histories of the Hartford and Newark Basins inferred from maturation indices of organic matter. In: Froelich, A.J., Robinson, G.R. (Eds.), Studies of the Early Mesozoic Basins of the Eastern United States: United States Geological Survey Bulletin 1776, pp. 58–62.

Ragland, P.C., 1991. Mesozoic igneous rocks. In: Horton Jr., J.W., Zullo, V.A. (Eds.), The Geology of the Carolinas. University of Tennessee Press, Knoxville, pp. 171–190.

Ragland, P.C., Hatcher, R.D., Whittington, D., 1983. Juxtaposed Mesozoic diabase dike sets from the Carolinas: a preliminary assessment. Geology 11, 394–399.

Ragland, P.C., Cummins, L.E., Arthur, J.D., 1992. Compositional patterns for early Mesozoic diabases from South Carolina to central Virginia. In: Puffer, J.H., Ragland, P.C. (Eds.), Eastern North American Mesozoic Magmatism. Geological Society of America Special Paper, vol. 268, pp. 301–331.

Rankin, D.W., 1994. Continental margin of the eastern United States: past and present. In: Speed, R.C. (Ed.), Phanerozoic Evolution of North American Continent-Ocean Transitions, Geological Society of America, DNAG Continent-Ocean Transect Volume, pp. 129–218.

Rast, N., 1988. Variscan-Alleghenian orogen. In: Manspeizer, W. (Ed.), Triassic-Jurassic Rifting, Continental Breakup and the Origin of the Atlantic Ocean Passive Margins, Part A. Elsevier, New York, pp. 1–27.

Ratcliffe, N.M., Burton, W.C., 1985. Fault reactivation models for origin of the Newark basin and studies related to eastern U.S. seismicity. In: Robinson, G.R., Froelich, A.J. (Eds.), Proceedings of the Second U.S. Geological Survey Workshop on the Early Mesozoic Basins of the Eastern United States. U.S. Geological Survey Circular, vol. 946, pp. 36–45.

Ratcliffe, N.M., Burton, W.C., D'Angelo, R.M., Costain, J.K., 1986. Low-angle extensional faulting, reactivated mylonites, and seismic reflection geometry of the Newark Basin margin in eastern Pennsylvania. Geology 14, 766–770.

Sachs, P.E., Stoddard, E.F., Berquist, R., Newton, C., 1999. A field guide to the geology of the fall zone region, North Carolina and Virginia state line: road log for CGS field trip. Geology of the Fall Zone Region along the North Carolina – Virginia State Line, Guidebook for the 1999 Meeting of the Carolina Geological Society, Emporia, Virginia.

Sanders, J.E., 1963. Late Triassic tectonic history of northeastern United States. Am. J. Sci. 261, 501–524.

Schlische, R.W., 1991. Half-graben basin filling models: new constraints on continental extensional basin evolution. Basin Res. 3, 123–141.

Schlische, R.W., 1992. Structural and stratigraphic development of the Newark extensional basin, eastern North America: implications for the growth of the basin and its bounding structures. Geol. Soc. Am. Bull. 104, 1246–1263.

Schlische, R.W., 1993. Anatomy and evolution of the Triassic-Jurassic continental rift system, eastern North America. Tectonics 12, 1026–1042.

Schlische, R.W., 1995. Geometry and origin of fault-related folds in extensional settings. AAPG Bull. 79, 1661–1678.

Schlische, R.W., 2003. Progress in understanding the structural geology, basin evolution, and tectonic history of the Eastern North American Rift System. In: LeTourneau, P.M., Olsen, P.E. (Eds.), The Great Rift Valleys of Pangea in Eastern North America. Tectonics, Structure, and Volcanism, vol. 1. New York, Columbia University Press, pp. 21–64.

Schlische, R.W., Ackermann, R.V., 1995. Kinematic significance of sediment-filled fissures in the North Mountain Basalt, Fundy rift basin, Nova Scotia, Canada. J. Struct. Geol. 17, 987–996.

Schlische, R.W., Anders, M.H., 1996. Stratigraphic effects and tectonic implications of the growth of normal faults and extensional basins. In: Beratan, K.K. (Ed.), Reconstructing the Structural History of Basin and Range Extension Using Sedimentology and Stratigraphy, Geological Society of America Special Paper, vol. 303, pp. 183–203.

Schlische, R.W., Olsen, P.E., 1990. Quantitative filling model for continental extensional basins with applications to early Mesozoic rifts of eastern North America. J. Geol. 98, 135–155.

Schlische, R.W., Withjack, M.O., 2005. The early Mesozoic Birdsboro central Atlantic margin basin in the Mid-Atlantic region, eastern United States. Disc. Geol. Soc. Am. Bull. 117, 823–828.

Schlische, R.W., Withjack, M.O., Olsen, P.E., 2003. Relative timing of CAMP, rifting, continental breakup, and basin inversion: tectonic significance. In: Hanes, W.E., McHone, J.G., Renne, P.R., Ruppel, C. (Eds.), The Central Atlantic Magmatic Province, Insights from Fragments of Pangea. Geophysical Monograph, vol. 136, Washington, D.C., American Geophysical Union, pp. 33–60.

Shaler, N.S., Woodworth, J.B., 1899. Geology of the Richmond basin, Virginia: U.S. Geological Survey Annual Report, No. 19, pp. 1246–1263.

Sheridan, R.E., et al., 1993. Deep seismic reflection data of EDGE U.S. Atlantic continent-margin experiment: implications for Appalachian sutures and Mesozoic rifting and magmatic underplating. Geology 21, 563–567.

Shipboard Scientific Party, 2003. Leg 210 Preliminary Report. ODP Preliminary Report 110 [Online]. Available from World Wide Web <http://www-odp.tamu.edu/publications/prelim/210_prel/210PREL.PDF>.

Sinclair, I.K., 1995a. Transpressional inversion due to episodic rotation of extensional stresses in Jeanne d'Arc basin, offshore Newfoundland. In: Buchanan, J.G., Buchanan, P.G. (Eds.), Basin Inversion, Geological Society Special Publication, vol. 88, pp. 249–271.

Sinclair, I.K., 1995b. Sequence stratigraphic response to Aptian-Albian rifting in conjugate margin basins: A comparison of the Jeanne d'Arc basin, offshore Newfoundland, and the Porcupine basin, offshore Ireland. In: Scrutton, R.A., Stoker, M.S., Shimmield, G.B., Tudhope, A.W. (Eds.), The Tectonics, Sedimentation and Paleooceanography of the North Atlantic Region. Geological Society Special Publication, vol. 90, pp. 29–49.

Sinclair, I.K., Evan, J.E., Albrechtsons, E.A., Sydora, L.J., 1999. The Hibernia Oilfield – effects of episodic tectonism on structural character and reservoir compartmentalization. In: Fleet, A.J., Boldy, S.A.R. (Eds.), Petroleum Geology of Northwest Europe: Proceedings of the 5th Conference, pp. 517–528.

Srivastava, S.P., Sibuet, J.-C., Cande, S., Roest, W.R., Reid, I.D., 2000. Magnetic evidence for slow seafloor spreading during the formation of the Newfoundland and Iberian margins. Earth Planet. Sci. Lett. 182, 61–76.

Steckler, M.S., Omar, G.I., Karner, G.D., Kohn, B.P., 1993. Pattern of hydrothermal circulation with the Newark basin from fission-track analysis. Geology 21, 735–738.

Stoddard, E.F., Delorey, C.M., McDaniel, R.D., Dooley, R.E., Ressetar, R., Fullagar, P.D., 1986. A new suite of post-orogenic dikes in the eastern North Carolina Piedmont: Part I. Occurrence, petrography, paleomagnetics, and Rb/Sr geochronology. Southeast. Geol. 27, 1–12.

Sutter, J.F., 1988. Innovative approaches to the dating of igneous events in the early Mesozoic basins of the eastern United States. In: Froelich, A.J., Robinson Jr., G.R. (Eds.), Studies of the Early Mesozoic Basins of the Eastern United States. U.S. Geological Survey Bulletin, vol. 1776, pp. 194–199.

Swanson, M.T., 1986. Preexisting fault control for Mesozoic basin formation in eastern North America. Geology 14, pp. 419–422.

Tankard, A.J., Welsink, H.J., 1987. Extensional tectonics and stratigraphy of Hibernia oil field, Grand Banks, Newfoundland. Am. Assoc. Pet. Geol. Bull. 71, 1210–1232.

Tanner, L.H., Brown, D.E., 2003. Tectonostratigraphy of the Orpheus graben, Scotian basin, offshore eastern Canada, and its relationship to the Fundy rift basin. In: LeTourneau, P.M., Olsen, P.E. (Eds.), The Great Rift Valleys of Pangea in Eastern North America. Sedimentology, Stratigraphy, and Paleontology, vol. 2. New York, Columbia University Press, pp. 59–68.

Tseng, H.Y., Onstott, T.C., Burruss, R.C., Person, M., 1996. Thermal and hydrogeological evolution of Taylorsville basin in Virginia: implications for subsurface geomicrobiology experiments. In: LeTourneau, P.M., Olsen, P.E. (Eds.), Aspects of Triassic-Jurassic Rift Basin Geoscience, State Geological and Natural History Survey of Connecticut Miscellaneous Reports, vol. 1, p. 54.

Turrin, B.D., 2000. $^{40}Ar/^{39}Ar$ mineral ages and potassium and argon systematics from the Palisade Sill, New York. EOS, 81, Abstract V72E-13.

van Veen, P.M., Skjold, L.J., Kristensen, S.E., Rasmussen, A., Gjelberg, J., Stølan, T., 1992. Triassic sequence stratigraphy in the Barents Sea. In: Vorren, T.O., Bergsager, Ø.A., Dahl-Stamenesm Holter, E., Johansen, B., Lie, E., Lund, T.B. (Eds.), Arctic Geology and Petroleum Potential, NPF Spec. Pub., vol. 2, pp. 515–538.

Vendeville, B., Hongxing, G., Jackson, M.P.A., 1995. Scale models of salt tectonics during basement-involved extension. Pet. Geosci. 1, 179–183.

Venkatakrishnan, R., Lutz, R., 1988. A kinematic model for the evolution of the Richmond basin. In: Manspeizer, W. (Eds.), Triassic-Jurassic Rifting, Continental Breakup and the Origin of the Atlantic Ocean Passive Margins, Part A New York, Elsevier, pp. 445–462.

Vogt, P.R., 1973. Early events in the opening of the North Atlantic. In: Tarling, D.H., Runcorn, S.K. (Eds.), Implications of Continental Drift to the Earth Sciences, New York, Academic Press, pp. 693–712.

Wade, J.A., Brown, D.E., Traverse, A., Fensome, R.A., 1996. The Triassic-Jurassic Fundy basin, eastern Canada: regional setting, stratigraphy, and hydrocarbon potential. Atlantic Geol. 32, 189–231.

Welsink, H.J., Dwyer, J.D., Knight, R.J., 1989. Tectono-stratigraphy of the passive margin off Nova Scotia. In: Tankard, A.J., Balkwill, H.R. (Eds.), Extensional Tectonics and Stratigraphy of the North Atlantic Margins, American Association of Petroleum Geologists Memoir, vol. 46, pp. 215–231.

Wheeler, G., 1939. Triassic fault-line deflections and associated warping. J. Geol. 47, 337–370.

Wise, D.U., 1992. Dip domain method applied to the Mesozoic Connecticut Valley rift basins. Tectonics 11, 1357–1368.

Withjack, M.O., Callaway, S., 2000. Active normal faulting beneath a salt layer: an experimental study of deformation patterns in the cover sequence. Am. Assoc. Pet. Geol. 84, 627–651.

Withjack, M.O., Olsen, P.E., Schlische, R.W., 1995. Tectonic evolution of the Fundy rift basin, Canada: evidence of extension and shortening during passive margin development. Tectonics 14, 390–405.

Withjack, M.O., Schlische, R.W., Olsen, P.E., 1998. Diachronous rifting, drifting, and inversion on the passive margin of central eastern North America: an analog for other passive margins. Am. Assoc. Pet. Geol. 82, 817–835.

Withjack, M.O., Schlische, R.W., Olsen, P.E., 2002. Rift-basin structure and its influence on sedimentation and stratigraphy. In: Renaut, R., Ashley, G.M. (Eds.), Continental Rift Basin Sedimentology, SEPM Special Publication, vol. 73, pp. 57–81.

In this chapter

14

Extensional tectonics and stratigraphy of the Mesozoic Jeanne d'Arc basin, Grand Banks of Newfoundland

Herman Welsink, Anthony Tankard†*
*Repsol Exploración SA, Madrid, Spain
†Tankard Enterprises, Calgary, Alberta, Canada

14.1 Introduction

The continental lithosphere beneath the Grand Banks and Orphan basin forms a broad platform that extends 450 km offshore Newfoundland. It is separated from the narrower shelves of Nova Scotia and Labrador by the Newfoundland and Charlie Gibbs fracture zones, respectively. The basins of the Grand Banks and Orphan basin (Fig. 14.1) developed by the reactivation of older basement fabrics. Extensional subsidence was episodic from the Late Triassic to Late Cretaceous. Importantly, the post-rift cover is relatively thin and allows detailed mapping. The Grand Banks was originally at the center of Pangea where it was surrounded by the northwest African, Iberian, and European continental plates. Late Jurassic–Cretaceous extension culminated in ocean opening by northward migration of sea-floor spreading, as Africa, then Iberia, and finally the Goban Spur-Porcupine Bank margin of the European plate separated.

How do we know the history of basin evolution? Four decades of exploration of the Grand Banks and Orphan basin has resulted in the acquisition of over 465,000 km of conventional reflection seismic, about 1.2 million CMP km of three-dimensional seismic (CMP refers to the Common Mid-Point method of 3D seismic acquisition), and several thousand kilometers of deep (20 s or more) seismic profiles. Whereas Lithoprobe East examines the structure of the continental crust and the processes of basin formation (de Voogd and Keen, 1987; Keen et al., 1987a,b), the focus of the SCREECH program is the transition between continental and oceanic crust in the nonvolcanic Newfoundland basin

Phanerozoic Rift Systems and Sedimentary Basins DOI: 10.1016/B978-0-444-56356-9.00013-4

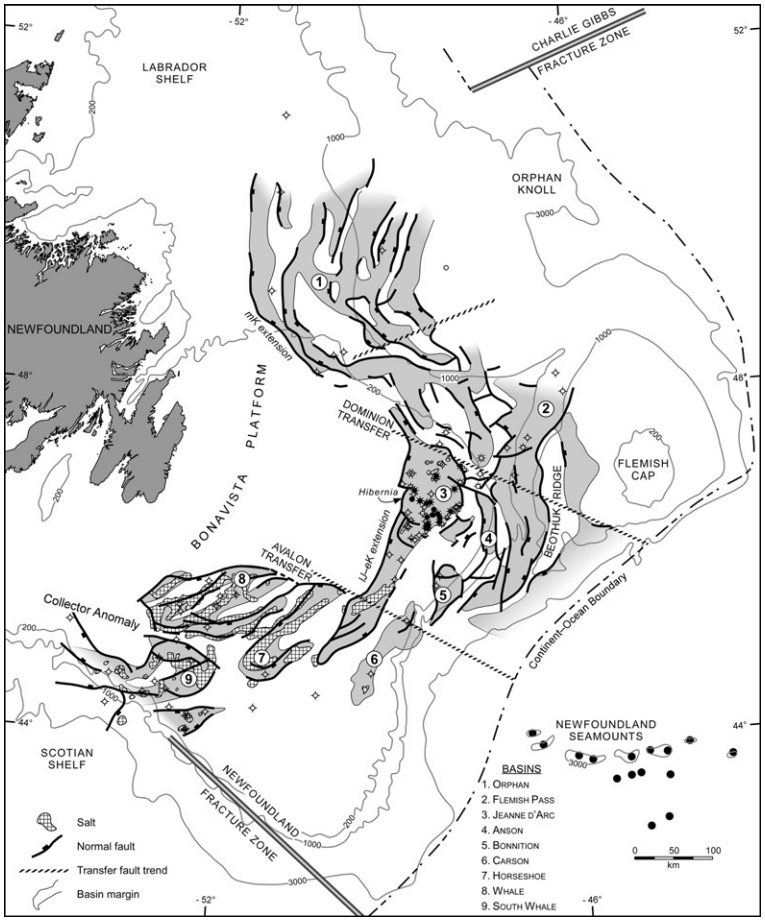

Figure 14.1 Principal structural elements of the Grand Banks and Orphan provinces, and showing exploration well control. Basin architecture is constructed from a compilation of about 75 seismic structure exploration maps. The seismic structure is integrated with gravity and magnetic data to show basin linkage. Newfoundland and Charlie Gibbs fracture zones separate these tectonic provinces from the narrower Scotian and Labrador shelves, respectively. The first-order Avalon and Dominion transfer faults separate the southern Grand Banks, central Grand Banks, and Orphan basin. These faults are believed to have penetrated the entire brittle crust, because they coincide with offsets of the Moho, and were able to confine extensional strain. Transpressional uplift created basement highs along the Avalon (Avalon uplift) and Dominion transfer zones. The smaller-scale second-order transfer faults accommodated different amounts and rates of extension. Bathymetric contours are in meters. *(Modified after Welsink et al., 1989a.)*

as part of ODP Leg 210 (Hopper et al., 2006; Lau et al., 2006a). There are 136 deep exploration and delineation wells in the basins of the Grand Banks, including 52 in the Jeanne d'Arc basin (Fig. 14.1). The Jeanne d'Arc is the best understood of these basins. It is more than 10,000 km^2 in area and up to 18 km deep; average drill depths are greater than 3700 m. Several papers describe the basin architecture and stratigraphy (Arthur et al., 1982; Enachescu, 1987, 1993; Grant et al., 1986; Hubbard, 1988; Karner et al., 1993; Meneley, 1986; Sinclair, 1993, 1995; Tankard and Welsink, 1987, 1988; Tankard et al., 1989).

The Jeanne d'Arc is an extensional basin. Whereas crustal stretching controlled the course of basin subsidence, the basin fill preserves a detailed account of how and when this took place. In this chapter, we investigate the interplay between regional extensional tectonics and basin evolution, and attempt to show that the formation of the Jeanne d'Arc basin is linked to the behavior of overlapping crustal plates. We describe the structural styles and their behavior, and show how the sedimentary fill reflects this activity. By integrating the structural and stratigraphic history of the Jeanne d'Arc basin, we are also able to examine the distribution and timing of tectonic linkages between old continental crust and new oceanic crust. These geodynamic interpretations are derived from petroleum exploration mapping and basin studies over many years, involving the integration of geophysical, geological, and biostratigraphic information.

14.2 Tectonic evolution

The pre-breakup reconstruction juxtaposes offshore Newfoundland's Flemish Cap and Orphan Knoll with Galicia Bank and Goban Spur, respectively (Fig. 14.2). Extension of the Grand Banks began in the earliest Carnian. The basins formed by reactivation of structures that already existed in the crystalline and meta-sedimentary Avalon basement. The Jeanne d'Arc succession is made up of unconformity-bounded sequences that record three stages of ocean opening and northward migration of sea-floor spreading (Fig. 14.3). The earliest record of spreading between Nova Scotia and northwest Africa is the 175-Ma East Coast Magnetic Anomaly (ECMA; Aalenian). At 118 Ma in the Aptian, chron M0, the propagating sea-floor jumped from the southern margin of the Grand Banks to the northern Newfoundland basin. At 84 Ma in the Santonian, chron 34, the Orphan basin separated from the Porcupine Bank-Goban Spur margin (Srivastava et al., 1988). Bay of Biscay opening dates to this Santonian event.

The first-order Avalon and Dominion transfer faults divide the platform between the Newfoundland and Charlie Gibbs fracture zones into three extensional provinces, each characterized by distinctive basin styles. We recognize this threefold subdivision by combining Bouguer gravity and magnetic compilations with the network of basin structures derived from seismic mapping (Figs. 14.1 and 14.4). Local perturbations outline the Mesozoic sedimentary basins. The boundary between the Avalon and Meguma terranes is a large-amplitude magnetic

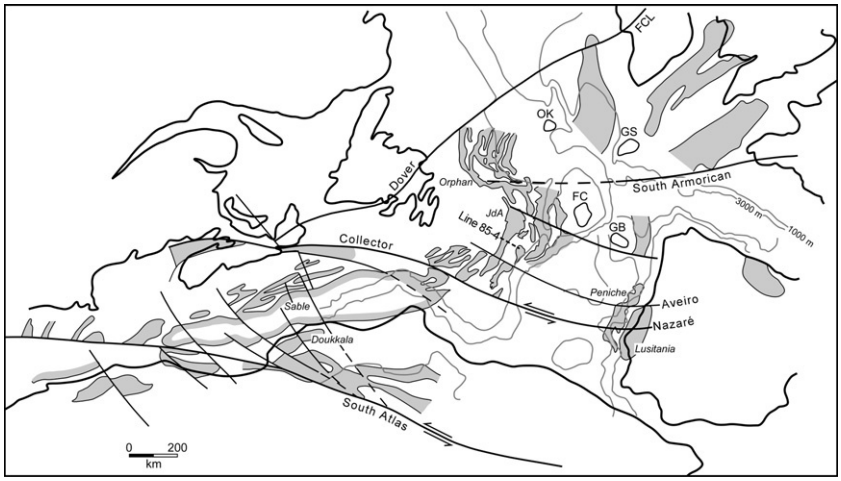

Figure 14.2 Pre-drift reconstruction showing structural linkages and basin distribution. Mesozoic extension reactivated fabrics that already existed in the basement. Reconstruction of the North Atlantic at chron M0 is on the basis of Klitgord and Schouten (1986), Srivastava and Tapscott (1986), and Klitgord et al. (1988). We correlate the Dover fault of Newfoundland with the Fair Head Clew Bay line (FCL) of Ireland and the Highland Boundary fault of Scotland (Max and Riddihough, 1975). The South Atlas fault is collinear with the hingeline and tract of basins off the United States (Klitgord et al., 1988). This study addresses the Late Jurassic–Early Cretaceous Jeanne d'Arc–northern Peniche–Galicia extensional tract, and the Early to Late Cretaceous Jeanne d'Arc–Orphan extensional tract. Line 85–4 is the location of the Lithoprobe deep seismic line shown in Fig. 14.5. FC, Flemish Cap; GB, Galicia Bank; JdA, Jeanne d'Arc basin; OK, Orphan Knoll; GS, Goban Spur. The important conjugate pairs are Sable–Doukkala, southern Grand Banks–southern Peniche–Lusitania, Jeanne d'Arc–northern Peniche, and Orphan–Goban Spur. *(Modified after Tankard and Balkwill, 1989.)*

anomaly, known as the Collector anomaly (Haworth and Lefort, 1979), either side of which sinistral strike-slip deformation has created the relatively shallow South Whale, Whale, and Horseshoe pull-apart basins (Fig. 14.1). The Avalon-Meguma boundary is associated with a step in the Moho from 11.5 to 10 s (Lithoprobe line 85–1; Tankard and Welsink, 1989). The Grand Banks between the Avalon and Dominion faults is characterized by linear gravity and magnetic trends, and a suite of subparallel but very deep half grabens.

Second-order transfer faults compartmentalize these three extensional provinces and their basins still further (Fig. 14.4). At map scale, the transfer faults are continuous traces rather than the broad band of *en echelon* threads that actually exist. The major normal faults commonly terminate against these cross-basin transfer faults. Within the basins, the larger transfer fault zones coincide with the trends of gravity anomalies. From this relationship, we are able to extrapolate these larger transfer fault trends regionally and can also recognize the linkage of the transfer faults with older basement strength anisotropies. In some

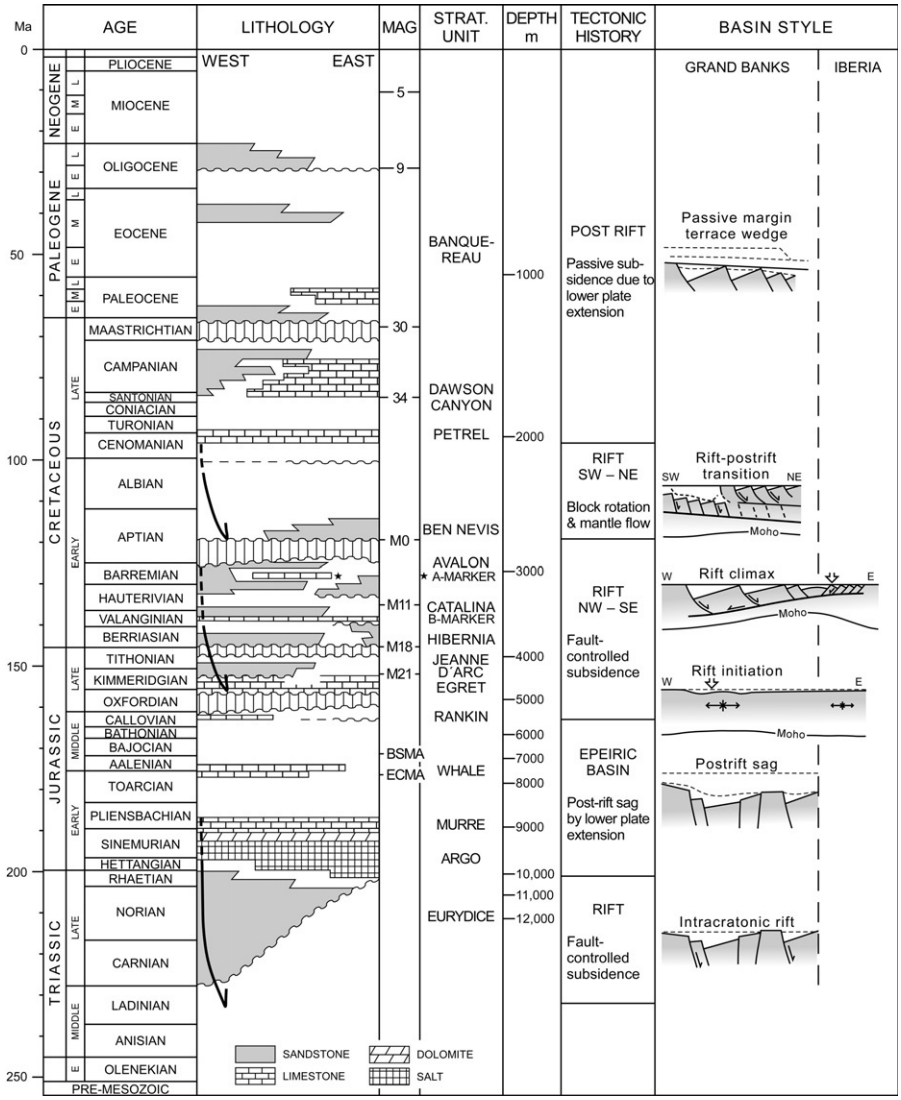

Figure 14.3 Stratigraphy and tectonic evolution, Jeanne d'Arc basin. The unconformities that mark the transition from one episode of subsidence to the next are late Callovian, early Aptian, early Cenomanian, and Maastrichtian. This long history of subsidence includes three prominent rift stages (shown by subsidence arrows) in the Carnian–Sinemurian, late Callovian–early Aptian (SE-directed extension), and mid-Aptian–Cenomanian (NE-directed extension). The East Coast Magnetic Anomaly (ECMA) marks the separation of northwest Africa, chron M0 the separation of the Iberia margin, and chron 34 the separation of the European-Greenland plate. Unconformity-bounded sequences are on the basis of seismic stratigraphy, well control, and biostratigraphy. Several prolific reservoir sequences were deposited during the mid-Mesozoic rift episode. Magnetic anomalies after Klitgord and Schouten (1986) and Srivastava et al. (1988). Time scale is that adopted by the ICS. *(Modified after Tankard et al., 1989.)*

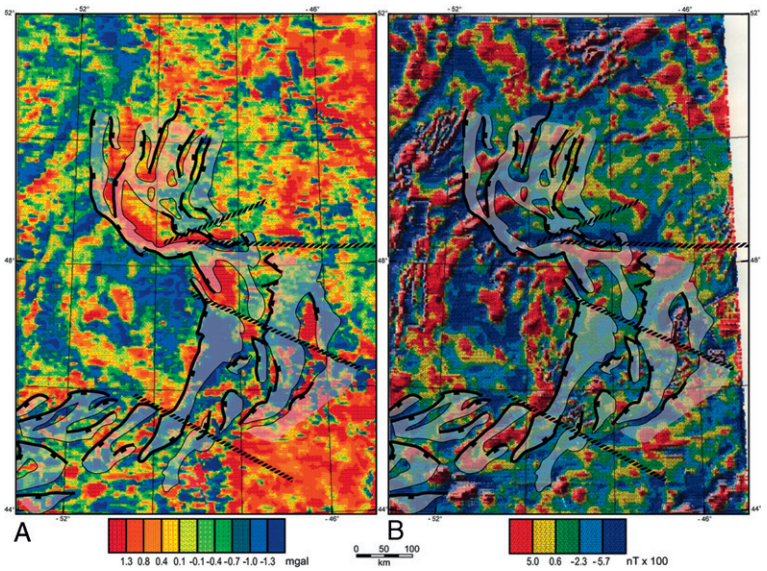

Figure 14.4
(A) First vertical derivative of Bouguer gravity with overlay of basins and their structural framework. (B) First vertical derivative of magnetic anomalies with overlay of basins and their structural framework. The principal basement trends are interpreted from both gravity and magnetic data.

areas, such as the Orphan basin, sparse seismic coverage and a thicker post-rift cover limit the structural analysis.

The basins of the *southern Grand Banks* formed along strike-slip and normal faults by reactivation of Paleozoic Appalachian structures. Basin depths are seldom greater than 8 km. Immense synkinematic salt diapirs have intruded the extensional basin fills, especially along basement faults (Balkwill and Legall, 1989). In contrast, the structural framework of the *central Grand Banks* is much simpler (Fig. 14.1). Late Callovian to early Aptian extension created a family of half grabens that are subparallel and separated by tilted fault blocks. The amount of extension measured is twice that of the southern Grand Banks, and the basins are consequently much deeper. The Jeanne d'Arc basin contains at least 18 km of Mesozoic and Cenozoic sediments. The principal basin-forming fault, the Murre fault, formed along older thrust-like dipping reflectors (Fig. 14.5), whereas many of the orthogonal fault sets coincide with conspicuous disruptions of magnetic anomalies (Tankard and Welsink, 1989). the The *northern extensional province* is the broad Orphan basin, a complex of small rift basins bounded by normal faults with structural relief generally less than 4 km (Keen et al., 1987a; Tankard and Welsink, 1989). The Orphan basin owes its structural evolution mainly to a mid-Aptian–Cenomanian episode of rifting which also resulted in over-deepening of the Jeanne d'Arc basin.

Extension by intracrustal detachment

Major basement faults controlled extension in the continental lithosphere. Several authors have explored the nature of Basin and Range-style intracrustal detachment faults (cf. Wernicke, 1981, 1985) as a means of accommodating

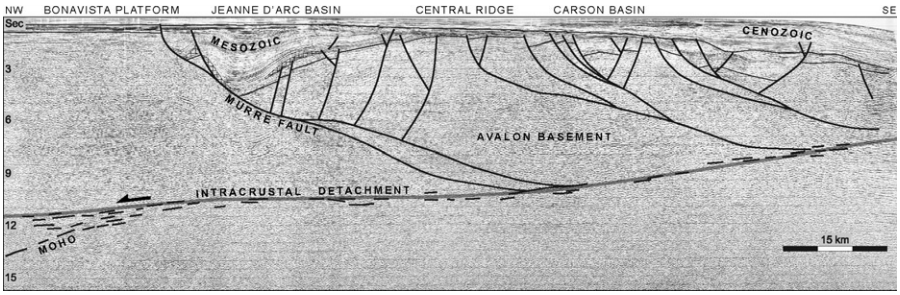

Figure 14.5 Lithoprobe East deep (20 s) seismic line 85–4A showing half graben shape of the Jeanne d'Arc basin, including rollover of the sedimentary basin fill and hanging-wall basement into the listric Murre fault. Depth-to-detachment calculations indicate that this fault soles at ~26 km along a band of sub-horizontal reflectors (10.5 s) that we interpret as a low-angle intracrustal detachment. This detachment separates upper plate from lower plate. The lower part of the Murre fault splays, which we think is in response to upward arching of the detachment due to late rift tectonic unloading, forming an extensional horse. See Fig. 14.2 for location.

extension and continental separation along the Atlantic margin of Canada (Kusznir and Egan, 1989; Tankard and Welsink, 1987, 1988; Tucholke and Whitmarsh, Chapter 1, Volume 1C; Welsink et al., 1989a). Extension is depth-dependent in this model, and the low-angle detachment fault forms a regional zone of decoupling between brittle upper crust and distributed plastic deformation in the lower crust and mantle. This depth-dependent extension controls basin geometry, the amount of fault-controlled extension, and subsidence history (Kusznir and Egan, 1989).

SE-oriented Grand Banks–Iberia extension

Considering the pronounced structural asymmetry of the Grand Banks–Iberia extensional tract, extensional failure may have occurred along a complex system of detachments dipping to the west, with the major basement faults being restricted to the brittle upper crust. Tankard and Welsink (1987) interpreted the geometry of the detachment surface initially by palinspastic restoration of balanced seismic profiles, and later from Lithoprobe deep seismic.

The continental crust beneath the Bonavista platform (Fig. 14.1) is 36 km thick, but thins to 17 km beneath Flemish Cap (Keen and Barrett, 1981). Estimates derived from cross-section balancing indicate that the Murre fault soles at ~26 km beneath the Jeanne d'Arc basin, and that a shallower depth-to-detachment of ~16 km is calculated for the Carson basin and Flemish Pass boundary faults. A continuous down-to-the-west detachment fault was inferred (Tankard and Welsink, 1987). This reconstruction was confirmed by Lithoprobe East deep seismic line 85–4A which shows the listric basin-forming faults detaching at progressively shallower depths toward the east (compare Figs. 14.5 and 14.6A; de Voogd and Keen, 1987). The zone of detachment is expressed as a band of weak, discontinuous reflectors rather than by a single strong reflective surface. The change to a smaller velocity gradient (Lau et al., 2006a) coincides with the detachment at the base of the upper crust. The hanging-wall basement rolls over into the listric Murre fault, where it resulted in rotational subsidence of the Jeanne d'Arc basin. Extensional rotation of fault-bounded horst blocks such as the Central Ridge above the intracrustal detachment caused them to maintain their elevation at regional levels, as is shown by depositional and erosional

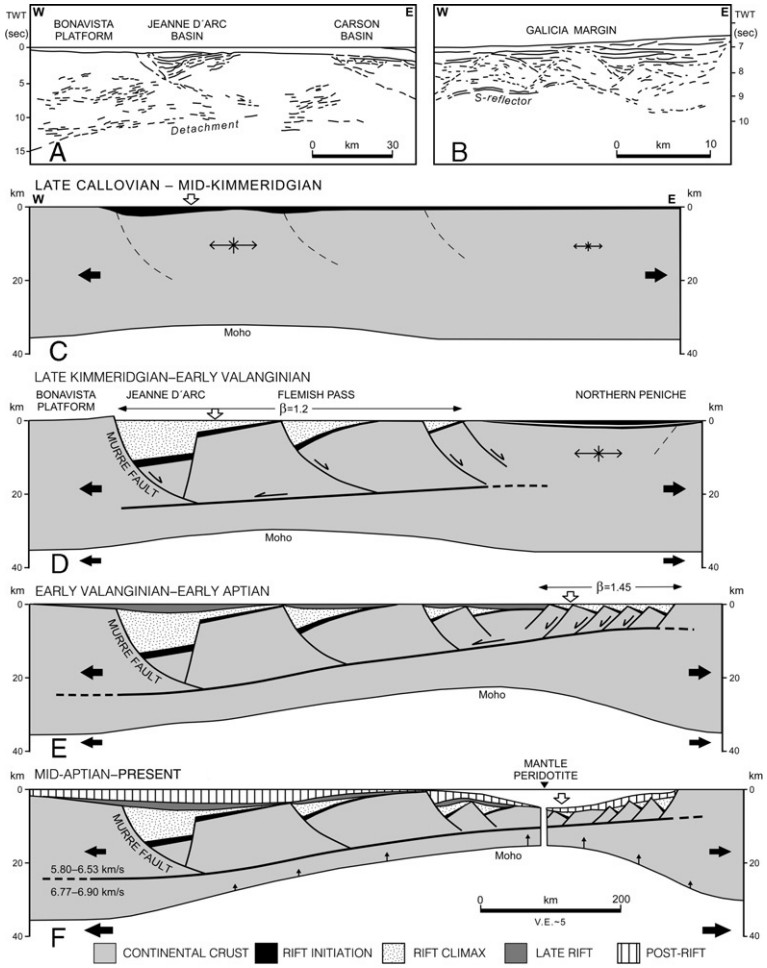

Figure 14.6 Reconstruction of Grand Banks–Iberia SE-oriented extension; late Callovian to early Aptian. With reference to the direction of shear, Iberia margin is proximal and the Grand Banks distal. (A) Distal: line tracing of reflector patterns, Lithoprobe East deep seismic line 85–4A *(after de Voogd and Keen, 1987),* showing listric normal faults merging with a westward-dipping band of reflectors. (B) Proximal: Galicia margin conventional seismic line GP 12 showing the 9.5-km-deep S-reflector, interpreted as a low-angle detachment, with detached allochthons above it *(after de Charpal et al., 1978).* The irregular S-reflector shape is due to velocity pull-up. (C) Onset of extension, on the Grand Banks a broad downwarp and argillaceous drape largely unassisted by faulting. We infer pure-shear processes with locus of upper crustal extension on the Grand Banks. (D) Brittle failure of the Grand Banks crust by basin faults which sole onto a low-angle detachment fault at ~26 km, 20% extension, thick synrift basin fill. The conjugate northern Peniche basin was still in a pre-rift state (Alves et al., 2006). Depth-to-detachment under the Jeanne d'Arc basin calculated from balanced cross-sections and Lithoprobe reflection seismic. Locus of extension Grand Banks, mechanism simple shear. The proximal Iberia margin stretched in pure shear. (E) Grand Banks basins were in late-stage rift subsidence and rheological weakening, while the climax of fault-controlled subsidence was the northern part of the Iberia margin (*op. cit.*), 45% extension. This implies development of an overall simple-shear detachment system for the first time, 25 Ma after the start of extension. Locus of extension Iberia margin. (F) Late stage extension, tectonic denudation, and shearing exposed serpentinized peridotites at the breakaway. A mantle core complex is inferred. Progressive tectonic unloading and isostatic rebound resulted in footwall uplift, and Aptian breakup unconformity. In Flemish Pass uplift resulted in erosion of the mid-Barremian through Aptian section (CNLOPB, 2006b). Size of arrows (black) indicates relative amounts of extension; arrows (white) locus of extension. This detachment model accounts for the geometry of the detachment surface, asymmetry of Grand Banks–Iberia margin extensional terrane, variable amounts of extension, and widespread erosion of Bonavista platform.

thinning of the Callovian–Aptian succession. Uplift only occurred late in the rift cycle because of tectonic unloading.

The Jeanne d'Arc and Flemish Pass basins of the Grand Banks, together with the conjugate margin basins of the northern part of the Iberian margin, including the Galicia, Porto, and Peniche basins (Alves et al., 2006; de Charpal et al., 1978; Reston et al., 1996; Tankard and Welsink, 1988), form a late Callovian–Aptian extensional tract. In our reconstruction (Fig. 14.2), the basins of the southern Grand Banks and the Newfoundland basin were opposite the Lusitania basin and southern Peniche basin, south of the Aveiro fault, where the climax of rifting was earlier (Alves et al., 2002; Balkwill and Legall, 1989; T. Alves, personal communication). The Grand Banks–northern Iberia conjugate pair appears to have shared an intracrustal detachment fault (Fig. 14.6). We correlate the deep detachment of the Grand Banks with an irregular reflective surface at about 9 s beneath the tilt-block basins of the west Iberian margin. The S-reflector at 9.5 km (9 s) beneath the Galicia margin was interpreted by Wernicke and Burchfiel (1982) as a low-angle shear zone with erosionally modified allochthons above it. A large-scale detachment model accounts for the westward-dipping asymmetry of the décollement, and the smaller fault-block spacing of the Iberian margin (10–50 km) compared to the Grand Banks (40–100 km). This is a two-dimensional reconstruction at the end of the extensional cycle. The character and timing of basin subsidence suggest that this extensional model evolved through at least four stages of coupled pure shear and simple shear.

1. The late Callovian–middle Kimmeridgian onset of extension on the Grand Banks (Fig. 14.6C) created a broad downwarp with an onlap stratigraphy. The 1300-m-thick argillaceous drape accumulated without significant fault disruption. Strain was apparently non-rotational. This basin fill correlates with a thin pre-rift stratigraphy in the west Iberian basins north of the Aveiro fault (Alves et al., 2006; Boillot et al., 1985). It appears that for the first 9 Ma (Fig. 14.3), the locus of extension was the Grand Banks crust, and that pure-shear processes dominated (cf. McKenzie, 1978).
2. The climax of fault-controlled subsidence in the Jeanne d'Arc basin was late Kimmeridgian to early Valanginian, marked by stratigraphic thickening and rollover into the listric boundary fault system (Fig. 14.6D). Deposition of coarse alluvial fans indicates that structural relief was substantial. Lithoprobe 85–4A shows that the Murre fault soled at ~26 km (10.5 s) onto a discontinuous reflective surface interpreted as a zone of detachment (Fig. 14.5). The average amount of upper crustal extension is 20%, although locally this may range up to 50% (e.g., Flemish Pass). In contrast, the conjugate Iberian margin remained in an unstructured pre-rift state. Strain accumulation on the Grand Banks appears to have resulted in brittle failure controlled by intracrustal detachment. The locus of Kimmeridgian–Valanginian extension remained the Jeanne d'Arc Grand Banks.
3. By Valanginian time, fault-controlled subsidence in the Jeanne d'Arc basin had diminished substantially, and the late-stage rift sequences (Catalina and

Avalon) were more argillaceous and marine. However, on the basis of ODP Legs 149 and 173, the early Valanginian to Aptian was the climax of rifting on the Iberian margin (Fig. 14.6E; Alves et al., 2006; Chian et al., 1999; Manatschal and Bernoulli, 1999; Wilson et al., 1996) when a train of allochthons detached and rotated above a 9-s-deep reflector (Alves et al., 2006; de Charpal et al., 1978; Reston et al., 1996). We have measured an average amount of extension of 45% on the northwest Iberia margin, but varying up to 120%. With development of the Galicia-Peniche rift system, extension was, for the first time, regionally partitioned across a zone of decoupling, implying widespread simple-shear extension. The locus of Valanginian–Aptian extension was the Iberia margin.

4. During these later stages of extension, in particular, tectonic unloading and isostatic compensation resulted in uplift of the footwall (Fig. 14.6F). The greatest amount of tectonic unloading and upward arching was near the rift-drift transition, dated approximately by the lower Aptian breakup unconformity in the Jeanne d'Arc basin (118 Ma chron M0). Lithospheric extension and arching locally resulted in reversal of dip (down-to-the-east) of the detachment beneath the Iberia margin (e.g., Wilson et al., 1989, their Fig. 21), and tectonic denudation of upper mantle peridotite. A 50-km-long ridge of peridotite, consisting of serpentinized harzburgite and lherzolite, was unroofed along the breakaway zone at the Galicia continent–ocean boundary (Boillot et al., 1980, 1989; Dean et al., 2000; Mauffret and Montadert, 1987). These peridotites are crosscut by subordinate dolerite dykes with a strongly constrained plateau-age of 122 Ma. Mylonitization and serpentinization, as well as a highly reflective surface, are attributed to detachment shearing as mantle rock was unroofed at the climax of extension (Boillot et al., 1989). This domelike exposure of mylonitic mantle footwall of the regional detachment fault, parallel to the breakaway zone, is interpreted as a mantle core complex (cf. Doblas and Oyarzun, 1989). Landward-dipping reflections in the Newfoundland basin also consist of serpentinized peridotite (drilled at ODP Site 1277; Lau et al., 2006b; Shipboard Scientific Party, 2004). Extension ended with ocean opening between Iberia and the Grand Banks.

Finally, this simple-shear extensional model is better able to explain the breakup unconformity than the McKenzie (1978) pure-shear model because the greatest amount of uplift due to tectonic unloading occurred late in the rift cycle.

NE-oriented Orphan basin extension

By Aptian time, sea-floor spreading had jumped from the southern Newfoundland basin to the edge of the Flemish Cap, thus initiating the final phase of extension between the Orphan basin and Goban Spur (Figs. 14.1 and 14.2). Orphan basin is a 450-km-wide tract of rift basins, typically with only 3–4 km (2 s) of structural relief. Lithoprobe deep seismic line 84–3 images the base of the crust at 11.5 s. Basin-forming normal faults form a crustal-scale listric fan which merges at

15–17 km (9 s) depth with an intracrustal décollement (Keen et al., 1987a; Tankard and Welsink, 1989). Seismic refraction data indicate that this is not a velocity boundary or basement strength anisotropy. We measure about 50% extension by cross-section balancing. The age of this rifting episode is mid-Aptian to late Cenomanian. The Jeanne d'Arc basin also participated in this phase of NE-directed extension, expressed in the asymmetric synrift geometries between the Aptian unconformity and the end-Cenomanian Petrel limestone (Figs. 14.1 and 14.3; Sinclair, 1995; Tankard and Welsink, 1987). Before the Aptian, the Dominion transfer had partitioned strain between the Grand Banks and Orphan provinces, but in this new extensional phase both regions were jointly affected.

After the mid-Aptian, extensional stresses were aligned approximately with the axis of the Jeanne d'Arc basin, thereby imposing a dip-slip sense of displacement on the cross-basin transfer faults, including the Dominion structure (Tankard et al., 1989). NE-directed extension resulted in domino-style rotation of these basement blocks and northward deepening of the basin floor across a series of fault-block steps (Fig. 14.7). The depth to the top of these tilted fault blocks in

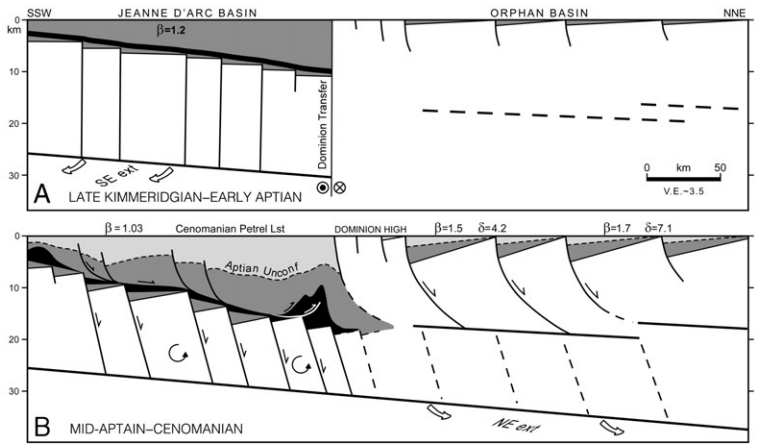

Figure 14.7 Interpretation of Jeanne d'Arc–Orphan basin NE-oriented extension; mid-Aptian–Cenomanian. (A) Until early Aptian, Dominion transfer partitioned strain between Jeanne d'Arc and Orphan. SE-directed extension of Jeanne d'Arc was accommodated by intracrustal detachment at 26 km (10.5 s) and upper plate dissected by transfer faults. (B) After mid-Aptian, NE-directed extension of Orphan basin by intracrustal detachment at 15–17 km on which listric basin faults merge (Lithoprobe East deep seismic line 84–3). In Jeanne d'Arc, the previous transfer faults were reactivated by anti-clockwise domino-style rotation, probably continuing under the Orphan detachment. Minimal upper crustal extension, implying basin deepening due to lower crust and mantle flow (see Keen et al., 1987a). Basin plunge resulted in gravity-driven detachment of the sedimentary cover above basement, distally buttressed by Dominion structure. Jurassic salt was expelled and formed distal Adolphus diapir complex.

the Jeanne d'Arc basin coincides with the level of Orphan basin detachment, 18 km and 15–17 km, respectively. We suggest that this array of domino-tilted blocks continued beneath the Orphan intracrustal detachment; line 85–3 is of variable quality and cannot resolve the deep structure. These various seismic structural interpretations together have intriguing consequences. First, Early Cretaceous SE-directed extension was accommodated by an intracrustal detachment at ~26 km beneath the Jeanne d'Arc basin (Fig. 14.5). Second, NE-directed extension of the Orphan basin in the mid-Cretaceous used a detachment at 15–17-km depth, and likely involved tilt-block rotation of the sub-detachment lithosphere as well. This arrangement suggests that the upper plate of the Grand Banks–Iberia extension became the lower plate, possibly an extensional wedge, of the Orphan basin extension.

Substantial basin deepening is attributed to lower crust and mantle flow. Modeled subsidence curves (Keen et al., 1987a) predict that subcrustal extension (δ) is everywhere greater than extension of the brittle crust (β). This would explain the northward plunge of the Jeanne d'Arc basin. The small amount of rotation of the basement blocks (<5% extension) is not enough to explain the observed over-deepening. A large positive gravity anomaly that forms an arcuate rim along the inboard edge of the Orphan basin is not associated with topography in the upper crust, and is attributed to flexure at the crust-mantle level (along latitude 48° in Fig. 14.4A; Welsink et al., 1989a). Regional subsidence and basin over-deepening continued until separation from the European continental plate in the Santonian (84 Ma chron 34; Srivastava et al., 1988) and opening of the Bay of Biscay.

Tectonic linkage between continental and oceanic lithosphere

The gross morphology of the extensional basins and their principal normal and cross-basin transfer faults were controlled by reactivation of preexisting weaknesses in the continental crust. These crustal weaknesses are interpreted from gravity and magnetic anomaly trends (Figs. 14.4 and 14.8). On the adjacent oceanic crust, relative plate motions are recorded in magnetic lineations and fracture zones (Srivastava and Tapscott, 1986). The calculated flow lines describe the relative motions between the North American, Iberian, and Eurasian plates.

The extensional architecture of the Grand Banks and the flow lines in the oceanic crust are perfectly matched. Trends of transfer faults and gravity-magnetic trends in the continental crust are largely collinear with the fracture zones and flow lines in the ocean floor, implying tectonic-structural linkage between continental and oceanic crust. This correlation is reinforced by the change in orientation from the NW–SE Grand Banks–Iberia extension to the SW–NE Orphan basin–Goban Spur extension. The chronology of continental extension and sea-floor spreading, including their periodic adjustments, is preserved in the Jeanne d'Arc basin

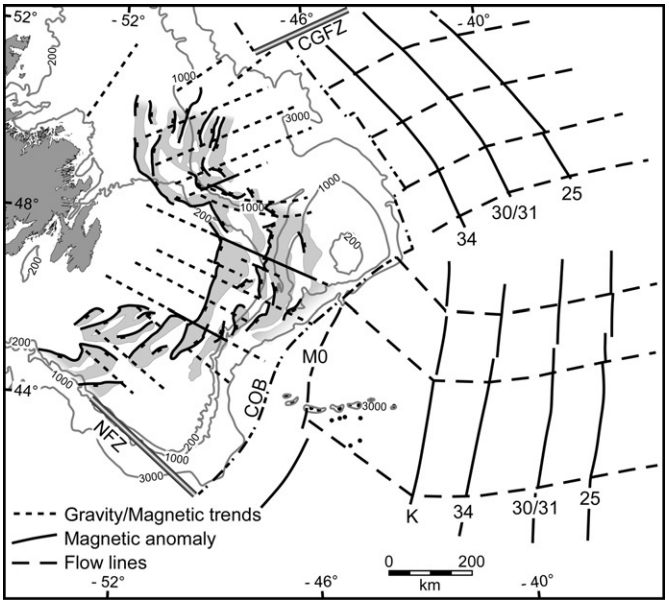

Figure 14.8 Structural framework of basin development in Grand Banks and Orphan provinces, derived by integrating seismic mapping with gravity and magnetic anomaly trends, compared with distribution of fracture zones and flow lines in oceanic crust. Flow lines derived from poles of rotation of the North Atlantic (Srivastava and Tapscott, 1986; Srivastava et al., 1988). Collinear structural trends due to SE-oriented and NE-oriented extensional events on continental and oceanic lithosphere suggest tectonic linkage. In the Jeanne d'Arc basin fill (Fig. 14.3), the unconformities at sequence boundaries and the ages of magnetic anomalies coincide, confirming the tectonic control of basin subsidence and the succession of stratigraphic sequences. CGFZ, Charlie Gibbs Fracture Zone; NFZ, Newfoundland Fracture Zone. *(Modified after Welsink et al., 1989a.)*

fill (Fig. 14.3). The unconformities in the basin fill mark periodic changes in the patterns of subsidence, while the ocean-floor magnetic anomalies record the course of sea-floor spreading. These are two sets of data that are dated by very different means. Nevertheless, there is an exceptionally close correspondence between the two, making the argument for tectonic linkage compelling.

The subdivision of the area between the Charlie Gibbs and Newfoundland fracture zones is interpreted from potential-field data and seismic structural mapping (Figs. 14.1 and 14.4). The southern and central Grand Banks have similar SW-striking basin fault patterns, despite being offset from each other across the Avalon transfer. The Orphan basin is marked by an arcuate array of faults that are generally NW-oriented. Although Tankard and Welsink (1987) emphasized a tectonic linkage between continental and oceanic crust, they did not elaborate on the structural framework within the Grand Banks and Orphan basin. This is

important because it facilitates precise structural linkage between conjugate margins, and explains the distribution of the sizes and shapes of structural complexes and basins alike, and the differences in timing of extension. Examples include the structural zones of the south Orphan–South Armorican fault, Dominion fault–Galicia Bank, Avalon fault–Aveiro fault, and Collector anomaly–Nazaré fault (Fig. 14.2), and the similarities of basin styles between them. Furthermore, because Mesozoic extension was guided by inherited basement fabrics, we suggest that the patterns of extension and ocean opening have a significant ancestry. These old perturbations of the brittle crust were probably able to influence the patterns of sea-floor behavior because they focused and accommodated the thermal effects of the subcrustal lithosphere.

In summary, the evolution of the Grand Banks basins and Orphan basin is attributed to the reactivation of old crustal fabrics and the orientation of extensional stresses. Differences in the amounts and styles of extension were accommodated by transfer faults that divide the region into distinct tectonic provinces. Failure of the Grand Banks during extension probably involved pure-shear and simple-shear processes before accumulated strain developed a system of low-angle intracrustal detachment faults. The Callovian–Aptian extension between the Grand Banks and Iberia developed a down-to-the-west detachment, while the mid-Aptian–Cenomanian Orphan basin extension was directed to the northeast. Extension involved a suite of overlapping, asymmetric crustal plates such that the upper plate of the SE-directed extension later became the lower plate to the NE-directed extension (Figs. 14.6 and 14.7).

14.3 Jeanne d'Arc structural styles

Subsidence of the Jeanne d'Arc basin was intermittent and controlled by faults rooted in preexisting basement structures. This discussion will focus on Callovian–Cenomanian events. It is difficult to fully interpret the underlying Triassic-Lower Jurassic section because of the limitations of seismic record length, and because the Callovian–Aptian extension was rooted in the earlier rift structures. Nevertheless, a conspicuous absence of seismic thickness and amplitude variations suggests that the Lower Jurassic post-rift accumulation was little affected by intrabasin structures.

Petroleum was generated and accumulated in the synrift sediments. The climax of extension in the Kimmeridgian–Barremian (Fig. 14.3) was controlled by NNE-oriented listric and planar fault sets and SE-striking transfer faults. Together these faults formed the asymmetric, funnel-shaped geometry of the half graben (Fig. 14.9). Small-displacement, right-lateral strike-slip movement along the transfer faults also created Riedel shears and tension gashes within the sedimentary cover. During the Aptian–Cenomanian, reservoirs were formed by erosion and deposition along the tilted edges of detached and rotated transfer blocks (i.e., structural blocks

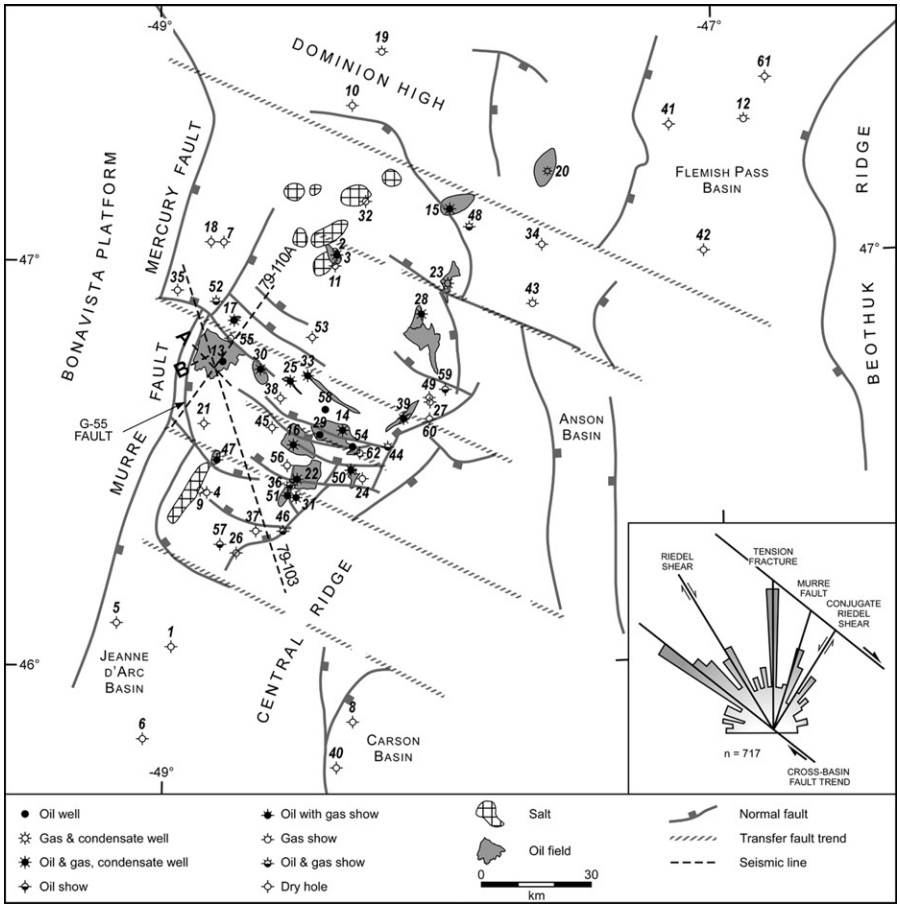

Figure 14.9 Variable extension of Jeanne d'Arc basin was accommodated along transfer faults that offset the margins of the basin, resulting in the irregular funnel-shaped geometry. Oil-field distribution is closely related to cross-basin faults. This map is simplified, but is on the basis of exploration seismic structure maps that are extrapolated regionally by correlation with gravity anomalies. Data for rose diagram (insert) mainly from the cover sequence. There is a 15°-clockwise rotation, best shown by transfer fault trends, because of detachment and rotational translation of the cover. Seismic line locations: 79–103 is Fig. 14.10, 79–110A is Fig. 14.12, A and B are conventional and high-resolution lines in Fig. 14.18. Exploration well locations are in order of spud dates: 1, Cormorant N-83. 2, Adolphus K-41. 3, Adolphus 2K-41. 4, Egret K-36. 5, Murre G-67. 6, Spoonbill C-30. 7, Flying Foam I-13. 8, Bonnition H-32. 9, Egret N-46. 10, Dominion O-23. 11, Adolphus D-50. 12, Gabriel C-60. 13, Hibernia P-15. 14, Ben Nevis I-45. 15, Tempest South G-88. 16, Hebron I-13. 17, Nautilus C-92. 18, Flying Foam West L-23. 19, Bonanza M-71. 20, Dana North I-43. 21, Rankin M-36. 22, Terra Nova K-08. 23, Trave E-87. 24, Voyager J-18. 25, Mara South C-13. 26, Port au Port J-97. 27, Archer K-19. 28, White Rose N-22. 29, Ben Nevis West B-75. 30, Mara M-54. 31, Beothuk M-05. 32, Conquest K-09. 33, Ben Nevis North P-93. 34, Panther P-52. 35, Mercury K-76. 36, Terra Nova K-17. 37, Gambo N-70. 38, Mara E-30. 39, Fortune G-57. 40, St. George J-55. 41, Lancaster G-70. 42, Kyle L-11. 43, Golconda C-64. 44, Bonne Bay C-73. 45, Avondale A-46. 46, South Brook N-30. 47, East Rankin H-21. 48, South Merasheen K-55. 49, Amethyst F-20. 50, Springdale M-29. 51, King's Cove A-26. 52, Thorvald P-24. 53, Botwood G-89. 54, Bonne Bay West C-23. 55, South Nautilus H-09. 56, Brent's Cove I-30. 57, Riverhead N-18. 58, Cape Race N-68. 59, Trepassey J-91. 60, Gros Morne C-17. 61, Tuckamore B-27.

between transfer faults). The northward plunge of the Jeanne d'Arc basin at this time resulted in gravitational collapse of the basin fill above basement.

Basement-involved faulting

Crustal extension was accommodated by movement along listric and planar normal faults. The Jeanne d'Arc basin owes its typical half-graben asymmetry to extensional subsidence along a listric boundary fault system (Fig. 14.10). The Murre fault is the principal basin-forming fault and soles at ~26 km (10.5 s) along a low-angle intracrustal décollement. Lithoprobe line 85–4A shows, at

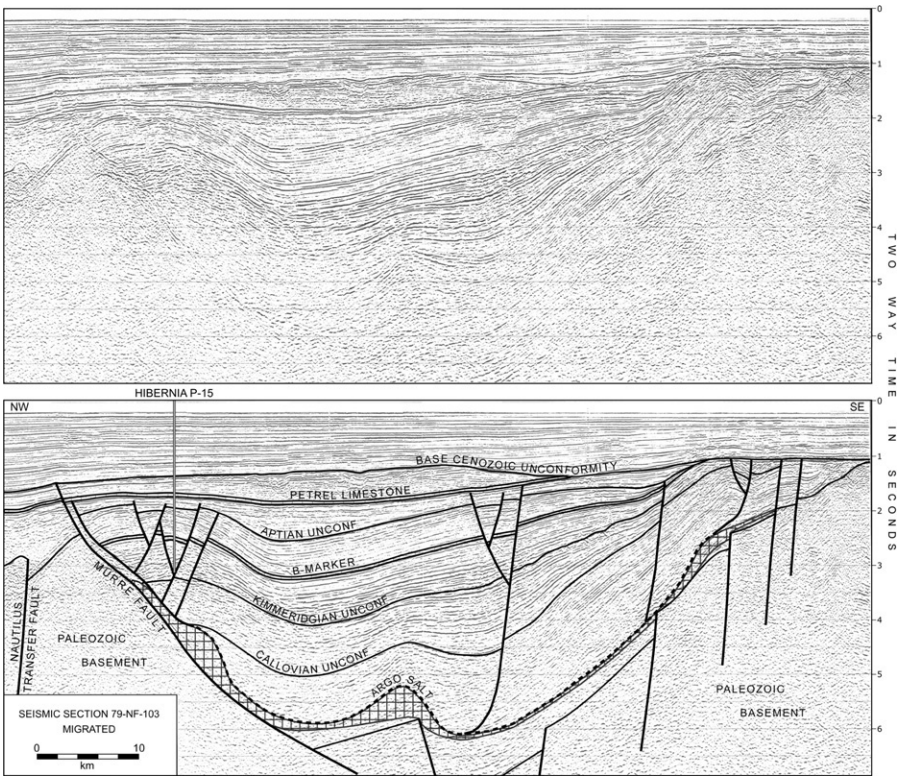

Figure 14.10 Seismic line 79-NF-103 showing half-graben asymmetry of Jeanne d'Arc basin and major unconformity-bounded sequences (see Fig. 14.9 for location). Late Jurassic–Early Cretaceous extension was accommodated by listric and planar faults that parallel the axis of the basin. The listric basin-forming Murre fault was active during late Callovian–early Aptian rifting, as shown by characteristic rollover of Hibernia structure. Unconformities merge on the eastern ramp of the basin, indicating persistent positive relief of the Central Ridge. Horst relief was maintained at regional levels by rotational transport, as an extensional allochthon, on an intracrustal detachment (Fig. 14.5). The Nautilus transfer fault offsets the Hibernia relay – hanging-wall ramp structure (Fig. 14.11). Post-Aptian detachment of the basin fill occurred above Argo salt and over-pressured Upper Jurassic shales, shown by broken line. Rotation of the cover above the detachment is indicated by folding along the eastern horst ramp. *(Seismic line courtesy of Geophysical Service Inc.)*

depth, a change in the path of the Murre fault plane, presumably in response to upward arching of the décollement due to extensional tectonic unloading late in the rift cycle (Figs. 14.5 and 14.6). Whether this shift was to maintain an efficient fault plane geometry or not, the result is an extensional horse or duplex.

The Murre fault is characterized by a listric geometry and rotation of the synrift succession into the fault plane (Fig. 14.10) (Welsink and Tankard, 1988). The Hibernia rollover structure on the Murre fault was later deformed by salt diapirism. Formation of synthetic fault sets created detached riders that impart a ramp-flat geometry to the floor of the basin. These riders significantly influenced later deformation of the basin fill. Extension along the system of listric faults also required accommodation within the hanging-wall, including rollover of the crustal rocks and development of antithetic and synthetic normal faults (Figs. 14.5 and 14.10). Together, these elements form a terraced horst ramp that ascends eastward to the Central Ridge.

Cross-basin transfer faults of various scales control the overall shape of the basin and also compartmentalize the basin internally. We have simplified the transfer faults as linear traces (Figs. 14.1, 14.4, and 14.9). However, detailed seismic structural mapping shows that these transfer faults are relatively broad transfer zones that consist of *en echelon* and gently sinuous strands, each of which relays strain from its neighbor (Tankard and Welsink, 1987, their Fig. 11). First-order transfer faults divide the basement into several extensional tracts characterized by distinct basin types and structural styles (Fig. 14.1): pull-apart basins of the southern Grand Banks, deep dip-slip basins of the central Grand Banks, and the arcuate Orphan basin complex. These faults penetrate the crust and locally offset the Moho, besides accommodating different levels and polarities of intracrustal detachment at lateral ramps. The Dominion transfer consecutively offsets several basins and forms the precipitous southern edge of the Flemish Cap. Secondary transfer faults have the more modest role of compartmentalizing the basins and accommodating differences in style and rates of extension within basins.

In plan view, the major basin-bounding faults are offset several kilometers across transfer faults (Fig. 14.9). But at depth Lithoprobe deep seismic line 85–4A shows that the individual fault segments share the same level of detachment (Fig. 14.5). These offsets of the upper parts of the normal faults were present from the beginning, but were accentuated as extension continued. For example, the Hibernia and Mercury structures are linked by a Z-shaped fault pattern formed by *en echelon* normal faults and the connecting Nautilus transfer fault (Figs. 14.1 and 14.9). The seismic expression and interrelationships of these faults are shown in Figs. 14.10 and 14.11. The offset listric fault traces are connected by an eroded ramp onlapped by synrift sediments. This is a typical relay structure in which the relay ramp transmits the displacement from one offset listric fault to the next (Larsen, 1988; Tankard et al., 1989). The relay ramp eventually failed and was offset across a transfer fault. Stratigraphic relationships between the Hibernia and Nautilus successions suggest that the evolution from

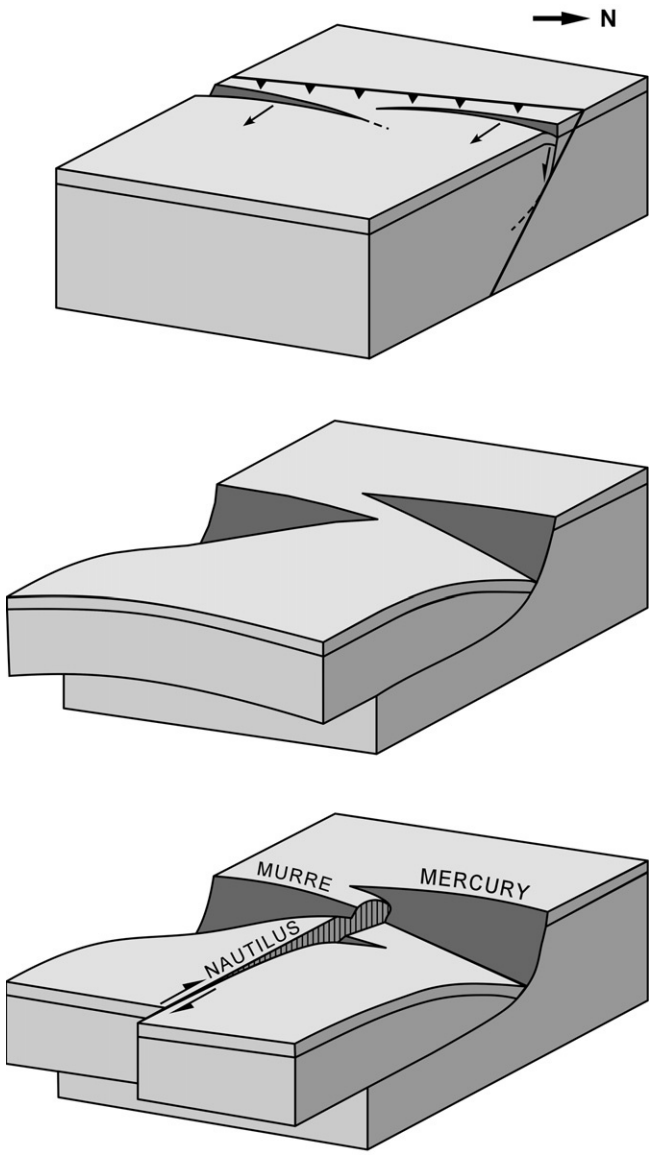

Figure 14.11 Evolution of a relay structure and transfer fault system based on seismic and well data from the Hibernia and Nautilus oil fields (see also Fig. 14.17). The listric faults were originally offset because they reactivated old basement structure. Increasing extensional strain resulted in breakdown of the relay ramp structure and development of a transfer fault. Preservation of the tip line of the Murre fault across the Nautilus transfer is mapped seismically *(sketch of relay structure inspired by Larsen, 1988; modified after Tankard et al., 1989).*

low-strain relay deformation to higher-strain transfer faulting occurred in the Early Cretaceous.

Transfer faults were the dominant structure in the Barremian. The intermittent nature of extension may have allowed periodic lockup and re-faulting of the relay system. Transfer faults are characteristic of all extensional terranes because the brittle, inhomogeneous crust cannot extend uniformly. On the Grand Banks, Paleozoic and Triassic deformation established the primary structural grain. The irregular margin of the Jeanne d'Arc basin with its transfer faults is not unique.

Fault analysis

Structural mapping of a basin should, ideally, be at the level of the basement reflection. In practice, the interval of economic interest and seismic mapping is well above basement; in the Jeanne d'Arc it is typically between 2 and 5 km depth. Most of the structures mapped reflect deformation of the sedimentary cover and do not everywhere show the precise location of underlying basement structure. The relationship of cover deformation to basement-involved faulting is best shown along the margins where the basin floor shallows. However, on a regional scale discrepancies are generally insignificant. Our structural analysis is on the basis of seismic structure maps at various scales and stratigraphic levels, the seismic expression of these structural styles, and construction of balanced cross-sections (cf. Gibbs, 1983). Basinwide cross-sections have also been compiled from reflection seismic and well data (Tankard et al., 1989, their Fig. 8). The timing of structural deformation is constrained by detailed palynological biostratigraphic analysis.

The distribution of the faults in the Jeanne d'Arc basin has a strong bias toward cross-basin trends. The rose diagram compilation (Fig. 14.9) resolves these patterns. Two major fault trends involve basement, namely, the NNE-striking extensional basin-forming faults such as the Murre fault, and the SE-striking cross-basin transfer faults. These fault trends coincide with gravity anomalies across the unextended Bonavista platform, not only suggesting that they are rooted in Paleozoic basement fabrics, but also explaining why the extensional faults and transfer faults are not quite orthogonal to each other.

The residual fault distribution is trimodal, but appears to be related kinematically to right-lateral strike-slip motion of the transfer faults. Riedel shear and conjugate Riedel shear trends formed as a result of the right-lateral shear couple. The conjugate form is subordinate. Bisecting these two trends is a prominent peak interpreted as tension fractures. Typical dogleg fault patterns formed where Riedel shears and tension fractures combined to connect transfer faults. Each of these fault types has been involved in the evolution of the Hibernia structure. However, the varying thicknesses of several stratigraphic sequences (e.g., the Hibernia and Avalon sequences) clearly are related to the behavior of the extensional and transfer faults. The G-55 fault (Fig. 14.9) formed late in the rift cycle by detachment and NE-translation of the basin fill.

Late Cretaceous detachment of the basin fill

The normal and transfer faults in the basement define the overall pre-Aptian basin framework. The next phase of extension in mid-Aptian–Cenomanian time was NE-oriented and caused significant disruption of the basement faults and sedimentary cover alike. Most conspicuous was transtensional displacement on the NNE-striking basin-bounding faults and domino-style rotation of the cross-basin faults (the old transfer faults). The floor of the Jeanne d'Arc basin deepened northward across down-stepping fault blocks to form an overall ramp-flat geometry (Fig. 14.12). (We mapped this array of basement structures from the dense grid of 3D seismic.) The northward-plunging basin resulted in massive gravitational failure of the sedimentary cover above basement. Translation of the detached cover created a listric fan and a new set of faults that were guided by the overall ramp-flat shape of the footwall (Figs. 14.12 and 14.13).

The detachment surface is asymmetric in profile like the basin. Depth-to-detachment calculations and seismic show that, at its deepest, detachment occurred principally on Lower Jurassic salt and over-pressured Upper Jurassic shales (Fig. 14.10; Welsink and Tankard, 1988). A large amount (~5 km) of rotational translation down the plunging axis of the basin is expressed in the extensional wedge-shaped sections between the Aptian unconformity and Petrel limestone (Fig. 14.12), as well as in the curved cross-basin faults (Fig. 14.13). The northward-directed listric rotation was translated into a strike-slip component along the older basin-bounding extensional faults. In the Hibernia field, SE-oriented normal faults and Riedel shears terminate at the G-55 fault which parallels the listric Murre fault. Whereas apparent throw on the G-55 fault ranges between 50 and 200 m, strike-slip movement was about 1.5 km, equivalent to the amount of extension southwest of Hibernia. Opposite the Mercury fault, the 5-km-high (4 s) Flying Foam structure formed as a marginal detachment fold above the ramp-flat of a basement rider (Tankard et al., 1989, their Fig. 12). The cover detachment responded very differently to the terraced ramp that forms the eastern margin of the basin because there was no salt or over-pressured shale to facilitate movement. Detached blocks of cover sediments are thin and are encapsulated within a network of shallow splays of the detachment fault system. Many cross-faults are offset with opposite dips ("scissor" faults).

Seismic and well data clearly show the sequence of fault development (Fig. 14.12). Initial displacement of the hanging-wall was substantial and interacted with the down-stepping footwall to form a hanging-wall anticline and syncline couple. The Avalon sequence of the Hibernia and Nautilus structures is deeply eroded and thinned across the structural culmination. Development of the anticline in the hanging-wall was accommodated by antithetic and synthetic faulting. Persistent rotation of the Hibernia structure is reflected in onlap onto its southern flank. Finally, a shortcut fault (cf. Gibbs, 1984) developed above the Nautilus transfer fault between the anticline and syncline, separating the

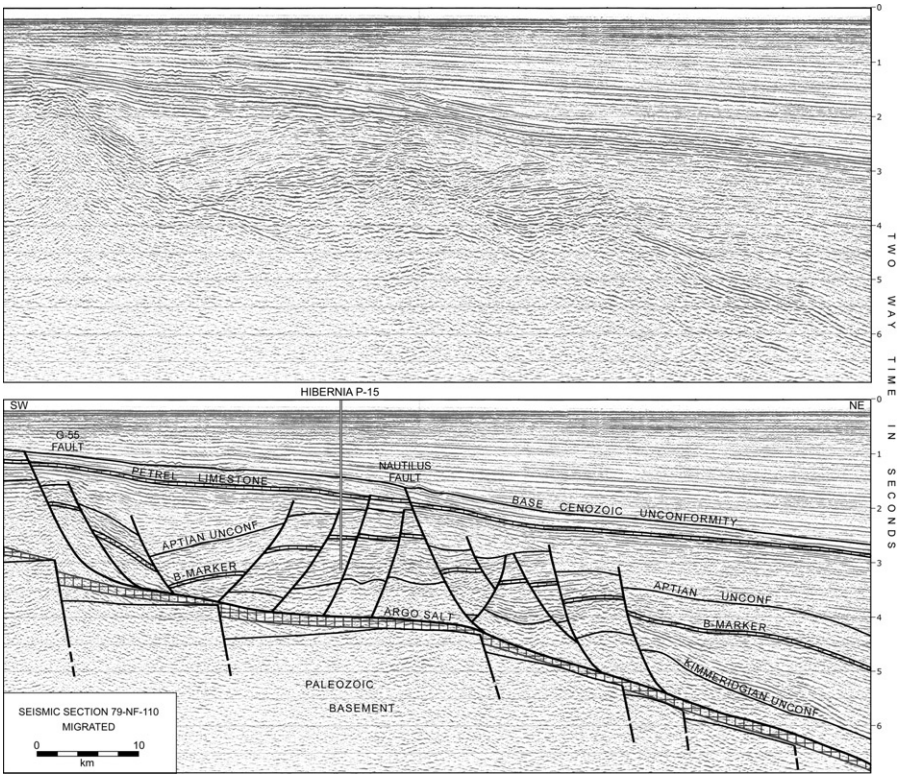

Figure 14.12 Seismic line 79-NF-110A is close and subparallel to the Murre fault margin of the basin (see Fig. 14.9 for location). Basement is regularly offset across fault-block steps, because the transfer faults were reactivated in a dip-slip sense after the mid-Aptian. The asymmetric basin fill between the Aptian unconformity and Petrel limestone marks the mid-Aptian–Cenomanian phase of NE-directed extension. The northward plunge resulted in gravitational failure of the cover above basement (Fig. 14.7). Detachment used the Argo salt and over-pressured shales. Down-stepping basement blocks impart a ramp-flat-ramp shape to the detachment surface, above which a listric fan and antithetic faults developed. The Hibernia structure was modified into a transverse ridge where the Nautilus shortcut fault separated the hanging-wall anticline and syncline. Tilting of the Hibernia hanging-wall ramp or transverse ridge is indicated by reflections that onlap the Aptian unconformity. Interpretation of this seismic line was constrained by a dense grid of cross-cutting seismic lines, including Hibernia 3D seismic coverage, and well control. *(Seismic line courtesy of Geophysical Service Inc.)*

Hibernia and Nautilus structures and forming a transverse ridge; displacement across this shortcut fault is 900 m. Faults in the hanging-wall apparently are genetically related to transfer fault trends.

Development of the supracrustal detachment and its associated structural patterns has important consequences for hydrocarbon exploration. They form

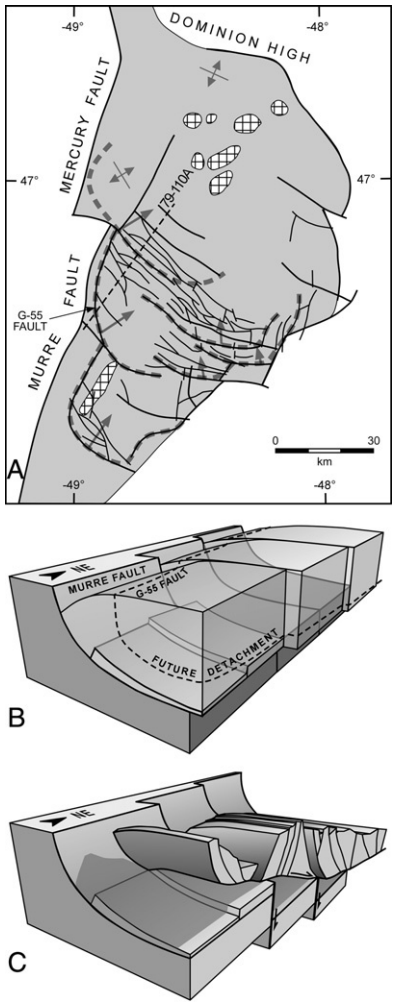

Figure 14.13 Jeanne d'Arc NW–SE extension occurred along listric normal extensional faults and cross-basin transfer faults. In mid-Aptian–Cenomanian time, NE-oriented extension caused domino-style reactivation of the cross faults, northward over-deepening, and detachment of the basin fill above basement. (A) Tip line of the cover detachment is shown in relation to basement faults. The G-55 fault hugs the Murre fault plane (Fig. 14.10), translating northward dip-slip movement into a strike-slip component with 1.5 km of displacement. The large Flying Foam marginal detachment fold formed opposite the Mercury structure. In the center of the basin, the cross faults are curved northward by translation; we measure 5.3 km of translation. Along the shallow, lower-angle ramp of the Central Ridge the detachment tip line is diffuse and splayed. (B) Extension accommodated by listric faults and transfer faults. (C) The northward-translated detached cover formed an anticline-syncline couple which broke up by antithetic and synthetic faulting. Translation caused the distal Adolphus diapirism.

structural traps and fault seals, and affect migration routes, dispersal patterns, and preservation of sedimentary facies. There is an association of clay smearing with this strike-slip component of displacement that may partly explain several of the dry wells around the margin of the Jeanne d'Arc basin (e.g., Hibernia G-55, Voyager J-18, Archer K-19, Trave E-87).

Large salt-cored structures in the Jeanne d'Arc basin include elongate pillows and piercement diapirs, several of which have been drilled, including Adolphus, Cormorant, Egret, and Hibernia (Figs. 14.7 and 14.13). Salt growth onto structural highs was partly induced by rotation of basement fault blocks. The Argo salt sheet facilitated detachment of the cover, but translation of this cover and loading caused expulsion of the salt to form the Adolphus cluster of salt pillows in the northern Jeanne d'Arc basin. Synkinematic salt growth was augmented by structural inversion where the Dominion high buttressed the displaced cover. The Egret diapir in the southern Jeanne d'Arc formed primarily by rotation of the underlying fault block.

In summary, cross-basin transfer faulting resulted in the conspicuous offset pattern along the margins of the Jeanne d'Arc basin, and internally compartmentalized the basin into east–west segments (Fig. 14.9). A new phase of NE-oriented extension from mid-Aptian to the Cenomanian reactivated and tilted these cross-basin structures. Large-scale failure of the basin fill resulted in gravitational translation and anti-clockwise rotation as the cover detached above salt and over-pressured shales (Figs. 14.10 and 14.12). The resulting structural patterns and relative movements influenced the maturation, migration, and trapping of hydrocarbons, reservoir distribution, and salt diapirism.

14.4 Stratigraphic response

The Jeanne d'Arc basin subsided through several distinct episodes, each with a unique tectonic history and characteristic seismic signature. In this section, we describe the depositional response to intermittent extension (Fig. 14.3).

Late Triassic–Middle Jurassic rift system

The earliest episode of rifting spanned ~30 Ma from the Carnian to the Sinemurian. This interval in the Jeanne d'Arc basin varies up to 2.5 km (1 s) thick between basement and the first strong reflector interpreted as an upper Sinemurian–Pliensbachian transgressive carbonate (Figs. 14.3 and 14.5). Diverging reflectors trace the basin asymmetry, but its original size is unknown. The early basin fill consists of thick argillaceous red beds and evaporites (Hubbard, 1988; Tankard and Welsink, 1988). Relevant wells are Hibernia I-46, Murre G-67, Cormorant N-83, and Spoonbill C-30.

The evaporite-carbonate stratigraphy overlying the red beds accumulated as a regional blanket without any obvious structural control, probably in response

to lower-plate extension. Rheological weakening and thermal relaxation resulted in a broad downwarp that straddled both conjugate margins (Tankard and Welsink, 1987). A monotonous succession of Pliensbachian–Bathonian calcareous mudstones and carbonates, uninterrupted by significant unconformities, reflects a long history of uniform subsidence. Furthermore, seismic shows little evidence of thickness or amplitude variation to indicate structural relief or fault activity. Transgression and basin deepening were most pronounced in the Toarcian; these sediments contain a shallow marine Tethyan fauna. Until the mid-Jurassic, this shallow basin remained underfilled, although periodic fluctuations of sea level did result in stacking of limestone-capped shale sequences. Farther south, continent–continent translation along the Newfoundland transform culminated in separation of northwest Africa, which is marked by a pronounced breakup unconformity in the Sable basin offshore Nova Scotia (Welsink et al., 1989b). This event correlates with the end-Toarcian limestone sheet in the Jeanne d'Arc basin.

Late Jurassic-Early Cretaceous extension

The intense episode of rifting from the end-Callovian to early Aptian lasted for 45 Ma, and established the structural architecture of the Jeanne d'Arc basin (Fig. 14.9). Subsidence was intermittent. The thick synrift succession is punctuated by numerous unconformities or limestone markers that approximate regional time lines (based on biostratigraphy), by which it is subdivided into six smaller sequences indicating a variable 4–10 Ma periodicity of basin subsidence.

The synrift succession is asymmetrical and has conspicuous rollover into the listric Murre fault, such as in the Hibernia structure, where it is characterized by pronounced stacking of terrigenous sediments (Fig. 14.10). The opposite margin is the terraced ramp of the Central Ridge horst block, an extensional allochthon, across which stratigraphic units wedge out by depositional and erosional thinning. Compared with the Hibernia margin, these sandstone intervals are relatively thin and clean, and facies tracts are laterally more continuous. The principal petroleum reservoir intervals include the Jeanne d'Arc, Hibernia, Avalon, and Ben Nevis sandstones (Fig. 14.3).

There were three stages of Late Jurassic–Early Cretaceous structural evolution and subsidence (Figs. 14.3 and 14.14). *First*, the late Callovian–middle Kimmeridgian onset of rifting over a 9-Ma period fragmented the preceding epeiric basin into smaller depocenters. But apart from minor subsidence along the principal basin-forming faults, there was little internal structural relief so that deposition of limestones and oil-prone shales formed an irregular blanket (Fig. 14.14A). *Second*, late Kimmeridgian–early Valanginian fault-controlled subsidence and high structural relief characterized the climax of rifting, and was accompanied by deposition of fluvial clastics in restricted marine and shallow basin environments (Fig. 14.14B).

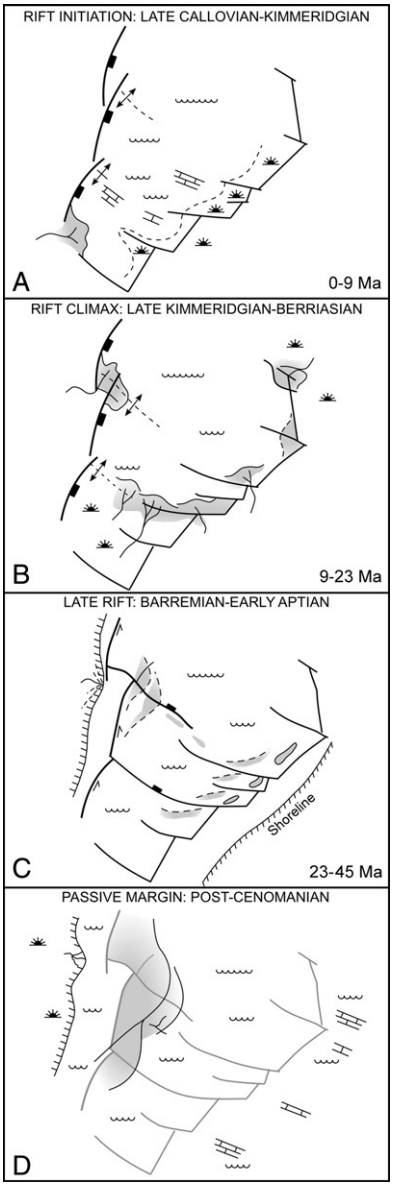

Figure 14.14 Mid-Mesozoic extension developed in three stages followed by regional post-rift subsidence. (A) Initiation of extension largely unassisted by brittle failure and faulting. Subtle structure started to develop only in the Kimmeridgian. Characterized by low structural relief and a broad calcareous-shale basin and source rock accumulation. (B) Fault-controlled rift climax, significant structural relief, alluvial and restricted marine depositional systems. (C) Late rift with decreasing fault intensity, low structural relief and basinwide drape, normal marine circulation. (D) Breakup and passive margin terrace wedge includes a Paleocene progradational fan complex. *(Modified after Tankard and Welsink, 1988.)*

This phase of subsidence lasted for 14 Ma. *Third*, late Valanginian–early Aptian subsidence over a 22-Ma period was slower, and syndepositional normal faulting much less intense. A shallow marine paleogeography spilled across the rift shoulders (Fig. 14.14C). The late Jeanne d'Arc was an underfilled basin with normal marine circulation. The Valanginian B marker limestone roughly separates the earlier closed basin system from this later open system (Figs. 14.3 and 14.10). Continental separation terminated the mid-Mesozoic episode of rifting.

Rift initiation: Late Callovian–middle Kimmeridgian

After a long period of flexural subsidence, the transition to an extensional regime began gradually in the late Callovian, expressed seismically by an unconformity and stratigraphic onlap along the southeastern margin of the basin (Figs. 14.3 and 14.10). Fault activity was subtle at best. Elsewhere sedimentation continued without significant interruption and the onset of late Callovian extension is marked by an increase in reflectivity (e.g., Rankin M-36). This incipient rift accumulation varies up to 1300 m or more in thickness and is dominated by argillaceous and calcareous rocks that accumulated in a shallow, low-relief euxinic environment. Calcareous shales are the principal source rock in the basin (Powell, 1985; von der Dick et al., 1989).

Subtle as it was, the onset of fault activity contributed toward an irregular, compartmentalized landscape of east–west basin segments (Figs. 14.9 and 14.14A). For example, the lower–middle Kimmeridgian source rock locally thins to 30 m (South Mara C-13) within a wedge of unconformities associated with cross-basin faults (Tankard and Welsink, 1987). Of the three periods of source-rock accumulation, two accumulated during this incipient extensional prelude: early–middle Kimmeridgian (26–143 m thick) and late Kimmeridgian (14–100 m thick; Tankard et al., 1989). These source rock shales form a southward-thickening wedge between Hibernia and Rankin (Fig. 14.9; Hibernia K-18 and Rankin M-36).

This stratigraphy shows that extension began gradually and without significant fault control. The equivalent on the Iberian margin (ODP 103) is a condensed section (Boillot et al., 1985); thus it is questioned whether a pervasive intracrustal detachment had yet developed. It appears that the locus of the early passive phase of subsidence was on the Grand Banks, and that subsidence was due to coaxial stretching (pure shear; cf. McKenzie, 1978).

Rift climax: Late Kimmeridgian–early Valanginian

For the next 14 Ma, subsidence was controlled by rotation along the listric Murre fault, which created substantial structural relief, and by transfer and antithetic faults (Fig. 14.14B). The Jeanne d'Arc and Hibernia sequences were deposited as progradational aprons around the margin of a restricted nonmarine to weak marine basin (Figs. 14.3, 14.10, and 14.14B). In each, after a vigorous start, there was a systematic change upwards to accumulation of argillaceous

sediments. It appears that initial structural relief was quickly established, and that intense fault activity was short-lived.

Of the entire synrift succession, the *Jeanne d'Arc sequence* contains the greatest volume of coarse terrestrial material, and was superimposed abruptly on the earlier argillaceous fill. A prominent structurally controlled dispersal system of deeply eroded fluvial channels and sandy fan-delta and delta front complexes occupied the southern apex of the basin (e.g., Terra Nova K-08 and K-18). Ubiquitous soft-sediment deformation is attributed to contemporaneous fault activity. In the Hibernia oil field, structural entry points fed a system of alluvial fans consisting of conglomerates, immature sandstones, and mudstones. The alluvial facies associations are arranged in upward-coarsening sequences up to 100 m thick (Fig. 14.15). Fringing basinal facies were deposited in weak marine environments, also as progradational upward-coarsening sequences (e.g., South Mara C-13). Conifer forests grew along the edge of the basin, supplying a rain of *Classopollis* pollens and woody material.

Extensional rotation maintained the positive elevation of the Central Ridge (Fig. 14.6). Eastward thinning seismic sequences and converging unconformities are evidence of this persistent topography (Fig. 14.10). Here, the Jeanne d'Arc succession consists of interbedded mudstones and sandstones deposited in shoal-water environments with periodic emergence: interpreted from sandstone maturity and coal spar, trace fossil assemblages, and tidal channels (Hebron I-13).

The *Hibernia sequence* was a repeat of this history. Listric normal faulting, extensional rollover, and fluvial influx reinvented the Late Jurassic tectonic landscapes, but noticeably absent were the conglomeratic facies, probably because structural relief and gradients were more subdued. Also similar to the Jeanne d'Arc paleogeography, fault activity quickly established topographic relief, after which there was general denudation, relaxation, and deposition of a thick mudstone cover. The *en echelon* left-stepping strands of the Murre and Mercury boundary faults were linked via a relay structure, while asymmetric rollover into the listric Murre fault from its tip point created a hanging-wall ramp. Brittle failure of the flexural hanging-wall ramp may explain the structural complexity of the Hibernia field. Hibernia and Nautilus wells record deposition across this structural complex. Hibernia isopachs are oblique to the Murre fault and trace the contours of the hanging-wall ramp to form a southwestward thickening wedge (Figs. 14.16 and 14.17A).

The Hibernia sandstone interval is up to 180 m thicks and was built by bedload rivers with associated floodplain and bay-margin facies associations which are attributed to a lobate fan-delta paleoenvironment (Figs. 14.14B and 14.15; Tankard and Welsink, 1987). Bedload rivers generally construct multilateral and stacked framework bodies as they change course by avulsion. Figure 14.16 shows the internal geometry of the Hibernia sequence on the basis of quantitative models to predict sand-body continuity. The asymmetry of the Hibernia sandstone wedge matches the geometry of the hanging-wall ramp. Interlaminated

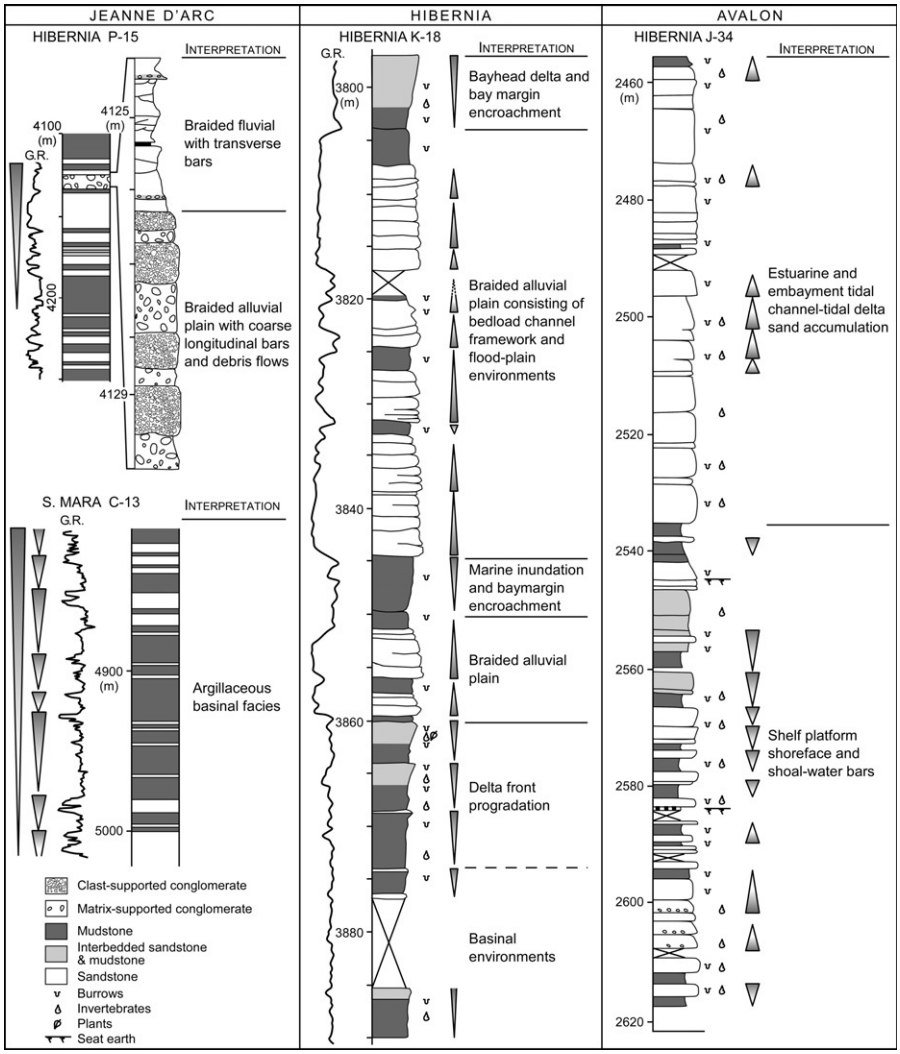

Figure 14.15 Measured sections of the Jeanne d'Arc, Hibernia, and Avalon sequences in the Hibernia oil field from continuously cored intervals (see Tankard and Welsink, 1987). *Jeanne d'Arc Sequence*, Kimmeridgian–Tithonian, compares alluvial-plain and basinal facies associations. The overall upward-coarsening distribution resulted from basinward progradation. Smaller scale cyclicity is attributed to rapid subsidence, which also explains the very sudden change from the earlier argillaceous drape to this stratigraphy. *Hibernia sequence*, Berriasian, built by bed-load river and floodplain deposits. *Avalon sequence*, upper Barremian, progradational shelf depositional systems, normal marine circulation. Widespread shoaling across the hanging-wall ramp (Fig. 14.17).

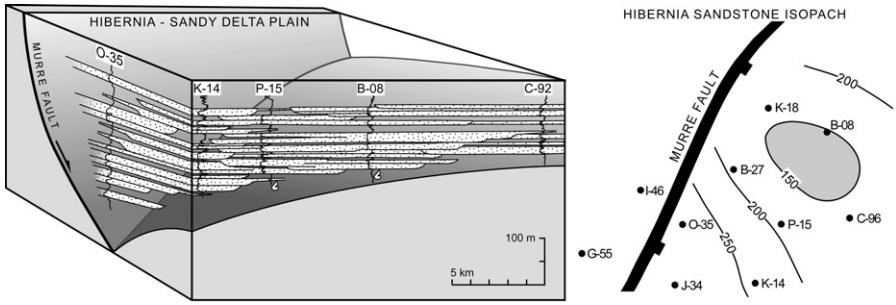

Figure 14.16 Stratigraphic fence diagram of Hibernia sandstones, Hibernia oil field, showing interpretation of alluvial architecture based on quantitative models (Tankard and Welsink, 1987). The three-dimensional wedge shape of this alluvial sandstone interval and its isopach distribution are the same as the hanging-wall ramp geometry (Fig. 14.17). Flexure is also suggested by the distribution of a thin, fossil-bearing (*Turritella* sp.) estuarine mudstone underlying this channel sandstone complex. Interlaminated mudstones in the deeper, southwestern part of the hanging-wall trough are burrowed and there are seat earths and preserved plant debris. In contrast, this section is oxidized across the structural culmination. Isopachs in meters.

mudstones in the depositional low are burrowed and contain seat earths and plant debris, whereas on the structural culmination these intervals are oxidized. The Nautilus C-92 sequence was also deposited on this structural culmination before younger faulting intervened.

Contemporaneous sedimentation along the shoaling Central Ridge margin of the basin formed a thinner onlapping sequence that is burrowed and contains a shelly fauna (e.g., Hebron I-13).

The Hibernia sandstone-mudstone succession records a generally underfilled basin with progressively less energetic sediment influx. This stage of basin subsidence ended with deposition of a 20–80-m-thick transgressive limestone, the lower Valanginian B marker, which forms a strongly reflective surface. Whereas the late Kimmeridgian–Berriasian Jeanne d'Arc and Hibernia depocenters were restricted marine and nonmarine with subnormal salinities, the B marker limestone marks a general change to normal salinities and open marine environments of deposition during the late Valanginian, Hauterivian, and Barremian. Furthermore, higher energy regimes with oxidizing conditions at the sediment-water interface are recognized below the B marker, but above it lower energy sedimentation with neutral or anoxic conditions at the sediment-water interface are more often identified.

Late stage extension: Late Valanginian–Barremian

Fault-controlled subsidence was most intense during Jeanne d'Arc and Hibernia time, albeit with decreasing intensity. Thereafter, the late Valanginian–Barremian denouement involved important modifications reflecting decay of the rift system. Faulting was initially still able to cause stratigraphic thickening and rollover. However, gradients were generally low, and the landscape was characterized by shallow-marine deposition that overlapped the rift shoulders. Regional downwarping lowered even the Bonavista platform west of the basin-forming Murre fault (Fig. 14.14C), presumably due to relaxation of extensional stresses. Catalina and Avalon shorelines were outside the half graben, and there are no terrestrial facies recognized in the preserved basin fill. Changes were less dramatic along the Central Ridge horst because translation maintained its positive relief.

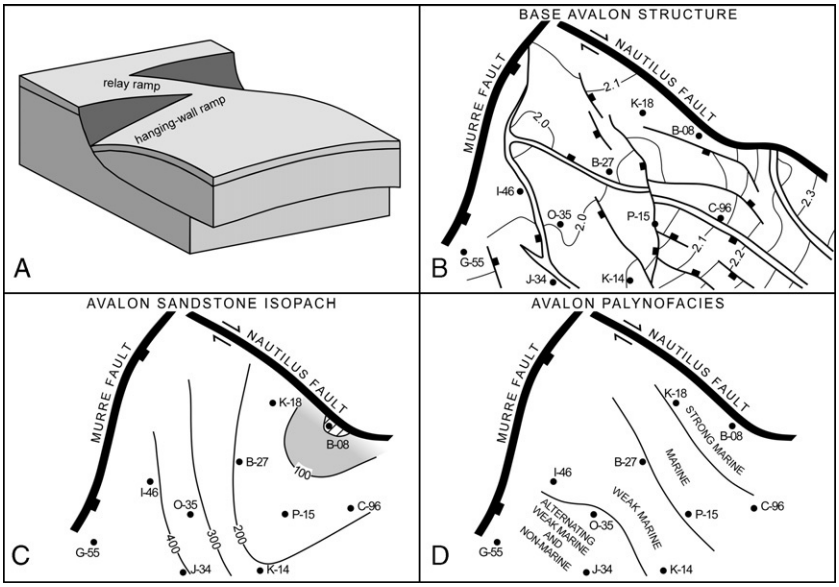

Figure 14.17 Relay ramp linkage between the offset Murre and Mercury faults during extension was coupled to a hanging-wall ramp where dip-slip subsidence along the Murre fault was asymmetric from the tip point of the fault plane. This asymmetric rotation created a hanging-wall ramp that appears to have been faulted at the onset of Avalon accumulation by flexural failure (contours in seconds). The hanging-wall ramp controlled depositional thinning, erosion, and oxidation within the Avalon (isopach lines are in meters; compare with Hibernia sandstone interval, Fig. 14.16). Lower Barremian ecozones of the Avalon sequence, based on the relative proportions of terrigenous and marine organic matter, show similar cross-trends of palynofacies (Tankard et al., 1989). Breakdown of the relay–hanging-wall ramp structure by the Nautilus shortcut fault (Fig. 14.11) took place after the Hauterivian.

There are several progradational sequences which are separated by transgressive mudstones, unconformities, or limestone drapes (Fig. 14.3). The composite Catalina and Avalon sandstones are the principal reservoirs. The intervening A marker consists of limestone and calcareous sandstone lenses that have distinct lithological and thickness variations across faults, and is more terrigenous across the crests of structures. Although conventionally interpreted as a timeline for the convenience of mapping, high-resolution, true-amplitude seismic profiles show that the A marker consists of several diachronous beds with an *en echelon* arrangement that intertongue with the bottomset deposits of the Avalon sequence. Deposition of this marker complex was synchronous with faltering extensional subsidence and deformation across the Hibernia hanging-wall ramp. Structural interpretation shows flexural failure of the hanging-wall ramp in early Avalon time, forming antithetic normal faults that trace the ramp contours (Fig. 14.17).

In the Hibernia–Rankin structural tract, the Avalon Formation is a southwestward-thickening wedge of interbedded mudstones and quartzose sandstones that were deposited in shelf and shore-zone environments (Fig. 14.15). The progradational facies are arranged in upward-coarsening units up to 50 m thick.

Thicker sandstone units formed by amalgamation.The overall geometry of the Avalon sequence mimics the shape of the trough above the hanging-wall ramp (Fig. 14.17). The Avalon was constructed by three overlapping depositional systems, which are separated by transgressive shale drapes. Subsidence along the Murre fault was initially relatively rapid and resulted in accumulation of a thick prism of clastics characterized by synsedimentary deformation (e.g., Hibernia G-55 and I-46). Slower rates of subsidence resulted in basinward offlap of the succeeding depositional units. High-resolution seismic (Fig. 14.18) shows the onlapping and downlapping character of the Avalon. The hummocky clinoform pattern, typical of progradation, is formed by variable amplitude and discontinuous reflections.

Reminiscent of Hibernia sedimentation, Avalon facies distribution was clearly controlled by flexural development and subsequent brittle failure of the hanging-wall ramp (Fig. 14.17). Northward thinning across the culmination resulted from non-deposition and erosion. For example, in Hibernia B-08 Avalon reservoir sandstones have been eroded entirely. Reworking around the edge of the ramp culmination deposited mature reservoir sandstones (e.g., Hibernia 0–35 and K-18) and oxidized mudstones (e.g., Hibernia B-27 and P-15). Maximum preservation of the stratigraphy was adjacent to the Murre fault, where limited reworking resulted in poorer quality reservoirs (e.g., Hibernia J-34). Similar trends are observed in the palynofacies, with strongest marine influence on the culmination of the hanging-wall ramp (Fig. 14.17D; early Barremian).

Persistent rotational topography of the Central Ridge maintained shoal-water environments there too (e.g., Hebron I-13). Local synsedimentary faulting caused abrupt thickening of the Avalon strata; examples include the Hebron–Ben Nevis and Hibernia–Nautilus offsets.

Timing and duration of fault activity during rifting

One of the joys of this study is not only the large amount of geophysical and drilling data, but also the detailed biostratigraphy that is available. For the crucial upper Callovian–Cenomanian interval, we have relied exclusively on palynological analyses.

Extension began gradually as a passive downwarp largely unaided by brittle failure of the crust, and deposition of a thick argillaceous blanket (Fig. 14.3). Transition from this low-relief early phase to fault-controlled high-relief subsidence was sudden. Each tectono-stratigraphic sequence started with relatively intense faulting and rollover, followed by denudation and rheological relaxation, as evidenced by the thick mudstone intervals, and was terminated by an

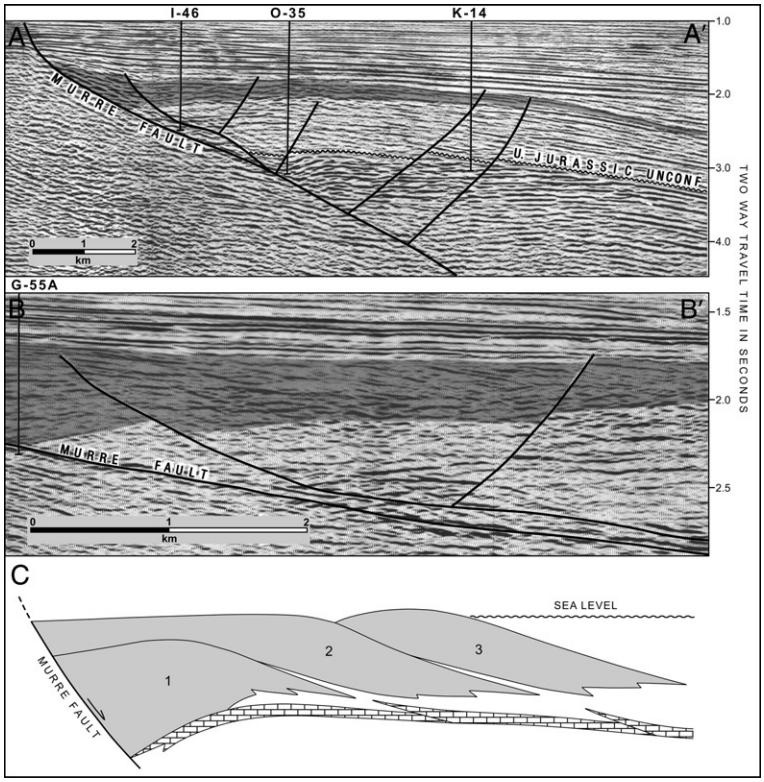

Figure 14.18 Seismic lines (Fig. 14.9 for location) and interpretive section showing offlapping character of Avalon depositional systems. (A) 3D seismic line 141 displays hummocky clinoform pattern indicative of progradation. (B) High-resolution seismic line 5052–82 shows the internal clinoform and downlap geometries of two depositional bodies, one stacked against the Murre fault, the other prograding basinward. This line is from an 82-km multi-channel seismic survey that was acquired with a 12–125-Hz frequency band and 2-ms sample rate. A maximum frequency of 50 Hz was achieved. Processing focused on stratigraphic rather than structural objectives. This seismic stratigraphic approach, emphasizing geometries based on reflection configuration, amplitude variations, and boundary relationships, has helped resolve the complex Avalon stratigraphy. This seismic interpretation was successfully tested by means of a detailed biostratigraphic study that emphasized correlation of communities of taxa. (C) The Avalon consists of three depositional systems separated by transgressive marine shale drapes. Subsidence was initially rapid and resulted in rollover and vertical stacking adjacent to the Murre fault plane. Slower rates of subsidence caused the two succeeding depositional systems to prograde basinward, as thinner units, in order to find sufficient accommodation (Tankard et al., 1989).

unconformity due to rebound. The Avalon lithosome geometries were investigated by means of high-resolution seismic. The Avalon consists of three offlapping depositional bodies that are mutually separated by transgressive shale drapes (Fig. 14.18). The first depositional package was accommodated largely by stacking and rollover against the Murre fault. But as fault activity decreased, the next two depositional packages were forced to find sufficient accommodation space by prograding farther basinward as thinner units. The periodicity of each tectono-stratigraphic sequence is 4–10 Ma, but it appears that intense faulting at the beginning of each phase had a duration not much more than 1 Ma, or probably considerably less. Of the 45-Ma duration of this mid-Mesozoic extensional episode, intense faulting accounted for only a very small part.

Post-rift subsidence

Transition to the post-rift era

The Aptian breakup unconformity marks the end of the Callovian–early Aptian period of extension, 45 Ma after its beginning, and transition to the next phase of extensional subsidence. It was also the end of a long period of uninterrupted marine sedimentation. Below this unconformity, diverse assemblages of dinoflagellates and other marine organic matter indicate more or less continuous marine conditions. But above it, the sediments contain durable, resistant types of organic matter from terrestrial sources and impoverished marine dinoflagellate assemblages indicative of higher energy environments with restricted marine circulation. A new period of NE-oriented extension in mid-Aptian–Cenomanian time initiated Orphan basin subsidence. At the same time, the Jeanne d'Arc basin was disrupted by transverse-block rotation and detachment of the plunging sedimentary cover (Figs. 14.12 and 14.13). Stratigraphic onlap and local wedges of unconformities show that fault-block rotation was syndepositional.

Upper Avalon sediments deposited along the crest of the Hibernia–Mara structural block in the late Barremian and early Aptian are relatively coarse and are attributed to fluvial–estuarine environments. Despite at least one major unconformity, these landscapes persisted into the Albian. Marginal marine sediments are also encountered in the Aptian–Albian Ben Nevis sequence (Fig. 14.3), consisting of medium to very coarse-grained channel sandstones that are bioturbated and contain shell material. Analysis of organic material from Hibernia wells suggests that Albian ecozones paralleled the rotated edges of the tilted fault blocks which anchored a cross-basin shoreline.

Shelf seas submerged the Grand Banks in the Late Cretaceous. By the end of the Cenomanian, terrigenous sediment starvation led to deposition of the highly reflective Petrel limestone, a shallow-water foraminiferal coccolithic limestone, or chalk (Fig. 14.3). The modern continental terrace wedge was built during the Cenozoic; it consists mostly of mudstones with unconformities incised by

glacio-eustatic sea-level fluctuations. Above the Jeanne d'Arc basin this Cenozoic cover thickens northward from 1 to 3 km in response to mantle flow (Keen et al., 1987a). Subtle adjustments of the earlier basin-forming faults to this flexural subsidence are reflected in local forced folding in the Cenozoic cover (Fig. 14.10). Initiation of flexural subsidence is marked by a Paleocene fan and immature oil-prone source rocks. Cenozoic deposits are particularly thick over the late-subsiding Orphan basin.

Structural disruption and oil generation

Petroleum accumulations in the Jeanne d'Arc basin are in upper Kimmeridgian–Aptian synrift reservoirs. These oils are correlated with the Kimmeridgian shales that form a geochemical marker throughout the basin. The reservoired oil and source rock have identical sterane biomarker distributions. *n*-Alkane compounds over the C_3–C_{35} molecular range predominate (von der Dick et al., 1989).The source beds are rich in amorphous marine sapropel with a primary dinoflagellate contribution and a secondary terrestrial component. Oil-prone Type II kerogen makes up 80–85% of the organic matter, with average TOC values of 3% (ranging up to 8%), and hydrogen index values typically 500–800 mg/g TOC. The source rock was probably deposited in a suite of east–west basin segments between primitive transfer faults (Fig. 14.14A). Subtle chemical variations in the expelled oil (e.g., Ben Nevis I-45) are attributed to admixture of terrestrial material from the fringes of these depocenters.

The timing of oil generation is estimated from maturity modeling which shows that it began in the late Aptian (~120 Ma), and that the peak of generation and expulsion was in the Eocene (~50 Ma) (Williamson, 1992). The oil and source rock are most mature in the deep northern part of the basin where the post-Kimmeridgian cover is 4–5 s (10 km) thick (Figs. 14.12 and 14.13). The late Aptian and Albian period was when the basin deepened northward due to mantle flow, causing the sedimentary fill to detach above basement. The source rocks are thermally immature in the southern part of the Jeanne d'Arc basin, but mature rapidly northward where they are involved with this large-scale structural disruption and deepening. Comparing the Rankin and Hibernia structures, Rankin M-36, which was drilled close to the southern splayed edge of the detachment tip line, has an erosionally condensed reservoir interval and petroleum source rocks that are still immature. In contrast, deepening of the Hibernia synrift rocks by transportation along the detachment resulted in complete reservoir preservation as well as source rock maturation. The Ben Nevis I-45 succession was also over-deepened in a hanging-wall syncline and isolated by a shortcut fault, entering the oil window in the Albian. The onset of maturation is clearly linked to late Aptian and Albian basin deepening and deformation.

Rift-related petroleum traps were formed before the onset of oil generation and expulsion, but the younger detachment above basement and its associated antithetic family of faults formed the conduits for migration. Apparently the

petroleum was locally sourced (von der Dick, 1989) and migrated northward up the gentle slopes of tilted structural blocks. Biodegradation affected only the structurally highest parts. For example, in the shallow Hebron I-13 reservoir the C_2–C_{13} *n*-alkanes have largely been removed. The only evidence of long-distance migration is recognized where highly mature oil is trapped above marginally mature Jurassic source rock along the gently sloping eastern ramp of the basin (*op. cit.*), reflecting the irregular system of anastomosing detachment splays. Oil in the Adolphus well has a distinctive sterane distribution attributed to a Paleogene source rock that owes its maturation to higher heat flows associated with the salt diapir complex (Fig. 14.13).

Petroleum exploration commenced in the 1960s and progressed through three distinct cycles (Fig. 14.19). The earliest exploration focused, albeit unsuccessfully, on salt piercement structures in the basins of the southern Grand Banks (Amoco and Imperial, 1973). Success came in 1979 with the discovery of the giant Hibernia oil field in the Jeanne d'Arc basin, 315 km offshore where the shelf is 80 m deep. It contains up to 1.2 billion barrels of oil and 1.8 tcf of gas (CNLOPB, 2006a). Subsequent discoveries have all been in the Jeanne d'Arc basin, including the Hebron–Ben Nevis, Terra Nova, Whiterose, Mara, Springdale, Nautilus, and South Tempest fields. The petroleum is sourced from the Kimmeridgian shales and structurally trapped in sandstones of Late Jurassic–Early Cretaceous age. Estimates are that 3 billion barrels of liquids (oil and NGL) and 6 tcf of gas have been discovered in the Jeanne d'Arc basin. The history of reserve additions (Fig. 14.19) shows that exploration was efficient, having found the largest fields first. This implies that the principal play type is now well explored,

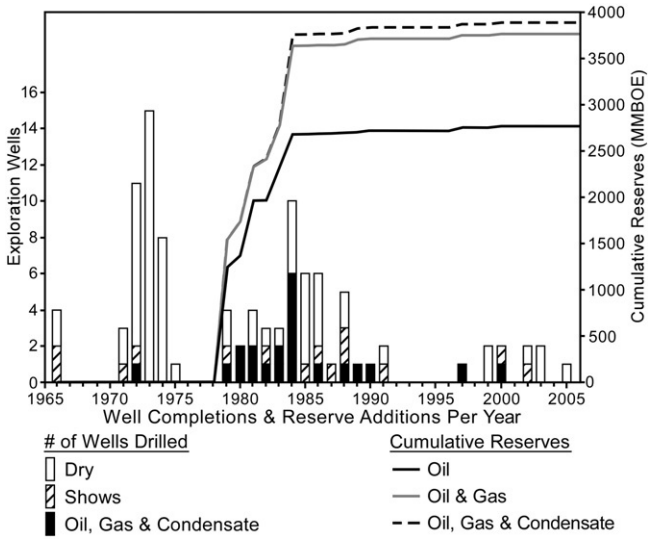

Figure 14.19 Exploration history of the Grand Banks showing petroleum reserves and the number of wells drilled annually. Early exploration tested unsuccessfully the salt piercement structures of the southern Grand Banks basins. The first major discovery of petroleum was in 1979 in the Hibernia structure of the Jeanne d'Arc basin; Hibernia P-15 was the discovery well. Estimates are that 3 billion barrels of liquids (oil and NGL) and 6 tcf of gas have been discovered in the Jeanne d'Arc basin. By the end of 2006, 103 exploration wells had been drilled, 52 of them in the Jeanne d'Arc basin with average drill depths of 3712 m. *(Data from CNLOPB, 2006a.)*

and recent exploration has added only meager reserves. Any significant new discoveries in the Jeanne d'Arc basin will likely be in a new play type, for example, the slivers of stratigraphy and reservoir rocks that are encapsulated between sealing splays of the marginal cover detachment system. An interesting aspect of the seismic acquisition is that there are about 1.2 million CMP km of 3D reflection seismic, mainly in the southern half of the Jeanne d'Arc, but it has not significantly resulted in exploration success; over 90% of the petroleum was discovered before there was 3D seismic available. Nevertheless, this 3D data set is invaluable in deciphering structural and stratigraphic detail.

14.5 Discussion

The mid-Mesozoic Jeanne d'Arc developed as a successor basin above an earlier rift system. This episode of extensional subsidence was complicated by sequential opening of the Atlantic as sea-floor spreading propagated northward. Extension occurred as a series of very intense episodes of fault reactivation. Although the variable strain was apparently focused onto the principal structural fabrics that already existed in the upper crust, the course of deformation was probably determined in the upper mantle.

There is an enormous amount of geophysical and drilling data. Each type of reflection seismic has its own unique application. For example, the large amount of 3D seismic is ideal for structural and stratigraphic interpretation, such as the down-stepping basement blocks in Fig. 14.12. Also important in this study is the wealth of biostratigraphic information to constrain subsidence. For the crucial upper Callovian–Cenomanian interval, the principal focus of exploration, we have resorted solely to the palynological work of W.A.M. Jenkins.

The large-scale mega-sequences embody the major episodes of basin evolution, events lasting tens of millions of years. The principal unconformities are the late Callovian, early Aptian (chron M0), early Cenomanian, and Maastrichtian (chron 30) boundaries that are expressed as distinct seismic reflectors and biostratigraphic hiatuses. This is the scale of crustal dynamics and plate kinematics. Seismic character, even at mid-crustal depths, is variable (Fig. 14.5), and there is no direct evidence of the nature of the deep crust or its acoustic signature. At an intermediate scale, the unconformity-bounded sequences record the basin responses to changes in extensional behavior and structural styles. Table 14.1 summarizes the variable scales of tectono-stratigraphy and suggests appropriate methods of seismic stratigraphic investigation.

We do not know how the early Mesozoic basins relate to each other because their basin-forming structures were reworked, but we have a better understanding of events from late Callovian to the Cenomanian (Figs. 14.1 and 14.5). Our reconstruction from the Bonavista platform, and Jeanne d'Arc and Flemish Pass basins to the conjugate Iberian margin is a two-dimensional transect. Extension

Table 14.1 Scales of tectono-stratigraphy and basin dynamics

Large-scale: Gross stratigraphic subdivision, 20–45 Ma periodicity. For example, upper Callovian–lower Aptian mega-sequence	Deep seismic reflection (>15 s), conventional seismic (7 s), and balanced-section constructions relate large-scale unconformity-bounded sequences to crustal and basin dynamics. Mega-sequences have generalized paleontology, and diagnostic genera and species defined geochronologically
Intermediate scale: Repetitive unconformity-bounded sequences, 4–10 Ma periodicity. For example, upper Barremian–lower Valanginian sequence	Conventional seismic (7 s) integrated with regional biostratigraphy to chronicle the history of episodic subsidence. Identified by means of refined paleontology and diagnostic species, subspecies, and varieties, defined geochronologically
Reservoir scale: 2–5 Ma periodicity. For example, *dimorphum–polonicum* beds (100 m), middle Oxfordian *tenuiserratum* zone, east flank of basin	Conventional 2D and 3D seismic requiring different scales of display, different processing (e.g., trace inversion, color displays of phase, frequency, anisotropy). Core studies, biostratigraphy, and palynofacies. Correlated and fingerprinted by individual biostratigraphic events or succession of events, defined biostratigraphically
Small or facies scale: <1 Ma periodicity. For example, upper *Subtilisphaera* shale in Avalon reservoir rocks at Hibernia	Conventional and high-resolution seismic, correlation of amplitude and facies characteristics including saturation, porosity, AVO, simultaneous trace inversion, bed thickness. Biota offers paleoenvironmental information, defined biostratigraphically

progressed through at least four steps (Fig. 14.6): (1) The late Callovian–middle Kimmeridgian onset of extension on the Grand Banks was a regional sag with an argillaceous fill largely unaccompanied by faulting, while its counterpart on the Iberia margin is a condensed section (Boillot et al., 1985). Pure shear is inferred. (2) The late Kimmeridgian to early Valanginian climax of fault-controlled extension on the Grand Banks was marked by rollover into the basin boundary faults and high structural relief. Simple-shear failure involved a detachment at ~26 km beneath the Jeanne d'Arc basin. In contrast, the conjugate Iberia margin was largely in a pre-rift state (Alves et al., 2006). (3) Fault-controlled subsidence of the Grand Banks basins had diminished by the Valanginian. However, the early Valanginian to Aptian was the main rifting phase on the Iberia margin north of the Aveiro fault (Alves et al., 2006), and on the Galicia margin basin faults soled on the 9-km-deep S-reflector (de Charpal et al., 1978; Reston et al., 1996). For the first time, extension was partitioned across an intracrustal zone of detachment. (4) Extension along this transect ended with ocean opening. On the Galicia margin a ridge of serpentinized peridotite marks the continent–ocean boundary. We interpret these rocks as a mantle core complex attributed to extensional unroofing and attenuation of the lower crust and upper mantle.

The thickness of the upper plate beneath the Bonavista platform is about 26 km (10.5 s), the level at which the intracrustal detachment also flattens, but considerably shallower under the Flemish Pass. The onset of fault-controlled subsidence that formed the rift system was 9 Ma after a gentle start that was unattended by faulting. Wernicke (1985) argues that late development of brittle failure may reflect the diachroneity between lower plate ductile deformation and upper plate brittle deformation. And so it may, except that across the Grand Banks–Iberia conjugate pair the absence of early structural control is more typical of pure-shear deformation. Only in our third stage of extension do we contemplate a fully developed intracrustal décollement, as a single low-angle fault zone, spanning the entire extensional tract (Fig. 14.6E). If during late Kimmeridgian–Berriasian time simple-shear deformation of the Grand Banks and pure-shear deformation of the Iberia margin coexisted, we wonder whether a nested system of two or three detachments would not be more likely. Unfortunately, the deep seismic does not resolve the intracrustal-fault geometries in this detail. Elsewhere extension has involved several levels of detachment and also symmetric extensional systems; examples include the Orphan basin (Keen et al., 1987a) and the transect Sable basin–Doukkala basin of Morocco (Heyman, 1989; Welsink et al., 1989b). Chian et al. (1995) observe that extension between the Labrador and southwest Greenland conjugate margins was initially symmetric, and that an asymmetric detachment fault only fully developed late in the rift cycle.

Regional tectonic unloading by extensional thinning and isostatic compensation resulted in footwall uplift and elevation of hot asthenosphere. Uplift and erosion were clearly greatest at the end of the rift cycle (Fig. 14.6), which is not the case with the pure-shear extensional model. The Aptian breakup unconformity in the Jeanne d'Arc basin is the same age as the earliest oceanic crust (chron M0; Srivastava et al., 1988). A lower Aptian unconformity is also the most important sequence boundary identified in other Atlantic margin basins. Besides being a breakup event on the Grand Banks, it also universally marks a fundamental change in terms of biostratigraphy, subsidence patterns, sedimentation, and marine circulation, even though ocean-opening was diachronous (Tankard and Balkwill, 1989).

Lithospheric extension and arching at the rift-drift transition locally resulted in an eastward reversal of dip of the intracrustal detachment beneath the west Iberia margin (e.g., Wilson et al., 1989), and tectonic denudation of upper mantle peridotite at breakup, interpreted as a mantle core complex (cf. Doblas and Oyarzun, 1989). The mylonitization and serpentinization, together with a highly reflective surface, are attributed to detachment shearing (Boillot et al., 1989). Tectonic unloading is also believed to have increased the slope of the detachment surface beneath the Jeanne d'Arc basin and Flemish Pass. Compared with the Jeanne d'Arc basin, uplift and erosion in the Flemish Pass stripped most of the mid-Barremian to Campanian section, except for a thin Albian unit (e.g., Mizzen L-11; CNLOPB, 2006b).

During the early phase of SE-oriented extension (Grand Banks–Iberia), the Dominion transfer confined extensional strain to the Jeanne d'Arc Grand Banks and excluded the Orphan basin. By the early Aptian, sea-floor spreading had jumped from the southern Newfoundland basin to the Flemish Cap, thus initiating Orphan basin extension (Fig. 14.1). This new episode of rifting is dated as mid-Aptian to late Cenomanian (~20 Ma). The listric basin-forming faults of the Orphan basin merge with a décollement at 15–17 km (Keen et al., 1987a). In the Jeanne d'Arc basin, this NE-oriented extension resulted in domino-style rotation of its cross-basin structures and a down-stepping basin floor (Figs. 14.7 and 14.12). We believe that this pattern of basement tilt-block rotation continued under the Orphan detachment, and was probably driven by the detachments below and above (i.e., the 26- and 17-km levels of detachment). However, extension by tilt-block rotation is too small to explain the pronounced northward plunge that we observe in the Jeanne d'Arc basin, suggesting that this phase of subsidence was caused mainly by mantle flow (*op. cit.)*. Pronounced uniform subsidence after the Cenomanian because of mantle flow affected both the Jeanne d'Arc and Orphan basins.

This reconstruction implies that the upper plate of the NW–SE Grand Banks–Iberia extension became the lower plate to the SW–NE Orphan extension. An arcuate gravity anomaly traces the tip line of the Orphan upper plate, crosscutting the magnetic signature of the lower plate (Fig. 14.4). Thus, in three dimensions, extension involved a suite of overlapping, asymmetric crustal plates. The history of this extension is preserved in the unconformity-bounded sequences within the basin. After continental fragmentation, there is a unique correlation between events in the continental basins and the sea-floor spreading record (Figs. 14.3 and 14.8). In this respect, the stratigraphic framework of the Jeanne d'Arc basin, which reflects adjustments in the patterns of subsidence, and the record of magnetic anomalies in the oceanic crust imply coupling between ocean floor and continental crust.

The fault-controlled rift system developed above a passive regional sag that was largely unassisted by significant fault accommodation. Stratigraphic control suggests that intense faulting may have lasted no longer than 1 Ma at the beginning of each increment, after which general decay or relaxation of the extensional stresses and deposition of thick mudstone intervals continued to deepen the basin. Three distinct patterns of subsidence characterize rift and post-rift subsidence: (1) Fault-controlled subsidence defines the overall half graben asymmetry. (2) In late-stage basin subsidence, fault activity is minor and petering out, and subsidence is attributed to rheological weakening, resulting in a basinwide saucer-shaped argillaceous cover. (3) In the final stage, the individual basins are yoked together in a regional downwarp attributed to lower crust and upper mantle flow.

In summary, the three-part evolution of the Grand Banks basins involving fault-controlled rift, saucer-shaped drape unassisted by faulting, and regional downwarp due to lower crust and upper mantle flow may be characteristic of rift

basin evolution in general. Depth-dependent extension is partitioned across the intracrustal zone of decoupling, resulting in an overall dichotomy between upper plate and lower plate extension. Several papers address the role of lower crust and mantle flow to explain basin subsidence in which there is little brittle deformation of the upper crust. Besides the Jeanne d'Arc basin (Tankard and Welsink, 1987), examples include the northern Carnarvon basin of Australia (Driscoll and Karner, 1998), the Dead Sea basin (Al-Zoubi and ten Brink, 2002), and the Cape basin of South Africa (Tankard et al., Chapter 14, this volume).

14.6 Conclusions

The mid-Mesozoic Jeanne d'Arc basin is thoroughly documented by an enormous amount of exploration seismic and numerous exploration wells drilled into the synrift fill. Basin subsidence resulted primarily from crustal stretching between the Grand Banks and the Iberian margin. It is important to remember that seismic records only the final configuration, at the completion of 45 million years of extension. From this seismic, we observe that, at least by the end of the process, extension was partitioned across a westward-dipping intracrustal detachment. This simple-shear reconstruction is elegant, but has two major deficiencies. First, it is clearly two dimensional. Second, the model presents only the finale, but does not explain how and when it got there.

The Jeanne d'Arc is an extensional basin. Its association of structural styles and stratigraphy is intimately linked to the history of crustal attenuation. The stratigraphy preserves the details of the way extension took place and when it happened. This record is not wanting. It shows that extension proceeded through at least four stages of asymmetric stretching involving both pure shear and simple shear, and that fully developed failure along a pervasive down-to-the-west detachment occurred only halfway through, 25 million years into a 45-million-year-long period of extension. The stratigraphic and seismic data are together able to show how extension occurred and the timing of each step. But this reconstruction is still two-dimensional.

A younger episode of extension from the mid-Aptian through Cenomanian modified the Jeanne d'Arc basin internally. This extension was due to stress fields oriented approximately northeast, from the Jeanne d'Arc to the Goban Spur. Extension of the Orphan basin occurred by intracrustal detachment. This NE-oriented extension affected the Jeanne d'Arc basin by domino-style rotation of its transverse basement blocks, a tilt-block arrangement that likely continued under the Orphan basin detachment because it probably depended upon the plane of detachment for translation. It appears that the upper plate of the SE-oriented Grand Banks–Iberia extension became the lower plate to the NE-oriented Orphan basin extension. However, tilt-block rotation cannot, alone, explain the contemporaneous northward deepening of the Jeanne d'Arc basin. Estimates from subsidence history

analysis indicate that subsidence was dominated by lower crust and mantle flow. We suggest that the lower crustal flow associated with the Grand Banks–Iberia extension continued unabated through the period of the Jeanne d'Arc–Orphan basin extension too, reorganization of stress fields notwithstanding.

Mesozoic extension of the Grand Banks and Orphan provinces and their surrounding conjugate margins involved both pure shear and simple shear, and also overlapping crustal plates that could switch polarity, so that an upper plate of one extensional tract could become the lower plate to another. Furthermore, the switchover from one extensional regime to the next appears to be continuous, rather than being tectonically compartmented. The Jeanne d'Arc is an extensional basin with a sedimentary fill that records the detail of how and when these events took place. Finally, whereas basin formation was accommodated by reactivation of preexisting fabrics in the brittle upper crust, there is substantial evidence that the course of extensional deformation was determined in the upper mantle.

Acknowledgments

We thank Miguel Galliski, Jeremy Hall, David Hawkins, Peter McGregor, and Andy Parmenter for assistance at various stages of this study, and Tiago Alves and Tony Jenkins for discussions on the timing of extension. An earlier draft of this paper was reviewed by Hugh Balkwill, Bob Meneley, and Paul Williams. Drafting was done by Carlos Espejon.

About the Authors

Herman Welsink is a senior geologist in the Regional Studies Group of Repsol Exploration in Madrid. He was born in Haarlem, The Netherlands, and graduated with a doctoraal in Geology from the University of Utrecht. Since 1981, Herman has worked in the oil industry, especially in the exploration of basins in Canada, Bolivia, Argentina, and other South American countries. His research interests and publications are concerned with the formation and structural deformation of sedimentary basins, tectonic-stratigraphic linkages, and the way these can be applied to petroleum exploration.

Anthony Tankard was born and educated in South Africa, and has a Ph.D. from Rhodes University. He has worked in various academic institutions in South Africa and North America and, since 1981, in the petroleum industry. Tony has undertaken regional studies and basin evaluations in South and East Africa, U.S. Appalachians, Canadian offshore basins, Burma, West Greenland, and most of the sub-Andean basins. His research and publications have been concerned mainly with the evolution of basins and their tectonic linkage, the sedimentary fill, and the development of models for petroleum accumulation.

Herman and Tony joined the petroleum industry at the same time and have since then collaborated on numerous exploration and research projects.

References

Alves, T.M., Gawthorpe, R.L., Hunt, D.W., Monteiro, J.H., 2002. Jurassic tectono-sedimentary evolution of the northern Lusitania basin (offshore Portugal). Mar. Pet. Geol. 19, 727–754.

Alves, T.M., Moita, C., Sandnes, F., Cunha, T., Monteiro, J.H., Pinheiro, L.M., 2006. Mesozoic-Cenozoic evolution of North Atlantic continental-slope basins: the Peniche basin, western Iberian margin. AAPG Bull. 90 (1), 31–60.

Al-Zoubi, A., ten Brink, U., 2002. Lower crustal flow and the role of shear in basin subsidence: an example from the Dead Sea basin. Earth Planet. Sci. Lett. 1999, 67–79.

Amoco and Imperial, 1973. Regional geology of the Grand Banks. Bull. Can. Pet. Geol. 21, 479–503.

Arthur, K.R., Cole, D.R., Henderson, G.G.L., Kushnir, D.W., 1982. Geology of the Hibernia discovery. In: Halbouty, M.T. (Ed.), The deliberate search for the subtle trap, American Association of Petroleum Geologists Memoir, vol. 32, pp. 181–195.

Balkwill, H.R., Legall, F.D., 1989. Whale basin, offshore Newfoundland: extension and salt diapirism. In: Tankard, A.J., Balkwill, H.R. (Eds.), Extensional tectonics and stratigraphy of the North Atlantic margins, American Association of Petroleum Geologists Memoir, vol. 46, pp. 233–245.

Boillot, G., Grimaud, S., Mauffret, A., Mougenot, D., Kornprobst, J., Mergoil, D.J., et al., 1980. Ocean continent boundary off the Iberian margin: a serpentinite diapir west of Galicia Bank. Earth Planet. Sci. Lett. 48, 23–39.

Boillot, G., et al., 1985. Evolution of a passive margin. Nature 317, 115–116.

Boillot, G., Mougenot, D., Girardeau, J., Winterer, E.L., 1989. Rifting processes on the west Galicia margin, Spain. In: Tankard, A.J., Balkwill, H.R. (Eds.), Extensional tectonics and stratigraphy of the North Atlantic margins, American Association of Petroleum Geologists Memoir, vol. 46, 363–377.

Chian, D., Louden, K.E., Reid, I., 1995. Crustal structure of the Labrador Sea conjugate margin and implications for the formation of nonvolcanic continental margins. J. Geophys. Res. 100, 24239–24253.

Chian, D., Louden, K.E., Minshull, T.A., Whitmarsh, R.B., 1999. Deep structure of the ocean-continental transition in the southern Iberia abyssal plain from seismic refraction profiles. Ocean Drilling Program (Legs 149 and 173) transect. J. Geophys. Res. 104, 7443–7462.

CNLOPB 2006a. Canada-Newfoundland and Labrador Offshore Petroleum Board. Available online at:http://www.cnlopb.nl.ca (accessed 16.10.06) (see Statistics; Field Statistics; Discovered Reserves and Resources: disc_rr.pdf).

CNLOPB 2006b. Canada-Newfoundland and Labrador Offshore Petroleum Board. Available online at:http://www.cnlopb.nl.ca (accessed 14.12.06) (see Publications; Other Publications; Schedule of Wells; North Grand Banks Wells; Mizzen L-11: well234.pdf).

Dean, S.M., Minshull, T.A., Whitmarsh, R.B., Louden, K.E., 2000. Deep structure of the ocean-continent transition in the southern Iberia abyssal plain from seismic refraction profiles. The IAM-9 transect at 40°20′. J. Geophys. Res. 105, 5859–5885.

de Charpal, O., Montadert, L., Guennoc, P., Roberts, D.G., 1978. Rifting, crustal attenuation and subsidence in the Bay of Biscay. Nature 275, 706–711.

de Voogd, B., Keen, C.E., 1987. Lithoprobe East: results from reflection profiling of the continental margin; Grand Banks region. Geophys. J. R. Astron. Soc. 89, 195–200.

Doblas, M., Oyarzun, R., 1989. "Mantle core complexes" and Neogene extensional detachment tectonics in the western Betic Cordilleras, Spain: an alternative model for the emplacement of the Ronda peridotite. Earth Planet. Sci. Lett. 93, 76–84.

Driscoll, N.W., Karner, G.D., 1998. Lower crustal extension across the northern Carnarvon basin, Australia: evidence for an eastward dipping detachment. J. Geophys. Res. 103, 4975–4991.

Enachescu, M.E., 1987. Tectonic and structural framework of the northeast Newfoundland continental margin. In: Beaumont, C., Tankard, A.J. (Eds.), Sedimentary basins and basin-forming mechanisms, Canadian Society of Petroleum Geologists Memoir, vol. 12, 117–146.

Enachescu, M.E., 1993. North Grand Banks, offshore Newfoundland: a sedimentary epeiric basin west of the Murre-Mercury fault. Mar. Pet. Geol. 10, 439–449.

Gibbs, A.D., 1983. Balanced cross-section construction from seismic sections in areas of extensional tectonics. J. Struct. Geol. 5, 153–160.

Gibbs, A.D., 1984. Structural evolution of extensional basin margins. J. Geol. Soc. Lond. 141, 609–620.

Grant, A.C., McAlpine, K.D., Wade, J.A., 1986. The continental margin of eastern Canada: geological framework and petroleum potential. In: Halbouty, M.T. (Eds.), Future petroleum provinces of the world, American Association of Petroleum Geologists Memoir, vol. 40, pp. 177–205.

Haworth, R.T., Lefort, J.P., 1979. Geophysical evidence for the extent of the Avalon zone in Atlantic Canada. Can. J. Earth Sci. 16, 552–567.

Heyman, M.A.W., 1989. Tectonic and depositional history of the Moroccan continental margin. In: Tankard, A.J., Balkwill, H.R. (Eds.), Extensional tectonics and stratigraphy of the North Atlantic margins, American Association of Petroleum Geologists Memoir, vol. 46, pp. 323–340.

Hopper, J.R., Funck, T., Tucholke, B.E., Holbrook, W.S., Louden, K.E., Larsen, H.C., 2006. A deep seismic reflection investigation of the Flemish Cap margin: implications for the origin of deep reflectivity and evidence for asymmetric opening of the North Atlantic between Newfoundland and Iberia. Geophys. J. Int. 164, 501–515.

Hubbard, R.J., 1988. Age and significance of sequence boundaries on Jurassic and Early Cretaceous rifted continental margins. AAPG Bull. 72, 49–72.

Karner, G.D., Driscoll, N.W., Weissel, J.K., 1993. Response of the lithosphere to in-plane force variations. Earth Planet. Sci. Lett. 114, 397–416.

Keen, C.E., Barrett, D.L., 1981. Thinned and subsided continental crust on the rifted margin of eastern Canada: crustal structure, thermal evolution and subsidence history. Geophys. J. R. Astron. Soc. 65, 443–465.

Keen, C.E., Stockmal, G.S., Welsink, H., Quinlan, G., Mudford, B., 1987a. Deep crustal structure and evolution of the rifted margin northeast of Newfoundland: results from LITHOPROBE East. Can. J. Earth Sci. 24, 1537–1549.

Keen, C.E., Boutilier, R., de Voogd, B., Mudford, B., Enachescu, M.E., 1987b. Crustal geometry and extensional models for the Grand Banks, eastern Canada: constraints from deep seismic reflection data. In: Beaumont, C., Tankard, A.J. (Eds.), Sedimentary basins and basin-forming mechanisms, Canadian Society of Petroleum Geologists Memoir, vol. 12, pp. 101–115.

Klitgord, K.D., Schouten, H., 1986. Plate kinematics of the central Atlantic. In: Vogt, P.R., Tucholke, B.E. (Eds.), The geology of North America, the western North Atlantic region. Decade of North American Geology Series, vol. M. Geological Society of America, pp. 351–378.

Klitgord, K.D., Hutchinson, D.R., Schouten, H., 1988. U.S. Atlantic continental margin; structural and tectonic framework. In: Sheridan, R.E., Grow, J.A. (Eds.), The geology of North America, the Atlantic continental margin, U.S. Decade of North American Geology Series, vol. I-2. Geological Society of America, pp. 19–55.

Kusznir, N.J., Egan, S.S., 1989. Simple-shear and pure-shear models of extensional sedimentary basin formation: application to the Jeanne d'Arc basin, Grand Banks of Newfoundland. In: Tankard, A.J., Balkwill, H.R. (Eds.), Extensional tectonics and stratigraphy of the North Atlantic margins, American Association of Petroleum Geologists Memoir, vol. 46, pp. 305–322.

Larsen, P.H., 1988. Relay structures in a Lower Permian basement involved extension system, east Greenland. J. Struct. Geol. 10, 3–8.

Lau, K.W.H., Louden, K.E., Funck, T., Tucholke, B.E., Holbrook, S., Hopper, J.R., et al., 2006a. Crustal structure across the Grand Banks – Newfoundland basin continental margin – I. Results from a seismic refraction profile. Geophys. J. Int. 167, 127–156.

Lau, K.W.H., Louden, K.E., Deemer, S., Hall, J., Hopper, J.R., Tucholke, B.E., et al., 2006b. Crustal structure across the Grand Banks – Newfoundland basin continental margin – II. Results from a seismic reflection profile. Geophys. J. Int. 167, 157–170.

Manatschal, G., Bernoulli, D., 1999. Architecture and tectonic evolution of non-volcanic margins: present day Galicia and ancient Adria. Tectonics 18, 1099–1119.

Mauffret, A., Montadert, L., 1987. Rift tectonics on the passive continental margin of Galicia (Spain). Mar. Pet. Geol. 4, 49–70.

Max, M.D., Riddihough, R.P., 1975. Continuation of the Highland Boundary fault in Ireland. Geology 3, 206–210.

McKenzie, D.P., 1978. Some remarks on the development of sedimentary basins. Earth Planet. Sci. Lett. 40, pp. 25–32.

Meneley, R.A., 1986. Oil and gas fields in the East Coast and Arctic basins of Canada. In: Halbouty, M.T. (Ed.), Future petroleum provinces of the world, American Association of Petroleum Geologists Memoir, vol. 40, pp. 143–176.

Powell, T.G., 1985. Paleogeographic implications for the distribution of Upper Jurassic source beds: offshore eastern Canada. Bull. Can. Pet. Geol. 33, 116–119.

Reston, T.J., Krawczyk, C.M., Klaeschen, D., 1996. The S reflector west of Galicia (Spain): evidence from prestack depth migration for detachment faulting during continental breakup. J. Geophys. Res. 101, 8075–8091.

Shipboard Scientific Party, 2004. Leg 210 summary. In: Tucholke, B.E., Sibuet, J.C., Klaus, A. (Eds.), Proceedings of the Ocean Drilling Program, Initial Reports, vol. 210, pp. 1–78.

Sinclair, I.K., 1993. Tectonism: the dominant factor in mid-Cretaceous deposition in the Jeanne d'Arc basin, Grand Banks. Mar. Pet. Geol. 10, 530–549.

Sinclair, I.K., 1995. Sequence stratigraphic response to Aptian–Albian rifting in conjugate margin basins: a comparison of the Jeanne d'Arc basin, offshore Newfoundland, and the Porcupine basin, offshore Ireland. In: Scrutton, R.A., Stoker, R.A., Shimmield, G.B., Tudhope, A.W. (Eds.), The tectonics, sedimentation and palaeoceanography of the North Atlantic region, Geological Society (London) Special Publication, vol. 90, pp. 29–49.

Srivastava, S.P., Tapscott, C.R., 1986. Plate kinematics of the North Atlantic. In: Vogt, P.R., Tucholke, B.E. (Eds.), The geology of North America, the western North Atlantic region. Decade of North American Geology Series, vol. M. Geological Society of America, pp. 379–404.

Srivastava, S.P., Verhoef, J., Macnab, R., 1988. Results from a detailed aeromagnetic survey across the northeast Newfoundland margin, part II: early opening of the North Atlantic between the British Isles and Newfoundland. Mar. Pet. Geol. 5, 324–337.

Tankard, A.J., Balkwill, H.R., 1989. Extensional tectonics and stratigraphy of the North Atlantic margins: introduction. In: Tankard, A.J., Balkwill, H.R. (Eds.), Extensional tectonics and stratigraphy of the North Atlantic margins, American Association of Petroleum Geologists Memoir, vol. 46, pp. 1–6.

Tankard, A.J., Welsink, H.J., 1987. Extensional tectonics and stratigraphy of Hibernia oil field, Grand Banks, Newfoundland. AAPG Bull. 71 (10), 1210–1232.

Tankard, A.J., Welsink, H.J., 1988. Extensional tectonics, structural styles and stratigraphy of the Mesozoic Grand Banks of Newfoundland. In: Manspeizer, W. (Ed.), Triassic-Jurassic rifting and the opening of the Atlantic Ocean. Elsevier, Amsterdam, pp. 129–165.

Tankard, A.J., Welsink, H.J., 1989. Mesozoic extension and styles of basin formation in Atlantic Canada. In: Tankard, A.J., Balkwill, H.R. (Eds.), Extensional tectonics and stratigraphy of the North Atlantic margins, American Association of Petroleum Geologists Memoir, vol. 46, pp. 175–195.

Tankard, A.J., Welsink, H.J., Jenkins, W.A.M., 1989. Structural styles and stratigraphy of the Jeanne d'Arc basin, Grand Banks of Newfoundland. In: Tankard, A.J., Balkwill, H.R. (Eds.), Extensional tectonics and stratigraphy of the North Atlantic margins, American Association of Petroleum Geologists Memoir, vol. 46, pp. 265–282.

Tankard, A., Welsink, H., Aukes, P., Newton, A.R., Stettler, E., 2012. Geodynamic interpretation of the Cape and Karoo basins, South Africa. In: Bally, A.W., Roberts, D.G. (Eds.), Principles of Phanerozoic Regional Geology. Elsevier, Amsterdam.

Tucholke, B.E., Whitmarsh, R.W., 2012. The Newfoundland – Iberia conjugate rifted margins. In: Bally, A.W., Roberts, D.G. (Eds.), Principles of Phanerozoic Regional Geology. Elsevier, Amsterdam.

von der Dick, H., 1989. Environment of petroleum source rock deposition in the Jeanne d'Arc basin off Newfoundland. In: Tankard, A.J., Balkwill, H.R. (Eds.), Extensional tectonics and stratigraphy of the North Atlantic margins, American Association of Petroleum Geologists Memoir, vol. 46, pp. 295–303.

von der Dick, H., Meloche, J.D., Dwyer, J., Gunther, P., 1989. Source-rock geochemistry and hydrocarbon generation in the Jeanne d'Arc basin, Grand Banks, offshore eastern Canada. J. Pet. Geol. 12, 51–68.

Welsink, H.J., Tankard, A.J., 1988. Structural and stratigraphic framework of the Jeanne d'Arc basin, Grand Banks. In: Bally, A.W. (Ed.), Atlas of seismic stratigraphy, 2, American Association of Petroleum Geologists Studies in Geology, vol. 27, pp. 14–21.

Welsink, H.J., Srivastava, S.P., Tankard, A.J., 1989a. Basin architecture of the Newfoundland continental margin and relationship to ocean crust fabrics during extension. In: Tankard, A.J., Balkwill, H.R. (Eds.), Extensional tectonics and stratigraphy of the North Atlantic margins, American Association of Petroleum Geologists Memoir, vol. 46, pp. 197–213.

Welsink, H.J., Dwyer, J.D., Knight, R.J., 1989b. Tectono-stratigraphy of the passive margin off Nova Scotia. In: Tankard, A.J., Balkwill, H.R. (Eds.), Extensional tectonics and stratigraphy of the North Atlantic margins, American Association of Petroleum Geologists Memoir, vol. 46, pp. 215–231.

Wernicke, B., 1981. Low-angle normal faults in the Basin and Range province-nappe tectonics in an extending orogen. Nature 291, 645–648.

Wernicke, B., 1985. Uniform-sense normal simple shear of the continental lithosphere. Can. J. Earth Sci. 22, 108–125.

Wernicke, B., Burchfiel, B.C., 1982. Modes of extensional tectonics. J. Struct. Geol. 4 (2), 105–115.

Williamson, M.A., 1992. The subsidence, compaction, thermal and maturation history of the Egret Member source rock, Jeanne d'Arc basin, offshore Newfoundland. Bull. Can. Pet. Geol. 40, 136–150.

Wilson, R.C.L., Hiscott, R.N., Willis, M.G., Gradstein, F.M., 1989. The Lusitanian basin of west-central Portugal: Mesozoic and Tertiary tectonic, stratigraphic, and subsidence history. In: Tankard, A.J., Balkwill, H.R. (Eds.), Extensional tectonics and stratigraphy of the North Atlantic margins, American Association of Petroleum Geologists Memoir, vol. 46, pp. 341–361.

Wilson, R.C.L., Sawyer, D.S., Whitmarsh, R.B., Zerong, J., Carbonell, J., 1996. Seismic stratigraphy and tectonic history of the Iberia abyssal plain. In: Whitmarsh, R.B., Sawyer, D.S., Klaus, A., Masson, D.G. (Eds.), Proceedings of the Ocean Drilling Program, Scientific Results 149, pp. 617–630.

In this chapter

15

The Recôncavo basin

Luciano P Magnavita,[1] *Peter Szatmari,*[2] *José A Cupertino,*[1] *Nivaldo Destro,*[1] *David Roberts*[3]

[1]Petrobras/E&P-EXP, Av. República do Chile 330, Centro, Rio de Janeiro, Brazil
[2]Petrobras/CENPES/PDGEO, Ilha do Fundão, Rio de Janeiro, Brazil
[3]Petrobras/CENPES/GEOT, Ilha do Fundao, Rio de Janeiro, Brazil

15.1 Introduction

The term "Recôncavo basin" is used in two senses in world literature. In the looser sense, it refers to the entire Recôncavo–Tucano–Jatobá rift system that extends for ~620 km across the continent in northeastern Brazil; but in a stricter sense, it should refer only to the southernmost part of this rift system, situated in the vicinity of the Atlantic Ocean, at and to the northeast of the city of Salvador, the capital of Bahia state, Brazil.

The Recôncavo basin is one of the key sedimentary basins of the Phanerozoic as it provides excellent outcrops well exposed on land of an entire rift sequence which is virtually devoid of igneous activity. It is the first basin in Brazil where exploration for petroleum was successful, with the discovery of the first producing Candeias, Dom João, and Água Grande oil fields in the late 1940s and early 1950s. The basin offers excellent opportunities to study in detail both sedimentary geology and tectonics and is surrounded by outcropping Precambrian basement, providing opportunities for excellent correlation with preexisting grain.

The lack of a significant post-rift section in the rift has been attributed to differential stretching of the lithosphere due to simple shear (Ussami et al., 1986), to continuous vertical and lateral heat loss after uniform stretching of the lithosphere (Milani and Davison, 1988), or to removal of the sedimentary record after massive regional erosion (Magnavita et al., 1994). In fact, vitrinite reflectance data indicate more than 1.5 km of erosion in the Recôncavo basin (Daniel et al., 1989). Also, the truncation of the sedimentary section toward the flexural border suggests that the rift occupied a much broader area than presently preserved (Magnavita, 1992).

The exhumation probably occurred during two main periods: the first, at the end of rifting, possibly as a consequence of elastic rebound on the continental breakup; the second, probably in the Paleogene (Oligocene), as indicated by generalized peneplanation in northeastern Brazil (Bigarella, 1975; King, 1956).

Phanerozoic Rift Systems and Sedimentary Basins DOI: 10.1016/B978-0-444-56356-9.00014-6

This chapter will examine three aspects of the Recôncavo basin. First, the general tectonic context, including the Recôncavo–Tucano–Jatobá rift system, the Northeast Brazilian Sergipe Microplate, and their relationship to continental breakup between South America and Africa during early Cretaceous time; second, the tectono-sedimentary evolution, major tectonic elements, and petroleum resources in the Recôncavo basin *sensu stricto;* and, finally, the thermal history of the Recôncavo and adjacent Camamu basins as determined from Fission Track Analysis (FTA).

The FTA results presented here were obtained by Cupertino (2000), from samples taken at outcrops and wells, totaling 33 samples of both crystalline basement rocks and sediments of various ages. The crystalline basement is composed of a high grade of metamorphic rocks (granulite facies) re-worked through the Upper Proterozoic and Cambrian. The well samples came from a lower Cretaceous sequence, obtained from cuttings. The thermal histories conceived here were obtained by the use of Gallagher's (1995) algorithm and represent a simplification of the actual situation. However, there is consistency in the identified episodes, as well as in the epochs in which they occurred.

15.2 The Recôncavo–Tucano–Jatobá rift system

Rifting along Brazil's South Atlantic margin took place from latest Jurassic(?) through early Cretaceous times, before and during the early Cretaceous basaltic volcanism of the Paraná basin, and followed the Precambrian tectonic framework. In the SW, along the northern margin of the Santos basin, rifting took place along ENE-trending late Proterozoic right-lateral strike-slip faults, but it propagated from Cabo Frio (latitude S22°) to the north along the NNE to N–S-directed Precambrian grain that parallels the major structural elements of the São Francisco craton which lies farther inland. Still farther to the north, before approaching Salvador, the eastern limit of the São Francisco craton turns to the east and reaches the coastline to continue as the limit of the Congo craton in Africa. The northward propagating rift passes across this limit undeflected to Salvador, already within the São Francisco craton. At Salvador (latitude 13°N), the rift bifurcates, repeating bifurcation of Archean through lower Proterozoic granulites. One branch continues its northward trend inland, along the Tucano basin, until it reaches the E–W-trending Pernambuco ductile shear zone, which marks the northern end of the São Francisco craton. Another branch follows from Salvador to the northeast, outlining the coastal basins of Sergipe-Alagoas (and Gabon in Africa), continuing to the eastern end of the same Pernambuco shear zone near Recife. The triangular block, composed mostly of outcropping Precambrian rocks, and embraced by these two rift branches in the west and east and by the Pernambuco shear zone in the north, constitutes the Northeast Brazilian or Sergipe Microplate (Fig. 15.1).

The microplate model (Milani et al., 1988; Szatmari and Milani, 1999; Szatmari et al., 1985) has provided a framework capable of accommodating some of the

Figure 15.1 The Recôncavo–Tucano–Jatobá rift system, in relation to the separating South American and African plates. The Northeast Brazilian Sergipe Microplate between the Tucano rift and Africa moved at first with Africa and subsequently rotated clockwise with South America relative to Africa *(modified after Szatmari and Milani, 1999)*.

key aspects of the other models as well. Thus, the megashear model (Cohen, 1985) proposed left-lateral wrenching in a wide NW-trending zone along the present NE-trending continental margin, relative to which the N–S-trending grabens including the Tucano rift formed as tension gashes. The double rifting model of Magnavita (1992) was based on the recognition of two tectonic phases in the region. Magnavita (1992) suggested that the first syn-rift phase occurred in the middle Rio da Serra local stage (Berriasian), when E–W extension across the Recôncavo–Tucano–Jatobá rift and adjacent basins was accommodated by

sinistral motion along the Pernambuco-Ngaoundere shear zone. In Magnavita's model, the block to the north of this shear zone stayed fixed, as evidence suggests that this was the last portion of South America to separate from Africa. The second syn-rift phase was related to the propagation of the South Atlantic opening. Assuming northward propagation in the earliest Aptian (local Jiquiá stage), relative clockwise rotation of South America with respect to Africa would cause NW–SE-oriented shear in the region. Further extension was transferred to the Atlantic margin, isolating the Recôncavo–Tucano–Jatobá rift which, in turn, started its post-rift evolution, marked by negligible thermal subsidence and diverse phases of erosion and final exhumation.

The discussion below is based on the microplate model, but incorporating into it these key elements of the other models.

One of the most striking features of the Recôncavo–Tucano–Jatobá rift system is the alternating polarity along the rift borders. In the south, in the central and southern Tucano and Recôncavo basins, the main fault is situated at the eastern, or southeastern borders of the basins, whereas the opposite margin is a hinge-line. Conversely, in the northern Tucano and Jatobá basins, the main fault is situated along the western or, in the Jatobá basin, the northern border, that is, on the side farthest from the Atlantic Ocean. These two polarities are separated by a major tectonic lineament along the Vaza-Barris river, whose nature is now established as a major transfer fault zone. It may be a transfer fault, strike-slip fault, or just a structure inherited from the Precambrian basement; in the southeast, near Aracaju, it runs along the axis of transpressional late Proterozoic folds. This tectonic lineament (the Vaza-Barris "fault" of Szatmari and Milani, 1999) which, from the Atlantic margin to the western border of the Tucano rift, marks the northeastern border of the Archean to early Proterozoic São Francisco craton. To the south of the Vaza-Barris transfer fault, the Central Tucano, South Tucano, and Recôncavo basins lie over the craton whereas to the north of it, the North Tucano and Jatobá basins lie over the Neoproterozoic, in part metasedimentary rocks of the Borborema province.

To the northwest of the Tucano rift, the Vaza-Barris transfer fault reaches the outcropping northern end of the São Francisco craton, near the Proterozoic E–W-trending Pernambuco-Ibimirim fault, which forms the northern end of the Recôncavo–Tucano–Jatobá rift system.

The Vaza-Barris transfer fault cuts through the Tucano rift between the northern and central Tucano basins, sharply offsetting the eastern border of the Tucano rift so that it becomes considerably wider and deeper directly to the south of the "fault." In this area, the Cícero Dantas low, seismic surveys record the thickest sequence of the entire rift system, more than 10 km and possibly over 17 km of layered sediments, perhaps including some of the latest Proterozoic sediments below the rift sequence. To the southeast, between the Tucano rift and the Atlantic Ocean, the SE-trending Vaza-Barris transfer fault cuts across the outcropping

late Proterozoic rocks of the Sergipe Microplate, reaching the Atlantic Ocean near Aracaju. It is nearly perpendicular to the NE-trending ocean margin where it separates two tectonic units: to the SW the granulites of the mostly Archean Salvador-Jacuípe horst, which forms a part of the São Francisco craton and divides the Recôncavo basin from the ocean; to the northeast the coastal Sergipe-Alagoas basin, lying over younger Precambrian metasediments. The left-lateral offset of the outcropping Precambrian border along the Vaza-Barris transfer fault near the Atlantic, between the Salvador-Jacuípe horst and the Sergipe-Alagoas basin, is approximately the same as that of the eastern border of the Tucano rift, so that the combined width of the northern Tucano and Sergipe-Alagoas basins to the north of the Vaza-Barris transfer fault is similar to the width of the central Tucano basin to the south of the fault zone (Fig. 15.1).

There are several other major structures within the Tucano rift which are related to its opening. One of the most important is the Caritá fault, that coincides with the Vaza-Barris "fault" at the eastern border of the Tucano basin, where it has a similar NW–SE trend, but which curves to the northwest and then to the north across the rift, so that it reaches the main border fault at the western border of the North Tucano basin. Another major fault is the Jeremoabo fault, which trends E–W across the eastern margin of the Tucano rift and formed along a reactivated late Proterozoic transpressional fault (Destro et al., 2003a).

15.3 Rift abortion, rift jump, and the origin and duration of the Northeast Brazilian Sergipe Microplate

Continental breakup between South America and Africa, becoming more active from the time of the Paraná flood basalt eruptions 132 Ma ago, took place by clockwise rotation of South America relative to Africa (Milani et al., 1988; Szatmari and Milani, 1999; Szatmari et al., 1985). As a result, a long and more or less simultaneous rift formed along the present continental margin from the Paraná hotspot to Salvador in the north, trending N–S between Cabo Frio and Salvador. North of Salvador, it continued to propagate northward up to where the E–W-trending Ibimirim-Pernambuco and, farther north, the Patos Proterozoic shear zones made further propagation impossible (Milani et al., 1988; Szatmari and Milani, 1999). Thus, northward propagation of the rift ended during extension in the earliest stages of rifting. Continued widening of the Recôncavo–Tucano rift therefore required first left-lateral motion along the Pernambuco-Ibimirim shear zone zone as suggested by Magnavita (1992), compensated by the opening of rifts north of the Ngaoundere fault zone, which mark the continuation of the Pernambuco shear zone inside Cameroon. Further widening of the Tucano rift resulted in its propagating perpendicularly to the east along the Pernambuco shear zone as South America rotated clockwise relative to both Africa and the

North Brazilian or Sergipe Microplate. This rotation created the E–W-trending and eastward-tapering Jatobá basin, along the Ibimirim-Pernambuco shear zone.

The Northeast Brazilian or Sergipe Microplate (Milani et al., 1988; Szatmari and Milani, 1999) became imperfectly coupled to the African continent, with a left-lateral wrench zone forming between the two, from Salvador toward Recife along what are now the Recôncavo, North Gabon, and Sergipe-Alagoas basins. Along this wrench zone, slivers were moving to the northeast relative to South America; the Salvador horst might have had its origin in one of these slivers. The Recôncavo basin, at the southern end of the Recôncavo–Tucano–Jatobá rift system, was in the vicinity of both the original N–S-trending Recôncavo–Tucano rift and the NE-trending wrench zone, its tectonic evolution being affected by both. As long as the Recôncavo–Tucano rift was free to extend, there was little extension along the NE-trending wrench zone, taking place largely along N–S-trending grabens that formed tension gashes. These grabens, filled by pre-Aptian sediments, are well expressed in the Sergipe-Alagoas basin.

Whereas the northern portion of the microplate was deformed relatively rigidly, the southern portion, including the southern tip that contains the Recôncavo basin, appears to have undergone partially ductile deformation, shown, among others, by the left-lateral drag of the Salvador-Jacuípe horst, along the NE–SW-trending Barra fault that marks the southern end of the Recôncavo basin, separating it from the offshore Camamu basin in the south. Although the sedimentary fill of the Camamu basin is similar to that of the Recôncavo basin, its structure is different. The main faults trend N–S, cut by NW–SE-trending transfer faults.

Differential rotation of the Sergipe Microplate, still attached partially to Africa and rotating with it relative to South America, created, along the northern margin of the microplate, the eastward-tapering Jatobá graben, together with its compressional counterpart and mirror image, the Arcoverde thrust wedge (Szatmari and Milani, 1999). This compressional structure tapers westward and widens to the east from Arcoverde township toward Recife. Crustal thickness in the compressional wedge originally increased eastward to the coast with increasing rotation of the microplate. However, the upper portion of the thrust wedge has been eroded along the Atlantic margin.

By the end of late Barremian to early Aptian times, the resistance created by the accumulated Arcoverde thrust wedge (Szatmari and Milani, 1999) made further rotation of the microplate and extension along the Recôncavo–Tucano–Jatobá rift system impossible, annealing the Sergipe Microplate to the South American plate and thus aborting further rifting in the Recôncavo–Tucano–Jatobá rift system. At the same time, extension was transferred to the NE-trending wrench zone between Salvador and Recife in the same manner as it has been transferred from the Suez Rift to the Dead Sea transform, where extension now is increasing in response to increased extension in the Red Sea. Extension in the eastern branch and annealing in the western branch

produced a sharp unconformity in the Recôncavo–Tucano rift system; the unconformity is overlain by late Aptian conglomerates. Along the eastern branch, the former wrench zone between Salvador and Recife, which by late Aptian times became the main zone of extension, late Aptian conglomerates of the Sergipe-Alagoas basin were overlain by a thick but relatively narrow evaporite sequence, with carbonates over the evaporites containing well-characterized ammonites of latest Aptian age in the Taquari member of the Riachuelo Fm: *Epicheloniceras*, *Diadococeras,* and *Eodouvilleiceras*. The late Aptian sequence is followed by Albian carbonates and siliciclastic rocks, cut by basement-involved faults that mark continued rifting in this area during late Aptian and Albian times. It took some time, during the Albian, for the rift to cross the thickest portion of the Arcoverde thrust wedge along the Pernambuco shear zone. Rifting in this area was accompanied by localized but intense igneous activity near Recife (microgranite, basalt, andesite, rhyolite) of Albian age, reflecting the great thickness and high temperatures of the crust during Albian rifting in the lower portion of the Arcoverde thrust wedge. By latest Albian times, rifting had been completed in the area.

15.4 Time span of rifting

The opening of the aborted Recôncavo basin, as well as the entire Recôncavo–Tucano–Jatobá rift system, was related to other rift basins along the Brazilian margin (Chang et al., 1992) in early Cretaceous times. The exact time of this opening is still subject to controversies because fossil content in the intracontinental Recôncavo basin are mainly lacustrine ostracods with lesser amounts of spores and pollens which, while good enough for detailed local correlation, are not best suited to correlation with other basins along the Brazilian margin and even less to correlation with marine basins around the world.

Therefore, as to the start of rifting, two lines of reasoning can be followed. According to the generally accepted model, based mostly on correlation of ostracods, spores, and pollens in the freshwater rift basin with globally accepted stratigraphic markers in other basins of the world, the pre-rift sequence (Aliança-Sergi Fms) of the Recôncavo basin is of uppermost Jurassic age, and the overlying Cretaceous rift sequence starts with Berriasian sediments ~144 Ma. This would make the deposition of the rift sequence of the Recôncavo basin last ~23 Ma, from 144 to 121 Ma, and make its petroleum source rocks, the Gomo and Tauá shales of the Candeias Fm of Berriasian age (Da Silva et al., 2000), older than the rift source rocks of the Campos basin. These ages are supported by preliminary data of Re–Os dating.

However, in the absence of more geochronological data, other models are also possible. The pre-rift sequence of the Recôncavo basin, composed of the lacustrine shales of the Aliança formation and the overlying lacustrine-fluvial sandstones

of the Sergi Fm, appears to correlate with the Botucatu-Pirambóia sandstones of the Paraná basin, deposited in a semi-arid environment. These sandstones interfinger with the flood basalts of the Paraná igneous province, which are well dated by the Ar-Ar method at about 132 ± 5 Ma, that is, of Valanginian age. Thus, the Botucatu sandstones, which directly underlie and interfinger with the basalts and by extension the correlating sequence of the Sergi-Aliança Fms in the Recôncavo basin, would also be of early Valanginian or Berriasian age, deposited directly before the extrusion of the flood basalts of the Paraná igneous province. These basalts are absent from the Recôncavo basin, distant from the Tristan de Cunha hotspot, and underlain by the thick and cold lithosphere of the São Francisco craton.

Thus, the sequence overlying the pre-rift Aliança-Sergi Fms of the Recôncavo basin including the basin's main petroleum source rocks, the Tauá and Gomo shales of the Candeias Fm would have been deposited in late Valanginian time(?). The world's well-defined Valanginian source rocks correspond to a negative excursion of $\delta^{13}C$, a Weissert oceanic anoxic event, reported from the Alps and the eastern Pacific in Valanginian time (Erba et al., 2004). The source rock in the southeast Brazilian basins (such as Campos) deposited over the basalts are also late Valanginian. Erba et al. (2004) suggest that the cause of this anoxic event was the emission of large amounts of CO_2 from the Paraná igneous province and from the oceanic ridges opening during the breakup of Gondwana; subsequently atmospheric CO_2 was rapidly consumed by weathering and the deposition of organic-rich Valanginian sediments (Erba et al., 2004). The rift sequence of the Recôncavo–Tucano–Jatobá rift system would follow the deposition of the Berriasian to early Valanginian pre-rift sediments of the Aliança-Sergi Fms. Thus, rift sedimentation would last somewhat shorter than in the traditional first model, from late Valanginian to the end of Barremian time, from $\sim$136 to 121 Ma, for $\sim$15 Ma.

In the discussion below, we shall follow the traditional stratigraphic model, attributing late Jurassic age to the pre-rift sequence and starting the rift sequence in Berriasian time.

The rift sequence of the Recôncavo basin is cut by a sharp unconformity overlain by the Aptian sandstones and conglomerates of the Marizal Fm that end the Cretaceous sequence of the Recôncavo. Conversely, on the Atlantic margin of the Sergipe Microplate, in the Sergipe-Alagoas basin, extension was minor until Aptian times, with little normal faulting mainly along N–S trends, but became intense from late Aptian times with the deposition of a thick salt sequence over Aptian conglomerates, overlain by Albian carbonates cut by thick-skin, basement-penetrating faults. The deposition of this second rift sequence along the eastern Atlantic margin of the Sergipe Microplate lasted from the late Aptian, to the end of the Albian, that is, from $\sim$115 Ma to $\sim$99 Ma, taking $\sim$16 Ma.

15.5 The Recôncavo basin *S.S.*

The Recôncavo basin *sensu stricto*, the main object of this study, extends for ~150 km in a north easterly direction from Salvador. To the southeast, it is bordered by the outcropping Salvador horst and its offshore extension, the Jacuípe horst, both composed of Archean granulites of the São Francisco craton. Part of the Jacuípe horst is terminated toward the Atlantic Ocean by a fault of Albian age; the Aptian sequence is missing but it is present in Gabon, on the conjugate, African margin.

Tectono-sedimentary evolution

Basin-fill of the Recôncavo–Tucano–Jatobá rift contains strata from Paleozoic to Cenozoic age, comprising pre-, syn-, and post-rift megasequences (Fig. 15.2). The syn-rift phase occurred during the Early Cretaceous, chiefly in the Neocomian, but rift evolution extended at least from Late Jurassic to Early Albian. The total sedimentary thickness exceeds 6 km in the main depocenter of the Recôncavo basin, the Camaçari-Miranga low, compared to more than 10 km in the Cícero Dantas low, in the Central Tucano basin.

The basal, pre-rift sequence is made up of the red shales and sandstones of the Aliança Fm, overlain by the sandstones of the Sergi Fm, both attributed to the late Jurassic (Table 15.1, Fig. 15.3). Whereas in the offshore Camamu basin to the south there is an erosional unconformity between the pre-rift and syn-rift sequence, in the Recôncavo basin such an unconformity cannot always be discerned. The shales were deposited in a playa-lake environment; the sandstones are fluvial to eolian. Dadoxylon trunks, belonging to Araucaria-type conifers, are common in the Sergi Fm, but their stratigraphic value is limited as dadoxylon taxa appear throughout the Mesozoic. These formations were deposited before, or during, initial rifting; their shape is tabular and only rarely cut by growth faults.

The tectono-sedimentary evolution of the basin is markedly asymmetrical, both in space and in time. In space, the main fault, the Salvador fault, runs along the SE border of the basin and has a maximum downthrow of ~6,000 m. It follows a NE–SW to N–S direction along the northwestern edge of the Salvador horst, bordered by conglomerates with excellent outcrops within the city of Salvador where an elevator links the upper and lower towns close to the fault scarp. Rapid movement along the fault in early Cretaceous time deposited thick conglomerates along the fault scarp and produced a rapidly deepening starved basin in which the Candeias (Gomo) source shales were deposited. At the northwestern, flexural border of the Recôncavo basin, the rise of the Precambrian rocks of the Aporá high along the hinge line was slower and more delayed.

Thus, a deep starved lake formed at the beginning of the rift sequence (Fig. 15.4) in which the organic-rich black shales of the Tauá and Gomo Members of the Candeias Fm were deposited. Between these and the Sergi Fm, the

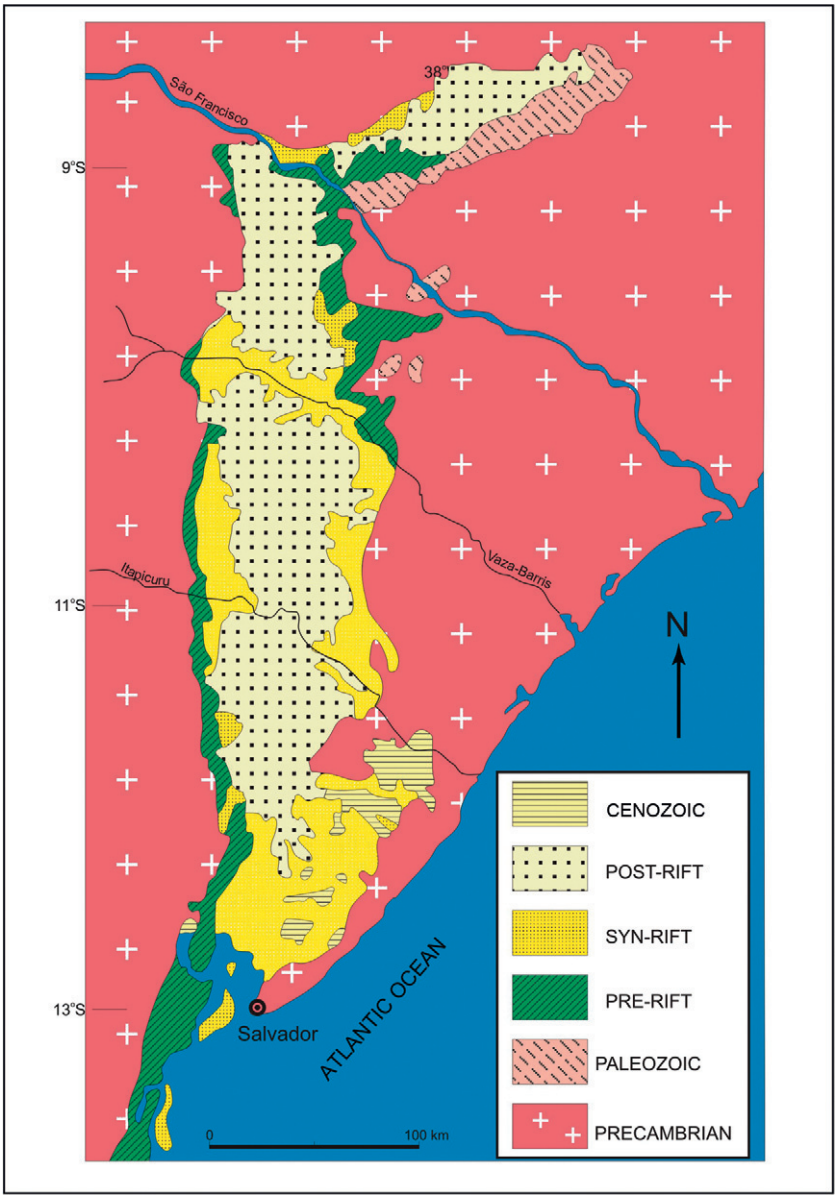

Figure 15.2
Distribution of pre-, syn-, and post-rift sediments *(after Magnavita, 1992)*.

lacustrine shales of the Itaparica Fm, dissected by sand dykes, and the fluvial to eolian sandstones of the Água Grande Fm provide a transition between the pre-rift and syn-rift sequences. The thick shale sequence of the Candeias Fm, with interfingering turbidites, thus characterizes the first phase of the evolution

Table 15.1 Stratigraphic table for the Recôncavo basin

Period	Epoch/Age	Group	Formation	Member	Environment	Lithology (main)
Cenozoic	Pliocene	Barreiras			Alluvial fan	Sandstone
L. Cretaceous (POST-RIFT)	Aptian		Marizal		Alluvial fan	Conglomerate
(SYN-RIFT)	Barremian	Massacará	Poço Verde			Shale
			São Sebastião		Fluvial	Sandstone
	Hauterivian	Ilhas	Pojuca	Santiago	Deltaic	Sandstone/ Shale
			Taquipe		Canyon fill	Sandstone/ Shale
	Valanginian		Marfim	Catu	Deltaic	Sandstone
			Salvador	Sesmaria	Fan-delta	Conglomerate
		Santo Amaro	Maracangalha	Pitanga/ Caruaçu	Lacustrine/ Turbidites – Sand debris	Shale/ Sandstone
	Berriasian		Candeias	Gomo	Lacustrine/ Turbidites	Shale
				Tauá	Lacustrine	Shale
(PRE-RIFT)			Água Grande		Fluvial/aeolian	Sandstone
U. Jurassic			Itaparica		Lacustrine	Shale
	Tithonian	Brotas	Sergi		Fluvial/aeolian	Sandstone
			Aliança	Capianga	Playa lake	Shale
				Boipeba	Fluvial/aeolian	Sandstone
Permian			Afligidos/ Santa Brígida	Cazumba/ Ingá	Playa lake	Shale
	Kungurian			Pedrão/ Caldeirão	Platform/tidal	Sandstone

of the Recôncavo rift proper, when sedimentation was still relatively slow, subsidence rapid, and lake waters deep. Sedimentation continued with the deposition of the Maracangalha Fm, similarly made up of lacustrine shales and turbidite sands, but already in somewhat less deep lake waters. During the late stages of the rift evolution, these shales were strongly deformed by the weight of the overlying sediments, forming shale diapirs that penetrate the entire rift

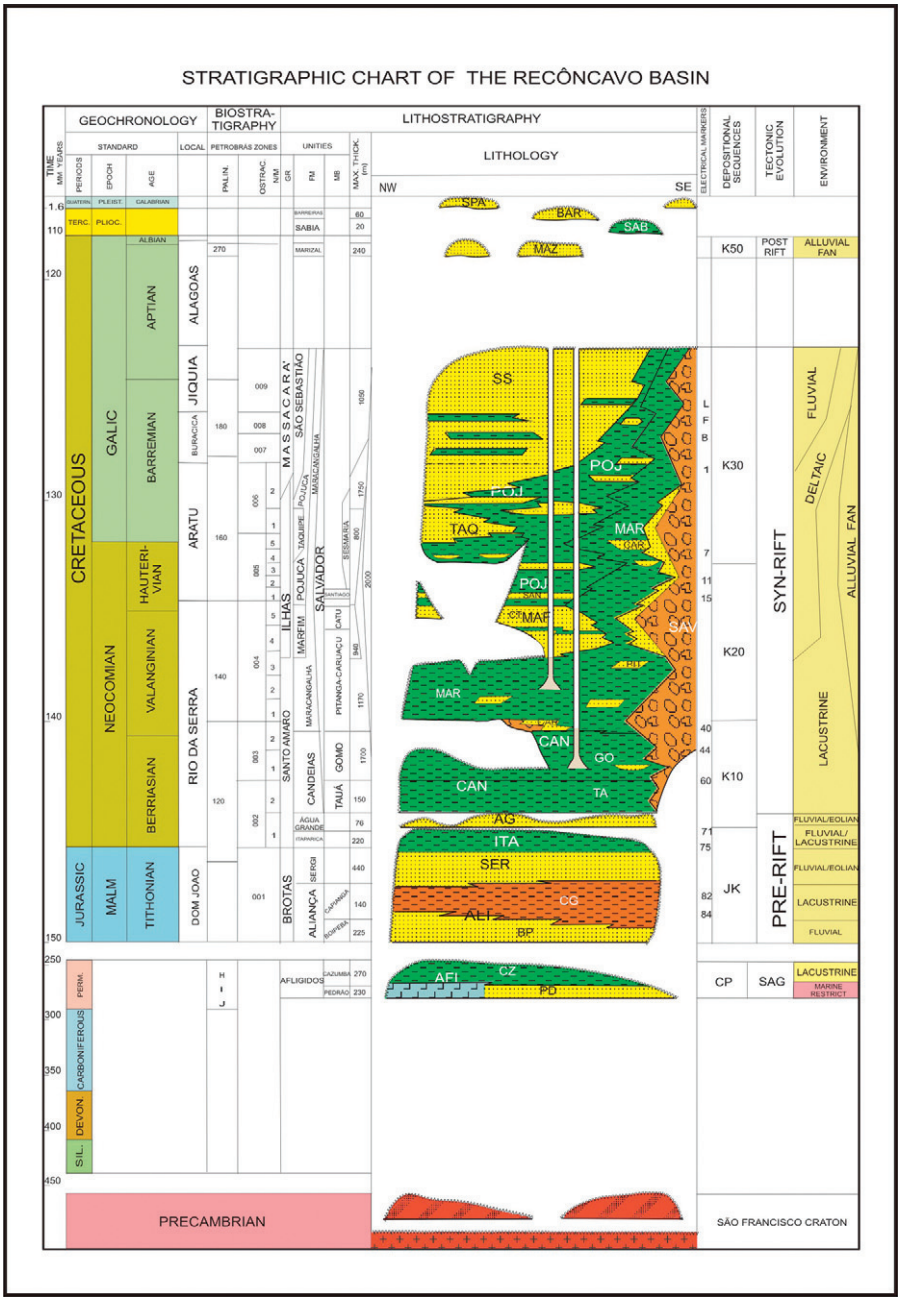

Figure 15.3
Stratigraphic chart of the Recôncavo basin *(after Caixeta et al., 1994).*

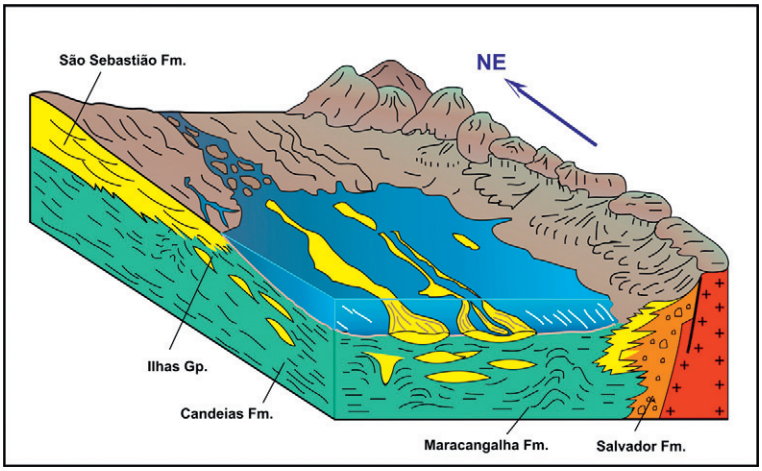

Figure 15.4 Syn-rift paleogeography of the Recôncavo basin *(adapted from Medeiros and Pontes, 1981).*

sequence, such as the famous Cinzento diapir. Similarly, many of the sandstones are affected by both syn-sedimentary and deep deformation; those of the Pitanga Mb display diapiric shapes and a texture resembling igneous intrusives. The Candeias and Maracangalha Fms together form the Santo Amaro group (Table 15.1, Fig. 15.3).

After the deposition of the shales and turbidites of the Santo Amaro group, sediment flux to the basin increased while subsidence decreased, so that the basin started to fill up. Two major sedimentary bodies formed: the Salvador conglomerates, composed of fan-delta sediments derived from the Salvador-Jacuípe horst and forming along its scarp; and the sediments of the Ilhas group, in which deltaic sandstones dominated (Marfim and Pojuca Fms). Also, within the Ilhas group (Table 15.1, Fig. 15.3) are the canyon-filling sediments of the Taquipe Fm, formed when lake level suddenly dropped in both the South Tucano and western Recôncavo basins.

The last phase of the syn-rift sequence was the deposition of the sediments of the Massacará group, composed predominantly of the fluvial red sandstones of the São Sebastião Fm. At this time, relief was already low, reflecting the slowdown of tectonic subsidence.

The rift sequence is cut by a major unconformity of Aptian age that marks the failure of the Recôncavo–Tucano–Jatobá rift system and the transfer of extension to the present Atlantic margin. The erosional surface cuts through all depositional sequences as well as the diapirs coming from the deeper portion of the rift sequence, such as the Cinzento diapir. The angular unconformity is overlain by the late Aptian alluvial fan conglomerates of the Marizal Fm.

15.6 Major tectonic elements of the Recôncavo basin: The Salvador and Mata-Catu faults

The boundary between the Recôncavo and Tucano basins is placed along the Aporá high. The Recôncavo basin is structurally characterized by an N30°–40°E-trending system of synthetic and antithetic extensional faults (Fig. 15.5). The basin is an eastward-tilted half-graben, with most basin asymmetry generated by a single border fault, the Salvador fault (Fig. 15.6). The shallower western-flexural side is bounded by faulted monoclines or unconformable ramps.

The general NE-trending faulted blocks are broken by a NW-oriented transfer zone (Aragão, 1994; Milani and Davison, 1988), the Mata-Catu fault, which controls a major oil trend in the basin. This fault zone not only controlled the traps, but also exerted an important role on oil migration, focusing fluid movement from the depocenter toward traps located far from the "oil kitchen" (Magnavita, 2000). More recently, as discussed below, this major cross-fault has been interpreted by Destro et al. (2003b) as a release fault, created to compensate the bending of the hanging-wall block along the Salvador border fault.

Release faults are distinct from the other type of cross-fault termed "transfer fault" (Gibbs, 1984, 1990). In the Recôncavo basin, the only cross-faults we have identified are release faults. Release faults have been described by Destro (1995), Stewart (2001) who used the term "stretch accommodation faults," and Destro et al. (2003a,b).

Distinct from transfer faults, which are predominantly strike-slip, release faults are normal and develop in the hanging-wall blocks of the main components of the extensional basins. The term "release" reflects a genetic aspect, that is, the releasing of the bending stresses of the hanging-wall blocks due to the variation of displacement along the strike of normal faults (Destro et al., 2003a,b).

Release faults form preferably in the strike ramps and die out within an individual hanging-wall without connecting distinct normal faults (Fig. 15.7). They are intimately associated with single normal faults, called "parent faults," which they do not cut at depth. Release faults are more common over the ramps because bending of the hanging-wall is greater there.

Because release faults are cross-faults of normal displacements they generally do not show compressional structures such as flower structures, *en échelon* folds, and Riedel-type geometries (Destro et al., 2003a,b). Additionally, since they form due to differential vertical displacements in the hanging-walls, they are compatible with regional plane strain deformation. In oblique extension, they may contribute to three-dimensional strain deformation. However, between the terminations of a parent fault, three-dimensional strain deformation does occur in the hanging-wall (Destro et al., 2003a,b).

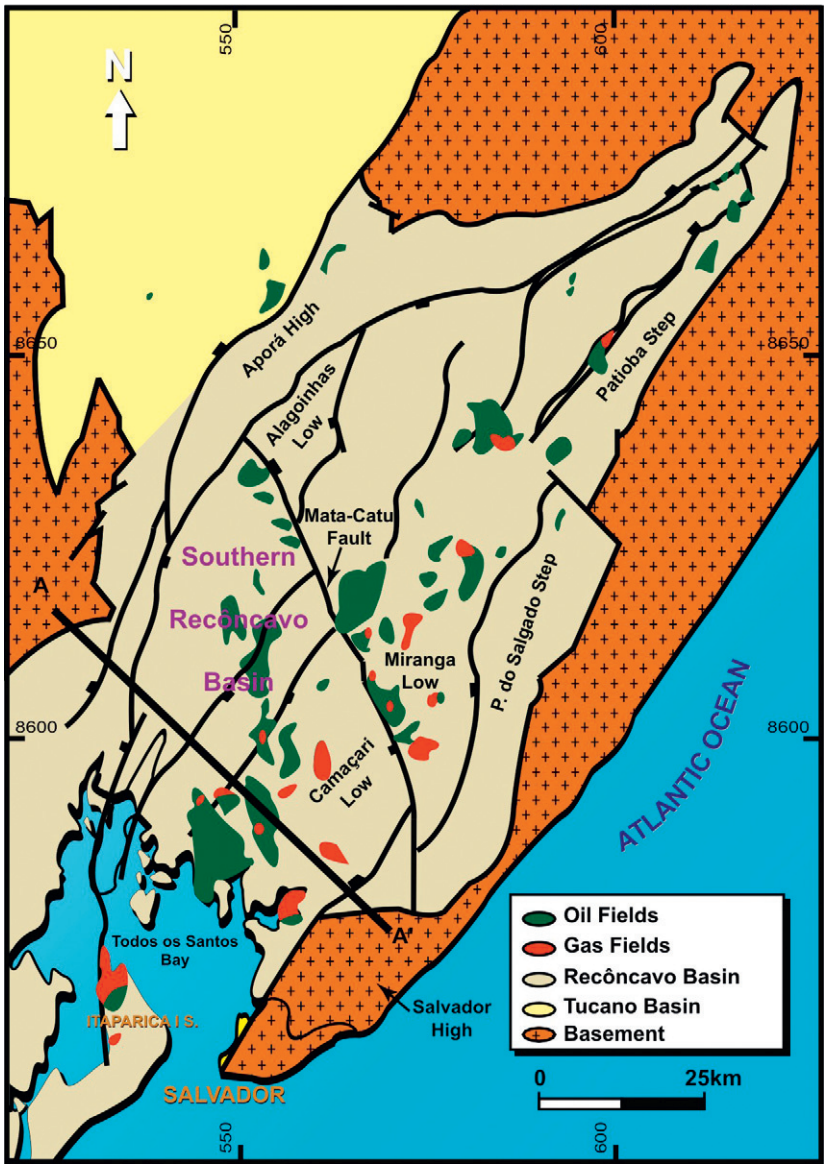

Figure 15.5 Structural framework and hydrocarbon fields of the Recôncavo basin. The line A–A′ refers to the cross-section in Fig. 15.6.

Along release faults the local stress field can strongly depart from the regional one, allowing the formation of release fractures and reverse faults (Fig. 15.8). As a result of footwall uplift and a consequent upward differential bending, footwall blocks may also display small-scale release faults (e.g., Destro et al., 2003a,b; Stewart, 2001).

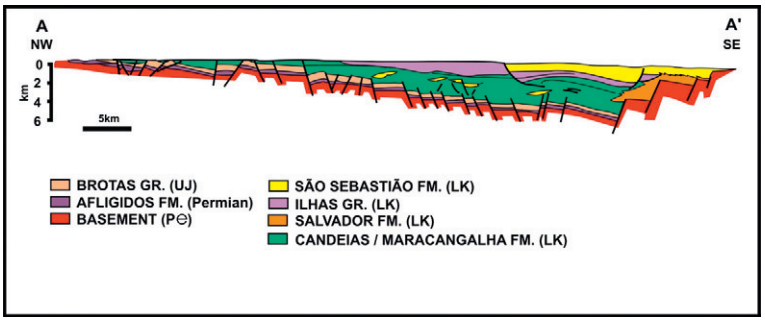

Figure 15.6
Section A–A′ across the Southern Recôncavo basin.

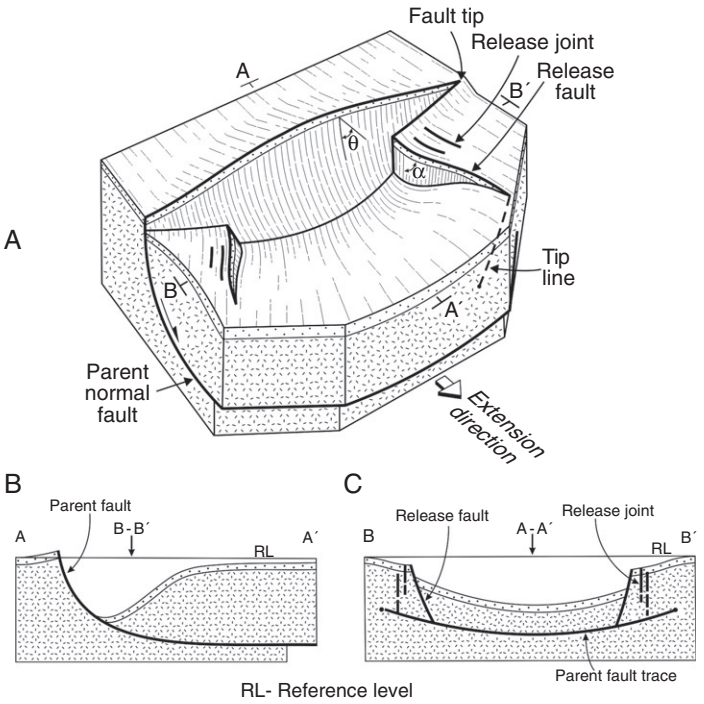

Figure 15.7 Block-diagram showing the displacement variation along the strike of a normal fault *(modified after Destro et al., 2003b)*. Release faults may be also present in the footwall block as a result of differential footwall uplift.

Since release faults represent areas of stronger stress release compared with the parent faults, they are also associated with developed salt and shale diapirs. This aspect also makes them favorable oil migration pathways. Because release faults form in areas where joints are enhanced, they may act as a focal point of relatively higher quality reservoir rock.

In the Recôncavo basin, the major North and South Mata-Catu cross-faults as well as several smaller cross-faults terminate against the Salvador fault to the

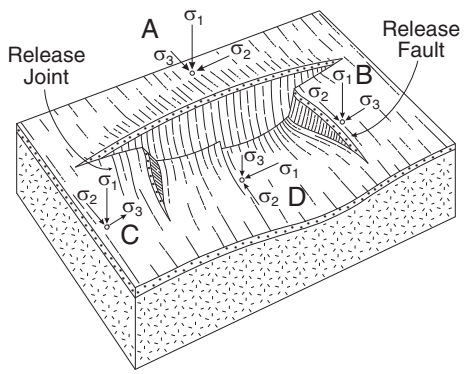

Figure 15.8 Orientation of stress field states around major normal faults and release faults (Destro et al., 2003b). (A) Regional stress field. (B) Rotation of the intermediate (σ_2) and the smallest (σ_3) principal stresses around the maximum principal stress (σ_1) axis causing the formation of a release fault. (C) Perpendicular to σ_3 release fractures may develop parallel to the release faults. (D) Reversion among the three principal stresses, forming a reverse fault.

southeast, or against the major Tombador and Paranaguá faults to the northwest (Fig. 15.9). Because they die out within the hanging-wall blocks toward the central areas of the basin, they have been interpreted as release faults (Destro et al., 2003b). The major Salvador border fault in the southeast and the Tombador and Paranaguá faults in the northwestern portion of the basin would have acted then as parent faults to the various release faults. Note that the South Mata-Catu fault is associated with the Salvador parent fault, while the North Mata-Catu fault is associated with the Tombador parent fault.

Following the classical work on transfer faults by Gibbs (1984), some authors (e.g., Magnavita, 1992; Milani and Davison, 1988) have interpreted the South and North Mata-Catu fault system as a single transfer fault, called the Mata-Catu fault, in which the sense of dip changes along its strike. The interpretation by Destro et al. (2003b) that the North and South Mata-Catu faults acted as separate release faults is based on the data by Aragão (1994), who mapped this fault system and portrayed it as being composed of two distinct faults dipping in opposite directions, instead of a single fault as previously thought; Destro et al.'s field data document slickenside striations showing a predominance of normal displacements on these faults. These authors also consider that release faults in the Recôncavo basin do not indicate regional three-dimensional strain because orthogonal rifting operated in this specific basin within the Recôncavo–Tucano–Jatobá rift system.

The maximum vertical displacement of the South Mata-Catu fault is about 3 km (Fig. 15.9), whereas the displacement of the Salvador fault, its parent fault, is about 6 km in this area.

Release faults and a number of release faulting-related cross-structures, including shale diapirs, release fractures, and a reverse fault, control the distribution of oil fields in the Recôncavo basin. Also, these structures contribute in particular ways to the formation of structural traps.

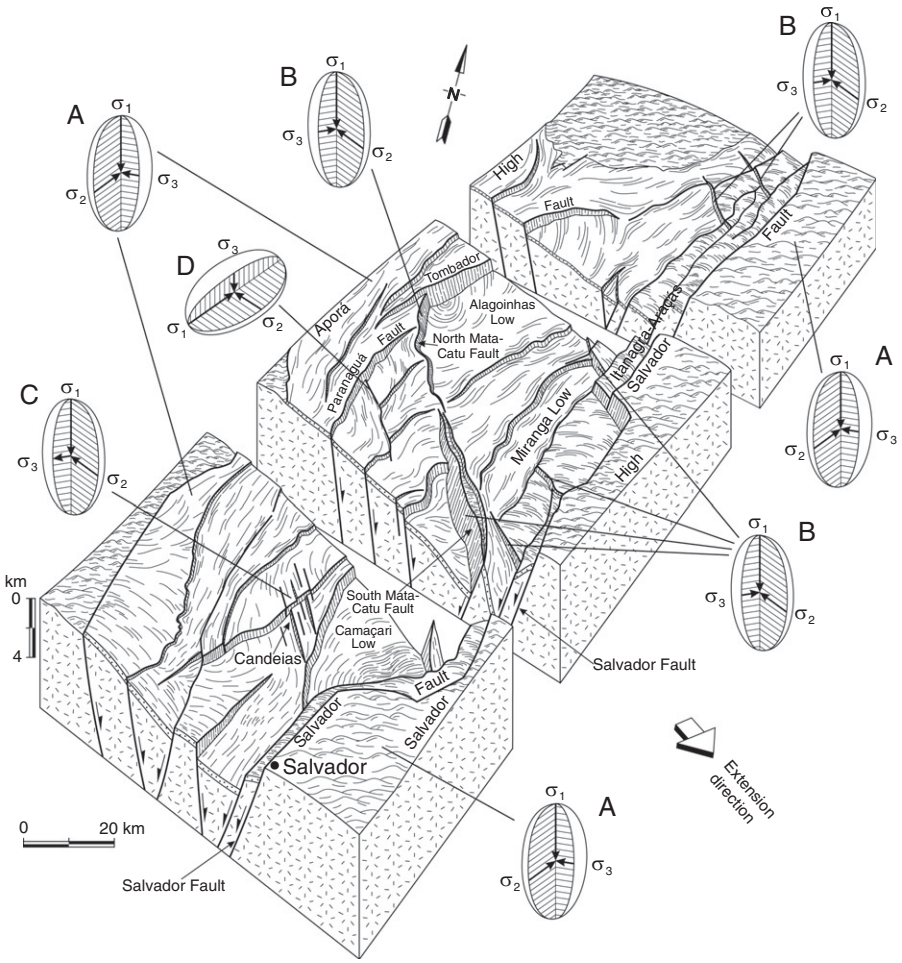

Figure 15.9 Major features of the Recôncavo basin, and associated local stress field ellipsoids *(modified after Destro et al., 2003b)*. (A) Regional stress field caused regional northwest-southeast extension. (B) Stress fields around the main release faults. The intermediate (σ_2) and the smallest (σ_3) principal stresses change their position. (C) σ_3 becomes smaller than the case in (B), causing the formation of open release fractures in the Candeias area. (D) Change in the position of the three principal stresses, causing the formation of the North Cassarongongo reverse fault.

The South and North Mata-Catu faults produced the most prolific petroleum trend in the Recôncavo basin, with oil fields located in their footwall blocks (see also Fig. 15.5). The fields along this trend produce almost only from the pre-rift Sergi reservoir, filled with oil generated from syn-rift source rocks.

The closure of the Miranga field, located in the Miranga low (Fig. 15.9), is due to shale diapirism from the Candeias formation developed parallel to the Itanagra-Araçás release fault as well as northeast-trending diapirs of the Candeias formation parallel to the Salvador fault. The diapirs formed along the Itanagra-Araçás fault are better developed than the ones formed parallel to the Salvador fault because, as seen above, the minimum principal stress (σ_3) in the release faults is smaller than the regional minimum principal stress (σ_3) parallel to the extension direction.

Open release fractures oriented across the rift axis are responsible for most of the oil production in the Candeias field. The fractures cut calcareous shales of the synrift Candeias formation at a depth of about 2000 m. They can be up to 0.5 cm open, with quartz crystals lining their walls and reaching up to 1 cm in length, and enclosing oil bubbles.

The Brejinho and Canabrava oil fields are located in the footwall block of the North Cassarongongo release fault in the western border of the Recôncavo rift (see Fig. 15.6). The North Cassarongongo fault is a rare example of a reverse release fault as presented above, which formed in the region of maximum throw of the major Paranaguá parent fault. The Cassarongongo field is situated on the footwall of the South Cassarongongo fault (Fig. 15.9), which dips northward and shows dip-slip motion.

15.7 Petroleum resources

Along the entire Recôncavo–Tucano–Jatobá rift system, the Recôncavo basin is the only one with established hydrocarbon production; in the South Tucano sub-basin, there are some small oil and gas fields; northward, no hydrocarbon accumulations have been found so far. The main source rocks are lacustrine freshwater shales of the Tauá and Gomo Members of Candeias Formation (Fig. 15.10), with TOC values ranging from 0.8% to 2.0% and hydrocarbon source potential of about 5 kg HC/ton rock (values of 10% TOC and 60 mg HC/g rock have been also reported by Mello et al., 1994). The oil window coincides with the main structural lows, and geochemical modeling of petroleum generation indicates that up to 80% of the petroleum was expelled at transformation ratios ($S_1/S_1 + S_2$) of about 0.5 (Mello et al., 1994). Based upon vitrinite reflectance, Aragão et al. (1998) placed the onset of oil generation between 800 and 2400 m, with peak conditions reached from 1500 to more than 3000 m in the deepest depocenters. The main reservoirs are sandstones of the pre-rift Sergi Formation, which may have 18% porosity and 800 millidarcys permeability.

The Recôncavo basin, the oldest petroleum-producing basin in Brazil, is in a mature stage of exploration. Commercial oil production started in 1941, and massive investments in the following decades led to the discovery of 85 oil and gas fields (see Fig. 15.5). Petroleum accumulation in the basin can be grouped into four basic systems, listed in order of importance: (1) the pre-rift Candeias-Sergi/Água Grande (!) system, (2) the syn-rift Candeias-Ilhas (!) system, (3) the syn-rift Candeias-Candeias (!) system, and (4) the syn-rift Candeias-Caruaçu (!) system. Principal reservoirs of the pre-rift system are the fluvial/aeolian Sergi and Água Grande Formations. Traps are typically structural (horsts and tilted blocks). Together they account for 57% of the proven oil volume of the basin (corresponding to 2.7 billion barrels). The second most important

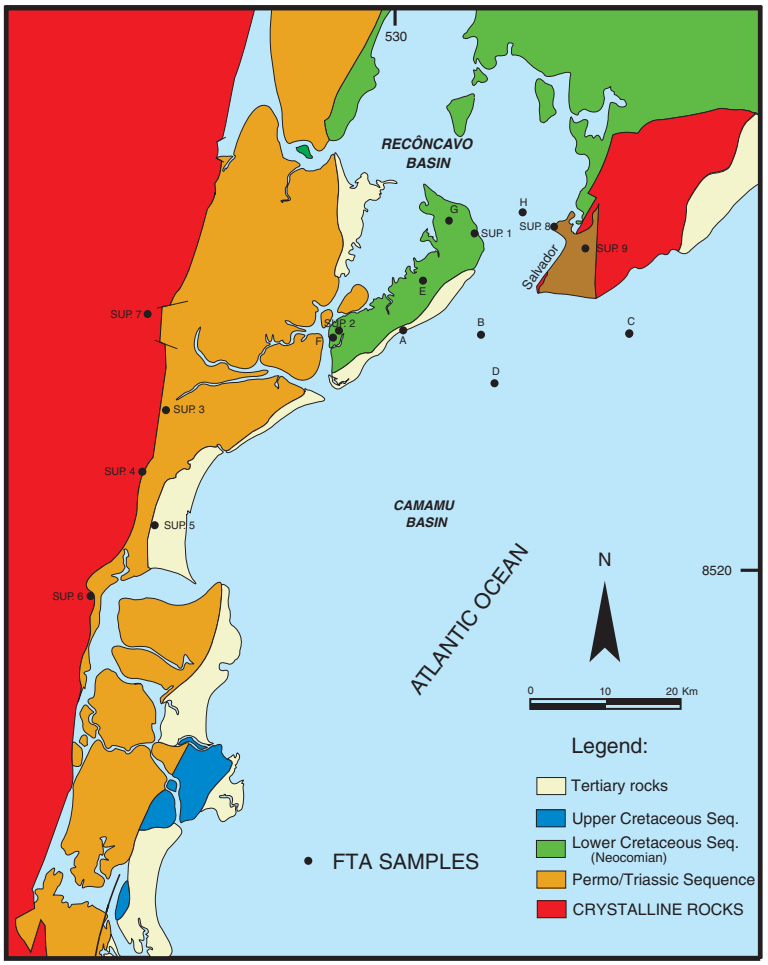

Figure 15.10
Geologic map of the Recôncavo and Camamu basins with FTA sample locations. City of Salvador is marked by dark brown color.

petroleum system is the syn-rift Ilhas system. Main reservoirs are deltaic sandstones forming structural (anticline), combined, and stratigraphic traps. Growth faults are common. Oil volume of this system corresponds to 27% of the total proven oil volume of the basin (ca. 1,265 billion barrels). Both stratigraphic and combined traps characterize the syn-rift Candeias system. Reservoirs are mainly lacustrine turbidites in northeastern and southern Recôncavo. Subordinate oil production comes from fractured shales. This petroleum system comprises 16% of the proven oil of the basin (corresponding to ca. 739 million barrels). Finally, the Caruaçu system, typified by massive gas-prone tight sandstones, constitutes the last frontier of the basin.

15.8 FTA in the Recôncavo basin

History of FTA

The method of FTA started to be used by geological studies in the 60 s. Nowadays, the application of this method has involved the study of the geological processes that affect the dynamics of the upper crust, especially in sedimentary basins. The technique provides parameters to study the thermal behavior, from deposition to burial, based on geological conditions that affect the stability of fission tracks; temperature is the main one (Naeser, 1979). Gallagher et al. (1998) described the application of this analysis to solve several geological problems, such as provenance studies, long-term structural and erosional evolution, and particularly modeling thermal history.

In the study of sedimentary basins, apatite is widely used for FTA because of the relatively high amounts of uranium present in its crystal lattice, the frequency in which it occurs in siliciclastic rocks, especially in sandstones, and its high susceptibility to spontaneous fission, even at the relatively low temperatures typical of sedimentary basins (Giles and Indrelid, 1998; Green et al., 1989a; Naeser, 1979). Among the contributions resulting from the application of the FTA method, the most important are dating of barren rocks (Carter et al., 1995), provenance studies (Rohrman et al., 1996), thermal histories of sedimentary basins (Zhao et al., 1996), passive margin evolution (Gallagher et al., 1995), and intracontinental rifts (Van der Beek et al., 1998).

Fission track data in the Recôncavo basin

The FTA results presented here were obtained by Cupertino (2000), from samples taken at outcrops and oil wells, totaling 33 samples of both crystalline basement rocks and sediments of various ages (Fig. 15.10). The crystalline basement is composed of high-grade metamorphic rocks (granulite facies) re-worked in the Cambrian. The well samples came from the lower Cretaceous sequence, obtained from cuttings.

The thermal histories conceived here were obtained by the use of Gallagher's (1995) algorithm and represent a simplification of the actual situation. However, there is consistency in the identified episodes, as well as in the epochs in which they occurred.

FT ages have shown themselves very useful for dating tectonic events in areas where the absence of igneous rocks does not permit use of conventional radiometric methods. Additionally, the study of track lengths aids understanding of the thermal evolution of the basin.

In the samples analyzed in the Recôncavo basin, FT ages vary between 188.5 $\pm$ 19.9 and 26.5 $\pm$ 2.4 Ma, encompassing a time interval between the Jurassic and the Oligocene. FT ages of basement surface samples are younger than the

Brasiliano orogenic system (between 580 and 420 Ma), the last event to affect the São Francisco craton. This permits us to infer that the FT ages obtained result from regional, long-term denudations, bringing to the surface apatites previously residing at depths of up to 4 km (approximately 110 °C temperature). Ages obtained from well samples show a decrease with depth, as well as a shortening of the average track length, a common occurrence in sedimentary basins.

The surface-sampled FT ages support the thesis that subsidence in rifts is distributed asymmetrically (Santos et al., 1990). While the western border sample (SUP7) begins to develop tracks at 205 Ma, at the faulted eastern border these only become stable at 148 Ma. The tracks reached stabilization temperature first on the western border (at about 145 Ma), reflecting that this region has always behaved as a platform zone, while the eastern border was uplifted throughout the rift's history. Figure 15.11 shows that the FT ages become older from south to north, besides the aforementioned differences. Thus, it is reasonable to assume that the Recôncavo–Tucano–Jatobá rift system was progressively abandoned from north to south. It is clear that the samples which were taken in the vicinity of the present continental margin are influenced by later processes, which makes it difficult to quantify the rate at which this abandonment occurred.

Numerical methods applied to the surface samples indicate the occurrence of two well-defined erosional phases (Fig. 15.12), one preceding the rift phase, between 200 and 150 Ma, and another during the Tertiary (from 63/52 Ma). The first uplift provided the source area for the pre-rift sequence sediments; using a geothermal gradient of 30 °C/km to estimate the erosion rate, 800 to 1000 m of crystalline rocks were eroded. The second phase represents the long-term uplift and denudation of the continental margin, when about 1700 m of rocks were eroded.

Another important aspect in the correlation between the basin borders is the erosion rate; at the faulted border this rate is much higher than at the flexural border. Using a present-day geothermal gradient (30 °C/km), it can be estimated that the erosion rate was 32 m/my at the faulted border against 18 m/my at the flexural border. The thermal stability shown by the samples at the flexural border is coherent with the idea that this margin acted as a sediment "bypass" zone since the start of the rift phase, while the rift shoulders to the east of the Salvador fault supplied the basin with sediments throughout its history. Figure 15.13 represents the temperature envelopes obtained by different algorithms for the observed track distribution at the western margin of the Camamu basin (SUP3). Assuming a constant geothermal paleogradient, the cooling was caused by a low erosion rate of the denudation during the rifting process (between 3 and 4.5 m/my), characteristic of the flexural margins of intracontinental rifts (Van der Beek et al., 1998).

Sample SUP9, collected from the roof of the Salvador fault, shows an asymmetric length distribution pattern, indicating that the sample underwent continuous

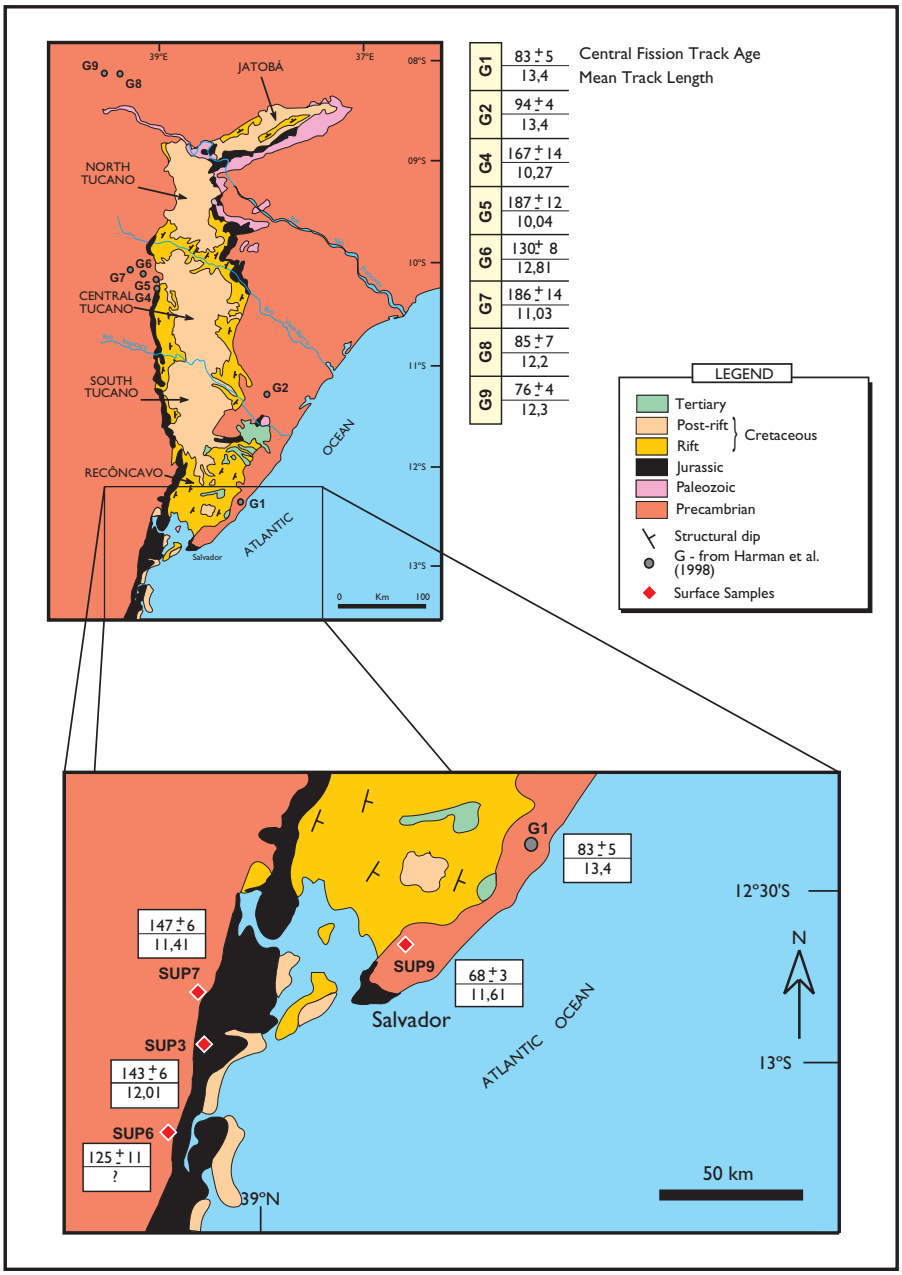

Figure 15.11 Geologic map with sample locations. The FT central ages decrease from north to south. G samples from Harman et al. (1998) *(modified from Cupertino, 2000)*.

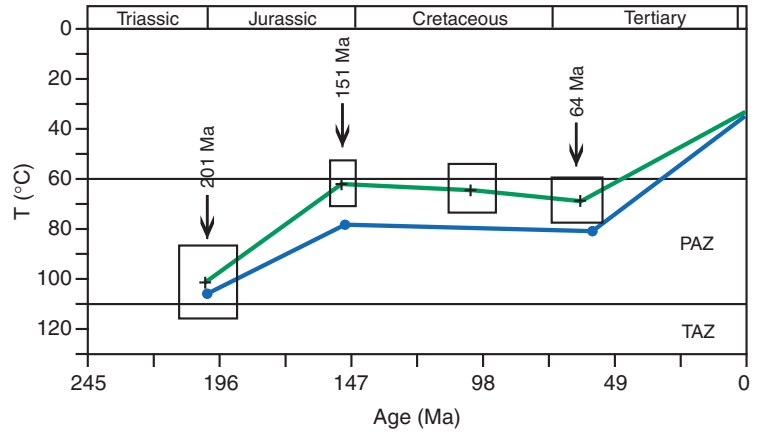

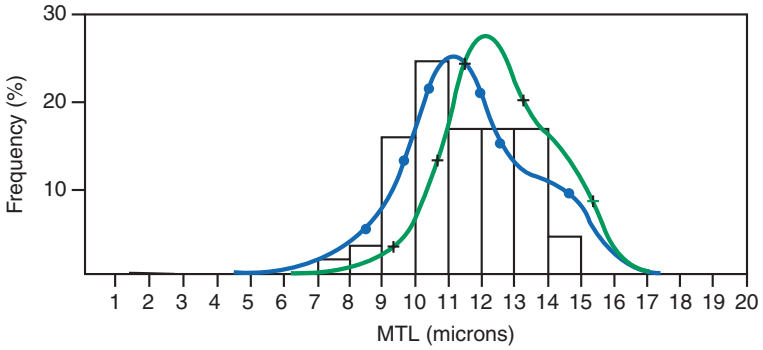

NUMERICAL MODELINGS			
Durango Laslett		F-apatite Carlson	
AGE	TEMP.	AGE	TEMP.
205	105	201	101
152	77	151	62
-	-	103	63
52	82	64	67
0	30	0	31

CALC. Data		OBS. Data.	
Durango Laslett	F-apatite Carlson		
147,2	157	147,4	Central age TF (Ma)
205	201	265	Oldest individual age (Ma)
11,7	12,5	11,4	- MTL (m)
2,0	1,7	1,6	Standard deviation (m)
0,65	0,62	-	R_o(%)

Figure 15.12
Simulations of thermal history for sample SUP7.

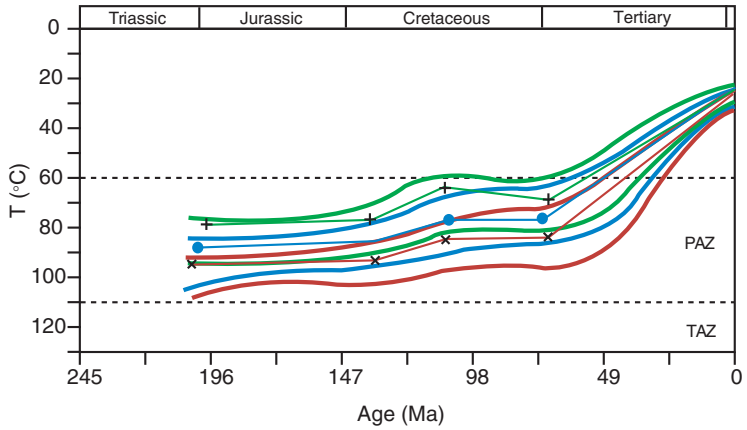

MODELINGS								
F-apatite Carlson —+—			Durango Laslett —●—			Durango Crowley —×—		
AGE	TEMP.	ΔTEMP.	AGE	TEMP.	ΔTEMP.	AGE	TEMP.	ΔTEMP.
196 ±10	80 ±6		200 ±11	90 ±5		200 ±12	96 ±5	
		-3			-6			-3
132 ±9	77 ±5		131 ±8	84 ±6		132 ±9	93 ±6	
		-12			-9			-9
107 ±6	62 ±5		106 ±6	75 ±8		105 ±6	82 ±8	
		+6			+3			+2
67 ±12	68 ±9		71 ±11	78 ±9		66 ±10	84 ±7	
		-43			-53			-59
0	25 ±3		0	25 ±3		0	25 ±3	

Figure 15.13
Simulations of thermal history for sample SUP3. FTA modeling by Carlson, Laslett, and Crowley algorithms all support a low erosion rate during the rift phase.

cooling throughout its history (Fig. 15.14). Numerical modeling indicates two phases of cooling. They also show that this area remained tectonically active until 91 Ma (Turonian/Cenomanian boundary) when the sample began to reside at temperatures of the order of 80 °C. A 35 °C/km paleogradient during the rift phase suggests that 1200 m of rock were eroded (24 m/my rate). There is evidence that there may have been a certain amount of heating altering the gradient of this region at 46 Ma; the temperature would pass from 74 to 102 °C. If the rock remained at the same depth, the geothermal gradient passed to 51 °C/km, which would imply a substantial rise of the heat flow to values known from proto-oceanic volcanic zones, such as the Red Sea (Lysak, 1992; Middleton, 1982) or rifts with associated volcanism (Ingersoll and Busby, 1995). When the tectonic subsidence in the Recôncavo rift ended, this area still acted as the source for the Atlantic margin basins. The modeling also shows a process of uplift and erosion of the eastern margin which began 46 Ma ago, and is still going on today. Using the present geothermal gradient, the erosion was about 2700 m at a rate of about 58 m/my.

The well samples tend to mark the subsurface conditions under which fission tracks developed; in this basin they suggest that each block has evolved independently of its neighbors. There are, however, some modeling attributes which are similar between wells, indicating that regional aspects are also being recorded. One of the best of the common points is related to the time when

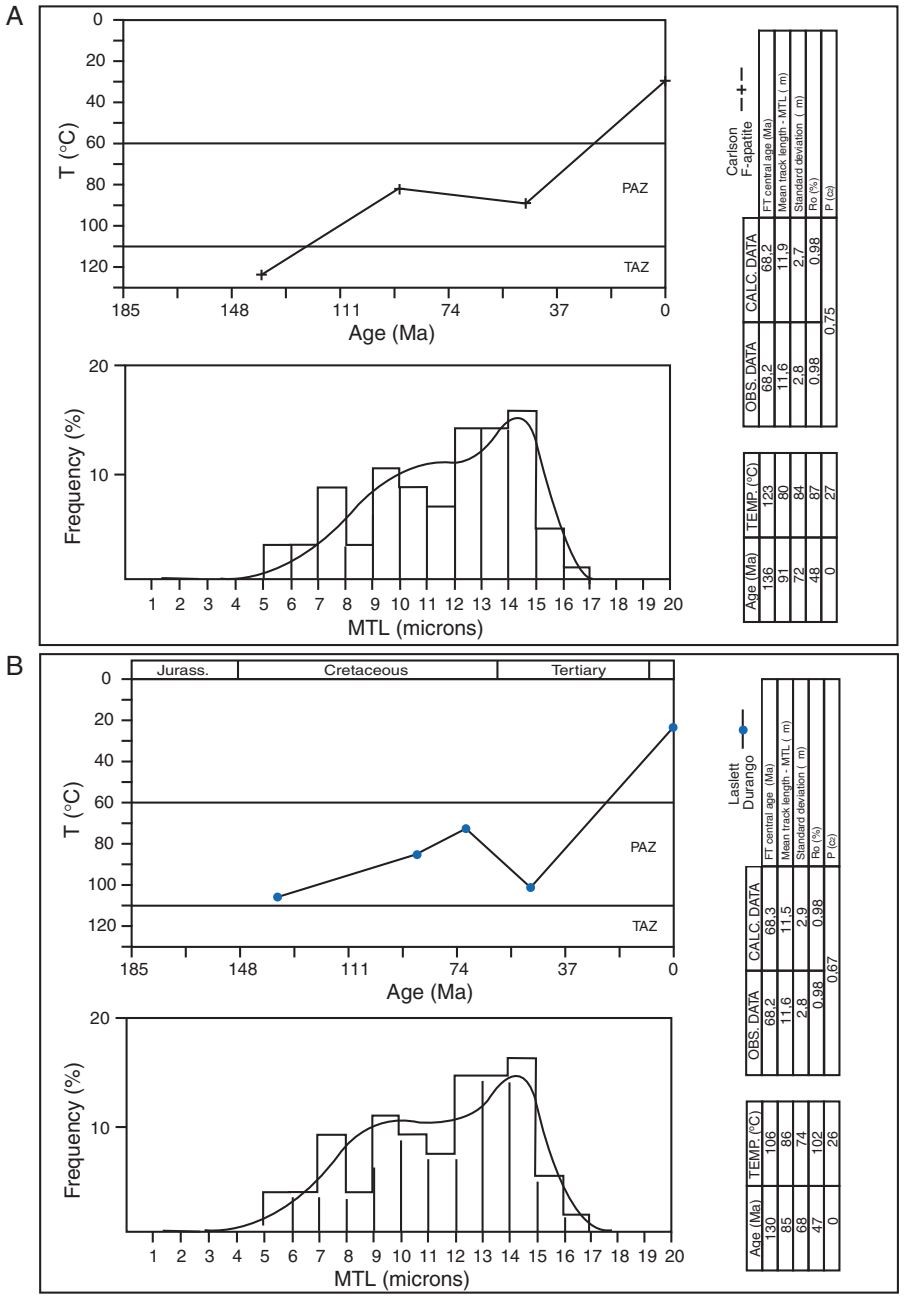

Figure 15.14
Simulations of thermal history for sample SUP9 using the Carlson (A) and Laslett (B) algorithms. Note that a heating event occurs in both models at 40–50 Ma.

the basin reached maximum subsidence with hydrocarbon generation taking place, in Berriasian time, about 144 to 137 Ma (Gradstein et al., 1994), during the early rift phase. This is in agreement with previous studies (Cupertino and Magnavita, 1987; Magnavita and Cupertino, 1988; Prosser, 1993), according to which subsidence is highest at the beginning of the extensional process. Using the FTA modeling the peak of subsidence is placed at 141 Ma.

The Lower Hauterivian (132 Ma) is marked by a strong erosion that affected many of the samples. At this point, the base level of the lake dropped with the consequent erosion of Valanginian sediments and rejuvenation of the source areas. The main evidence for this unconformity is based on the absence and re-worked strata of some ostracod biozones (Picarelli and Grillo, 1996). The FTA thermal reconstruction did not record any major alteration during Aptian time and we assume that the western border of the Camamu basin continued to act as the source area even after the end of the rift phase (Dias, 1998; Magnavita et al., 1994). The geothermal paleogradient of this epoch probably did not alter significantly and the local uplift should be the cause of cooling recorded in the sample B3 (Fig. 15.15). This interval probably represents a halt in sedimentation during a period of tectonic inversion. The amount of material eroded during this period depends on the paleotemperature. Assuming the present geothermal gradient (22 °C/km according to Zembruscki and Thomaz Filho, 1984), this event may have removed up to 600 m of sediment; with higher

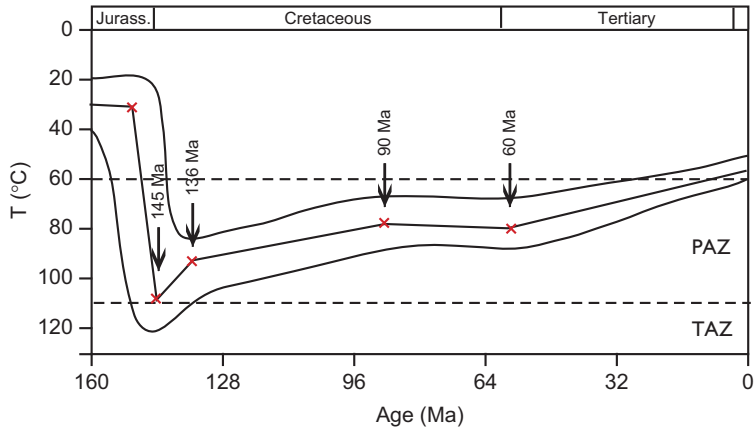

F-APATITE	CARLSON
AGE (Ma)	TEMP. (°C)
201±5	30±5
150±5	32±5
145±3	110±5
136±3	93±6
90±6	80±6
60±6	83±5
0	61±3

Figure 15.15
Simulations of thermal history for sample B3 using Carlson's kinetic modeling.

paleotemperatures (geothermal gradient 35 °C/km) the erosion would have been less than 400 m. Figure 15.16 illustrates the profile of subsidence at depth based on the fission track data (thermal history). Minor oscillations are due to method artifacts and, therefore, should not be considered. These samples reflect the main events: greatest subsidence at about 142 Ma, first period of uplift at about 128 Ma, and a second uplift at 56 Ma.

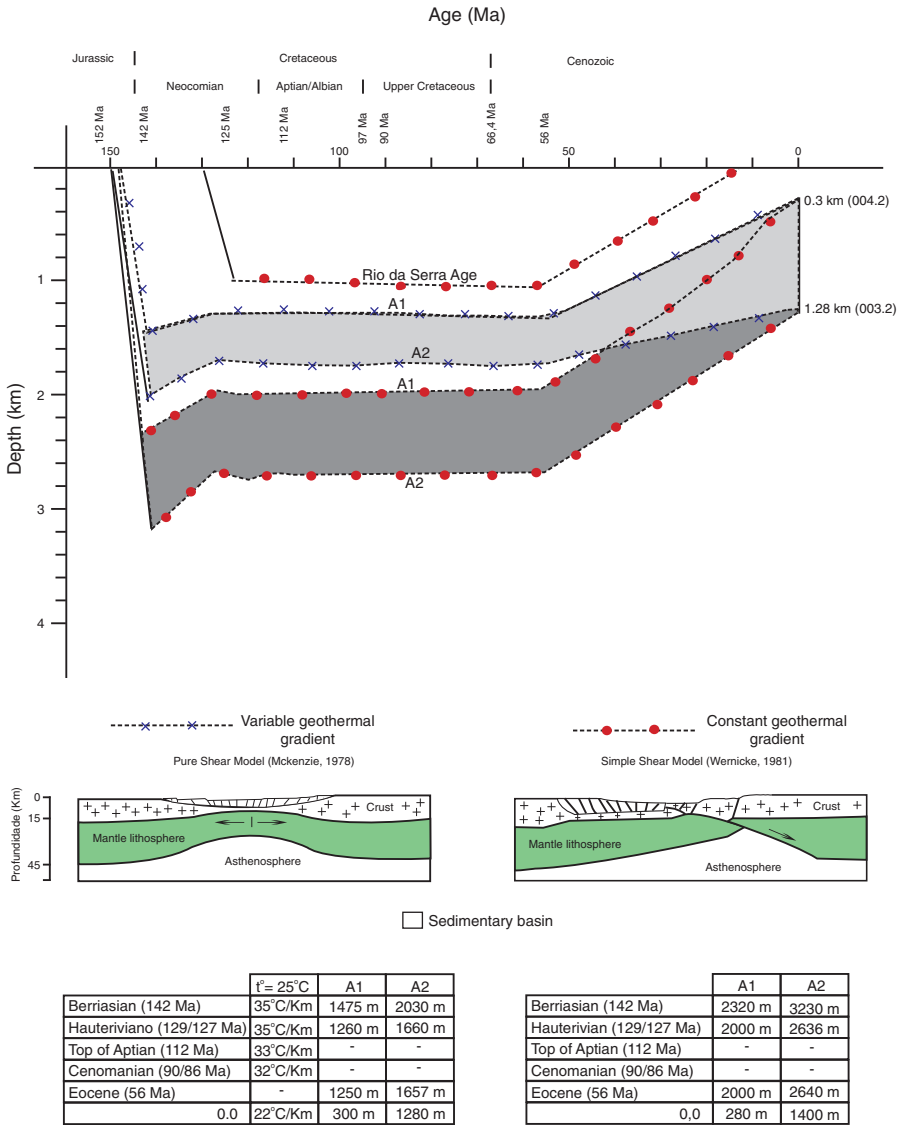

	t°= 25°C	A1	A2
Berriasian (142 Ma)	35°C/Km	1475 m	2030 m
Hauteriviano (129/127 Ma)	35°C/Km	1260 m	1660 m
Top of Aptian (112 Ma)	33°C/Km	-	-
Cenomanian (90/86 Ma)	32°C/Km	-	-
Eocene (56 Ma)	-	1250 m	1657 m
0.0	22°C/Km	300 m	1280 m

	A1	A2
Berriasian (142 Ma)	2320 m	3230 m
Hauterivian (129/127 Ma)	2000 m	2636 m
Top of Aptian (112 Ma)	-	-
Cenomanian (90/86 Ma)	-	-
Eocene (56 Ma)	2000 m	2640 m
0,0	280 m	1400 m

Figure 15.16 FTA subsidence and uplift events recognized in well A (samples A1 and A2) using two different paleogradients: (1) A constant pattern (simple shear); (2) highest gradient during the rift phase (pure shear).

From 67 Ma to present, the region was subjected to continuous cooling. This gradual decrease of temperature is interpreted as related to the accelerated erosion along the entire eastern coastline of Brazil. If the present geothermal gradient (23 °C/km) is valid for all that period, then about 1800 m of rocks were eroded (27 m/my erosion rate).

When the thermal history is too complex, it is difficult to find a good fit between observed and calculated data. The simulation of sample C1 (Fig. 15.17) suggests that the area was subjected to more than two thermal events. The large amount of short tracks indicates that this sample stayed for a long time at the limit of the total annealing zone.

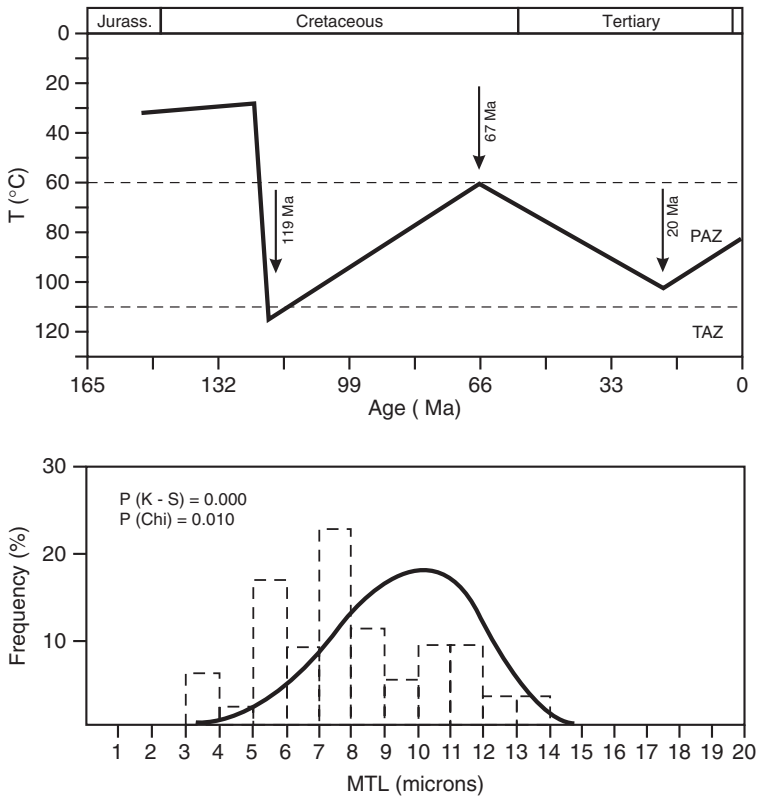

AGE (Ma)	TEMP. (°C)
123	28
119	114
67	61
20	101
0	81

OBS. DATA	CALC. DATA	
50,4	47,62	FT central age (Ma)
94,7	121	Oldest individual age (Ma)
8,11	9,57	Mean Track Length - MTL (mm)
2,58	2,07	Standard deviation (mm)
0,65	0,7	R_o (%)
0,01		P (c_2)

Figure 15.17 Simulations of thermal history for sample C1.

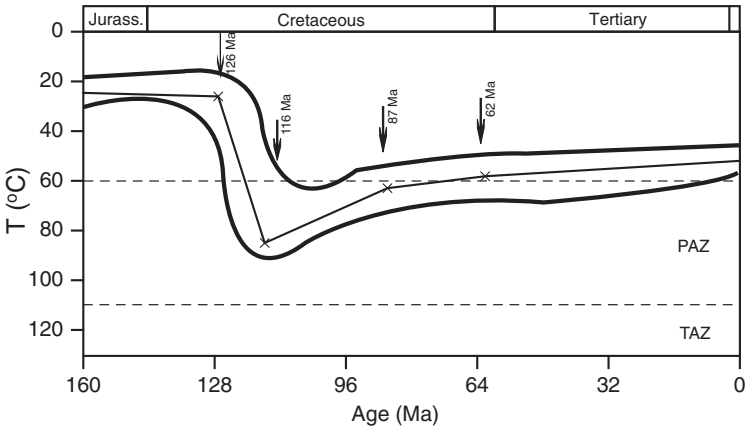

AGE (Ma)	TEMP. (°C)
195 + 8	23 + 2
126 + 4	25 + 2
116 + 4	82 + 5
87 + 4	64 + 6
62 + 11	57 + 4
0	50 + 2

Figure 15.18
Simulations of thermal history for sample D1.

The simulation of sample D1 (Fig. 15.18) shows a first thermal event related to the rift subsidence phase that takes place directly after deposition. Its stratigraphic age is 121 Ma, close to the age at the first point of inflexion (126 $\pm$ 4 Ma). This observation permits two conclusions: (1) Tectonic subsidence at the end of the rift phase is decreasing; (2) tectonic subsidence goes beyond the limit of the Barremian. Thus, based on FT lengths, the rift phase in these basins may have lasted until early Aptian times. Erosion started at about 116 Ma, first at a high rate (40 m/my for a gradient of 24 °C/km), and decreased to the Campanian/Santonian boundary. Modeling shows an inflexion point at 62 Ma (Paleocene). Cenozoic erosion was minor, and the erosional rate did not exceed 5 m/Ma.

To the south of Itaparica Island, the basement is relatively shallow. Modeling of sample F2 (Fig. 15.19) infers temperatures high enough ($\pm$115 °C) to reduce the FT age. The asymmetric curve that envelops the length tracks shows a slow and continuous cooling. The peak of tectonic subsidence was about 146 Ma, at the beginning of the Berriasian. Assuming a gradient of 35 °C/km, it can be estimated that the rocks were at a depth of about 2500 m. Unlike the other areas of the basin, these samples remain at that depth for a shorter period. This means that without erosion, temperatures would drop to about 98 °C.

The modeling for well H is shown on Fig. 15.20. After an initial subsidence, the sample cooled, reaching its lowest temperature at 126 Ma (49 °C). This event coincides with the time when the Recôncavo basin was exposed to the regional

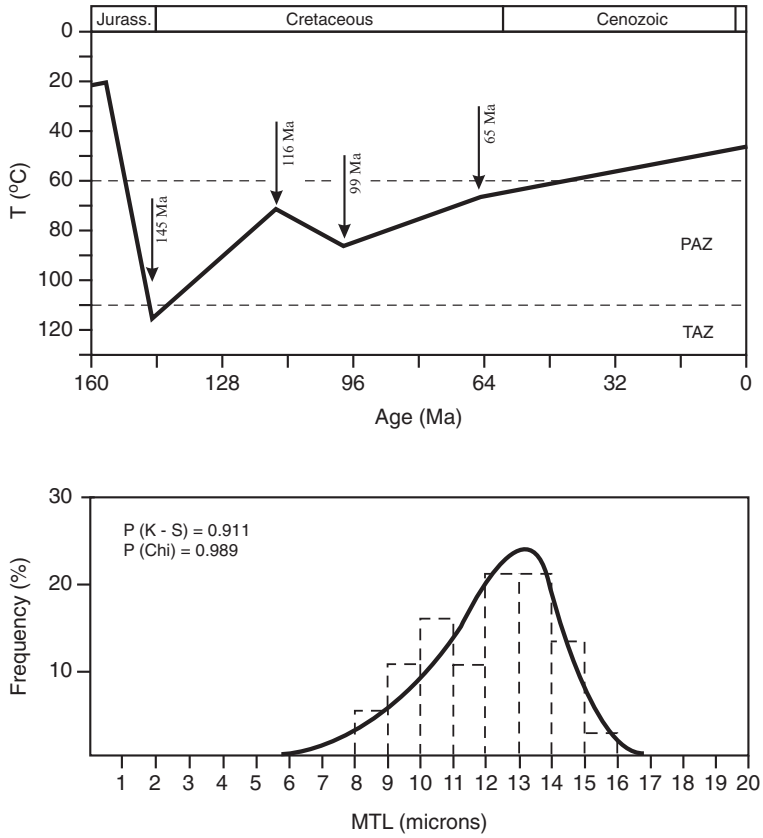

AGE (Ma)	TEMP. (°C)
215	25
157	21
145	115
116	70
99	85
65	66
0	45

OBS. DATA	CALC. DATA	
101,1	101,2	FT central age (Ma)
174,1	150	Oldest individual age (Ma)
12,09	12,24	Mean Track Length - MTL (mm)
1,85	1,89	Standard Deviation (mm)
0,99		P (c_2)

Figure 15.19 Best correlations obtained by simulations of thermal history for sample F2.

erosion that created the Hauterivian unconformity. Assuming that the temperature difference was 5 °C (g.g. = 30 °C/km), the erosion would amount to 160 m. A better correlation occurs between 140 and 130 Ma. From 126 Ma on, a second phase of heating starts, reaching maximum value (78 °C) at 110 Ma. To reach this temperature only through the burial of sediments, it is necessary for subsidence to be fast, so that it should be tectonically controlled. In the interval between 110 and 57 Ma, temperature remains constant, about 70 °C,

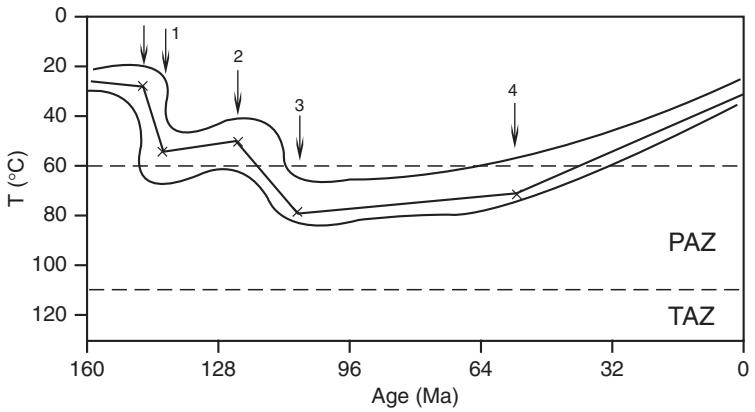

EVENT			1	2	3	4	5
Age (Ma)	–	146 ± 5	143 ± 2	126 ± 6	110 ± 2	57 ±4	0
Temperature (°C)	–	26 ±3	54 ±7	49 ±7	78 ±5	72 ±5	30 ±2

Figure 15.20 Simulations of thermal history for sample F3.

in the zone of partial track extinction. The small decrease of temperature (−6 °C) may result from the normalization of the heat flow.

During Paleocene/Eocene time, the basin was submitted to a process of positive epeirogenesis that resulted in at least 1000 m of sediment being eroded. The most recent regional event is due to the formation of the relief that acted as the source area for the Cenozoic sediments deposited in the deepwater region of the Camamu basin (Cupertino, 2000). Erosion in the emergent part, from Miocene to recent time, was slow and continuous, resulting in the erosion of more than 1500 m of rock, both from the crystalline basement and from the sediments. Differential movements caused by isostatic adjustment between different regions of the rift has caused Cenozoic erosion to be more pronounced in some compartments than the others, as can be seen in the modeling results.

15.9 Conclusions

With its huge dataset from exploration and extremely well-exposed sedimentary sequences, the early Cretaceous Recôncavo basin, Brazil's first oil producer, provides unique opportunities to study the structure, stratigraphy, and tectonic framework of a non-volcanic rift basin and its relationship to the Precambrian basement in surface outcrops. It forms the southern end of the inland Recôncavo–Tucano–Jatobá rift system, 620 km long, whose propagation to the north was arrested by the transverse Pernambuco ductile shear zone. This caused final

rifting and continental breakup to propagate along an alternative path from Salvador to the NE, along the northern Gabon and Sergipe-Alagoas basins, forming the present continental margin. Between the two rift zones lies the triangular Sergipe Microplate, bordered to the north by the Pernambuco shear zone. Rifting in the west and thrusting in the east along this shear zone reflects counterclockwise rotation of the microplate.

Both rift zones, and the microplate between them, are cut in two by the NW–SE-trending Vaza-Barris lineament that marks the NE border of the São Francisco craton. To the NE of this lineament, the North Tucano and Jatobá basins lie over late Proterozoic basement, with their main boundary faults being located on their landward, western or northwestern borders. Conversely, to the SW of this lineament, the Central Tucano, South Tucano, and Recôncavo basins lie over Archean to early Proterozoic cratonic basement and their main boundary faults are located on their oceanward eastern or southeastern borders. In the NE–SW-trending Recôncavo basin, the border fault and lesser border-parallel faults trend NE–SW. Cross-faults, of which the Mata-Catu fault system is the most important, trend NW–SE and have been interpreted as transform faults. Recent studies suggest that the coaxial Mata and Catu faults formed separately as release faults in the hanging-wall block of border faults.

The Recôncavo basin is filled by pre-rift and syn-rift sediments overlying Paleozoic relics and cratonic basement. The pre-rift sediments are eolian, fluvial, and lacustrine sands and shales; the sandstones of the Sergi Fm are the main oil reservoir. The overlying rift sediments, up to 6000 m thick, start with the organic-rich shales of the Candeias Fm deposited in a deep lake created by rapid early subsidence. They are the main source rocks of the basin, brought in contact along faults with the Sergi reservoirs. The overlying sedimentary sequence is increasingly sandy, reflecting decreasing subsidence and gradual fill-up of the basin, passing ultimately into the fluvial sandstones of the São Sebastião Fm. There are several shale diapirs rising from the Candeias Fm. These shale diapirs, together with the entire rift sequence, are cut by an angular unconformity overlain by the conglomerates and sandstones of the Marizal Fm, correlated with similar lithologies beneath ammonite-bearing latest Aptian strata in the Sergipe-Alagoas basin. The ages of the underlying rift and pre-rift sequences are based on freshwater ostracods and microflora, defining local stages whose precise correlation with the international stratigraphy is not fully defined. These correlations place the pre-rift sequence into the late Jurassic and the rift sequence into the early Cretaceous.

Along the entire Recôncavo–Tucano–Jatobá rift system, the Recôncavo basin is the only one with established hydrocarbon production. It is the oldest petroleum-producing basin in Brazil in a mature stage of exploration, with the discovery of 85 oil and gas fields. The main source rocks are lacustrine freshwater shales

of the Tauá and Gomo Members of the Candeias Formation; the main reservoirs are sandstones of the pre-rift Sergi Formation.

Application of the Fission Track Analysis (FTA) technique by Cupertino (2000) provides important information on the subsidence, uplift, and erosion history of the Recôncavo rift. The most important conclusions based on that technique are the following.

The surface samples show that the western margin became tectonically stable early (132 Ma) compared to the opposite margin (91 Ma), a pattern typical of half-graben geometry. The rate of erosion of 4.3–3.0 m/my obtained in FTA modeling for the samples of the flexural margin in the NW is much lower than the 24 m/my obtained over the Salvador horst along the border fault in the SE, indicating that along the faulted border relief was always more prominent. Fission track modeling, both in the southern portion of the Recôncavo basin and farther south in the northern portion of the Camamu basin, indicate that the greatest subsidence took place between 144 and 137 Ma (Berriasian). Monte Tracks simulations suggest that about 132 Ma (Hauterivian) the region may have been affected by an erosional process (cooling), affirming the importance of the pre-Hauterivian unconformity. FTA simulations of thermal histories suggest different evolution of tectonically isolated blocks, probably with local isostatic compensations. The FTA data indicate that, after a regional heating (66 Ma), uplift and erosion occurred along the present continental margin (starting about 60–50 Ma ago) resulting in the loss of about 2700 m of the sedimentary section at a mean rate of 58 m/my.

Acknowledgments

The authors gratefully acknowledge the revision and constructive comments made by E.J. Milani, the help received at Petrobras to do this work, and the permission to publish.

References

Aragão, M.A.N.F., 1994. Arquitetura, estilos tectônicos e evolução da Bacia do Recôncavo, Brasil. Boletim do III Simpósio sobre o Cretáceo do Brasil, 3, Boletim, Rio Claro, pp. 165–167.

Aragão, M.A.N.F., Trindade, L.A.F., Araújo, C.V., Silva, O.B., Scartezini, A.A., Oswald, F.H., Canário, J.A., & Garcia, A.P., 1998. Distribution and controls of lacustrine source rocks in the Recôncavo Basin. Brazil. AAPG International Conference & Exhibition, Extended Abstracts, Rio de Janeiro p. 306.

Bigarella, J.J., 1975. The Barreiras Group in Northeast Brazil. Anais da Academia Brasileira de Ciências 47, 365–393.

Caixeta, J.M., Bueno, G.V., Magnavita, L.P., Feijó, F.J., 1994. Bacias do Recôncavo. Tucano e Jatobá. Bol. Geoci. PETROBRAS 8 (1), pp. 163–172.

Carter, A., Bristow, C., Hurford, A.J., 1995. The application of fission track analysis to dating of barren sequences: examples from red beds in Scotland and Thailand. In: Dunay, R.E., Hailwood, E.A. (Eds.), Non-bioestratigraphical Methods of Dating and Correlation, Geological Society of London Special Publication, vol. 89.

Chang, H.K., A.M.F. Figueiredo, R.O. Kowsmann, and A.A. Bender, 1992. Tectonics and stratigraphy of the EastBrazil Rift: an overview: Tectonophysics, v. 213, p. 97–138.

Cohen, C.R., 1985. Accumulation and structural evolution of Recôncavo basin, northeastern Brazil. Am. Assoc. Pet. Geol. Bull. 69, 65–76.

Cupertino, J.A., 2000. Evolução tectono-climática na fase rifte das Bacias de Camamu, parte norte, e sul do Recôncavo, com ênfase na utilização de isótopos estáveis e traços de fissão. Tese de Doutorado, vol. 2. Universidade Federal do Rio Grande do Sul, Porto Alegre, Brasil (illus).

Cupertino, J.A., Magnavita, L.P., 1987. Configuração estrutural das bacias do Tucano e Jatobá. I Seminário de Tectônica da Petrobrás (TECTOS) Cenpes/PETROBRAS.

Daniel, L.M.F., Mato, L.F., 1989. Geoquímica e modelos de migração de hidrocarbonetos no Campo de Rio do BU - integração com o Compartimento Nordeste da Bacia do Recôncavo, Bahia. Bol. Geoci. PETROBRAS 3 (3), pp. 201, 214.

Da Silva, H.T.F., Caixeta, J.M., Magnavita, L.P., Sanches, C.P., 2000. Syn-rift lacustrine deep-water deposits: Examples from the Berriasian sandy strata of the Recôncavo Basin, northeastern Brazil. AAPG Studies in Geology, vol. 46, pp. 209–224.

Destro, N., 1995. Release fault: a variety of cross fault in linked extensional fault systems in the Sergipe-Alagoas basin, northeast Brazil. J. Struct. Geol. 17, 615–629.

Destro, N., Alkmim, F.F., Magnavita, L., Szatmari, P., 2003a. The Jeremoabo transpressional transfer fault, Recôncavo–Tucano Rift, NE Brazil. J. Struct. Geol. 25 (8), 1263–1279.

Destro, N., Szatmari, P., Alkmim, F.F., Magnavita, L.P., 2003b. Release faults, associated structures, and their control on petroleum trends in the Recôncavo Rift, northeast Brazil. Bull. Am. Ass. Petrol. Geol. 87 (7), 1123–1144.

Dias, J.L., 1998. Análise Sedimentológica e Estratigrafia do Andar Aptiano em parte da margem Leste do Brasil e no Platô das Malvinas – Considerações Sobre as Primeiras Incursões e Ingressões Marinhas do Oceano Atlântico Sul Meridional. Tese de Doutorado, vol. 2. Universidade Federal do Rio Grande do Sul, Porto Alegre, Brasil (illus.).

Erba, E., Bartolini, A., Larson, R.L., 2004. Valanginian Weissert oceanic anoxic event. Geology 32 (2), 149–152.

Gallagher, K., 1995. Evolving temperature histories from apatite fission-track data. Earth Planet. Sci. Lett. 136, 421–435.

Gallagher, K., Hawkeworth, C.J., Mantovani, M.S.M., 1995. Denudation, fission track analysis and long-term evolution of passive margin topography: application to the southeast Brazilian margin. J. South Am. Earth Sci. 8 (1), 66–77.

Gallagher, K., Brown, R., Johnson, C., 1998. Fission Track Analysis and its applications to geological problems. Ann. Rev. Earth Planet. Sci. 26, 519–572.

Gibbs, A.D., 1984. Structural evolution of extensional basin margins. J. Geol. Soc. Lond. 141, 609–620.

Gibbs, A.D., 1990. Linked fault families in basin formation. J. Struct. Geol. 12, 795–803.

Giles, M.R., Indrelid, S.L., 1998. Divining burial and thermal histories from indicator data: application & limitations. In: Van den Haute, P., de Corte, F. (Eds.), Advances in Fission-Track Geochronology. Selection of papers presented at the International Workshop on Fission-Track Dating, Ghent, Belgium, 1996. Kluwer Academic Publishers, Dordrecht, pp. 115–149, 311.

Gradstein, F.M., Agtenberg, F.P., Ogg, J.G., Hadenbol, J., Van Veen, P., Thierry, J., Huang, Z., 1994. A Mesozoic time scale. J. Geophys. Res. 99 (B12), 24.05–24.074.

Green, P.F., Duddy, I.R., Gleadow, A.J.W., Lovering, J.F., 1989. Apatite fission track analysis as palaeotemperature indicator for hydrocarbon exploration. In: Naeser, N.D, McCullogh, T.H. (Eds.), Thermal History of Sedimentary Basins. Springer-Verlag, pp. 181–195, 319.

Harman, R., Gallagher, K., Brown, R., Raza, A., Bizzi, L., 1998. Accelerated denudation and tectonic/geomorphic reactivation of the cratons of northeastern Brazil during the Late Cretaceous. J. Geophys. Res. 103 (B11), 27091–27105.

Ingersoll, R.V., Busby, C.J., 1995. Tectonics of sedimentary basins. In: Busby, C.J., Ingersoll, R.V. (Eds.), Tectonics of Sedimentary Basins. Blackwell Science, USA, pp. 1–51.

Lysak, S.V., 1992. Heat flow variations in continental rifts. Tectonophysics 208, 309–323.

Magnavita, L.P., 2000. Deformation mechanisms in porous sandstones: implications for development of fault seal and migration paths in the Recôncavo Basin, Brazil, *in* M.R. Mello and B.J. Katz, eds., Petroleum systems of South Atlantic margins: AAPG Memoir 73, p. 195–212.

Magnavita, L.P., 1992. Geometry and kinematics of the Recôncavo–Tucano–Jatobá rift, Northeast Brazil. Ph.D. dissertation, University of Oxford, Oxford, U.K., p. 493.

Magnavita, L.P., Cupertino, J.A., 1988. A new approach to the geological configuration of the Lower Cretaceous Tucano and Jatobá basins, northeastern Brazil. Rev. Bras. Geoci. 18 (2), 222–230.

Magnavita, L.P., Davison, I., Kusznir, N.J., 1994. Rifting, erosion, and uplift history of the Recôncavo-Tucano-Jatobá Rift, northeast Brazil. Tectonics 13 (2), pp. 367–388.

Medeiros, R.A., Ponte, F.C., 1981. Roteiro geológico da Bacia do recôncavo (Bahia). PETROBRAS/SEBA, Relatório Interno, 63 p.

Mello, M.R., Mohriak, W.U., Koutsoukos, E.A.M., Bacoccoli, G., 1994. Selected petroleum systems in Brazil, *in*, L.B. Magoon & W.G. Dow, eds., The Petroleum System - from Source to Trap. AAPG Memoir 60, pp. 499-512.

Middleton, M.F., 1982. Tectonic history from vitrinite reflectance. Geophys. J. Res. Aust. Soc. 68, 121–132.

Milani, E.J., Davison, I., 1988. Basement control, and transfer tectonics in the Recôncavo–Tucano–Jatobá rift, Northeast Brazil. Tectonophysics 18, 41–70.

Milani, E.J., Lana, M.C., Szatmari, P., 1988. Mesozoic rift basins around the Northeast Brazilian Microplate (Recôncavo–Tucano–Jatobá, Sergipe–Alagoas). In: Manspeizer, W. (Ed.), Triassic–Jurassic rifting, Developments in Geotectonics, vol. 22, pp. 833–858, Ch. 34.

Naeser, C.W., 1979. Thermal history of sedimentary basins: fission trck dating of subsurface rocks. In: Scholle, P.A., Schluger, P.R. (Eds.), Aspects of Diagenesis, Society of Economic Paleontologists and Mineralogists, Special Publication, vol. 26, pp. 109–112.

Picarelli, A.T., Grillo, J.L., 1996. Paleogeografia das bacias de Camamu e Almada e integração bioestratigráfica com a Bacia do Recôncavo. Cenpes/Divex/Sebipe, E & P Bahia Relatório Interno.

Prosser, S., 1993. Rift-related linked depositional systems and their seismic expression. In: Willians, G.D., Dobb, A. (Eds.), Tectonics and Seismic Sequence Stratigraphy. Geological Society of London Special Publication, vol. 71, pp. 35–66.

Rohrman, M., Andriessen, P., Van Des Beek, P., 1996. The relationship between basin and margin thermal evolution assessed by fission track thermochronology: an application to offshore southern Norway. Basin Res. 8, 45–63.

Santos, C.F., Cupertino, J.A., Estrella Braga, J.A., 1990. Síntese sobre a geologia das Bacias do Recôncavo, Tucano e Jatobá. In: Raja Gabaglia, G.P., Milani, E.J., et al. (Eds.), Origeme evolução da Bacias Sedimentares. PETROBRÁS, CENSUD, Rio de Janeiro, pp. 235–266.

Stewart, S.A., 2001. Displacement distributions on extensional faults: implications for fault stretch, linkage and seal. Bull. Am. Assoc. Pet. Geol. 85, 587–599.

Szatmari, P., Milani, E.J., 1999. Microplate rotation in northeast Brazil during South Atlantic rifting: analogies with Sinai microplate. Geology 27, 1115–1118.

Szatmari, P., Milani, E.J., Lana, M.C., Conceição, J.C., Lobo, A., 1985. How South Atlantic rifting affects Brazilian oil reserves distribution. Oil Gas J. January 14, 107–113.

Ussami, N., et al., 1986. Crustal detachment during South Atlantic rifting and formation of Tucano-Gabon basin system. Nature 322, pp. 629–632.

Van der Beek, P., Mbede, E., Andriessen, P., Delvaux, D., 1998. Denudation history of the Malawi and Rukwa Rift flanks (East African Rift System) from apatite fission track thermochronology. J. Afr. Earth Sci. 26, 363–385.

Zembruscki, S.G., Thomaz Filho, A., 1984. Correlação geotérmica dos campos de hidrocarbonetos do Recôncavo. PETROBRÁS – CENPES. Rio de Janeiro, Relatório Interno inédito, 38.

Zhao, M.W., Behr, H.J., Ahrendt, H., Wemmer, K., Ren, Z.L., Zhao, Z.Y., 1996. Thermal and tectonic history of the Ordos Basin, China: evidence from Apatite Fission Track Analysis, Vitrinite Reflectance and K-Ar dating. AAPG Bull. 80 (7), 1110–1134.

In this chapter

16

The Dniepr-Donets Basin

Randell Stephenson, Sergiy Stovba†*
*School of Geosciences, University of Aberdeen, Aberdeen, Scotland
†SPK-Geoservice, Kyiv, Ukraine

16.1 Introduction

The Dniepr-Donets Basin (DDB) is located in the south eastern part of the East European Craton along a NW-SE trending axis between the present-day Ukrainian Shield and Voronezh Massif (Fig. 16.1). It is part of the same rift basin system as the shallower Pripyat Trough to the north west (mainly in Belarus) and the inverted Donbas Basin (Donbas Foldbelt – DF) and its south eastward extension to the south east (straddling the Ukraine-Russia border). The DDB is the most important hydrocarbon province of Ukraine, accounting for 85% of the Ukraine's oil and gas production. The most recent published estimate, made at the beginning of 2004, of ultimate recoverable reserves in established accumulations (produced and remaining reserves) is 266×10^6 tons of oil, 132.7×10^6 tons of gas-condensate, and 2352×10^9 m^3 gas (Prygarina et al., 2005). The average annual production during the past years comes to some 2.0×10^6 tons of oil, 1×10^6 tons of gas-condensate and 16×10^9 m^3 of gas (Prygarina et al., 2005), but this meets only a fraction of the total hydrocarbon requirements of the Ukraine.

The DDB is one of the deepest basins of Europe (up to 19 km of sediment fill; Stovba et al., 1996). The Upper Devonian syn-rift sequence, which was deposited in a shallow-marine environment and contains significant quantities of salt, is overlain by a thick post-rift sequence of Carboniferous age and younger. Structural reactivation, including inversion and salt tectonics, has played an important role in forming the present-day basin architecture. Major post-rift structural reactivations took place at the beginning of the late Visean and in the middle of the Serpukhovian, in the Early Permian and between the Mesozoic and Cenozoic (Stovba and Stephenson, 1999; Stovba et al., 1996). Salt movements occurred during the whole history of basin formation starting with the Late Devonian rift stage (Stovba and Stephenson, 2003). A series of cross-sections – based on interpreted, depth-converted regional seismic profiles acquired in the 1980s and 1990s, through the basin – located in Fig. 16.1, is shown

Phanerozoic Rift Systems and Sedimentary Basins DOI: 10.1016/B978-0-444-56356-9.00015-8

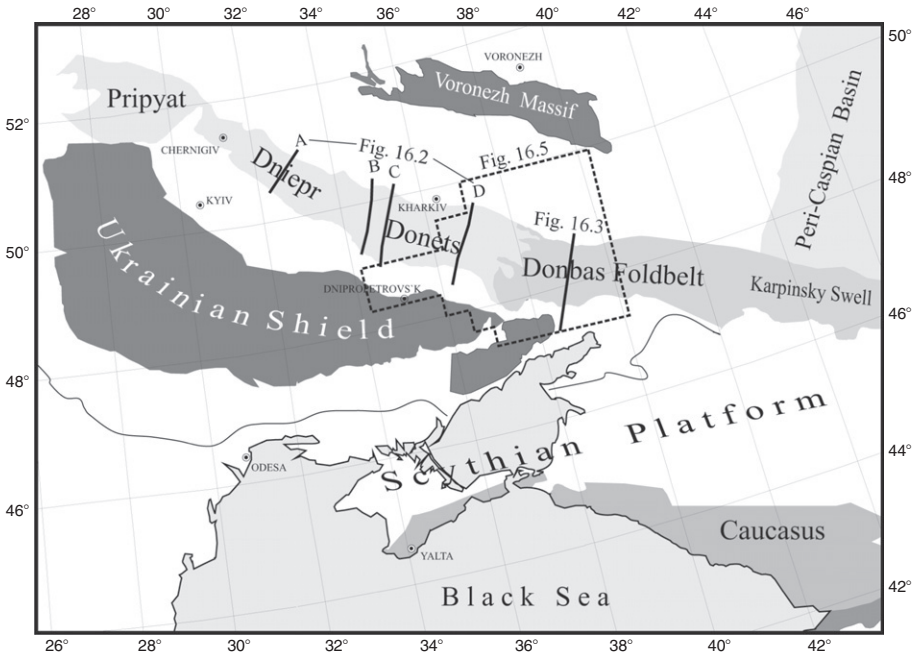

Figure 16.1
Regional setting of the DDB; the shaded region corresponds to the extent of the Late Devonian rift; post-rift sediments overlie the flanks of the rift up to the Ukrainian Shield and Voronezh Massif. Lines show the locations of cross-sections in Figs. 16.2 and 16.3 and the dashed box indicates the location of Fig. 16.5.

in Fig. 16.2. A cross-section of the inverted DF segment, including the entire crust, is shown in Fig. 16.3. This is based on deep seismic reflection profiling ("DOBREflection") carried out in 2000 and 2001 (Maystrenko et al., 2003; Stovba et al., 2005).

A number of tectonic subsidence models of the DDB have been published, including 2-D forward models, along profiles in the Dniepr (Kusznir et al., 1996; Starostenko et al., 1999) and Donets (Stovba et al., 2003) segments, and 1- and 2-D inverse models throughout the DDB (van Wees et al., 1996) and in the Dniepr segment (Poplavskii et al., 2001). Although these studies employed a variety of modelling approaches, with significant differences in how they were parameterised, a common result of all of them was that conventional concepts of rift basin subsidence (involving syn-rift crustal thinning and post-rift thermal re-equilibration) sufficed to explain the regional basin architecture of the DDB. Some key inferences of these models included the probable role of additional mantle heating ("active" rifting, implying possible mantle plume involvement; Stovba et al., 2003; van Wees et al., 1996), regional uplift prior to and during rifting (also consistent with mantle plume effects; Kusznir et al., 1996), the importance of post-rift tectonic reactivations (van Wees et al., 1996), and the high degree of crustal thinning, almost to continental break-up, in the south easternmost segment of the basin (Donets segment adjacent to DF; Stovba et al., 2003; van Wees et al., 1996; cf. DOBREfraction '99 Working Group et al., 2003).

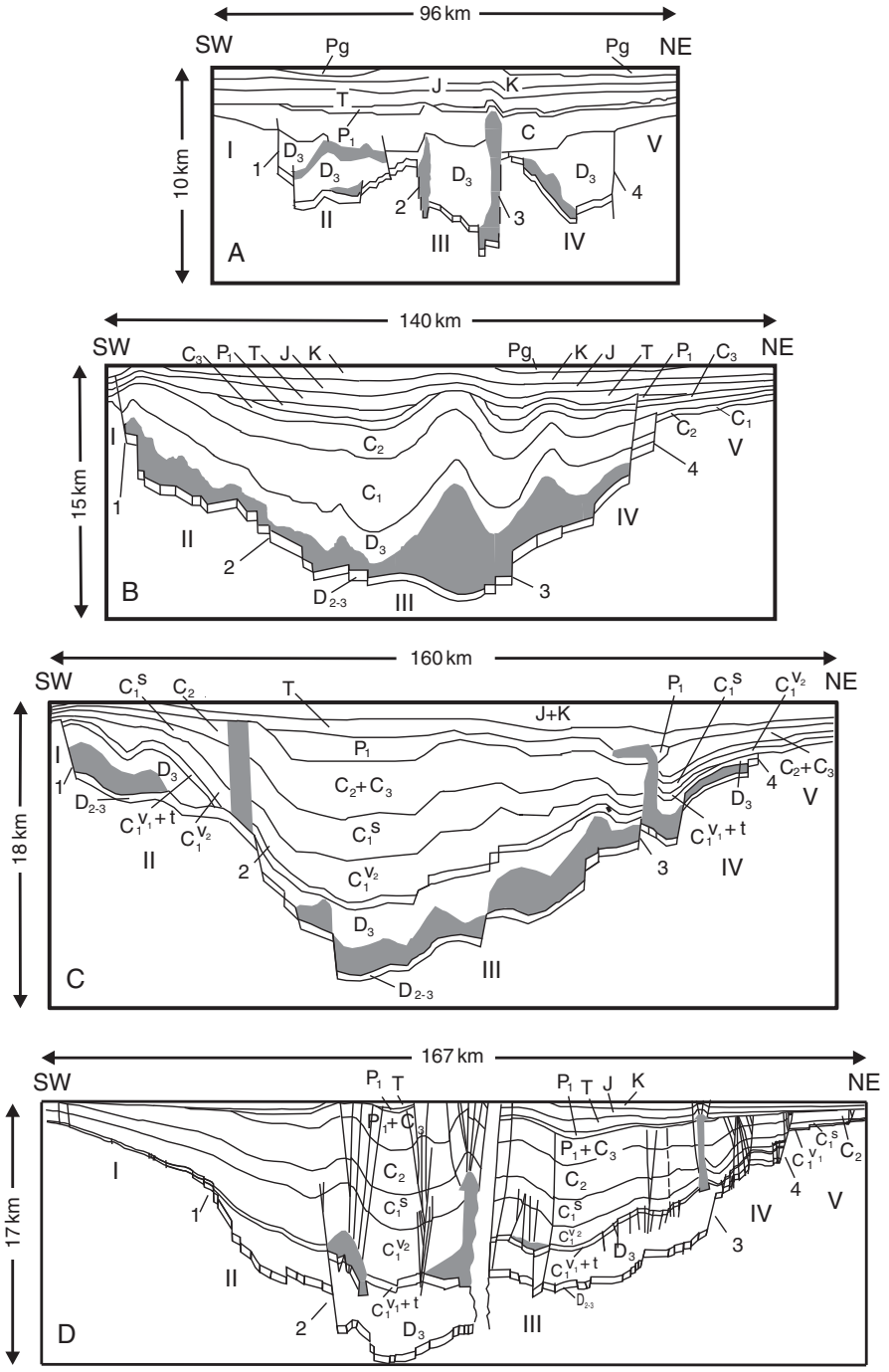

Figure 16.2 (See legend on next page)

Figure 16.2 Structural cross-sections through the DDB, based on depth-converted versions of interpreted regional seismic reflection profiles (from Stovba and Stephenson, 1999; Stovba et al., 1996). For locations, see Fig. 16.1. Shaded areas represent salt bodies. The rift has a generally symmetric structure and is subdivided into an axial, deepest part (III) and adjacent southern and northern "preflank" zones (II and IV), separated from the axial zone either by large displacement faults or a system of obliquely dipping blocks separated by faults with moderate throw (labelled 2 and 3). The pre-flank zones are separated from the southern and northern rift shoulders (I and V) by regionally extensive, large amplitude boundary faults (labelled 1 and 4). Abbreviations: $D_{2\text{-}3}$, Middle Devonian-Upper Devonian; D_3, Upper Devonian; C, Carboniferous; C_1, Lower Carboniferous, t-Tournaisian, v_1-lower Visean, v_2-upper Visean, s-Serpukhovian; C_2, Middle Carboniferous (Ukrainian/Russian usage – for example, Bashkirian and Moscovian); C_3, Upper Carboniferous (Ukrainian/Russian usage – for example, Kasimovian and Gzelian); P_1, Lower Permian; T, Triassic; J, Jurassic; K, Cretaceous; K_2, Upper Cretaceous; Pg, Palaeogene.

16.2 Tectono-stratigraphic successions of the DDB

The sedimentary succession of the DDB can be readily subdivided into pre-, syn- and post-rift series, corresponding to pre-late Frasnian ($D_{2\text{-}3}$), late Frasnian-Famennian (D_3) and post-Devonian units, respectively (Fig. 16.4). Rifting may have begun slightly earlier in the south east, propagating north eastwards (cf. Stephenson et al., 2001). The post-rift succession is well developed, displaying evidence of multiple extensional reactivations as well as compressional tectonic events. A lack of stratigraphy of suitable age in the DF (due to the uplift, deformation and erosion affecting it) and, therefore, an absence of diagnostic structural relationships led to uncertainty regarding the timing and nature of post-rift tectonic events controlling its development (cf. Fig. 16.5). However, by comparing the exposed and drilled geology of the DF with seismic images from the adjacent Donets segment of the DDB (e.g., Fig. 16.2D), Stovba and Stephenson (1999) demonstrated that the main pre-inversion events affecting the DF do not significantly differ from the DDB. This has been confirmed by subsequent structural studies (Saintot et al., 2003a,b) and by DOBREflection (cf. Stovba et al., 2005).

Pre-rift succession

The oldest sediments in the DDB are Eifelian to Middle Frasnian, so-called "undersalt", pre-rift sediments. These were deposited in platformal terrestrial and shallow marine environments and comprise sandstones, siltstones, clays and carbonates. These pre-rift Devonian sediments correlate with equivalent Devonian sequences of the East European Platform (Eisenverg, 1988). They are characterised by homogeneous lithofacies, an average thickness of 300–400 m and a series of stratigraphic gaps, the most significant being between the Eifelian and Givetian and between Givetian and Frasnian. Thickness variations of the pre-rift succession are independent of the modern basement relief. The sequence is observed only locally on the rift shoulders. The pre-rift sediments were probably deposited over a much wider area but were truncated during syn-rift uplift of

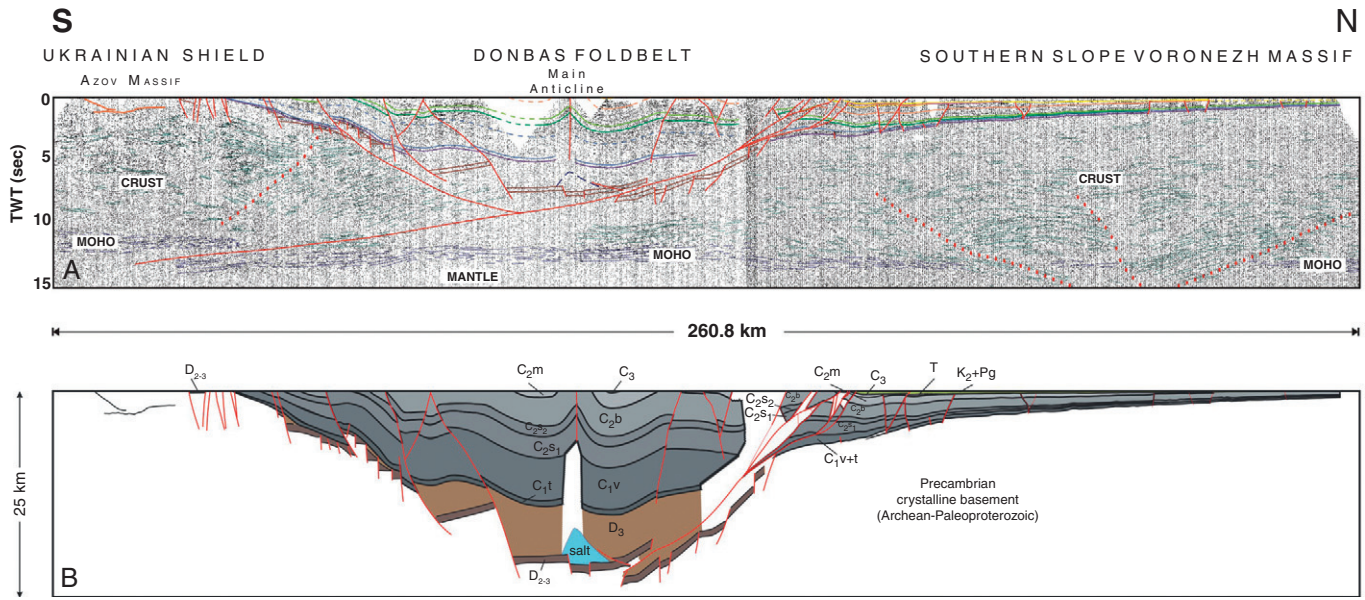

Figure 16.3 (A) The full DOBREflection profile, compiled from the DOBREflection-2000 data set (left part; Maystrenko et al., 2003) and the DOBREflection-2001 data set (right part; Stovba et al., 2005) with interpretation and (B) segment of depth-converted DOBRE profile showing the subsurface architecture (stratigraphic key as in Fig. 16.2) of the Donbas Foldbelt part of the DDB in greater detail. For location, see Figs. 16.1 and 16.5.

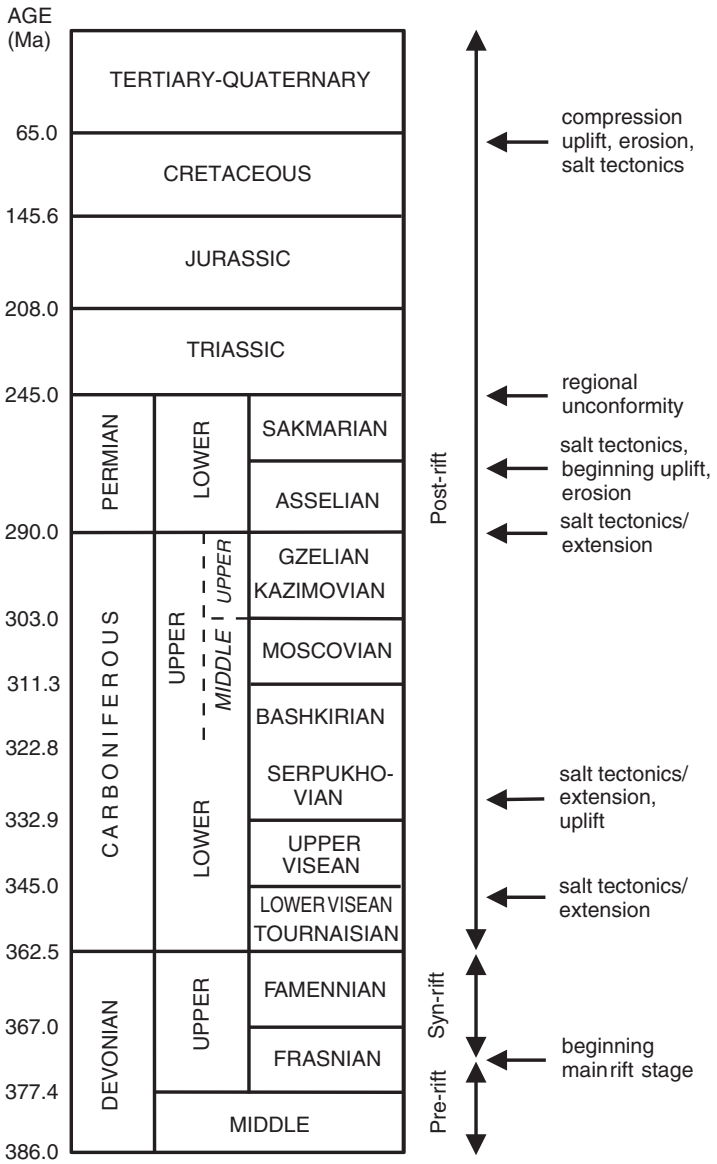

Figure 16.4 Summary chrono-stratigraphic column for the Dniepr-Donets Basin showing the main tectonic phases discussed in the text *(from Stephenson et al., 2001)*. The subdivision of Upper Carboniferous into separate Middle and Upper units corresponds to common usage in Russian and Ukrainian literature.

the rift flanks. Similarly, they are locally absent atop intrabasinal structural highs developed during rifting.

There is no evidence for the presence of a coaxial but narrower Riphean-aged graben underlying the DDB as reported in much of the older literature (e.g., Chekunov et al., 1992). This was based on DSS velocity models but is

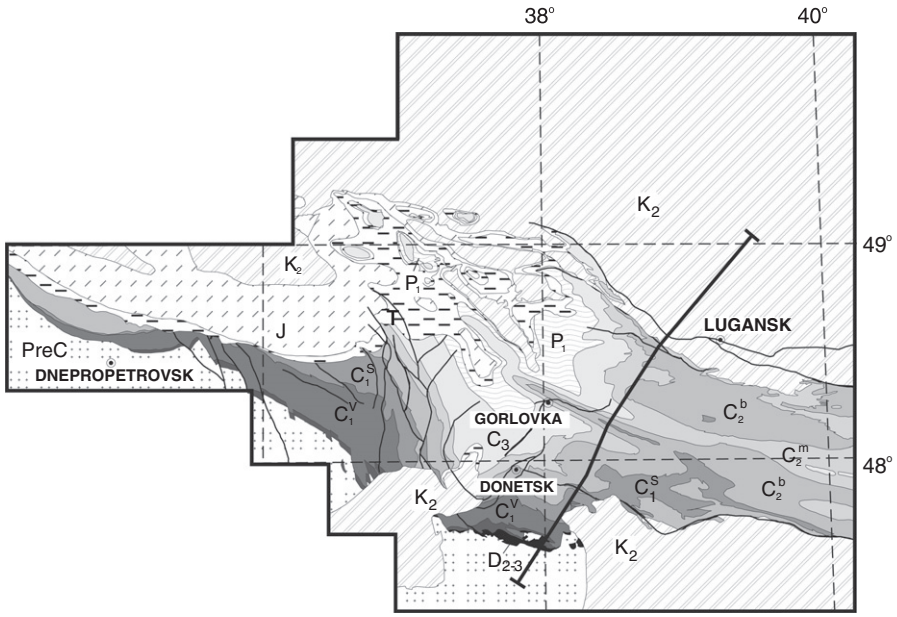

Figure 16.5 Cenozoic subcrop map of the DF and surrounding areas. For location see Fig. 16.1. Also shown is the location of the DOBRE deep seismic reflection profile (Fig. 16.3).

not observed on seismic reflection profiles recorded up to 12 s TWT (Stovba et al., 1996). No strata older than Middle Devonian have been encountered in any of the numerous boreholes that penetrate basement beneath the Palaeozoic sediments of the DDB or adjacent Pripyat Trough (Chirvinskaya and Sollogub, 1980; Eisenverg, 1988). Rather, the Devonian-Carboniferous succession revealed by the reflection data is much thicker than inferred from the earlier velocity models and occupies the deeper parts of the section hitherto thought to be Riphean strata (cf. Stovba et al., 1996). Therefore, tectonic models suggesting that a precursor Riphean rift basin was reactivated during the Devonian cannot be supported.

Syn-rift structures and sedimentary succession

Although modified by post-rift tectonic and especially salt movements (Stovba and Stephenson, 2003), the basic architecture of the DDB seen in Fig. 16.2 was developed during its Late Devonian rifting stage. High and laterally variable syn-rift subsidence rates, accompanied by the development of grabens and half-grabens, resulted in a wide range of local depositional environments and considerable palaeogeographic heterogeneity both in space and time, intense volcanism and multidirectional tectonic movements (Stovba et al., 1996).

The main marginal faults, as well as numerous smaller faults of variable polarity, were activated during the initial rifting stages of the DDB and these cut the

basement and overlying pre-rift Devonian sediments into 2–5 km wide small blocks. Fault throws were in the range 50–300 m with fault orientations ranging from sub-parallel to highly oblique to the strike of the rift axis. Smaller faults are in general beyond the resolution of the seismic data. Subsequently, most syn-rift fault displacement appears to be confined to the main border faults (labelled 1 and 4 in Fig. 16.2) and two or more sub-parallel faults (labelled 2 and 3), subdividing the basin into an axial zone and so-called northern and southern "pre-flank" zones.

The rift margins are characterised regionally either by pervasive faults, exhibiting displacements from hundreds of metres to 2–4 km, or by sets of less developed faults, displaying various displacements. Major faults dip at 70–80° and, based on DSS studies (Chekunov, 1994), may affect a significant part of the crust, as also seen in deep seismic reflection profiles crossing the related Pripyat Trough basin to the north west (e.g., Juhlin et al., 1996).

Syn-rift deposits in the DDB reach a maximum thickness of about 4 km (e.g., Stovba et al., 1996; Ulmishek et al., 1994). They overlie the pre-rift sequence discordantly and are absent on some interior fault blocks, due to reduced sedimentation and subsequent erosion. Much of the lower part of the syn-rift sequence consists of Frasnian salt, called the "lower salt", that alternates with clastics and carbonates in a complex laterally variable pattern. The depositional thickness of the Frasnian series is at least 1000 m and reaches a maximum (up to 2 km) in the axial zone of the south eastern part of the DDB. The upper part of the syn-rift series consists of a thinner Famennian "upper salt" that thickens in the north western part of the DDB.

Syn-rift volcanic and intrusive rocks, consisting of a variety of alkali basalts and their differentiates and associated pyroclastics, occur in two main series of late Frasnian and late Famennian age and attain thicknesses of more than 2000 m (e.g., Wilson and Lyashkevich, 1996).

Post-rift succession and tectonic reactivations

There is no evidence of syn-depositional faulting affecting Tournaisian and earliest Visean units, which were apparently deposited under tectonically quiescent conditions (e.g., Stovba et al., 1996). Therefore, the syn-rift phase *sensu stricto* is considered to have terminated by the end of the Devonian and, in general, the Carboniferous and younger post-rift sedimentary basin of the DDB has the configuration of a broad syncline centred on the rift axis, overlapping the rift shoulders and increasing in thickness depth towards the south east (Fig. 16.2). Seismic profiles published by Stovba et al. (1996) clearly demonstrate, however, that the DDB was affected during its Permo-Carboniferous evolution by a series of post-rift extensional reactivations, generally synchronous with salt movements, but tectonic in origin: namely, at the end of the early Visean, during the middle Serpukhovian and during latest Carboniferous-earliest Early Permian

times. These events increased in intensity towards the south east, being minor to not observed in the north western DDB (Stovba and Stephenson, 2003).

The Carboniferous succession is represented by continental deposits in the north western part of the DDB (e.g., Dvorjanin et al., 1996; Izart et al., 1996; Ulmishek et al., 1994). Elsewhere in the DDB it is characterised by continuous rhythmic sedimentation and comprises mainly siliciclastic rocks (with some clastic-carbonate sequences) deposited in shallow marine and lagoonal environments. There is little variation in the position of the basin depocentre. Only in the axial part of the south eastern DDB, where the Lower Carboniferous includes marine carbonates, did the depth of deposition exceed 200 m. Exposed and drilled Lower Carboniferous sediments in the DF are mainly marine limestones overlain by sandy-clay deposits interbedded by thin coal and limestone beds. Middle and Upper Carboniferous successions are exposed throughout most of the DF and consist mainly of arenaceous-argillaceous rocks interbedded with coal and limestone. With the exception of coal beds and sandy-clay continental intercalations most were deposited in a shallow-marine environment. Carboniferous sediments in the DDB reach thicknesses of 11 km, with a maximum depth of their base at about 15 km (Stovba et al., 1996). The present-day maximum thickness of Carboniferous sediments in the DF area is about 15 km based on the DOBREflection profile (Fig. 16.3).

The effects of the post-rift tectonic reactivation events can be seen in the DDB in the regional cross-sections (Fig. 16.2). In particular, the early Visean extensional reactivation is demonstrated in Fig. 16.2D where normal faulting was accompanied by the intrusion of Devonian salt into lower Visean strata. There is no evidence of uplift, either of the basin or its flanks. Stovba and Stephenson (1999) documented faulting on the northern part of this profile, younger than Late Carboniferous and older than Triassic, interpreted to be Early Permian in age, reactivating the boundary fault of the rift. The same fault was active at the end of early Visean and in the middle of Serpukhovian. The stratigraphic thicknesses show that during the remainder of the Carboniferous and during the Mesozoic, no further conspicuous faulting took place. The intensity of each of the Permo-Carboniferous extensional events increases in the DDB south eastwards towards the DF, but it is difficult to document in the DF. Saintot et al. (2003b) inferred a transtensional paleostress field in the DF that could be of this age. Additional evidence of Early Permian extensional deformation along the northern margin of the DF, documented widely but generally not in published literature, is presented and discussed by Stovba and Stephenson (1999). Elsewhere in the DF, Upper Cretaceous sediments directly overlie block-faulted and rotated Devonian and Carboniferous strata (cf. Fig. 16.3). The lack of a Permian-Early Cretaceous sedimentary record prevents a definite interpretation of the age of these faults. However, there is no evidence for Mesozoic extensional deformation in the DDB, with the exception of minor, Late Cretaceous normal faults associated with salt movements (see below). Therefore, it is likely that

faulting and block rotation seen along the south western margin of the DF are part of the widespread phase of Early Permian extension (transtension) seen throughout the DDB (Stovba and Stephenson, 1999).

The lowermost Lower Permian sediments are represented by monotonous sand-shale series containing rare interbeds of limestone and coal that, similar to the Upper Carboniferous, reflect coastal-continental facies. Asselian sediments consist of five to seven layers of rock salt, separated by clastics and carbonates and also include numerous beds of gypsum, anhydrite and dolomite. The thickness of salt layers and percent volume increases upward in the section (Eisenverg, 1988). The Sakmarian part of the series consists of a single salt layer likely representing redeposited Devonian salt dissolved from diapirs piercing the depositional surface in the Early Permian (Stovba and Stephenson, 2003). In the southern pre-shoulder zone of the DDB, the Lower Permian sequence abruptly decreases in thickness and pinches out as a result of a decrease in depositional thickness as well as subsequent erosion. In contrast, its thickness decrease towards the northern shoulder of the basin is far more gradual. There are no Early Permian sediments preserved within the DF, although Upper Carboniferous and Lower Permian sediments are documented beneath the eastern extension of the northern margin of the DF.

A general absence of Upper Carboniferous and Lower Permian sediments in the north westernmost part of the DDB can be explained by a decrease in the rate of post-rift subsidence within a platform-wide regime of relative sea-level fall. Elsewhere within the DDB, the basin margins, particularly the southern one, were exposed during Early Permian times while the axial part of the basin continued to subside (cf. Fig. 16.2). Uplift of the southern margin of the DDB was very short-lived, lasting no more than 2–3 Myr between the late Asselian and early Sakmarian (Stovba et al., 1996). Extensive erosion occurred with progressively older sediments subcropping beneath the erosion surface in the direction of the Ukrainian Shield; by implication, considerable erosion of the Ukrainian Shield may also have occurred. Locally more than 2 km of Upper and Lower Carboniferous were eroded at this time and during an ensuing dormant phase, which lasted until the Triassic. The widespread regional Permian unconformity observed throughout the DDB is therefore interpreted to be the result of the Early Permian event followed by a relative sea-level low stand during the later Permian.

Sedimentation resumed in the DDB in the Triassic, a time of tectonic quiescence, rising sea levels, and the resumption or continuation of post-rift subsidence. Most of the Mesozoic succession, comprising both marine and continental sediment sections, occurs throughout the area, overlying the rift axis as well as its flanks. Exceptions are the Upper Triassic and Lower Jurassic units, which occur only in the south eastern part of the DDB, and the Upper Cretaceous marls and chalks, which were eroded from large parts of the southern flank. The Upper Cretaceous succession was, as a whole, characterised by Chirvinskaya and

Sollogub (1980) as "close to" platform type, although subsidence coincident with the Devonian rift axis exceeds that of the marginal zones (cf. Fig. 16.3). It is up to 2000 m thick in the central part of the DDB with maximum thicknesses of the Triassic, Jurassic and Cretaceous units being 900, 700 and 1000 m, respectively.

An angular unconformity between the Triassic and Jurassic has been documented (Eisenverg, 1988). Triassic and Jurassic sequences thin smoothly in the direction of the DF, perhaps due to reduced subsidence, but also because of the later erosional truncation (Stovba and Stephenson, 1999). In the DF, Mesozoic sediments are preserved only along the basin margins. Along the northern margin, 150–200 m thick Triassic sediments occur locally in the vicinity of exposed Palaeozoic rocks, while the Jurassic is absent. East of Lugansk (Fig. 16.3), the Mesozoic section contains only Upper Cretaceous units. Similarly, on the southern margin of the DF, only Upper Cretaceous sediments are preserved. They reach a thickness greater than 500 m and rest on eroded Palaeozoic strata or the basement (Fig. 16.5). The present-day limits of the Mesozoic sequences in the DF are clearly erosional, indicating that the original depositional area may have been considerably larger (e.g., Ulmishek et al., 1994). Further, no marginal facies or developments are observed near the erosional edges of the Mesozoic successions. It is therefore likely that the entire area of the DF underwent post-rift subsidence during the Mesozoic and that, depending on relative sea-level variations, Mesozoic successions were deposited within its confines but were later eroded.

There is little evidence of post-rift magmatic activity in the DDB; however, this is not the case for the DF, where igneous rocks of Early Carboniferous, Early Permian, and Mesozoic ages have been reported. New results and discussion of earlier ones are presented by Alexandre et al. (2004).

A widespread angular unconformity in the DDB developed at the end of Cretaceous-beginning of Palaeogene (Kabyshev et al., 1998). The magnitude of inferred relative uplift increases towards the Ukrainian Shield and, as during the Early Permian, its maximum occurred in the area bordering the DF. In this area, Upper Cretaceous, Jurassic and Triassic sediments were eroded (cf. Fig. 16.5). In the axial part of the south eastern DDB, there are local folds, domes and salt diapirs defining linear trends, which correspond to the trends of the main folds of the DF as seen on the Cenozoic subcrop map (Fig. 16.5). Within the DF itself, structural relationships determining the age of formation of folds, thrust and reverse faults can be observed only near its margins, where Lower Permian, Mesozoic and Cenozoic sediments are preserved. Stovba and Stephenson (1999) reported that no single geological section could be found in the published literature showing tightly constrained, structurally defined pre-Triassic folding or reverse faulting in the DF. In contrast, where Cretaceous sediments are present, for example, along the northern margin of the DF, reverse faults and/or folds younger than the Cretaceous sediments and exposed at the

surface are relatively common. Reverse faulting of Late Cretaceous age is also evident on the southern margin of the DF (Stovba and Stephenson, 1999). Saintot et al. (2003a,b) determined that the palaeostress field associated with compressional structures found in the Cretaceous sediments on the margins of the DF is identical to that recorded by the outcropping Carboniferous sediments. Thus, it can be concluded that the inversion of the DDB and formation of the DF occurred mainly in the Late Cretaceous (cf. Stephenson et al., 2001; Stovba and Stephenson, 1999). The DOBREflection profile (Fig. 16.3) shows that the shortening of the DF occurred at the crustal scale as a "mega-pop-up", which involved a major detachment fault through the entire crust and an associated back-thrust (Maystrenko et al., 2003).

The Cenozoic section of the DDB unconformably overlies Upper Cretaceous and older series and reaches a maximum thickness of 500 m to the north west DDB (Eisenverg, 1988). The Palaeogene consists mainly of sands, clays and marls and the Neogene mainly of sands with clayey interbeds.

16.3 Salt tectonics in the DDB

The distribution and style of salt kinematics in the DDB and, importantly, its temporal relationship with tectonic events has been described in detail by Stovba and Stephenson (2003). Salt structures in the DDB formed episodically, with flow beginning during the deposition of syn-rift sediments directly overlying the Frasnian salt. At least half of all present-day known salt structures began forming during the rift stage (Stovba and Stephenson, 2003). Primary salt structures also controlled the subsequent development of many salt pillows and diapirs. The distribution of salt structures in the DDB is shown in Fig. 16.6.

Initiation of the post-rift phases of salt movements in the DDB is intimately related to regional tectonic reactivations in the basin documented by seismic and other data. In particular, the onset of distinct episodes of salt movement coincides with the onset of distinct periods of extensional tectonic reactivation recorded in the late Visean, middle Serpukhovian and Early Permian, and with compressional tectonic inversion at the end of the Cretaceous. Some salt structures display phases of growth beginning with all of the tectonic reactivation events whereas others display phases of growth beginning with only one or some of them. The intensity of tectonic reactivation in the DDB increases to the south east towards the DF (Stovba and Stephenson, 1999), and the number of salt structures displaying growth during all periods of tectonic reactivation also increases in this direction. It should be noted, however, that the post-rift succession thickness gradient follows the same trend.

Concordant (pillows and anticlines) and discordant (diapirs) salt structures formed during every phase of salt movement in the DDB. Though the onset of these phases during post-rift basin evolution coincided with the onset of tectonic

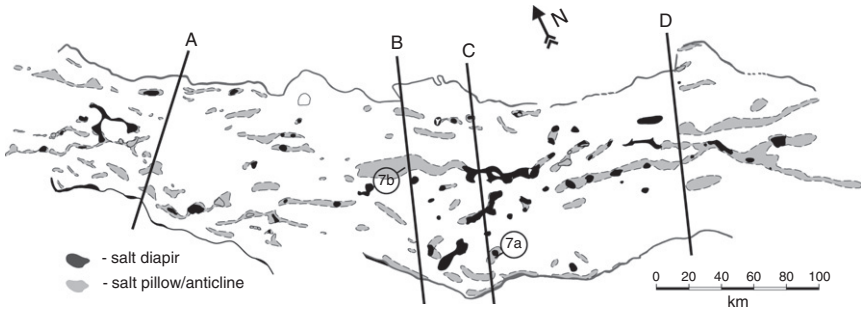

Figure 16.6
A sketch map showing the distribution of the main concordant (grey) and discordant (black) salt structures in the DDB, based on seismic and well data *(modified from Stovba and Stephenson, 2003)*. Salt has been penetrated in boreholes for many of the salt structures. In the axial zone, concordant salt bodies are inferred to correlate with anticlinal structures seen in seismic data and are along strike of known salt diapirs. Solid lines with numbers indicate the locations of seismic and geological sections displayed in Fig. 16.7. The approximate locations of the depth-converted regional seismic sections seen in Fig. 16.2 are also shown.

reactivations, the duration of periods of active halokinesis, especially when salt became extrusive, generally exceeded the duration of the corresponding regional tectonic event. Periods of halokinesis were followed by periods of quiescence during which diapirism was frozen and up to several kilometres of sediments could be deposited above it before the next regional tectonic event triggered renewed salt movement (Stovba et al., 1996).

Figure 16.6 demonstrates the relationship between salt daipir growth and regional tectonics. The salt structure shown in Fig. 16.7A formed episodically in the late Visean, middle Serpukhovian and Early Permian. The growth of this structure was accompanied by the development of a rim-syncline. A significant proportion of the upper Visean sediments (up to one-third in the north and up to one-half to the south of the structure) was accumulated within this primary rim-syncline. The subsidence that provided the accommodation space for these Visean sediments was produced by the outflow of Frasnian salt from the salt series itself into the core of the salt anticline. The thinning of the Tournaisian-lower Visean succession towards the top of the structure is related to erosion in the earliest late Visean, occurring simultaneously with the formation of the rim-syncline. The late Visean growth phase was followed by a period of quiescence prior to renewed uplift after the deposition of the lower Serpukhovian succession. A period of quiescence also preceded the renewal of salt flow after the deposition of Late Carboniferous sediments, inferred to have occurred in the earliest Early Permian (Stovba and Stephenson, 1999). The timing of this tectonic event is more clearly demonstrated in Fig. 16.7B. This concordant salt structure is typical of those forming mainly at the end of Carboniferous-Early Permian. This is evinced by the erosive truncation of Carboniferous sediments on the crest of the structure and by the onlap of Early Permian deposits on the flanks of the structure. Quiescence is indicated until the latest Carboniferous but the structure was active in the Early Permian, the onset of growth coinciding with the onset of latest Carboniferous regional extension although the duration of salt flow was longer than the duration of the short-lived tectonic event. After a period of quiescence in the Mesozoic, the growth of this structure was renewed in latest Cretaceous-earliest Tertiary times when the regional compressional tectonic event affected the DDB (leading to its inversion).

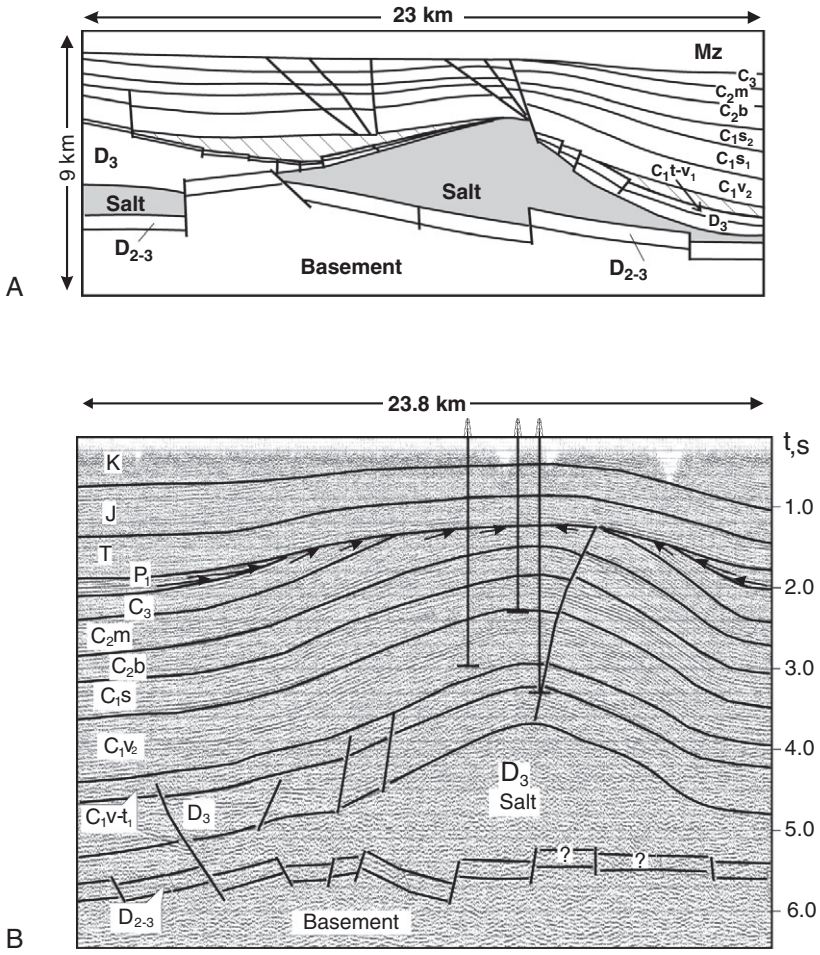

Figure 16.7 (A) Depth converted seismic section (located in Fig. 16.6) showing a salt anticline that formed during three stages of tectonic reactivation in the DDB. The formation of this salt structure was accompanied by the development of primary rim-synclines in the late Visean, Serpukhovian, and at the end of Carboniferous (Early Permian). The crosshatched part of the upper Visean was deposited during outflow of Devonian salt from beneath the primary rim-syncline towards the core of the salt structure. (B) Seismic section (located in Fig. 16.2) showing a salt structure formed mainly at end Carboniferous-Early Permian times with renewed growth in latest Cretaceous-Early Tertiary time; C_2, Middle Carboniferous (Ukrainian/Russian usage – b-Bashkirian and m-Moscovian); Mz, Mesozoic, with other stratigraphic symbols as in Fig. 16.2.

16.4 Hydrocarbon occurrence in the DDB

Hydrocarbon exploration began in 1936 and has resulted in the discovery of about 200 oil and gas accumulations. Most of these are contained in Carboniferous to Permian series that were deposited during the post-rift stage of the basin evolution (Fig. 16.8). The Devonian syn-rift series contains only a small part of the total reserves of the DDB, in contrast to the Pripyat Trough where the Devonian syn-rift series is the main hydrocarbon producer (Ulmishek et al., 1994). Additional oil and gas accumulations are reservoired in the Precambrian basement and in the Triassic and Jurassic. Areas that were strongly affected by compressional tectonic reactivation contain only minor hydrocarbon reserves. The

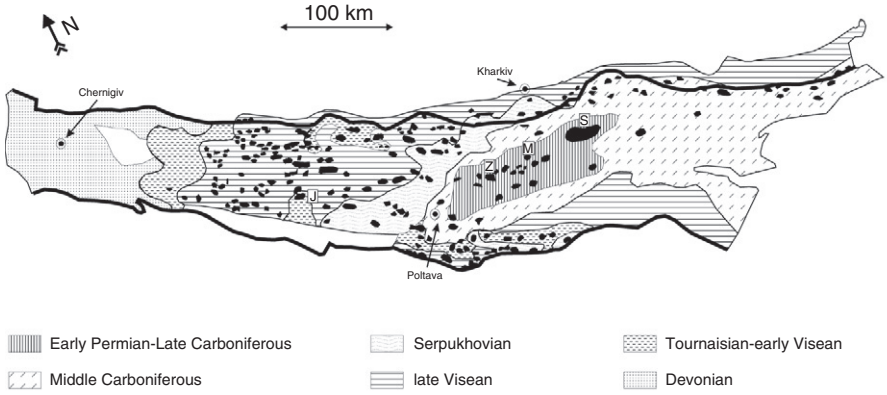

Figure 16.8 The distribution of hydrocarbon accumulations in the DDB (oil, gas-condensate, and gas fields shown in black), in relation to the age of the dominant productive formations. Fields referred to in the text are indicated as such: S, Shebelynka; M, Melykhivka; Z, Zakhidno-Krestyshche; J, Jablunivka *(after (Kabyshev et al., 1998)*.

most significant fields are Shebelynka, Zakhidno-Krestyshche, Melychivka and Jablunivka, the locations of which are shown in Fig. 16.8.

The main oil and gas generating source rocks of the DDB are marine Tournaisian-early Visean, late Visean and Serpukhovian shales, which have an average TOC content of 1.5–2.3% and a maximum of up to 5–6% (Kabyshev et al., 1998). The Early Carboniferous sequence in the north western part of the basin lies partly in the gas window, the rest being in the oil window, while all of this sequence is in the gas generation window in the southeastern part of the basin. Middle Carboniferous strata, comprising coals and shales, are ubiquitous, have a TOC content in the 0.6–0.9% range, and have entered the gas window in the basin centre and the oil window along the basin flanks. The Late Carboniferous and Early Permian sediments of the axial part of the DDB contain coal and shales with TOC of 0.2–1.1% that have reached conditions for oil and gas generation only in the deepest, southeastern part of the DDB. Mesozoic source rocks are absent and are immature for the generation of hydrocarbons (Kabyshev et al., 1989, 1998).

"Primary" hydrocarbon accumulations of the DDB, meaning those associated with short lateral and vertical migration distances and having closely associated source rocks, occur in a variety of structural (fault blocks, anticlines), stratigraphic (Devonian reefs, sand pinch-outs) and combination (unconformity) traps that developed during and shortly after the deposition of the relevant strata. They include small Devonian-hosted reservoirs and stacked reservoir/seal pairs (2–6 levels) occurring in the cyclical Early Carboniferous series (Kabyshev et al., 1998). "Secondary" accumulations, those associated with a greater degree of vertical migration from deeper levels, are trapped in structures related to the diapiric ascent of Devonian salt that occurred in conjunction with post-rift tectonic movements (cf. Stovba and Stephenson, 2003). Salt diapirs associated with hydrocarbon reservoirs in the prolific Late Carboniferous-Early Permian

series are broken by faults that have facilitated migration from below. Most of these traps developed during Mesozoic times and are characterised by a high fill ratio (Kabyshev et al., 1998). Mesozoic-hosted reservoirs contain oil and gas that has migrated from older formations through gaps in the regional Permian salt seal. Sealing conditions, in general, are most favourable in the middle parts of the DDB but deteriorate towards the shallower, north western parts of the basin, where shales are sandier, and towards its deeper southeastern parts, where shales are more brittle due to their greater degree of diagenesis.

16.5 Regional tectonic setting of the DDB

Shatsky (1946) considered the DDB to be a type example of an aulacogen. Clearly being a "failed rift" in the sense that it did not itself lead to continental break up and ocean crust formation, there remains disagreement on whether the DDB rift represents the failed third arm of a triple-rift system, the other arms of which ultimately formed a passive continental margin (e.g., Saintot et al., 2003a,b). Indeed, subsequent to Shatsky's work and until quite recently, some authors (e.g., Chekunov et al., 1992; Volozh et al., 1999) have regarded the DDB to be part of a very long, singular intracontinental rift system, including the Karpinsky Swell (on the northern margin of the northern Caucasus domain; Fig. 16.1), that crosses the Caspian Sea and continues into western Asia. Such a model appears at least in part to be untenable within a plate tectonic framework.

Related to the question of whether the DDB is a failed arm of a triple rift junction or not is the age of its initial rifting stage. Shatsky (1946) and later writers considered it to have been initiated as one of a set of Neoproterozoic (Riphean) rifts cross-cutting the East European craton (EEC), some of which (including the DDB and the closely related Peri-Caspian Basin) were thought to have been very long-lived and only strongly reactivated in Late Palaeozoic times. Scattered Neoproterozoic strata are exposed within the Ukrainian shield (e.g., Chekunov et al., 1992) and Neoproterozoic sediments of continental affinity reportedly underlie Devonian sediments in the north westernmost part of the DDB rift system and in its farthest south eastern extent, near the northeast end of the Azov Sea but nowhere else (e.g., Stephenson et al., 2001). However, Stovba et al. (1996) clearly showed from regional near-vertical reflection seismic profiling that what was thought to be Neoproterozoic is, in fact, part of the Late Palaeozoic (middle Devonian and younger) platformal and rift-related sedimentary sequence. Thus, the peri-cratonic rifting that formed the DDB is convincingly not older than Late Palaeozoic, followed by several extensional reactivations in Permo-Carboniferous times as described earlier.

In a pioneering plate tectonic synthesis of former Soviet Union geology, Zonenshain et al. (1990) represented the DDB as the failed arm of a Late Devonian rift system that led to the development of subsequently closed, small ocean

basins along the southern margin of the EEC (see also Kostyuchenko et al., 2004; Saintot et al., 2003b; Saintot et al., 2006). In their palaeogeographic and palaeotectonic reconstructions, Nikishin et al. (1996) appear to hold to this view though it is not explicitly expressed as such. A critical issue in this respect would seem to be the tectonic origins and age of the oldest sediments in the Peri-Caspian Basin. Some authors (e.g., Volozh et al., 2003) argue strongly and without equivocation that these are undoubtedly at least as old as Early Palaeozoic based primarily on the presence of sediments of this age on the northern, peri-cratonic platformal margin of the basin. However, others suggest that definitive evidence of the age of these very deeply buried and inaccessible sediments simply does not exist and that a tectonic scenario in which the basin is due to Late Devonian rifting (contemporaneously with the DDB, therefore) fully and more satisfactorily fits available observations than other ones (e.g., Brunet et al., 1999). At best, this remains an open question.

Devonian rifting was accompanied by major magmatic activity (Wilson and Lyashkevich, 1996) and probably by the uplift of the Ukrainian Shield and the Voronezh Massif, which together form a large radius dome that is transected by the DDB (e.g., Stephenson et al., 1993) (Fig. 16.1). Rifting crosscuts the structural grain of the underlying craton as determined by Shchipansky and Bogdanova (1996), with major boundaries within the basement thought to provide conduits for magma expulsion during rifting. The geochemical signature of rift-related magma (Wilson and Lyashkevich, 1996) plus the sheer volume of magma suggests that the origin of the DDB is mantle-plume related (e.g., Chekunov, 1994), as has also been inferred from various more recent subsidence-modelling studies mentioned earlier (e.g., Kusznir et al., 1996; Poplavskii et al., 2001; Starostenko et al., 1999; van Wees et al., 1996). However, there is no clear indication that the intensity of magmatism increases to the southeast in the direction of the supposed triple junction, although the depth of the basin increases significantly in this direction. Potential field anomalies indicate that mafic rocks have also intruded the crust beneath the sedimentary basin. Magnetic anomalies in the Dniepr segment, indicative of both supracrustal and crustal depth sources, correlate well with igneous bodies known to lie within the sedimentary sequence (Orlyuk and Pashkevich, 1994; Stephenson et al., 2001). Gravity modelling has long suggested the presence of a high-density lower crustal body along the rift axis interpreted as an "axial dyke" related to rifting (Starostenko et al., 1986). Yegorova et al. (1999, 2004) show that this feature extends the entire length of the DDB to its culmination at the Karpinsky swell, taking a 120° bend to the northeast parallel to the recognisable margin of the EEC at this culmination, providing some evidence that this could have been the triple-rift junction locus.

Deep seismic sounding (DSS; e.g., Chekunov et al., 1992; Ilchenko, 1996; Stephenson et al., 2006) and more recent wide-angle reflection-refraction (WARR) seismic studies (DOBREfraction '99 Working Group et al., 2003) show that the amount of crustal thinning beneath the DDB increases to the south

east, concurrently with increasing sedimentary thickness (cf. Stephenson et al., 2001). The most recent profile is DOBRE (DOBREfraction '99 Working Group et al., 2003), crossing the inverted DF segment of the DDB. The sedimentary basin itself is well-defined, overlying a main crustal layer that thins significantly beneath the main sedimentary depocentre. In turn, a high velocity lower crustal layer thickens significantly in the same part of the profile. The shape of the sedimentary basin is asymmetric, with the steepest crystalline basement surface on the south western margin of the basin whereas the asymmetry of the high velocity layer displays its steepest upper surface beneath the north eastern margin of the basin. The high velocity layer has been interpreted as a zone of crustal underplating or "rift-pillow" (DOBREfraction '99 Working Group et al., 2003). The asymmetry may be evidence of some degree of so-called "simple-shear" rather than "pure-shear" during rifting. The Moho depth is more or less constant across the DF (40 $\pm$ 2 km). The lower crustal high velocity layer has presumably incorporated (and been thickened by) mantle-derived magmas during the rifting process. A minimum of 10% but as much as 50% of the high velocity layer comprises mantle material, implying somewhat more than 50% thinning of the pre-rift crystalline crust beneath this part of the rift basin and a maximum crustal "stretching factor" of as much as 2.25–2.5 (DOBREfraction '99 Working Group et al., 2003), a figure that compares favourably with what has been inferred from subsidence modelling in the vicinity of the DOBREfraction profile (Stovba et al., 2003).

About the Authors

Randell Stephenson is professor of lithosphere geophysics at the University of Aberdeen in Scotland. His university degrees are from Carleton University (B.Sc. and M.Sc.) and Dalhousie University (Ph.D.) in Canada, after which he did a postdoctoral fellowship at the Australian National University and worked as a Research Scientist at the Geological Survey of Canada (focused mainly on Arctic Canada) before moving to the VU University in Amsterdam in 1989 and to Aberdeen in 2009. A key area of research interest during this time has been the geology and tectonic history of south eastern Europe, in particular the intraplate sedimentary basins, and the tectonic events they record, overlying the southern part of the East European Craton and its – poorly defined – southern margin. Much of this work was carried out in collaboration with Ukrainian, Romanian and Russian colleagues in the framework of the European Science Foundation's EUROPROBE Programme. He coordinated the compilation of a DNAG-style lithosphere transect, developed for the 2004 IGC in Florence, across the Ukrainian Shield, Crimea, western Black Sea, Anatolia, Cyprus, eastern Mediterranean Sea and Sinai Peninsula. An important active research target is the Black Sea, in particular the pre-Cretaceous history of its margins.

Sergiy Stovba works at the consulting company "SPK-Geoservice" (Ukraine), which he founded in 2010 . He completed his studies as a geophysicist at Kyiv University in 1979 after which he worked for the State Geophysical Company Ukrgeofisika (Ukraine) and the Scientific Research Institute of the Oil and Gas Industry "Naukanaftogas", an institute of the National Joint-Stock Company "Naftogas of Ukraine". Simultaneously with his time at Ukrgeofisika he was a post-graduate student at Kyiv State University (1982–1986) leading to a Ph.D. degree from the Institute of Geophysics of the National Academy of Science in 1990, and in 2008 he obtained the degree of Doctor of Sciences from the same institute. His research has included reflection/refraction seismic surveys, seismo-stratigraphic interpretation, tectonics, basin analysis, salt tectonics, numerical modelling, paleogeography and geological/geophysical mapping. He was a participant of a number of international projects including the GeoRift project of EUROPROBE; the Peri-Tethys Programme; IGCP Project No. 369; INTAS Projects 93-3346, 96-1701, and 97-0743; TRANSMED and MEBE. He has published on the geology and tectonics of the Dniepr-Donets Basin, Donbas Foldbelt, and Black Sea.

References

Alexandre, P., Chalot-Prat, F., Saintot, A., Wijbrans, J., Stephenson, R., Wilson, M., et al., 2004. $^{40}Ar/^{39}Ar$ Dating of magmatic activities in the Donbas Foldbelt and the Scythian Platform (Eastern Europe). Tectonics 23 (5), TC5002, doi: 10.1029/2003TC001582.

Brunet, M.F., Volozh, Y.A., Antipov, M.P., Lobkovsky, L.I., 1999. The geodynamic evolution of the Precaspian Basin (Kazakhstan) along a north-south section. Tectonophysics 313, 85–106.

Chekunov, A.V., 1994. The geodynamics of the Dniepr-Donets rift syneclise. Geophys. J. 16 (3), 3–13 (in Russian).

Chekunov, A.V., Gavrish, V.K., Kutas, R.I., Ryabchun, L.I., 1992. Dnieper-Donets paleorift. Tectonophysics 208, 257–272.

Chirvinskaya, M.V., Sollogub, V.B., 1980. Deep Structure of the Dniepr-Donets Aulacogen According to Geophysical data. Naukova Dumka, Kiev, 178 pp. (in Russian).

DOBREfraction '99 Working Group, Grad, M., Gryn, D., Guterch, A., Janik, T., Keller, R., Lang, R., et al., 2003. "DOBREfraction '99" – velocity model of the crust and upper mantle beneath the Donbas Foldbelt (east Ukraine). Tectonophysics 371, 81–110.

Dvorjanin, E.S., Samoyluk, A.P., Egurnova, M.G., Zaykovsky, N.Y.a., Podladchikov, Y.u., Van Den Belt, F.J.G., et al., 1996. Sedimentary cycles and paleogeography of the Dnieper Donets Basin during the late Visean-Serpukhovian based on multiscale analysis of well logs. Tectonophysics 268, 169–187.

Eisenverg, D.E. (Ed.), 1988. Geology and Oil and Gas Occurrences of the Dniepr-Donets Depression: Stratigraphy. Naukova Dumka, Kiev, 148 p. (in Russian).

Ilchenko, T., 1996. The Dniepr-Donets Rift: deep structure and evolution from DSS profiling. Tectonophysics 268, 83–98.

Izart, A., Briand, C., Vaslet, D., Vachard, D., Coquel, R., Maslo, A., 1996. Stratigraphy and sequence stratigraphy of the Moscovian of the Donets Basin. Tectonophysics 268, 189–209.

Juhlin, C., Stephenson, R.A., Klushin, S., 1996. Reappraisal of deep seismic reflection Profile VIII across the Pripyat Trough. Tectonophysics 268, 99–108.

Kabyshev, B.P., et al., 1989. Geology and Oil and Gas habitat in the Dniepr-Donets Depression. Academy Nauk Ukrainskoy CCP, Institute of Geology. Naukova Dumka, Kiev, 201 p. (in Russian).

Kabyshev, B., Krivchenkov, B., Stovba, S., Ziegler, P.A., 1998. Hydrocarbon habitat of the Dniepr-Donets Depression. Mar. Pet. Geol. 15, 177–190.

Kostyuchenko, S.L., Morozov, A.F., Stephenson, R.A., Solodilov, L.N., Vedrentsev, A.G., Popolitov, K.E., et al., 2004. The evolution of the southern margin of the East European Craton based on seismic and potential field data. Tectonophysics 381, 101–118.

Kusznir, N.J., Stovba, S.M., Stephenson, R.A., Poplavskii, K.N., 1996. The formation of the northwestern Dnieper-Donets Basin: 2-D forward and reverse syn-rift and post-rift modelling. Tectonophysics 268, 237–256.

Maystrenko, Y.u., Stovba, S., Stephenson, R., Bayer, U., Menyoli, E., Gajewski, D., et al., 2003. Crustal-scale pop-up structure in cratonic lithosphere: DOBRE deep seismic reflection study of the Donbas Foldbelt, Ukraine. Geology 31, 733–736.

Nikishin, A.M., Ziegler, P.A., Stephenson, R.A., Cloetingh, S.A.P.L., Furne, A.V., Fokin, P.A., et al., 1996. Late Precambrian to Triassic history of the East-European craton: dynamics of sedimentary basin evolution. Tectonophysics 268, 23–63.

Orlyuk, M.I., Pashkevich, I.K., 1994. Evaluation of consolidated crust magnetization of the Dnieper-Donets aulacogen. Dokl. Acad. Sci. Ukraine 5, 125–128 (in Ukrainian).

Poplavskii, K.N., Podladchikov, Y.u.Y.u., Stephenson, R.A., 2001. Two-dimensional inverse modeling of sedimentary basin subsidence. J. Geophys. Res. 106 (B4), 6657–6672.

Prygarina, T.M., Lukin, O.E., Kabyshev, B.P., Demjanenko, I.I., Polyschuk, M.B., 2005. Probable hydrocarbon resources of the Eastern oil-and-gas bearing region. Geology 1, 15–18 (in Ukrainian).

Saintot, A., Stephenson, R.A., Stovba, S.M., Maystrenko, Y.u., 2003a. Structures associated with inversion of the Donbas Foldbelt. Tectonophysics 373, 181–207.

Saintot, A., Stephenson, R.A., Brem, A., Stovba, S.M., Privalov, V., 2003b. Palaeostress field reconstruction and revised tectonic history of the Donbas fold-and-thrust belt (Ukraine and Russia). Tectonics 22, 1059 10.1029/2002TC001366.

Saintot, A., Stephenson, R.A., Stovba, S., Brunet, M.-F., Yegorova, T., Starostenko, V., 2006. The evolution of the southern margin of Eastern Europe (Eastern European and Scythian platforms) from the latest Precambrian-Early Palaeozoic to the Early Cretaceous. In: Gee, D.G., Stephenson, R.A. (Eds.), European Lithosphere Dynamics, Geological Society of London, Memoir 32, 481–505.

Shatsky, N.S., 1946. The great Donets basin and the Wichita system; comparative tectonics of ancient platforms. Akad. Nauk SSSR Izv., Ser. Geol. 6, 57–90.

Shchipansky, A., Bogdanova, S., 1996. The Sarmatian crustal segment: Precambrian correlation between the Voronezh Massif and the Ukrainian Shield across the Dniepr-Donets Aulacogen. Tectonophysics 268, 109–126.

Starostenko, V.I., Kozlenko, V.G., Oganesyan, S.M., Shen, E.L., Oganesyan, M.G., Yegorova, T.P., Dyadura, G.V., 1986. 3-D distribution of the density in the crust of the Dnieper Graben. Geophysical Journal 8, 3–19 (in Russian).

Starostenko, V.I., Danilenko, V.A., Vengrovitch, D.B., Kutas, R.I., Stovba, S.M., Stephenson, R.A., et al., 1999. A new geodynamical-thermal model of rift evolution, with application to the Dnieper-Donets Basin, Ukraine. Tectonophysics 313, 29–40.

Stephenson, R.A., Chekunov, A., Ilchenko, T., Kaluzhna, L., Baranova, Y.e., Starostenko, V., et al., 1993. Continental rift development in Precambrian and Phanerozoic Europe: EUROPROBE and the Dnieper-Donets rift and Polish Trough basins. Sed. Geol. 86, 159–175.

Stephenson, R.A., Stovba, S.M., Starostenko, V.I., 2001. Pripyat-Dniepr-Donets Basin: implications for rift geodynamics and northern Peri-Tethyan tectonic history. Mém. Mus. Nat. Hist. Nat. 186, 369–406.

Stephenson, R.A., Yegorova, T., Brunet, M.-F., Stovba, S., Wilson, M., Starostenko, V., Saintot, A., Kusznir, N., 2006. Late Palaeozoic intra- and pericratonic basins on the East European Craton and its margins. In: Gee, D.G., Stephenson R.A. (Eds.), European Lithosphere Dynamics, Geological Society of London, Memoir 32, 463–479.

Stovba, S.M., Stephenson, R.A., 1999. The Donbas Foldbelt: its relationships with the uninverted Donets segment of the Dniepr-Donets Basin, Ukraine. Tectonophysics 313, 59–83.

Stovba, S.M., Stephenson, R.A., 2003. Style and timing of salt tectonics in the Dniepr-Donets Basin (Ukraine): implications for triggering and driving mechanisms of salt movement in sedimentary basins. Mar. Pet. Geol. 19, 1160–1189.

Stovba, S.M., Stephenson, R.A., Kivshik, M., 1996. Structural features and evolution of the Dniepr-Donets Basin, Ukraine, from regional seismic reflection profiles. Tectonophysics 268, 127–147.

Stovba, S.M., Maystrenko, Y.u.P., Stephenson, R.A., Kusznir, N.J., 2003. The formation of the south-eastern part of the Dniepr-Donets basin: 2-D forward and reverse syn-rift and post-rift modelling. Sed. Geol. 156, 11–33.

Stovba, S.M., Tolkunov, A.P., Stephenson, R.A., 2005. Regional investigations of geological structure and evolution of the Donbas Foldbelt (DOBRE international project). Problems of the Petroleum and Natural Gas Industry, Kyiv, pp. 21–34.

Ulmishek, G.E., Bogino, V.A., Keller, M.B., Poznyakevich, Z.L., 1994. Structure, stratigraphy and petroleum geology of the Pripyat and Dniepr-Donets basins, Belarus and Ukraine. AAPG Mem. 59, 125–156.

van Wees, J.D., Stephenson, R.A., Stovba, S.M., Shimanovsky, V., 1996. Tectonic variation in the Dniepr-Donets Basin from automated modelling of backstripped subsidence curves. Tectonophysics 268, 257–280.

Volozh, Y.u.A., Antipov, M.P., Leonov, Y.u.G., Morozov, A.F., Yurov, Y.u.G., 1999. Setting of the Karpinsky Swell. Geotectonics 1, 28–43, (in Russian).

Volozh, Y.u.A., Antipov, M.P., Brunet, M.F., Garagash, I.A., Lobkovskii, L.I., Cadet, J.P., 2003. Pre-Mesozoic geodynamics of the Precaspian Basin (Kazakhstan). Sed. Geol. 156, 35–58.

Wilson, M., Lyashkevich, Z.M., 1996. Magmatism and the geodynamics of rifting of the Pripyat-Dniepr-Donets rift, East European Platform. Tectonophysics 268, 65–81.

Yegorova, T.P., Stephenson, R.A., Kozlenko, V.G., Starostenko, V.I., Legostaeva, O.V., 1999. 3-D gravity analysis of the Dnieper-Donets Basin and Donbas Foldbelt, Ukraine. Tectonophysics 313, 41–58.

Yegorova, T.P., Stephenson, R.A., Kostyuchenko, S.L., Baranova, E.P., Starostenko, V.I., Popolitov, K.E., 2004. Structure of the lithosphere below the southern margin of the East European Craton (Ukraine and Russia) from gravity and seismic data. Tectonophysics 381, 81–100.

Zonenshain, L.P., Kuzmin, M.I., Natapov, L.M., 1990. Geology of the USSR: a Plate Tectonic Synthesis. Am. Geophys. Union Geodyn. Ser. 21, 242.

In this chapter

17

Sedimentary basins of the late Mesozoic extensional domain of China and Mongolia

S.A. Graham,* T. Cope,† C.L. Johnson,‡ Bradley Ritts§

*Department of Geological and Environmental Sciences, Stanford University, Stanford, California, USA

†Department of Geosciences, DePauw University, Greencastle, Indiana, USA

‡Department of Geology and Geophysics, University of Utah, Salt Lake City, Utah, USA

§Chevron Asia Pacific Exploration and Production, Singapore

17.1 Introduction

Much of eastern China and eastern Mongolia was extended during the Late Jurassic and Early Cretaceous. As noted by various authors (Li et al., 1995; Ren and Li, 1998), the extended area of eastern Asia was remarkably comparable to the Cenozoic Basin and Range province of North America: it covered a comparably vast area (Fig. 17.1), was characterized by structurally controlled topography, was dominated by normal faults and subsidiary strike-slip faults, and featured basins dominated by facies characteristic of internal drainage. The Mesozoic Asian system persisted for 30 m.y. or less, whereas the North American Basin and Range system has been extending for over 40 m.y., with a period of widespread high-strain extension for ca. 20 m.y. (Dickinson, 2002).

Recent decades of investigation have revealed that the history and character of the North American Basin and Range system are complex. Extension and associated magmatism has been heterogeneous in time and space (Burchfiel et al., 1992; Dickinson, 2002). Early in the history of the province, some regions were characterized by remarkable zones of high strain extension, whereas other areas were substantially unaffected. In the latest Cenozoic, high rates and magnitudes of strain have been less important, and more conventional rift structuring has been typical.

The region typified by late Mesozoic extension in eastern Asia is proving to be equally complicated, although full understanding of the region is still years

Phanerozoic Rift Systems and Sedimentary Basins DOI: 10.1016/B978-0-444-56356-9.00016-X

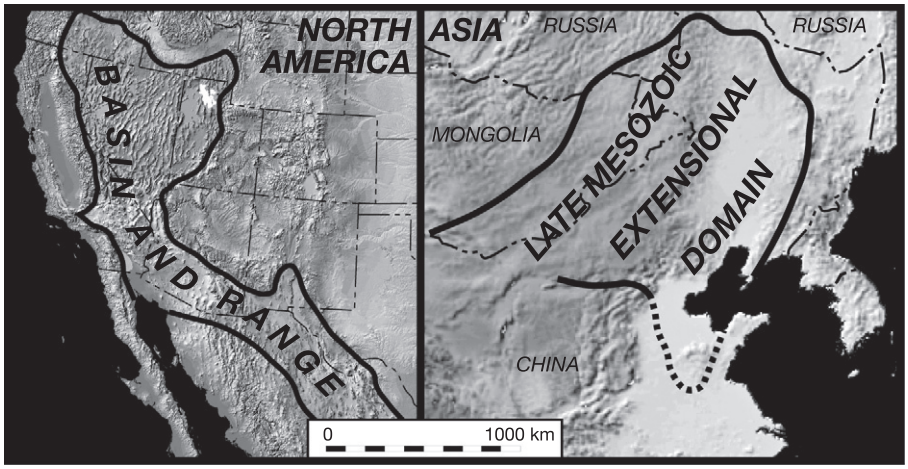

Figure 17.1 Same-scale comparison of the areas encompassed by the North American Basin and Range province and the late Mesozoic extensional domain of China and Mongolia. Approximate boundary of late Mesozoic extension from Ren et al. (2002).

away. Basins of the region vary from small to large conventional low-strain extensional basins, to transtensional basins, to rapidly filled basins associated with high-strain extensional metamorphic core complexes (Fig. 17.2). Magmatism is widespread (Graham et al., 2001; Meng et al., 2003). Temporal variations in styles and rates of extension also characterize the east Asia extensional domain. The sheer geographic scale of the two intracontinental regions indicates that plate scale tectonic processes have been operative (Fig. 17.1).

Nevertheless, important differences exist between the Asian and North American extensional provinces. The Asian basins display a remarkable diversity of sizes, in part reflecting an underlying control on basin size and bounding faults by pre-existing crustal structure. Certainly, basin-bounding normal faults in America have been demonstrated to reactivate Mesozoic and early Cenozoic thrust faults (e.g., Gries, 1983), but in eastern Asia the pre-rift substrate, an amalgam of crustal materials of variable dimensions, uncratonized and significantly shortened only a few tens of million years prior to extension (e.g., Johnson et al., 2001; Zheng et al., 1991), exerted a fundamental control on rifting. As a first approximation, the region is underlain, from north to south, by accreted Paleozoic arc terranes in southern Mongolia (Lamb and Badarch, 1997), a crushed late Paleozoic flysch basin along the China–Mongolia border marking the Junggar–Hegen–Solon suture (Zhang et al., 1984), and North China cratonal basement tectonized during the early Mesozoic (Davis et al., 1998). Furthermore, the puzzling, close geographic and temporal bracketing of the Asian extended domain by contractile orogenic belts (Fig. 17.2) differs from the American Basin and Range province. Finally, the crust of the Asian Mesozoic extensional domain remains thick, as emphasized by Meng et al. (2003).

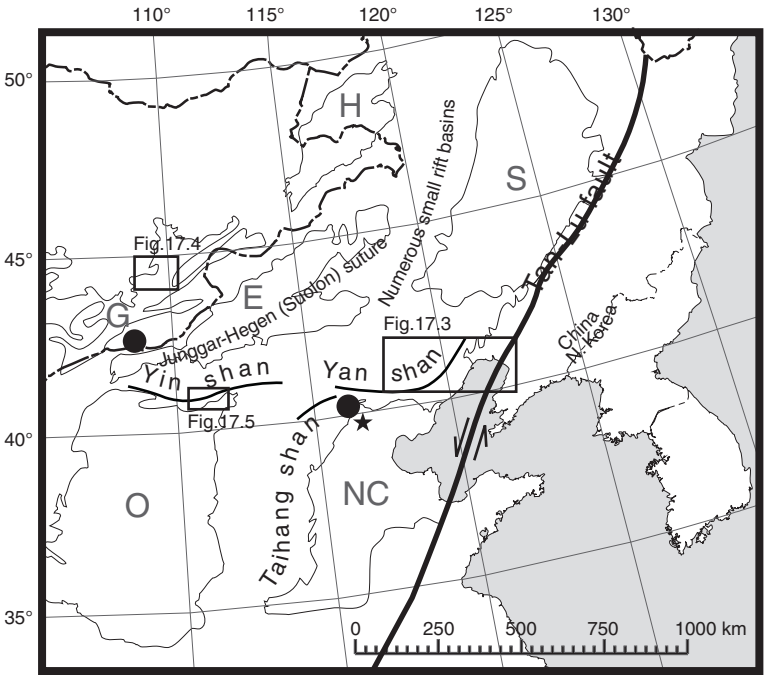

Figure 17.2 Map of northeastern China and eastern Mongolia, showing major Jurassic-Cretaceous extensional basins (stippled), Mesozoic contractile basins (ruled), and Cenozoic extensional basins (cross-hatched), and selected features of the pre-extension basement. Locations of Figures 17.3–17.5 shown (boxes). E, Erlian basin; NC, North China basin; S, Songliao basin; G, Gobi basin; H, Hailar basin; O, Ordos basin. Metamorphic core complexes of Cretaceous age shown by black circles: O, Yagan-Onch Harhyan; Y, Yunmeng Shan; H, Hohhot.

In this paper, we illustrate representative structures and basins of the east Asia Mesozoic extensional domain. Meng et al. (2003) offer additional details of the system. We do not treat the largest basins of the region, the Songliao, Erlian, and Hailar-Tamsag basins (Fig. 17.2), which are discussed separately by Li (this volume), but instead, focus on the diverse and less well-known basins and structural features of the province. These features do not contribute significantly to petroleum reserves of the province, but they do afford important insights into the timing and origins of the extensional episode.

17.2 Basins and structures associated with low-strain extension

Introduction

The history of intracontinental extension in Mesozoic eastern Asia includes many characteristics common to low-strain provinces worldwide (e.g., Gawthorpe and Leeder, 2000). Specifically, rift structures broadly define horst and graben geometries bounded by high angle normal faults. These initially isolated nonmarine depocenters demonstrate rapid facies changes and development of multiple synrift sequences. Increasing fault displacement and linkages resulted in more continuous and interconnected subbasins as rifting progressed. Basin evolution departs from general models of low-strain extension in that rifting ended

abruptly with a basin-inversion event rather than developing a significant postrift sequence reflecting thermal subsidence (Meng et al., 2003). This departure is largely a function of the frequency of intracontinental deformation events during the amalgamation of Asia, as well as the heterogeneous basement structures that characterize the prerift substrate of southern Mongolia. In addition, the role of strike-slip faulting is poorly understood and may play a larger role in late Mesozoic rifting and post-rift basin sequences in the China-Mongolia border region than previously recognized.

Northeastern China

The late Mesozoic extensional province in northeast China extends from the Mongolian border eastward to the Tan-Lu fault (Fig. 17.2). As many as 200 rift basins and subbasins, each bounded by northeast-trending normal faults, developed within this broad area during mid-Cretaceous time (Dou, 1997; Lin et al., 2001; Meng et al., 2003). Well-documented examples of late Mesozoic basins related to this rifting event include a number of coal-bearing half-graben basins in Inner Mongolia (Li et al., 1984), the Erlian basin of northern China (E, Fig. 17.2, Lin et al., 2001), and Late Jurassic-Early Cretaceous half-grabens which exist beneath the extensive Cenozoic post-rift fill of Songliao basin (S, Fig. 17.2; Dou, 1997; Xue and Galloway, 1993).

The rift system is superimposed upon a complex and heterogeneous basement fabric consisting of multiple Paleozoic suture zones and Mesozoic belts of intracontinental shortening, most notably the Yanshan fold-thrust belt (Fig. 17.2). The Yanshan belt, and the coeval Yinshan fold-thrust belt farther west (Fig. 17.2), together comprise one of the largest and longest-lived zones of intracontinental shortening in Asia (Davis et al., 1998, 2001). Rift basins of Cretaceous age developed both within the Yanshan belt and along its northern periphery. Rifting closely followed, and perhaps overlapped, Late Jurassic-Early Cretaceous shortening in the Yanshan region. North of Beijing, major Yanshan thrust structures are intruded by a plutonic suite that yields ages of 132–129 Ma (Davis et al., 1998, 2001), indicating that the bulk of thrusting was completed by this time. Low-strain extension in the Yanshan region began ca. 130–121 Ma, the age range of volcanic units interbedded with and underlying syn-rift fill throughout the area. Lower Cretaceous strata associated with rifting in the Yanshan region comprise humid climate, coal-bearing fluvial, alluvial, and lacustrine facies associations (Fig. 17.3) that thicken and coarsen toward basin-bounding normal faults. These strata contain an abundant and diverse faunal assemblage, including the well-known Jehol biota that contains feathered dinosaur remains (Zhou et al., 2003).

The occurrence, geometry, and fill of rift basins in the Yanshan region was strongly influenced by the orientation of preexisting thrust trends relative to the Early Cretaceous stretching direction. Throughout most of its length, the Yanshan fold-thrust belt (and its Yinshan counterpart farther west, Fig. 17.2)

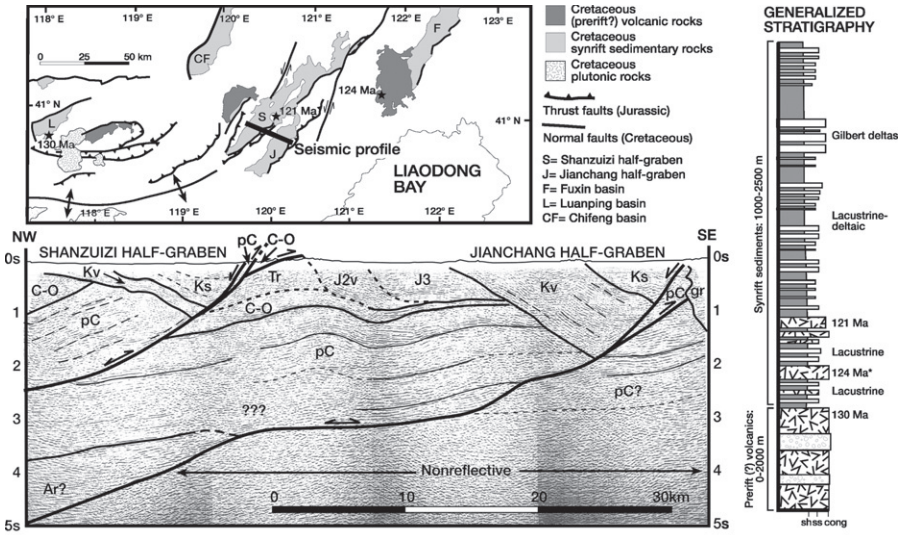

Figure 17.3 NW-SE time-migrated seismic line showing extensional basins developed atop the eastern Yanshan fold-thrust belt, Liaoning Province, China. Cretaceous normal faults bounding two half-graben basins (Shanzuizi basin and Jianchang basin) sole into Jurassic thrust faults at depth. Near-surface seismic interpretation is calibrated to surface exposures where these relationships are well exposed. Mesozoic structural trends plunge northeast, allowing for good control at depth. Geographic locations and stratigraphic position of $^{40}Ar/^{39}Ar$ ages shown; age denoted with asterisk from Swisher et al. (1999). Stratigraphic section generalized from outcrops in western Liaoning Province and northeastern Hebei Province. pC, Precambrian sedimentary rocks; C-O, Cambrian-Ordovician sedimentary rocks; Tr, Triassic clastic strata; J2v, Middle Jurassic volcanic and volcaniclastic strata; J3, Upper Jurassic clastic strata; Kv, Cretaceous volcanic rocks; Ks, Cretaceous fluvial-lacustrine strata; gr, Cretaceous(?) granite.

trends strongly east-west and contains numerous large-offset features verging both north and south. In its easternmost extent, however, fold and thrust structures in the Yanshan belt trend northeast (Fig. 17.2) and are strongly southeast vergent. The Early Cretaceous stretching direction, as derived from the orientation of basin-bounding normal faults throughout northeast China, was to the northwest-southeast and apparently uniform throughout the extensional province. Early Cretaceous rift basins are widespread throughout the eastern segment of the Yanshan belt, where thrust structures were favorably oriented to be reutilized as normal faults in extension. Along western segments of the Yanshan belt, where stretching direction was oriented oblique to basement fabrics, normal faults of Cretaceous age are common, but evidence for widespread rift basin development within the thrust belt is generally lacking.

Cretaceous rift basins developed atop the eastern, northeast-trending segment of the Yanshan belt are characterized by numerous southeast-deepening

half-graben basins which occupy the core and periphery of the preexisting orogen and reactivate southeast vergent Jurassic-Cretaceous thrust structures as normal faults (Fig. 17.3). Normal faults that bound these half-graben uniformly dip to the northeast and sole into the older thrust faults in outcrop. Basin-bounding normal faults have shallow dips ($\sim 25^{\circ}$ in surface exposures), and the basins they bound seldom exceed 1–2 km in depth (Fig. 17.3). The fill of Jianchang and Shanzuizi basins (Fig. 17.3) comprises dominantly shallow lacustrine siltstone and sandstone punctuated by the occurrence of 2–6 m thick progradational gilbert delta complexes, fluvial sandstone, and coal. A tuff from the base of the Shanzuizi basin fill yields an $^{40}Ar/^{39}Ar$ biotite inverse isochron age of 121 ± 4 Ma; this is compatible with 124–125 Ma ages obtained from tuffaceous lacustrine strata elsewhere in Liaoning Province that broadly constrain the onset of rifting (Swisher et al., 1999).

Within the western, east-west trending segment of the Yanshan belt, Lower Cretaceous lacustrine strata are lacking. Instead, intermediate volcanic and volcaniclastic units dominate (135–122 Ma; Davis et al., 2001; Niu et al., 2003). These unconformably overlie deformed Jurassic-Cretaceous strata and structures. Lacustrine rift basin development in this area was restricted to basement-floored regions external to, and north of, the fold-thrust belt. One such basin, Luanping basin, lies immediately north of the Yanshan belt within Archean crystalline basement. Luanping basin is bounded by steeply dipping normal faults along its northern and western margins that together define a northwest-southeast extension direction in keeping with the rest of the province. A minimum of 3 km of organic-rich lacustrine shale, siltstone, and marl fill the basin and coarsen and thicken toward both fault-bounded margins. The basin fill unconformably overlies Jurassic strata related to contractile deformation in the Yanshan region. A welded tuff beneath the lowermost lacustrine strata in Luanping basin yields an $^{40}Ar/^{39}Ar$ biotite plateau age of 130 ± 0.5 Ma, providing a lower limit on the timing of extension.

Southeastern Mongolia

Extension in the East Gobi basin (EGB) of southeastern Mongolia (Fig. 17.2) began in Late Jurassic time and continued through the Early Cretaceous, as recorded by up to 3 km of nonmarine and volcaniclastic strata filling late Mesozoic-aged grabens and half-grabens (Fig. 17.4). Parallel fault systems broadly define the basin, which spans approximately 500 km in length from northeast to southwest. At the southwestern edge of the EGB, Early Cretaceous rifting is characterized by high-strain extension and formation of the Yagan-Onch Hayrhan detachment fault and metamorphic core complex (Webb et al., 1999). In contrast, the region near the active oil fields around Zuunbayan (Fig. 17.4) demonstrates characteristics of low-strain extension, including high-angle normal faults that border multiple subbasins (Johnson, 2004).

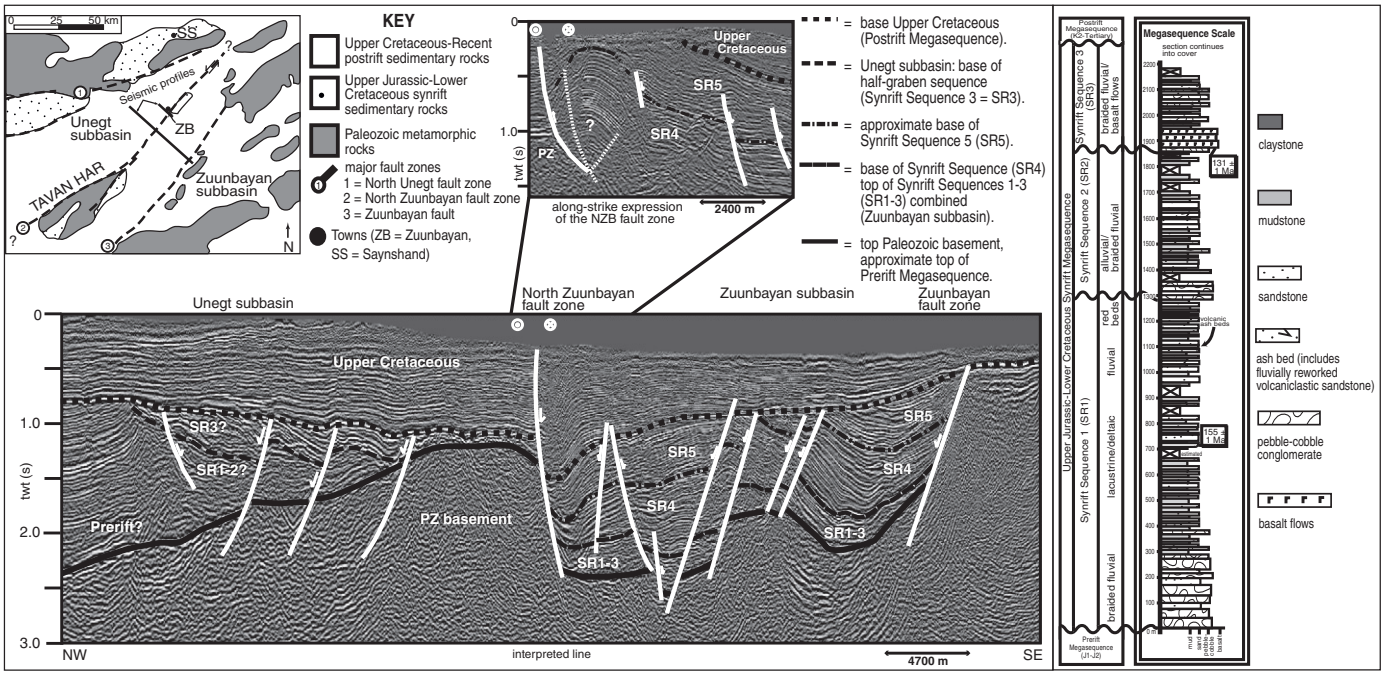

Figure 17.4 Regional seismic profile showing rift structure and prerift, synrift, and postrift megasequences of the East Gobi basin, Mongolia. Location of line shown in inset map. Vertical axis is in two-way travel time. Smaller seismic profile is from a parallel line several km away. Note high angle faults bounding major rift features, which were reactivated during a transpressional mid-Cretaceous basin inversion. Seismic data are from Johnson (2004). Stratigraphic section generalized from outcrops in the Unegt subbasin (Graham et al., 2001; Johnson and Graham, 2004a) is typical of Mongolian sector low-strain rift-basin fill.

Prerift, synrift, and postrift stratigraphic megasequences are well-expressed on seismic reflection profiles near Zuunbayan (Johnson, 2004; Traynor and Sladen, 1995; Fig. 17.4), and can be correlated to outcrop exposures particularly along the northern margin of the EGB and at other basement uplifts (Graham et al., 2001). Basement rocks in southeastern Mongolia mainly consist of Paleozoic-aged volcanic arc sequences (spanning Ordovician-Carboniferous sequences) that accreted prior to Mesozoic time as part of a closing ocean basin along the northern margin of the North China block (Lamb and Badarch, 1997). Although Precambrian rock units are mapped in parts of the EGB (e.g., Tavan Har locality, Fig. 17.4; Yanshin, 1989), this interpretation is largely based on the high grade of metamorphism and inferred relative age relations between crystalline metamorphic rocks and "younger" Paleozoic units. No absolute age data are currently available to support this age assignment, and in fact recent studies suggest at least an overprint of a much younger metamorphic event (latest Triassic) at Tavan Har (Lamb et al., 1999). Thus, basement rocks underpinning late Mesozoic rift basins in southeastern Mongolia are relatively young and also distinctly heterolithic, particularly compared to the more homogeneous "microcontinent" crust of the Precambrian North China block. Evidence for poly-phase reactivation of major structures, particularly as long-lived strike-slip faults, may in part reflect this basement heterogeneity (Johnson, 2004).

Prerift units also include Lower-Middle Jurassic strata of the Khamarkhavoor Formation. Locally, this unit is up to 1 km thick, and it contains widespread coal beds that distinguish it from the rest of the Mesozoic sequence. These strata appear to predate (and are offset by) the main extensional structures of the EGB, and they also lack the bimodal volcanic units common to the overlying synrift Mesozoic sequence (Graham et al., 2001). The basin setting for these units is poorly constrained, but they correlate in age and depositional style to lower Mesozoic foreland and intermontane deposits found in western Mongolia (Hendrix et al., 2001) and may reflect a related prerift contractile event in the EGB.

The synrift megasequence of southeastern Mongolia includes up to 3 km of preserved basin fill (Fig. 17.4). Five distinct synrift sequences are defined based on unconformable relations and indications of regional changes in depositional style (Graham et al., 2001). Nonmarine basin fill includes alluvial and fluvial deposits as well as widespread lacustrine and perilacustrine facies, particularly in Lower Cretaceous units at the basin center near Zuunbayan (Fig. 17.4; Johnson et al., 2003). Seismic-stratigraphic units show asymmetric growth patterns that thicken into horst-bounding normal faults, supporting the interpretation of a synrift basin setting for these sequences. Rhyolitic ash beds and basalt flows are also common, and provide radiometric constraints on the timing of rifting, from at least 155–126 Ma (Graham et al., 2001). Mapping of seismic reflection data indicates that the earliest phase of rifting (during Late Jurassic time) was characterized by isolated depocenters that coalesced into larger, more

continuous subbasins during Early Cretaceous time as displacement on extensional faults increased, and fault systems linked to form more continuous structures (Johnson, 2004). Synrift fluvial-lacustrine strata of the EGB also form the major source, reservoir, and seal units for hydrocarbon accumulations in the subsurface near Zuunbayan (Johnson et al., 2003).

The main period of rift-related subsidence ended abruptly during ~mid-Cretaceous time (early Cenomanian; Graham et al., 2001). A major basin-reorganization event is reflected by a regionally recognized angular unconformity between deformed synrift strata as young as Aptian-Albian, and relatively undeformed Upper Cretaceous strata of the postrift megasequence (Fig. 17.4). Synrift normal faults were reactivated as thrust faults during this event, as indicated by reverse drag of synrift strata seen on seismic data (Fig. 17.4). Mapping at Tavan Har and correlation to seismic data suggest that this basin inversion event may reflect transpressional movement along a major basin-dividing strike-slip fault (the North Zuunbayan fault). Although poorly understood, outcrop and subcrop relations suggest that this was a long-lived structure with multiple phases of movement as old as Triassic and reactivated as recently as Cenozoic (Johnson, 2004).

17.3 Basins and structures associated with high-strain extension

Introduction

High-strain extensional styles are increasingly recognized across the northeast China-Mongolia Early Cretaceous extended region (Fig. 17.2). Structurally, high-strain extension is marked by the presence of detachment faults, low-angle normal faults of regional extent upon which large amounts of extension (at least tens of kilometers) are accommodated (Davis and Lister, 1988; Lister and Davis, 1989). The low-angle regional nature of detachment faults results in efficient accommodation of extension, and thus, these faults are found in regions that undergo large magnitudes and high rates of extension (Friedmann and Burbank, 1995). In northeast China and southern Mongolia, many of these detachment faults control formation of extensional metamorphic core complexes, which are created when tectonic removal of the upper plate of the detachment unloads the lower plate, resulting in isostatic uplift and doming. The resultant metamorphic core complex is characterized by a domal lower plate composed of mid- or lower crustal metamorphic rocks separated from a lower-grade upper plate by the detachment fault, which is usually characterized by a mylonitic shear zone overprinted by brittle fault rocks (Davis et al., 1986; Lister and Davis, 1989). The upper plate of detachment faults, whether in metamorphic core complexes or not, often contains syn-extensional sedimentary basins, termed "supradetachment basins" by Friedmann and Burbank (1995). Supradetachment basins can be distinguished based on their structural setting in the upper

plate of a detachment and on a variety of sedimentary characteristics, including dominance of footwall provenance, transverse deposystems, coarse sediment, proximal sedimentary facies distributed across the basin, and relatively thin sequences of strata (Friedmann and Burbank, 1995).

The recognition of extensional detachments, metamorphic core complexes, and supradetachment basins in eastern Asia has only begun, with a few documented examples and several probable systems that remain undescribed. Documented examples range from the Yagan-Onch Hayrhan metamorphic core complex in the southern Mongolia-China border region (Meng, 2003; Webb et al., 1999; Zheng and Zhang, 1993), through the Ertomiao and Hohhot metamorphic core complexes in Inner Mongolia (Darby, 2003; Davis et al., 2002), to several examples in eastern Inner Mongolia and the Liaoning provinces (Davis et al., 1996; Darby 2004). All of these detachment fault systems share a common basement; they overlie or are in close proximity to the Jurassic-earliest Cretaceous Yinshan-Yanshan fold-thrust belt (Darby, 2003; Darby et al., 2001; Davis et al., 1998). Other documented detachment systems in eastern China lie outside this area, including structures along the Mesozoic Qinling-Dabie orogen (e.g., Webb et al., 1999; Zhang et al., 1999). Of all the high-strain extensional structures in this region, the Hohhot detachment is part of the most thoroughly documented metamorphic core complex and is associated with well-developed and well-exposed supradetachment basins (Davis et al., 2002). Because the structural characteristics and tectonics of the Hohhot detachment and Hohhot metamorphic core complex are well-constrained, and because associated supradetachment basins are widespread, we detail this system below as an excellent type example of east Asian high-strain extensional systems and sedimentary basins.

Hohhot detachment: Structural setting

The Hohhot detachment system lies within the Daqing Shan north of Hohhot, the capitol of the Inner Mongolia Autonomous Region (Fig. 17.2). The detachment stretches along-strike in an east-west direction for more than 120 km (Fig. 17.5) and accommodates at least 40 km of top to the southeast extension in its central portion, where the Hohhot metamorphic core complex is developed (Davis et al., 2002). The age of extension on the Hohhot detachment is constrained to approximately 125–121 Ma by $^{40}Ar/^{39}Ar$ hornblende and biotite cooling ages in the footwall of the detachment, cross-cutting relationships, and $^{40}Ar/^{39}Ar$ dating of volcanics in synextensional sedimentary basins (Davis et al., 2002).

The Hohhot metamorphic core complex consists of the Hohhot extensional detachment fault, the Daqing Shan antiform, a roughly east-west trending culmination of metamorphic and plutonic rocks, and a folded upper plate of pre-Cretaceous crystalline and sedimentary units and Lower Cretaceous synextensional strata (Davis et al., 2002). On the south flank of the Daqing Shan

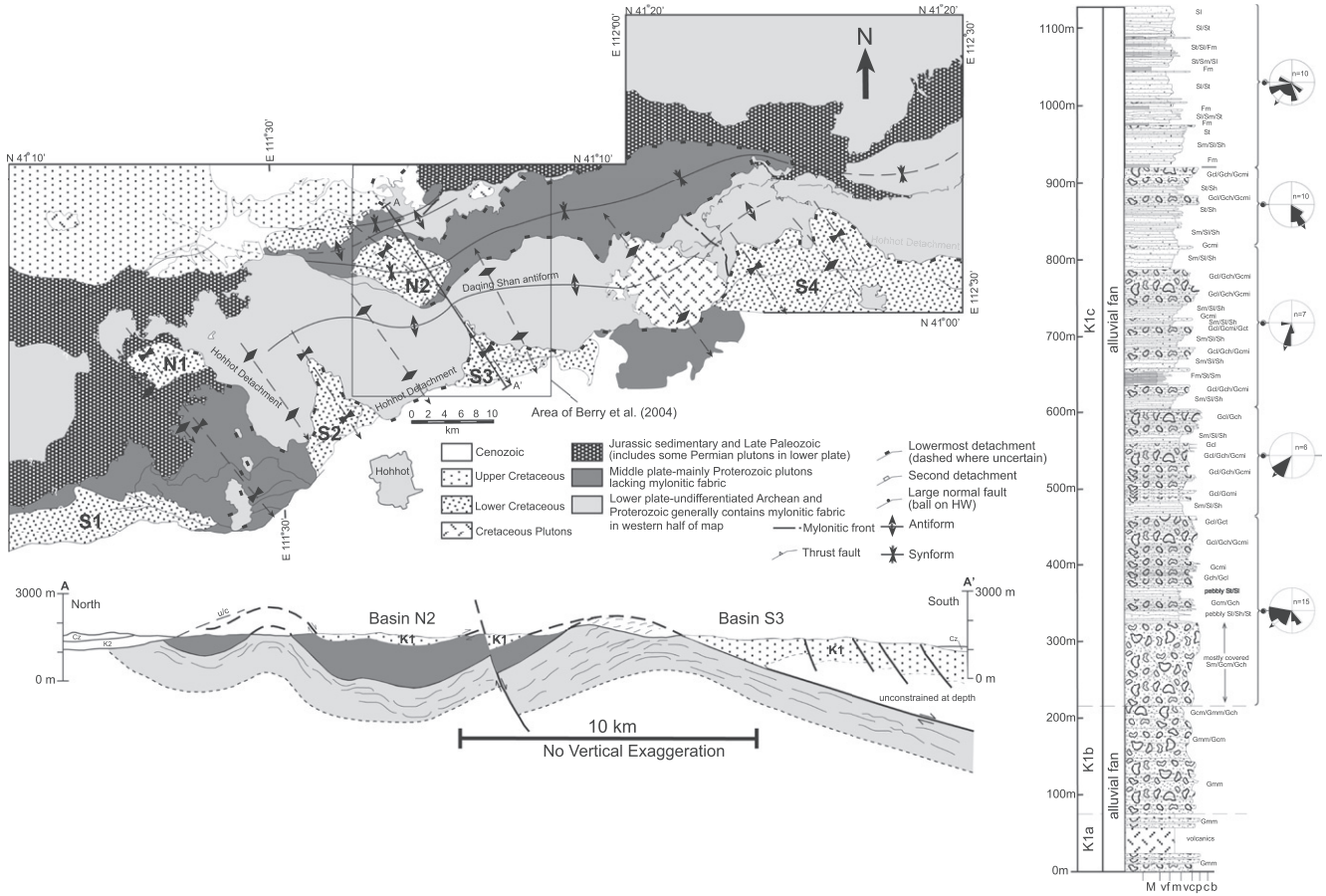

Figure 17.5 Structure, basin development, and typical stratigraphy associated with the Hohhot detachment fault and metamorphic core complex, near Hohhot, Inner Mongolia, China. See Fig. 17.2 for location of area. Note low angle normal faulting, folding of detachment fault, and doming of lower plate metamorphic rocks. Basin fill sequences, such as that shown at the right from basin S1 (north is to the top on paleocurrent diagrams), are dominated by very coarse grained alluvial and fluvial strata; limited accommodation precludes development of thick lacustrine sequences.

antiform, the Hohhot detachment fault is a south-dipping low-angle (15–30°) mylonitic normal fault system with a brittle overprint (Fig. 17.5); this fault is the master detachment. It is corrugated into synforms and antiforms with hinges parallel to the NW-SE extension direction (Davis et al., 2002). Synformal corrugations in the detachment preserve numerous Lower Cretaceous nonmarine clastic basins (Ritts, 2010). On the northern flank of the Daqing Shan antiform, two detachment faults are stacked and synformally folded, with top-to-the south slip on both splays (Fig. 17.5; Davis et al., 2002). The lower detachment separates mylonitic rocks from overlying non-mylonitic rocks, primarily Proterozoic crystalline rocks and Permian granitic gneisses. The upper detachment carries a succession of Cretaceous volcanic and sedimentary rocks (basin N2 in Fig. 17.5) that are highly deformed by normal faulting related to extension. The lower, oldest, detachment was the original detachment, but with extension, the footwall was progressively unloaded, triggering isostatic uplift and bringing lower plate rocks to the surface. The resultant antiformally folded detachment was deactivated and a new splay propagated to the surface to accommodate further extension (Davis et al., 2002). The new splay, in turn, was also antiformally folded due to continued uplift with further unloading. The Hohhot detachment, on the southern flank of the Daqing Shan antiform, is the youngest fault splay and accommodated the remaining extension (Davis et al., 2002).

Hohhot detachment: Supradetachment basins

The eastern Daqing Shan contain at least six distinct Lower Cretaceous basins that formed synchronously with extension along the underlying Hohhot detachment (Fig. 17.5). Because of their structural position above the Hohhot detachment, and their synchronous evolution with the detachment (demonstrated by $^{40}Ar/^{39}Ar$ dating of intercalated volcanic rocks, cross-cutting relationships, and basin analysis) these basins are, by definition, supradetachment basins (Friedmann and Burbank, 1995). The six basins together comprise a *supradetachment basin system* which is defined here as a series of supradetachment basins that form in the upper plate of a detachment or linked detachments and that can be ascribed to a specific structural depozone within that system.

Basins N1 and S1–S4 (Fig. 17.5) all formed in the upper plate of the youngest splay of the Hohhot detachment, whereas basin N2 formed above an older splay of the detachment and is now located in the synformal keel of the Hohhot metamorphic core complex (Davis et al., 2002). Of the basins in the upper plate of the youngest splay of the Hohhot detachment, basins N1, S2, and S3 directly overlie, and are cut by, the Hohhot detachment, and basin S1 is bounded by a low-angle brittle normal fault that is wholly within the upper plate of the Hohhot detachment.

All of the supradetachment basins share the basic sedimentologic and stratigraphic characteristics of supradetachment basins as defined by Friedmann

and Burbank (1995), although different depozones, particularly the upper plate basin depozone represented by basin S1, have some marked variation peculiar to their structural setting. All six basins are relatively thin; the maximum stratigraphic thickness is ~1200–1400 m and the thinnest basin is basin N2 with less than 400 m of strata. Strata in the basins are overwhelmingly dominated by conglomerate (Fig. 17.5), frequently cobble to boulder grade, that were deposited by streamflow and sheetflood-dominated alluvial fan depositional systems. Large (some more than 2 km long and 100 m thick) gravity-driven slide blocks are common in basins S2, S3, N1, and N2, also demonstrating the coarse-grained, proximal nature of the basins' depositional systems.

In each basin, sediment is derived from the lower plate, with only relatively minor amounts from the upper plate, and then only early in the basin's evolution. The fluvial and alluvial fan depositional systems that delivered the sediment filled the basin transversely from either the detachment breakaway or the domal core of the metamorphic core complex; paleocurrents in each basin are to the south-southeast, parallel to the extension direction. Finally, in each basin, facies are laterally uniform over the scale of the exposed basin, as is stratigraphic thickness.

These shared characteristics of the Lower Cretaceous Daqing Shan basins are consistent with the supradetachment basin model of Friedmann and Burbank (1995), and vary considerably from characteristics expected for half-graben or graben basins (Gawthorpe and Leeder, 2000). For example, half-graben basins are typically marked by strongly asymmetrical facies distributions, with coarse material deposited by mass wasting restricted to the fault margin of the basin and immediately juxtaposed with deepwater or axial facies, dominance of hangingwall and axial provenance, and wedge geometry in cross section with the deepest part of the basin proximal to the basin-bounding fault (Gawthorpe and Leeder, 2000).

Basin S1 and its basin-bounding low-angle normal fault are wholly restricted to the upper plate of the Hohhot detachment (Fig. 17.4). The low-angle normal fault that bounds the northern edge of basin S1 is a brittle structure that has not accommodated large amounts of slip. It probably soles into the Hohhot detachment at depth, and may represent an incipient new splay of the Hohhot detachment (B. Darby, personal communication). Because basin S1 is southward of the uplifted footwall of the Hohhot detachment, it is dominated by coarse conglomerate delivered by south-flowing transverse depositional systems and derived from the lower plate, as in the other basins. However, enhanced subsidence in the hanging-wall of the S1 basin-bounding fault provided additional accommodation space in the center of the basin that influenced facies distribution and architecture in ways not observed in the other basins. Specifically, finer-grained sediments and lower-energy depositional systems are preserved along the central part of the basin-bounding fault, where the amount of relative

hanging-wall subsidence and fault slip rate were at their maximum. Composed of a limited lacustrine facies dominated by organic-rich coaly mudstone and intercalated fan delta conglomerate and pebbly sandstone with slump and dewatering structures, these facies grade laterally into pebble-boulder alluvial fan conglomerate derived from the lower plate of the Hohhot detachment that spilled over and around the eastern and western ends of the basin-bounding upper plate fault.

17.4 Implications

The Late Jurassic-Early Cretaceous extensional province of eastern China and Mongolia was a vast continental interior region of localized nonmarine deposition, remarkably similar in topography and structure to the Cenozoic Basin and Range province of North America (Fig. 17.1). The Asian basins include conventional low-strain rift graben, as well as high-strain basins associated with extensional metamorphic core complexes. Unlike the North American Basin and Range province, temporal and spatial distribution trends of the two basin end-member types have yet to be conclusively demonstrated, although Meng et al. (2003) proposed an evolutionary linkage between the two rift modes. All basins contain exclusively nonmarine fill, varying from relatively modest total thickness, very coarse-grained sequences in the high-strain setting basins, to thick accumulations of fine-grained lacustrine facies with coarse marginal facies in the low-strain basins. As in all nonmarine basins, climate is a major factor in determining the character of facies, whereas both tectonism and climate control the stratigraphic architecture (Graham et al., 2001; Johnson and Graham, 2004b). The deepest water lacustrine facies are best developed in the largest basins of the region, where accommodation was maximized along major basin-bounding faults. The larger basins tended to evolve from initially isolated sets of grabens, which over time became linked to form larger, lacustrine-dominated entities.

The Asian basins demonstrate pronounced structural control, including both localization of basins by the fabric of the underlying accretionary basement, as well as reactivation of specific faults. The regional pattern of extension abruptly terminated in the mid-Cretaceous with an episode of basin inversion. Only the largest of the basins, notably Songliao (Li, this volume), display a clearly discernible pattern post-rift thermal subsidence (termed the "sag" phase in local literature).

The scale of the province and duration of extension suggest that extension was driven by plate-scale processes. No single extensional driver has yet been convincingly demonstrated, but a variety of mechanisms have been advanced (Fig. 17.6): (1) backarc extension behind the Pacific margin arc of Asia (Ren et al., 2002; Traynor and Sladen, 1995; Watson et al., 1987); (2) extension associated with the closing of the Mongol-Okhotsk seaway

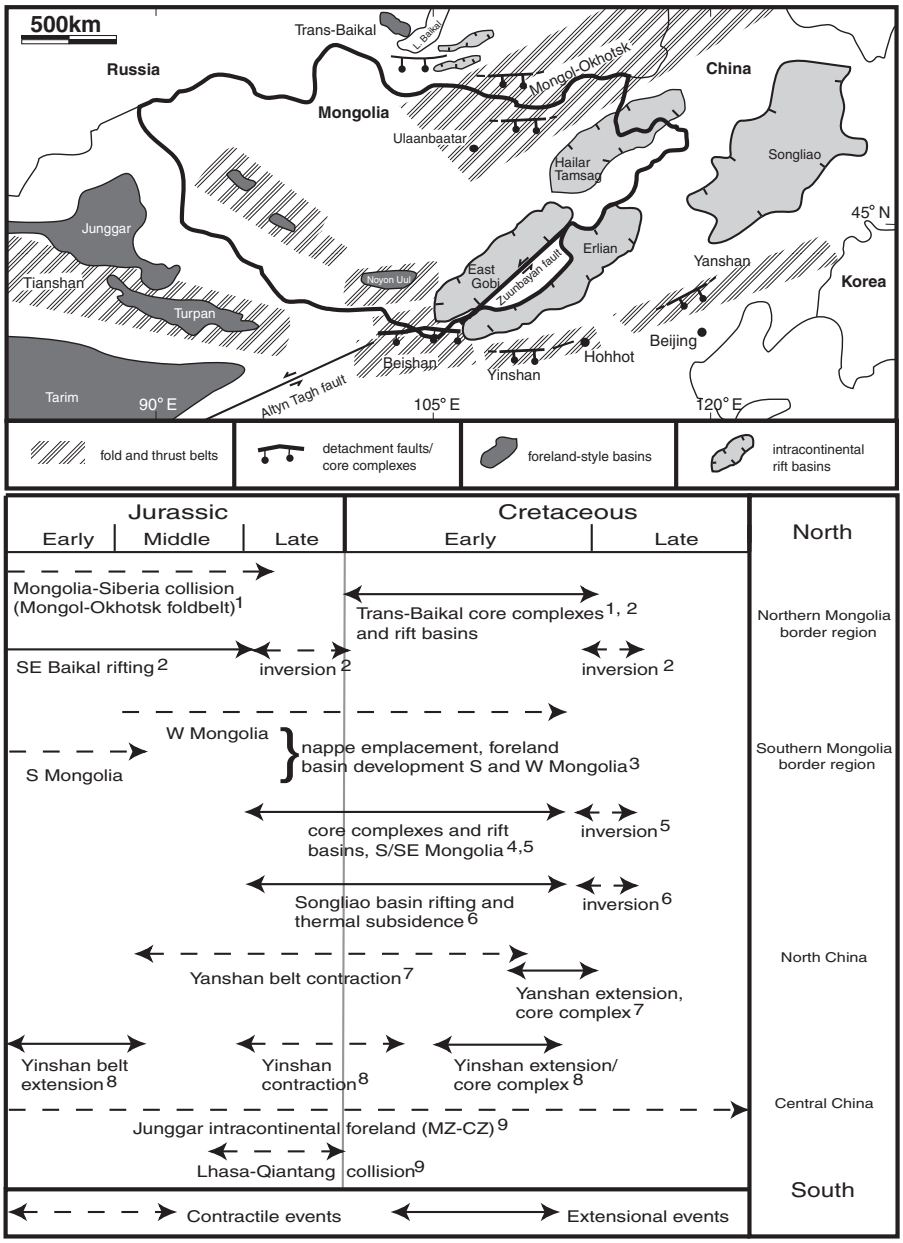

Figure 17.6 Tectonic features and temporal relations associated with the late Mesozoic extensional domain of China and Mongolia *(modified from Graham et al., 2001). References to features/ timing: 1. Zorin (1999); 2. Van der Beek et al. (1996); 3. Hendrix et al. (1996), Zheng et al. (1991); 4. Webb et al. (1999), Johnson et al. (2001); 5. Graham et al. (2001), Johnson (2004); 6. Li (this volume); 7. Davis et al. (1996); 8. Darby et al. (2001); 9. Hendrix et al. (1992).*

(Graham et al., 2001); (3) transtension associated with collisional tectonics (Kimura et al., 1990; Lamb et al., 1999); (4) gravitational collapse of orogenically thickened crust (Junggar–Hegen–Solon suture, Yinshan-Yanshan belt) (Graham et al., 2001; Traynor and Sladen, 1995) or orogenic collapse

followed by compensatory mid-lower crustal flow (Meng et al., 2003). The first two of these seem less able to explain the most interior of the rift basins, >1000 km from any continental margin, but may explain at least in part large basins, such as Songliao, of eastern China. The third driver, transtension, seem most likely to have been important only locally near large faults. Thus, orogenic collapse or some modification thereof (cf. Meng et al., 2003) seems a likely driver for regional extension in the Late Jurassic-Early Cretaceous.

Many basins of the Asian extensional system are petroliferous. Most notably, the Songliao basin contains Daqing oil field, the largest field in China (Li, this volume). In general, the prospectivity of basins in the province is directly related to basin size and thickness of fill. Basins with a greater history of accommodation host better developed lacustrine petroleum source-rock facies and greater burial facilitated maturation. Thus, the most continentward of the low-strain basins tend to be the least petroliferous, as do the relatively modest-thickness high-strain basins. High heat flow, typical of rift settings, somewhat offsets minimal burial in some basins: the deepest grabens of the EGB contain at most only 3 km of fill, yet are petroliferous (Johnson, 2004; Prost, 2004).

Many of the Asian basins contain numerous complicated, smallish structural traps (e.g., Erlian basin, Meng et al., 2003; Li, this volume), and erratically developed nonmarine reservoir facies and poor quality reservoir sand (Johnson and Graham, 2004b); hence reserves can be modest. In Songliao basin, however, the sequential history of early rift subsidence, optimum lacustrine source facies deposition, development of interleaved reservoir facies, inversion to enhance trapping, and burial maturation produced a world-class petroleum accumulation in Daqing field.

Acknowledgments

We acknowledge support by the member companies of the Stanford-China Industrial Affiliates Program; NSF grants EAR9315941 and EAR9708207 to Graham, an NSF grant, NSF Career Grant, and an ACS-PRF grant to Ritts. Nescor Energy and Roc Oil Company provided logistical support in Mongolia, and Roc Oil Company and the Petroleum Authority of Mongolia granted permission to publish seismic data. We appreciate helpful discussions with G.A. Davis, B. Darby, Zheng Yadong, A. Berry, G. Badarch, and D. Badamgarav.

References

Burchfiel, B.C., Cowan, D.S., Davis, G.A., 1992. Tectonic overview of the Cordilleran orogen in the western United States. In: Burchfiel, B.C., Lipman, P.W., Zoback, M.L. (Eds.), The Cordilleran orogen: Conterminous U.S. Geological Society of America Geology of North America G-3, pp. 407–479.

Darby, B.J., 2003. Mesozoic intraplate deformation in the east Asian tectonic collage: the enigmatic northwest Ordos region, China. Ph.D. dissertation, University of Southern California, 174.

Darby, B.J., 2004. The newly discovered Waziyu metamorphic core complex. Yiwulu Mountains, western Liaoning Province, north China. Earth Sci. Front. 11, 145–155.
Darby, B.J., Davis, G.A., Zheng, Y., 2001. Structural evolution of the southwestern Daqing Shan, Yinshan belt, Inner Mongolia, China. Geol. Soc. Mem. 194, 199–214.
Davis, G.A., Lister, G.S., Reynolds, S.J., 1986. Structural evolution of the Whipple and South Mountains shear zones, southwestern United States. Geology 14, 7–10.
Davis, G.A., Lister, G.S., 1988. Detachment faulting in continental extension; perspectives from the Southwestern U.S. Cordillera. In: Clark, S.P., Burchfiel, B.C., Suppe, J. (Eds.), Processes in continental lithospheric deformation. Geol. Soc. Am. Spec. Pap. 218, 133–159.
Davis, G.A., Qian, X., Zheng, Y., Yu, H., Wang, C., Tong, H.M., et al., 1996. Mesozoic deformation and plutonism in the Yunmeng Shan: a Chinese metamorphic core complex north of Beijing, China. In: Yin, A., Harrison, T.M. (Eds.) The Tectonic Evolution of Asia. Cambridge University Press, pp. 253–280.
Davis, G.A., Cong, W., Zheng, Y.D., Zhang, J.J., Zhang, C.H., Gehrels, G.E., 1998. The enigmatic Yinshan fold-and-thrust belt of northern China: new views on its intraplate contractional styles. Geology 26, 43–46.
Davis, G.A., Zheng, Y., Darby, B.J., Spell, T.L., 2002. Geometric and temporal evolution of an extensional detachment fault, Hohhot metamorphic core complex, Inner Mongolia, China. Geology 30, 1003–1006.
Davis, G.A., Zheng, Y., Wang, C., Darby, B.J., Zhang, C., Gehrels, G., 2001. Mesozoic tectonic evolution of the Yanshan fold and thrust belt, with emphasis on Hebei and Liaoning provinces, northern China. Geol. Soc. Am. Mem. 194, 171–197.
Dickinson, W.R., 2002. The Basin and Range Province as a composite extensional domain. Int. Geol. Rev. 44, 1–38.
Dou, L., 1997. The Lower Cretaceous petroleum system in NE China. J. Pet. Geol. 20, 475–488.
Friedmann, S.J., Burbank, D.W., 1995. Rift basins and supradetachment basins: intracontinental extensional end members. Basin Res. 7, 109–127.
Gawthorpe, R.L., Leeder, M.K., 2000. Tectono-sedimentary evolution of active extensional basins. Basin Res. 12, 195–218.
Graham, S.A., Hendrix, M.S., Johnson, C.L., Badamgarav, D., Badarch, G., Amory, J., et al., 2001. Sedimentary record and tectonic implications of late Mesozoic rifting, southeast Mongolia. Geol. Soc. Am. Bull. 113, 1560–1579.
Gries, R., 1983. North-south compression of Rocky Mountain foreland structures. In: Lowell, J.D. (Ed.), Rocky Mountain Foreland Basins and Uplifts. Rocky Mountain Association of Geologists, pp. 9–32.
Hendrix, M.S., Graham, S.A., Carroll, A.R., Sobel, E.R., McKnight, C.L., Schulein, B.J., et al., 1992. Sedimentary record and climatic implications of recurrent deformation in the Tian Shan: evidence from Mesozoic strata of the north Tarim, south Junggar and Turpan basins, northwest China. Geol. Soc. Am. Bull. 104, 53–79.
Hendrix, M.S., Graham, S.A., Amory, J.Y., Badarch, G., 1996. Noyon Uul (King Mountain) syncline, southern Mongolia: early Mesozoic sedimentary record of the tectonic amalgamation of central Asia. Geol. Soc. Am. Bull. 108, 1256–1274.
Hendrix, M.S., Beck, M.A., Badarch, G., Graham, S.A., 2001. Triassic synorogenic sedimentation in southern Mongolia: Early effects of intracontinental deformation. Geol. Soc. Am. Mem. 194, 413–434.
Johnson, C.L., 2004. Polyphase evolution of the East Gobi basin: sedimentary and structural records of Mesozoic-Cenozoic intraplate deformation in Mongolia. Basin Res. 16, 79–100.
Johnson, C.L., Graham, S.A., 2004a. Sedimentology and reservoir architecture of a synrift lacustrine delta, southeastern Mongolia. J. Sediment. Res. 74, 770–785.
Johnson, C.L., Graham, S.A., 2004b. Cycles in perilacustrine facies of Upper Mesozoic rift basins, southeastern Mongolia. J. Sediment. Res. 74, 786–804.

Johnson, C.L., Webb, L.E., Graham, S.A., Hendrix, M.S., Badarch, G., 2001. Sedimentary and structural records of late Mesozoic high-strain extension and strain partitioning, East Gobi basin, southern Mongolia. In: Hendrix, M.S., Davis, G.A. (Eds.), Paleozoic and Mesozoic tectonic evolution of central and eastern Asia. Geological Society of America Memoir 194, pp. 413–434.

Johnson, C.L., Greene, T.J., Zinniker, D.A., Moldowan, M.J., Hendrix, M.S., Carroll, A.R., 2003. Geochemical characteristics and correlation of oil and nonmarine source rocks from Mongolia. AAPG Bull. 87, 817–846.

Kimura, G., Tasaki, T., Kono, M., 1990. Mesozoic collisional extrusion tectonics in eastern Asia. Tectonophysics 181, 15–23.

Lamb, M.A., Badarch, G., 1997. Paleozoic sedimentary basins and volcanic-arc systems of southern Mongolia; new stratigraphic and sedimentologic constraints. Int. Geol. Rev. 39, 542–576.

Lamb, M.A., Hanson, A.D., Graham, S.A., Badarch, G., Webb, L.E., 1999. Left-lateral sense offset of upper Proterozoic to Paleozoic features across the Gobi Onon, Tost, and Zuunbayan faults in southern Mongolia and implications for other Central Asian faults. Earth Planet. Sci. Lett. 173, 183–194.

Lister, G.S., Davis, G.A., 1989. The origin of metamorphic core complexes and detachment faults formed during Tertiary continental extension in the northern Colorado River region, U.S.A. J. Struct. Geol. 11, 65–94.

Li, S., Li, B., Yang, S., Huang, J., Li, Z., 1984. Sedimentation and tectonic evolution of late Mesozoic faulted coal basins in north-eastern China. In: Rahmani, R.A., Flores, R.M. (Eds.), Special Publication of the International Association of Sedimentologists 7, pp. 387–406.

Li, S., Mo, X., Yang, S., 1995. Evolution of Circum-Pacific basins and volcanic belts in East China and their geodynamic background. J. China Univ. Geosci. 6, 48–58.

Lin, C., Eriksson, K., Li, S., Wan, Y., Ren, J., Zhang, Y., 2001. Sequence architecture, depositional systems, and controls on development of lacustrine basin fills in part of the Erlian Basin, Northeast China. AAPG Bull. 85, 2017–2043.

Meng, Q.R., 2003. What drove late Mesozoic extension of the north China – Mongolia tract? Tectonophysics 369, 155–174.

Meng, Q.R., Hu, J.M., Jin, J.Q., Zhang, Y., Xu, D.F., 2003. Tectonics of the late Mesozoic wide extensional basins system in the China-Mongolia border region. Basin Res. 15, 397–415.

Niu, B., He, Z., Song, B., Ren, J., 2003. Zhangjiakou Group volcanic rock SHRIMP age and significance. Geol. Bull. China 22, 140–141.

Prost, G.L., 2004. Tectonics and hydrocarbon systems of the East Gobi basin, Mongolia. AAPG Bull. 88, 483–514.

Ren, J., Li, S., 1998. Comparison between the faulted basin system in northeastern Asia and the extension of the Basin and Range Province in western North America: Dizhi Keji Qingbao. Geol. Sci. Technol. Inf. 17, 7–11.

Ren, J., Tamaki, K., Li, S., Zhang, J., 2002. Late Mesozoic and Cenozoic rifting and its dynamic setting in eastern China and adjacent areas. Tectonophysics 344, 175–205.

Ritts, B.D., Berry, A.K., Johnson, C.L., Darby, B.J., Davis, G.A., 2010. Early Cretaceous supradetachment basins in the Hohhot metamorphic core complex. Inner Mongolia, China. Basin Res. 22, 45–60.

Swisher III, C.C., Wang, Y., Wang, X., Xu, X., Wang, Y., 1999. Cretaceous age for the feathered dinosaurs of Liaoning, China. Nature 400 (6739), 58–61.

Traynor, J.J., Sladen, C., 1995. Tectonic and stratigraphic evolution of the Mongolian People's Republic and its influence on hydrocarbon geology and potential. Mar. Pet. Geol. 12, 35–52.

Van der Beek, P., Delvaux, D., Andreissen, P., Levi, K., 1996. Early Cretaceous denudation related to convergent tectonics in the Baikal region, southeast Siberia. J. Geol. Soc. 153, 515–523.

Watson, M.P., Hayward, A.B., Parkinson, D.N., Zhang, Z.M., 1987. Plate tectonic history, basin development, and petroleum source rock deposition, onshore China. Mar. Petrol. Geol. 4, 205–225.

Webb, L.E., Graham, S.A., Johnson, C.L., Badarch, G., Hendrix, M.S., 1999. Occurrence, age, and implications of the Yagan-Onch Hayrhan metamorphic core complex, southern Mongolia. Geology 27, 143–146.

Xue, L., Galloway, W.E., 1993. Genetic sequence stratigraphic framework, depositional style, and hydrocarbon occurrence of the Upper Cretaceous QYN formations in the Songliao lacustrine basin, northeastern China. AAPG Bull. 77, 1792–1808.

Yanshin, A.L., 1989. 1:1,500,000 Map of Geologic Formations of the Mongolian People's Republic. Academia Nauka USSR, 2 sheets.

Zhang, J., Zheng, Y., 1999. Multistage extension and age dating of the Xiaoqinling metamorphic core complex, central China. Acta Geol. Sinica 73, 139–147.

Zhang, Z.M., Liou, J.G., Coleman, R., 1984. An outline of the plate tectonics of China. Geol. Soc. Am. Bull. 95, 295–312.

Zheng, Y., Zhang, Q., 1993. The Yagan metamorphic core complex and extensional detachment fault in Inner Mongolia. Acta Geol. Sinica 67, 301–309.

Zheng, Y., Wang, S., Wang, Y., 1991. An enormous thrust nappe and extensional metamorphic core complex in Sino-Mongolian boundary area. Sci. China B 34, 1145–1152.

Zhou, Z., Barrett, P., Hilton, J., 2003. An exceptionally preserved Lower Cretaceous ecosystem. Nature 421, 807–814.

Zorin, Y.A., 1999. Geodynamics of the western part of the Mongolia-Okhotsk collisional belt, Trans-Baikal region (Russia) and Mongolia. Tectonophysics 306, 33–56.

In this chapter

18

Songliao/Erlian rifts

Li Desheng
Chinese Academy of Geosciences, 20 Institution Road, P.O. Box 910, Beijing, China

18.1 Introduction

In the Early Paleozoic, the area of N.E. China was an open sea between the Siberian and Sino-Korean cratons. During the Middle and Late Paleozoic, the sea of central Asia and Mongolia retreated as the Siberian and Sino-Korean cratons converged involving subduction beneath each craton. The resulting Paleozoic fold belts between the Siberian and Sino-Korean cratons are characterized by elongated southwardly convex anticlinoria and synclinoria (Fig. 18.1) involving complex flysch and volcanic formations which formed the new basement of the region.

At the end of Jurassic, the Kula plate began to subduct toward the northwest and underneath the Eurasia plate. Due to the tensile stresses associated with rising mantle, a series of Mesozoic rifts were formed, such as the Songliao rift, the Erlian rift, and the Hailaer rift (Fig. 18.2). The regional geology and tectonic regime of these basins are summarized in Table 18.1.

18.2 The Songliao Basin

The Songliao basin covers an area of 260,000 km^2 in the northeast part of China and is one of the world's most prolific oil and gas producing basins (Fig. 18.3). The basin is a Mesozoic intraplate rift depression which overlies basement composed of Paleozoic metamorphic rocks intruded by Hercynian granites. The depth to the Moho ranges from about 27 km beneath the depression to more than 35 km below the surrounding mountains. The deep-seated mantle high beneath the Songliao Basin strikes NNE and coincides with the overlying Cretaceous depression (Fig. 18.4).

The tectonic evolutionary stages for the Songliao basin can be described as follows (Fig. 18.5):

1. *Hercynian basement formation:* The Hercynian movements of the late Paleozoic created large-scale crustal uplifts that were associated with strong magmatic activity primarily involving the emplacement of granites.

Phanerozoic Rift Systems and Sedimentary Basins DOI: 10.1016/B978-0-444-56356-9.00017-1

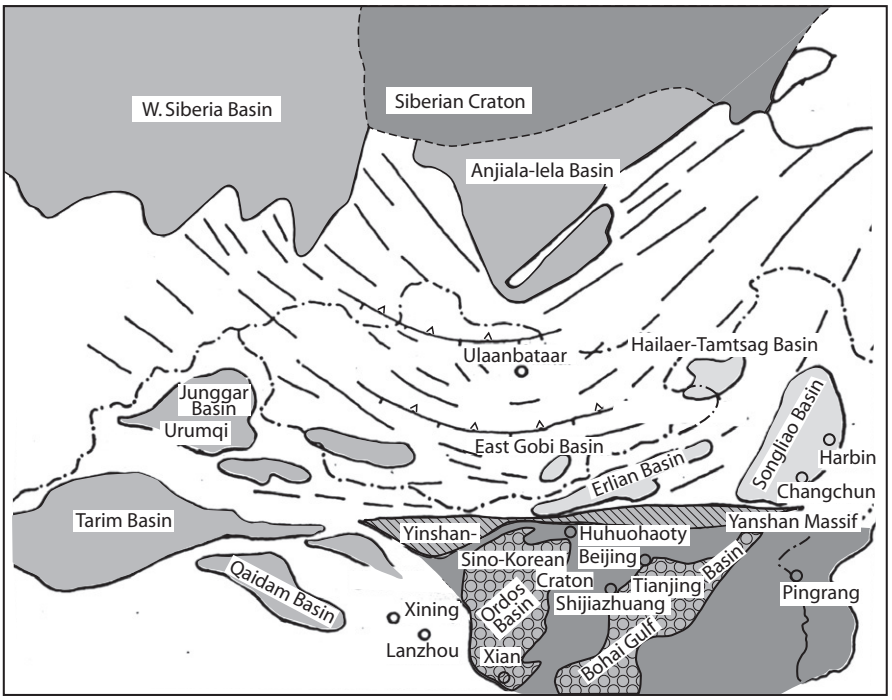

Figure 18.1
Tectonic outline between Siberian and Sino-Koran craton *(after Fei Baosheng et al., 1994, modified).*

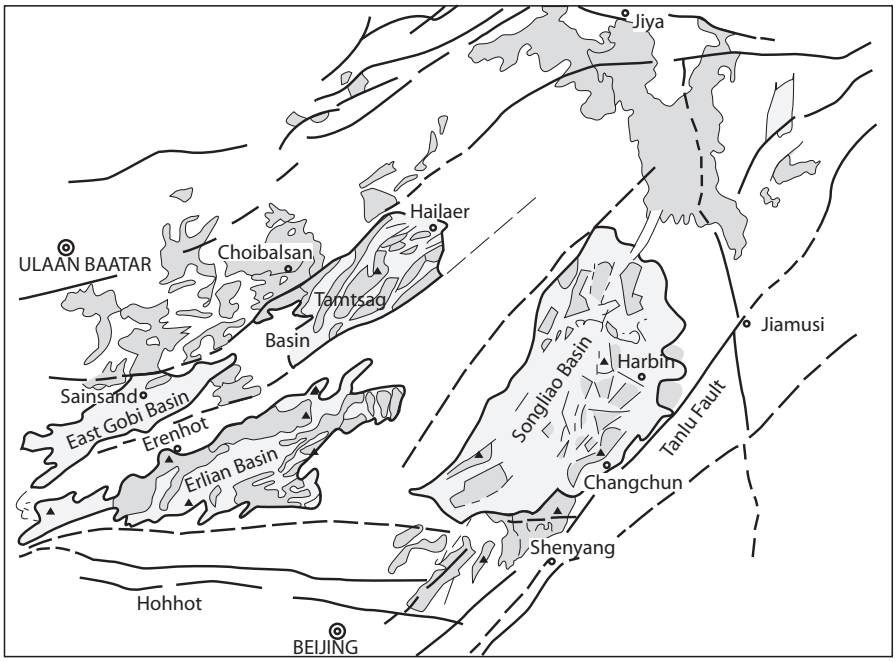

Figure 18.2
Mesozoic rifts of northeastern China and Mongolia *(after Hu Jianyi et al., 1944, modified).*

Table 18.1 Regional structural features of the Mesozoic rift basins of Northeastern China and Mongolia

Basin Name	Songliao	Erlian	Hailear
Area (10^4 km^2)	26	10	4
Morphology	Plain, grassland	Desert, grassland	Grassland
Basement	Pz folded	Pz folded	Pz folded
Sedimentray overburdens	J, K, R, Q	J, K, R, Q	J, K, R, Q
Thickness of sediments (km)	4–6	3–5	3–5
Magnetic features	Broad, positive	NEE trend positive	NE trend positive
Gravity features (mgal)	Bouguer 10–20	Bouguer −60∼−140	Bouguer −50∼−70
Crustal thickness (km)	27–35	42–44	41–43
Geothemal gradient (°C/km)	35–40	25–40	26–30
Magmatic activities	Q basalt	Mz, Kz basalts	Q basalt
Earthquakes	Weak	Weak	Weak
HC-Bearing strata	k_1	k_1	k_1
Basin structural type	Mz rift	Mz rift	Mz rift

2. *Rift stage:* During the Late Jurassic and Early Cretaceous, extensional stresses induced block faulting at the junctures of different tectonic units during the Yanshanian phase. This resulted in the formation of a series of crustal fracture systems which subsequently evolved into numerous, discrete rifts of varying sizes (Fig. 18.6).
3. *Sag stage:* Rapid subsidence during the Early and Late Cretaceous led to the deposition of interbedded sand and petroliferous shale sequences of deltaic origin, as well as shallow and deep lacustrine facies (Fig. 18.7).
4. *Inversion stage:* Near the end of the Late Cretaceous, the Sea of Japan began to open, thus inducing compressional stresses. These exerted a strong influence on the Songliao Basin resulting in inversion forming alternating anticlinal and synclinal trends. The area of the lacustrine basin was significantly reduced and elevated to its present topographic position.

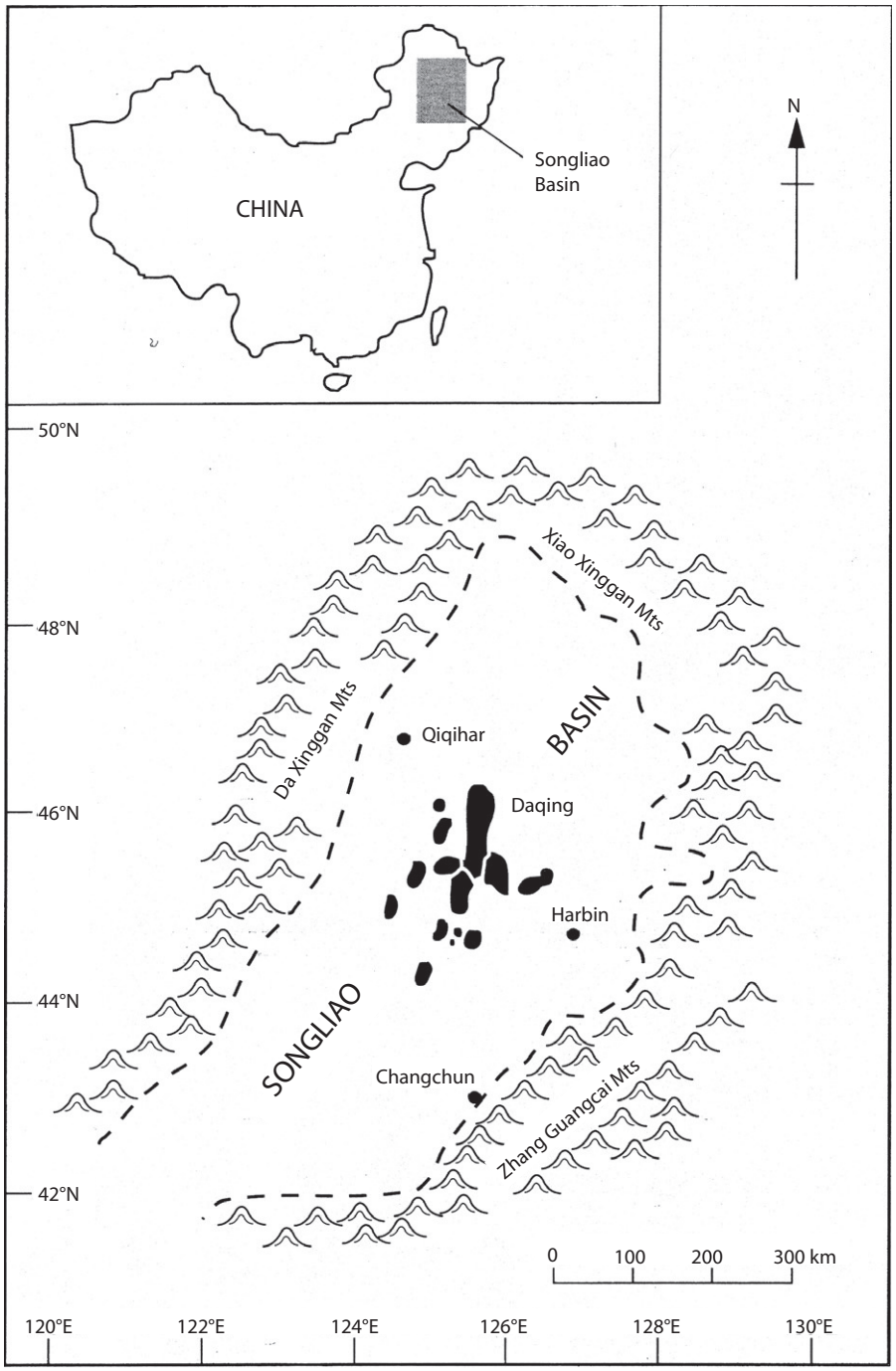

Figure 18.3 The location of the Songliao Basin.

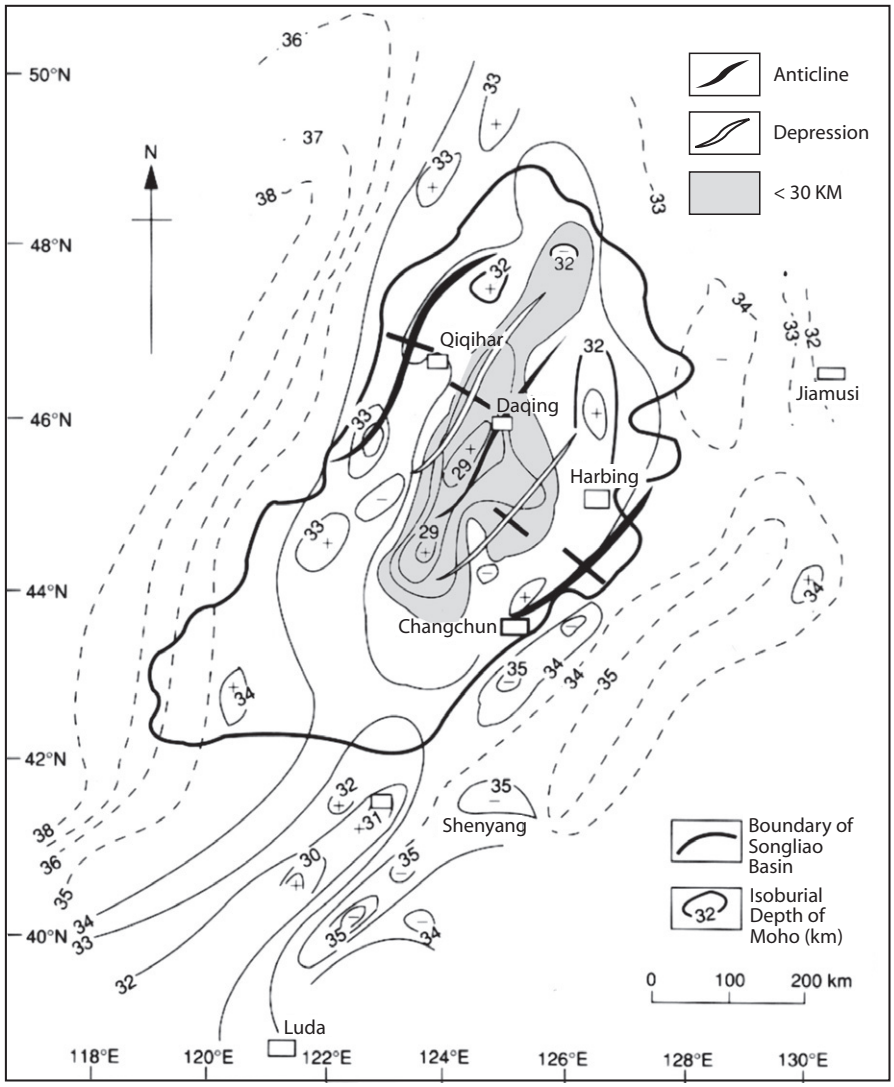

Figure 18.4
Depth to Moho in the Songliao Basin and its surrounding areas.

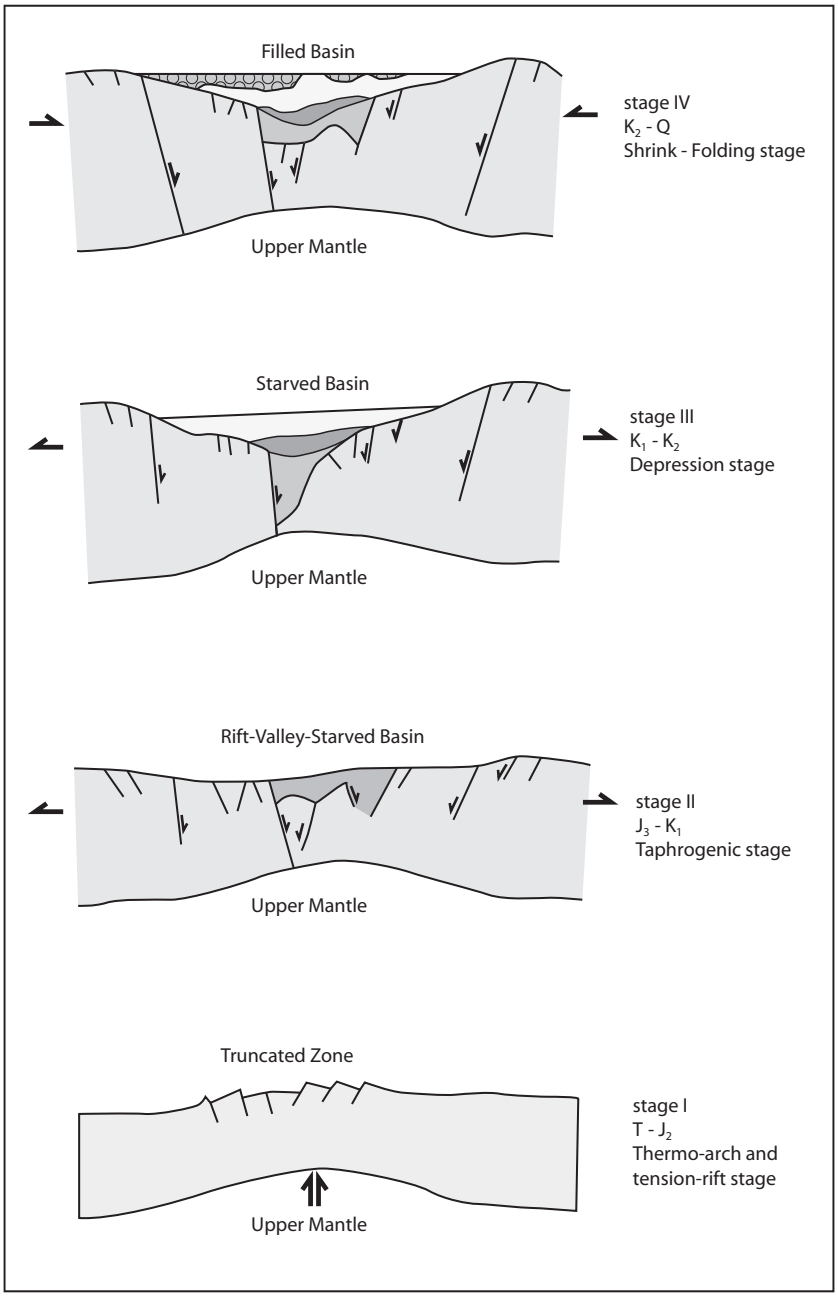

Figure 18.5
Tectonic evolution of Songliao basin.

Figure 18.6
Location of the Jurassic rifts in the Songliao area.

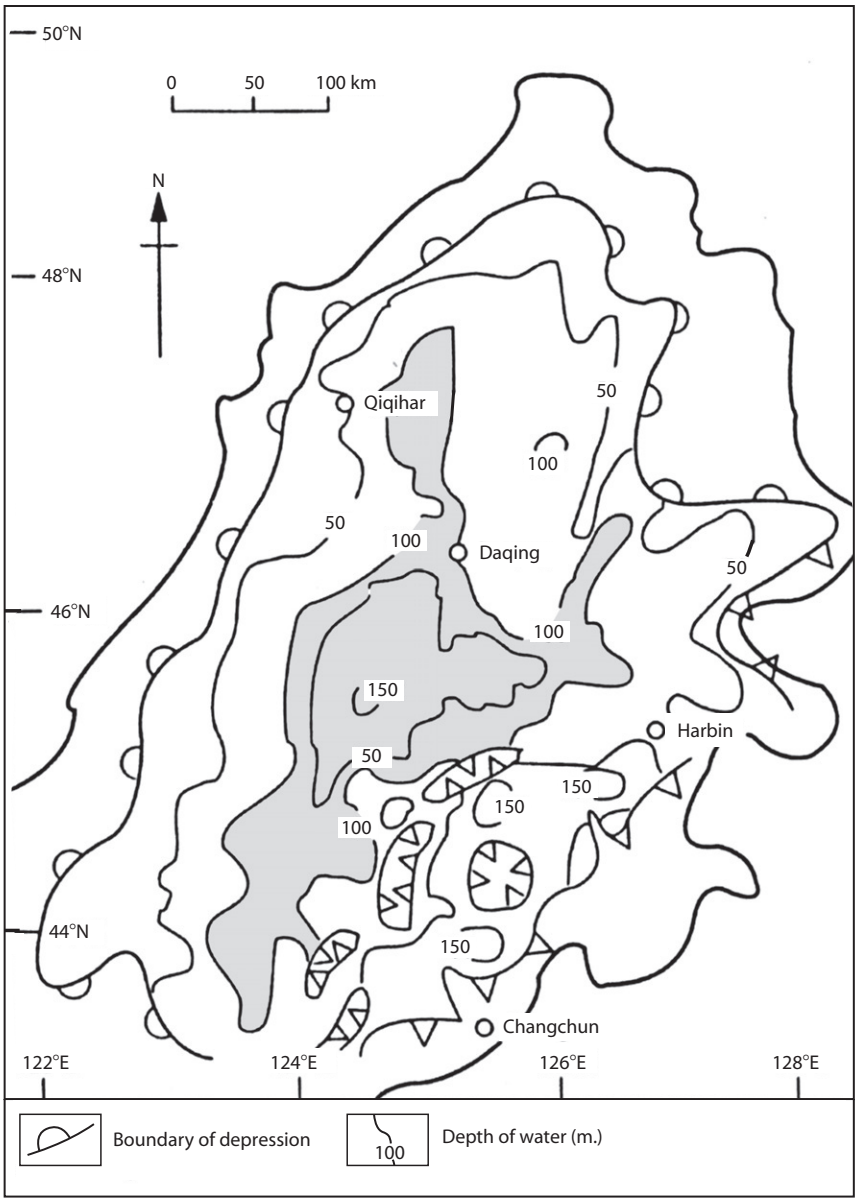

Figure 18.7
Location of the Lower Cretaceous basin.

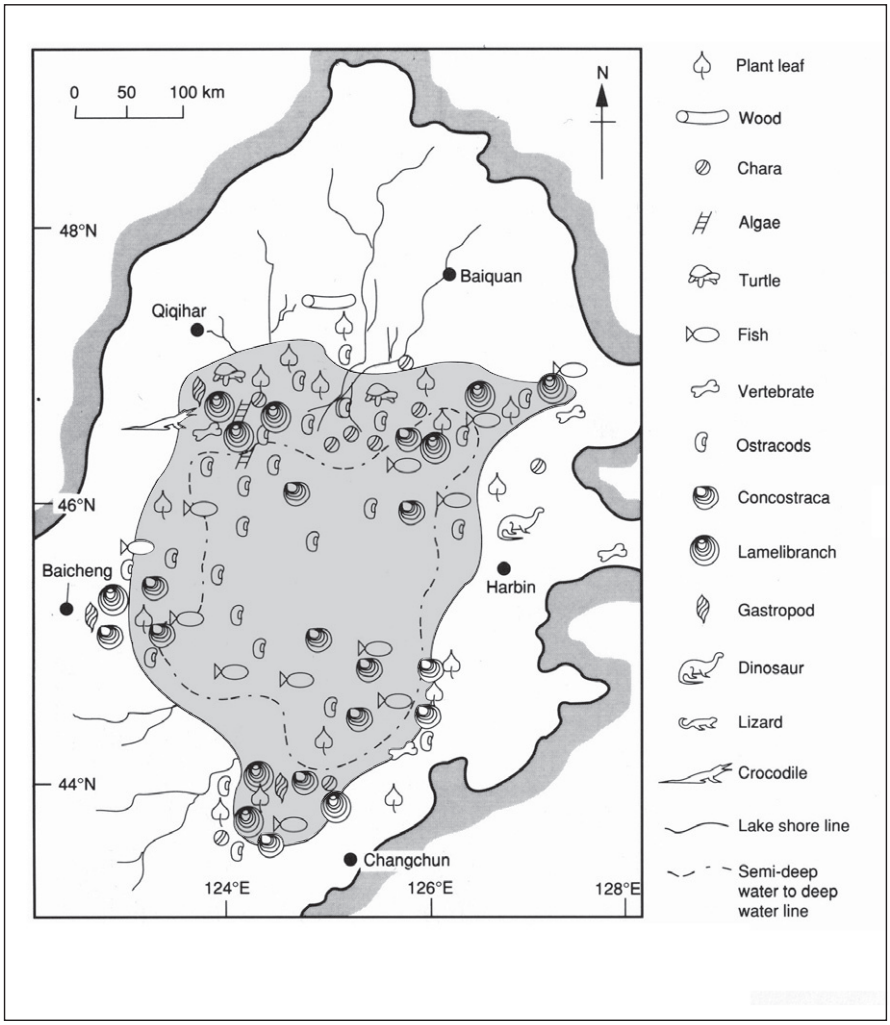

Figure 18.8 Faunal distribution during deposition of the Lower Cretaceous Qingshankou Formation.

Fossils are very abundant in all the strata and include continental and aquatic plants, continental and amphibious animals such as dinosaurs, lizards, turtles, and insects, and great numbers of aquatic organisms such as conchostraca, chara, gastropods, and ostracods. Some genera of lamellibranchs, fish, and algae (Fig. 18.8) lived in both shallow and deep lakes. No marine fossils have been found in the Cretaceous formations of the Songliao Basin which were deposited in fresh to brackish water lacustrine environments.

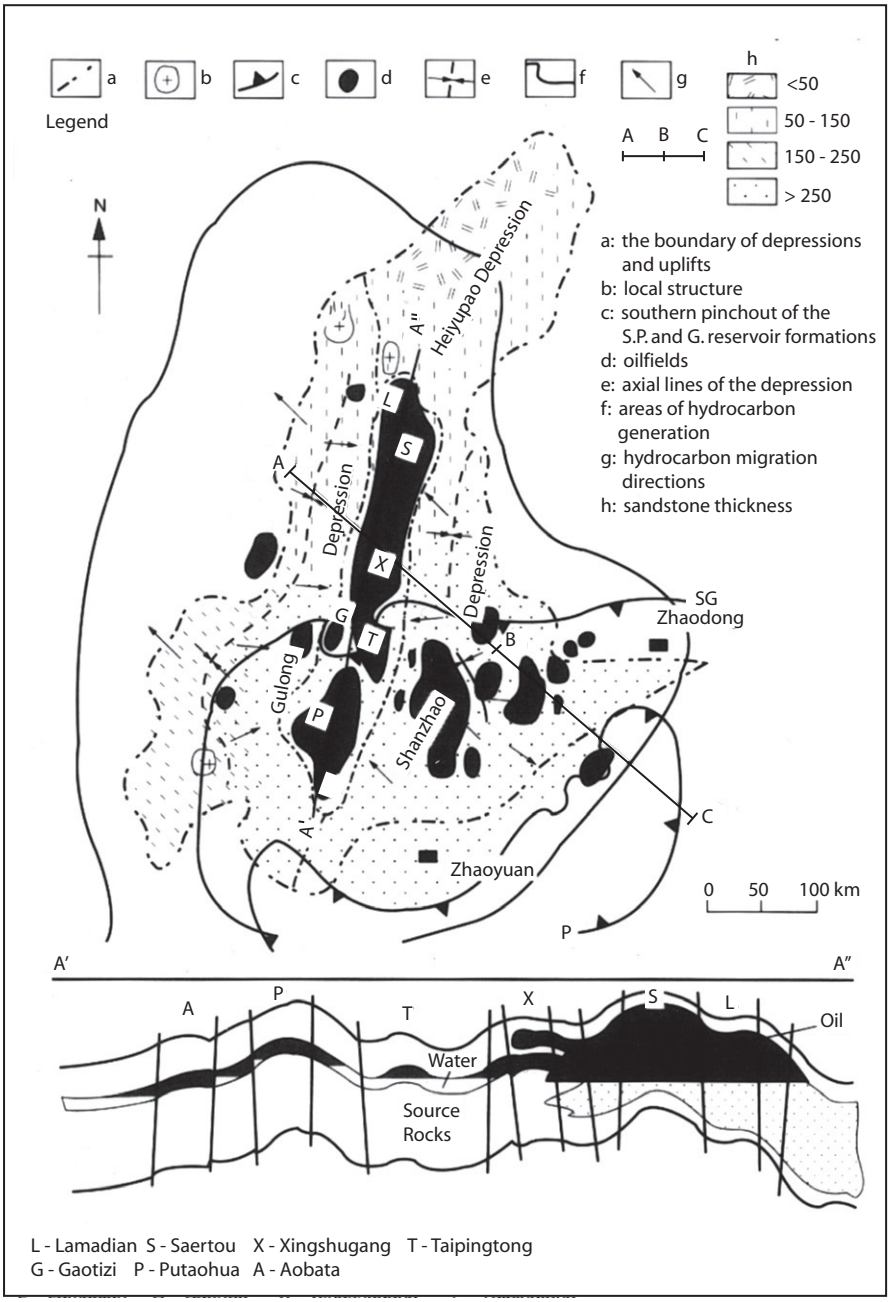

Figure 18.9
Geography of the Supergiant Daqing oilfield.

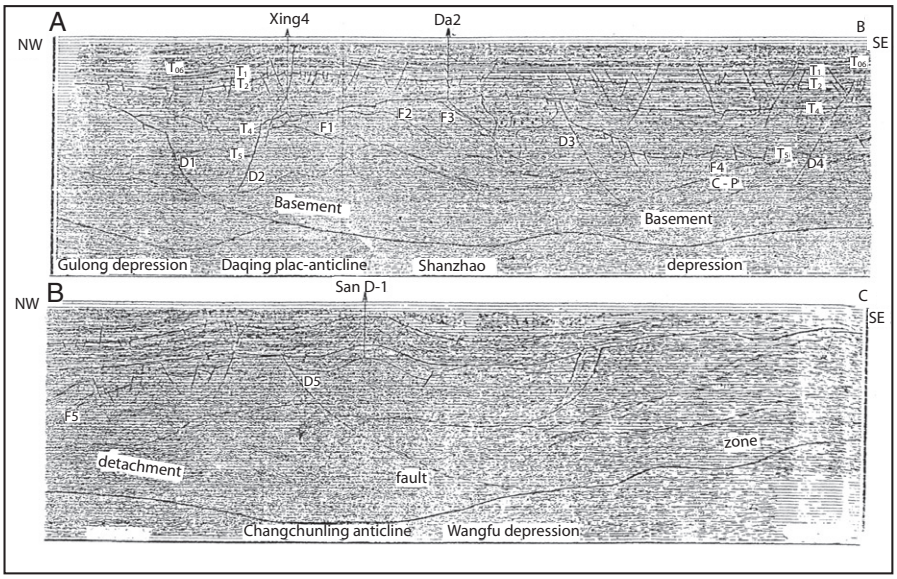

Figure 18.10 Regional seismic profile across Songliao Basin Line 85-Songl *(after Wu Qizhi et al., 1997)* location in Fig. 18.8.

Hydrocarbon accumulations in the Songliao Basin

Large-scale domal anticlines are the most important hydrocarbon traps. For example, the giant Daqing oilfield, located in the center of the Songliao Basin, is a domal anticline belt striking 15°NE, about 140 km long and 20–30 km wide (Figs. 18.9–18.11). There are 7 aligned domal structures (from north to south: Lamadian, Saerto, Xingshugang, Taipingtong, Gaotaizi, Putaohua, and Aobaota) within a total area of 2000 km^2 with a 600 m high closure. The discovery well, Songj1-3, tested 20 tons/day (140 bbl/day) of crude oil on 26 September 1959. Another discovery well, Sa-66, tested a higher flow rate of 200 tons/day (1400 bbl/day) on 11 March 1960. As a result, a 41 km^2 pilot development area was put into production in June 1960. Since then, a 920 km^2 proven area, including the Saerto, Xingshugang, and Lamadian oilfields, has been progressively developed. The peak production of 50 million tons/a (1 million bbl/day) has been maintained from 1976 to the present. Cumulative oil production to the end of 2002 was 1.72 billion tons (12 billion bbl).

Figure 18.12 shows that oil-bearing reservoirs of the Daqing oilfield can be divided into three main groups, the lower Albian Saerto and Putaohua reservoir groups, and the upper Aptian Gaotaizi reservoir group. Within the Saerto and Putaohua groups, there are 5 reservoir sandstone zones (S1, S2, S3, P1, and P2), 14 reservoir sandstone subzones, and 45 individual sandstone beds. The pay thickness of the reservoir sandstone zones is 30–40 m in the Lamadian oilfield, 20–30 m in the Saerto oilfield, and 10–20 m in the Xingshugang oilfield. Stratigraphic analysis shows that each sandstone bed thins from north to south, interfingering with the adjacent source rocks.

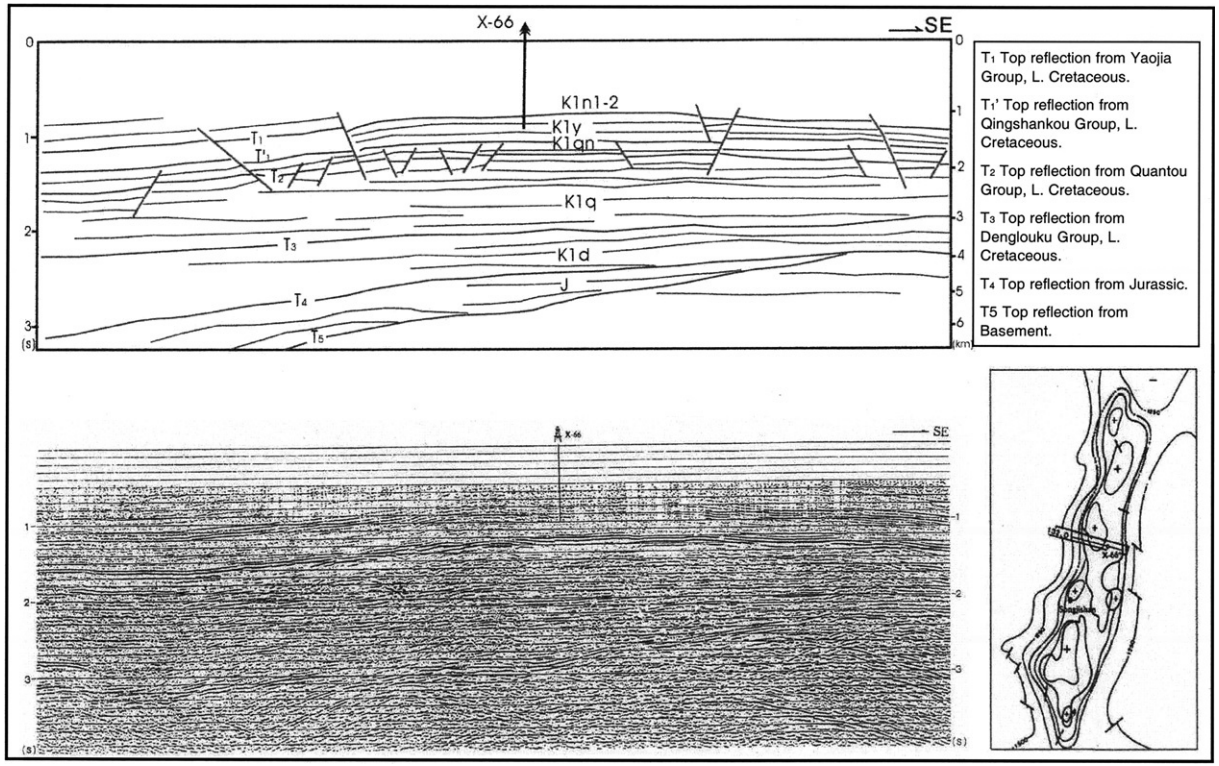

Figure 18.11
Seismic profile across Daqing-Xingshugang plac-anticline Line 132.0. X: Location Xingshugang oil field (see Fig. 18.9).

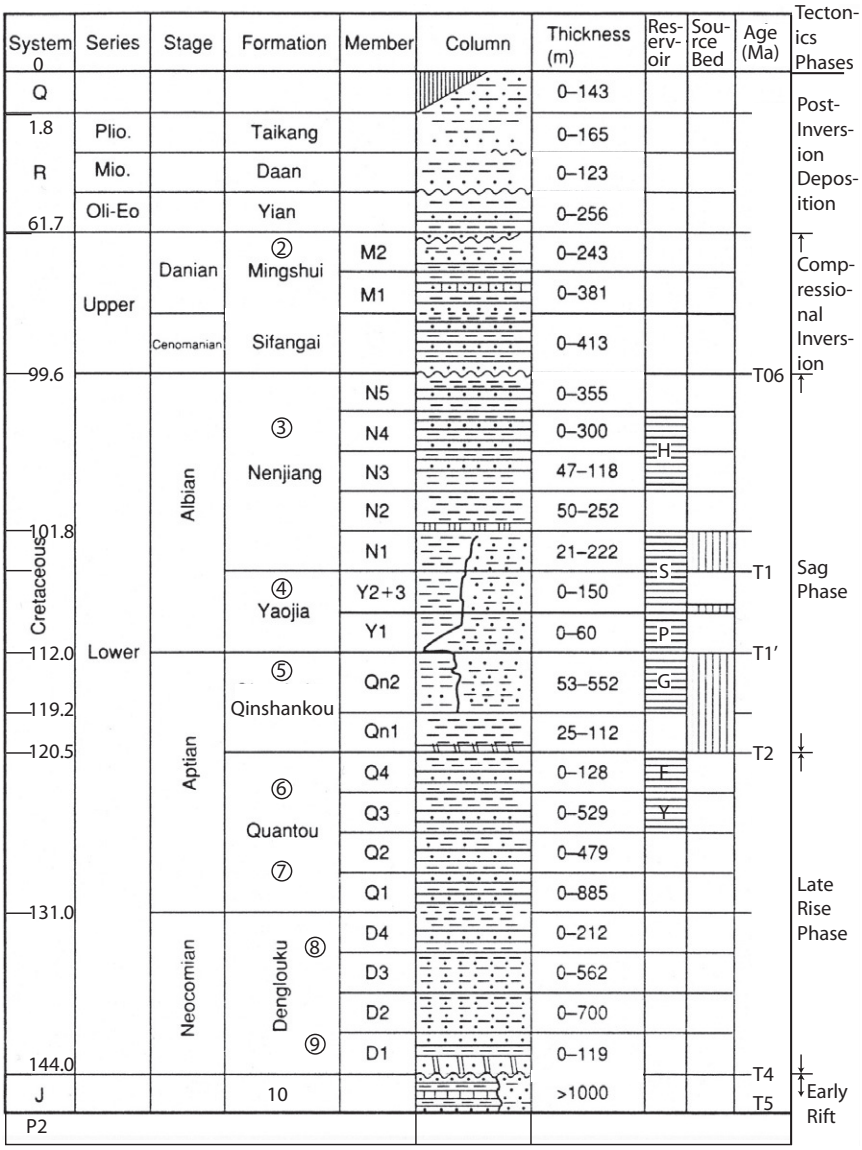

Figure 18.12 The lower Cretaceous reservoir formations in the Songliao basin.

Table 18.2 Average porosity and permeability of the reservoir sandstone zones of Daqing oilfield

Reservoir sandstone zone	Average porosity (%)	Average permeability (md)
S1	26.7	552
S2	27.7	880
S3	27.8	519
P1	27.2	973
P2	26.6	562

The average porosity and permeability of the 5 reservoir sandstone zones are shown in Table 18.2. The reservoir sandstones are mainly fine-grained sandstones with subrounded to subangular grains and a typical mineral composition of 30–35% quartz, 35–40% feldspar, and 10% matrix fragments. Cement contributes 5–10% clay and 1–5% calcareous minerals.

Crude oil properties include a specific gravity (d_4^{20}) of 0.8593 (API 33°) in the axial part of the domal anticline and 0.8658 (API 32°) on the flanks of the structure. The viscosity at 50 °C is 18 cp in the axial part of the structure and 23.3 cp on the flank, while the pour point is 25 °C. The oils are high wax sweet crude, with a wax content of 27.7%, a sulfur content of 0.055%, and a salt content of 31.6 mg/L.

18.3 The Erlian Basin

The Erlian Basin is a Mesozoic rift, located in the mid-northern part of the Inner Mongolia Autonomous Region of China. To its east are the Daxingan mountains, to the south are the Yinshan mountains, and to the north is the China-Mongolia international boundary. The basin is about 1000 km long, about 220 km wide and its areal extent is about 10×10^4 km^2. The sedimentary thickness of the Mesozoic and Cenozoic is about 2000–6000 m. There are five depressions (Manite, Wulanchabu, Chuanjing, Wunite, and Tenggeer) and one uplift (Sunite), dissected by many normal faults into 53 sags and 21 swells (Fig. 18.13). Since 1981, 11 oilfields have been found in the Erlian Basin. They range in size from middle to small, with a proven area total of 190 km^2 and proven reserves (in place) total 200 million tons. Since 1990, annual oil production reached 1 million tons (or 20,000 bopd) with cumulative oil production of 13.73 million tons to the end of 2002.

The Erlian Basin is located in the transitional area between the Sino-Korean and Siberian cratons. It is a composite Mesozoic rift system located between these two cratons. The basement underlying the Erlian basin consists of lower Paleozoic metamorphic and deformed, imbricated Permo-Carboniferous sediments and volcanics. The rift fill consists Jurassic of lower and middle early Cretaceous clastics, overlain by an upper early Cretaceous sag basin (Fig. 18.14).

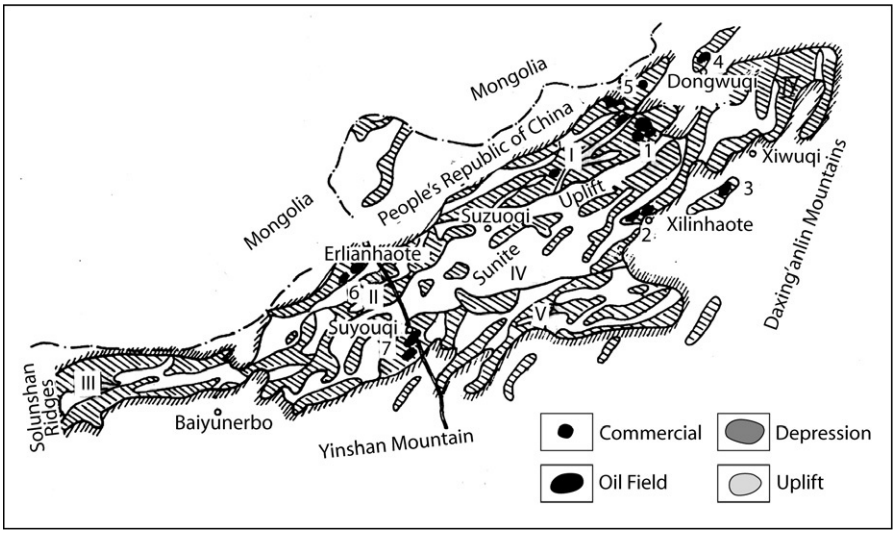

Figure 18.13 The tectonic units and the oilfields of the Erlian basin.

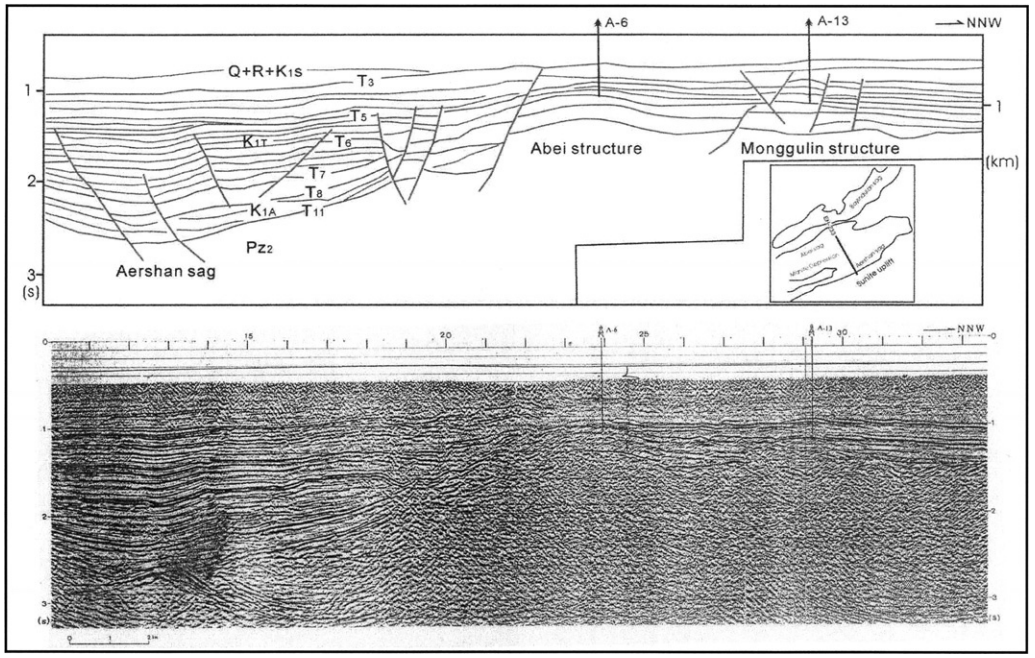

Figure 18.14
Seismic Profile Line EH-323 cross Manite Depression. Erlian basin.

According to the characteristics of its sediments, igneous activity, structural development, and isotope age, the evolution of this basin can be divided into four phases:

1. Triassic plate collision period: During the Indosinian orogeny, the Sino-Korean craton and Siberian plate collided again, forming east-west trending ramps, nappes, and folds. Beyond the end of the Triassic, regional uplift continued, so that most of the Triassic sediments are now absent in this area.
2. Early and middle Jurassic conversion period: During the Early and middle Jurassic, the Paleo-Asian tectonic regime ended, and the Pacific tectonic regime began. Deposition of the Early and middle Jurassic of Erlian Basin was controlled by syn-depositional normal faults that re-activated earlier reverse faults.
3. Upper Jurassic and lower Cretaceous rifting period: During the upper Jurassic and lower Cretaceous, major rifts formed. The rifting is divided into 2 stages: that is, (a) an early faulted depression and infilling stage and (b) a later phase of strong faulting associated with the formation of a deep lake.
4. Upper Cretaceous inversion and uplift period: In the Late Cretaceous, the Songliao basin continued to subside. The source rocks in the above two basins are older in the west and younger in the east. Pacific plate subduction lasted from the Late Cretaceous into the Cenozoic.

Twenty-nine sags in the Erlian Basin have been drilled and 19 of them are proven to have good hydrocarbon generation conditions. Commercial oil has been found in nine sags, that is, the Anan, Saihantala, Erennaoer, Jiergalangtu, Abei, Bayindula, Wuliyastai, Honghaoershute, and Hurenbug sags, in 20 petroliferous structures (Fig. 18.13).

Because of its complex tectonic evolution, there are several trap types in the Erlian Basin. The main trap types are structural including anticline and fault blocks. Other trap types include buried-hill traps, stratigraphic traps, and structural-lithologic traps. The various types of reservoir rocks in this basin include sandstones, conglomerates, andesites, tuffs, and metamorphics, but sandstones and conglomerates are the main reservoirs.

Further reading

Dou, L.R., Chang, L., 2003. Fault linkage patterns and their control on the formation of petroleum systems of the Erlian basin, eastern China. Mar. Pet. Geol., 20, 1213–1224.

Fei , B., (2002). Tectonic characteristics and Hydrocarbon habitats in Erlian Basin, China. In: Li, D., et al. (Eds.), Tectonics of Petroleum Basin in China, pp. 386–409 (in Chinese).

Golonka, J., Krobicki, M., Pajak, J., Giange, N. V., Zuchiewicz, W., 2006. Global Plate Tectonics and Paleogeography of Southeast Asia . AGH University of Science and Technology, Arkadia, pp. 1– 127.

Hu, W., Cai, C., Wu, Z., Li, J., 1998. Structural style and its relation to hydrocarbon exploration in the Songliao Basin, northeast China. Mar. Pet. Geol., 15, 41–55.

Hu, W.S., Lu, B.Q., Zhang, W.J., Mao, Z.G., Leng, J., Guan, D.Y., 2005. An approach to the tectonic evolution and dynamics of Songliao basin. Chin. J. Geol., 40, 16–31 (in Chinese).

Li, D., 1987. Geological characteristics of hydrocarbon generation and distribution in the Songliao basin, China. In: Kumar, P.K., Dwivedi, P., Banerjie, V., Gupta, V. (Eds.), Petroleum Geochemistry and Exploration in the Afro-Asian Region. Balkema, Rotterdam, pp. 191–195.

Li, D., 1995a. Hydrocarbon Habitat in the Songliao rift basin, China. In: Lambiase, J.J. (Ed.), Hydrocarbon Habitat in Rift Basins. Geol. Soc. Spec. Publ., 80, 317–329.

Li, D., 1995b. Petroleum Generation in the Nonmarine Qingshankou formation (Lower Cretaceous), Songliao Basin, China. In: Lambiase, J.J. (Ed.), Petroleum Source Rocks. Springer-Verlag, Germany, pp. 131–148.

Li, J.Y., 2006. Permian geodynamic setting of Northeast China and adjacent regions: closure of the Paleo-Asian Ocean and subduction of Paleo-Pacific Plate. J. Asian Earth Sci., 26, 207–224.

Liang, S., 2002. The evolution of inner Mongolia rifts and petroleum systems. In: Li, D., et al. (Eds.), Tectonics of Petroleum Basin in China, pp. 372–385 (in Chinese).

Liu, H., 1986. Geodynamic scenario and structural styles of Mesozoic and Cenozoic Basins in China. AAPG Bull., 70, 377–395.

Liu, J., 2001. Cenozoic episodic volcanism and continental rifting in northeast China and possible link to Japan Sea development as revealed from K-Ar chronology. Tectonophysics, 339, 385–401.

Ren, J., Liwei X., 2002. Tectonics of petroleum-bearing regions on the continent of China. Episodes, 25 (4), 227–235.

Ren, J., Tamaki, K., Li, S.T., Zhang, J.X., 2002. Late Mesozoic and Cenozoic rifting and its dynamic setting in Eastern China and adjacent areas. Tectonophysics, 344, 175–205.

Sha, J., Hirano, H., Yao, X., Pan, Y., 2008. Late Mesozoic transgressions of eastern Heilogjiang and their significance in tectonics, in coal and oil accumulation in northeast China. Paleogeogr. Paleoclimatol. Paleoecolo., 263, 119–130.

Wang, F., Zhou, X.-H., Zhang, L.C., Ying J.-F., Zhang, Y.-T., Wu, F.-Y., Zhu, R.-X., 2006 . Late Mesozoic volcanism in the Great Xing'an Range (NE China): Timing and implications for the dynamic setting of NE- Asia. Earth Planet. Sci. Lett., 251,179–198.

Wei, H-H., Liu, J.-L., Meng, Q-R., 2010. Structural and sedimentary evolution of the southern Songliao Basin, northeast China, and implications for hydrocarbon prospectivity. AAPG Bull. 94, 533–566.

Wu, Q., 1997. Tectonic Evolution and Hydrocarbon Accumulation of Petroliferous Basins in China. Petroleum Industry Press, p. 80 (in Chinese).

Yang, W., Li, Y., Gao, R., 1985. Formation and evolution of non-marine petroleum in Songliao basin, China. AAPG Bull., 69, 1112–1122.

Zhang, F.Q., Chen, H.L., Yu, X., Dong, C.W., Yang S.F., Pang, Y.M., Batt, G.E., (2010). Early Cretaceous volcanism in the northern Songliao Basin, NE. China, and its geodynamic implication. Gondwana Res., 19,163–176.

In this chapter

19

Inverted rift-basins of northern Egypt

T.G. Bevan, A.R. Moustafa†*
*BP Exploration (Alpha) Ltd., Mumbai, India
†Department of Geology, Ain Shams University, Cairo, Egypt

19.1 Introduction

Mesozoic extensional rift-basins in northern Egypt are part of the greater Tethyan passive margin (Guiraud, 1998; Guiraud and Bosworth, 1999; Keeley, 1994). Within the overall northward-thickening passive margin sequences, several discrete E–W to ENE–WSW oriented half-graben basins initiated in the Jurassic and continued to subside through the Cretaceous, such as the Abu Gharadig, Alamein, Matruh, and Shoushan basins (Fig. 19.1).

The Jurassic–Cretaceous extensional basins of northern Egypt cover an area that was termed the "Unstable Shelf" by Said (1962). To the south of this basinal area lies the "Stable Shelf," which is characterized by predominantly continental sediments of Mesozoic to Paleozoic age that overlie relatively shallow Precambrian basement (Fig. 19.1). The boundary between these provinces lies between the Abu Gharadig Basin and the Bahariya Ridge indicated by gravity, magnetic, seismic, and borehole data. However, more isolated Mesozoic-age rift-basins also occur within the "Stable Shelf" area, such as the Dakhla, Beni Suef, El Miniya, Asyut, Kharga, Kom Ombo, Nuqura, Kharit, and Misaha Basins (see Dolson et al., 2001; Taha, 1992).

Sedimentation during the Late Cretaceous was interrupted during the Santonian by the development of inversion-related folds across northern Egypt (Guiraud and Bosworth, 1997; Moustafa, 1988; Sultan and Halim, 1988). The fold-belt, termed the "Syrian-Arc" by Krenkel (1925), extends from the Western Desert, the Eastern Desert, and North Sinai. The Syrian Arc fold-belt has been described from well-exposed outcrops such as Gebel Maghara in north Sinai (Moustafa, in preparation; Moustafa and Khalil, 1989), Abu Roash, west of Cairo (Moustafa, 1988), and at Wadi Araba in the Eastern Desert (Moustafa and Khalil, 1995). At Wadi Araba, sediments were folded, uplifted, and eroded, such that an angular unconformity developed at the onset of a Late Cretaceous (Campanian) transgression. This resulted in Campanian-age open-marine carbonates lying unconformably on steeply dipping Santonian-age clastics (Moustafa and Khalil, 1995).

Phanerozoic Rift Systems and Sedimentary Basins DOI: 10.1016/B978-0-444-56356-9.00018-3

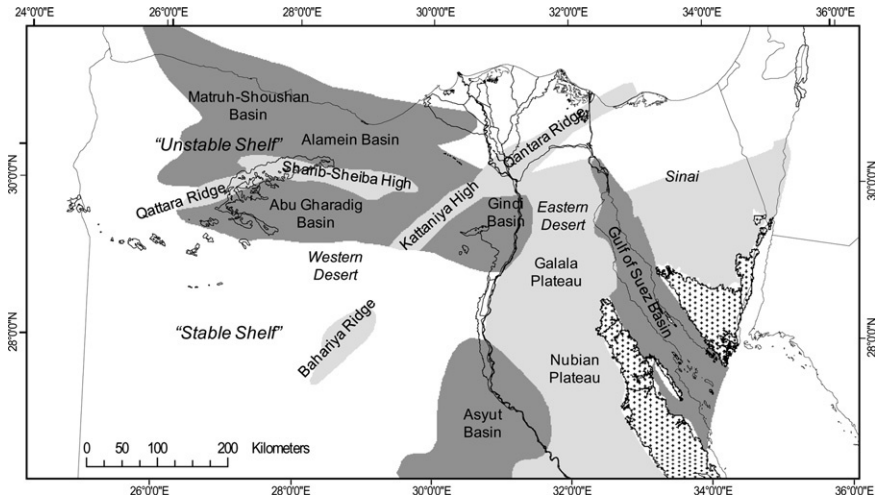

Figure 19.1 Paleozoic and Mesozoic basins in the Western Desert and Sinai *(after Dolson et al., 2001)*. Dark gray denotes main basinal areas, light gray platforms and ridges, and crosses basement.

Subsurface studies in the Western Desert have also shown the presence of inverted faults (e.g., Moustafa et al., 1998), which form important hydrocarbon-producing trends and show that the Syrian Arc inversion fold-belt extends across the whole of northern Egypt. Seismic and well data in the vicinity of the folds have also shown that the inversion did not end in the Late Cretaceous, but continued through to the Oligo-Miocene period. Late Cretaceous to Eocene carbonate sequences in particular show considerable thickness variations in the vicinity of the inversion structures, due to the development of the folds as growth-anticlines at relatively high sea level conditions during these times.

Moustafa et al. (2003) have shown from the Bahariya Oasis that the effects of the compression of the Syrian-Arc fold-belt are not confined to the "Unstable Shelf" of northern Egypt, but were felt at least as far south as the Bahariya Ridge (Fig. 19.1). The cause of the Syrian-Arc fold-belt has been attributed by Guiraud and Bosworth (1997) to changes in the Africa–Arabia plate motion with respect to the Eurasian plate. Counterclockwise rotation of the Africa–Arabia plate from a generally east to northeast movement to a northerly convergence coincided with the onset of inversion at the end of the Santonian.

In this chapter, we present seismic and outcrop data across northern Egypt to reveal the geometrical differences in the structural style of the inversion as it developed from the Santonian to the Oligo-Miocene. We also show that there are examples of compressional deformation occurring over a wide area of northern Egypt, beyond the "Unstable Shelf" area, including the Paleozoic basin of southwest Egypt. We also place the structural geometries in the context of the petroleum systems of the Western Desert and describe the implications for the maturation, migration, and trapping of hydrocarbons.

19.2 Basin stratigraphy

The stratigraphic succession of northern Egypt is shown in Fig. 19.2, which defines the tectono-sequences described here.

Tectono-sequence 1: Paleozoic

The Paleozoic extends across the whole of northern Egypt with two exceptions; on the margins of the Gulf of Suez/Red Sea (Red Sea Hills and Sinai), where the

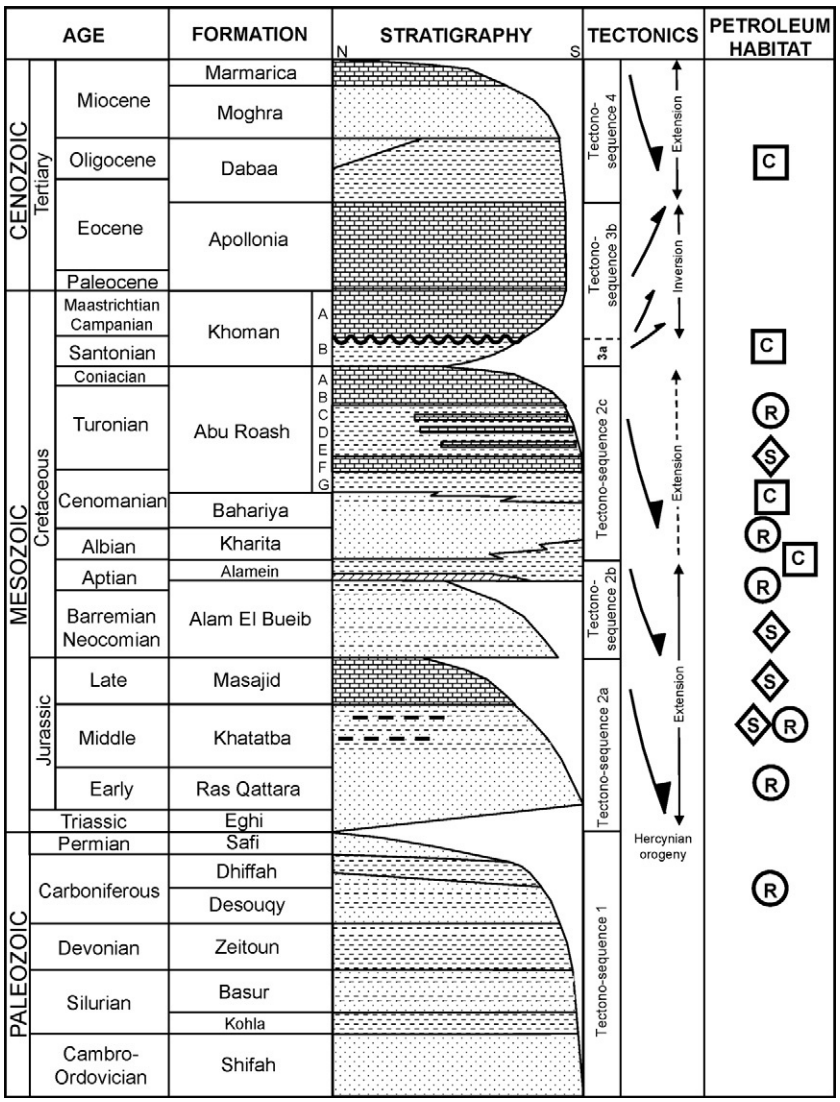

Figure 19.2 Stratigraphic section. For petroleum habitat, S = source, R = reservoir, C = seal.

Paleozoic has been removed in part due to Cenozoic rift-related uplift, exposing basement at the surface, and the Paleozoic is absent in the subsurface in the lower Nile Valley. Here, well data indicate the presence of an approximately 30 km wide N–S trending ridge on which the Jurassic lies directly on basement. This basement ridge occurs south of the Gindi Basin and extends 400 km to the south (Guiraud and Bosworth, 1999, their Figure 6).

In north Sinai, the Paleozoic is typically up to 500 m thick, but in the Ghazalat Basin, in the central Western Desert, and to the west of the Qattara Depression around Siwa, it exceeds 3000 m in thickness. Permian- to Cambrian-age marine and shallow-marine sandstone and shale sequences occur in a broad basin that extends westward to the Kufra Basin in Libya (see Boote et al., 1998; Guiraud and Bosworth, 1999; Lüning et al., 2000). In the Eastern Desert and Sinai, the Paleozoic is the predominantly fluvial and shallow-marine "Nubia Sandstone" sequence, of poorly constrained age due to lack of biostratigraphic markers, except for the presence of a Lower Carboniferous marine carbonate sequence in the Gulf of Suez region. Otherwise, the "Nubia Sandstone" term is lithostratigraphic and applies to an undifferentiated group of clastic sediments ranging from Cambrian to Early Cretaceous age.

According to Keeley and Massoud (1998) and Keeley (1994), the Paleozoic of the Ghazalat Basin was inverted during a Tournasian tectonic event. Subsequent erosion completely removed the Devonian section in the southeast Western Desert, and this section is only preserved in the northwest (Keeley and Massoud, 1998). Between 2.0 and 2.5 km of Lower Paleozoic strata may also have been eroded in southern Israel and Sinai (Kohn et al., 1997), prior to the more recent Gulf of Suez border fault uplift-related erosion.

Tectono-sequence 2: Jurassic to Coniacian

Tectono-sequence 2 is defined on the basis of being syn-rift during the opening of the Tethys margin and the development of rift-basins on the greater Tethyan passive margin. Within this syn-rift tectono-sequence, there are three distinct cycles of transgressive sedimentation marking three subsequences, in the Jurassic (2a), Early Cretaceous (2b), and Late Cretaceous (2c).

Tectono-sequence 2a comprises a transgressive sequence from the non-marine clastics of the Lower Jurassic Ras Qattara Formation, the shallow-marine mixed clastics and carbonates of the Middle Jurassic Khatatba Formation, and the shallow-marine carbonates of the Upper Jurassic Masajid Formation. The Khatatba Formation is the major source-rock for the Western Desert, containing gas-prone shales and oil- and gas-prone coals. The overlying Masajid Formation also contains oil-prone marine carbonates and shales.

A major regression at the start of the Early Cretaceous marks the base of tectono-sequence 2b with deposition of the non-marine to shallow-marine clastics of the

Alam El Bueib Formation. The transgression reached its maximum with the marine deposition of the Aptian-age Alamein Dolomite and Dahab Shale at the end of tectono-sequence 2b.

Jurassic and Lower Cretaceous sediments are commonly deposited in half-graben syn-rift wedges in the Western Desert. The Alamein Dolomite is a good seismic marker defining the top of the Jurassic–Lower Cretaceous syn-rift tectono-sequence. The relatively thin Alamein Dolomite and Dahab Shale Formations represent a regional maximum flooding event at a time when there was a decrease in the dominantly fault-controlled sedimentation in many of the Western Desert basins. The Alamein Dolomite and Dahab Formations were deposited across the region and are only absent, through nondeposition or erosion, over the Sharib–Sheiba High (Fig. 19.1). There is a major unconformity between the Masajid and Alam El Bueib Formations (Sultan and Halim, 1988), and the clastics of the Alam El Bueib Formation generally show more dramatic thickening into basin-controlling faults than the underlying Jurassic, indicating that growth and extension on the faults was greater in the Early Cretaceous than during the Jurassic. According to Guiraud and Bosworth (1999), continental rifting was active during the Early Cretaceous in North Africa and Arabia, producing predominantly E–W oriented rift-basins.

Albian-aged regressive clastic sequences unconformably overlie the Dahab Shale and represent the base of another transgressive cycle. The fluvial to shallow-marine Kharita Formation marks the base of tectono-sequence 2c and is followed by the shallow-marine clastics of the Bahariya Formation, which are Early Cenomanian in age. The transgression continued into the Late Cenomanian, when carbonates of the basal Abu Roash Formation were deposited (the Abu Roash G Member). This was the first in the series of carbonate, shale, and sandstone cycles of the Abu Roash Formation (termed the Abu Roash A to G Members), which included the deposition of an oil-prone carbonate source-rock (the Abu Roash F Member). In the Gulf of Suez, the Abu Roash Formation is stratigraphically equivalent to the Nezzazat Group, which is comprised of the Matulla, Wata, and Raha Formations.

The Albian- to Coniacian-age tectono-sequence 2c in many areas could be considered to be a post-rift sequence to the earlier Jurassic and Early Cretaceous syn-rift sequences, as it typically has a more uniform isopach, thickening generally to the north toward the open-marine Tethys basin. However, on some major extension faults such as the Mubarak and Abu Gharadig Faults (Fig. 19.3), this tectono-sequence continues to expand into the hangingwalls of these faults. Extension and fault-related subsidence therefore remained active during the Late Cretaceous.

Tectono-sequence 3: Santonian to Late Eocene

The base of tectono-sequence 3 is marked by a regressive phase of deposition in the Santonian. The Khoman B Member shales were deposited in relatively restricted basins that were previously tectonically active (Said, 1990).

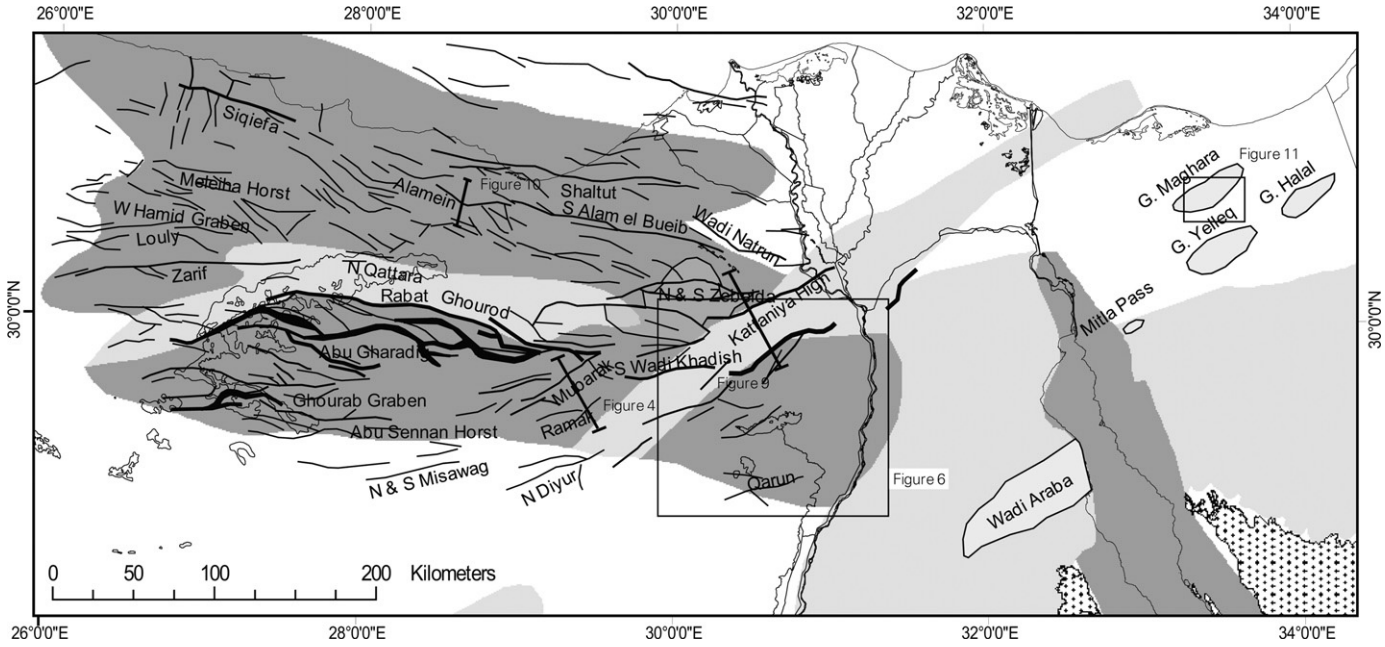

Figure 19.3 Regional fault map of the northern Western Desert, with locations of other figures as shown. Basins and highs are as in Fig. 19.1.

The major phase of transgression, starting in the Campanian, led to increased sea levels in the latest Cretaceous to Eocene, and to the deposition of the chalks and limestones of the Khoman A and Apollonia Formations in the Western Desert. Lithostratigraphic equivalents in the Gulf of Suez region are the Esna and Sudr for the Khoman A, and the Mokattam, Darat, and Thebes Formations for the Apollonia.

Following deposition of the Khoman B Member, the first Syrian-Arc inversion event occurred which resulted in folding, faulting, uplifting, and subsequent erosion of the Santonian and older formations in the cores of the inversion anticlines, such as at Wadi Araba on the western side of the Gulf of Suez (Moustafa and Khalil, 1995). There is a major angular unconformity between the Khoman B and the Khoman A Members, indicating that the first major phase of inversion occurred at the end of Khoman B deposition in the Late Santonian.

The chalks and limestones in tectono-sequence 3 show dramatic thickness variations about the inversion structures, indicating that inversion occurred throughout this period of deposition. Over the crests of the hangingwall inversion anticlines, the Khoman A and Apollonia Formations thin considerably, but deposition continued above the footwalls and in the hangingwalls away from the immediate inverted anticlines.

The impact on the thickness of formations of the Santonian inversion and subsequent growth of the structures during the Late Senonian to Eocene can be seen in isopachs around the Wadi Araba anticline on the northern Gulf of Suez. Figure 19.4 illustrates a series of isopachs based on well data of the Santonian–Coniacian-age Matulla Formation (Khoman B to Abu Roash B equivalent) in tectono-sequence 2c, the Maastrichtian–Campanian Sudr Formation (Khoman A equivalent) in tectono-sequence 3a, and the Paleocene and Eocene-age Esna and Thebes Formations (Apollonia equivalent) in tectono-sequence 3b. The Matulla and Sudr Formation isopachs are regionally uniform to the south or east of the Wadi Araba structure; however, toward the structure the isopach thins to zero, as the formation has been removed due to erosion over the crest of the structure. By contrast, the Esna and Thebes Formation isopachs increase in thickness toward the inversion structure before thinning over the crest. Here, local depocenters developed in front of the inversion structure. The growth of structures such as Wadi Araba also impacted on the deposition of facies in the Late Senonian. Well data show that the Brown Limestone, the major oil-prone carbonate source-rock for the Gulf of Suez, is absent north of a line defined by the southern edge of the inversion structure, suggesting that the structure provided topographical relief which controlled the distribution of organic matter and resulting source facies.

Similar dramatic thickening of the Apollonia Formation in front of inversion anticlines is clear in the Gindi basin that lies to the south of the Kattaniya inverted basin (Abd El-Aziz et al., 1998). The Apollonia Formation reaches a maximum

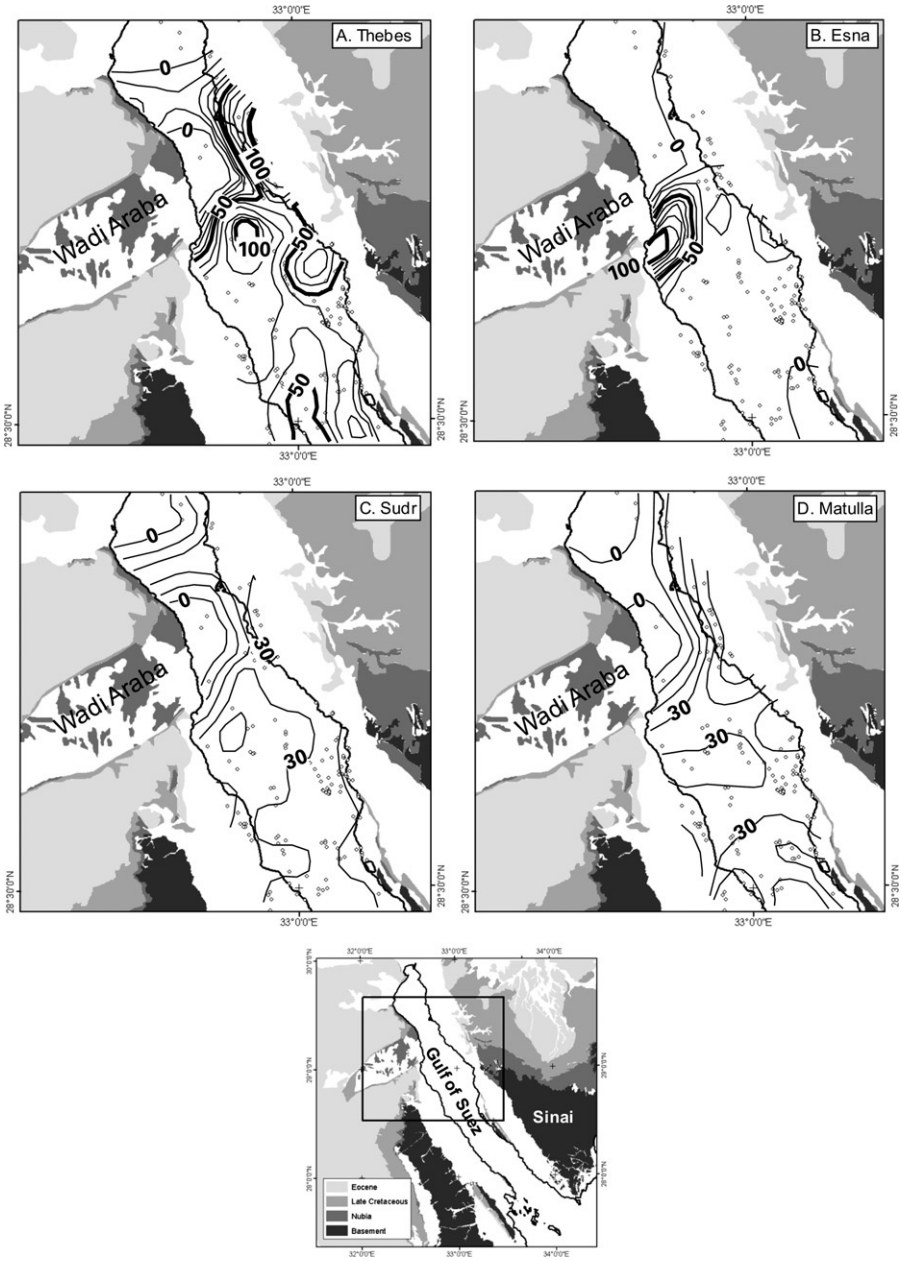

Figure 19.4
Eocene to Late Cretaceous isopach maps around the Wadi Araba Inversion, northern Gulf of Suez. Gray shades represent outcrop of Eocene (lightest), Upper Cretaceous, Lower Cretaceous (Nubia), and Basement (darkest). (A) Eocene-age Thebes Formation, (B) Paleocene-age Esna Formation, (C) Maastrichtian–Campanian-age Sudr Formation, equivalent to the Khoman A Formation, (D) Santonian–Coniacian-age Matulla Formation, equivalent to the Khoman B to Abu Roash B Formations. Circles represent well data points, contour intervals 10 m.

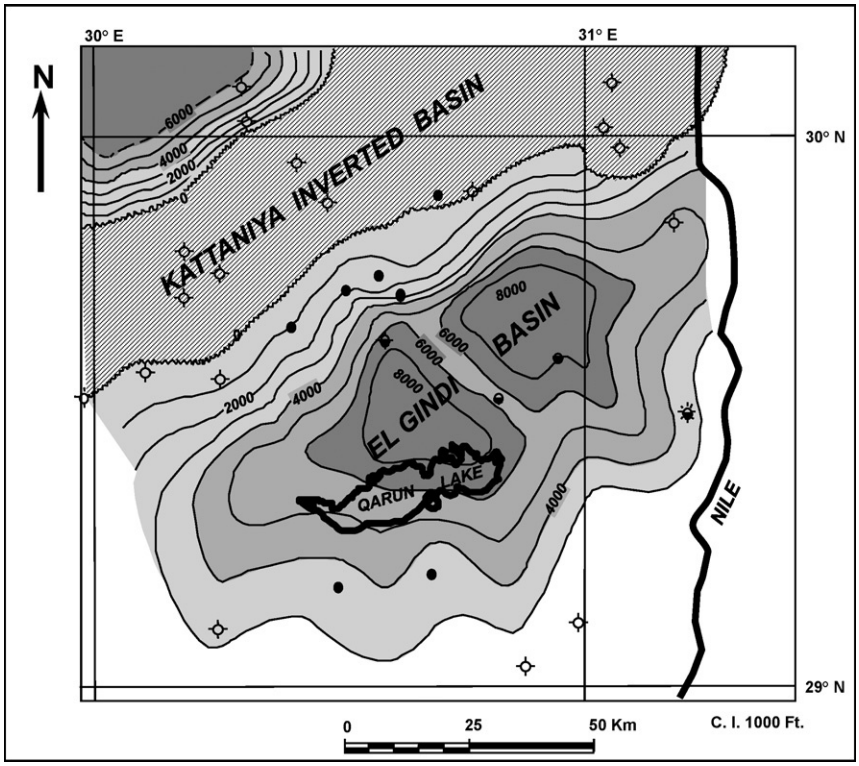

Figure 19.5
Isopach map of the Apollonia Formation in the Gindi basin south of the Kattaniya inverted basin *(after Abd El-Aziz et al., 1998)*.

thickness equal to 2440 m in the Gindi basin (Fig. 19.5). The depocenter of the syn-inversion Apollonia Formation lies to the southeast of the inverted Jurassic–Early Cretaceous basin, now forming the Kattaniya High. The Khoman Formation also shows abrupt thickening to the southeast of the inverted basin but its depocenter lies relatively closer to the inverted basin (Fig. 19.6). This indicates that, during this later phase of basin inversion and growth anticline development, the deposition of the Khoman A Member and Apollonia Formation occurred with continued migration of the depocenter away from the inverted basin.

Tectono-sequence 4: Late Eocene to Pliocene

The Late Eocene–Oligocene Dabaa and Miocene Moghra marine clastics unconformably overlie the Apollonia Formation. In the vicinity of the inversion folds, this has an angular relationship. The Marmarica Formation represents the Middle Miocene part of this sequence.

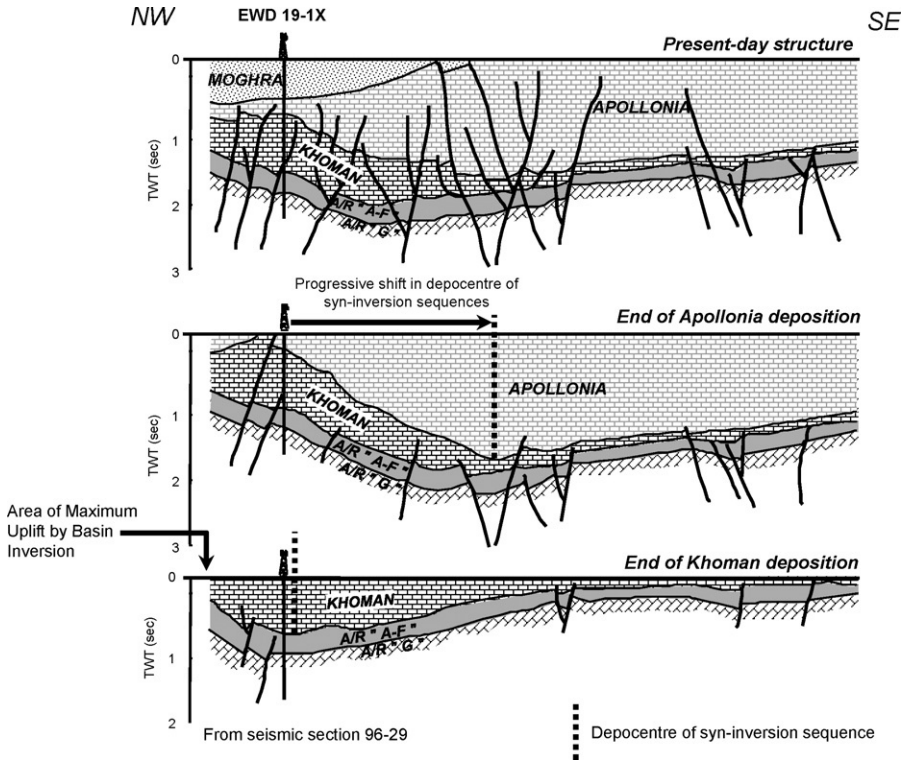

Figure 19.6 Palinspastic reconstruction of a geoseismic section extending from the Kattaniya inverted basin to the Gindi basin *(after Abd El-Aziz et al., 1998)*.

Growth on the inversion structures such as the Mubarak Anticline continued through the Oligocene and into the Early Miocene, as evidenced by the relief on the structure in the Dabaa and Moghra Formations. Contemporaneous with continued growth on the anticlines in the Eastern Desert and Sinai was the initiation of the Gulf of Suez rift and associated basaltic igneous activity, in the Late Oligocene–Early Miocene, due to regional NE–SW extension as the Arabian plate began to separate from the African plate. Oligo-Miocene intrusive and extrusive basalts are found in several locations, some of which appear near major inversion structures, for example, in the northern Gulf of Suez, in the Cairo-Suez area to the north of the Wadi Araba inversion, in northern Fayoum along the southern edge of the Kattaniya inversion (Gebel Qatrani), and 200 km to the southwest of Cairo in the Bahariya Depression (Meneisy, 1990).

Inversion geometries in northern Egypt

In this section, we describe some specific examples of inversion geometries using seismic and outcrop data.

Western Desert: Mubarak inversion

The Mubarak structure is a major inversion anticline lying between the Abu Gharadig and Gindi Basins and lies on the trend to the SW of the Kattaniya High (Figs. 19.1 and 19.3). The structure is a doubly plunging anticline some 50 km wide and 100 km long that trends N70°E and comprises a main northerly anticline with subsidiary subparallel folds to the south. In cross-section (Fig. 19.7), the structure can clearly be interpreted as an inverted half-graben, with the southerly dipping north-bounding fault acting as the major inverted extensional fault. To the southeast, north-dipping antithetic faults are also inverted.

Well data and seismic interpretation of the inversion structure indicate that the Jurassic to Upper Cretaceous sediments thicken in to the hangingwall of the main fault, with the most significant growth occurring during the deposition of the Kharita and Alam El Bueib Formations. The Upper Cretaceous Abu Roash and Khoman B intervals show a more uniform isopach, and the top of this interval marks the significant unconformity between the Khoman B and Khoman A, as the main hangingwall anticline of the structure was inverted during Khoman B deposition. Due to continued growth of the anticline during the Late Cretaceous to Eocene interval of relatively high sea level, the Khoman A and Apollonia Formations thin onto the inversion anticline, whereas on the flanks to the northwest (on the footwall) and southeast, the formations maintain regionally thick isopachs. On the southeast flank of the anticline, small reverse faults occur due to layer-parallel flexural shortening within the fold. Deformation is not restricted to the half-graben, as on the northwest flank of the hangingwall anticline, a footwall syncline is developed. The top Apollonia surface also shows truncation indicating that the anticlinal crest was elevated and subsequently eroded during the Oligo-Miocene regression following Apollonia deposition. The fold continued to grow during the deposition of the Dabaa Formation in the Oligo-Miocene, as indicated by the relief on the top Apollonia surface, which is onlapped by the Dabaa Formation.

Figure 19.8 illustrates a restoration of a simplified true-scale model of the Mubarak inversion and shows restored stages at the present-day, end Apollonia, end Khoman B, and end Alamein time. The magnitude of the inversion on the Mubarak Fault was not enough to remove the net extension on the fault, but the inversion was sufficient to generate over 1.5 km of vertical relief in the core of the resultant hangingwall anticline. The footwall syncline developed at the initial inversion phase at the end of the Khoman B deposition, as the Khoman A and Apollonia maintain a uniform isopach above the footwall and then thin over the growth anticline.

Western Desert: Kattaniya High

Along strike to the northeast of the Mubarak inversion anticline is the Kattaniya High, which is one of the most dramatic examples of basin inversion in the

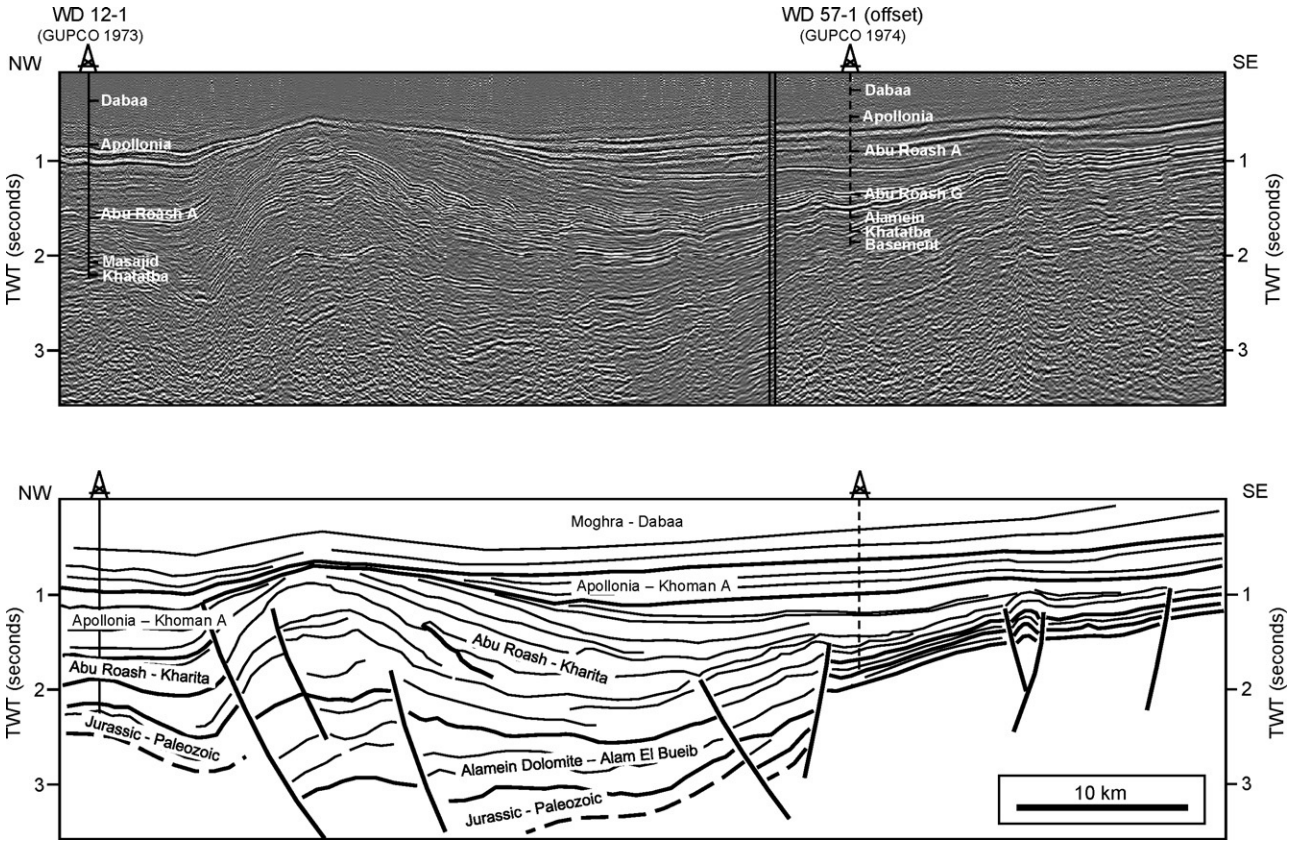

Figure 19.7 Composite 2D seismic lines (WQ85-37B and WQ85-35A) and line drawing interpretation over the Mubarak Inversion structure. Vertical exaggeration is approximately 3:1.

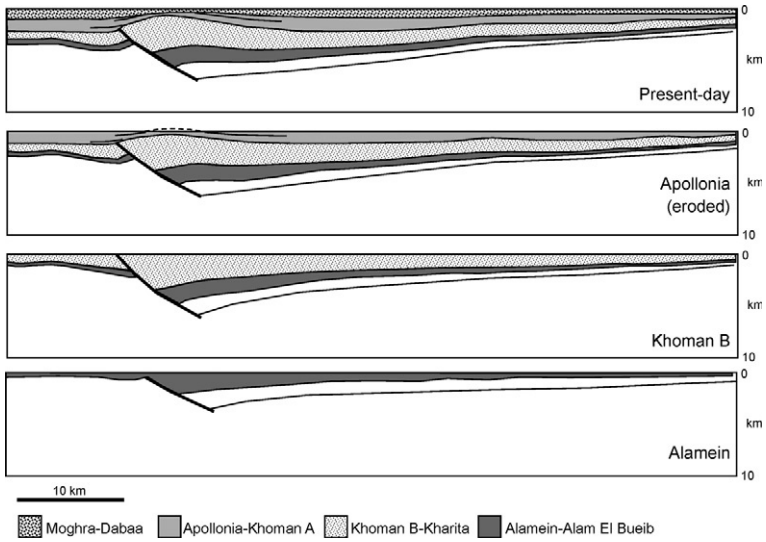

Figure 19.8 Restoration sequence of a 1:1 simplified interpretation across the Mubarak Inversion.

Western Desert. Here, Jurassic sediments in the hangingwall of the main Kattaniya Fault have almost been brought to the surface as a result of inversion. As with the Mubarak structure, the main fault of the Kattaniya inversion is on the northern side of the fold axis and dips to the south. This is a similar doubly plunging anticline, some 35 km wide by 70 km long. Figure 19.9 is a line drawing from seismic over the Kattaniya High. Well data have been projected onto the line to indicate the extent of the inversion; wells T56-1 and T57-1 (both drilled by BP in the 1970s) penetrated vastly different sections, even though the wells are just 5 km apart. T56-1 penetrated the footwall sequence similar to the down-dip Natrun Ghibli E-1 well; however, T57-1 encountered the Jurassic Masajid Formation approximately at the same depth as the Apollonia Formation in T56-1. The total thickness of Jurassic sediments in T57-1 (2789 m) is over twice that in Natrun Ghibli E-1 (1267 m) and is actually more because the base of the Jurassic was not reached in T57-1. Interpretation of the seismic and well data together shows that T57-1 was drilled in the inverted hangingwall of a Jurassic half-graben. The Dabaa Formation clastics unconformably overlie the Lower Cretaceous sequences over the crest of the structure, effectively removing any top seal to the main hangingwall anticline. To the south of this major inversion anticline (drilled by the T56-1 and T57-1 wells) the depocenters of the Khoman and Apollonia shift southward as shown in Fig. 19.6. Also, to the south of the main inverted fault lie smaller parasitic reverse faults with associated fault-propagation folds. These lie beneath the thicker Apollonia top seal interval and have been proved to be successful oil traps (e.g., the Qarun oil field, discovered by the El Sagha-2X well in 1995) Nemec (1996).

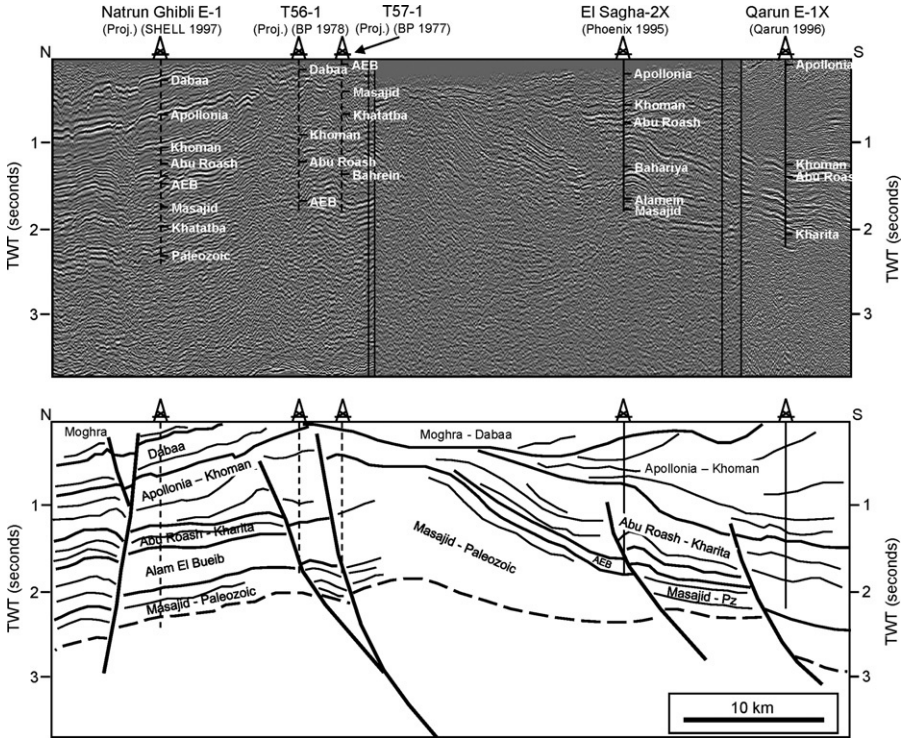

Figure 19.9 Composite 2D seismic lines (LVO-20, SQ3-150, 9402-Hi55-25) and line drawing interpretation over the Kattaniya High. Vertical exaggeration is approximately 3:1.

Western Desert: Alamein

The Alamein inversion trend (see Fig. 19.3) lies in the Alamein Basin, north of the Sharib–Sheiba High. The trend is oriented WSW–ESE and is approximately 70 km in length and 30 km wide. It consists of a series of anticlines that are of a much smaller scale compared to the Mubarak–Kattaniya structures, measuring less than 10 km in length. They are associated with a series of relatively small oil pools (e.g., the Aghar, Razzak, Alamein, and Burg El Arab fields). Figure 19.10 is a three-dimensional seismic line and interpretation across the Razzak structure. Well and seismic data show that the structure has hangingwall extensional growth geometries in the Alamein to Alam El Bueib (tectono-sequence 2b) and Abu Roash to Kharita (tectono-sequence 2c) intervals. The Razzak Fault was inverted in the Early Senonian to generate folding and minor erosion over the crest of the resultant hangingwall anticline, prior to the deposition of the Khoman and Apollonia Formations. Unlike the major inversions to the south, there is no major isopach variation over the anticline of the Apollonia–Khoman interval. However, erosion over the structure at the top of the Apollonia Formation and deformation of the base Dabaa Formation indicates that the Razzak fault continued to invert into the Oligocene.

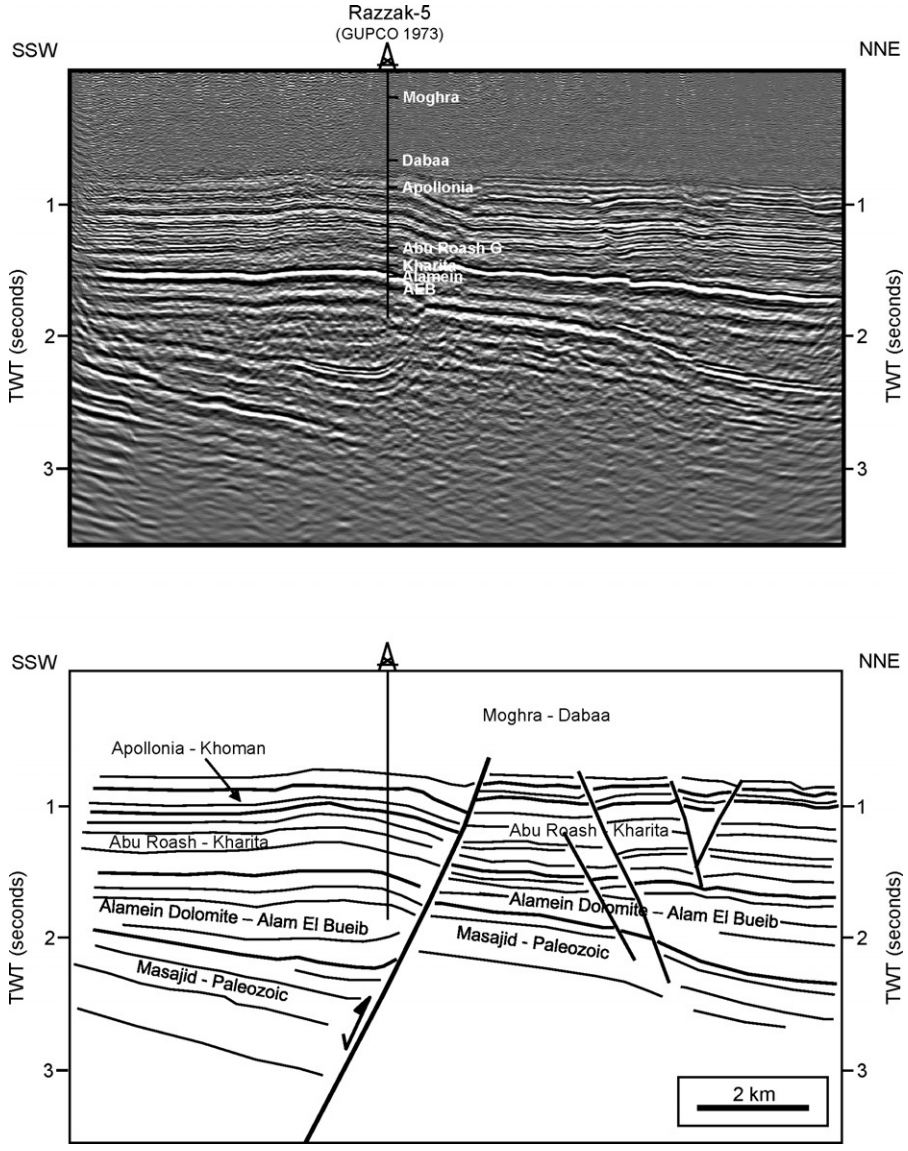

Figure 19.10 Arbitrary 3D seismic line and line drawing interpretation over the Razzak Field, Alamein Inversion trend. Vertical exaggeration is approximately 2:1.

North Sinai: Gebel Maghara

Three major inversion anticlines are located in north Sinai: namely, Gebel Maghara, Gebel Yelleq, and Gebel Halal (Fig. 19.3). These NE–SW oriented folds are 40–50 km long and about 20 km wide. They have gentle NW-dipping flanks (5–15°) and steep SE-dipping flanks that are vertical to overturned in places and associated with steep NW-dipping reverse faults. The three major folds of north

Sinai represent fault-propagation folds formed by inversion of Jurassic–Early Cretaceous extensional basins. Jurassic syn-rift rocks are over 1900 m thick in the Gebel Maghara area (Al-Far, 1966) and 3234 m thick in the core of Gebel Halal fold (Jenkins, 1990). Taking into consideration the fact that the Gebel Halal fold lies to the south of the latitude of the Gebel Maghara fold, the thick Jurassic section in the two areas represents separate half-graben basins with NW-dipping basin-bounding faults on the southern sides. Changes in thickness of the Aptian rocks across the basin-bounding fault are clear in the Gebel Maghara area indicating that basin subsidence continued during that time (Moustafa et al., in preparation). The Cenomanian–Turonian section of northern Sinai represents post-rift rocks deposited after basin subsidence ceased before the Cenomanian. Basin inversion started in Santonian time (e.g., Areif El Naqa area; Bartov et al., 1980) and continued during the Early Tertiary as indicated by the deposition of a syntectonic debris flow between Danian and Upper Paleocene rocks and within the Lower Eocene rocks on the southern side of the Gebel Maghara fold, as well as by the folding of Lower-Middle Eocene rocks (Moustafa et al., in preparation).

Detailed field mapping of the Gebel Maghara area (Moustafa, in preparation) indicates the existence of three main asymmetric, NE–SW oriented, SE verging anticlines (Fig. 19.11). These folds are bounded on their southeastern sides by steeply dipping reverse faults. The northern (Hamayir) and the central (Mahgara) reverse faults are well exposed and dip at angles exceeding 50° NW whereas the southernmost reverse fault is concealed and is only visible on reflection seismic sections. The

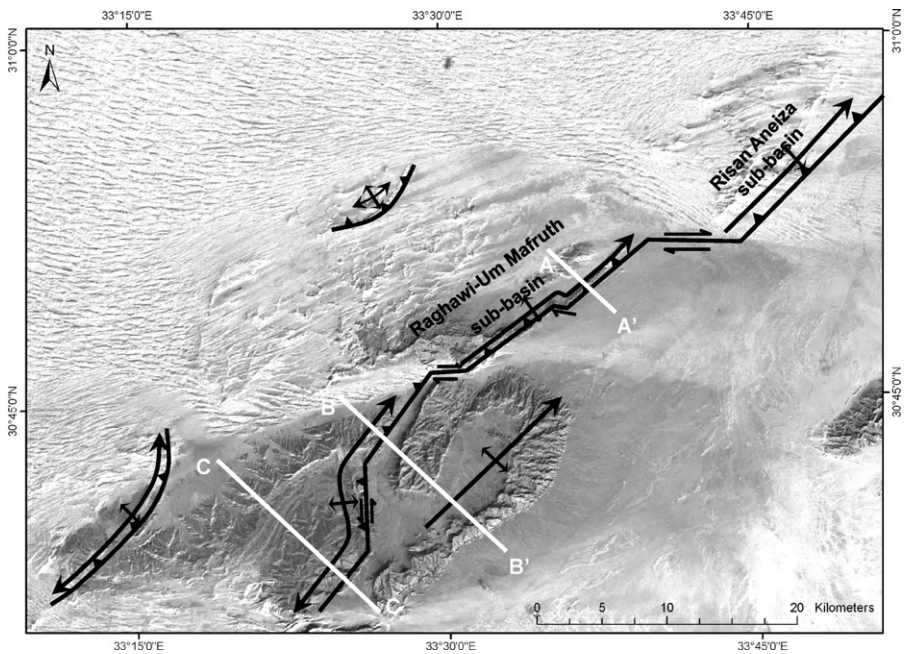

Figure 19.11 Landsat TM images showing the main structures of Gebel Maghara area *(after Moustafa, in preparation).* NE–SW oriented faults are main basin-bounding faults, whereas E–W and N–S faults are transfer faults. NE–SW oriented faults were reactivated by reverse slip during basin inversion whereas transfer faults were reactivated by oblique-slip movement.

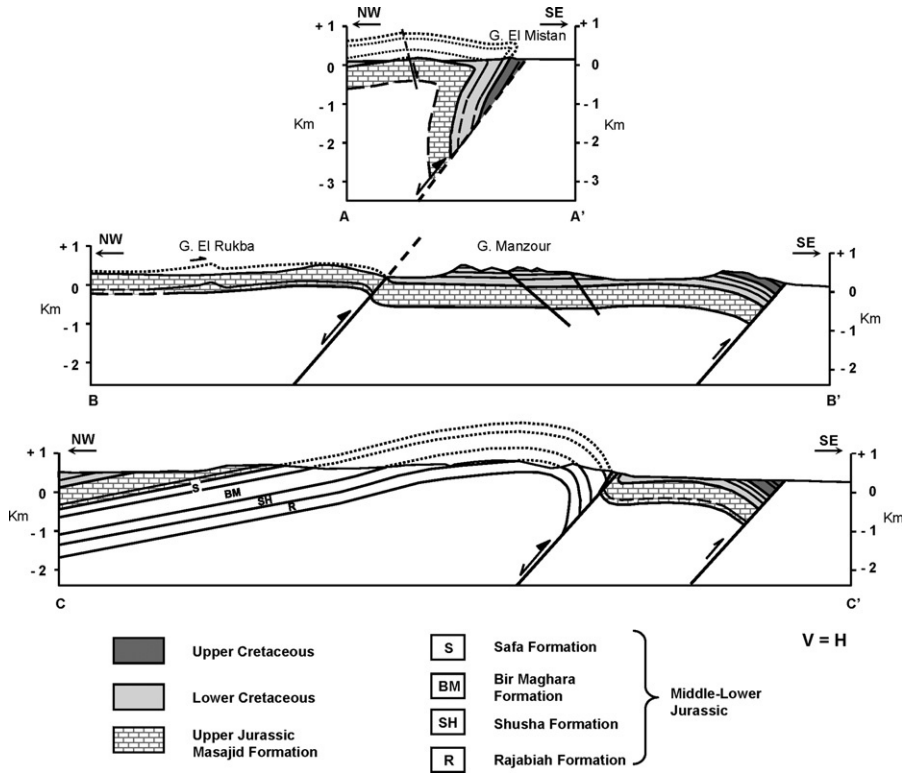

Figure 19.12 True-scale (1:1) structural cross-sections of Gebel Maghara area, locations on Fig. 19.11 *(after Moustafa, in preparation)*.

asymmetric folds on the hangingwall of these reverse faults have very steep, vertical to overturned southeastern flanks lying in the immediate vicinity of the reverse faults and show structural relief equal to about 2 km (e.g., Fig. 19.12).

The Maghara reverse fault has a zigzag geometry with three different fault trends. These are NE–SW oriented segments with pure reverse slip, WNW–ESE oriented fault segments with right-lateral oblique slip, and NNE–SSW oriented segments with left-lateral oblique slip. The zigzag geometry of the Maghara reverse faults affects the geometry of the hangingwall anticline as indicated by the change in its trend with changes in the orientation of the fault (Fig. 19.12). This indicates that the WNW–ESE and NNE–SSW oriented fault segments are not tear faults dissecting the NE–SW oriented reverse fault. On the contrary, they represent early transfer faults during the Jurassic–Aptian extensional phase of deformation of the area. This also explains why the main axis of the extensional basin and of the inversion structure is laterally shifted from one locality to the other (Fig. 19.12).

A reflection seismic section, extending from Gebel Maghara to the eastern side of Gebel Yelleq (Fig. 19.13), clearly shows the inverted basins of both areas.

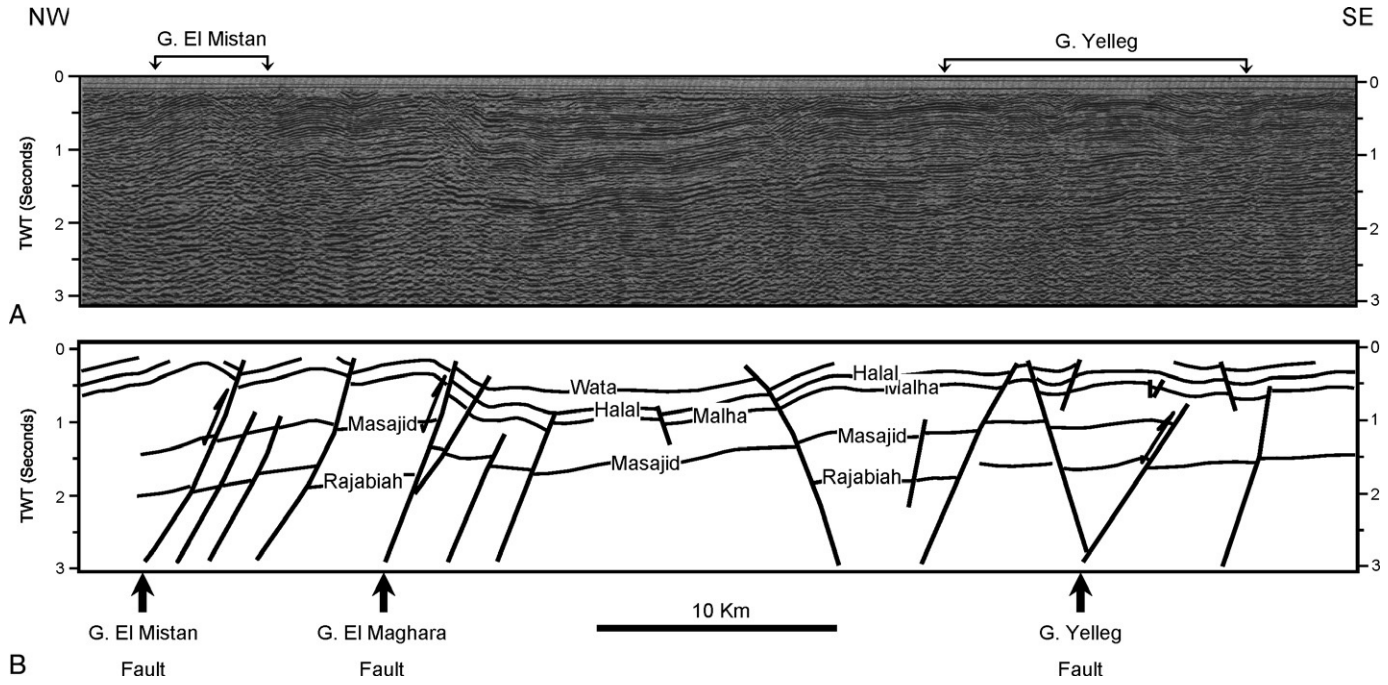

Figure 19.13 2D seismic line (CS91-05) and line drawing interpretation across the Gebel Maghara and Gebel Yelleq inverted structures.

It also shows the thicker Jurassic–Early Cretaceous syn-rift section in the two basins compared to the intervening area. The Gebel Yelleq extensional basin had a graben-like geometry with two oppositely dipping faults on the NW and SE sides of the basin. The SE bounding fault is currently a blind reverse fault that dies within the Lower Cretaceous section and is overlain by a steep monocline (dip is up to 52° SE; Gibali, 2003) representing a fault-propagation fold. The NW bounding fault is also associated by a hangingwall anticline due to basin inversion (Fig. 19.13). This clearly indicates that the two faults bounding the NW and SE sides of Gebel Yelleq extensional basin were reactivated by reverse slip during basin inversion. The seismic section also shows the regional northwestward dip of the syn-rift sequences is opposite to the original direction of dip during basin extension, when the dip would have been toward the main boundary faults. Such dip reversal represents total basin inversion (i.e., reverse slip due to basin inversion exceeds early normal slip during extensional deformation). Any hydrocarbon migration from syn-rift source-rocks would thus be directed toward the inversion anticlines. The Halal-1 exploratory well (drilled in 1976) is a failed test for hydrocarbons in the crest of the Gebel Halal inversion anticline, where the Jurassic was encountered at just 750 m below the surface.

Southwestern Desert

In the far west of Egypt, south of the Siwa Oasis, a series of 1970s vintage two-dimensional seismic lines show that compressional structures are not restricted to the Syrian-Arc in northern Egypt. Figure 19.14 is a 180-km-long seismic line (UER-101) oriented NNW–SSE lying some 100 km south of the Siwa oasis. The line intersects GPC well Dessouky-1 (drilled in 1972) in which the Kharita Formation (tectono-sequence 2c) unconformably overlies the Carboniferous Dhiffah Formation (tectono-sequence 1). Paleozoic strata and overlying Late Cretaceous to Eocene sediments are predominantly flat lying, except for the presence of relatively narrow, vertical folds. The folding can be seen to affect the whole stratigraphic interval from Apollonia and Khoman Formations near the surface, and links down to basement-cored reverse faults. Given the age of the youngest deformed strata is Eocene, it is suggested that these fault-propagation folds were generated by Eocene-age reactivation of preexisting (possibly Hercynian) reverse faults, or are Eocene-aged reverse faults. The location of the compressional features is also approximately along strike from the Kattaniya and Bahariya trends, which would be near the northern edge of the "Stable Shelf" basement platform.

Impact of inversion on petroleum system evolution

The examples of inversion structures presented here have hydrocarbon pools associated with them, developed to varying degrees and at different locations. To understand the relationships between inversion, trapping, and migration, three of the structures (Razzak, Mubarak, and Kattaniya) have been stylized in Fig. 19.15 to illustrate the main components of the petroleum system.

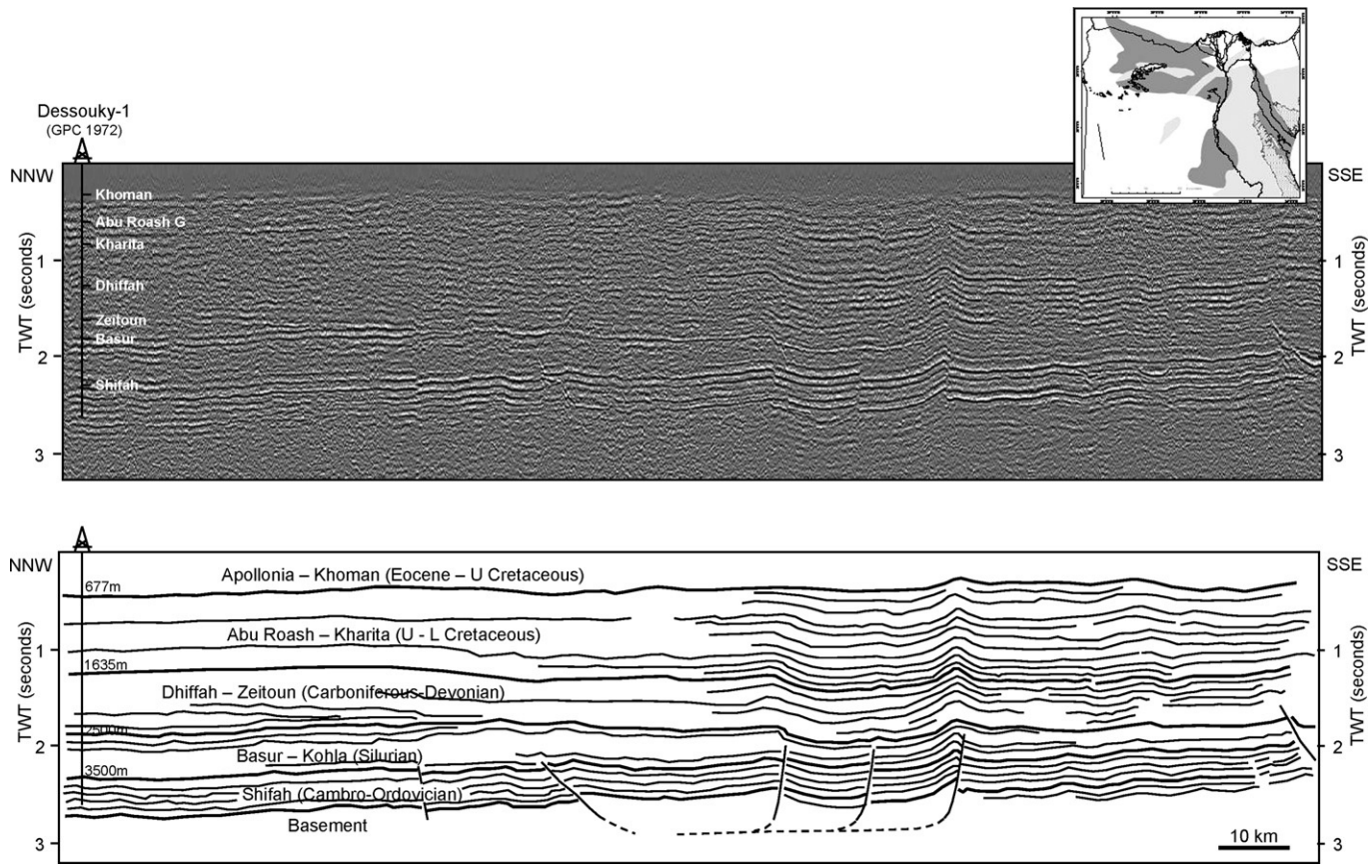

Figure 19.14 2D seismic line (UER-101) and line drawing interpretation over the Paleozoic Ghazalat Basin, showing Late Cretaceous-age compressional structures. Inset: location map. Vertical exaggeration is approximately 10:1.

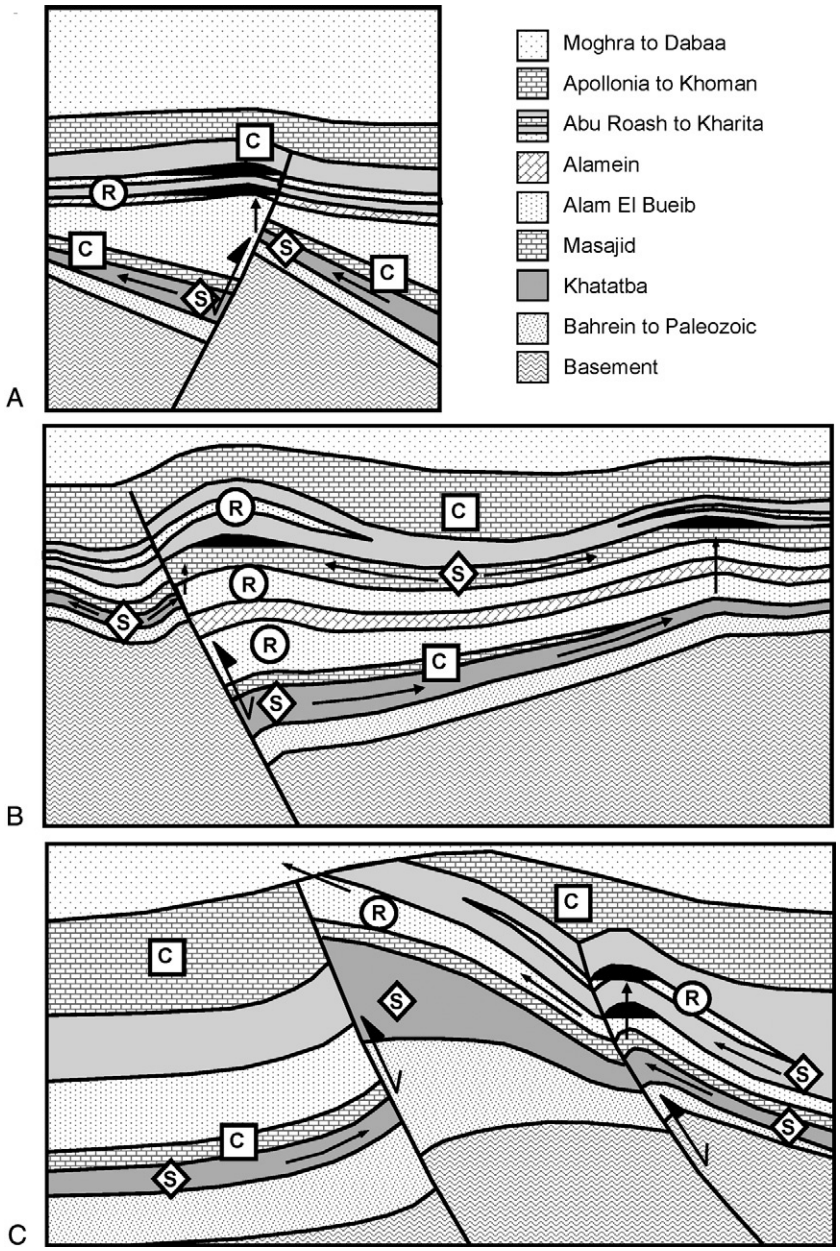

Figure 19.15 Potential charge scenarios of structures associated with inversion structures. The examples from the Western Desert illustrate increasing severity of inversion with subsequent variations on the petroleum system migration patterns. (A) Razzak, (B) Mubarak, (C) Kattaniya. For petroleum habitat, S = source, R = reservoir, C = seal, small arrows indicate hydrocarbon migration flow directions.

The Razzak inversion structure (Fig. 19.15A) is relatively very mild, but with the hangingwall anticlinal flexure developed enough to create a closed structure. Oil is reservoired in the Bahariya and Alamein Dolomite Formations, and is sealed by the Abu Roash Formation. Oils are sourced from the underlying Jurassic and the hangingwall anticline lies above the focus point where the Jurassic in the footwall intersects the Razzak Fault. Hydrocarbon migration would have traveled up-dip, from the kitchen to the north, to the footwall crest and then vertically through the Alam El Bueib Formation as far as the regional top seal (Abu Roash). Mature hydrocarbons on the hangingwall side of the fault would migrate up-dip and therefore away from the hangingwall anticline.

A more severe inversion structure such as the Mubarak anticline (Fig. 19.15B) has a similar migration pattern to Razzak, except that the charge from the footwall to the hangingwall anticline is very limited because the footwall developed a synclinal geometry. The majority of mature hydrocarbons will migrate away from the hangingwall and only a limited kitchen area adjacent to the fault will thus be available for charging the hangingwall structures. The hangingwall anticline may also be charge limited from the Jurassic due to the presence of a tight Masajid limestone seal above the source. The major anticline is effectively charge de-focused for the Jurassic, because hydrocarbons migrate laterally up-dip away from the structure. However, any structure that is present due to inversion on antithetic faults at the edges of the half-graben may receive charge where it is focused beneath the reservoir. Younger source-rocks such as the Abu Roash F become mature where there has been significant syn-inversion deposition and burial, which is typically in basinal synclines between inversion anticlines. In structures such as the Mubarak anticline, hydrocarbons will migrate from the kitchens toward any adjacent structural high and hence the shallower Abu Roash reservoirs are more likely to be charged (e.g., the Karama Fields located on the southern margin of the inversion).

In the examples of the most severe inversion, such as the Kattaniya High (Fig. 19.15C), the inversion results in the hangingwall anticline reservoirs becoming breached and source-rocks "switched off," due to being elevated to shallower depths than those of maturation. While there may be the potential for migration from the footwall source-rocks, however, to date only shows have been reported from wells drilled on the main structural high. Structures that are successfully charged on the Kattaniya High are the smaller-scale fault-propagation folds, which sit on the southern flank of the inverted half-graben (e.g., the Qarun Field). These structures have remained unbreached and received charge from down-dip Jurassic and Abu Roash F source-rocks to the south in the Gindi Basin.

19.3 Conclusions

Northern Egypt has undergone regional north–south oriented Jurassic to Cretaceous extension and has been subsequently inverted during the Latest Cretaceous (WNW–ESE compression) to Oligocene (NW–SE compression).

In the Western Desert, Jurassic to Early Cretaceous deposition occurred in a series of half-graben bounded mainly by south-dipping extensional faults that are counter-regional to the Tethys passive continental margin to the north. By contrast, extensional basins developed in northern Sinai (e.g., Gebel Maghara) are bounded by north-dipping faults. The present-day Nile approximately defines a N–S "accommodation zone" between these dip provinces.

Inversion occurred in at least two distinct phases. Initially this occurred in the Santonian, marked by the top Khoman B angular unconformity, which resulted in uplift and erosion, and second during the Early Tertiary, during which inversion was synchronous with significant basin growth in the Abu Gharadig and Gindi Basins. This resulted in thick Khoman A to Apollonia deposition and burial/maturation of the Abu Roash F Member.

Although the Syrian-Arc inversion was generated by relative rotations and convergence between the Africa and Eurasia plates, there appears to be no relationship between the severity of inversion and the distance to the plate boundary. Generally, faults with the largest amount of normal slip formed in the early rift phase (e.g., basin/rift-bounding faults) and experienced the largest amount of reverse slip during basin inversion. This observation does not change whether the basin-bounding fault is dipping away from the direction of the compressive stress (e.g., in the north Western Desert) or toward the direction of the compressive stress (e.g., the north Sinai inverted structures). In counter-regional examples, basins are inverted as the footwall wedge pushed underneath the hangingwall basin-depocenter. In addition, the northern edge of the basement platform (the "Stable Shelf") area acted as a buttress, and defines a line to the north of which there is significant inversion. However, platform areas that did not go through the rifting phase are still deformed by the regional compressive stress. Examples of platform compression occur in the Paleozoic basin; in the western part of the Western Desert, and the Bahariya–Diyur platform. It appears that only the Sharib–Sheiba High, to the north of the Abu Gharadig Basin, failed to invert in the same way as individual Mesozoic extensional faults. This major basement-cored high in the central Western Desert appears to have been passive and remained a high-throughout Mesozoic basin development.

The magnitude of basin inversion has a distinct impact on the hydrocarbon potential of a given structure. In the major inversions (e.g., Kattaniya High and the north Sinai folds), the hangingwall basins are inverted such that the main reservoir and source-rock sections are brought to the surface and are thus breached, as well any previous mature source-rocks becoming non-generative. However, any less severe inversion structures that remain buried by the post-Eocene section will have a better chance of preserving the structural geometry, and therefore top seal.

In hangingwall geometries such as at the Mubarak anticline where the geometry of the deeper syn-rift sequences are more planar than the overlying folded

post-rift, migration from the syn-rift source-rocks beneath the main inversion anticlines will be carried up-dip along any permeable formations and beneath any local top seals. Major hangingwall inversion anticlines like these have the potential to be de-focused and consequently not charged.

Similarly, the magnitude of inversion has an impact on lateral migration; total inversion, as in north Sinai, has reversed the dip direction of the early syn-rift Jurassic source-rocks. In this case, syn-rift source-rocks are deeply buried and lateral charge will be directed toward the large inversion anticline that is affected by crestal extension fractures and faults, which will reduce trap integrity. Migration of hydrocarbons from later source-rocks will also be controlled by the dip direction of the inverted basin. In contrast to the syn-rift sequences, as post-rift kitchens tend to lie in the synclines between inversion anticlines, such that lateral migration is generally toward the anticlinal axes. These structures can therefore be more successful at shallower reservoir levels.

Acknowledgments

The authors thank BP/GUPCO for permission to publish this chapter and EGPC for permission to use the seismic sections from the Western Desert and north Sinai.

References

Abd El-Aziz, M., Moustafa, A.R., Said, S.E., 1998. Impact of basin inversion on hydrocarbon habitat in the Qarun Concession, Western Desert, Egypt, Proceedings of the 14th EGPC Exploration & Production Conference, Cairo, vol. 1, pp. 139–155.

Al-Far, D.A., 1966. Geology and coal deposits of Gebel El Maghara (North Sinai). Geological Survey of Egypt, Paper No. 37, p. 59.

Bartov, Y., Lewy, Z., Steinitz, G., Zak, I., 1980. Mesozoic and Tertiary stratigraphy, paleogeography and structural history of the Gebel Arief en Naqa area, eastern Sinai. Israel J. Earth Sci. 29, 114–139.

Boote, R.D., Clark-Lowes, D.D., Traut, M., 1998. Paleozoic petroleum systems of North Africa. Petroleum Geology of North Africa, Geological Society Special Publication No. 132, Geological Society of London, pp. 7–68.

Dolson, J.C., Shann, M.V., Matbouly, S.I., Hammouda, H., Rashed, R.M., 2001. Egypt in the twenty-first century: petroleum potential in offshore trends. GeoArabia 6, 211–230.

Gibali, H., 2003. Structural Setting of Gebel Yelleg and Gebel El Falig and its Relationship to the Hydrocarbon Potentialities of North Sinai, Egypt. M.Sc. Thesis. Ain Shams University, p. 150.

Guiraud, R., 1998. Mesozoic rifting and basin inversion along the northern African Tethyan margin: an overview. In: Macgregor, D.S., Moody, R.T.J., Clark-Lowes, D.D. (Eds.), Petroleum Geology of North Africa, Geological Society Special Publication No. 132, Geological Society of London, pp. 217–229.

Guiraud, R., Bosworth, W., 1997. Senonian basin inversion and rejuvenation of rifting in Africa and Arabia: synthesis and implications to plate-scale tectonics. Tectonophysics 282, 39–82.

Guiraud, R., Bosworth, W., 1999. Phanerozoic geodynamic evolution of northeastern Africa and the northwestern Arabian platform. Tectonophysics 315, 73–108.

Jenkins, D.A., 1990. North and Central Sinai. In: Said, R. (Ed.), The Geology of Egypt., A.A. Balkema, Rotterdam, pp. 361–380.

Keeley, M.L., 1994. Phanerozoic evolution of the basins of Northern Egypt and adjacent areas. Geologische Rundcshau 83, 728–742.

Keeley, M.L., Massoud, M.S., 1998. Tectonic controls on the petroleum geology of NE Africa. In: Macgregor, D.S., Moody, R.T.J., Clark-Lowes, D.D. (Eds.), Petroleum Geology of North Africa, Geological Society Special Publication No. 132, Geological Society of London, pp. 265–282.

Krenkel, E., 1925. Geologie der Erde, Geologie afrikas, Bd. I. Gerbrüder Borntraeger, 461 pp.

Kohn, B.P., Feinstein, S., Foster, D.A., Steckler, M.S., Eyal, M., 1997. Thermal history of the eastern Gulf of Suez. II. Reconstruction from apatite fission track and 40Ar/39Ar K-feldspar measurements. Tectonophysics 283, 219–239.

Lüning, S., Craig, J., Loydell, D.K., Storch, P., Fitches, B., 2000. Lower Silurian "hot-shales" in North Africa and Arabia: regional distribution and depositional model. Earth Sci. Rev. 49, 121–200.

Meneisy, M.Y., 1990. Vulcanicity. In: Said, R. (Ed.), The Geology of Egypt, A.A. Balkema, Rotterdam, pp. 157–172.

Moustafa, A.R., 1988. Wrench tectonics in the north Western Desert of Egypt (Abu Roash area, southwest of Cairo), Middle East Research Centre, Ain Shams University, Earth Science Series, vol. 2, pp. 1–16.

Moustafa, A.R., in preparation. Structural architecture of late Cretaceous-Early Tertiary inverted structures in northern Sinai (Gebel Maghara area), Egypt. J. Struct. Geol.

Moustafa, A.R., Khalil, M.H., 1989. North Sinai structures and tectonic evolution: MERC, Ain Shams University. Earth Sci. Ser. 3, 215–231.

Moustafa, A.R., Khalil, M.H., 1995. Superposed deformation in the northern Suez Rift, Egypt: relevance to hydrocarbon exploration. J. Pet. Geol. 18 (3), 245–266.

Moustafa, A.R., El-Badrawy, R., Gibali, H., 1998. Pervasive E-ENE oriented faults in northern Egypt and their effect on the development and inversion of prolific sedimentary basins. Proceedings of the 14th Petroleum Conference, EGPC, Cairo, vol. 1, pp. 51–67.

Moustafa, A.R., Saoudi, A., Moubasher, A., Ibrahim, I.M., Molokhia, H., Schwartz, B., 2003. Structural setting and tectonic evolution of the Bahariya Depression, Western Desert, Egypt. GeoArabia 8, 91–124.

Moustafa, A.R., Kuss, J., Bassiouni, M.A., Morsi, A., Speijer, R., Bachmann, M., in preparation. Tectonic evolution of Gebel Maghara area. Northern Sinai, Egypt.

Nemec, M.C., 1996. Qarun oil field, Western Desert, Egypt. Proceedings of 13th EGPC Petroleum Conference, pp. 140–164.

Said, R., 1990. Cretaceous paleogeographic maps. In: Said, R. (Ed.), The Geology of Egypt. A.A. Balkema, Rotterdam, pp. 439–449.

Said, R., 1962. The Geology of Egypt. Elsevier, p. 377.

Sultan, N., Halim, M.A., 1988. Tectonic framework of northern Western Desert, Egypt & its effect on hydrocarbon accumulations. Proceedings of 9th EGPC Petroleum Conference, EGPC Egyptian General Petroleum Corporation, Cairo, vol. 2, pp. 1–22.

Taha, M.A., 1992. Mesozoic rift basins in Egypt: their southern extension and impact on future exploration, Proceedings of 11th EGPC Petroleum Conference, EGPC Egyptian General Petroleum Corporation, Cairo, vol. 2, pp. 1–19.

Index

Note: Page numbers *f* indicate figures and *t* indicate tables.

C

K

L

N

O

P

Q

R